

## INFORMATION TO USERS

This manuscript has been reproduced from the microfilm master. UMI films the text directly from the original or copy submitted. Thus, some thesis and dissertation copies are in typewriter face, while others may be from any type of computer printer.

**The quality of this reproduction is dependent upon the quality of the copy submitted.** Broken or indistinct print, colored or poor quality illustrations and photographs, print bleedthrough, substandard margins, and improper alignment can adversely affect reproduction.

In the unlikely event that the author did not send UMI a complete manuscript and there are missing pages, these will be noted. Also, if unauthorized copyright material had to be removed, a note will indicate the deletion.

Oversize materials (e.g., maps, drawings, charts) are reproduced by sectioning the original, beginning at the upper left-hand corner and continuing from left to right in equal sections with small overlaps.

Photographs included in the original manuscript have been reproduced xerographically in this copy. Higher quality 6" x 9" black and white photographic prints are available for any photographs or illustrations appearing in this copy for an additional charge. Contact UMI directly to order.

ProQuest Information and Learning  
300 North Zeeb Road, Ann Arbor, MI 48106-1346 USA  
800-521-0600

UMI<sup>®</sup>



**University of Alberta**

**Structural and Functional Studies of Succinyl-CoA Synthetase**

by

Michael A. Joyce



**A thesis submitted to the Faculty of Graduate Studies and Research in partial fulfillment of  
the requirements for the degree of Doctor of Philosophy.**

**Department of Biochemistry**

**Edmonton, Alberta**

**Spring 2000**



**National Library  
of Canada**

**Acquisitions and  
Bibliographic Services**

**395 Wellington Street  
Ottawa ON K1A 0N4  
Canada**

**Bibliothèque nationale  
du Canada**

**Acquisitions et  
services bibliographiques**

**395, rue Wellington  
Ottawa ON K1A 0N4  
Canada**

*Your file Votre référence*

*Our file Notre référence*

**The author has granted a non-exclusive licence allowing the National Library of Canada to reproduce, loan, distribute or sell copies of this thesis in microform, paper or electronic formats.**

**The author retains ownership of the copyright in this thesis. Neither the thesis nor substantial extracts from it may be printed or otherwise reproduced without the author's permission.**

**L'auteur a accordé une licence non exclusive permettant à la Bibliothèque nationale du Canada de reproduire, prêter, distribuer ou vendre des copies de cette thèse sous la forme de microfiche/film, de reproduction sur papier ou sur format électronique.**

**L'auteur conserve la propriété du droit d'auteur qui protège cette thèse. Ni la thèse ni des extraits substantiels de celle-ci ne doivent être imprimés ou autrement reproduits sans son autorisation.**

**0-612-59978-7**

**Canada**

**University of Alberta**

**Library Release Form**

**Name of Author:** Michael A. Joyce

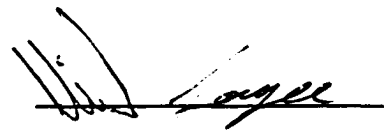
**Title of Thesis:** Structural and Functional Studies of Succinyl-CoA Synthetase

**Degree:** Doctor of Philosophy

**Year this Degree Granted:** 2000

Permission is hereby granted to the University of Alberta to reproduce single copies of this thesis to lend or sell such copies for private, scholarly, or scientific research purposes only.

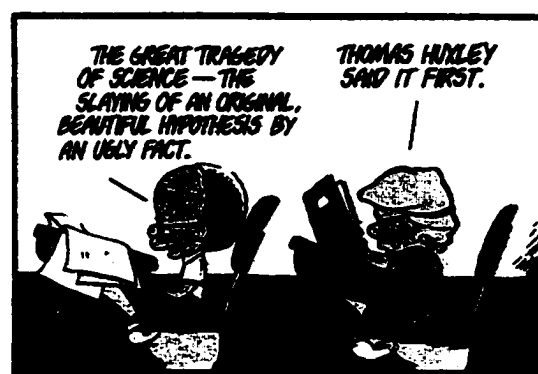
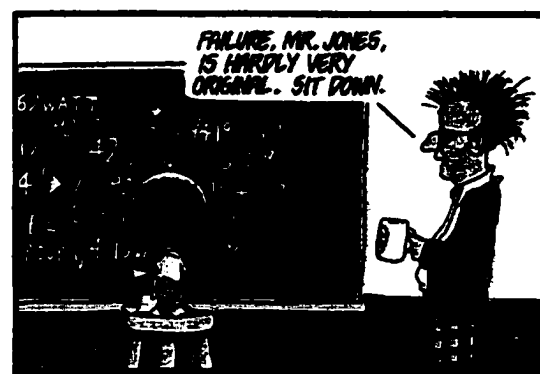
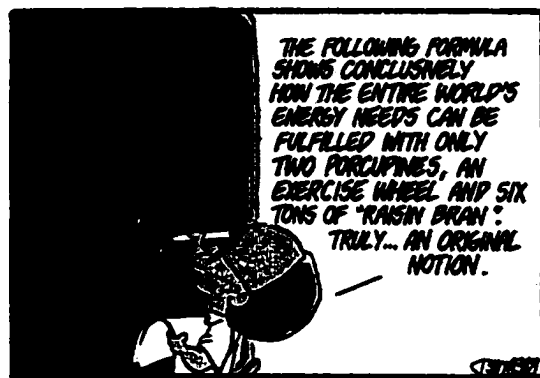
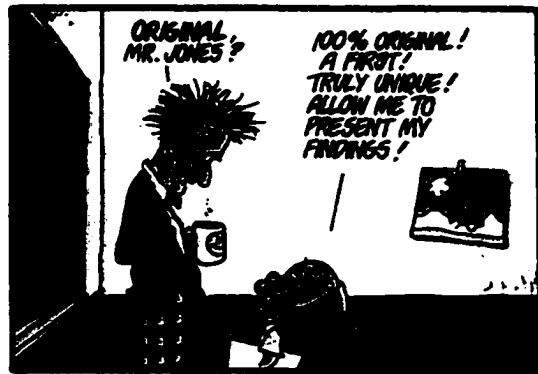
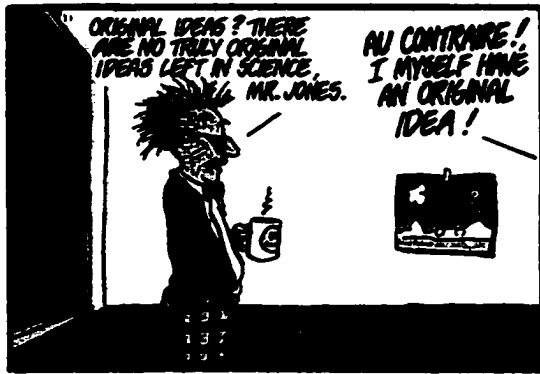
The author reserves all other publication and other rights in association with the copyright in the thesis, and except as hereinbefore provided, neither the thesis nor any substantial portion thereof may be printed or otherwise reproduced in any material form whatever without the author's prior written permission.



Michael A. Joyce  
9617-83 Avenue  
Edmonton, Alberta, Canada  
T6C 1C1

**Date submitted:** Dec 21, 1999

Quote Page





B. Breathed

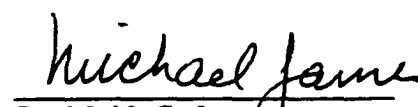
University of Alberta

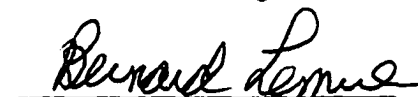
Faculty of Graduate Studies and Research


The undersigned certify that they have read, and recommended to the Faculty of Graduate Studies and Research for acceptance, a thesis entitled Structural and Functional Studies of Succinyl-CoA Synthetase submitted by Michael A. Joyce in partial fulfillment of the requirements for the degree of Doctor of Philosophy.

  
Dr. W. A. Bridger

  
Dr. W. T. Wolodko

  
Dr. M. N. G. James

  
Dr. B. Lemire

  
Dr. W. Gallin

  
Dr. R. F. Colman

Date: Dec 6, 1999

## Abstract

Succinyl-CoA synthetase (SCS) catalyzes the reversible interchange of purine nucleoside diphosphate, succinyl-CoA and  $P_i$  with purine nucleoside triphosphate, succinate and CoA via a phosphorylated histidine (H246 $\alpha$ ) intermediate. Two major themes have been investigated. The first theme was the folding of a thermostable form of SCS, and the second, and more prominent, was the investigation of the location of the nucleotide binding site and its implications for enzymatic catalysis.

To study the folding of a thermostable form of SCS, the enzyme from *Thermus aquaticus* was cloned and expressed. Examination of the folding of *T. aquaticus* SCS revealed that, although more stable than the *E. coli* enzyme, the value of  $\Delta G_u^{H_2O}$  for *T. aquaticus* SCS was in the mid-range for mesophilic proteins, indicating that the stabilization of *T. aquaticus* SCS was due to a change in the dependence of  $\Delta G_u^{H_2O}$  on temperature. Comparison of the unfolding and refolding of *T. aquaticus* SCS to that of *E. coli* SCS revealed that, although the equilibrium intermediates may be similar, the kinetics of refolding are very different.

Investigation of the nucleotide binding site in SCS began with the identification of two potential nucleotide binding sites in the  $\beta$ -subunit. These have been differentiated by photoaffinity labeling with 8-N<sub>3</sub>-ATP, by site-directed mutagenesis, and by x-ray crystallography. Using 8-N<sub>3</sub>-ATP as a suitable analogue for ATP, two tryptic peptides from the N-terminal domain of the  $\beta$ -subunit (an ATP-grasp fold) were labeled with 8-N<sub>3</sub>-ATP. Furthermore, mutant protein with changes in the N-terminal domain (G53 $\beta$ V-R54 $\beta$ E) could be phosphorylated by succinyl-CoA and  $P_i$  but not by nucleoside triphosphate. Mutant protein designed to probe nucleotide specificity (P20 $\beta$ Q) had a lower  $K_{m(app)}$  for GTP by over five times compared to wild-type SCS. Mutations in the C-terminal domain of the  $\beta$ -subunit designed to disrupt one loop of the Rossmann fold (I322 $\beta$ A, and R324 $\beta$ N-D326 $\beta$ A) had the greatest effect on the binding of succinate and CoA.

To determine the x-ray crystallographic structure of the enzyme with nucleotide bound, crystals of phosphorylated *E. coli* SCS were soaked in a series of different solutions successive experiments. The first experiment revealed only that the enzyme was dephosphorylated; and the successful experiment revealed ADP-Mg<sup>2+</sup> bound in the ATP-grasp fold of the N-terminal domain of each  $\beta$ -subunit. Thus, the nucleotide-binding site is located in the N-terminal domain of the  $\beta$ -subunit. The specific interactions of the nucleotide-Mg<sup>2+</sup> complex with SCS were described and compared to other nucleotide



binding proteins. Nucleotide binding in the N-terminal domain of the  $\beta$ -subunit implies that there are two partial active sites  $\sim 35 \text{ \AA}$  apart, and that the H246 $\alpha$  loop moves between them during catalysis. A hypothetical model of the histidine-containing loop in the “down” position to interact with the nucleotide was constructed. In part to test this model, mutagenesis of a glutamate residue in each of the active sites was carried out, and indicated that a charged residue in proximity to His 246 $\alpha$  is required in both sites.

## Acknowledgments

I am indebted to, and grateful for the help of both of my supervisors Dr. Bridger, and Dr. Wolodko . I would like to thank Dr. Bridger for providing resources and opportunities over the course of my graduate studies, and for allowing me to pursue my own direction in my investigations. I would like to thank Dr. Wolodko for his help and advice throughout my graduate studies, particularly for his careful inspection of manuscripts, his seemingly endless patience, and the carrot cakes.

I am grateful for the assistance and advice of everyone in the laboratory: Dr. Marie Fraser for teaching me crystallographic data processing, and refinement techniques; Ed Brownie for his advice and assistance with protein purification, and his relaxed attitude; the other graduate students, Dave Ryan, Darrin Bailey, and Chris Rochet, for scientific discussions, and for turning off gels late at night when I wanted to go home; and the undergraduate students, Jennette Vander Velde for her efforts at mutagenic PCR and Ziya Scaper for her charming presence.

I would also like to thank a number of people who have assisted me in my graduate work: members of my supervisory committee, Dr. Michael James, and Dr. Bernie Lemire for their guidance and advice during my graduate studies; Dr. Cyril Kay, Kimio Oikawa, and Les Hicks for their help in carrying out the circular dichroism, and sedimentation experiments; Dr. Bob Hodges, Brian Trippet, and Lorne Burk for their assistance with the mass spectrometry, and for allowing me to invade their laboratory to do HPLC; Jack Moore for protein and peptide sequencing; Jo Parish for writing the PLOTDIST set of programs, and for early-morning coffee; Perry D'Obrenan and Rita Witford for the DNA sequencing and oligonucleotide synthesis; and Roger Bradley for his photography work, and for finding me a corner to finish writing in; University Parking Services for price gouging, countless tickets in an empty parking lot, and numerous late-night towing experiences, including one on Christmas eve which was especially pleasant.

I would especially like to thank Dr. Richard Morgan whose advice in all matters was excellent, and interest in all subjects infectious. Dr. Morgan taught me to be curious about things simply because you were interested, that even small observations were at least interesting, and often the most informative observations. His influence is one of the major reasons that I have endeavored to do biochemistry.

I would like to thank my family and friends whose support, encouragement and social gatherings make life worth living. I would like to offer an apology to any members of the waterpolo team who may have caught a stray elbow after a failed experiment.

My most sincere and heartfelt thanks goes to my mate, Agnes Barabas, for her support and patience, and for putting up with many late nights and not enough attention.

My research was supported by a studentship from the Alberta Heritage Foundation for Medical Research, and Walter Johns tuition scholarships and the resources in the laboratory were funded by a grant from the Medical Research Council of Canada.

# Table of Contents

<b>Chapter 1. Introduction</b>	1
<b>Part A. Succinyl-CoA Synthetase in Metabolism</b>	2
<b>Part B. Structural Organization of Succinyl-CoA Synthetases</b>	8
Sources of Succinyl-CoA Synthetase	8
Subunit Composition and Quaternary Structure of SCS	9
<b>Part C. Primary Structure of Succinyl-CoA Synthetase</b>	10
Genetic Polymorphism of Succinyl-CoA Synthetase	10
Structural Organization of Succinyl-CoA Synthetase Genes	25
<b>Part D. The Reaction Catalyzed by Succinyl-CoA Synthetase</b>	28
The Specificity of Succinyl-CoA Synthetase for Substrates	28
The Reaction Mechanism of Succinyl-CoA Synthetase	29
Substrate Synergism	34
Conformational Changes Associated with Catalysis	37
Kinetic Measurements and Binding Constants	39
Alternating Sites Cooperativity	43
Regulation of Succinyl-CoA Synthetase	44
<b>Part E. Structural and Functional Relationships of SCS</b>	47
Folding of Succinyl-CoA Synthetase	47
The Crystal Structures of Succinyl-CoA Synthetase	49
<b>Part F. Thesis Objectives</b>	56
<b>References</b>	59

<b>Chapter 2. Cloning and Expression of Succinyl-CoA Synthetase</b>	<b>66</b>
<b>Introduction</b>	<b>66</b>
<b>Materials and Methods</b>	<b>67</b>
Section I: Cloning of <i>Neurospora crassa</i> SCS.	67
Purification of <i>Neurospora crassa</i> SCS.	67
Protein Sequencing of <i>N. crassa</i> SCS.	68
PCR of <i>N. crassa</i> Genomic DNA and cDNA Libraries.	68
Screening of <i>N. crassa</i> cDNA Libraries Using a Fragment of the $\beta$ -subunit cDNA.	69
Purification of Antibody Specific for the $\alpha$ -Subunit of <i>N. crassa</i> SCS.	70
Expression Screening of <i>N. crassa</i> cDNA Libraries.	71
Section II: mRNA Expression Studies of Pig SCS.	71
Isolation and Reverse Transcription of mRNA from Pig Tissues.	71
PCR of Reverse Transcribed mRNA from Pig Tissues.	71
Cloning and Sequencing of the PCR Products.	72
Section III: Cloning and Expression of <i>T. aquaticus</i> SCS.	72
Cloning and Sequencing of the Translationally Linked Genes for the $\alpha$ - and $\beta$ -Subunits of <i>T. aquaticus</i> SCS.	72
Expression of the Translationally Linked Genes for the $\alpha$ - and $\beta$ -Subunits of <i>T. aquaticus</i> SCS.	73
Mutagenesis of the Start Codon and the Ribosome Binding Site of the $\alpha$ -Subunit Gene of <i>T. aquaticus</i> SCS.	75
Expression of <i>T. aquaticus</i> SCS from pT7-7Taq <sub>ATG</sub> and pT7-7Taq <sub>RBS</sub> .	76
Purification and Refolding of <i>T. aquaticus</i> SCS from Inclusion Bodies.	77

Direct Sequencing of the PCR Product Generated from <i>T. aquaticus</i> Genomic DNA.	78
Independent Cloning of the <i>T. aquaticus</i> $\alpha$ - and $\beta$ -Subunit Genes, and Their Assembly in an Expression Vector that is Not Translationally Coupled.	78
Comparison of the Levels of Expression of <i>T. aquaticus</i> SCS Subunits and Whole Enzyme when Cells are Grown at 22 °C and 37 °C.	82
Labeling of the <i>T. aquaticus</i> SCS with [ <sup>35</sup> S]-Methionine.	82
N-Terminal Sequencing and Mass Spectrometry of the Subunits of <i>T. aquaticus</i> SCS.	83
<b>Results and Discussion</b>	84
Section I: Cloning of <i>Neurospora crassa</i> SCS.	84
Cloning a Fragment of the $\beta$ -Subunit of <i>N. crassa</i> SCS.	84
Screening a cDNA library of <i>N. crassa</i> for the $\alpha$ - and $\beta$ -Subunit Genes.	87
Section II: Expression of mRNA for the GTP-Specific $\beta$ -Subunit of SCS in Newborn Pig Tissues.	90
Section III: Cloning and Expression of <i>T. aquaticus</i> SCS	92
Cloning and Expression of Translationally Coupled SCS Subunit Genes from <i>T. aquaticus</i> .	92
Mutagenesis of the Start Codon and Ribosome Binding Site of the <i>T. aquaticus</i> SCS $\alpha$ -Subunit Gene.	95
Purification and Refolding of <i>T. aquaticus</i> SCS from Inclusion Bodies.	96
Direct Sequencing of PCR Products from the <i>T. aquaticus</i> SCS Genes.	99
Independent Cloning and Expression of the Subunits of <i>T. aquaticus</i> SCS.	100
Expression of Active, Thermostable, and Soluble <i>T. aquaticus</i> SCS.	102
Labeling of <i>T. aquaticus</i> SCS with [ <sup>35</sup> S]-Methionine.	106
<b>References</b>	110

<b>Chapter 3. Folding of <i>T. aquaticus</i> SCS</b>	112
<b>Introduction</b>	114
<b>Materials and Methods</b>	116
Purification of <i>T. aquaticus</i> SCS.	116
Analysis of the pH Profile of <i>T. aquaticus</i> SCS.	119
Steady State Kinetic Analysis of <i>T. aquaticus</i> SCS.	119
Activity of <i>T. aquaticus</i> , <i>E. coli</i> , and Pig Heart SCS at Different Temperatures and Denaturant Concentrations.	120
Gel Filtration Chromatography of <i>T. aquaticus</i> SCS.	120
Far UV-CD of <i>T. aquaticus</i> Whole Enzyme and Isolated Subunits in Guanidine HCl.	121
Sedimentation Equilibrium Analysis.	122
Refolding of <i>T. aquaticus</i> SCS.	123
Correlation Between Relative Stability and Amino Acid Substitutions in Pig heart, <i>E. coli</i> and <i>T. aquaticus</i> SCS.	123
Potential Ion Pairs in Pig heart, <i>E. coli</i> and <i>T. aquaticus</i> SCS.	124
Comparison of the Pig heart, <i>E. coli</i> and <i>T. aquaticus</i> SCS Amino Acid Sequences for Residues that Stabilize Secondary Structure.	126
<b>Results</b>	127
Characterization of the Quaternary Structure of <i>T. aquaticus</i> SCS.	125
Enzymology of <i>T. aquaticus</i> SCS.	128
Equilibrium Unfolding of <i>T. aquaticus</i> SCS.	129
Refolding of <i>T. aquaticus</i> SCS.	145
The Kinetics of Refolding <i>T. aquaticus</i> SCS.	146
Characterization of the Partially Folded <i>T. aquaticus</i> SCS.	149
Comparison of the Pig Heart, <i>E. coli</i> and <i>T. aquaticus</i> SCS Amino Acid Sequences.	153

<b>Discussion</b>	158
Equilibrium Unfolding of <i>T. aquaticus</i> SCS, and Comparison to <i>E. coli</i> SCS.	158
Thermodynamic Constants Derived from the Equilibrium Unfolding.	160
Kinetics of Refolding <i>T. aquaticus</i> SCS.	162
An Intermediate in the Refolding of <i>T. aquaticus</i> SCS.	163
Sequence Analysis of Three SCS Enzymes of Increasing Stability.	164
<b>References</b>	166
<b>Chapter 4. Photoaffinity Labeling of <i>E. coli</i> SCS with 8-N<sub>3</sub>-ATP</b>	170
<b>Introduction</b>	170
<b>Materials and Methods</b>	173
Photolabeling of <i>E. coli</i> SCS by [ $\alpha$ - <sup>32</sup> P]-8-N <sub>3</sub> -ATP.	173
Inactivation of SCS Activity by 8-N <sub>3</sub> -ATP.	174
Determination of the K <sub>m(app)</sub> of SCS for 8-N <sub>3</sub> -ATP.	174
Investigation of the Kinetic Relationship between 8-N <sub>3</sub> -ATP and ATP.	175
Photolabeling and Mass Spectrometry of SCS Subunits.	175
Photolabeling of SCS by 8-N <sub>3</sub> -ATP for Purification and Sequencing or Mass Spectrometry of Labeled Peptides.	176
<b>Results</b>	177
Photolabeling of SCS by 8-N <sub>3</sub> -ATP.	177
Is 8-N <sub>3</sub> -ATP a Substrate for SCS?	180
Does 8-N <sub>3</sub> -ATP Compete with ATP for Binding to SCS?	183
Inactivation of SCS by 8-N <sub>3</sub> -ATP.	183
Mass Spectrometry of SCS Subunits Labeled by 8-N <sub>3</sub> -ATP.	183

Isolation of 8-N <sub>3</sub> -ATP Photolabeled Peptides from SCS.	190
<b>Discussion</b>	195
<b>References</b>	199
<b>Chapter 5. Mutagenesis of Residues in Two Potential Nucleotide Binding Sites in <i>E. coli</i> SCS</b>	202
<b>Introduction</b>	202
<b>Materials and Methods</b>	206
Construction of Site-Directed Mutants in the $\beta$ -Subunit of SCS.	206
Expression and Purification of SCS Mutants.	207
Steady State Kinetic Analyses of SCS Mutants.	208
Phosphorylation Reactions Catalyzed by SCS Mutants.	211
<b>Results</b>	211
Site-Directed Mutagenesis of Residues in the N-Terminal Domain of the $\beta$ -Subunit.	211
Site-Directed Mutagenesis of Residues in the C-Terminal Domain of the $\beta$ -Subunit.	219
Site-Directed Mutagenesis of Residues in Both Domains of the $\beta$ -Subunit.	227
<b>Discussion</b>	232
<b>References</b>	235



<b>Chapter 6. Studies of the ADP-Bound Form of SCS</b>	<b>237</b>
<b>Introduction</b>	<b>237</b>
<b>Materials and Methods</b>	<b>238</b>
Protein Purification and Crystallization.	238
Soaking of ADP into Crystals of SCS.	238
Data Collection, Processing and Refinement.	239
Site Directed Mutagenesis of Glu 208 $\alpha$ and Glu 197 $\beta$ .	241
Expression and Purification of SCS Mutants.	242
Steady State Kinetic Analyses of SCS Mutants.	242
Phosphorylation Reactions Catalyzed by SCS Mutants.	242
<b>Results</b>	<b>243</b>
Crystallographic Structures of SCS Soaked with ADP.	243
Modeling of the Active Site Loop into Site II.	249
Site-Directed Mutagenesis of a Glutamate Residue in Each of Site I and II.	256
<b>Discussion</b>	<b>266</b>
Crystallographic Structures of SCS Soaked with ADP.	266
Comparison of the ADP-Bound Form of SCS to Other Nucleotide Binding Proteins.	273
Modeling and Mutagenesis of <i>E. coli</i> SCS.	281
<b>References</b>	<b>283</b>

<b>Chapter 7 Conclusions and Final Discussion</b>	287
<b>Summary</b>	287
Folding and Stability of <i>T. aquaticus</i> SCS.	287
The Nucleotide Binding Site of SCS.	288
<b>Significance and Future Prospects</b>	290
Investigation of the Folding of <i>T. aquaticus</i> SCS.	290
Comparison of the Folding of Thermophilic and Mesophilic SCS.	291
The Substrate Binding Sites of SCS.	292
Comparison of the Catalytic Mechanism of SCS to that of Other Synthetases and Phosphotransferases.	292
Investigation of the Proposed Conformational Change in SCS.	293
Investigation of Residues Directly Involved in Catalysis by SCS.	296
Investigation of the Function of the Rossmann Fold in the C-terminal Domain of the $\beta$ -Subunit.	299
<b>Appendices</b>	304
Appendix 1. Data base Accession Numbers for SCS Subunits	304
Appendix 2. Strains of <i>E. coli</i>	305
Appendix 3. Diagram of Site-Directed Mutagenesis by Overlap Extension	306
Appendix 4. Residues Used in the Structural Alignment of the Small Subdomain of the N-Terminal Domain of the $\beta$ -Subunit of <i>E. coli</i> SCS with DD-ligase.	307
Appendix 5. Residues Used in the Structural Alignment of the Large Subdomain of the N-Terminal Domain of the $\beta$ -Subunit of <i>E. coli</i> SCS with DD-ligase.	308
Appendix 6. Residues Used in the Structural Alignment of <i>E. coli</i> and Pig Heart SCS.	309
Appendix 7. Residues Used in the Structural Alignment of Native <i>E. coli</i> SCS and the ADP-Soaked Models of SCS.	310

## Table of Figures

Figure 1-1.	Metabolic pathways that utilize succinate or succinyl-CoA.	3
Figure 1-2.	Alignment of the $\alpha$ -subunits of SCS.	13
Figure 1-3.	Alignment of the $\beta$ -subunits of SCS.	17
Figure 1-4.	Phylogenetic tree of the amino acid sequences of the $\alpha$ -subunits of SCS.	20
Figure 1-5.	Phylogenetic tree of the amino acid sequences of the $\beta$ -subunits of SCS.	21
Figure 1-6.	Use of the binding energy of substrates by enzymes to achieve catalysis.	31
Figure 1-7.	Some of the resonance structures that are available to both phosphoguanidines and to phosphohistidine.	32
Figure 1-8.	Reactions of succinate, phosphate and CoA.	35
Figure 1-9.	Schematic representation of the conformational changes of the active site phosphohistidine.	38
Figure 1-10.	Kinetic schemes for SCS from <i>E. coli</i> and pig heart.	40
Figure 1-11.	Model for the regulation of expression of the genes for <i>E. coli</i> SCS.	46
Figure 1-12.	Ribbon diagram of the physiologically relevant tetramer of <i>E. coli</i> SCS.	51
Figure 1-13.	Close-up view of one active site of <i>E. coli</i> SCS.	54
Figure 1-14.	Superposition of the ribbon diagram for an $\alpha\beta$ -dimer of <i>E. coli</i> SCS with pig heart SCS.	55
Figure 2-1.	Cloning scheme for the cloning and assembly of the $\alpha$ - and $\beta$ -subunits of <i>T. aquaticus</i> SCS.	80
Figure 2-2.	Sequencing the N-terminus of the subunits of <i>N. crassa</i> SCS.	85
Figure 2-3.	Sequence of a fragment of the $\beta$ -subunit of <i>N. crassa</i> SCS.	86
Figure 2-4.	Western blot with antibodies to the $\alpha$ -subunit of rat liver SCS.	88
Figure 2-5.	Representative secondary screening of either <i>N. crassa</i> expression library or <i>N. crassa</i> cDNA library.	89

Figure 2-6.	PCR of reverse transcribed mRNA from pig tissues.	91
Figure 2-7.	Time course of expression of <i>T. aquaticus</i> SCS from the plasmids pT7-7Taq12 and pT7-7Taq13.	93
Figure 2-8.	Expression of <i>T. aquaticus</i> SCS from the plasmids pT7-7Taq <sub>ATG</sub> and pT7-7Taq <sub>RBS</sub> .	97
Figure 2-9.	Refolding of <i>T. aquaticus</i> SCS extracted from inclusion bodies.	98
Figure 2-10.	Expression of the $\alpha$ -subunit and $\beta$ -subunit of <i>T. aquaticus</i> SCS.	103
Figure 2-11.	Time course for the expression of soluble <i>T. aquaticus</i> SCS.	104
Figure 2-12.	Expression of soluble, active, and thermostable <i>T. aquaticus</i> SCS.	105
Figure 2-13.	Time course of degradation of [ <sup>35</sup> S]-methionine labeled subunits and whole <i>T. aquaticus</i> SCS.	107
Figure 2-14.	Quantification of the degradation of [ <sup>35</sup> S]-methionine labeled subunits and whole <i>T. aquaticus</i> SCS.	108
Figure 3-1.	SDS-PAGE analysis of the purification of <i>T. aquaticus</i> SCS.	118
Figure 3-2.	Initial evaluation of potential ion pairs in the $\alpha$ -subunit of <i>T. aquaticus</i> SCS.	125
Figure 3-3.	Determination of the quaternary structure of <i>T. aquaticus</i> SCS.	130
Figure 3-4.	The pH profile of the activity of <i>T. aquaticus</i> SCS.	131
Figure 3-5.	Hanes-Wolf plots for <i>T. aquaticus</i> SCS.	132
Figure 3-6.	Temperature profile of SCS.	133
Figure 3-7.	Denaturation of SCS.	134
Figure 3-8.	Denaturation of <i>T. aquaticus</i> SCS monitored by CD.	137
Figure 3-9.	Quaternary structure determination of <i>T. aquaticus</i> SCS in 0.9 M guanidine HCl, pH 7.4.	138
Figure 3-10.	Quaternary structure determination of <i>T. aquaticus</i> SCS in 1.8 M guanidine HCl, pH 7.4.	139
Figure 3-11.	Gel Filtration chromatography of <i>T. aquaticus</i> SCS in 1.8 and 3 M guanidine HCl.	140
Figure 3-12.	Separated subunits of <i>T. aquaticus</i> retain their native conformation in benign buffer.	142

Figure 3-13.	Denaturation of <i>T. aquaticus</i> SCS subunits monitored by far-UV CD.	143
Figure 3-14.	The refolding of <i>T. aquaticus</i> requires high concentrations of arginine and buffer exchange.	147
Figure 3-15.	Temperature and concentration dependence of the kinetics of refolding of <i>T. aquaticus</i> SCS.	148
Figure 3-16.	Temperature dependence of native and refolded <i>T. aquaticus</i> SCS.	150
Figure 3-17.	Hanes-Wolf plots for refolded <i>T. aquaticus</i> SCS.	151
Figure 3-18.	Gel filtration chromatography of refolded <i>T. aquaticus</i> SCS.	152
Figure 3-19.	Comparison of the amino acid composition of different SCS enzymes.	154
Figure 3-20.	Amino acid replacements in more stable SCS enzymes (pig heart to <i>E. coli</i> to <i>T. aquaticus</i> ).	155
Figure 3-21.	Models of the dependence of free energy on temperature.	161
Figure 4-1.	Stereo ribbon diagram of an $\alpha\beta$ -dimer of SCS with ATP modeled into the C-terminal domain of the $\beta$ -subunit.	171
Figure 4-2.	Modeling of ADP into the N-terminal domain of the $\beta$ -subunit of SCS.	172
Figure 4-3.	Autoradiogram of SCS photolabeled at pH 6.4 and 7.8 as analyzed by SDS-PAGE.	178
Figure 4-4.	Saturation of photolabeling of SCS by $[\alpha\text{-}^{32}\text{P}]\text{-}8\text{-N}_3\text{-ATP}$ , and prevention of photolabeling by ATP and GTP.	179
Figure 4-5.	Photolabeling of SCS in the absence and presence of substrates.	181
Figure 4-6.	Plot of the initial velocity of SCS activity versus concentration of $8\text{-N}_3\text{-ATP}$ .	182
Figure 4-7.	Reciprocal plots showing the "inhibition" of SCS by $8\text{-N}_3\text{-ATP}$ with ATP as the variable substrate.	184
Figure 4-8.	Correlation of photolabeling of the $\beta$ -subunit with inhibition of SCS.	185
Figure 4-9.	Reverse phase HPLC of SCS photolabeled by $8\text{-N}_3\text{-ATP}$ .	187
Figure 4-10.	Electrospray mass spectra of the subunits of SCS.	188

Figure 4-11.	Electrospray mass spectra of the subunits of SCS irradiated in the presence of a saturating concentration of 8-N <sub>3</sub> -ATP.	189
Figure 4-12.	Purification of photolabeled peptides of SCS by Al <sup>3+</sup> affinity chromatography.	192
Figure 4-13.	Purification of photolabeled peptides of SCS by reverse phase HPLC.	193
Figure 4-14.	Electrospray mass spectra of tryptic peptides from photolabeled SCS.	194
Figure 4-15.	Ribbon diagram of one αβ-dimer of <i>E. coli</i> SCS.	198
Figure 5-1.	Diagram of ATP modeled into the C-terminal domain of the β-subunit of SCS showing some residues that may interact with the nucleotide.	204
Figure 5-2.	Modeling of ADP into the N-terminal domain of the β-subunit of SCS.	205
Figure 5-3.	SDS-PAGE of purified mutants of <i>E. coli</i> SCS.	209
Figure 5-4.	Analysis of wild-type and mutant SCS by far-UV circular dichroism.	210
Figure 5-5.	Double reciprocal plots of the rate of succinyl-CoA formation versus substrate concentration for SCS with the mutation G53βV-R54βE.	212
Figure 5-6.	Time course of phosphorylation by NTP of wild-type and one mutant of SCS with changes in the N-terminal domain of the β-subunit.	213
Figure 5-7.	Time course of phosphorylation by succinyl-CoA and P <sub>i</sub> of wild-type and one mutant of SCS with changes in the N-terminal domain of the β-subunit.	214
Figure 5-8.	Stereo view of the superposition of residues from the N-terminal domains of <i>E. coli</i> and pig heart SCS on the ADP from DD-ligase.	217
Figure 5-9.	Double reciprocal plots of the rate of succinyl-CoA formation versus substrate concentration for SCS with the mutation P20βQ.	218
Figure 5-10.	Double reciprocal plots of the rate of succinyl-CoA formation versus substrate concentration for SCS with the mutation I322βA.	220
Figure 5-11.	Double reciprocal plots of the rate of succinyl-CoA formation versus substrate concentration for SCS with the mutation I322βG-R324βP.	221

Figure 5-12.	Double reciprocal plots of the rate of succinyl-CoA formation versus substrate concentration for SCS with the mutation I322 $\beta$ A-D326 $\beta$ N.	222
Figure 5-13.	Double reciprocal plots of the rate of succinyl-CoA formation versus substrate concentration for SCS with the mutation R324 $\beta$ N-D236 $\beta$ A.	223
Figure 5-14.	Time course of phosphorylation by NTP of wild-type SCS and mutants with changes in the C-terminal domain of the $\beta$ -subunit.	225
Figure 5-15.	Time course of phosphorylation by P <sub>i</sub> and succinyl-CoA of wild-type SCS and mutants with changes in the C-terminal domain of the $\beta$ -subunit.	226
Figure 5-16.	Hanes-Wolf plots for protein with the mutations G35 $\beta$ V-R54 $\beta$ E-I322 $\beta$ A.	228
Figure 5-17.	Double reciprocal plots of the rate of succinyl-CoA formation versus substrate concentration for SCS with the mutations G35 $\beta$ V-R54 $\beta$ E-R324 $\beta$ N.	229
Figure 5-18.	Time course of phosphorylation by NTP of wild-type SCS and mutants with changes in both domains of the $\beta$ -subunit.	230
Figure 5-19.	Time course of phosphorylation by P <sub>i</sub> and succinyl-CoA of wild-type SCS and mutants with changes in both domains of the $\beta$ -subunit.	231
Figure 6-1.	Stereo diagrams of difference electron density in the $\alpha$ -subunit.	244
Figure 6-2.	Stereo diagrams of difference electron density in the N-terminal domain of the $\beta$ -subunit.	245
Figure 6-3.	Stereo diagrams of electron density in the $\alpha$ -subunit.	246
Figure 6-4.	Stereo diagrams of electron density in the N-terminal domain of the $\beta$ -subunit.	247
Figure 6-5.	Superposition of native and dephosphorylated SCS around the phosphohistidine.	250
Figure 6-6.	Nucleotide binding site of SCS.	251
Figure 6-7.	Stereo diagrams showing the coordination of the Mg <sup>2+</sup> ion in the $\beta$ -subunit of SCS.	252
Figure 6-8.	Superposition of native and dephosphorylated SCS around the CoA.	253
Figure 6-9.	Model of the His 246 $\alpha$ loop at site II.	255
Figure 6-10.	Hanes-Wolf plots for the <i>E. coli</i> SCS mutant E208 $\alpha$ D.	257

Figure 6-11. Hanes-Wolf plots for the <i>E. coli</i> SCS mutant E208 $\alpha$ Q.	258
Figure 6-12. Time course of phosphorylation by NTP of wild-type SCS and the Glu 208 $\beta$ mutant protein.	259
Figure 6-13. Time course of phosphorylation by succinyl-CoA and P <sub>i</sub> of wild-type SCS and the Glu 208 $\beta$ mutant protein.	260
Figure 6-14. Hanes-Wolf plots for the <i>E. coli</i> SCS mutant E197 $\beta$ D.	262
Figure 6-15. Hanes-Wolf plots for the <i>E. coli</i> SCS mutant E197 $\beta$ Q.	263
Figure 6-16. Time course of phosphorylation by NTP of wild-type SCS and the Glu 197 $\beta$ mutant protein.	264
Figure 6-17. Time course of phosphorylation by succinyl-CoA and P <sub>i</sub> of wild-type SCS and the Glu 197 $\beta$ mutant protein.	265
Figure 6-18. Stereo diagram superposing the ADP-bound and native models of an $\alpha\beta$ -dimer to show the conformational shift.	269
Figure 6-19. Changes in the vicinity of the Mg <sup>2+</sup> ion.	270
Figure 6-20. Stereo diagram of the superposition of the ADP in SCS with that in DD-ligase.	272
Figure 6-21. Stereo diagram of the superposition of the ADP in SCS with that in cyclic AMP dependant protein kinase	278
Figure 6-22. Stereo diagram of the superposition of the ADP in SCS with that in Ribonucleotide reductase.	279
Figure 6-23. Stereo diagram of the superposition of the ADP in SCS with that in p12 ras.	280
Figure 7-1. Proposed mechanism of the attack of the thiol group of CoA on succinyl-phosphate.	298



## Table of Tables

Table 1-1.	The Exchange Reactions Catalyzed by Succinyl-CoA Synthetase.	30
Table 1-2.	Apparent Michaelis Constants for Succinyl-CoA Synthetase.	41
Table 2-1.	SCS Activity During the Purification of Inclusion Bodies.	100
Table 3-1.	Thermodynamic Parameters for the Unfolding of <i>T. aquaticus</i> SCS.	144
Table 3-2.	Ion Pairs in SCS from Pig Heart, <i>E. coli</i> , and <i>T. aquaticus</i> .	157
Table 4-1.	Summary of Kinetic Parameters of SCS for ATP, ADP or 8-N <sub>3</sub> -ATP.	195
Table 5-1.	Primers for Mutagenic PCR.	206
Table 5-2.	Apparent Kinetic Parameters of Wild-Type SCS Proteins.	215
Table 6-1.	Statistics for the Two X-ray Diffraction Data Sets.	240
Table 6-2.	Primers for Mutagenesis via PCR.	241
Table 6-3.	Refinement Statistics.	248
Table 6-4.	Kinetic Parameters of Wild-type and Mutant SCS Proteins	266
Table 6-5.	Equivalent Residues that Contact the ADP-Mg <sup>2+</sup> Complex in SCS and DD-ligase.	274

## List of Abbreviations and Symbols

ADP	adenosine 5'-diphosphate
AMPPCP	$\beta,\gamma$ -methyleneadenosine 5'-triphosphate;
ATP	adenosine 5'-triphosphate
ATP $\gamma$ S	adenosine 5'-O-(3 thiotriphosphate)
ADP $\beta$ S	adenosine 5'-O-(2 thiodiphosphate)
8-N <sub>3</sub> -ATP	8-azidoadenosine 5'-triphosphate
cAPK	cyclic adenosine monophosphate dependent protein kinase
cDNA	complementary deoxyribonucleic acid
CoA	coenzyme A
Da	Dalton
$\Delta G_u^{H_2O}$	free energy of unfolding in the absence of denaturant
DD-ligase	D-ala:D-ala ligase
DTT	dithiothreitol
$E_{260\text{ nm}}$	molar extinction coefficient at the designated wavelength
$E_a$	activation energy
EDTA	ethylenediaminetetraacetic acid
E-P	covalent enzyme-phosphate intermediate
E-succinyl-P	non-covalent enzyme with bound succinyl-phosphate
far-UV CD	far-ultraviolet circular dichroism
GDP	guanosine 5'-diphosphate
GTP	guanosine 5'-triphosphate
GuHCl	guanidine hydrochloride
$[\text{GuHCl}]_{1/2}$	concentration of GuHCl resulting in half maximal denaturation
HPLC	high performance liquid chromatography
IDP	inosine 5'-diphosphate
IPTG	isopropyl- $\beta$ -D-thiogalactopyranoside
ITP	inosine 5'-triphosphate
$k_{\text{cat}}$	catalytic constant (turnover number)
$K_d$	dissociation constant
$K_{\text{eq}}$	equilibrium constant
$K_m$	Michaelis constant
MOPS	3-[N-morpholino]propanesulfonic acid
mRNA	messenger RNA
NDP	adenosine or guanosine 5'-diphosphate
NMR	nuclear magnetic resonance
NTP	adenosine or guanosine 5'-triphosphate
PAGE	polyacrylamide gel electrophoresis

PCR	polymerase chain reaction
PDB	protein data base
$P_i$	inorganic phosphate
PMSF	phenylmethylsulfonyl fluoride
RNR R1	ribonucleotide reductase
rpm	revolutions per minute
PRR	proton relaxation rate
RT-PCR	reverse transcribed PCR
PVDF	polyvinylidene difluoride
SCS	succinyl-CoA synthetase
SDS	sodium salt of lauryl sulfate
Tris HCl	tris(hydroxymethyl)aminomethane hydrochloride
U	Units: $\mu$ moles of succinyl-CoA produced per minute
5'-UTR	5' untranslated region
3'-UTR	3' untranslated region
$V_{max}$	maximum rate of enzyme activity under saturating substrate conditions
X-gal	5-bromo-4-chloro-3-indolyl- $\beta$ -D-galactopyranoside

Specific amino acid residues in given subunits of SCS are designated by the one or three letter code followed by the residue number and either  $\alpha$  or  $\beta$  to indicate the subunit.

#### Abbreviations used in x-ray crystallography:

k	scale factor to minimize the difference between data sets
$ F_{o(native)} $	structure factor amplitude observed for the native crystal
$ F_{o(soak)} $	structure factor amplitude observed for the crystal after soaking
$\alpha_{(native)}$	phase calculated from the native structure
$I_i$	individual measurement of an intensity
I	observed intensity averaged from all equivalent reflections
$ F_o $	observed structure factor amplitude
$ F_c $	calculated structure factor amplitude
rms	root mean square
$\sigma$	standard deviation

## Chapter One Introduction

---

In 1937, Hans Krebs proposed that the reaction of pyruvate with oxaloacetate to produce citrate led to the closure of the citric acid cycle. His hypothesis for this cycle was based on previous work, which had shown that succinate, malate,  $\alpha$ -ketoglutarate and citrate were rapidly oxidized by muscle tissue during respiration. As well, the addition of succinate, fumarate, malate or oxaloacetate to muscle tissue stimulated respiration beyond that required for simple oxidation of these compounds (1). It had also been shown that succinate could be converted to fumarate, malate or oxaloacetate in that order. This sequence made up the four carbon dicarboxylic acid portion of the citric acid cycle. Martius *et al.* showed that citrate was rearranged to isocitrate, and subsequently decarboxylated to yield  $\alpha$ -ketoglutarate (1). This sequence made up the tricarboxylic acid portion of the citric acid cycle. Other experiments had shown that  $\alpha$ -ketoglutarate could be oxidatively decarboxylated to yield succinate (1). Thus, the reaction of pyruvate with oxaloacetate to produce citrate resulted in the unification of the two halves of the citric acid cycle, and accounted for the oxidation of pyruvate by muscle tissue.

Elucidation of the reaction catalyzed by succinyl-CoA synthetase (SCS) began when it was observed that enzyme preparations capable of the oxidative decarboxylation of  $\alpha$ -ketoglutarate to succinate also esterified inorganic phosphate (2, 3). Furthermore, these preparations produced inorganic phosphate from ATP when incubated with both succinate and CoA. Kaufman proposed that the oxidative decarboxylation of  $\alpha$ -ketoglutarate took place in two steps with succinyl-CoA as an intermediate (4). Subsequently he found that the activity which catalyzed the formation of succinyl-CoA from  $\alpha$ -ketoglutarate was separable from the activity which catalyzed the conversion of succinyl-CoA to succinate (5). These two activities were catalyzed by  $\alpha$ -ketoglutarate dehydrogenase and succinyl-CoA synthetase, respectively. Succinyl-CoA synthetase was shown to be responsible for both the esterification of inorganic phosphate if succinyl-CoA was provided, and the

release of inorganic phosphate from ATP if CoA and succinate were provided (6, 5). Thus, the reaction catalyzed by succinyl-CoA synthetase was firmly established to be part of the citric acid cycle. SCS catalyzes the interconversion of the high-energy thioester bond ( $\Delta G_{\text{hydrolysis}}^{\circ} = -7.53$  kcal/mol) in succinyl-CoA with the high-energy phosphoanhydride ( $\Delta G_{\text{hydrolysis}}^{\circ} = -7.29$  kcal/mol) bond in nucleoside triphosphates (7), by the following reaction:



(where NDP and NTP are purine nucleoside di- and triphosphates, respectively).

## Part A. Succinyl-CoA Synthetase in Metabolism

In respiring aerobes the reaction catalyzed by SCS in the forward direction (as shown above) is the substrate-level phosphorylation step of the citric acid cycle, which conserves the energy of the thioester bond as a nucleoside triphosphate, and results in the conversion of succinyl-CoA to succinate (Fig. 1-1 [I]). This is thought to be the primary function of SCS in most organisms (8, 9). Some primitive eukaryotes, which lack the reactions of a complete citric acid cycle, still use SCS in a manner analogous to its function in the citric acid cycle. Rumen ciliates and trichomonad flagellates lack mitochondria and metabolize carbohydrates by fermentation (10). In these organisms, organelles, which morphologically resemble mitochondria and are called hydrogenosomes, convert the pyruvate generated by glycolysis to acetyl-CoA. The high-energy thioester bond in acetyl-CoA is conserved by CoA transferase which transfers the CoA moiety to succinate, generating succinyl-CoA. The subsequent substrate-level phosphorylation of ADP is catalyzed by SCS (Fig. 1-1 [II])(10). Thus, the succinyl-CoA is recycled to succinate and the energy from the thioester bond of acetyl-CoA is ultimately conserved in ATP. These

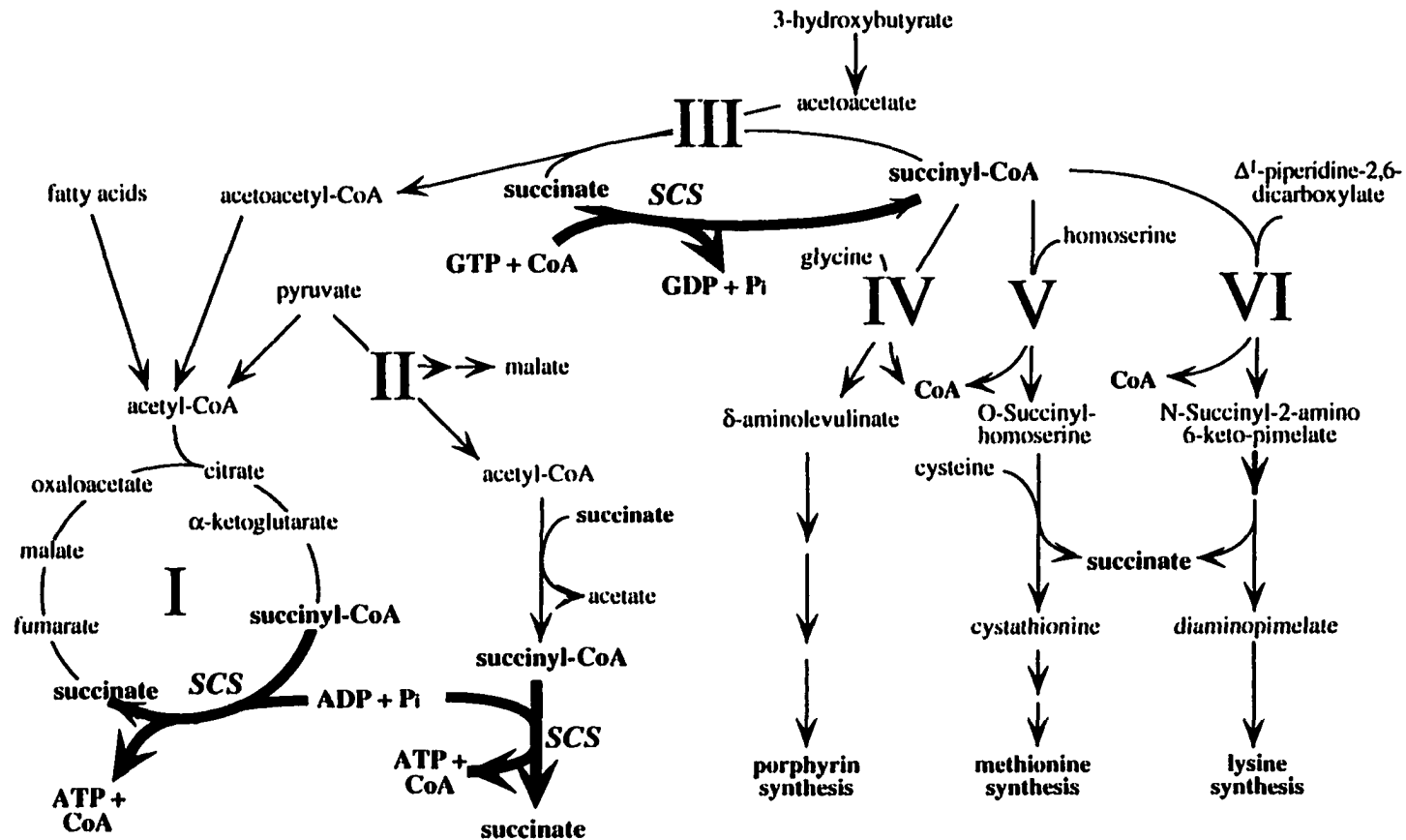


**Figure 1-1. Metabolic pathways that utilize succinate or succinyl-CoA.** The reactions catalyzed by SCS are shown by the bold arrows. The roman numerals denote the following pathways: I, citric acid cycle; II, pyruvate reduction in hydrogenosomes; III, ketone body metabolism; IV porphyrin synthesis; V, methionine synthesis; VI, lysine synthesis. Adapted from Voet and Voet (7). The direction of the reversible reaction catalyzed by SCS has been postulated to be dependent on the ratio of the concentration of NTP to NDP in a cell or organelle, and thus this dependence and the direction of the reaction is indicated by the bold arrows and the appropriate nucleotide.

reactions are also used for energy metabolism in the mitochondria of Trypanosomatids, which are the first eukaryotes to diverge from the common eukaryotic lineage and retain mitochondria (11). The existence of the same metabolic pathway in mitochondria and hydrogenosomes supports the hypothesis that mitochondria and hydrogenosomes have a common origin (12).

In the reverse direction the reaction catalyzed by SCS is important in ketone body metabolism (Fig. 1-1 [III]). In mammals, ketone bodies such as acetoacetate and D- $\beta$ -hydroxybutyrate are produced in liver mitochondria when acetyl-CoA accumulates in amounts greater than can be oxidized by the citric acid cycle. These ketone bodies are released into the blood and are catabolized by peripheral tissues. Some tissues, such as heart and kidney, use ketone bodies as their major source of metabolic energy. Other tissues, such as skeletal muscle and brain, increase their use of ketone bodies when blood glucose levels are low. The utilization of ketone bodies begins with the conversion of D- $\beta$ -hydroxybutyrate to acetoacetate by  $\beta$ -hydroxybutyrate dehydrogenase. The acetoacetate is activated by the transfer of CoA from succinyl-CoA by succinyl-CoA:3-ketoacid CoA transferase (CoA transferase) yielding acetoacetyl-CoA. A second molecule of coenzyme A is then added by thiolase yielding two molecules of acetyl-CoA which can be oxidized by the citric acid cycle (7).

High levels of succinyl-CoA must be maintained during ketone body metabolism (13, 14) because the  $K_m$  of CoA transferase for succinyl-CoA is 4.2 mM (15), approximately two orders of magnitude greater than the  $K_m$  of SCS for the same substrate (30  $\mu$ M) (16). Under conditions where ketone bodies are the major source of metabolic energy, and in the absence of any control on the activity of SCS, the breakdown of succinyl-CoA by SCS to make NTP would be greater than the use of succinyl-CoA by CoA transferase to activate acetoacetate. Thus, the citric acid cycle would eventually come to a halt due to the lack of acetyl-CoA, because succinyl-CoA is not available for the activation of acetoacetate by CoA transferase. It has been proposed that the direction in

which the reaction catalyzed by SCS proceeds is determined by the ratio NTP to NDP (17, 14). Since the  $K_{eq}$  for the reaction catalyzed by SCS is approximately one (18), a high ratio of NTP to NDP will lead to the production of succinyl-CoA which can then be used by CoA transferase to activate acetoacetate. Thus, there appears to be an apparent contradiction: the reaction catalyzed by SCS is required to proceed in the forward direction (in the citric acid cycle) and also in the reverse direction (to supply succinyl-CoA for acetoacetate activation). This contradiction may be resolved by the simultaneous existence of two different SCS activities, one that is specific for adenosine nucleotides, and one that is specific for guanosine nucleotides. Thus, SCS specific for ADP/ATP (functioning in the citric acid cycle), will readily respond to the energy changes of the cell because the ratio of ATP to ADP varies about one depending on the metabolic state of the cell (see bold arrow in Figure 1-1 section [I]) (17, 14). Since the value of the GTP to GDP ratio in mammalian mitochondria has been estimated to be 100 or higher, a GDP/GTP specific enzyme would be expected to maintain the high level of succinyl-CoA required by CoA transferase during ketone body metabolism (see bold arrow in Figure 1-1 [II]) (17, 14).

Studies of the levels of citric acid cycle enzymes of *Trypanosoma brucie* suggested that the ADP/ATP-specific SCS is associated with the citric acid cycle (19). The life cycle of *T. brucie* consists of two dramatically different stages, one occurs in the bloodstream of the mammalian host, and the other in the gut of the insect vector. In the bloodstream, *T. brucie* is entirely dependent on glucose and cannot utilize fatty acids or amino acids because in this stage the parasite lacks a functional citric acid cycle. However, in the insect gut, glucose is scarce and the main energy source is amino acids (20). *T. brucie* has both an ADP/ATP-specific SCS activity and a GDP/GTP-specific SCS activity. Depressed levels of citric acid cycle enzymes, including the ADP/ATP-specific SCS activity, were observed when lysates of the bloodstream form of *T. brucie* were examined. In contrast, lysates from the procyclic form found in the insect gut revealed a functional citric acid cycle and elevated levels of ADP/ATP-specific SCS activity. The levels of GDP/GTP-specific



activity remain approximately the same in both forms of *T. brucie* (19). This is consistent with the role of the ADP/ATP-specific SCS activity in the citric acid cycle.

Studies with mammalian tissues have suggested that a GDP/GTP-specific SCS activity is responsible for the high levels of succinyl-CoA required during ketone body metabolism. In support of this, a correlation between a GDP/GTP-specific SCS activity and the utilization of ketone bodies has been shown in various tissues (17, 21, 14, 22, 23) For example, in rats, diabetic ketoacidosis can be induced by treatment with streptozotocin (22). During this condition, elevated levels of ketone bodies are present in the blood, and tissues such as the brain, which normally use glucose as an energy source, now use ketone bodies. There is a 5-10 fold increase in the levels of GDP/GTP-specific SCS activity when lysates of brain tissue from streptozotocin treated rats are compared to those from untreated rats (22). This is consistent with the role of the GDP/GTP-specific SCS activity in ketone body metabolism.

Succinyl-CoA is also an essential anabolic precursor in the synthesis of porphyrin, methionine and lysine (Fig. 1-1, [IV-VI]). This role is best illustrated by the observation that anaerobic organisms, which can not oxidize acetate via the citric acid cycle, still require SCS activity for biosynthesis. When *E. coli* is grown on glucose, the activity of the glycolytic pathway is high, and thus enzymes that play a role in energy metabolism would be expected to have high activity. However, there is a 10-fold decrease in SCS activity when *E. coli* is grown on glucose (24). Therefore, SCS is regarded as serving a predominantly biosynthetic role in enteric bacteria.

Porphyrins are metal binding compounds including heme, cobalamine, phycobilin, and chlorophyll, that are all synthesized from a common precursor,  $\delta$ -aminolevulinic acid. This precursor is synthesized by the condensation of succinyl-CoA and glycine, liberating  $\text{CO}_2$  and CoA in the process (Fig. 1-1 [IV]). Studies with mice concluded that a GDP/GTP-specific SCS activity was responsible for the elevated levels of succinyl-CoA required during porphyrin synthesis (25, 26). Administration of 3,5-dicarbethoxy-1, 4-

dihydrocollidine to the mice caused chemically induced hepatic porphyria, a condition characterized by failure of the negative feedback inhibition which normally regulates the porphyrin biosynthesis pathway. This led to increased levels of porphyrin precursors, and thus an increased demand for succinyl-CoA. Consistent with this, an increase in the levels of GDP/GTP-specific SCS activity was observed when 3,5-dicarbethoxy-1, 4-dihydrocollidine was administered to mice (26). This is consistent with the hypothesis that a GDP/GTP-specific SCS activity is responsible for the synthesis of succinyl-CoA used as a precursor of  $\delta$ -aminolevulinic acid. In other studies, SCS isolated from soybean callus and *Rhodospseudomonas sphearoides*, a photosynthetic bacterium, was inhibited by protoporphyrin and hemin (27, 28). The negative regulation of SCS by the products of heme biosynthesis further solidifies the role of SCS in heme biosynthesis.

One of the precursors in the synthesis of methionine is cystathionine. In plants and bacteria, cystathionine is synthesized from homoserine and cysteine (7). The succinate portion of Succinyl-CoA is added to homoserine, liberating CoA, in a reaction catalyzed by homoserine acyl transferase. In the subsequent reaction the succinate is displaced by cysteine. Thus succinyl-CoA serves to activate homoserine for the attachment of cysteine to generate cystathionine (Fig. 1-1 [V]). Succinyl-CoA is used to facilitate the ring opening of  $\Delta^1$  piperidine-2,6 dicarboxylate in the early stages of the synthesis of lysine (Fig. 1-1[VI]).

Recently, Johnson *et al.* (29, 30) have carried out a thorough study on the tissue-specific expression of SCS. They purified both ADP/ATP- and GDP/GTP-specific activities from various pigeon tissues, and found that only the GDP/GTP-specific activity was present in liver, and only the ADP/ATP-specific activity was present in breast tissue. Other tissues contained a mixture of the two activities: the ratios of GDP/GTP-specific activity to ADP/ATP-specific activity in kidney, brain, and heart were 7, 1, and 0.1, respectively. Tissues that were highly dependent on oxidative metabolism contained high levels of ADP/ATP-specific SCS activity, while tissues that utilized ketone bodies or

played a predominately biosynthetic role, contained high levels of GDP/GTP-specific activity (30). This is consistent with the hypothesis that ADP/ATP-specific SCS participates in the citric acid cycle and GDP/GTP-specific SCS participates in ketone body metabolism and in biosynthetic roles. Thus, the combination of separate nucleotide pools and the nucleotide specificity of SCS alleviates the apparent conflict between the requirement for the degradation of succinyl-CoA (in the citric acid cycle) and the synthesis of succinyl-CoA for use in ketone body metabolism and biosynthesis (the bold arrows in Figure 1-1).

## **Part B. Structural Organization of Succinyl-CoA Synthetases**

### ***Sources of Succinyl-CoA Synthetase***

SCS from a number of sources has been studied, (31-36, 28, 37-40, 22, 23, 26, 41, 30) but the highest yields of pure enzyme have been obtained from *E. coli* (42-46) and pig heart (47-49), and thus these enzymes are the best characterized ones. Initially, SCS was purified from *E. coli* grown on succinate as the carbon source (50). The development of an overexpression system (51, 52) has led to the production of sufficient amounts of *E. coli* SCS for characterization and for x-ray crystallography (53-55). Improvements in the purification of the GDP/GTP-specific enzyme from pig heart (56, 57), and the development of an expression system (58, 59) has also led to the purification of sufficient quantities for x-ray crystallography (60). The recent cloning of GDP/GTP- and ADP/ATP-specific SCS from pigeon (29) foretell the development of expression systems for these enzymes. Thus, sufficient amounts of these enzymes will be produced, and will allow for the examination of the basis for the differences in the nucleotide specificity. As has been discussed above, this is one of the major functional distinctions between SCS from different organisms and tissues.

### ***Subunit Composition and Quaternary Structure of Succinyl-CoA Synthetase***

Characterization of the quaternary structures of SCS has revealed that oligomeric structure is another major distinction of SCS from different organisms. All SCS enzymes characterized thus far are comprised of two subunits, designated  $\alpha$  and  $\beta$ , with approximate molecular masses of 31 kDa and 42 kDa, respectively (9, 61, 58, 62, 29, 30). However, SCS with two different quaternary structures have been observed in different species, one from all gram negative bacteria that have been examined (63, 38, 64), and a second from all other organisms and eukaryotic tissues (48, 38, 39, 64, 65). The molecular mass of purified *E. coli* SCS had been estimated by gel filtration to be between 140 and 160 kDa (42, 43, 46), indicating an  $\alpha_2\beta_2$  tetrameric enzyme. The existence of tetrameric *E. coli* SCS has been confirmed by cross-linking studies (66), and also by x-ray crystallography which showed that *E. coli* SCS was a dimer of  $\alpha\beta$ -dimers (54, 55). Active enzyme sedimentation studies proved that the active species were non-dissociating  $\alpha_2\beta_2$ -tetramers (65). SCS from pig heart, on the other hand, has a molecular mass of approximately half that of *E. coli* SCS as estimated by gel filtration, indicating an  $\alpha\beta$ -dimeric enzyme (48, 56-58, 67). Active enzyme sedimentation studies showed that SCS from pig heart was a non-associating  $\alpha\beta$ -dimer (65). This has also been confirmed by x-ray crystallography (60). The enzyme from other eukaryotic species is similar in size to pig heart SCS (38, 39), as is SCS from a number of gram positive bacteria (38, 64). Given the clear distinction between the species which have dimeric SCS and those that have tetrameric SCS, it is surprising that SCS from *Trichomonas vaginalis* has been reported to have a molecular mass of 150 kDa whereas SCS from *Trichomonas foetus* has a molecular mass of 70 kDa (41).

The functional significance of the tetrameric/dimeric quaternary structure is not known. Reasons for the formation of higher oligomers in multi-subunit enzymes include, formation of a shared active site, increased stability and solubility, decreased osmotic

pressure within the cell, and the formation of a functional unit (68). A dimeric form of *E. coli* SCS has been constructed by specific mutagenesis of residues at the tetramer interface (67). This dimeric enzyme had kinetic properties which were identical to those of the wild-type tetrameric enzyme (67). Thus, the tetrameric quaternary structure is not required *per se* for catalysis. It is possible that the tetrameric structure is required for the increased stability of *E. coli* SCS. In support of this idea, it was noted by Bailey *et al.* (67) that the dimeric form of *E. coli* SCS was somewhat less stable and less soluble than the wild-type enzyme.

## **Part C. Primary Structure of Succinyl-CoA Synthetase**

### ***Genetic Polymorphism of Succinyl-CoA Synthetase***

The large number of amino acid sequences of different SCS now available permits the examination and comparison of the primary structures of SCS in order to determine evolutionary relationships. Moreover, such comparisons often provide clues as to the basis for, and significance of, structural and functional differences between SCS enzymes. The genes encoding SCS have been characterized from a number of sources. Genome sequencing projects have contributed greatly to the number of known sequences of SCS (69-82). An alignment of the deduced amino acid sequence of various SCS is shown in Figure 1-2 for the  $\alpha$ -subunits, and in Figure 1-3 for the  $\beta$ -subunits. These alignments were done initially with the PIMA multiple sequence alignment program (83, 84) and subsequently improved manually. The data base accession numbers for each sequence are given in Appendix 1. Three sequences have not been included in this alignment, the genes from *Synechocystis sp.*, the  $\alpha$ -subunit gene of *Pyrococcus horikoshii* and a second  $\alpha$ -subunit gene from *E. coli*. These sequences are much more divergent than the other SCS sequences, and they do not contain the active site histidine at the position equivalent to 246 $\alpha$  (using the *E. coli* numbering system). Although they are similar to other SCS genes,

they are not likely to function in a manner similar to the well characterized species of SCS, and may represent pseudo-genes or other activities entirely. Thus, comparison of these sequences to the other SCS sequences is not likely to yield productive information because these genes are no longer subject to evolutionary pressure. The corresponding secondary structure of *E. coli* SCS (derived from the x-ray crystallographic structure of *E. coli* SCS) is also noted in Figures 1-2 and 1-3. The position of an amino acid located in a loop on the surface of the protein is denoted in red. Similar to other proteins, insertions and deletions of amino acids most often occur in these surface loops.

Figures 1-4 and 1-5 show dendograms for the  $\alpha$ - and  $\beta$ -subunits, derived from these sequence alignments using the ClustalX (85) and TREEVIEW (86) programs. The length of the lines joining the different species is proportional to the number of differences between SCS enzymes. The  $\alpha$ - and  $\beta$ -subunits fall into three major groups that correspond to the taxonomic domains, eubacteria, archaeobacteria, and eukaryotes. The majority of the eukaryotic sequences have extensions at the N-terminus, which are most likely mitochondrial signal sequences. In the sequence alignments, the segregation of the three groups is most obvious in the  $\beta$ -subunit, where there is a seven residue insertion in the sequences from eukaryotes, and a separate seven residue deletion in the sequences from archaeobacteria. The SCS amino acid sequences from three species, *Mycobacterium tuberculosis*, *Streptomyces coelicolor*, and *Aquifex aeolicus* 2, do not segregate into the group that corresponds to their taxonomic group, but align in the group corresponding to the archaeobacteria. There are examples of other proteins from *Mycobacterium tuberculosis* and *Streptomyces coelicolor* whose amino acid sequences align within the archaeobacterial domain (87, 88). The similarity between the primary structure of SCS from the two mesophilic parasitic eubacteria, and that from thermophilic archaeobacteria may be due to the relatively high G+C content of the genomes of these two organisms (89, 80). It is thought that the high G+C content of the genomes of thermophilic organisms is due to the required increase in the melting point of their DNA. The increased G+C content is reflected

**Figure 1-2. Alignment of the amino acids of the  $\alpha$ -subunits of SCS.** Amino acid positions that are 85% identical over all species are highlighted in pink, and those which have 85% similarity, if conservative substitutions are allowed, are highlighted in blue. The allowed substitutions are: E or D; K or R; S or T; F Y or W; M L I or V. The abbreviations are: ECOLI, *Escherichia coli*; HAEIN, *Haemophilis influenzae*; COXBU, *Coxiella brunetii*; RICPR, *Rickettsia prowazekii*; AQUAE, *Aquifex aeolicus*; BASCU, *Bacillus subtilis*; CHLTR, *Chlamydia trachomatis*; MYCTU, *Mycobacterium tuberculosis*; STRCO, *Streptomyces coelicolor*; ARCFU, *Archaeoglobus fulgidus*; METJA, *Methanococcus jannachii*; METTH, *Methanobacterium thermoautotrophicum*; THEAQ, *Thermus aquaticus*; THEFL, *Thermus flavus*; Malate, malate thiokinase from *Methylobacterium extroquens*; PIG108/57, pig heart isoforms PH108 or PH57; RAT, rat liver; BIRD-A/G, ATP-specific pigeon breast or GTP specific pigeon liver, (note: these sequences are the same for this subunit); CAEEL, *Caenorhabditis elegans*; ARATH, *Arabidopsis thaliana*; DICDI, *Dictyostelium discoideum*; SACCE, *Saccharomyces cerevisiae*; SCHPO, *Schizosaccharomyces pombe*; TRIVA, *Trichomonas vaginalis*; CIT-HU, human ATP citrate lyase; CIT-SO *Sordaria macrospora* ATP citrate lyase. Data base accession numbers are listed in Appendix 1. The sequences were obtained from the National Center for Biotechnology Information (NCBI @ [www.ncbi.nlm.nih.gov](http://www.ncbi.nlm.nih.gov)). The alignment was initially done using the PIMA program (83, 84), and then adjusted manually. The secondary structure from *E. coli* SCS (55) is indicated.  $\alpha$ -helix is denoted by an 'a',  $\beta$ -sheet by a 'b', a  $3_{10}$  helix by a '3', and turns by 'T'. Positions shown in red indicate residues in exposed loops.

2\* Struct ----- --TTTTTTTaaaaaT TTTaaaaa\*\*\*\*\* 25
1 ECOLI ----- MSILIDRNRKRVICQ GFPGSQGTFRSEQAI 29
2 HAELN ----- MAILIDRNRKRVICQ GFPGSQGTFRSEQAL 29
3 COXBU ----- MSILIDRNRKRVICQ GFPGSQGTFRSEQAI 29
4 RICPR ----- MAILINKRNRKRVICQ GFPGSQGTFRSEQAI 29
5 AQUAE1 ----- MAILVNRKDRRVVQ GITGREGSPRKRCK 29
6 BASCU ----- MSVFDNRKDRRVVQ GITGSTALPRTKQML 29
7 CHLTR ----- MLELSKDRRRTVQ GITGREGSPRTTCV 29
8 MYCTU ----- MT HMSIFLSRDNRVVQ GITGSEAVRRTARML 32
9 STRCO ----- HAIYLYKESRNLVQ GMFGABQKRRTFRML 29
10 ARCFU1 ----- MM DVALLDNRNRVIVQ GITGFGSPQAKRML 32
11 ARCFU2 ----- HAIIVDERKRVVQ GITGYGKFRTERML 29
12 METJA ----- HVLR DRMLLDNRRAIVQ GITGREGSPRTKQML 34
13 MEYTH ----- MRG SIMILLEDNRRLVQ GITGREGSPRTKQML 33
14 THEAQ ----- MLLVNRDRRVVQ GITGREGSPRTKQML 28
15 THEFL ----- VLVNDRDRRVVQ GITGREGSPRTKQML 28
16 MaLate ----- MSILIDNRKRVVQ GITGREGSPRKRMI 28
17 FIG108 ----- MASGSSGLA AARLLRSRFLQQNG IRH ----- CSYTAS RKHLVDRNRKRVICQ GFPGSQGTFRSQAL 63
18 FIG57 ----- MASGSSGLA AARLLRSRFLQQNG IRH ----- CSYTAS RKHLVDRNRKRVICQ GFPGSQGTFRSQAL 63
19 RAT ----- MVSQSSGLA AARLLSRFLQQNG IRH ----- GSYTAS RKNLYDKNRKRVICQ GFPGSQGTFRSQAL 63
20 BIRD-A ----- CSYTAS RKNLYDKNRKRVICQ GFPGSQGTFRSQAL 36
21 BIRD-G ----- CSYTAS RKNLYDKNRKRVICQ GFPGSQGTFRSQAL 36
22 CABEL1 ----- MLS QQIANNARTLQGA ----- RFYAST YNNLIKDKNRKRVICQ GFPGSQGTFRSQML 54
23 CABEL2 ----- M ASTLASAARAATRAA VTR ----- SVYNDT RNNLAKNSKRVVQ GFPGSQGTFRSQML 55
24 ARATH1 LKQPCIGRSRDFSDL FAIPAAAAAARQSA LSLHWYSLAPS ----- GQLLRL LRQVFDNRNRVIVQ GITGNGGTFRTRQAI 77
25 ARATH2 ----- MSRQVARL ----- IGSLSKARCRST GGSEVP ----- PSCQSL TSLIQRSRFPASDHPH PAAVVFDNRNRVIVQ GITGNGGTFRTRQAI 78
26 DICDI ----- M ----- ISA-GHIDRN ----- FG ----- KRPFST KPSVLDNRKRVICQ GFPGSQGTFRSQAI 48
27 SACCE ----- MLR STVSKASLKIQRPH RES ----- IPYDNT IRNLKPKDRRVVQ GFPGSQGTFRSALSQ 57
28 SCHPO ----- MFKIQTITLLTSLR RFSSSSQLK ----- N ----- SK ----- SLYBQT IPNLINDNRKRVVQ GFPGSQGTFRSQOHM 61
29 TRIVA2 ----- MLSSSFERNLH QLLFFIDNRKRVVQ GI-GNQQGPHSRMLR 40
30 TRIVA3 ----- MLSSSFERNLH QLLFFIDNRKRVVQ GI-GNQQGPHSRMLR 40
31 TRIVA1 ----- MLAGDSRNLH KPLFFIDNRKRVVQ GI-GNQQGPHSRMLR 40
32 AQUAE2 ----- ----- MAKSLFITSF LKPRYKPKDMEKQNN VGTKYLNRKRVIVV GITGREASQVTESEA 57
33 CIT-HU ----- ----- RSLQGKST -TLFSRHTKALVW GHO-CGLDFDVIYC 515
34 CIT-SO ----- ----- RPLSPLPA HALFNEKTRCFVY GLQ-CGMLDFDFIC 80

2\* Struct aTtbhbhbhbTTTTT TbbbTT----- bbbbTTaaaaaaaT TbbbbTTT333aaa aaaaaTTTTTbhbhb TTTTTTaaaaa\*\*\* 111
1 ECOLI AAGTQVGGVTEGNG GTTHLG----- LEVNTVREVAATG ATASVIVEAPFQD SILEALDAGLKIT IREGITLDMKLVK 109
2 HAELN AAGTQLGGVSEENG GTTHLG----- LEVNTVREVAENIG VTAIVEVSEAFQD ALEALDAGGLVIC IREGITLDMKLVK 109
3 COXBU EYGTVHGGVTEGNG GQSHLG----- LEVNSVREVAEETS ADAMIEPVEAFFFQD SILEAVDAGRLAVC IREGITLDMKLVK 109
4 RICPR EYGTVHGGVTEGNG GETHLN----- LEVNTVREVAKATG ANASVIVEEPFFAAD SILEALDAGIELVVC IREGITLDMKLVK 109
5 AQUAE1 EYGTVVAGVTEGNG GMEVEG----- IPEVNTVREVAKEG ANCSLIVEAFFAAD AIVEALDAGIELVIC IREGITLDMKLVK 109
6 BASCU EYGENLVGGVTEGNG GTEAEG----- VEVNTVREVAQTG ANASVIVEAFFAAD ADEAVDAGGLVIC IREGITLDMKLVK 109
7 CHLTR AGENVFGVTEGNG GQQLFD----- LEPVDSVLEAQAATG CRASIEVEEPPFAAE AIEAEDAGIELVIC IREGITLDMLEVA 109
8 MYCTU RAGIQIVGGVNRKA GITVTHEKGGRLIK ERVGSVAEMEKTG ADVETVVEPPTFAK AIEALDAIEPLVW IREGITPQDTAYAW 122
9 STRCO AAGSDVGGVNERJA GRVDFDNRT----- VEVSGSVRERKERTG ADVVEVEVEPPFAEA AVVEAADAGGLAVV IREGITPQDSVALT 113
10 ARCFU1 DYGNKVGGVTEGNG GSEVHG----- IPEVNTVREVAEIN ADTSLIVEAFFFAD AIEFAEDAGELAVC VEGIEPLDMELTH 110
11 ARCFU2 NYGNKVAGVTEGNG GTEVLG----- VPEVDSVREVAEAD ANASVIVEAFFAAD AVMEAADAGELVIC IREGITPQDMLKY 107
12 METJA EGGKLVGGVTEGNG GQNVHG----- VPEVDSVREVAEAD ANASVIVEAFFFAD AVFEALDAGELVW IREGITPQDMEFV 112
13 MEYTH EYGERLVAGVTEGNG QQEFLG----- VPEVNSVEVTEEMD VNASTIVEAFFFAD AAFESIK-HLDLAVI IREGITPQDSQJIM 110
14 THEAQ DYGNKVAGVTEGNG GTEVLG----- VEVYDVKREVAHE VDASTIVEAFAAAD AALEAARNGEPLVW IREGITPLDMVAV 106
15 THEFL DYGNKVAGVTEGNG GTEVLG----- VPEVDVKREVAHE VDASTIVEAFAAAD AALEAARNGEPLVW IREGITPLDMVAV 106
16 MaLate AGENVFGVTEGNG GRTNCG----- VPEVNTVREVAEATG ATTSITVEAFFFAD AIMEAADAGGLAVCS IREGITPQDMMRVK 102
17 FIG108 EYGENLVGGVTEGNG GRTHLG----- LEVNTVREVAEQTG ATASVIVEPPFFAAA AINEALDMEVPLVVC IREGITPQDMMRVK 142
18 FIG57 EYGENLVGGVTEGNG GRTHLG----- LEVNTVREVAEQTG ATASVIVEPPFFAAA AINEALDMEVPLVVC IREGITPQDMMRVK 142
19 RAT EYGNKLGGVTEGNG GRTHLG----- LEVNTVREVAEQTG ATASVIVEPPFFAAA AINEALDAEPLVVC IREGITPQDMMRVK 142
20 BIRD-A DYGENLVGGVTEGNG GRTHLG----- LEVNSVREVAEQTG ASASVIVEPPFFAAA AINEALDAEPLVVC IREGITPQDMMRVK 115
21 BIRD-G DYGENLVGGVTEGNG GRTHLG----- LEVNSVREVAEQTG ASASVIVEPPFFAAA AINEALDAEPLVVC IREGITPQDMMRVK 115
22 CABEL1 EYGNLVGGVNRKA GTEHLG----- LEVNSVREVAEQTG ADASVIVEAFAANG AIEBAMDAEPLVVC IREGITPQDMMRVK 133
23 CABEL2 EYGNLVGGVSENA GQTHLG----- EPEVGSVAEMKRIG ADATVIVEAAGNAR AIEBAMDAEGLVA IREGITPQDMMRVK 124
24 ARATH1 EYGNKLVAGVTEGNG GTEHLG----- LEVNTVREVAEATK ANASVIVEAFFAAA AIEBGLAREGLVIC IREGITPQDMMRVK 156
25 ARATH2 EYGNKLVAGVTEGNG GTEHLG----- LEVNSVREVAEATK ANASVIVEAFFAAA AIEBGLAREGLVIC IREGITPQDMMRVK 157
26 DICDI EYGENLVGGVSPGNG GQKHLG----- EPEVNTVREVAEATG ANASVIVEPPFFAAA AIEBGLAREGLVIC IREGITPQDMMRVK 127
27 SACCE EYGENLVGGVNRKA GQTHLG----- QPEVNSVREVAEATG ACASAVEPPFFAAA AIEBGLAREGLVIC IREGITPQDMMRVK 136
28 SCHPO DYGNKVAGVTEGNG GETHLG----- EPVGTVEVAEATK ADASVIVEPPFFAAA AIEBGLAREGLVIC IREGITPQDMMRVK 140
29 TRIVA2 EYGNKVAGVNRKA GKTIAG----- EPVNTVREVAEKRTD ANASLIVEAFAANG ACTBAEACNGELVIC IREGITPQDMMRVK 119
30 TRIVA3 QYGNKVAGVNRKA GSTIAG----- EPVNTVREVAEKRTD ANASLIVEAFAANG ACTBAEACNGELVIC IREGITPQDMMRVK 119
31 TRIVA1 QYGNKVAGVNRKA GTTIAG----- EPVNTVREVAEKRTD ANASLIVEAFAANG ACTBAEACNGELVIC IREGITPQDMMRVK 119
32 AQUAE2 LYEGFLVGVTEGNG GTEVAG----- VEVNTVREVALSSPE----- TGLVVEEASVID AVIEALDAGGLVYI VREVPIRDTVIFY 140
33 CIT-HU SRDPSVAMVPEPT GDERQFVNGKEILL IPEVKNDAEMKRLS VDVLINDEAGLSAYD SIMHEMLAQRTYAI IAREGPEALTRKLI 615
34 CIT-SO KRSPFSVAGLIPFG QOFVSIVNGISEILL EPYQVEQVAKALD VDVVVNEASRSVYS SIMHEMLAQRTYAI IAREGPEARRAREIA 180

Reproduced with permission of the copyright owner. Further reproduction prohibited without permission.



2' Struct aaaaaa--TTbbTT TTbbbb-----TTTb bbbTTT333TTTTb bbbTTTaaaaaaa aaaaTTTTbbbbbT 187

1	ECOLI	VKLDEA--GVNLRIGP NCRGRLT	-----	RGEC	KIGDMPGHIRKGRV	GIVSRSGTLYEAVK	QTYDVGQOSTCVGI	178
2	HAELN	QKNET--GVNLRIGP NCRGRLT	-----	RGEC	KIGDMPGHIRKGRV	GIVSRSGTLYEAVK	QTYDVGQOSTCVGI	178
3	COXBU	AYLRQH--PDVLRIGP NCRGRLT	-----	RGEC	KIGDMPGHIRKGRV	GIVSRSGTLYEAVN	QTYDVGQOSTCVGI	179
4	RICPR	RALLGS--KTRLRIGP NCRGRLT	-----	RGEC	KIGDMPGHIRKGRV	GIVSRSGTLYEAVA	QTYDVGQOSTCVGI	178
5	AQUAE1	DYMLKRYENARGVGR NCRGRLT	-----	RGEA	KVGLMPGHIFKRGCI	GIVSRSGTLYEAAV	QLTKVGLGOSTAVGI	180
6	BASCU	RFMEGR--KTRLRIGP NCRGRLT	-----	RGEC	KIGDMPGHIRKGRV	GIVSRSGTLYEAVH	QLSEAGVQOSTAVGI	178
7	CHLTR	SLMEKS--ASSLRIGP NCRGRLK	-----	RGCV	KIGDMPGYIHLPGKV	GIVSRSGTLYEAVH	QLTQRKIGQSTCVGI	178
8	MYCTU	AVNLEAGHRTLRIGP NCRGRLS	-----	RGQS	IAGDEPANTVGRPE	GIVSRSGTLYEAVF	ELR--DLGFSTAIGI	190
9	STRCO	AHARANG--TRVIGP NCRGRLT	-----	RGQS	WAGLPPDPTKGRV	GIVSRSGTLYEAVL	ELR--DIGFSTCVGI	180
10	ARCFUL	RRLREV--KSMVIGP NCRGRLS	-----	RGRS	KVGLLPPORSTQGNL	GIVSRSGTLYEAVI	NLTKVGLGOSTVAVGI	181
11	ARCFU2	WRVKEAG--AT--LRIGP NCRGRLS	-----	RGRT	KIGDMPVQVIFKGNV	GIVSRSGTLYEAVL	NLTKVGLGOSTVAVGI	178
12	MEIJA	NYASRMG--VT--LRIGP NCRGRLS	-----	RGVQ	KIGDMPVQVIFKGNV	GIVSRSGTLYEAVL	QIDQVGFVSTCVGI	183
13	MEIYH	EYASRMG--KT--VIGP NCRGRLT	-----	RGVQ	KIGDMPVQVIFKGNV	GIVSRSGTLYEAVL	QIDQVGFVSTCVGI	181
14	THEAQ	EETKALG--SRVIGP NCRGRLS	-----	RGET	KIGDMPGHVFRKGRV	GIVSRSGTLYEAAA	ALSOAGLGLTTTVGI	177
15	THEFL	EETKALG--SRVIGP NCRGRLS	-----	RFLP	KIGDMPGHVFRKGRV	GIVSRSGTLYEAAA	ALSOAGLGLTTTVGI	177
16	MaLate	LRRVYPKRKRIVVIGP NCRGRLS	-----	RGKS	KIGDMPGHTYLPKGV	GIVSRSGTLYEAAA	QMKELGIGDSTVAVGI	169
17	PIG108	HRLLRQG--KTRLRIGP NCRGRLNRFLEAVY	ITSRVFTCTQOEYR	-----	KIPLLPG--TRSDIM	GIVSRSGTLYEAVH	QTYDVGQOSTCVGI	230
18	PIG57	HRLLRQG--KTRLRIGP NCRGRLN	-----	RGEC	KIGDMPGHIRKGRV	GIVSRSGTLYEAVH	QTYDVGQOSTCVGI	213
19	RAT	HRLLRQG--KTRLRIGP NCRGRLN	-----	RGEC	KIGDMPGHIRKGRV	GIVSRSGTLYEAVH	QTYDVGQOSTCVGI	213
20	BIRD-A	HRLVRQD--KTRLRIGP NCRGRLN	-----	RGEC	KIGDMPGHIRKGRV	GIVSRSGTLYEAVH	QTYDVGQOSTCVGI	186
21	BIRD-G	HRLVRQD--KTRLRIGP NCRGRLN	-----	RGEC	KIGDMPGHIRKGRV	GIVSRSGTLYEAVH	QTYDVGQOSTCVGI	186
22	CAEEL1	SRLLRQN--KTRLRIGP NCRGRLS	-----	ADQC	KIGDMPGHIRKGRV	GIVSRSGTLYEAVH	QTYDVGQOSTCVGI	204
23	CAEEL2	NRLLRQN--KTRLRIGP NCRGRLS	-----	SDCC	KIGDMPGHIRKGRV	GIVSRSGTLYEAVH	QTYDVGQOSTCVGI	205
24	ARATH1	AALNSQS--KTRLRIGP NCRGRLK	-----	RGEC	KIGDMPGYIHKPGKI	GIVSRSGTLYEAVF	QTYDVGQOSTCVGI	227
25	ARATH2	HALNSQS--KTRLRIGP NCRGRLK	-----	RGEC	KIGDMPGYIHKPGKI	GIVSRSGTLYEAVF	QTYDVGQOSTCVGI	228
26	DICD1	YLNRQN--KTRLRIGP NCRGRLK	-----	RGEC	KIGDMPGHIRKGRV	GIVSRSGTLYEAVA	QTYDVGQOSTCVGI	198
27	SACCE	EMLTQDQ--KTRLRIGP NCRGRLN	-----	ERKV	KIGDMPKTIQVAGCI	GIVSRSGTLYEAVQ	QTYDVGQOSTCVGI	208
28	SCHPO	DILKQDQ--KTRLRIGP NCRGRLN	-----	RGCC	KIGDMPSHIRKPGCI	GIVSRSGTLYEAVN	QTYDVGQOSTCVGI	211
29	TRIVA2	KVMKET--GCQLIGP NCRGRLQ	-----	RGHT	KIGDLPINIFNNGCI	GIVSRSGTLYEAAV	ATTQVGLGOSTVAVGI	190
30	TRIVA3	KVMKET--GCQLIGP NCRGRLQ	-----	RGHT	KIGDLPINIFNNGCI	GIVSRSGTLYEAAV	ATTQVGLGOSTVAVGI	190
31	TRIVA1	KVMKET--GCQLIGP NCRGRLQ	-----	RGHT	KIGDLPINIFNNGCI	GIVSRSGTLYEAAV	ATTQVGLGOSTVAVGI	190
32	AQUAE2	HYAKER--GVTIVGP TSLGCIIV	-----	FRIBAR	IGGQSPSTAYADGL	VILSRSGGTTTTTAR	MFKRRNGVYVALAL	214
33	CIT-HU	KKADQK--GVTIVGP AVVGGIK	-----	RGCF	KIGDMPGHTYLPKGV	VAVSRSGGMSBELAN	IISRTIDGVYEGVAL	691
34	CIT-SO	VYAKKK--GVTIVGP AVVGGIK	-----	RGCF	KIGDMPGHTYLPKGV	VAVSRSGGMSBELAN	IISRTIDGVYEGVAL	256

2' Struct TTTTTTTTaaaaaa aaaTTTTTTbbbbb bTTTTTaaaaaaa aaT-----TTTbbb bbTTTT--TTTTTTP/TTTTTTTTTTTaaa 273

1	ECOLI	GGDPTGSENFIDILE	MFEDPQTEAVVIG	KIGGABREAAAYIK	EHV----	TKPVVY	IAGVAP--RGRMG	HGALTAGGKTADE	261
2	HAELN	GGDPTGSENFIDILE	RFQDPEIEAVVIG	KIGGABREAAAYIK	DAN----	TKPVVY	IAGVAP--RGRMG	HGALTAGGKTADE	261
3	COXBU	GGDPTGSENFIDILE	MFEDPQTEAVVIG	KIGGABREAAAYIK	SNV----	KKPVVY	IAGVAP--RGRMG	HGALTAGGKTADE	262
4	RICPR	GGDPTGSENFIDILE	MFEDPQTEAVVIG	KIGGABREAAAYIK	QSK----	IKPVVY	IAGVAP--RGRMG	HGALTAGGKTADE	262
5	AQUAE1	GGDPTGSENFIDILE	MFEDPQTEAVVIG	KIGGABREAAAYIK	KEV----	DKPVVY	IAGVAP--RGRMG	HGALTAGGKTADE	263
6	BASCU	GGDPTGSENFIDILE	MFEDPQTEAVVIG	KIGGABREAAAYIK	AMN----	TKPVVY	IGGQAP--RGRMG	HGALTAGGKTADE	261
7	CHLTR	GGDPTGSENFIDILE	MFEDPQTEAVVIG	KIGGABREAAAYIK	QHS----	SKPVVY	IAGVAP--RGRMG	HGALTAGGKTADE	261
8	MYCTU	GGDPTGSENFIDILE	MFEDPQTEAVVIG	KIGGABREAAAYIK	TNV----	SKPVVY	VAGVAP--RGRMG	HGALTAGGKTADE	273
9	STRCO	GGDPTGSENFIDILE	MFEDPQTEAVVIG	KIGGABREAAAYIK	AHV----	TKPVVY	IAGVAP--RGRMG	HGALTAGGKTADE	263
10	ARCFUL	GGDPTGSENFIDILE	MFEDPQTEAVVIG	KIGGABREAAAYIK	-QM----	SKPVVY	IAGVAP--RGRMG	HGALTAGGKTADE	263
11	ARCFU2	GGDPTGSENFIDILE	MFEDPQTEAVVIG	KIGGABREAAAYIK	-EM----	SKPVVY	VAGVAP--RGRMG	HGALTAGGKTADE	260
12	MEIJA	GGDPTGSENFIDILE	MFEDPQTEAVVIG	KIGGABREAAAYIK	-QM----	SKPVVY	IAGVAP--RGRMG	HGALTAGGKTADE	265
13	MEIYH	GGDPTGSENFIDILE	MFEDPQTEAVVIG	KIGGABREAAAYIK	-QM----	SKPVVY	IAGVAP--RGRMG	HGALTAGGKTADE	263
14	THEAQ	GGDPTGSENFIDILE	MFEDPQTEAVVIG	KIGGABREAAAYIK	DHM----	KKPVVY	IGGQAP--RGRMG	HGALTAGGKTADE	260
15	THEFL	GGDPTGSENFIDILE	MFEDPQTEAVVIG	KIGGABREAAAYIK	DHM----	KKPVVY	IGGQAP--RGRMG	HGALTAGGKTADE	260
16	MaLate	GGDPTGSENFIDILE	MFEDPQTEAVVIG	KIGGABREAAAYIK	ENF----	SKPVVY	VAGVAP--RGRMG	HGALTAGGKTADE	251
17	PIG108	GGDPTGSENFIDILE	MFEDPQTEAVVIG	KIGGABREAAAYIK	QHN--SGPKSPVSE	IAGVAP--RGRMG	HGALTAGGKTADE	317	
18	PIG57	GGDPTGSENFIDILE	MFEDPQTEAVVIG	KIGGABREAAAYIK	QHN--SGPKSPVSE	IAGVAP--RGRMG	HGALTAGGKTADE	300	
19	RAT	GGDPTGSENFIDILE	MFEDPQTEAVVIG	KIGGABREAAAYIK	ENH--SGPKSPVSE	IAGVAP--RGRMG	HGALTAGGKTADE	300	
20	BIRD-A	GGDPTGSENFIDILE	MFEDPQTEAVVIG	KIGGABREAAAYIK	ENH--SGPKSPVSE	IAGVAP--RGRMG	HGALTAGGKTADE	273	
21	PIG-B	GGDPTGSENFIDILE	MFEDPQTEAVVIG	KIGGABREAAAYIK	ENH--SGPKSPVSE	IAGVAP--RGRMG	HGALTAGGKTADE	273	
22	CAEEL1	GGDPTGSENFIDILE	MFEDPQTEAVVIG	KIGGABREAAAYIK	ENH--SGPKSPVSE	IAGVAP--RGRMG	HGALTAGGKTADE	291	
23	CAEEL2	GGDPTGSENFIDILE	MFEDPQTEAVVIG	KIGGABREAAAYIK	SRN--SGPKSPVSE	IAGVAP--RGRMG	HGALTAGGKTADE	312	
24	ARATH1	GGDPTGSENFIDILE	MFEDPQTEAVVIG	KIGGABREAAAYIK	ENH--SGPKSPVSE	IAGVAP--RGRMG	HGALTAGGKTADE	292	
25	ARATH2	GGDPTGSENFIDILE	MFEDPQTEAVVIG	KIGGABREAAAYIK	AS---GTEKPVVY	IAGVAP--RGRMG	HGALTAGGKTADE	312	
26	DICD1	GGDPTGSENFIDILE	MFEDPQTEAVVIG	KIGGABREAAAYIK	DN---PTKPVVY	IAGVAP--RGRMG	HGALTAGGKTADE	282	
27	SACCE	GGDPTGSENFIDILE	MFEDPQTEAVVIG	KIGGABREAAAYIK	ENH--SGPKSPVSE	IAGVAP--RGRMG	HGALTAGGKTADE	298	
28	SCHPO	GGDPTGSENFIDILE	MFEDPQTEAVVIG	KIGGABREAAAYIK	ANASRSTPKPVVY	IAGVAP--RGRMG	HGALTAGGKTADE	299	
29	TRIVA2	GGDPTGSENFIDILE	MFEDPQTEAVVIG	KIGGABREAAAYIK	KT--KLTQKPVVY	IAGVAP--RGRMG	HGALTAGGKTADE	276	
30	TRIVA3	GGDPTGSENFIDILE	MFEDPQTEAVVIG	KIGGABREAAAYIK	KT--KLTQKPVVY	IAGVAP--RGRMG	HGALTAGGKTADE	276	
31	TRIVA1	GGDPTGSENFIDILE	MFEDPQTEAVVIG	KIGGABREAAAYIK	KT--KLTQKPVVY	IAGVAP--RGRMG	HGALTAGGKTADE	276	
32	AQUAE2	GGDPTGSENFIDILE	MFEDPQTEAVVIG	KIGGABREAAAYIK	RYLTKRNVKPVVY	VAGVAP--RGRMG	HGALTAGGKTADE	300	
33	CIT-HU	GGDPTGSENFIDILE	MFEDPQTEAVVIG	KIGGABREAAAYIK	E---GRLTKPVVY	CIGVAP--RGRMG	HGALTAGGKTADE	778	
34	CIT-SO	GGDPTGSENFIDILE	MFEDPQTEAVVIG	KIGGABREAAAYIK	Q---GLTKPVVY	AVGAP--RGRMG	HGALTAGGKTADE	343	

2*	Struct	aaaaaaTTTbTTT	333aaaaa-----	-----	-----	288
1	ECOLI	KFAAEAAAGVKIVRS	LADIGEALRIVLK--	-----	-----	289
2	HAEIN	KIAALEAAGVTCVKS	LAETGEALRKLKSS	KN-----	-----	293
3	COXBU	KVAALEAAGVVFVKS	PAETGRGVREATGMS	TH-----	-----	294
4	RICFR	KVEALEAAGVITRS	PADIGRTMLDLANKI	-----	-----	292
5	AQUAE1	KKALEAAGAVVVEN	PAKIGETVAKILKVI	ELEBERTSDAE	-----	305
6	BASCU	KKKEAAGGTEVAET	PSVHGTELLKVLKEK	NLFETCKNH	-----	300
7	CHLTR	KQEAERQAGVTVVES	LALIGEAVASVLKPR	-----	-----	291
8	MYCTU	KQEALEAAGVKVGT	FSAEALARETLLSL	-----	-----	303
9	STRCO	KKALESVGVVVGST	PTEIARRHVLQALDVP	GGAAPDGAARDGARA	-----	308
10	ARCFU1	KMAALEAAGARVAET	LLDVVKEVRRVLE	-----	-----	291
11	ANCFU2	KIKALEAAGARVGT	FHEVAELVAEIL	-----	-----	287
12	METJA	KKALEAAGAVVAKN	ISDTPKLLAGILGK	-----	-----	294
13	METTH	KKALEAAGAVVDR	PSAIVDETRAQIGVR	-----	-----	293
14	THEAQ	KLRVAEAGIPVADT	IDRIVELVKKALG	-----	-----	288
15	THEFL	KLRVAEAGIPVADT	IDRIVELVKKALG	-----	-----	288
16	Malate			-----	-----	251
17	FIG108	KITALQSAGVVVMS	PAQLGTTTYKEFEKR	KHLZKQNE	-----	355
18	FIG57	KITALQSAGVVVMS	PAQLGTTTYKEFEKR	KHLZKQNE	-----	338
19	RAT	KISALQSAGVIVSMS	PAQLGTCMYKEFEKR	KML	-----	333
20	BIRD-A	KIAALQAGVVVMS	PAQLGSTTYKEFEKR	KLL	-----	306
21	BIRD-G	KIAALQAGVVVMS	PAQLGSTTYKEFEKR	KLL	-----	306
22	CAEEL1	KINALREAGVVVYDS	PAKLGTSMTAFILGK	I	-----	322
22	CAEEL2	KIEALRNAMVVVYDS	PAKLGVAHQKALLG	-----	-----	321
24	ARATH1	KIKSLRDAGVKVVES	PAKLGAAHFELPQER	GLLK	-----	345
24	ARATH2	KIKSLRDAGVKVVES	PAKIGSAMVELPQER	GLLQ	-----	347
26	DICDI	KIEALQAGVTVVFS	PAKLGTEILRQNE	-----	-----	310
27	SACCE	KKQALRDVGVAVVES	FGYLGQALLDQFAKF	K	-----	329
28	SCHPO	KFAALEAAGVRIERS	PATLGSLIVVEELNKL	KH	-----	331
29	TRIVA2	KYKALEAAGVRIARH	FGNMGKFIPEEMKRL	GKI	-----	309
30	TRIVA3	KYKALEAAGVRIARH	FGNMGKFIPEEMKRM	GKI	-----	309
31	TRIVA1	KYKALEAAGVRIARH	FGNMGKFIPEEMKRM	GKI	-----	309
32	AQUAE2	KIRMNEVGKETGLV	KVAEFYHDLVNCIEE	LGVPRDFEDSTPGCK	VEPLVRTIDPETCEFKPD	368
33	CIT-HU	KNQALKEAGVVFPRS	FDELGELIQSVYEDL	VANGVIVPAQEVPPP	...	823
34	CIT-SO	KNKSMREAGVVPDT	FDEMPALLKQVYDKL	VADGTTIVPAPEVVP	...	386

**Figure 1-3. Alignment of the amino acids of the  $\beta$ -subunits of SCS.** Amino acid positions that are 85% identical over all species are highlighted in pink and those which have 85% similarity, if conservative substitutions are allowed, are highlighted in blue. The allowed substitutions are: E or D; K or R; S or T; F Y or W; M L I or V. The abbreviations are: ECOLI, *Escherichia coli*; COXBU, *Coxiella brunetii*; HAEIN, *Haemophilis influenzae*; BASCU, *Bacillus subtilis*; RIPR, *Rickettsia prowazekii*; AQUAE, *Aquifex aeolicus*; Malate, malate thiokinase from *Methylobacterium extroquens*; CHLTR, *Chlamydia trachomatis*; THEAQ, *Thermus aquaticus*; THEFL, *Thermus flavus*; MYCTU, *Mycobacterium tuberculosis*; STRCO, *Streptomyces coelicolor*; ARCFU, *Archaeoglobus flugidus*; METJA, *Methanococcus jannaschii*; METTH, *Methanobacterium thermoautotrophicum*; HUMAN-A/G, ATP- or GTP-specific SCS from human; PIG-A/G, ATP- or GTP-specific SCS from pig; MOUSE-A/G, ATP- or GTP-specific SCS from mouse; BIRD-A/G, ATP-specific SCS from pigeon breast or GTP-specific SCS from pigeon liver; CAEEL, *Caenorhabditis elegans*; ARATH, *Arabidopsis thaliana*; TRIVA, *Trichomonas vaginalis*; NEOFR, *Neocallimastix frontalis*; SCHPO, *Schizosaccharomyces pombe*; SACCE, *Saccharomyces cerevisiae*; CIT-HU, human ATP citrate lyase. The database accession numbers are given in Apendix I. The sequence alignment was generated initially by the program PIMA (83,84) and modified manually. The secondary structure from *E. coli* SCS (55) is indicated.  $\alpha$ -helix is denoted by an 'a',  $\beta$ -sheet by a 'b', a  $3_{10}$  helix by a '3', and turns by 'T'. Positions shown in red indicate residues in exposed loops.

2' Struct	-----	-----	-----	-----	-----	-----	-----	-----	-----
1 ECOLI	-----	-----	-----	-----	-----	-----	-----	-----	55
2 COXBU	-----	-----	-----	-----	-----	-----	-----	-----	55
3 HAEIN	-----	-----	-----	-----	-----	-----	-----	-----	55
4 BASCU	-----	-----	-----	-----	-----	-----	-----	-----	55
5 RICFR	-----	-----	-----	-----	-----	-----	-----	-----	55
6 AQUAE1	-----	-----	-----	-----	-----	-----	-----	-----	55
7 MaLate	-----	-----	-----	-----	-----	-----	-----	-----	55
8 CELTR	-----	-----	-----	-----	-----	-----	-----	-----	55
9 THEAQ	-----	-----	-----	-----	-----	-----	-----	-----	54
10 THEFL	-----	-----	-----	-----	-----	-----	-----	-----	54
11 MYCTU	-----	-----	-----	-----	-----	-----	-----	-----	54
12 STRCO	-----	-----	-----	-----	-----	-----	-----	-----	54
13 ARCFU1	-----	-----	-----	-----	-----	-----	-----	-----	55
14 ARCFU2	-----	-----	-----	-----	-----	-----	-----	-----	54
15 MEIUA	-----	-----	-----	-----	-----	-----	-----	-----	52
16 MEITH	-----	-----	-----	-----	-----	-----	-----	-----	54
17HUMAN-A	-----	-----	-----	-----	-----	-----	-----	-----	65
18 FIG-G	-----	-----	-----	-----	-----	-----	-----	-----	78
19MOUSE-G	-----	-----	-----	-----	-----	-----	-----	-----	65
20 BIRD-G	-----	-----	-----	-----	-----	-----	-----	-----	52
21 CABEL2	-----	-----	-----	-----	-----	-----	-----	-----	75
22 ARATH	-----	-----	-----	-----	-----	-----	-----	-----	84
23 TRIVA2	-----	-----	-----	-----	-----	-----	-----	-----	62
24 TRIV13	-----	-----	-----	-----	-----	-----	-----	-----	63
25 TRIVA1	-----	-----	-----	-----	-----	-----	-----	-----	65
26HUMAN-A	-----	-----	-----	-----	-----	-----	-----	-----	71
27 FIG-A	-----	-----	-----	-----	-----	-----	-----	-----	70
28MOUSE-A	-----	-----	-----	-----	-----	-----	-----	-----	71
29 BIRD-A	-----	-----	-----	-----	-----	-----	-----	-----	58
30 CABEL1	-----	-----	-----	-----	-----	-----	-----	-----	79
31 NDOFR	-----	-----	-----	-----	-----	-----	-----	-----	48
32 SCHFO	-----	-----	-----	-----	-----	-----	-----	-----	78
33 SACCE	-----	-----	-----	-----	-----	-----	-----	-----	86
34 AQUAE2	-----	-----	-----	-----	-----	-----	-----	-----	55
35 CIT-HU	-----	-----	-----	-----	-----	-----	-----	-----	68
2' Struct	T-----	Tbb	bbTTaaaaa	aaTTTTTbbbbTTT	aaaaa	---aTT	TbbbbTTTTTTTTTT		
1 ECOLI	A-----	-----	-----	-----	-----	-----	-----	-----	136
2 COXBU	A-----	-----	-----	-----	-----	-----	-----	-----	136
3 HAEIN	A-----	-----	-----	-----	-----	-----	-----	-----	136
4 BASCU	A-----	-----	-----	-----	-----	-----	-----	-----	136
5 RICFR	A-----	-----	-----	-----	-----	-----	-----	-----	136
6 AQUAE1	A-----	-----	-----	-----	-----	-----	-----	-----	135
7 MaLate	A-----	-----	-----	-----	-----	-----	-----	-----	136
8 CELTR	N-----	-----	-----	-----	-----	-----	-----	-----	136
9 THEAQ	A-----	-----	-----	-----	-----	-----	-----	-----	128
10 THEFL	A-----	-----	-----	-----	-----	-----	-----	-----	128
11 MYCTU	A-----	-----	-----	-----	-----	-----	-----	-----	128
12 STRCO	A-----	-----	-----	-----	-----	-----	-----	-----	128
13 ARCFU1	A-----	-----	-----	-----	-----	-----	-----	-----	128
14 ARCFU2	A-----	-----	-----	-----	-----	-----	-----	-----	128
15 MEIUA	A-----	-----	-----	-----	-----	-----	-----	-----	126
16 MEITH	A-----	-----	-----	-----	-----	-----	-----	-----	127
17HUMAN-G	GVF-NSGLK--GGNH	LTKDPNVVQGLAKQM	IGYNLAINQTPREGV	KVWKWMAEALDISR	ETFLAITMDSRNGP	VLVGSPOGSDIEIV			152
18 FIG-G	GVF-SSGLK--GGNH	LTKDPEVVOGLAKQM	IGYNLAINQTPREGV	KVWKWMAEALDISR	ETFLAITMDSRNGP	VLVGSPOGSDIEIV			165
19MOUSE-G	GVF-NSGLK--GGNH	LTKDPRVVOGLAKQM	IGYNLAINQTPREGV	KVWKWMAEALDISR	ETFLAITMDSRNGP	VLVGSPOGSDIEIV			152
20 BIRD-G	GVF-NSGLK--GGNH	LTKDKPIVQGLAKQM	IGYNLAINQTPREGV	KVWKWMAEALDISR	ETFLAITMDSRNGP	VLVGSPOGSDIEIV			139
21 CABEL2	GKF-INGNGIGGGVF	ITKDKMALEAIDEM	IGKRLVINQTPSEGV	RVDKVMAEAGVDIQR	ETFLAVIMDSRNGP	VVVASPDGGMDIEIV			164
22 ARATH	GTF-KSGLK--GGNH	IVKR-DEABEIAKQM	LQQLVINKQTPGQK	VSKWVLECKLSLVM	EMFSTLIDRSKSGP	LIIACKNGGISTEDL			170
23 TRIVA2	GHMKEIGFK--SGNH	FVKSADAAKIAKEM	LGHHLVINQTKGDGL	LQQAVMESDPVEVGR	ELMFAILEDRTQSP	VVIASTEGGVEIEIV			150
24 TRIV13	GHMKEIGFK--SGNH	FVKSADAAKIAKEM	LGHHLVINQTKGDGL	LQQAVMESDPVEVGR	ELMFAILEDRTQSP	VVIASTEGGVEIEIV			151
25 TRIVA1	GHMLETGFK--SGNH	FVKSADAAKIAKEM	LGHHLVINQTKGDGL	LQQAVMESDPVEVGR	ELMFAILEDRTQSP	VVIASTEGGVEIEIV			153
26HUMAN-A	GTF-ESGLK--GGNH	IVFSPPEAKAVSSQM	IGKQLFTIQIGENGR	ICNQVLCERRVYFR	EYFALTMBSFQGP	VLIGSSQGGNIEIV			158
27 FIG-A	GTF-ESGLK--GGNH	IVFSPPEAKAVSSQM	IGKQLFTIQIGENGR	ICNQVLCERRVYFR	EYFALTMBSFQGP	VLIGSSQGGNIEIV			157
28MOUSE-A	GTF-TSGLK--GGNH	IVFSPPEAKAVSSQM	IGKQLFTIQIGENGR	ICNQVLCERRVYFR	EYFALTMBSFQGP	VLIGSSQGGNIEIV			158
29 BIRD-A	GTF-EGGLK--GGNH	IVFSPPEAKAVSSQM	IGKQLFTIQIGENGR	ICNQVLCERRVYFR	EYFALTMBSFQGP	VLIGSSQGGNIEIV			145
30 CABEL1	GTF-SSGLK--GGNH	IVFSPPEAKAVSSQM	IGKQLFTIQIGENGR	ICNQVLCERRVYFR	EYFALTMBSFQGP	VLIGSSQGGNIEIV			166
31 NDOFR	GTF-DSGLK--GGNH	IVFSPPEAKAVSSQM	IGKQLFTIQIGENGR	ICNQVLCERRVYFR	EYFALTMBSFQGP	VLIGSSQGGNIEIV			135
32 SCHFO	GTF-DSGLK--GGNH	IVFSPPEAKAVSSQM	IGKQLFTIQIGENGR	ICNQVLCERRVYFR	EYFALTMBSFQGP	VLIGSSQGGNIEIV			165
33 SACCE	GTF-DTGYK--GGNH	IVFSPPEAKAVSSQM	IGKQLFTIQIGENGR	ICNQVLCERRVYFR	EYFALTMBSFQGP	VLIGSSQGGNIEIV			173
34 AQUAE2	A-----	-----	-----	-----	-----	-----	-----	-----	129
35 CIT-HU	L-----	-----	-----	-----	-----	-----	-----	-----	147

2' Struct		aaat333TTTTTTTTTTTTTTTTTaaasaaaaa	aTT-Taaasaaaaa	asasasaaaaaTtbbb	bbbbbb--bTTT	TbbbTTTTbbbT333
1	ECOLI	AEETPELHVAIDP	LGGMPYQGRGAPK	LGL-EGLKVOQPKI	FAGTITFLERLAL	IKINREVI---TRQG
2	COXBU	AKESPELHVAIDP	AIGLQPFQCRGEPG	LGLQDLKQMSFDI	WAGTITFLERLAL	IKINREVI---TRQG
3	HAEIN	VNSPELHVAIDP	LFGGLPYQGRGAPK	LGL-SGANKQFDI	FAGTITFLERLAL	IKINREVI---TRQG
4	BASCU	AERTPELHVAIDP	AVGLQGVQARETAA	INIKPELVGAQEM	I-GGKALEVERKCSI	AKINREVI---TQGG
5	RICFR	AEKMEPELHVAIDP	AIGLQPFQGRGAPK	LGF-KINQAKQKEI	WAGTITFLERLAL	IKINREVI---TRQG
6	AQUAEI	VKENPELHVAIDP	ELGLMPYQAREAPK	LAL---PVKEASTA	IK-TQTESLQASL	VEINREVI---TRQG
7	Malate	AKKEPELHVAIDP	AVGLQGVQARETAA	LGL-NIKQVSAVKT	INNSRAFDCCGEM	IKINREVI---TRQG
8	CHLTR	AEKQPELHVAIDP	SGKLYGQVLRGAPK	MEW-DQITADQGR	IQGLQCCYKQASL	IKINREVI---TRQG
9	THEAQ	AEERPELHVAIDP	HNGFRPFPEARWKR	AGL-EGNLAK-LAQV	EAVALRAREGVDAI	AKINREVI---TMDG
10	THEFL	AEERPELHVAIDP	HNGFRPFPEARWKR	AGL-EGNLAK-LAQV	EAVALRAREGVDAI	AKINREVI---TMDG
11	MYCTU	AATKPELHVAIDP	VGVNLDFAFSZABQ	GHL-PAEVLDTAVT	TAKNRELVAEDAVL	VEINREVI---TFPH
12	STRCO	AARRPELHVAIDP	ATGVHATAVRLAQA	AGL-----PFQIVDT	IVRANRIVREDALL	VEINREVI---TAEQ
13	ARCFU1	AAKHPELHVAIDP	LWGLADYEVKRLFR	AGF-EGRFPQMFDI	IKKQNDIFAYEAIL	TKINREVI---TDEG
14	ARCFU2	AAKHPELHVAIDP	LWGLADYEVKRLFR	AGF-EGRFPQMFDI	IKKQNDIFAYEAIL	TKINREVI---TDEG
15	MEUJA	AEKNPELHVAIDP	RKEFLPYARWVKE	AKL-PSNLEIGVADV	YKGLAKIPELDAIM	VEINREVI---TRDG
16	MEYTH	AARSPELHVAIDP	LDFLPEAREZARK	MGL-ESELPVSGV	IKKQVLEPKVDAIL	AKINREVI---SDGS
17	HUMAN-G	AASNPELHVAIDP	FEKIKDSQARMAEN	LGF-VGLKSOAADQ	YTKNLEFLKIDAIQ	VEINREVI---TFEG
18	PIG-G	AASNPELHVAIDP	FEKIKDSQARMAEN	LGF-LGFLQNAADQ	IKKQVLEFLKIDAIQ	VEINREVI---TFEG
19	MOUSE-G	AASNPELHVAIDP	FEKIKDSQARMAEN	LGF-LGFLQNAADQ	YTKNLEFLKIDAIQ	VEINREVI---TFEG
20	BIRD-G	AVTSPPELHVAIDP	FEKIKDSQARMAEN	LGF-KGFLQQAADQ	IKKQVLEFLKIDAIQ	VEINREVI---TFEG
21	CAEEL2	AERTPELHVAIDP	QMGTEGQSLAKADQ	LGF-EGLKIGVAADQ	IKKQVLEFLKIDAIQ	VEINREVI---TDEG
22	ARATH	AEKPELHVAIDP	FAGITDEDAKVVGD	LAP-KAADKQSIQ	WGLYELFRKDCIM	IKINREVI---TSTN
23	TRIVA2	AAKHPELHVAIDP	VEGTRDVAIVNLSKQ	LGL-TGAVYNGVZE	WQKDKLVKVGSDAIQ	VEINREVI---TMDG
24	TRIV3	AAKHPELHVAIDP	VEGTRDVAIVNLSKQ	LGL-TGAVYNGVZE	WQKDKLVKVGSDAIQ	VEINREVI---TMDG
25	TRIVA1	AAKHPELHVAIDP	VEGTRDVAIVNLSKQ	LGL-TGAVYNGVZE	WQKDKLVKVGSDAIQ	VEINREVI---TMDG
26	HUMAN-A	AAETPELHVAIDP	VEGTRDVAIVNLSKQ	MCF-PRIIVSAEEN	WVQKLSFLKIDAIM	IKINREVI---DSGD
27	PIG-A	AAETPELHVAIDP	VEGTRDVAIVNLSKQ	MCF-PRIIVSAEEN	WVQKLSFLKIDAIM	IKINREVI---DSGD
28	MOUSE-A	AAETPELHVAIDP	VEGTRDVAIVNLSKQ	MCF-PRIIVSAEEN	WVQKLSFLKIDAIM	IKINREVI---DSGD
29	BIRD-A	AAETPELHVAIDP	VEGTRDVAIVNLSKQ	MCF-PRIIVSAEEN	WVQKLSFLKIDAIM	IKINREVI---DSGD
30	CAEEL1	AAETPELHVAIDP	VEGTRDVAIVNLSKQ	MCF-PRIIVSAEEN	WVQKLSFLKIDAIM	IKINREVI---DSGD
31	NEOFR	AAETPELHVAIDP	VEGTRDVAIVNLSKQ	MCF-PRIIVSAEEN	WVQKLSFLKIDAIM	IKINREVI---DSGD
32	SCHFO	AAETPELHVAIDP	VEGTRDVAIVNLSKQ	MCF-PRIIVSAEEN	WVQKLSFLKIDAIM	IKINREVI---DSGD
33	SACCE	AAETPELHVAIDP	VEGTRDVAIVNLSKQ	MCF-PRIIVSAEEN	WVQKLSFLKIDAIM	IKINREVI---DSGD
34	AQUAE2	EPKQVPELHVAIDP	LYEHRVRYNLYE	LGF---MFLVRLKSEV	IARMDAFAWGAEL	LEINREVI---TRQG
35	CIT-HU	AJAKPELHVAIDP	PEIDKHLVHA	---	PDKKELASF	LEINREVI---TRDG
2' Struct		333TaaaTTTTT333	TTaaaaaa-aatTbb	bbbTTTTbbbTta	asasasaaaaaT---	-TTTTTTTTbbbT T-TTaaaaaa
1	ECOLI	LERQPELHVAIDP	EDPREAQA-AQMEIN	YKLDGNGICMNGA	GLMATADEIKL---	HGG-EPNPELDVGG
2	COXBU	LYRQPELHVAIDP	EDPREAQA-AQMEIN	YKLDGNGICMNGA	GLMATADEIKL---	HGG-EPNPELDVGG
3	HAEIN	LFRQPELHVAIDP	EDPREAQA-AQMEIN	YKLDGNGICMNGA	GLMATADEIKL---	HGG-EPNPELDVGG
4	BASCU	LYRQPELHVAIDP	EDPREAQA-AQMEIN	YKLDGNGICMNGA	GLMATADEIKL---	HGG-EPNPELDVGG
5	RICFR	LFRQPELHVAIDP	EDPREAQA-AQMEIN	YKLDGNGICMNGA	GLMATADEIKL---	HGG-EPNPELDVGG
6	AQUAEI	LFRQPELHVAIDP	EDPREAQA-AQMEIN	YKLDGNGICMNGA	GLMATADEIKL---	HGG-EPNPELDVGG
7	Malate	LYRQPELHVAIDP	EDPREAQA-AQMEIN	YKLDGNGICMNGA	GLMATADEIKL---	HGG-EPNPELDVGG
8	CHLTR	LYRQPELHVAIDP	EDPREAQA-AQMEIN	YKLDGNGICMNGA	GLMATADEIKL---	HGG-EPNPELDVGG
9	THEAQ	LERHPDLELHVAIDP	EDPREAQA-AQMEIN	YKLDGNGICMNGA	GLMATADEIKL---	HGG-EPNPELDVGG
10	THEFL	LERHPDLELHVAIDP	EDPREAQA-AQMEIN	YKLDGNGICMNGA	GLMATADEIKL---	HGG-EPNPELDVGG
11	MYCTU	DERQPELHVAIDP	EDPREAQA-AQMEIN	YKLDGNGICMNGA	GLMATADEIKL---	HGG-EPNPELDVGG
12	STRCO	DERQPELHVAIDP	EDPREAQA-AQMEIN	YKLDGNGICMNGA	GLMATADEIKL---	HGG-EPNPELDVGG
13	ARCFU1	DERQPELHVAIDP	EDPREAQA-AQMEIN	YKLDGNGICMNGA	GLMATADEIKL---	HGG-EPNPELDVGG
14	ARCFU2	DERQPELHVAIDP	EDPREAQA-AQMEIN	YKLDGNGICMNGA	GLMATADEIKL---	HGG-EPNPELDVGG
15	MEUJA	AERH-NEEPELHVAIDP	EDPREAQA-AQMEIN	YKLDGNGICMNGA	GLMATADEIKL---	HGG-EPNPELDVGG
16	MEYTH	LYRHPDLELHVAIDP	EDPREAQA-AQMEIN	YKLDGNGICMNGA	GLMATADEIKL---	HGG-EPNPELDVGG
17	HUMAN-G	EPKQKIDFAMDKSE	NEPTINEA-ARYDEK	YKLDGNGICMNGA	GLMATADEIKL---	HGG-EPNPELDVGG
18	PIG-G	EPKQKIDFAMDKSE	NEPTINEA-ARYDEK	YKLDGNGICMNGA	GLMATADEIKL---	HGG-EPNPELDVGG
19	MOUSE-G	EPKQKIDFAMDKSE	NEPTINEA-ARYDEK	YKLDGNGICMNGA	GLMATADEIKL---	HGG-EPNPELDVGG
20	BIRD-G	EPKQKIDFAMDKSE	NEPTINEA-ARYDEK	YKLDGNGICMNGA	GLMATADEIKL---	HGG-EPNPELDVGG
21	CAEEL2	AERKPELHVAIDP	EDPREAQA-AQMEIN	YKLDGNGICMNGA	GLMATADEIKL---	HGG-EPNPELDVGG
22	ARATH	AERKPELHVAIDP	EDPREAQA-AQMEIN	YKLDGNGICMNGA	GLMATADEIKL---	HGG-EPNPELDVGG
23	TRIVA2	HYRQPELHVAIDP	EDPREAQA-AQMEIN	YKLDGNGICMNGA	GLMATADEIKL---	HGG-EPNPELDVGG
24	TRIV3	HYRQPELHVAIDP	EDPREAQA-AQMEIN	YKLDGNGICMNGA	GLMATADEIKL---	HGG-EPNPELDVGG
25	TRIVA1	HYRQPELHVAIDP	EDPREAQA-AQMEIN	YKLDGNGICMNGA	GLMATADEIKL---	HGG-EPNPELDVGG
26	HUMAN-A	AYRQKIDFAMDKSE	EDERDKER-AKANEN	YKLDGNGICMNGA	GLMATADEIKL---	HGG-EPNPELDVGG
27	PIG-A	AYRQKIDFAMDKSE	EDERDKER-AKANEN	YKLDGNGICMNGA	GLMATADEIKL---	HGG-EPNPELDVGG
28	MOUSE-A	AYRQKIDFAMDKSE	EDERDKER-AKANEN	YKLDGNGICMNGA	GLMATADEIKL---	HGG-EPNPELDVGG
29	BIRD-A	AYRQKIDFAMDKSE	EDERDKER-AKANEN	YKLDGNGICMNGA	GLMATADEIKL---	HGG-EPNPELDVGG
30	CAEEL1	EPKQKIDFAMDKSE	NEPTINEA-ARYDEK	YKLDGNGICMNGA	GLMATADEIKL---	HGG-EPNPELDVGG
31	NEOFR	EPKQKIDFAMDKSE	NEPTINEA-ARYDEK	YKLDGNGICMNGA	GLMATADEIKL---	HGG-EPNPELDVGG
32	SCHFO	EPKQKIDFAMDKSE	NEPTINEA-ARYDEK	YKLDGNGICMNGA	GLMATADEIKL---	HGG-EPNPELDVGG
33	SACCE	EPKQKIDFAMDKSE	NEPTINEA-ARYDEK	YKLDGNGICMNGA	GLMATADEIKL---	HGG-EPNPELDVGG
34	AQUAE2	EPKQKIDFAMDKSE	NEPTINEA-ARYDEK	YKLDGNGICMNGA	GLMATADEIKL---	HGG-EPNPELDVGG
35	CIT-HU	EPKQKIDFAMDKSE	NEPTINEA-ARYDEK	YKLDGNGICMNGA	GLMATADEIKL---	HGG-EPNPELDVGG

2' Struct aaTTTTTbbbbbbT TTTTaaaaaaaaaaaaaaT--TTTTbbbb bbTTTaaaaa TTTT----bbbTTaaaaa aaaaaTTTT

1	ECOLI	LSDKRVKAEIVMIFG	GIIVRCILDIDGELI	VAEFG--VNVKVVVR	LEGNNALGAKKED	SGLN----	ITAAKG	LIDAAQVVVAVEGK	388
2	COXBU	VSDKNVGTIVMIFG	GIIVRCILDIDGELI	VKEFG--IDVSNVVR	LEGNNALGAKKED	SCHN----	ITAAKG	PADRAEQIVKQVGI	389
3	BACIN	LIDPSVVEIVMIFG	GIIVRCILDIDGELI	VMEFG--VRVNVVVR	LEGNNALGAKKED	SDVN----	ITAAQS	LQQGAEIIVNKAAGE	388
4	BASCU	LSDKNVGTIVMIFG	GIIVRCILDIDGELI	TRQFG--LITSEVVR	LEGNNALGAKKED	SGLN----	ITSAES	MADGAKIVSLV---	385
5	RICPR	LSDKNVGTIVMIFG	GIIVRCILDIDGELI	AKDGG--LKNVNVVR	LEGNNALGAKKED	SULK----	ITPAHD	LADAKKIVELAIR	386
6	AQUAE1	MADPNVKAIVMIFG	GIIVRCILDIDGELI	SRGGE--LRVSEVVR	LEGNNALGAKKED	SGLN----	ITLAED	MDEGAKKAVELANKQ	384
7	Malate	LSDKNVKAIVMIFG	GIIVRCILDIDGELI	AREFK--LDRVNVVR	LEGNNALGAKKED	SGLD----	ITTADT	LITEAAKAVEACHGA	390
8	CHLTR	LSDKSVVVEIVMIFG	GIIVRCILDIDGELI	MQGGK--ETEPVVR	LEGNNALGAKKED	AGIP----	CEFVTS	MSBGAELAVQLSR--	386
9	THEAQ	LKDFWVGVVIMIFG	GIIVRCILDIDGELI	LEBGL--LTKVNVVR	VAGTAEBAKLLZ-	-GCP----	VVMYPT	SIEBAKIVAVHVGGA	377
10	THEFL	LKDFWVGVVIMIFG	GIIVRCILDIDGELI	LEBGL--LTKVNVVR	VAGTAEBAKLLZ-	-GCP----	VVMYPT	SIEBAKIVAVHVGGA	377
11	MYCTU	LGDQNKSVIVMIFG	GIIVRCILDIDGELI	LGMGDEANNEVVR	LEGNNALGAKKED	ANHP----	LWTLVAT	MDEBAKAAELASA-	387
12	STRCO	LSDPVRSTIVMIFG	GIIVRCILDIDGELI	LDEVR--LITSEVVR	LEGNNALGAKKED	RAHF----	LEBQAT	MDEBARRARLATA-	375
13	ARCFL1	LKDFNVVVEIVMIFG	GIIVRCILDIDGELI	LDEVP--RNVSEVVR	LEGNNALGAKKED	YSSNGARIEFVES-	IEBARRAVELAG--	383	
14	ARCFL2	LKDFNVVVEIVMIFG	GIIVRCILDIDGELI	LADV--ST--VNVVR	LEGNNALGAKKED	FAKDRPNFHI--VET-	MEBARRAVELAE-	379	
15	METJA	LSNRNVKIVMIFG	GIIVRCILDIDGELI	KEH--RNVSEVVR	LEGNNALGAKKED	HGIP----	YETS	MEBARRAVELAE-	364
16	METH	LSHPSVVEIVMIFG	GIIVRCILDIDGELI	RDAR--RNVSEVVR	LEGNNALGAKKED	AGIP----	FETS	LEBAKAVFLAKH--	364
17	HUMAN-G	TADPKVEALVIMIFG	GIIVRCILDIDGELI	CRELE--LKVSEVVR	LEGNNALGAKKED	SGLP----	ITSAID	LEBAKAVASVAKK	404
18	FIG-G	TADPKVEALVIMIFG	GIIVRCILDIDGELI	CRELE--LKVSEVVR	LEGNNALGAKKED	SGLP----	ITSAVD	LEBAKAVASVTKK	417
19	MOUSE-G	TADPKVEALVIMIFG	GIIVRCILDIDGELI	CRELE--LKVSEVVR	LEGNNALGAKKED	SGLP----	ITSAVD	LEBAKAVASVAKK	404
20	BIRD-G	TADPKVEALVIMIFG	GIIVRCILDIDGELI	CRELE--LKVSEVVR	LEGNNALGAKKED	SGLP----	ITSAVD	LEBAKAVASVAKK	391
21	CAEEL2	SQPSVKAIVMIFG	GIIVRCILDIDGELI	VNKIG--LNVSEVVR	LEGNNALGAKKED	SGLK----	ITSAID	LIDGAKAVKAAGE	415
22	ARATH	TSDEKVAIVMIFG	GIIVRCILDIDGELI	AKEVA--LKVSEVVR	LEGNNALGAKKED	SGMK----	LITADD	LIDNAEKAVKALAH-	425
23	TRIVA2	SSQPHKVAIVMIFG	GIIVRCILDIDGELI	FKKVG--LKVSEVVR	LEGNNALGAKKED	SGLP----	ITPADN	LIDNGIKAVKAAGE	402
24	TRIVI3	SSQSHKVAIVMIFG	GIIVRCILDIDGELI	FKKVG--LKVSEVVR	LEGNNALGAKKED	SGLP----	ITPADN	LIDNGIKAVKAAGE	398
25	TRIVI1	SQPSVKAIVMIFG	GIIVRCILDIDGELI	FKKVG--LNVSEVVR	LEGNNALGAKKED	SGLP----	ITSAID	LIDGAKAVKAAGE	405
26	HUMAN-A	SDK-KVLAIVMIFG	GIIVRCILDIDGELI	VKILE--IKVSEVVR	LEGNNALGAKKED	SGLK----	ITACDD	LDEARAVVVKLSEIV	409
27	FIG-A	SDK-KVLSIVMIFG	GIIVRCILDIDGELI	VKICE--IKVSEVVR	LEGNNALGAKKED	SGLK----	ITACDD	LDEARAVVVKLSEIV	408
28	MOUSE-A	SDK-KVLAIVMIFG	GIIVRCILDIDGELI	VKILE--IKVSEVVR	LEGNNALGAKKED	SGLK----	ITACDD	LDEARAVVVKLSEIV	409
29	BIRD-A	SDK-KVLAIVMIFG	GIIVRCILDIDGELI	VKILE--IKVSEVVR	LEGNNALGAKKED	SGLK----	ITACDD	LDEARAVVVKLSEIV	396
30	CAEEL1	ADKQVSAIVMIFG	GIIVRCILDIDGELI	ARELD--LKVSEVVR	LEGNNALGAKKED	SGLR----	ITPCDN	LDEARAVVVKLSNIV	418
31	NEOFR	SDKA-VSALIVMIFG	GIIVRCILDIDGELI	VKEILG--LKVSEVVR	LEGNNALGAKKED	SGLS----	ITLADD	LDEARAVVVKLANVV	387
32	SCHFO	TNDPKVAIVMIFG	GIIVRCILDIDGELI	VSALN--LNVSEVVR	LEGNNALGAKKED	SGLR----	ITSPDD	LDEARAVVVKLSEIV	422
33	SACCE	LSNRNVAIVMIFG	GIIVRCILDIDGELI	ARELE--VRVSEVVR	LEGNNALGAKKED	SGVK----	ITSEFE	LDEARAVVVKLSEIV	426
34	AQUAE2	LSKP--GIRAVLIDG	GIIVRCILDIDGELI	.....KLDPSNIVVR	LEGNNALGAKKED	AFKDCGIGIEYDGA	LPILEAVVVKLELLD	390	
35	CIT-HU	SLMTR--DCKILLIG	GIIVRCILDIDGELI	IR.....KEHEVTEVVR	LEGNNALGAKKED	VGKTIPIPIVFGTE	THMELVGVHAPAJ	423	
9	THEAQ	A-----	-----	-----	-----	-----	-----	378	
10	THEFL	A-----	-----	-----	-----	-----	-----	378	
12	STRCO	ASTAGAG	-----	-----	-----	-----	-----	383	
14	ARCFL2	V-----	-----	-----	-----	-----	-----	380	
16	METH	L-----	-----	-----	-----	-----	-----	365	
23	TRIVA2	KLI-----	-----	-----	-----	-----	-----	405	
24	TRIVI3	KL-----	-----	-----	-----	-----	-----	405	
25	TRIVI1	KF-----	-----	-----	-----	-----	-----	407	
26	HUMAN-A	TLAKQAVDVKQFLP	I-----	-----	-----	-----	-----	426	
27	FIG-A	TLINQAQVDVVKQFLP	I-----	-----	-----	-----	-----	425	
28	MOUSE-A	TLAKQAVDVKQFLP	I-----	-----	-----	-----	-----	426	
29	BIRD-A	TLAKQAVDVKQFLP	I-----	-----	-----	-----	-----	413	
30	CAEEL1	DLARAVVVKLSEIV	I-----	-----	-----	-----	-----	435	
31	NEOFR	GLAKENKIKIKEN-	-----	-----	-----	-----	-----	402	
32	SCHFO	DVNVSEFLP	-----	-----	-----	-----	-----	433	
34	AQUAE2	KQAKKLEBEEQIKG	GHTFTDQASDLGM	-----	-----	-----	-----	436	
35	CIT-HU	ENQPTTAHIANFL	NAQRETSTPAPRT	-----	-----	-----	-----	454	

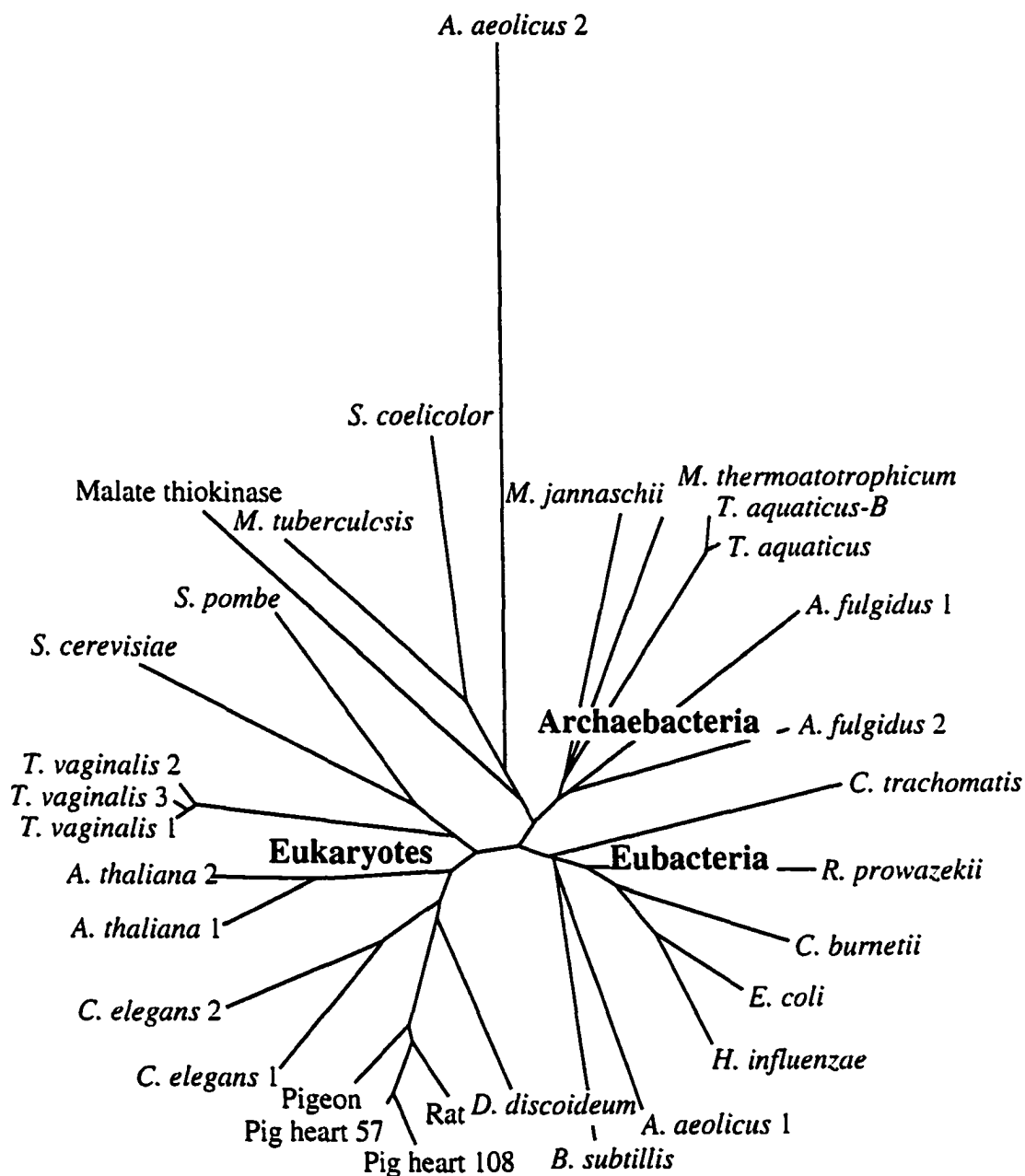


**Figure 1-4. Phylogenetic tree for the amino acid sequences of the  $\alpha$ -subunits of SCS.** The three taxonomic domains are shown in bold. The tree was generated using the alignment in Figure 1-2, and the programs CLUSTAL W (85) and TREE VIEW (86). The data base accession numbers are listed in Appendix 1.

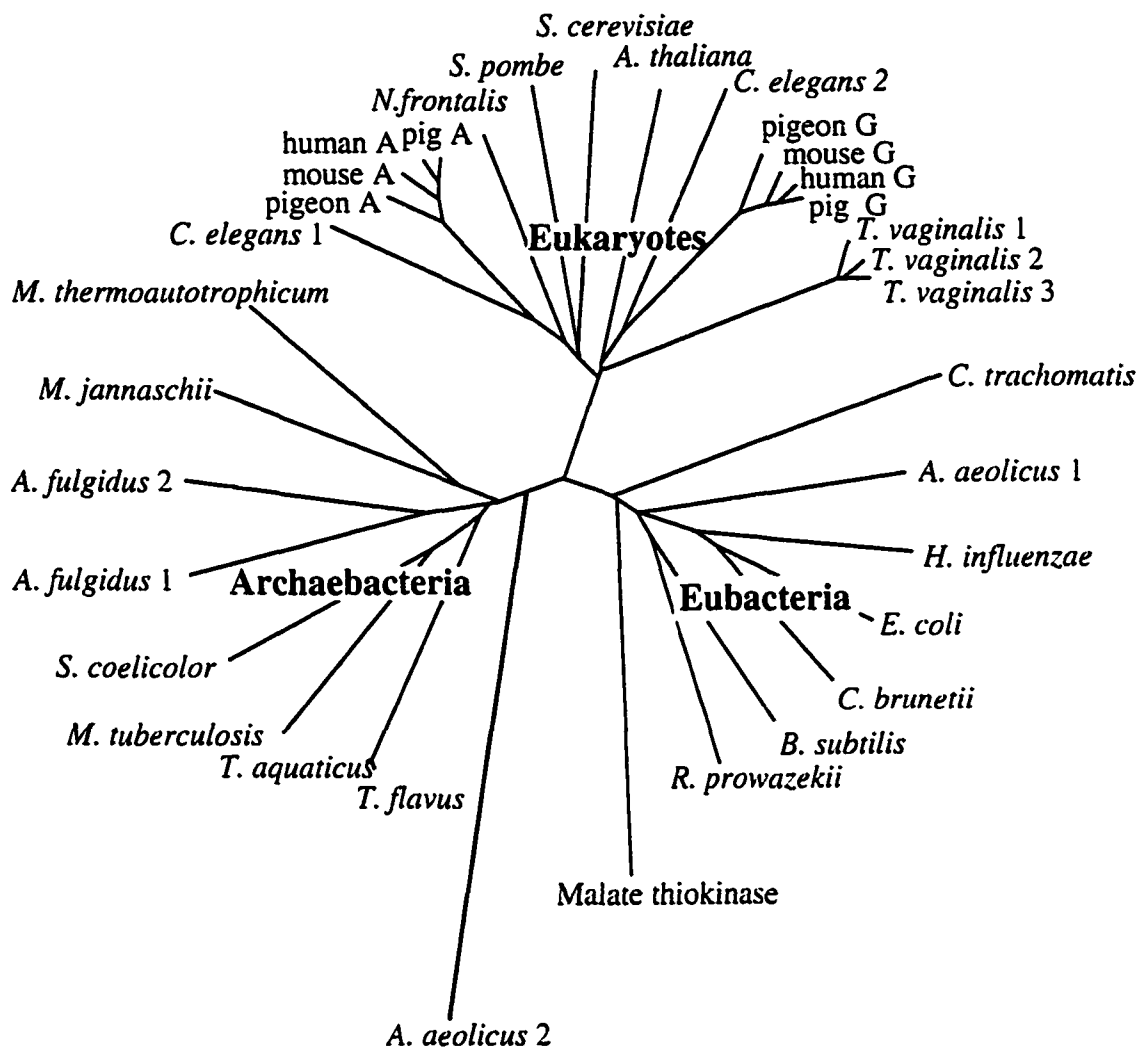


**Figure 1-5. Phylogenetic tree for the amino acid sequences of the  $\beta$ -subunits of SCS.** The three taxonomic domains are shown in bold. The tree was generated using the alignment in Figure 1-3, and the programs CLUSTAL W (85) and TREE VIEW (86). The data base accession numbers are listed in Appendix I.



in a bias toward amino acid residues that have codons with a high G+C content (89). The amino acid alignment of SCS from the high G+C content mesophilic eubacteria thus reflects the bias for codons with a high G+C content, leading to the placement of amino acid residues in a finite number of positions regardless of the mesophilic or thermophilic nature of the organism. The segregation of the second set of *Aquifex aeolicus* genes in the archaeobacterial group may be due to the thermophilicity of *A. aeolicus*, however this segregation may not be functionally significant because these genes are the most distantly related of the SCS sequences. There are several groups of residues that are absolutely conserved in all other species of SCS (see the shaded areas of Figures 1-2 and 1-3) which are not conserved in the second set of genes from *Aquifex aeolicus*, including the sequence around the active site histidine. This implies that these genes code for proteins that may no longer perform the same function as other SCS proteins, and thus are not under the same evolutionary pressure. In addition, relatively large differences between these sequences and other SCS sequences may lead to their inappropriate placement in the archaeobacterial domain. For example, the  $\alpha$ -subunit sequences in the group containing malate thiokinase, *M. tuberculosis*, *S. coelicolor*, and *A. aeolicus*, could be placed as a branch within the eubacterial domain without disturbing the relative evolutionary relationships. This has not been done because the sequences for their  $\beta$ -subunits align within the archaeobacterial group.

Some enzymes that catalyze reactions similar to the reaction catalyzed by SCS also display sequence similarity with SCS. Malate thiokinase functions in the serine cycle of the methylotroph, *Methylobacterium extorquens*, and as the name suggests, catalyzes the same reaction as SCS except malate thiokinase uses malate instead of succinate (90). Malate thiokinase from *Methylobacterium extorquens* segregates into either the eubacterial ( $\beta$ -subunit) or archaeobacterial ( $\alpha$ -subunit) domains. The mechanism for the reaction catalyzed by ATP citrate lyase is also similar to that catalyzed SCS: the formation of acetyl-CoA and oxaloacetate from citrate and CoA is accompanied by the hydrolysis of ATP to ADP, and

proceeds through the formation of a citryl-CoA intermediate. ATP citrate lyase from a number of organisms has been sequenced (91-93), and the C-terminus of this enzyme contains regions that are similar to the  $\alpha$ -subunit of SCS. Using the improved similarity searches of Altschul *et al.* (94, 95), Galperin and Koonin have detected similarities between the N-terminus of ATP citrate lyase and the N-terminus of the  $\beta$ -subunit of SCS (96). These similarities imply that catalysis of a similar reaction places similar evolutionary pressures on all of these enzymes, and indicates a common origin for the genes that encode ATP citrate lyase, malate thiokinase and SCS.

The functional differences in the nucleotide specificity of SCS are reflected in the alignment of the  $\beta$ -subunits of SCS. Johnson *et al.* (29) noted that the genes for the  $\beta$ -subunit of mammalian SCS segregate into two groups. Each group corresponded to SCS specific for either adenosine or guanosine nucleotides. The genes for the  $\beta$ -subunit of SCS from fungi all segregate into the ADP/ATP-specific group, whereas those for *Arabidopsis thaliana* and *Trichomonas vaginalis* segregate into the GDP/GTP-specific group near the point of divergence. The segregation of the fungi in the ADP/ATP-specific group is consistent with the reported nucleotide specificity of SCS from *Saccharomyces cerevisiae* (38). Based on the sequence alignment, SCS from *Arabidopsis thaliana* segregates into the GDP/GTP-specific group. The database report confirms that it is GDP/GTP-specific, in contrast to previous reports that all plants examined were ADP/ATP-specific (97, 33-35, 28). The ADP/ATP-specific enzymes have C-terminal extensions when compared to the GDP/GTP-specific enzymes. The differences in sequence between the ADP/ATP- and GDP/GTP-specific SCS families extend throughout the entire sequence of the  $\beta$ -subunit and suggest that their respective cDNA's are likely to be coded for by two separate genes. In the case of hemoglobin, the separate genes for the multiple species are thought to have arisen by gene duplication (7). The genes for the ADP/ATP- and GDP/GTP-specific SCS enzymes may have also arisen in this manner, and if so, the phylogenetic tree shown in Figure 1-5 indicates that the gene duplication event would have

occurred early in the eukaryotic lineage. Several other duplication events are indicated by the dendrogram, however they would be relatively recent gene duplications giving rise to paralogous genes. There are two recently diverged genes for the  $\beta$ -subunit in *Archaeoglobus fulgidus*, and three in *Trichomonas vaginalis*. No function has been ascribed to these duplicated genes.

Unlike the amino acid sequences of the  $\beta$ -subunits, those of  $\alpha$ -subunits do not segregate into groupings that are representative of functional differences (like nucleotide specificity). In general, the amino acid sequences of different SCS isozymes from a single species resemble each other more than they resemble SCS from other species. Thus, unlike the  $\beta$ -subunit, the alignments of the sequences for the  $\alpha$ -subunit indicate that only relatively recent gene duplications have occurred. Within the eukaryotic domain, the sequences of SCS align according to the expected evolutionary relationships of their respective organisms, the mammalian sequences are closely related, and the sequences from single celled eukaryotes are on a separate branch from the sequences from multicellular eukaryotes. Similar to the  $\beta$ -subunit, there are two genes that encode the  $\alpha$ -subunit in *Archaeoglobus fulgidus*, and three in *Trichomonas vaginalis*. In *T. vaginalis* the proteins expressed by these genes have been implicated in adhesion to the urogenital tract (98). In addition, unlike the  $\beta$ -subunit, there are two genes that encode the  $\alpha$ -subunit in *Caenorhabditis elegans*, and two different cDNAs have been cloned from flower buds and the epidermis of *Arabidopsis thaliana*. These cDNAs have differences along their entire sequence, implying that they are coded for by two separate genes. This is unlike the two cDNAs that have been cloned from fetal pig heart tissue, which differ only in an insertion, and arise from differential splicing of the  $\alpha$ -subunit gene (99). The absence of segregation of the  $\alpha$ -subunits into groups corresponding to ADP/ATP- and GDP/GTP-specific enzymes implies that the basis for nucleotide specificity lies in the  $\beta$ -subunit. This correlates well with the finding that the ADP/ATP-specific enzyme isolated from pigeon

muscle and GDP/GTP-specific enzyme isolated from pigeon liver, differ only in the  $\beta$ -subunit (30).

### ***Structural Organization of Succinyl-CoA Synthetase Genes***

Examination of the context in which the SCS genes are found in relation to each other and to those for other citric acid cycle and metabolic enzymes reveals that it is only the expression of the functional unit ( $\alpha\beta$ -dimer) that is conserved. The organization of the genes into groups with other citric acid cycle or metabolic enzymes occurs in relatively few species. The first SCS genes to be investigated were from *E. coli*. They are found in a cluster that encodes several citric acid cycle enzymes, and are located at the end of an operon which expresses four genes, *SucA* (the E1 dehydrogenase component of the  $\alpha$ -ketoglutarate dehydrogenase complex), *SucB* (the E2 succinyltransferase component of the same complex), *SucC* (the  $\beta$ -subunit of SCS), and *SucD* (the  $\alpha$ -subunit of SCS) (100). The *SucC* and *SucD* genes are translationally coupled: the stop codon of *SucC* overlaps with the ATG of the *SucD* (100). A ribosome binding site is located in the *SucC* coding region, upstream of the initial ATG for *SucD* (100). It is thought that the coexpression of these genes ensures the production of equimolar amounts of both subunits. In the same manner, the coexpression of the  $\alpha$ -ketoglutarate dehydrogenase genes with the SCS genes correlates with the report of specific association between these two enzymes (101). The genes in *Rhizobium leguminosarum* are also organized in a gene cluster (*mdh-SucCDAB*, where 'mdh' codes for malate dehydrogenase) which may constitute an operon (102). The genes for SCS from 8 other eubacteria, 4 archaeobacteria, 2 yeast, and the  $\alpha$ -subunit of pig heart have now been characterized (69, 70, 72-76, 99, 77, 79-81).

In eubacteria, the genes encoding the  $\alpha$ - and  $\beta$ -subunits of SCS are in close proximity to each other, and the  $\alpha$ -subunit gene follows the  $\beta$ -subunit gene. In some species, *Haemophilus influenzae* and *Coxiella brunetii*, the genes encoding the  $\alpha$ - and  $\beta$ -subunits are translationally coupled as in *E. coli* SCS and in one species, *Coxiella brunetii*,

they are organized in an operon that is similar to that in *E. coli*. Other eubacterial species, *Bacillus subtilis*, *Chlamydia trachomatis*, *Aquifex aeolicus*, *Streptomyces coelicolor*, and *Mycobacterium tuberculosis*, the subunit genes are separated by only 15-30 nucleotides, enough space for a ribosome binding site, and likely constitute an operon. In *Rickettsia prowazekii* the subunit genes are separated by approximately 200 nucleotides, indicating that the  $\alpha$ -subunit most likely has a separate promoter. The second set of SCS genes from *Aquifex aeolicus* is the exception to these observations. The genes coding for the two subunits are separated by  $2.7 \times 10^5$  nucleotides, and the 5'-end of the  $\alpha$ -subunit gene has a 16 nucleotide overlap with a cell cycle protein.

The corresponding genes from archaeobacteria span a wide range of genomic organization; in some species, *Thermus aquaticus*, and *Thermus flavus*, the subunit genes are translationally coupled in a similar manner to those in *E. coli*. In other species, *Methanobacterium thermoautotrophicum*, and *Archaeoglobus fulgidus*, the subunit genes are separated by only 4-15 nucleotides. In *Methanococcus jannachii* the  $\alpha$ -subunit gene is separated from the  $\beta$ -subunit gene by  $6.2 \times 10^5$  nucleotides, and is transcribed in the opposite direction. In both sets of SCS genes in *Archaeoglobus fulgidus*, the gene for the  $\alpha$ -subunit precedes that for the  $\beta$ -subunit. This is the reverse order to that found for other SCS subunit genes in proximity to one another.

The SCS genes in eukaryotic species have been less well characterized. Consistent with the back migration of genes from the primitive mitochondria into the nucleus, the  $\alpha$ - and  $\beta$ -subunit genes in yeast are found on different chromosomes and contain no introns. The  $\alpha$ -subunit gene from pig heart has been partially characterized and contains at least one intron which can be differentially spliced (99). Thus, in keeping with the hypothesis that one gene is an independent unit of heredity, the function of SCS is conserved but the organization and expression of the two subunits in relation to each other and to other citric acid cycle enzymes is not.

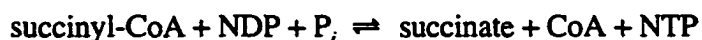
Given the translational coupling associated with some of the genes for SCS, it is worth noting that there is only one gene which codes for ATP citrate lyase in rat, human and *C. elegans*. The N-terminus of the translated protein is similar to the  $\beta$ -subunit of SCS, and the C-terminus is similar to the  $\alpha$ -subunit. However, in *Sordaria macrospora*, a fungus, a relatively small gene for ATP citrate lyase that is only similar to the  $\alpha$ -subunit of SCS, has been isolated (93). Nowrousian *et al.* (93) make the observation that the ATP citrate lyase isolated from animals and yeast is a homotetramer, while that from the filamentous fungi, *Aspergillus nidulans* and *Penicillium spiculisporum*, consists of two different subunits. Thus, in the filamentous fungi ATP citrate lyase is likely to be encoded by two genes.

Thus, the genomic organization displayed by SCS and related enzymes spans a wide spectrum of possible genomic arrangements. They range from expression of a single polypeptide (ATP citrate lyase) to separate polypeptides that are translationally coupled and expressed as part of a larger operon (*E. coli* and *Rhizobium leguminosarum*) to expression on their own operon, with and without translational coupling, to separate expression of the gene for each subunit. This indicates that not even the gene is conserved, but the functional unit. The conservation of functional units within and among SCS and related enzymes may be extended even further; the N-terminal domain of the  $\beta$ -subunit of SCS is structurally similar to the ATP-grasp fold that is found in D-ala:D-ala ligase (DD-ligase) (103, 55). This similarity could not be detected by the current sequence searching programs. However, Alschul *et al.* (94, 95) have developed new methods of data base searching that can detect the similarity between the N-terminal domain of SCS and other proteins that contain the ATP-grasp fold (96). It unclear whether this indicates a common origin for this fold, or if this is an example of convergent evolution.

## Part D. The Reaction Catalyzed by Succinyl-CoA Synthetase

### *The Specificity of Succinyl-CoA Synthetase for Substrates*

Early work on the citric acid cycle established that the overall reaction catalyzed by SCS was as follows:



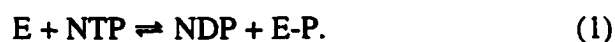
(where NDP and NTP are purine nucleoside di- and triphosphates, respectively). Later work characterized the nature of the substrates that could be used by *E. coli* SCS. SCS from *E. coli* displays a high degree of specificity with regard to succinate. A number of organic acids were tested as substrates for the complete reaction, and malate at high concentrations (91 mM) was about 3% as effective as succinate (104). Dephospho-CoA (CoA which is lacking the phosphoryl group at the 3' position of the ribose sugar) was an adequate replacement for CoA, while 4-phosphopantetheine was about 1000 times less effective and oxy-CoA (CoA which has an oxygen atom in place of the sulfur) was not a substrate. These results are consistent with the formation of a covalent bond between succinate and the sulfhydryl group of CoA. As discussed earlier the nucleotide specificity of SCS varies. The nucleotide preference for the *E. coli* enzyme is ADP/ATP > GDP/GTP > IDP/ITP (105). The eukaryotic isozymes are specific for either ADP/ATP or GDP/GTP but not both (58, 30). SCS from plants is apparently specific for ADP/ATP (97, 33-35, 28), except for that from *Arabidopsis thaliana* which may be specific for GDP/GTP. The pig heart enzyme can also use 8-aza-GTP (47) and 6-thio GTP (48). Like most reactions involving nucleotide di- and triphosphates, this reaction also requires divalent metal ions. Mg<sup>2+</sup> ions are the most effective followed, in decreasing order of effectiveness, by Mn<sup>2+</sup> and Co<sup>2+</sup> ions (42).

Mn<sup>2+</sup> ion binding has been studied using both proton relaxation rates (PRR) (106) and electron paramagnetic resonance (EPR) (107). Using PRR, it was determined that *E.*

*coli* SCS contained  $3.5 \pm 0.7$  metal ion binding sites, and that Mn-ADP was bound at 1.8 sites (106).

### ***The Reaction Mechanism of Succinyl-CoA Synthetase***

The ability of SCS to carry out several enzyme catalyzed exchange reactions has led to a hypothesized reaction mechanism consisting of three partial reactions. The exchange reactions are shown in Table 1-1. The substrates and products in each of these exchange reactions are a subset of the substrates and products that are associated with the corresponding partial reactions implying the existence of distinct intermediates. Later work showed that these intermediates could be used by the enzyme to catalyze the corresponding partial reactions. The first exchange reaction observed was that between  $\beta$ -[ $^{32}\text{P}$ ]-ADP and ATP in the presence of  $\text{Mg}^{2+}$  ions (31). Kaufman postulated the formation of a phosphorylated enzyme intermediate. This was later confirmed by the production of phosphorylated enzyme upon incubation of *E. coli* SCS with  $\gamma$ -[ $^{32}\text{P}$ ]-ATP (108, 43, 109). Pig heart SCS was also phosphorylated by  $\gamma$ -[ $^{32}\text{P}$ ]-GTP (110). Together these measurements indicated that the first partial reaction was:



The phosphorylated residue in SCS was found to be a histidine (108, 110), more specifically, 3-phosphohistidine (111). Later kinetic analyses confirmed that the initial rate of formation of the phosphorylated enzyme intermediate was as great as initial steady state rate for the overall reaction, and that the phosphorylated enzyme was an obligatory intermediate (112). The site of phosphorylation was found in the  $\alpha$ -subunit (113), and the peptide  $244\alpha\text{-MGH}(\text{PO}_3)\text{AGAIAGGK-255}\alpha$  was subsequently isolated (109). Mutagenesis of the active site histidine to Asp or Asn led to an inactive enzyme that could not be phosphorylated by ATP (114, 115).

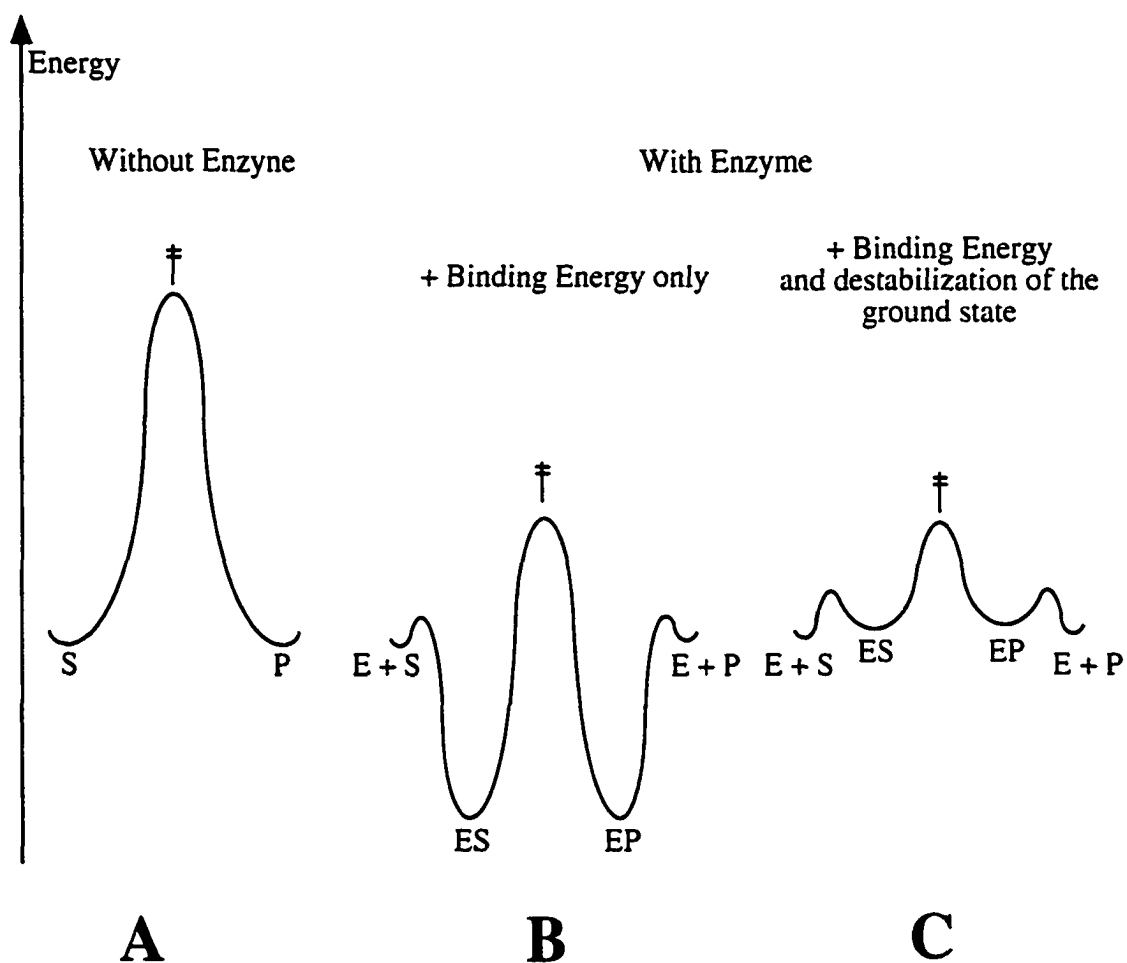


Table 1-1 The Exchange Reactions catalyzed by Succinyl-CoA Synthetase.

Exchange Reaction	Required Substrates	Stimulated by:
$\beta$ -[ <sup>32</sup> P]-ADP with ATP <sup>a</sup>	Mg <sup>2+</sup>	succinyl-CoA <sup>b</sup> , or succinate P <sub>i</sub> and CoA <sup>b</sup> , or CoA <sup>c</sup>
<sup>32</sup> P <sub>i</sub> with ATP	Mg <sup>2+</sup>	succinyl-CoA <sup>b</sup> , or succinate and CoA <sup>b</sup>
$\gamma$ -[ <sup>32</sup> P]ATP with SCS-P	Mg <sup>2+</sup>	CoA <sup>d</sup> , or desulfo-CoA <sup>c</sup>
[ <sup>18</sup> O]-P <sub>i</sub> with succinate <sup>a</sup>	succinyl-CoA	-
[ <sup>14</sup> C]-succinate with succinyl-CoA <sup>a</sup>	P <sub>i</sub> and Mg <sup>2+</sup>	ATP <sup>b</sup>

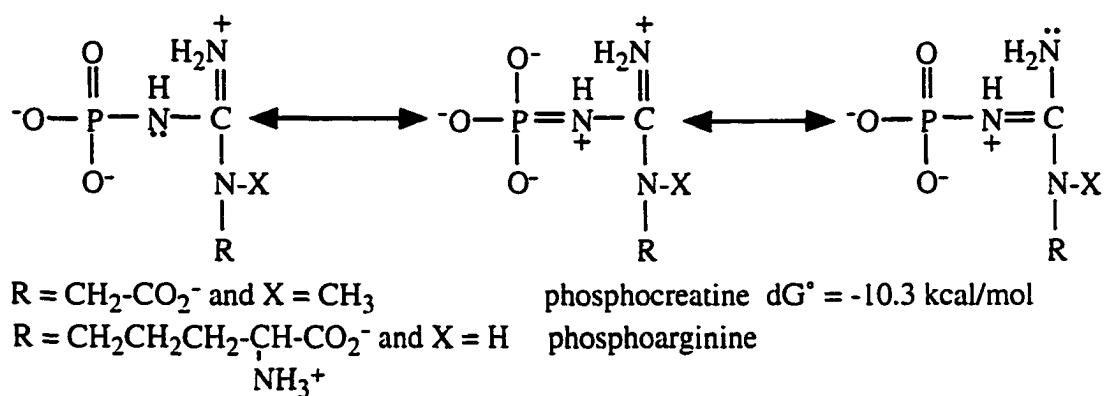
Exchange reactions observed by: <sup>a</sup> (97, 31, 43) and (116), or by <sup>b</sup> (112), <sup>c</sup> (117), <sup>d</sup> (43)

Jencks (118) proposed that enzymes stimulate catalysis by two general methods: first, they increase the effective concentration of the substrates by bringing them into proximity; and second, they must differentially stabilize the ground state and the transition state of the enzyme-substrate complex (Fig. 1-6). This principle is illustrated by this partial reaction catalyzed by SCS. The energy of binding nucleotide may be used to facilitate the formation of the phosphoenzyme intermediate. Two lines of evidence indicate that the energy of formation of a phosphohistidine is greater than that liberated by ATP cleavage. First, calculations of the free energy of hydrolysis for the phosphohistidine in pyruvate phosphate dikinase (119) and Enzyme I of the phosphotransferase system (120) indicated that this free energy is twice the free energy of hydrolysis of the phosphoanhydride bond in ATP. Second, the resonance structures that are available to the phosphohistidine are similar to those that are available to phosphoguanidinium groups, which also have free energies of hydrolysis that are greater than that of ATP (Fig. 1-7). This suggests that the formation of phosphorylated



**Figure 1-6. Use of the binding energy of substrates by enzymes to achieve catalysis.** A. The energy diagram for the uncatalyzed reaction of substrates (S) to produce products (P). B. The energy diagram that results if both the transition state ( $\ddagger$ ) and the enzyme-substrate/product (ES/EP) complex are stabilized to the same extent. It is obvious that this does not lead to catalysis. C. The energy diagram that results if some of the energy from binding substrates is "used" to destabilize the ground state complexes. This figure was adapted from Jencks (118)

A



B

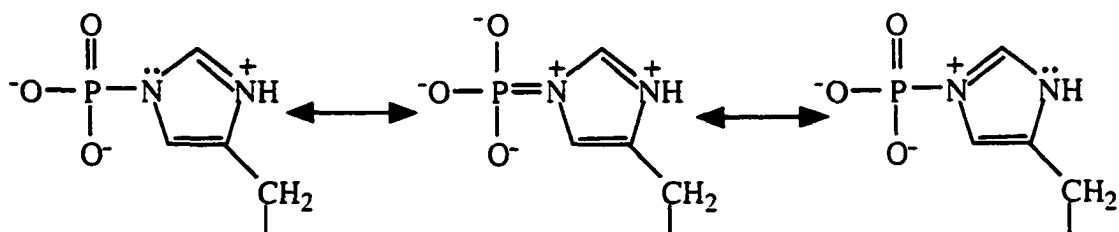


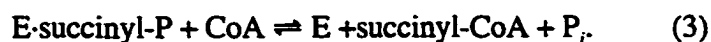
**Figure 1-7. Some of the resonance structures that are available to both phosphoguanidinium and to phosphohistidine.** A. Resonance structures that are available to phosphocreatine and to phosphoarginine. Adapted from Voet and Voet (7). B. Similar resonance structures that are available to phosphohistidine.

SCS from ATP should be disfavoured, yet the equilibrium constants for this partial reaction were  $K_{eq} = 31$  ( $\Delta G^\circ = -2.0$  kcal/mol) for the *E. coli* enzyme (43) and  $K_{eq} = 2.1$  ( $\Delta G^\circ = -0.4$  kcal/mol) for the pig heart enzyme (56). This is consistent with the observation that freshly purified SCS is normally found to be phosphorylated. Thus, since the formation of phosphorylated enzyme from ATP is favoured, despite the higher energy of the phosphohistidine, SCS may 'use' the energy that is available upon binding ATP to favour the formation of phosphorylated SCS.

The second exchange reaction, initially reported by Cohn, (121) was the exchange of an oxygen atom between inorganic phosphate and succinate during the oxidation of  $\alpha$ -ketoglutarate in mitochondria. This was later shown to occur during the reaction catalyzed by SCS (122, 116). The exchange of an oxygen atom between inorganic phosphate and the carboxyl group of succinate was explained by the formation of a succinyl-phosphate intermediate. Succinyl-phosphate is unstable, difficult to detect, and is not produced in any significant quantities when all of the substrates are present in the reaction mixture. However, it was confirmed as an intermediate by its detection following incubation of  $\gamma$ -[ $^{32}\text{P}$ ]-ATP and succinate with equal amounts of enzyme (123). Using NMR, succinyl-phosphate (succinyl-P) was also detected when enzyme was incubated with ATP and succinate (124). Furthermore, exogenously supplied succinyl- $^{32}\text{P}$  can phosphorylate the enzyme, and in conjunction with partial reaction (1), produced ATP from exogenously added ADP (123). These results proved that the second partial reaction was



(where E·succinyl-P indicates a non-covalent enzyme complex with succinyl-phosphate). Nishimura and Meister (123) found that exogenously added succinyl-phosphate could also react with CoA to produce succinyl-CoA, again in the presence of substrate quantities of enzyme. It was suggested that the final partial reaction was



However, under the proper conditions (pH 6.9 as opposed to pH 7.4) succinyl-phosphate also reacts non-enzymatically with CoA at rates which approach the enzyme catalyzed rate (125). It was thus suggested that the enzyme only positions the reactants for the final step in the reaction but does not stabilize the transition state (126). Fumaryl-phosphate (succinyl-phosphate with a *trans* double bond) or the monoethyl ester of succinyl-phosphate did not react with CoA, but maleyl-phosphate (succinyl-phosphate with a *cis* double bond) reacted at a rate greater than the rate of reaction of succinyl-phosphate with CoA (125). Thus, the mechanism for the non-enzymatic reaction of CoA with succinyl-phosphate was proposed to proceed via the formation of a cyclic anhydride intermediate (Fig. 1-8A). However, the enzyme catalyzed reaction is not likely to proceed through a cyclic intermediate. Maleyl-phosphate cannot be utilized by SCS to catalyze the formation of ATP, nor can maleate dephosphorylate the enzyme (126, 104). In addition, fumarate, which does not participate in the non-enzymatic reaction, can dephosphorylate the enzyme, although not with the same efficiency as succinate. Thus the enzyme catalyzed reaction likely proceeds via an in line nucleophilic attack by the thiol group of CoA on the carbonyl carbon of the phosphorylated carboxylate group of succinyl-phosphate. The difficulty in detection of succinyl-phosphate has led to the proposal that the last two partial reactions proceed in a concerted fashion (Fig. 1-8B) (9). In the x-ray crystallographic structure, the relative positions of the thiol group of CoA and the phosphohistidine allow for this possibility, however it seems more likely that the reaction proceeds in two rapid steps, as is shown in Figure 1-8C.

### ***Substrate Synergism***

During studies of the exchange reactions, it was noted that the rate of  $\text{ATP} \rightleftharpoons \text{ADP}$  exchange was slower than the rate of the overall reaction, and that the addition of the other substrates stimulated this exchange (Table 1-1) (43, 112, 45, 126, 124). This effect was

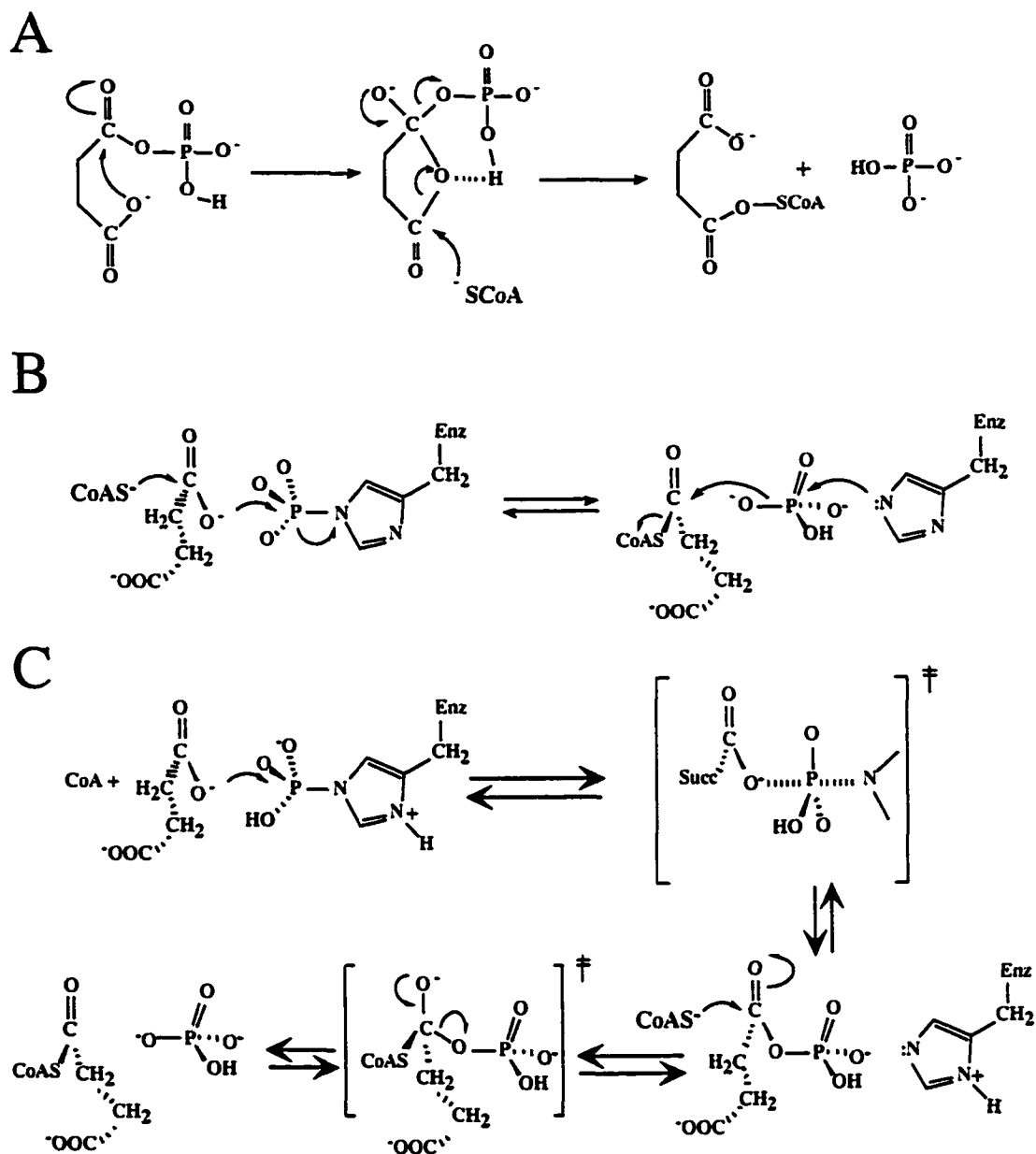


**Figure 1-8. Reactions of succinate, phosphate and CoA.** A. The proposed reaction mechanism for the non-enzymatic reaction of succinyl-phosphate with CoA to generate succinyl-CoA(125). B. The proposed concerted reaction mechanism for the synthesis of succinyl-CoA from phosphorylated enzyme, succinate, and CoA (9). C. The reaction mechanism for the production of succinyl-CoA from phosphorylated enzyme, succinate and CoA, including the likely transition states.

called substrate synergism, and is defined as the acceleration of a partial reaction by substrates that are not directly involved in that partial reaction. Grinnell and Nishimura (45) reported that CoA stimulated the  $\text{ATP} \rightleftharpoons \text{ADP}$  exchange in a concentration dependent manner that matched the binding of CoA. Hildebrand and Spector noted that the non-reactive CoA analogue, desulfo-CoA, stimulated the synthesis of ATP from succinyl-phosphate in the presence of enzyme (126). The most complete study on the substrate synergism shown by *E. coli* SCS was done by Bridger *et al.* (112). They showed that the greatest stimulation of the  $\text{ATP} \rightleftharpoons \text{ADP}$  exchange reaction occurred when succinyl-CoA was included. They also showed that the succinate  $\rightleftharpoons$  succinyl-CoA exchange reaction was greatly stimulated by the addition of ATP. Substrate synergism is also exhibited by the pig heart enzyme, which is an  $\alpha\beta$ -dimer with only one active site (127). The mechanistic rationale for substrate synergism is that the binding of the other substrates produces changes in the conformation of the enzyme which enhances catalysis of the exchange reaction. In the light of Jencks' proposal (118) outlined earlier, substrate synergism can be thought of as the use of the binding energy of substrates which are not involved in the exchange reaction to destabilize the ground state (or to stabilize the transition state) of those substrates that are involved.

Evidence of conformational changes that occur upon the binding of substrates supports the mechanistic rationale for substrate synergism. Fluorescence studies using enzyme labeled with dansyl chloride indicated that there were changes in the flexibility of the bound label upon the binding of CoA (128). Smaller changes were observed with the other substrates. Later studies showed that both ATP and CoA protected against the quenching of tryptophan fluorescence by acrylamide (129). Multiple changes in the proton relaxation rate (PRR) due to four bound  $\text{Mn}^{2+}$  ions were observed when substrates were bound (106). Consistent with the dansyl chloride labeling results, a large decrease in enhancement of the PRR was observed upon the addition of CoA to the enzyme. The addition of substrates that should bind to the same binding site resulted in very different

effects on enhancement of the PRR. The addition of succinyl-CoA resulted in an increase in the PRR enhancement, whereas addition of succinate and CoA together resulted in a decrease in the PRR enhancement. Intuitively, bound succinate and CoA should occupy the same binding site as succinyl-CoA, and thus induce the same conformation in the enzyme. However, in this case, the conformation of the active site responded differently to these substrates. Thus, the conformation of SCS must be exquisitely sensitive to the presence of the bond between succinate and CoA.

### ***Conformational Changes Associated with Catalysis***

A number of phenomena have been attributed to conformational changes that occur during the catalysis of the reaction catalyzed by SCS. The first of these, substrate synergism, was discussed above. The second, phosphorylation, has also been associated with these conformational changes (127). Phosphorylation of SCS results in a more stable form of the enzyme. Upon storage dephosphorylated *E. coli* SCS loses activity 100 times faster than phosphorylated SCS. In addition, the rate of inactivation of the dephosphorylated *E. coli* SCS by trypsin was two orders of magnitude greater than that of the phosphorylated enzyme.

The best evidence for the conformational changes that may occur during catalysis of the reaction comes from  $^{31}\text{P}$  NMR experiments (124, 130, 131). Resonance from the phosphohistidine, which was observed at 4.8 ppm, was shifted downfield and broadened by the addition of CoA to the enzyme (124). The broadening of the resonance was interpreted as two exchanging conformations of the phosphohistidine. The subsequent addition of the competitive inhibitor, 2,2'-difluorosuccinate caused the resonance to shift back upfield and sharpen to a resonance consistent with only one conformation. The model proposed was that one of the two conformations of the phosphohistidine interacts with ADP and the other with succinate. Thus, in the absence of substrates, the phosphohistidine



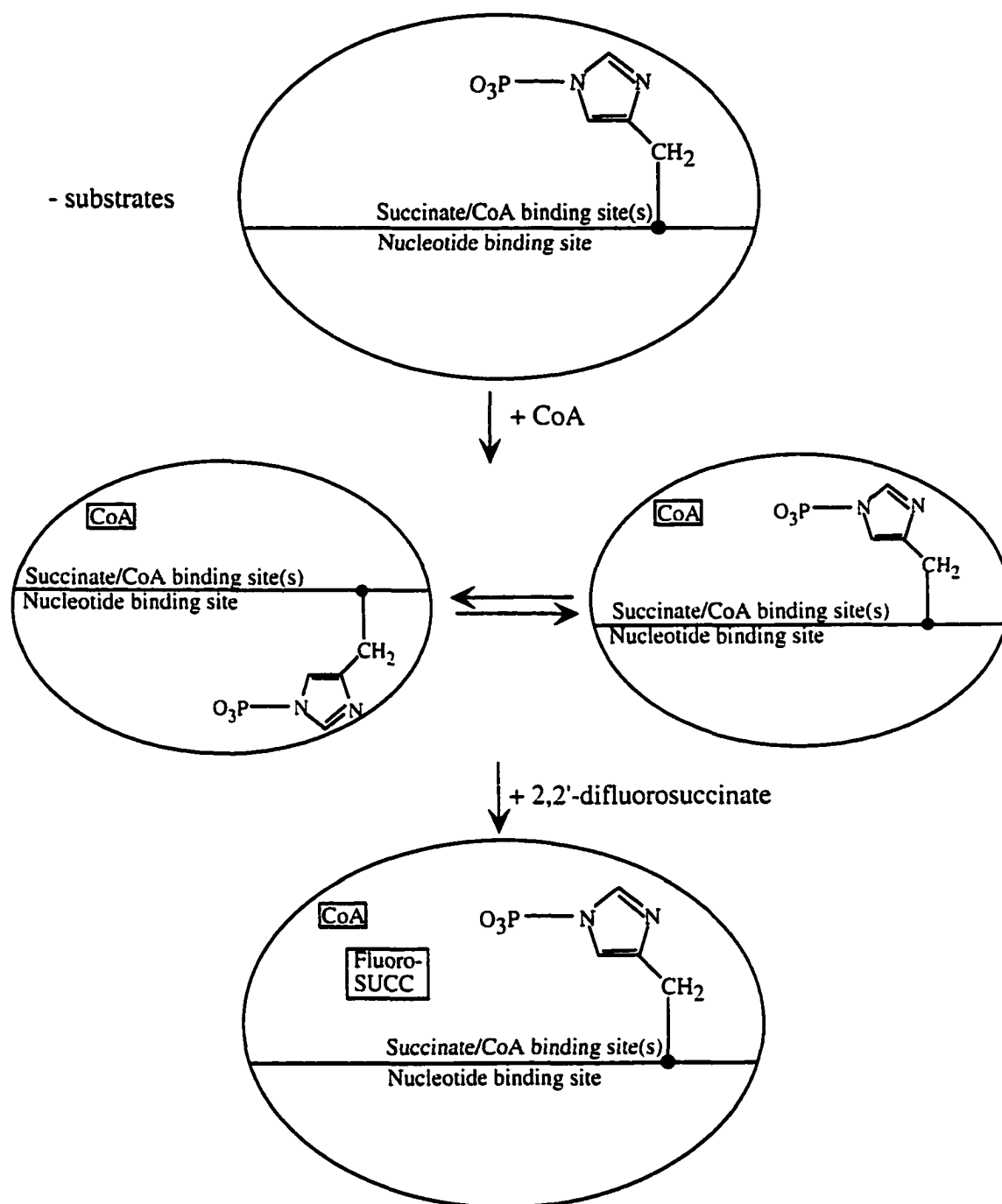


**Figure 1-9. Schematic representation of the conformational changes of the active site phosphohistidine.** Partial reactions (2) and (3) ( $E\text{-P} + \text{succinate} + \text{CoA} \leftrightarrow \text{succinyl-CoA} + \text{P}_i + E$ ) are thought to occur with the histidine in the succinate/CoA binding conformation, and partial reaction (1) ( $E\text{-P} + \text{ADP} \leftrightarrow \text{ATP} + E$ ) is thought to occur with the histidine in the nucleotide binding conformation. Adapted from Vogel and Bridger (124).

is found in the conformation which can react with succinate. The addition of CoA to SCS causes exchange between the two conformations, and the addition of 2,2'-difluorosuccinate "freezes" the phosphohistidine back in the succinate reactive conformation (Fig. 1-9) (124, 131). Thus, this model is also consistent with the increase in the rate of the  $\text{ATP} \rightleftharpoons \text{ADP}$  exchange reaction by CoA (112, 45), and the increase in the rate of the synthesis of ATP from succinyl-phosphate and ADP by desulfo-CoA (126).

### ***Kinetic Measurements and Binding Constants***

The reaction catalyzed by SCS has three substrates and three products, and thus the interpretation of initial rate kinetics and product inhibition patterns is very complex (9). Despite this, an extensive steady state kinetic analysis using initial rates has been done for both the *E. coli* (16, 132) and pig heart (47) enzymes. The proposed kinetic schemes based on these results are shown in Figure 1-10. The order of substrate attachment and product release for the reaction catalyzed by *E. coli* SCS is as follows: ATP is added to the enzyme first, followed by the random addition of succinate and CoA forming the ternary complex. This is followed by the random dissociation of the products succinyl-CoA and  $\text{P}_i$  from the enzyme, and lastly by the dissociation of ADP (Fig 1-10A) (16, 132). Although this is the major pathway, there are indications that other, minor, pathways exist (127, 132, 9). Interpretation of the initial rate kinetics and product inhibition pattern for the pig heart enzyme suggested a more complex mechanism where CoA and GTP add randomly to the enzyme, and the products succinyl-CoA and GDP dissociate last from the enzyme in random order. The last substrate to bind to the enzyme is succinate, which can bind either before or after the dissociation of the first product,  $\text{P}_i$  (Fig. 1-10B) (47). The partial reactions that have been characterized for SCS involve the formation of succinyl-phosphate as an intermediate, and thus dissociation of phosphate from the enzyme prior to the addition of succinate represents the formation of an abortive complex and no net catalysis can occur (47).

The source of the

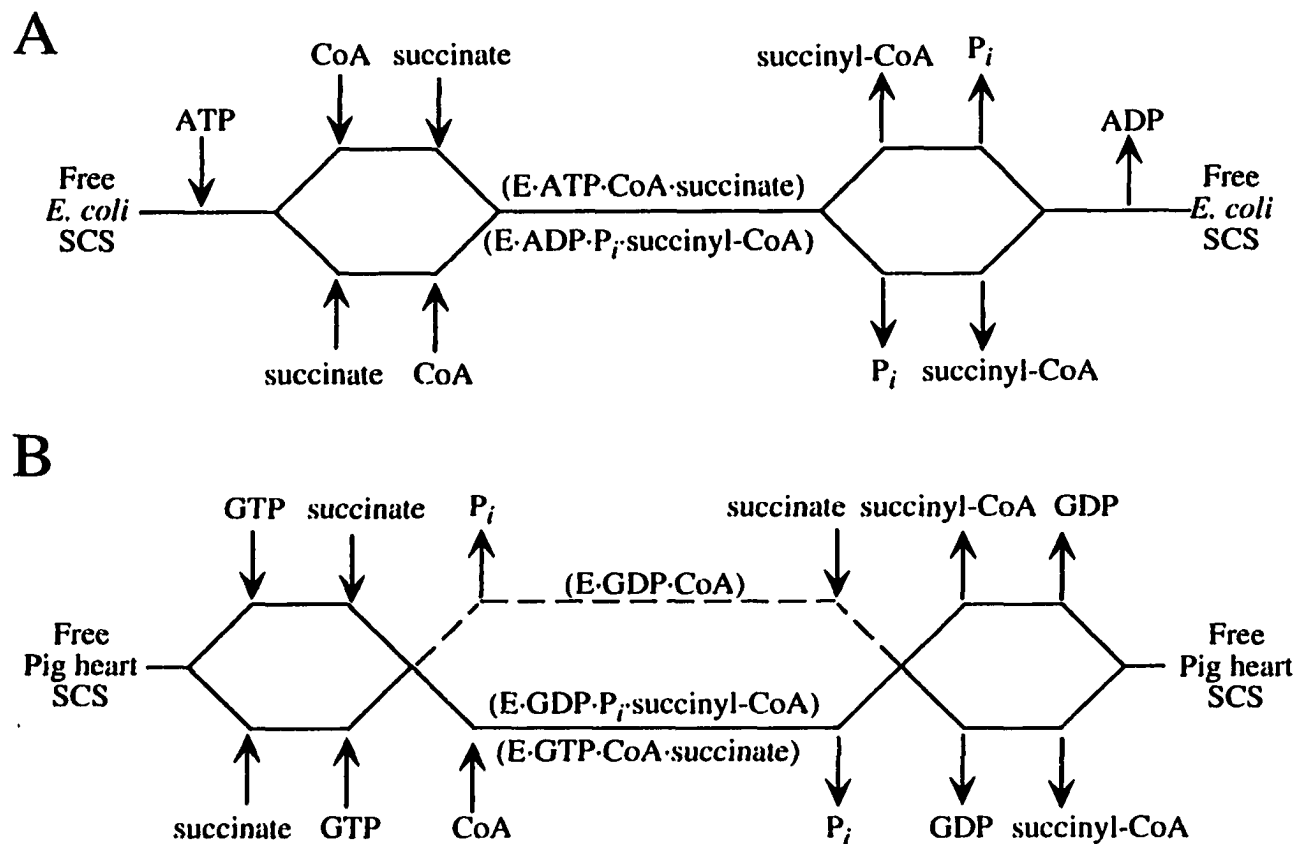


**Figure 1-10. Kinetic schemes for succinyl-CoA synthetase from *E. coli* (A) and pig heart (B).** The order of substrate addition and product release were deduced from steady state kinetic measurements. Productive catalysis proceeds through the ternary complexes E·NDP·P<sub>i</sub>·succinyl-CoA and E·NTP·CoA·succinate, where E is enzyme and NDP/NTP is adenosine di-/triphosphate for *E. coli* SCS or guanosine di-/triphosphate for pig heart SCS. Adapted from Moffet and Bridger (16, 132) and Cha and Parks (47).

differences in the kinetic pathways for pig heart and *E. coli* SCS may be the relative instability of the phosphorylated form of pig heart SCS when compared to *E. coli* SCS (as determined by the values of  $K_{eq}$  for the ATP/ADP exchange reaction). This is reflected in the formation of the abortive complexes caused by the dephosphorylation of pig heart SCS.

The Michaelis constants associated with all of the substrates have been determined for SCS from *E. coli* (16, 132), GDP/GTP-specific SCS from pig heart (47), artichoke (34), ADP/ATP-specific SCS from pigeon muscle (30), and GDP/GTP-specific SCS from pigeon liver, (30). These values are compiled in Table 1-2. In addition, the dissociation constants of some of the substrates with *E. coli* SCS have also been measured (133, 127). The  $K_{m(app)}$  values for the substrates that contain a nucleotide moiety (CoA, succinyl-CoA, ATP, ADP, GTP, and GDP) are one to two orders of magnitude lower than the values for succinate and phosphate.

Table 1-2. Apparent Michaelis Constants for Succinyl-CoA Synthetase.

Enzyme:	ATP/GTP <sup>a</sup> (M)	Succinate (M)	CoA (M)	ADP/GDP <sup>a</sup> (M)	P <sub>i</sub> (M)	Succinyl- CoA (M)
<i>E. coli</i> <sup>b</sup>	2.0 x 10 <sup>-5</sup>	1.0 x 10 <sup>-4</sup>	1.5 x 10 <sup>-6</sup>	1.2 x 10 <sup>-5</sup>	2.6 x 10 <sup>-3</sup>	7.7 x 10 <sup>-6</sup>
Pigeon breast <sup>c</sup>	5.5 x 10 <sup>-5</sup>	5.1 x 10 <sup>-3</sup>	3.2 x 10 <sup>-5</sup>	7.0 x 10 <sup>-6</sup>	2.3 x 10 <sup>-3</sup>	8.6 x 10 <sup>-5</sup>
Artichoke <sup>d</sup>	1.4 x 10 <sup>-4</sup>	2.0 x 10 <sup>-3</sup>	2.2 x 10 <sup>-6</sup>	1.2 x 10 <sup>-4</sup>	1.4 x 10 <sup>-3</sup>	5.6 x 10 <sup>-5</sup>
Pig heart <sup>e</sup>	1.0 x 10 <sup>-5</sup>	8.0 x 10 <sup>-4</sup>	2.0 x 10 <sup>-5</sup>	8.0 x 10 <sup>-6</sup>	6.0 x 10 <sup>-4</sup>	3.0 x 10 <sup>-5</sup>
Pigeon liver <sup>f</sup>	3.6 x 10 <sup>-5</sup>	4.9 x 10 <sup>-3</sup>	3.2 x 10 <sup>-5</sup>	2.5 x 10 <sup>-4</sup>	7.2 x 10 <sup>-4</sup>	7.2 x 10 <sup>-5</sup>

<sup>a</sup> Either ATP/ADP or GTP/GDP was used during kinetic analysis, depending on the enzyme source: ATP and ADP were substrates for the *E. coli*, pigeon breast, and artichoke enzymes, while GTP and GDP were substrates for the pig heart, and pigeon liver enzymes.

Data obtained from: <sup>b</sup> (16, 132), <sup>c</sup> (30), <sup>d</sup> (34), <sup>e</sup> (47).

Jencks' proposal (118) that the enzymes use the specific binding energy of substrates to destabilize the ground state relative to the transition state can be used as a

framework to examine the  $K_m$  values of succinate and phosphate. The decrease in entropy of the bound substrate occurs at the expense of the intrinsic binding energy that is available to the substrate. The amount of binding energy that is left over is the observed binding energy, which is reflected in the  $K_m$  of the substrate. Thus, specific binding requires that the substrate be held tightly by the enzyme, and this results in a large loss in entropy that is reflected in a relatively high  $K_{m(app)}$  (118). SCS is known to be highly specific for both phosphate and succinate.

A number of organic acids were tested for activity with *E. coli* SCS, and the results showed that four carbon dicarboxylic acids with a substituent on the  $\alpha$ -carbon (malate, methylenesuccinate, and methylsuccinate) could substitute for succinate (126, 104). No other organic acids were substrates for the entire reaction. The similarity of the reactive group of these compounds with the reactive group of succinate (the carboxyl group) supports the hypothesis that if these compounds do bind the enzyme, they are bound in a conformation that cannot react, indicating that although the  $K_m$  for succinate is relatively high, SCS is very specific for succinate. Thus, much of the intrinsic binding energy of the non-reactive portion of succinate is used to lower the free energy of activation, and the remainder is the observed binding energy.

The specificity of SCS for phosphate has been investigated by studying the ability of sulfate, nitrate and arsenate ions to inhibit succinyl-CoA synthesis. However, unlike the carboxyl groups of the compounds that resemble succinate, sulfate and nitrate have very different reactivities when compared to phosphate, and thus the specificity of SCS for phosphate may simply be a consequence of its reactivity, and not of the ability of SCS to bind phosphate tightly. The reactivity of arsenate ion is similar to that of phosphate, except that mixed anhydrides of arsenate are unstable and are rapidly hydrolyzed by water (134). Consistent with the hypothesis that the specificity of SCS for phosphate reflects the reactivity of the phosphate ions, arsenate ions can bind to the enzyme, ( $K_{m(app)} = 27 \mu\text{M}$ ) and participate in the arsenolysis of succinyl-CoA (114).

### ***Alternating Sites Cooperativity***

The controversial hypothesis that *E. coli* SCS is an enzyme that exhibits alternating sites cooperativity arose from early studies that indicated that the *E. coli* enzyme could apparently incorporate only one phosphate per tetramer (i.e. half of sites reactivity) (43, 46, 127). Bild *et al.* measured the exchange between [<sup>18</sup>O]-phosphate and succinate per ATP cleaved, and found that there was an increase in oxygen exchanged at lower concentrations of ATP (135). This was interpreted as multiple rounds of binding, and partial reaction, followed by release of the original substrates, all without the release succinyl-CoA. Pig heart SCS, an  $\alpha\beta$ -dimer with only one active site, did not exhibit this behavior. To account for these observations, an alternating sites cooperativity model was proposed where the binding of ATP and phosphorylation of the enzyme at the second “unoccupied” active site stimulates the formation and release of succinyl-CoA at the first active site. Additional studies provided support for this hypothesis (136-138). *E. coli* SCS can be thiophosphorylated by ATP $\gamma$ S to a stoichiometry of one thiophosphate/tetramer. The enzyme can then be dethiophosphorylated by succinate and CoA (which presumably form succinyl-CoA). The relatively slow rate of dethiophosphorylation could be stimulated by ATP, but not by non-hydrolyzable ATP analogues (137). This behavior was also attributed to alternating sites cooperativity.

Throughout the development of the model for alternating sites cooperativity in *E. coli* SCS, there have been reports that contradicted the predictions made by this model. For example, other early studies found that two moles of phosphate per tetramer could be incorporated using either ATP or succinyl-CoA and P<sub>i</sub> (43, 45). It was argued that the lower stoichiometries of phospho-enzyme intermediate could be attributed to low specific activity enzyme. Mann *et al.* (115) showed that two phosphates per tetramer could be incorporated by dephosphorylation of the enzyme prior to incubation with ATP. Nishimura and Mitchell (139) found that in the oxygen exchange experiments of Bild *et al.*,

the succinyl-CoA was not efficiently trapped, and thus it could be released, and subsequently rebind the enzyme. Nishimura and Mitchell also found that the dimeric pig heart enzyme exhibited the same dethiophosphorylation behavior as the *E. coli* enzyme (140). Thus, the dethiophosphorylation of tetrameric *E. coli* SCS was also consistent with a model in which phosphorylation of the enzyme stimulates the release of succinyl-CoA at one active site (140). The alternating sites cooperativity model was more directly tested by Bailey *et al.* who found that a dimeric mutant of *E. coli* SCS had essentially the same Michaelis constants as the wild-type enzyme and also exhibited the same dethiophosphorylation behavior as wild-type enzyme (67). In addition, they found that dethiophosphorylation of both dimeric and tetrameric *E. coli* SCS proceeded more quickly in the presence of phosphate, independent of the presence of ATP. This is consistent with a model in which the presence of a phosphate (either covalently bound or not) at the phosphohistidine binding site stimulates the release of succinyl-CoA. X-ray crystallographic studies of *E. coli* SCS showed that the histidines in both active sites were phosphorylated (54, 55). Thus, the tetrameric *E. coli* SCS is a dimer of dimers with two independent active sites, and alternating sites cooperativity is therefore unlikely to play a role in catalysis by SCS.

### ***Regulation of Succinyl-CoA Synthetase***

Although the direction of the reaction catalyzed by SCS (succinyl-CoA synthesis, or breakdown) is likely to be controlled by the intracellular nucleotide pools, an enzyme which is at the juncture of many biosynthetic and catabolic pathways would still be expected to be under tight regulatory control. SCS from *E. coli* tested with a variety of nucleotides, coenzymes and intermediates of both porphyrin synthesis and the citric acid cycle, and was inhibited only by fumarate, citrate, oxaloacetate, and to a lesser extent malate (46). The extent of inhibition observed was of the same order of magnitude, or even lower than the product inhibition by succinate. As discussed earlier when considering

the biosynthetic roles of SCS, the enzymes from soybean callus and *Rhodospseudomonas spheroides* were shown to be inhibited by protoporphyrin and hemin (27, 28). It has been suggested that the mammalian enzyme is subject to similar control by the products of porphyrin synthesis (25). The ADP/ATP-specific SCS activity from bovine heart is inhibited by GDP, and the GDP/GTP-specific SCS activity from the same tissue is inhibited by ADP (23). The GDP/GTP-specific SCS from pigeon liver exhibited very strong substrate inhibition with GDP. The inhibition of this SCS isozyme by ATP was not studied. There are several reports that SCS from *Dictyostelium discoideum* can be allosterically regulated by GDP (141, 142, 62, 143). In these studies, phosphorylation of the  $\alpha$ -subunit of SCS with GTP was stimulated by the addition of small amounts of GDP in lysates. However, the concentrations of GTP used were far below the levels required to phosphorylate a significant portion of the enzyme. Similar experiments done with *E. coli* SCS also revealed stimulation of phosphorylation by small amounts of GDP. This stimulation was dependent on a component that could be separated from SCS by ammonium sulfate fractionation (144, 145). The protein purity and concentrations were similar to those in the *D. discoideum* studies. Thus, there are indications that some SCS isoforms can be regulated by various metabolic products, but further studies on purified SCS (and other components) are needed.

Expression of *E. coli* SCS is regulated by two promoters, one upstream of the *sucA* gene, and a second, stronger promoter upstream of the *sdh* operon (146). This is illustrated in Figure 1-11. The first promoter is expressed under control of the IHF protein, and the second, stronger promoter is regulated, by the ArcA and Fnr proteins, in response to oxygen availability and carbon source. As discussed in the section SCS in Metabolism (p 2-8), different mammalian tissues express different levels of ADP/ATP- and



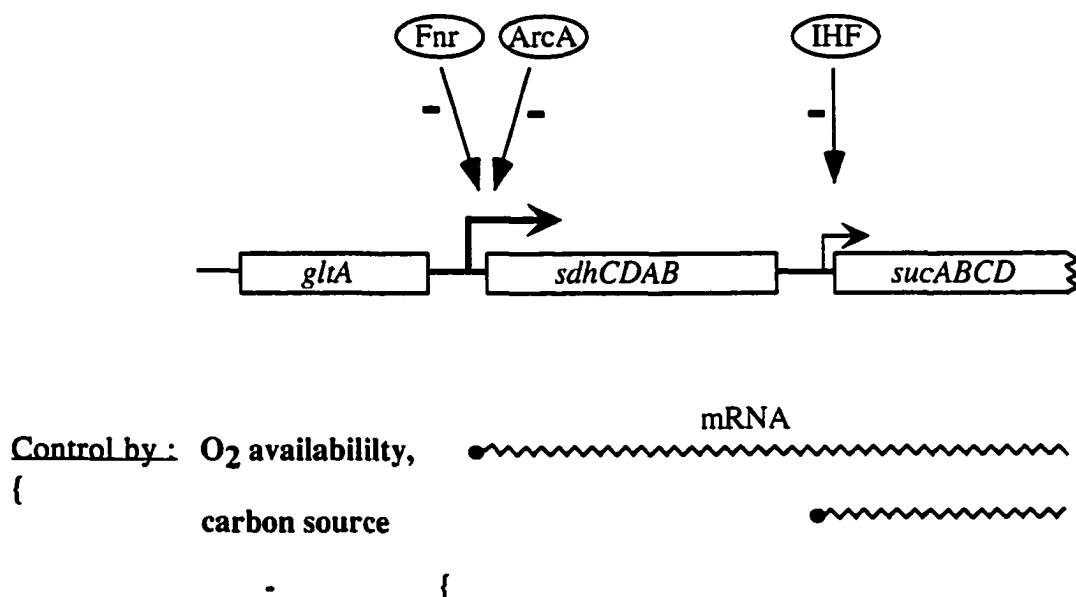


**Figure 1-11. Model for the regulation of expression of the genes for *E. coli* SCS.** *gltA* represents the gene for citrate synthase, *sdhCDAB* represents the genes for succinate dehydrogenase, and *sucABCD* represents the genes for  $\alpha$ -ketoglutarate dehydrogenase (*sucAB*) and SCS (*sucCD*). The *sucABCD* genes are transcribed from the weak *suc* promoter under control of the IHF protein, and also from the stronger *sdh* promoter under control of the Arc A and Fnr proteins. Negative regulation of a promoter by a protein is indicated by a minus sign. Transcription from the *sdh* promoter is regulated in response to oxygen availability and carbon source. The mRNA transcript originating from each operon is represented by the jagged line. Adapted from Park *et al.* (146).

GDP/GTP-specific SCS activity (21, 147, 22, 23, 26). Recent studies have examined the levels of expression of mRNA for SCS isoforms in mammalian tissues (99, 29). Johnson *et al.* (29) concluded that the levels of mRNA for  $\beta$ -subunit of ADP/ATP-specific SCS were generally high in tissues that were highly dependent on oxidative metabolism, whereas the levels of mRNA for  $\beta$ -subunit of GDP/GTP-specific SCS were high in tissues that were involved in biosynthesis. The expression of the different  $\beta$ -subunit isoforms was not mutually exclusive, for example, heart tissue had high levels of both isoforms. The levels of the mRNA for the  $\alpha$ -subunit also varied, but Johnson *et al.* (29) were not able to distinguish a pattern. In addition, the relative levels of ADP/ATP-specific and GDP/GTP-specific mRNA did not correlate with the levels of enzyme activity in tissues, indicating that there may be additional levels of control (29). Ryan *et al.* (99) found that the two different isoforms of the  $\alpha$ -subunit of SCS in pig tissues arose from the differential splicing of a single transcript. One was called PH $\alpha$ -57 and the other PH $\alpha$ -108. The mRNA for PH $\alpha$ -57 isoform was present in heart, muscle, liver, and brain, while the mRNA for PH $\alpha$ -108 isoform was present in only heart and muscle tissue (99). These results indicate that the expression of SCS is well controlled.

## **Part E. Structural and Functional Relationships of SCS**

### ***Folding of Succinyl-CoA Synthetase***

The folding and assembly of *E. coli* SCS has been extensively characterized *in vitro*. Subunits can be separated by gel filtration in the presence of denaturants, and subsequently refolded by dilution of the denaturant (148-150). Yields of refolded enzyme can approach 90% of the original activity (150). This is consistent with the finding that folding of SCS *in vivo* does not require the GroEL/ES chaperone (151). Refolding is dependent on protein concentration and falls off rapidly below 35  $\mu\text{g/ml}$  (149). In addition, the recovery of activity during refolding is first order with respect to each of the subunits and second order overall (149). It was observed that maximal refolding was dependent on

the presence of ATP or  $P_i$  in the refolding mixture (148-150). A non-hydrolysable analogue of ATP did not stimulate refolding (148). Circular dichroism measurements indicate that although the secondary structure refolds within one minute, the recovery of full activity takes up to 25 minutes (150). Crosslinking studies indicated that tetrameric enzyme species formed at an intermediate rate, while the formation of dimers remained at a constant low level during refolding (150). The recovery of activity was approximately the same as the appearance of tetramers when refolding was conducted in the presence of ATP (152) or phosphate ions (149). ATP could be added to the refolding mixture up to 10 minutes after the initiation of refolding and full activity could be recovered (150). Addition of ATP after 60 minutes however, had no effect. These results are consistent with a model for the refolding of *E. coli* SCS where the overall secondary structure forms quickly, followed by the association of the subunits to form dimers (either  $\beta\beta$  or  $\alpha\beta$ ), and then quickly by the association of the dimers into inactive tetramers (presumably  $(\alpha\beta)_2$ ). This is followed by a step probably involving conformational changes that are associated with phosphorylation of the enzyme by ATP (150) or the presence of phosphate ions. The association of the structured monomers into dimers is consistent with the finding that the rate limiting step in assembly is bimolecular. The requirement of ATP or  $P_i$  for refolding is consistent with the observation that dephosphorylated SCS is not stable when stored in the absence of phosphate (127). These results can be rationalized using the crystal structure of *E. coli* SCS. There are two phosphate binding sites per  $\alpha/\beta$  dimer, one is found in the N-terminal domain of the  $\beta$ -subunit, and the other is the phosphohistidine binding site located between the  $\alpha$ -subunit and the C-terminal domain of the  $\beta$ -subunit. The phosphohistidine is stabilized by two helix dipoles, one from a helix in the  $\alpha$ -subunit and one from a helix in the  $\beta$ -subunit (54). Thus, in the absence of phosphate or ATP, these structures may be unstable.

Much less is known about the folding of mitochondrial SCS, either *in vitro* or *in vivo*. When the  $\alpha$ -subunit of the rat liver enzyme was translated *in vitro*, it had extra amino

acids on the N-terminus that were not present in the mature protein as isolated from mitochondria (153). These amino acids have the potential to form an amphipathic  $\alpha$ -helix and resemble the mitochondrial signal sequences that direct other proteins synthesized in the cytosol to the mitochondria (58, 153, 154, 155). When the  $\alpha$ -subunit of rat liver SCS was translated *in vitro* in a reticulocyte lysate, it was translocated across the membrane of added mitochondria (153). Translocation was accompanied by the proteolytic cleavage of the 27 residues at the N-terminus which comprised the mitochondrial signal sequence. The translocation was ATP-dependent and was inhibited by compounds that diminish the mitochondrial membrane potential. The refolding of pig heart SCS *in vitro* was less productive than the refolding of *E. coli* SCS, and has been shown to be dependent on the addition of glycerol or ethylene glycol, and not on the presence of GTP (156). The requirement for high levels of ethylene glycol or glycerol for refolding of pig heart SCS may reflect the high protein concentrations that are found in the mitochondrial matrix or the participation of chaperones. It is interesting to note that when the  $\beta$ -subunit of SCS is purified from hydrogenosomes of *Trichomonas vaginalis*, the first 9 amino acid residues that are encoded for by the gene are missing. In addition, these missing residues have the potential to form an amphipathic  $\alpha$ -helix, and are similar to mitochondrial presequences (157). This similarity between proteins found in hydrogenosomes and those imported into mitochondria provides additional support for the hypothesis that mitochondria and hydrogenosomes are related organelles (12).

### ***The Crystal Structures of Succinyl-CoA Synthetase***

The x-ray crystal structures of the *E. coli* SCS (54, 55) and pig heart SCS (60) have been solved and refined to 2.3 and 1.9 Å, respectively. In the *E. coli* SCS crystals, the packing unit was an octamer, i.e. two tetramers pack together. Thus, there were two possible choices for the physiologically relevant tetramer, one where the two  $\alpha\beta$ -dimers were related to each other by a crystallographic two-fold axis, and a second where the  $\alpha\beta$ -

dimers were related by a non-crystallographic two-fold axis. Each possible tetramer had approximately the same buried surface area between the  $\alpha\beta$ -dimers. Choice of the physiologically relevant tetramer was resolved by mutation of residues at both of the possible  $\alpha\beta$ -dimer-dimer contact regions (67). In retrospect, the correct tetramer had a slightly larger buried surface area. The physiologically relevant tetramer is portrayed in Figure 1-12. The  $\alpha$ -subunits pack at the  $\alpha\beta$ -dimer-dimer interface, and are shown in yellow.

The  $\alpha$ - and  $\beta$ -subunits both contain distinct N- and C-terminal domains (54, 55). Both domains in the  $\alpha$ -subunit contain a Rossmann fold. A CoA molecule is bound by the Rossmann fold in the N-terminal domain of the  $\alpha$ -subunit. Previous studies showed that oxidized CoA disulfide was bound to Cys 325 $\beta$ , and that this binding was inhibited by analogues of CoA (158). This observation was thought to indicate that the CoA binding site was located in the  $\beta$ -subunit, and illustrates the need for caution in the interpretation of experiments using affinity analogues. The active site histidine (H246 $\alpha$ ) is phosphorylated and is found in a 23 residue loop in the C-terminal domain of the  $\alpha$ -subunit. This loop extends from the C-terminal domain of the  $\alpha$ -subunit and lies between it and the C-terminal domain of the  $\beta$ -subunit. The C-terminal domain of the  $\beta$ -subunit is linked to the N-terminal domain by a seven residue hydrophilic link. The N-terminal domain of the  $\beta$ -subunit consists of two subdomains, a sulphate ion is seen bound to one, and the other contains residues that interact with the N-terminal domain of the  $\alpha$ -subunit of the other  $\alpha\beta$ -dimer. The loop that binds the sulphate ion resembles the P-loop of other nucleotide binding folds. The nucleotide binding consensus sequence is GxxGxGKS/T (159), and the sequence in SCS is GGRGKxGG.

There is no succinate or nucleotide bound to either *E. coli* or pig heart SCS. The succinate binding site is presumed to be in the vicinity of the thiol group of CoA and the

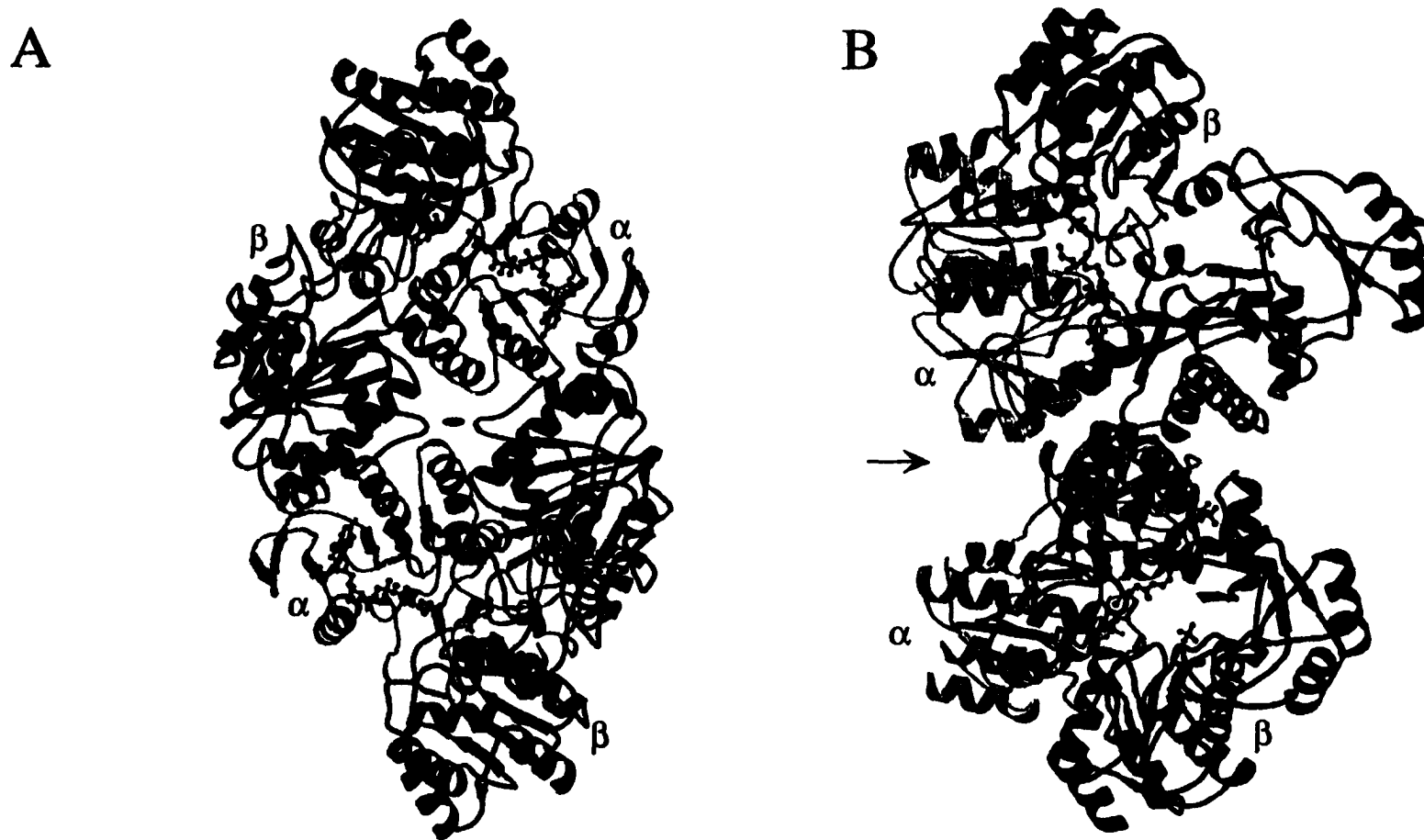


**Figure 1-12. Ribbon diagram of the physiologically relevant tetramer of *E. coli* succinyl-CoA synthetase.** In (A) the diagram of the tetramer is oriented about the crystallographic two-fold axis (denoted by the black oval). The tetramer is turned by approximately 90° in (B), and the approximate position of the two-fold axis is shown by the arrow. The  $\alpha$ -subunits are depicted in yellow, and the  $\beta$ -subunits in green. The molecules of CoA are drawn as cyan ball and stick models, the phosphohistidines are coloured mauve, and the sulfate ion, in the N-terminal domain of the  $\beta$ -subunits, red. This and all other structural figures in this thesis except Figures 6-2 to 6-5 were drawn using the program MOLSCRIPT (161).

phosphoryl group of the phosphohistidine. The binding site for NTP/NDP could be in either of two possible sites. There is an unoccupied Rossmann fold in the C-terminal domain of the  $\beta$ -subunit, which is where Cys 325 $\beta$  is located. The N-terminal domain of the  $\beta$ -subunit also resembles the nucleotide binding domain of the ATP-grasp family of nucleotide binding proteins (103, 55). However, this site is located approximately 35 Å from the active site phosphohistidine.

Each active site of *E. coli* SCS is thought to be located in a deep cleft between the  $\alpha$ -subunit and the C-terminal domain of the  $\beta$ -subunit of one  $\alpha\beta$ -dimer (54, 55). The N3-phosphohistidine is stabilized by residues from both of these domains. One oxygen atom of the phosphate is within hydrogen bonding distance of the hydroxyl groups of Ser 153 $\alpha$ , and Thr 155 $\alpha$ , and the main chain amide nitrogen of Gly 154 $\alpha$ . A second oxygen atom is within hydrogen bonding distance of the main chain nitrogen of residues Ala 266 $\beta$  and Gly 267 $\beta$ . The phosphate of the phosphohistidine lies between the N-termini of two  $\alpha$ -helices, called the “power helices”, one from the  $\alpha$ -subunit and the other from the  $\beta$ -subunit (Fig. 1-13). The residues in these two helices are highly conserved in all species of SCS and malate thiokinase (Fig. 1-2 and 3). The dipole moments of these power helices are thought to stabilize the charge on the phosphate moiety.

The nucleotide portion of the CoA molecule is bound in the N-terminal domain of the  $\alpha$ -subunit, and the pantothenic acid and  $\beta$ -mercaptoethylamine portions extend to within 7Å of the phosphate group of the phosphohistidine (located in the C-terminal domain of the  $\alpha$ -subunit). There is also a water molecule, in position for a nucleophilic attack on the phosphate moiety, positioned 3.3Å from the phosphate atom of the phosphohistidine which is thought to represent the carboxylate oxygen of succinate (55). The N1 atom of the imidazole group of the phosphohistidine is oriented to interact with the carboxyl group of Glu 208 $\alpha$ . The postulated mechanism of phosphorylation of SCS was a nucleophilic attack by the N3 atom of His 246 $\alpha$  on the phosphoryl group of ATP or succinyl-phosphate (131). However, the favored tautomer of histidine in solution has the

lone pair of electrons on N1 (160). Vogel and Bridger (131) predicted that an anionic group could stabilize the tautomer with the lone pair of electrons on the N3 position by forming a hydrogen bond with a hydrogen on N-1 (131). Glu 208 $\alpha$  is positioned to fulfill this role. The presence of the negative charge in the vicinity of N-1 may limit the resonance structures that are available to the phosphohistidine (Fig 1-7) thus leading to a lowering of the energy required to phosphorylate the histidine (discussed earlier in the section The Reaction Mechanism of SCS p 30) The functional importance of the residues discussed above is reinforced by their conservation in almost all species of SCS as well as malate thiokinase.

The x-ray crystallographic structure of the pig heart enzyme has been solved in both the phosphorylated and dephosphorylated forms. Neither contained bound CoA. The models are essentially the same as that for the *E. coli* enzyme, except that the pig heart enzyme is an  $\alpha\beta$ -dimer and all domains are in a more open conformation (Fig. 1-14) in the pig heart model (60). As seen in the *E. coli* model, there is a sulphate ion bound in the N-terminal domain of the  $\beta$ -subunit. In the pig heart model, there is a six residue insertion in the N-terminal domain of the  $\beta$ -subunit (as compared to the amino acid sequence of *E. coli* SCS) that forms a short two stranded antiparallel  $\beta$ -sheet that occurs just after the loop that binds the sulphate ion. An additional sulphate ion is found bound where the 5'  $\beta$ -phosphate of the CoA is located in *E. coli* SCS. There is also a second four residue insertion that forms a larger loop in the  $\alpha$ -subunit. This loop is located well away from the active site.

The source of the relative instability of phosphorylated pig heart SCS (when compared with *E. coli* SCS) is not immediately evident. The residues that interact with the phosphohistidine in pig heart SCS are the same as those in *E. coli* SCS. The difference in the free energy of the two phosphorylated forms is less than the bond energy of one hydrogen bond (43, 56), and at the resolution of the *E. coli* and pig heart SCS models, small differences in hydrogen bond length cannot be evaluated. However, pig heart SCS





**Figure 1-13. Close-up view of one active site of *E. coli* succinyl-CoA synthetase.** The  $\alpha$ -subunit is shown in yellow, and the  $\beta$ -subunit in green. The two power helices are shown in full colour, as is the active site loop. The active site phosphohistidine residue and CoA molecule are shown as ball and stick models in mauve and cyan, respectively. A water molecule is a light blue dot, and the main chain nitrogen atoms of residues 153 $\alpha$  - 155 $\alpha$  are blue. The side chains of Ser 153 $\alpha$  and Thr 155 $\alpha$  are also shown.

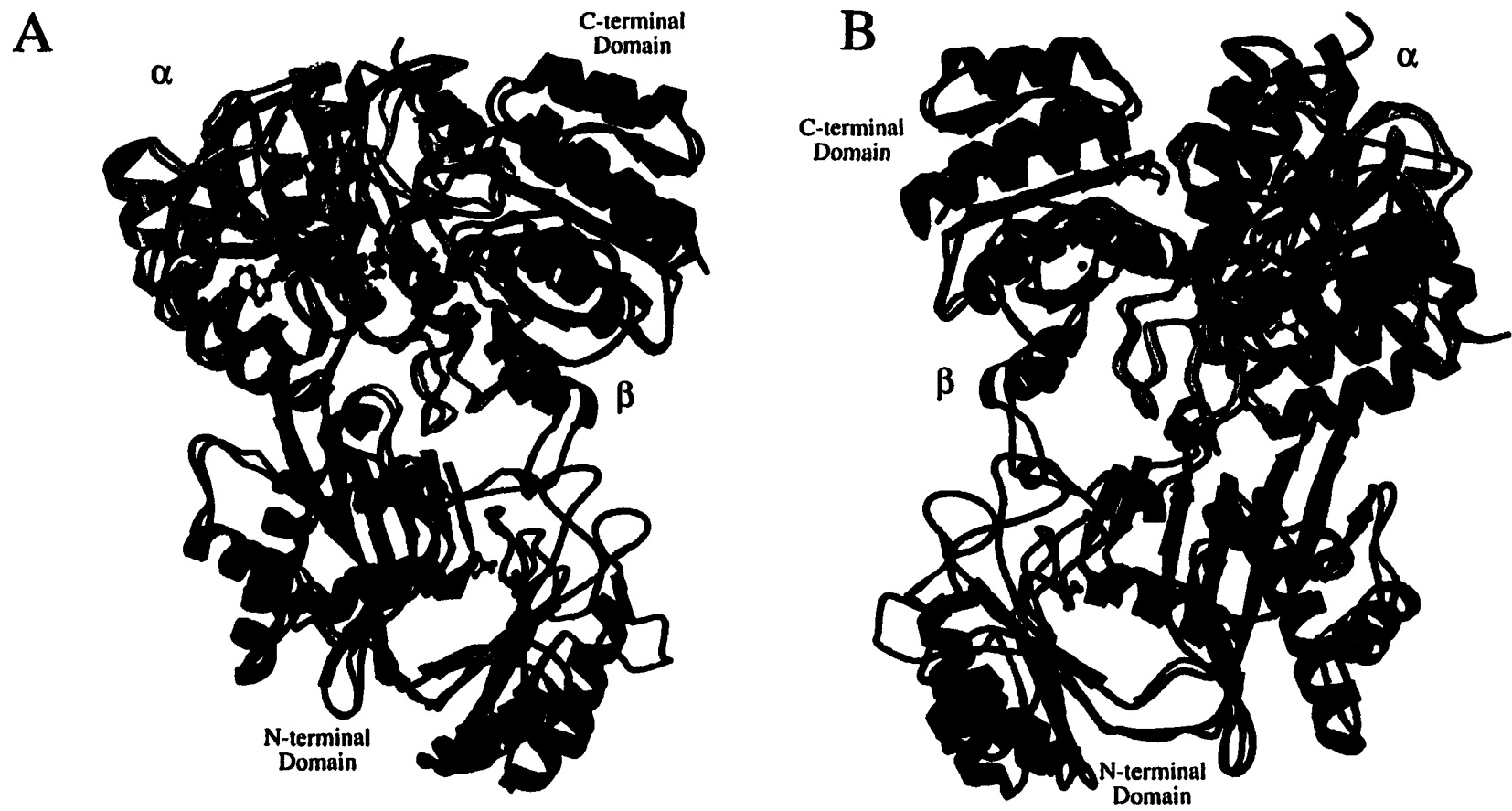


**Figure 1-14. Superposition of the ribbon diagrams for an  $\alpha\beta$ -dimer of *E. coli* SCS with pig heart SCS. In (A) the diagram is oriented to show the CoA molecule clearly, and is turned by approximately 90° in (B) to show the sulfate ion bound in the N-terminal domain of the  $\beta$ -subunit. The  $\alpha$ -subunit of *E. coli* SCS is shown in yellow, and the  $\beta$ -subunit in green. In the *E. coli* SCS model, the CoA molecule is shown as a cyan ball and stick model, the phosphohistidine residue is coloured mauve, and the sulfate ion is red. The subunits of pig heart SCS are coloured grey, the phosphohistidine and two sulfate ions are shown as black ball and stick models. There is a  $Zn^{2+}$  ion in the C-terminal domain of the  $\beta$ -subunit of the pig heart model that is displayed in blue.**

has an extra ionic interaction between Arg 256 $\alpha$ , which resides in the phosphohistidine loop, and Asp 227 $\beta$ . The equivalent residue in *E. coli* SCS is a glycine. The extra ionic interaction may be the reason that pig heart SCS does not need to be phosphorylated in order to refold. The crystal structures of SCS from *E. coli* and pig heart SCS thus provide a framework which can be used to rationalize past observations about the function of SCS. These crystal structures can also be used to develop and test hypotheses about the role of specific amino acid residues in the function of SCS.

## **Part F. Thesis Objectives**

It is clear from the preceding discussion that many aspects of the function of SCS are well established. The metabolic roles and reaction mechanism of SCS have been extensively investigated, and the recent proliferation of genomic sequencing projects has created a large database for sequence comparisons. In addition, the x-ray crystallographic structures of the *E. coli* and pig heart enzymes are now known. There are however many questions which remain unanswered, and the crystal structures of SCS open whole new avenues for exploration. The research in this thesis has two major themes: the first is the stability of SCS, and the second and more prevalent is the nucleotide binding site. Specifically, the goals of the research contained in this thesis are listed below:

1. In Chapter 2 there were three goals: the first was to clone ATP-specific SCS from *Neurospora crassa* for use in the investigation of the nucleotide specificity of SCS; the second was to clone thermostable SCS from *Thermus aquaticus* for use in the investigation of the stability of SCS; and the third was to study the expression of the mRNA for the  $\beta$ -subunit of GTP-specific pig heart SCS in pig tissues to see if it was expressed in manner consistent with the expression of the GTP-specific SCS activity, and thus was consistent with the proposed metabolic role of GTP-specific SCS.

2. The first major theme of this thesis is addressed in Chapter 3. In this chapter the goal was to probe the basis for the stability of SCS. Toward this end, the enzyme from *Thermus aquaticus* was characterized and its stability was compared to that of the *E. coli* and pig heart enzymes. The basis for the increased stability of *T. aquaticus* SCS when compared to *E. coli* SCS and of *E. coli* SCS compared to pig heart SCS was studied using sequence comparisons and the crystallographic structures of *E. coli* and pig heart SCS.
3. Investigation of the second major theme of this thesis begins in Chapter 4. The goal of the investigations in this chapter was to locate the nucleotide binding site of *E. coli* SCS using the photoactivated analogue 8-N<sub>3</sub>-ATP. Toward this end, specificity of SCS for 8-N<sub>3</sub>-ATP as a substrate was confirmed first. Then 8-N<sub>3</sub>-ATP was used to photolabel *E. coli* SCS, and tryptic peptides that were labeled by the 8-N<sub>3</sub>-ATP were subsequently isolated and identified.
4. The goal of Chapter 5 was to study the role of residues found in both of the potential nucleotide binding sites in the  $\beta$ -subunit of *E. coli* SCS by mutagenesis. These potential nucleotide binding sites (one in the C-terminal domain, and one in the N-terminal domain) were predicted by examination of the crystallographic structures of SCS and comparison to the structures of other nucleotide binding proteins. Specific residues that were predicted to be involved in binding nucleotide in each of the sites were changed by mutagenesis, and the effects of these changes were evaluated using steady state and single turnover enzyme kinetics.
5. The goal of the investigations in Chapter 6 was to determine the structure of nucleotide bound to *E. coli* SCS, and to examine the role of residues that were implicated in catalysis. The former goal was achieved by soaking high concentrations of ADP and Mg<sup>2+</sup> into crystals of native SCS, collecting diffraction data and generating electron density maps that compared the native and the ADP-Mg<sup>2+</sup>-bound forms of *E. coli* SCS. This was followed by model building and structure refinement. In addition, the roles that the two glutamate residues, one in the nucleotide binding site and one in the phosphohistidine binding site,

play in catalysis were studied by mutagenesis. Glu 208 $\alpha$  and Glu 197 $\beta$  were both changed, and the effects of these changes were monitored by steady state and single turnover enzyme kinetics.

**References:**

1. Krebs, H. A. (1970) *Perspect. Biol. Med.* 14, 154-170.
2. Ochoa, S. (1944) *J. Biol. Chem.* 155, 87-103.
3. Hunter, F. E. J., & Hixon, W. H. (1949) *J. Biol. Chem.* 181, 67-82.
4. Kaufman, S. (1951) in *Phosphorus Metabolism* (Eds. W. D. McElroy and B. Glass, Johns Hopkins Press, Baltimore) Vol. 1, 370-374.
5. Kaufman, S., Gilvarg, C., Cori, O., & Ochoa, S. (1953) *J. Biol. Chem.* 203, 869-888.
6. Hift, H., Ouellet, L., Littlefield, J. W., & Sanadi, D. R. (1953) *J. Biol. Chem.* 204, 565-579.
7. Voet, D., & Voet, J. G. (1995) *Biochemistry*, 2nd Ed., John Wiley and Sons, Inc., New York
8. Hager, L. P. (1962) *The Enzymes Vol. VI*, 387-399.
9. Bridger, W. A. (1974) in *The Enzymes* (Boyer, P. D., ed) Vol. X, 3 Ed., pp. 581-606, Academic Press Inc., New York
10. Muller, M. (1988) *Ann. Rev. Microbiol.* 42, 465-488.
11. Hellemond, J. V., Opperdoes, F. R., & Tielens, A. G. M. (1998) *Proc. Natl. Acad. Sci. USA* 95, 3036-3041.
12. Cavalier-Smith, T. (1987) *Ann. N. Y. Acad. Sci.* 503, 55-71.
13. Ottaway, J. H., & McMinn, C. L. (1979) *Biochem. Soc. Trans.* 7, 411-412.
14. Ottaway, J. H., McClellan, J. A., & Saunderson, C. L. (1981) *Int. J. Biochem.* 13, 401-410.
15. Hersh, L. B., & Jenks, W. P. (1967) *J. Biol. Chem.* 242, 3468-3480.
16. Moffet, F. J., & Bridger, W. A. (1970) *J. Biol. Chem.* 245, 2758-2762.
17. McClellan, J. A., & Ottaway, J. H. (1980) *Comp. Biochem. Physiol.* 67B, 679-684.
18. Lynn, R., & Guynn, R. W. (1978) *J. Biol. Chem.* 253, 2546-2553.
19. Jenkins, T. M., Eisenthal, R., & Weitzman, P. D. J. (1988) *Biochem. Biophys. Res. Commun.* 151, 257-261.
20. Bowman, K., Ropars, M., & Deshusses, J. (1982) *Experientia* 38, 533-534.
21. Hamilton, M. L., & Ottaway, J. H. (1981) *FEBS Lett.* 123, 252-254.
22. Jenkins, T. M., & Weitzman, P. D. J. (1986) *FEBS Lett.* 205, 215-218.

23. Weitzman, P. D. J., Jenkins, T. M., Else, A. J., & Holt, R. A. (1986) *FEBS Lett.* 199, 57-60.
24. Sanwal, B. D. (1970) *Bacteriol. Rev.* 34, 20-28.
25. Labbe, R. F., Kurumada, T., & Onisawa, J. (1965) *Biochim. et Biophys. Acta* III, 403-415.
26. Jenkins, T. M., & Weitzman, P. D. J. (1988) *FEBS Lett.* 230, 6-8.
27. Burnham, B. F., & Lascelles, J. (1963) *Biochem. J.* 37, 462-469.
28. Wider, E. A., & Tigier, H. A. (1970) *FEBS Lett.* 9, 30-32.
29. Johnson, J. D., Mehus, J. G., Tews, K., Milavetz, B. I., & Lambeth, D. O. (1998) *J. Biol. Chem.* 273, 27580-27586.
30. Johnson, J. D., Muhonen, W. W., & Lambeth, D. O. (1998) *J. Biol. Chem.* 273, 27573-27579.
31. Kaufman, S., & Alivisatos, S. G. A. (1955) *J. Biol. Chem.* 216, 141-152.
32. Burnham, B. F. (1963) *Acta Chem. Scand.* 17, suppl., 123-128.
33. Nandi, D. L., & Waygood, E. R. (1965) *Can. J. Biochem. Physiol.* 43, 1605-1614.
34. Palmer, J. M., & Wedding, R. T. (1966) *Biochim. Biophys. Acta* 113, 167-174.
35. Bush, L. P. (1969) *Plant Physiol.* 44, 347-350.
36. Meshkova, N. P., & Matveeva, L. N. (1970) *Biokhimiya* 35, 374-381.
37. Hansford, R. G. (1973) *FEBS Lett.* 31, 317-332.
38. Weitzman, P. D. J., & Kinghorn, H. A. (1978) *FEBS Lett.* 88, 255-258.
39. Ball, D. J., & Nishimura, J. S. (1980) *J. Biol. Chem.* 255, 10805-10812.
40. Weitzman, P. D., & Jaskowska-Hodges, H. (1982) *FEBS Lett.* 143, 237-240.
41. Jenkins, T. M., Gorrell, T. E., Müller, M., & Weitzman, P. D. J. (1991) *Biochem. Biophys. Res. Commun.* 179, 892-896.
42. Gibson, J., Upper, C. D., & Gunsalus, I. C. (1967) *J. Biol. Chem.* 242, 2474-2477.
43. Ramaley, R. F., Bridger, W. A., Moyer, R. W., & Boyer, P. D. (1967) *J. Biol. Chem.* 242, 4287-4298.
44. Bridger, W. A., Ramaley, R. F., & Boyer, P. D. (1969) *Methods Enzymol.* 13, 70-75.
45. Grinnell, F. L., & Nishimura, J. S. (1969) *Biochemistry* 8, 562-568.
46. Leitzmann, C., Wu, J.-Y., & Boyer, P. D. (1970) *Biochemistry* 9, 2338-2346.

47. Cha, S., & Parks, R. E. J. (1964) *J. Biol. Chem.* 239, 1961-1977.
48. Cha, S., Cha, C. J. M., & Parks, R. E. J. (1967) *J. Biol. Chem.* 242, 2577-2581.
49. Cha, S. (1969) *Methods Enzymol.* 13, 62-69.
50. Knight, E. J. (1961), Ph. D. Thesis, University of Illinois, Illinois, Urbana
51. Buck, D., Spencer, M. E., & Guest, J. R. (1986) *J. Gen. Microbiol.* 132, 1753-1762.
52. Buck, D., & Guest, J. R. (1989) *Biochem. J.* 260, 737-747.
53. Wolodko, W. T., James, M. N. G., & Bridger, W. A. (1984) *J. Biol. Chem.* 259, 5316-5320.
54. Wolodko, W. T., Fraser, M. E., James, M. N. G., & Bridger, W. A. (1994) *J. Biol. Chem.* 269, 10883-10890.
55. Fraser, M. E., James, M. N. G., Bridger, W. A., & Wolodko, W. T. (1999) *J. Mol. Biol.* 285, 1633-1653.
56. Brownie, E. R., & Bridger, W. A. (1972) *Can. J. Biochem.* 50, 719-724.
57. Murakami, Y., & Nishimura, J. S. (1974) *Biochim. Biophys. Acta* 336, 252-263.
58. Bailey, D. L., Wolodko, W. T., & Bridger, W. A. (1993) *Protein Sci.* 2, 1255-1262.
59. Ryan, D. G. (1994) Thesis, University of Alberta, Edmonton
60. Fraser, M. E. *personal communication.*
61. Nishimura, J. S. (1986) in *Advances in Enzymology* (Meister, A., ed) Vol. 58, pp. 141-172, Wiley, New York
62. Um, H. D., & Klein, C. (1993) *Biochem J.* 295, 821-826.
63. Kelly, C. J., & Cha, S. (1977) *Arch. Biochem. Biophys.* 178, 208-217.
64. Weitzman, P. D. J. (1981) *Adv. Microb. Physiol.* 22, 185-244.
65. Wolodko, W. T., Kay, C. M., & Bridger, W. A. (1986) *Biochemistry* 25, 5420-5425.
66. Teherani, J. A., & Nishimura, J. S. (1975) *J. Biol. Chem.* 250, 3883-3890.
67. Bailey, D. L., Fraser, M. E., Bridger, W. A., James, M. N. G., & Wolodko, W. T. (1998) , *J. Mol Biol* 285, 1655-1666.
68. Eisenstein, E., & Schachman, H. K. (1989) in *Protein Function* (Creighton, T. E., ed), pp. 135-176, IRL Press, Oxford, UK
69. Wilson, R. *et al.* (1994) *Nature* 368, 32.
70. Fleischmann, R. D. *et al.* (1995) *Science* 269, 496-512.



71. Fraser, C. M. *et al.* (1995) *Science* 270, 397-403.
72. Bult, C. J. *et al.* (1996) *Science* 273, 1066-1072.
73. Goffeau, A. *et al.* (1996) *Science* 274, 546-551.
74. Blattner, F. R. *et al.* (1997) *Science* 277, 1453-1462.
75. Klenk, H.-P. *et al.* (1997) *Nature* 390, 364-370.
76. Kunst, F. *et al.* (1997) *Nature* 390, 249-255.
77. Smith, D. R. *et al.* (1997) *J. Bacteriol.* 179, 7135-7155.
78. Tomb, J.-F. *et al.* (1997) *Nature* 388, 539-547.
79. Andersson, S. G. *et al.* (1998) *Nature* 396, 133-140.
80. Cole, S. T. *et al.* (1998) *Nature* 393, 537-544.
81. Deckert, G. *et al.* (1998) *Nature* 392, 353-357.
82. Fraser, C. M. *et al.* (1998) *Science* 281, 375-379.
83. Smith, R. F., & Smith, T. F. (1990) *Proc. Natl. Acad. Sci. USA* 87, 118-122.
84. Smith, R. F., & Smith, T. F. (1992) *Protein Engineering* 5, 35-41.
85. Thompson, J. D., Higgins, D. G., & Gibson, T. J. (1994) *Nucleic Acids Res.* 22, 4673-4680.
86. Page, R. D. M. (1996) *Comp. Appl. in Biosci.* 12, 357-358.
87. Tiboni, O., Cammarano, P., & Sanangelantoni, A. M. (1993) *J. Bacteriol.* 175, 2961-2969.
88. Siebers, B., Klenk, H.-P., & Hensel, R. (1998) *J. Bacteriol.* 180, 2137-2143.
89. Wright, F., & Bibb, M. J. (1992) *Gene* 113, 55-65.
90. Chistoserdova, L. V., & Lidstrom, M. E. (1994) *J. Bacteriol.* 176, 7398-7404.
91. Elshourbagy, N. A., Near, J. C., Kmetz, P. J., Sathe, G. M., Southan, C., Strickler, J. E., Gross, M., Young, J. F., Wells, T. N., & Groot, P. H. (1990) *J. Biol. Chem.* 265, 1430-1435.
92. Elshourbagy, N. A., Near, J. C., Kmetz, P. J., Wells, T. N., Groot, P. H., Saxty, B. A., Hughes, S. A., Franklin, M., & Gloger, I. S. (1992) *Eur. J. Biochem.* 204, 491-499.
93. Nowrousian, M., Masloff, S., Poggeler, S., & Kuck, U. (1999) *Mol. Cell. Biol.* 19, 450-460.
94. Alschul, S. F., & Gish, W. (1996) *Methods Enzymol.* 266, 460-480.

95. Alschul, S. F., Madden, T. L., Schaffer, A. A., Zhang, J., Zhang, Z., Miller, D. J., & Lipman, D. J. (1997) *Nucleic Acids Res.* 25, 3389-3402.
96. Galperin, M. Y., & Koonin, E. V. (1997) *Prot. Sci.* 6, 2639-2643.
97. Kaufman, S. (1955) *J. Biol. Chem.* 216, 153-164.
98. Engbring, J. A., & Alderete, J. F. (1998) *Mol. Microbiol.* 28, 305-315.
99. Ryan, D. G., Lin, T., Brownie, E., Bridger, W. A., & Wolodko, W. T. (1997) *J. Biol. Chem.* 272, 21151-21159.
100. Buck, D., Spencer, M. E., & Guest, J. R. (1985) *Biochemistry* 24, 6245-6252.
101. Porpaczy, Z., Sumegi, B., & Alkonyi, I. (1983) *Biochim. Biophys. Acta* 749, 172-179.
102. Walshaw, D. L., Wilkinson, A., Mundy, M., Smith, M., & Poole, P. S. (1997) *Microbiology* 143, 2209-2221.
103. Murzin, A. G. (1996) *Curr. Opin. in Struct. Biol.* 6, 386-394.
104. Robinson, J. L., Benson, R. W., & Boyer, P. D. (1969) *Biochemistry* 8, 2503-2508.
105. Murakami, K., Mitchell, T., & Nishimura, J. S. (1972) *J. Biol. Chem.* 247, 6247-6252.
106. Buttlare, D. H., Cohn, M., & Bridger, W. A. (1977) *J. Biol. Chem.* 252, 1957-1964.
107. Lam, Y. F., Bridger, W. A., & Kotowycz, G. (1976) *Biochemistry* 15, 4742-4748.
108. Upper, C. D. (1964), Thesis, University of Illinois, Urbana.
109. Wang, T., Jurasek, L., & Bridger, W. A. (1972) *Biochemistry* 11, 2067-2070.
110. Cha, S., Cha, C.-J. M., & Parks, R. E. J. (1965) *J. Biol. Chem.* 240, 3700-3702.
111. Hultquist, D. E., Moyer, R. W., & Boyer, P. D. (1966) *Biochemistry* 5, 322-331.
112. Bridger, W. A., Millen, W. A., & Boyer, P. D. (1968) *Biochemistry* 7, 3608-3616.
113. Bridger, W. A. (1971) *Biochem. Biophys. Res. Commun.* 42, 948-954.
114. Majumdar, R., Guest, J. R., & Bridger, W. A. (1991) *Biochim. Biophys. Acta* 1076, 86-90.
115. Mann, C. J., Mitchell, T., & Nishimura, J. S. (1991) *Biochemistry* 30, 1497-1503.
116. Cohn, M. (1959) *J. Cell. Comp. Physiol.* 54, 157-169.
117. Grinnell, F., & Nishimura, J. S. (1969) *Biochemistry* 8, 4126-4130.

118. Jencks, W. P. (1987) *Cold Spring Harbor Symp. Quant. Biol.* 52, 65-73.
119. Milner, Y., Michaels, G., & Wood, H. G. (1978) *J. Biol. Chem.* 253, 878-883.
120. Weigel, N., Kukuruzinska, M. A., Nakazawa, A., Waygood, E. B., & Roseman, S. (1982) *J. Biol. Chem.* 257, 14477-14491.
121. Cohn, M. (1951) in *Phosphorus Metabolism* (Eds. W. D. McElroy and B. Glass, Johns Hopkins Press, Baltimore) Vol. 1, 374-376.
122. Hager, L. P. (1957) *J. Amer. Chem. Soc.* 79, 4864-4869.
123. Nishimura, J. S., & Meister, A. (1965) *Biochemistry* 4, 1457-1462.
124. Vogel, H. J., & Bridger, W. A. (1982) *J. Biol. Chem.* 257, 4834-4842.
125. Walsh, C. T. J., Hildebrand, J. G., & Spector, L. B. (1970) *J. Biol. Chem.* 245, 5699-5708.
126. Hildebrand, J. G., & Spector, L. B. (1969) *J. Biol. Chem.* 244, 2606-2613.
127. Moffet, F. J., Wang, T., & Bridger, W. A. (1972) *J. Biol. Chem.* 247, 8139-8144.
128. Prasad, A. R. S., Nishimura, J. S., & Horowitz, P. M. (1982) *Biochemistry* 21, 5142-5147.
129. Prasad, A. R. S., Nishimura, J. S., & Horowitz, P. M. (1983) *Biochemistry* 22, 4272-4275.
130. Vogel, H. J., Bridger, W. A., & Sykes, B. D. (1982) *Biochemistry* 21, 1126-1132.
131. Vogel, H. J., & Bridger, W. A. (1983) *Biochem. Soc. Trans.* 11, 315-323.
132. Moffet, F. J., & Bridger, W. A. (1973) *Can. J. Biochem.* 51, 44-55.
133. Moffet, F. J. (1972) *Thesis*, University of Alberta, Edmonton Alberta.
134. Harting, J., & Velick, S. F. (1954) *J. Biol. Chem.* 207, 867-878.
135. Bild, G. S., Janson, C. A., & Boyer, P. D. (1980) *J. Biol. Chem.* 255, 8109-8115.
136. Wolodko, W. T., O'Connor, M. D., & Bridger, W. A. (1981) *Proc. Natl. Acad. Sci. USA* 78, 2140-2144.
137. Wolodko, W. T., Brownie, E. R., O'Connor, M. D., & Bridger, W. A. (1983) *J. Biol. Chem.* 258, 14116-14119.
138. Williams, S. P., & Bridger, W. A. (1987) *Biochemistry* 26, 4483-4487.
139. Nishimura, J. S., & Mitchell, T. (1984) *J. Biol. Chem.* 259, 2144-2148.
140. Nishimura, J. S., & Mitchell, T. (1985) *J. Biol. Chem.* 260, 2077-2079.
141. Um, H. D., & Klein, C. (1991) *J. Prot. Chem.* 10, 391-401.

142. Anshutz, A. L., Um, H. D., Seigel, N. R., Veron, M., & Klein, C. (1993) *Biochem Biophys Acta* 1162, 40-46.
143. Um, H. D., & Klein, C. (1994) *J. Prot. Chem.* 13, 177-185.
144. Birney, M., Um, H. D., & Klein, C. (1996) *J. Bacteriol.* 178, 2883-2889.
145. Birney, M., Um, H. D., & Klein, C. (1997) *Arch. Biochem. Biophys.* 347, 103-112.
146. Park, S., Chao, G., & Gunsalus, R. P. (1997) *J. Bacteriol.* 179, 4138-4142.
147. Steiner, A. W., & Smith, R. A. (1981) *J. Neurochemistry* 37, 582-593.
148. Pearson, P. H., & Bridger, W. A. (1975) *J. Biol. Chem.* 250, 4451-4455.
149. Wolodko, W. T., & Bridger, W. A. (1987) *Biochem. Cell Biol.* 65, 452-457.
150. Khan, I. A., & Nishimura, J. S. (1988) *J. Biol. Chem.* 263, 2152-2158.
151. Fong, G., & Bridger, W. A. (1992) *Biochemistry* 31, 5661-5664.
152. Kahn, I. A., & Nishimura, J. S. (1988) *J. Biol. Chem.* 263, 2152-2158.
153. Majumdar, R., & Bridger, W. A. (1990) *Biochem. Cell Biol.* 68, 292-299.
154. Henning, W. D., Upton, C., Majumdar, R., McFadden, G., & Bridger, W. A. (1988) *Proc. Natl. Acad. Sci. U.S.A.* 85, 1432-1436.
155. Ryan, D. G., & Bridger, W. A. (1991) *J. Mol. Biol.* 219, 165-174.
156. Nishimura, J. S., Ybarra, J., Mitchell, T., & Horowitz, P. M. (1988) *Biochem. J.* 250, 429-434.
157. Lahti, C. J., d'Oliveira, C. E., & Johnson, P. J. (1992) *J. Bacteriol.* 174, 6822-6830.
158. Collier, G. E., & Nishimura, J. S. (1978) *J. Biol. Chem.* 253, 4938-4943.
159. Saraste, M., Sibbald, P. R., & Whittinghofer, A. (1990) *Trends in Biochem. Sci.* 15, 430-434.
160. Blomberg, F., Maurer, W., & Ruterjans, H. (1977) *J. Am. Chem. Soc.* 94, 8149-8159.
161. Kraulis, P. J., (1991) *J. Appl. Crystallgr.* 24, 946-950.

## **Chapter Two      Cloning and Expression**

---

### **Introduction**

As outlined in Chapter 1, there are many differences between SCS enzymes from different sources. *E. coli* SCS for example, prefers ATP as substrate over GTP, which is preferred over ITP (1). On the other hand, SCS from mammalian species is strictly specific for either ATP or GTP (2, 3), and it has been suggested that different metabolic roles are fulfilled by mammalian SCS isozymes with different nucleotide specificities (4, 5). In addition, the quaternary structure of SCS also differs between eubacterial species. SCS from gram negative bacteria was found to be tetrameric whereas that from the gram positive bacteria was dimeric (6). SCS from pig heart was also found to be dimeric (7-9). The reasons for the different quaternary structures are not clear, however it has been suggested that tetrameric *E. coli* enzyme is more stable and more soluble (10). Prior to the cloning of the ATP-specific mammalian SCS, described below, SCS specific for GTP (from pig heart) and multi-specific SCS (from *E. coli*) were the primary subjects of investigation. This chapter is divided into three sections, and each deals with the cloning, or attempted cloning, of alternate isoforms of SCS.

To facilitate the investigation of the structural determinants of the nucleotide specificity of SCS, I attempted to clone an ATP-specific SCS. It was reasoned that comparison of ATP-specific SCS with both GTP-specific SCS from pig heart and multi-specific SCS from *E. coli* would yield information about the amino acids involved in determining nucleotide specificity. The SCS activity from *Neurospora crassa* had been shown to be specific for adenosine nucleotides (11). Two approaches were used to clone an ATP-specific SCS from *N. crassa*. In the first, the protein sequence of the N-terminus of both subunits of SCS from *Neurospora crassa* was determined by Edman degradation, and used to design degenerate primers for PCR. In the second, an antibody which

recognized the  $\alpha$ -subunit of *N. crassa* SCS was used to screen *N. crassa* expression libraries.

Prior to the work of Johnson *et al.* (12) relatively little was known about the expression of mammalian SCS isoforms. In mammals, different levels of SCS activity specific for either ATP or GTP had been found in different tissues, and a GTP-specific SCS from pig heart had been isolated and cloned (13, 5, 14-16, 2). Studies on the  $\alpha$ -subunit of pig heart SCS revealed two isoforms generated by differential splicing of at least one intron (17). The mRNA for these two isoforms of SCS was differentially regulated in pig tissues, but not in a manner that was consistent with the levels of SCS activity in the different pig tissues. It was reasoned that if the  $\alpha$ -subunit was not responsible for the expression of specific isoforms of SCS then perhaps the  $\beta$ -subunit was. To investigate this possibility, expression levels of the mRNA for the  $\beta$ -subunit of SCS in different pig tissues were determined by RT-PCR.

By creating a dimeric form of *E. coli* SCS, Bailey *et al.* found that neither the catalytic activity nor substrate efficiency depended on the presence of tetrameric enzyme (2). It was suggested that the dimeric enzyme was less stable than the tetrameric enzyme. To further investigate the determinants of the stability of SCS, the enzyme from the thermophile *Thermus aquaticus* was cloned, and the protein was expressed.

## Materials and Methods

### SECTION I: Cloning of *Neurospora crassa* SCS.

*Purification of N. crassa* SCS. A stock of *N. crassa* was obtained from Craig Wilson (University of Kansas Medical Center, Fungal Genetics Stock Center), and SCS was purified from cells grown from this stock by Ed Brownie. Cells were grown in Vogals media (150 g/L sodium citrate, 250 g/L potassium phosphate, 100 g/L  $\text{NH}_4\text{NO}_3$ , 10g/L  $\text{MgSO}_4$ , 5 g/L  $\text{CaCl}_2$ , 5g/L biotin) supplemented with sucrose (40g/L) for 72 h at 30

°C. Cells were harvested by centrifugation, and SCS was purified essentially according to the methods used for the purification of *E. coli* SCS (18).

*Protein Sequencing of N. crassa SCS.* The subunits of *N. crassa* SCS were separated by SDS PAGE using 12 % (w/v) acrylamide gels (19). The separated subunits were then transferred onto PVDF membranes (250 mA for 45 min at 4 °C) using a Mini Trans-Blot Transfer Cell (Bio-Rad Laboratories). The PVDF membrane was then lightly stained using coomassie blue in 25 % (v/v) methanol, and the bands which corresponded to the  $\alpha$ - and  $\beta$ -subunits were excised. They were then subjected to amino acid sequencing by Edman degradation with a Hewlett Packard 1005A peptide sequencer.

*PCR of N. crassa Genomic DNA and cDNA Libraries.* Degenerate primers for PCR of each subunit of *N. crassa* SCS were designed based on the protein sequence of the N-termini of the subunits and; for the  $\alpha$ -subunit, on a conserved sequence in the active site loop (RMGHAGAD); and for the  $\beta$ -subunit, on a conserved sequence in the C-terminal domain (NIFGGIVR). The reaction mixture for PCR consisted of 0.01% (w/v) gelatin, 50 mM KCl, 1.5 mM MgCl<sub>2</sub>, 10 mM Tris HCl, pH 8.3, 200  $\mu$ M each of dATP, dTTP, dGTP, and dCTP, 0.25-7  $\mu$ M of each primer, and 2.5 units of *Taq* polymerase. A 100 ng sample of *N. crassa* genomic DNA, prepared according to the methods in Molecular Cloning: A Laboratory Manual (20), or a library of *N. crassa* DNA in  $\lambda$  Zap (obtained from the laboratory of Dr. Frank Nargang) was used as template. The primers for PCR of the  $\alpha$ -subunit were: the 5' N-terminal primer, 5' CGT CTA GAA A(C/T)A A(A/G)G A(C/T)A C(A/T/G/C)A A(A/G)G T(A/T/G/C)A T(C/T)A C 3' , and the 3' active site primer, 5' CCG GAG CTC AT(A/T/G/C) GC(A/T/G/C) CC(A/T/G/C) GC(A/G) TG(A/T/G/C) CCC AT 3'. The nucleotides in brackets represent degenerate positions and the underlined nucleotides represent *Xba* I and *Sst* I restriction sites that were incorporated to facilitate cloning of the PCR products. The primers for the  $\beta$ -subunit were: the 5' N-terminal primer, 5' GCT CTA GAT GAA (A/G)AT (C/T)CA (C/T)GA (A/G)TA (C/T)CA (A/G)GG 3', and the 3' (conserved) primer, 5'CCG GGA GCT CAC (A/G)AT

(A/T/G/C)CC (A/T/G/C)CC (A/G)AA (A/G)AT (A/G)TT (A/T/G/C)AC 3'. Each PCR reaction was initially heated at 96 °C for 5 min to denature the template DNA. This was followed by 30 cycles (using a Techne PHC-2 thermocycler) of annealing for 30 s at a temperature between 42 °C and 52 °C, polymerase extension for 2 min at 72 °C and denaturation for 30 s at 94 °C.

For cloning, the PCR products were isolated by phenol/chloroform extraction and ethanol precipitation (20). The products were then digested with both *Xba* I and *Sst* I according to the manufacturer's instructions in the appropriate buffer (Bethesda Research Laboratories). These digestion products were purified again by phenol/chloroform extraction and ethanol precipitation and incubated overnight at 15 °C in the presence of similarly digested and purified pUC19 vector, T4 DNA ligase, and the appropriate buffer (New England Biolabs Inc.). Following transformation into competent *E. coli* JM103 cells (20), plasmid DNA which contained PCR products was isolated and sequenced. Sequencing was done using either dideoxy sequencing (21) with the Sequenase 2.0 DNA sequencing kit (United States Biochemical Corp.) and 8 M urea/6 % (w/v) acrylamide gels (22), or with an Applied Biosystems Model 373 Automated Sequencer.

*Screening of N. crassa cDNA Libraries Using a Fragment of the  $\beta$ -Subunit cDNA.* The fragment of the  $\beta$ -subunit that was obtained by PCR was used to screen the *N. crassa* DNA library that was propagated in *E. coli* Y1090 cells. The genotype for all *E. coli* strains used in this thesis are listed in Appendix 2. First, the DNA fragment was labeled with digoxigenin-11-dUTP using random primers and Klenow fragment polymerase according to the specifications in the Genius DNA Labeling and Detection Kit (Boehringer Mannheim GmbH). Second, the  $\lambda$  Zap DNA library was propagated in XL1-Blue cells, the plaques plated according to the methods in Molecular Cloning: A Laboratory Manual (20), and these plaques were then blotted onto Hybond-N Nylon membranes (Amersham International pIc), in duplicate, according to manufacturer's instructions. Finally, the labeled fragment of the  $\beta$ -subunit cDNA was hybridized to these plaques on the



membranes. The hybridization was carried out at 62 °C, followed by two washes at 59 °C. Subsequently an anti-digoxigenin antibody conjugated to alkaline phosphatase was used to detect the labeled fragment. The blots were developed by colorimetric detection using nitroblue tetrazolium salt and 5-bromo-4-chloro-3-indolyl phosphate, all according to the procedure described in the Genius DNA Labeling and Detection Kit. Nine plaques gave a positive signal in duplicate blots were then picked, and propagated; single plaques were isolated using repeated rounds of screening (called secondary and tertiary screens). The method for detection of the hybridized probe on the secondary and tertiary blots was chemiluminescence followed by autoradiography. In this case, the alkaline phosphatase cleaves phosphate from 4-methoxy-4-(3-phosphatephenyl)-spiro-1,2-dioxetane-3,2'-adamantane (Boehringer Mannheim GmbH) which subsequently decays to a phenolate ion and emits light. The procedure was carried out according to the manufacturer's specifications.

DNA libraries were contained the  $\lambda$  Zap phage which have the following structure: insert DNA from the organism of interest (*N. crassa*) has been cloned into the *EcoR* I sites from the phagemid pBluescript; the pBluescript has been inserted into the genome of  $\lambda$  phage. The pBluescript phagemid can be excised and packaged into M13 filamentous phage particles as single stranded DNA using a helper phage. The M13 phage particles can then be used to infect cells resulting in a plasmid which can be propagated in those cells. The  $\lambda$  Zap phage particles were isolated from the tertiary screens and used to transfect *E. coli* XL-1 Blue cells (obtained from Stratagene Cloning Systems), and the pBluescript was excised and packaged using the VCSM13 helper phage (obtained from Stratagene Cloning Systems) according to manufacturer's specifications. The single stranded DNA was then isolated and sequenced by dideoxy sequencing (21).

*Purification of Antibody Specific for the  $\alpha$ -Subunit of N. crassa SCS.* Serum from rabbits injected with the  $\alpha$ -subunit of rat liver SCS was found to cross-react with the  $\alpha$ -subunit from *N. crassa*. The serum also cross-reacted with some components in the lysate

of *E. coli* Y1090 cells. The component of the serum that reacted with *E. coli* proteins was depleted from the serum by repeated incubation of the serum with nitrocellulose that had been impregnated with the lysate from *E. coli* Y1090 cells.

*Expression Screening of N. crassa cDNA Libraries.* The  $\lambda$  Zap DNA library that was used above can also be used as an expression library by inducing protein production from the *lac z* promoter. The library was propagated as before, and proteins were expressed and blotted onto IPTG-impregnated nitrocellulose membranes, in duplicate, and according to the procedures in *Molecular Cloning: A Laboratory Manual* (20). The membranes were then blocked and incubated with the purified rat liver antisera, followed by removal of the rat liver antisera and incubation with goat anti-rabbit antibodies conjugated to alkaline phosphatase. The membranes were then developed as described before. Six single plaques that gave a positive signal in duplicate were then isolated and sequenced as described before.

## **SECTION II: mRNA Expression Studies of Pig SCS.**

*Isolation and Reverse Transcription of mRNA from Pig Tissues.* Samples of brain, muscle, liver, and heart tissue from newborn piglets was frozen in liquid nitrogen, sealed and stored at -70 °C. The mRNA was subsequently isolated and reverse transcribed by David Ryan (17). Samples were also mock reverse transcribed (i.e. no reverse transcriptase was added) for use as negative controls for the subsequent PCR reactions.

*PCR of Reverse Transcribed mRNA from Pig Tissues.* PCR was carried out as described earlier, except that each primer concentration was 0.25  $\mu$ M. The primers for amplification of the cDNA for the full length  $\beta$ -subunit were: the 5' UTR (untranslated region) primer (5' CCG GCG GCC CCC GTG GCA GC 3') and the 3' UTR primer (5' ATC TCT TCT TAT GGG AAA AC 3'). The annealing temperature for amplification of the full length  $\beta$ -subunit cDNA was 52 °C. As controls for the amount of mRNA present in the tissues, the cDNA for  $\beta$ -actin was also amplified with the following primers: 5' TGG

AAT CCT GTG GCA TCC ATG AAA C 3' and 5' TAA AAC GCA GCT CAG TAA CAG TCC G 3'.

*Cloning and Sequencing of the PCR Products.* The PCR products for the  $\beta$ -subunit of pig SCS were purified and cloned into the cloning vector pCR2.1 using the Invitrogen TA cloning kit (Invitrogen Corp.), according to the manufacturer's specifications. This kit uses a strategy to clone the PCR products that takes advantage of the 3' overhanging A's that Taq DNA polymerase incorporates into amplified DNA. This strategy is illustrated for the *T. aquaticus* subunits in Figure 2-1A and B. The site into which the PCR products are ligated has 5' overhanging T's that the amplified DNA fragment can anneal to. This site resides in the *lac Z* gene, and after transformation into the *lac Z* (-) *E. coli* strain INV $\alpha$ F', colonies that contained an insert were selected by their white colour on plates containing 50  $\mu$ g/ml ampicillin, X-gal and IPTG. The plasmid DNA from a colony that contained insert were then sequenced using an Applied Biosystems Model 373 Automated Sequencer.

### **SECTION III: Cloning and Expression of *T. aquaticus* SCS.**

*Cloning and Sequencing of the Translationally Linked Genes for the  $\alpha$ - and  $\beta$ -Subunits of *Thermus aquaticus* SCS.* The genes for the  $\alpha$ - and  $\beta$ -subunits of *Thermus aquaticus* SCS were amplified from *T. aquaticus* genomic DNA by PCR with primers directed to the 5' end of the gene for the  $\beta$ -subunit and the complement of the 3' end of the gene for the  $\alpha$ -subunit. Since the sequence of the  $\beta$ -subunit of *T. aquaticus* SCS was not available at that time, the sequence from the  $\beta$ -subunit of *T. flavus* SCS was used to design the 5' primer (for the  $\beta$ -subunit). The 5' primer incorporated an *Nde* I site that contained the start GTG codon in the sequence of the gene for the  $\beta$ -subunit from *Thermus flavus* (23). The 3' primer incorporated an *EcoR* I site after the stop codon of the  $\alpha$ -subunit gene from *T. aquaticus* (24). The sequence for the 5' primer was: 5' CGA TGC CAT ATG AAC CTG CAC GAG TAT CAA GCG 3', and the sequence for the 3' primer was 5' CCG GAT GAA TTC CAG CCC AGG GCC TTC TTG ACC AG 3'; the primer

sequences that do not match those in *T. flavus* or *T. aquaticus*, respectively, are shown in bold print and the restriction endonuclease sites are underlined. The conditions for the PCR reaction were the same as those described for the amplification of the pig heart cDNAs, except that 125 µg of *T. aquaticus* genomic DNA was used as template, the annealing step was carried out at 48 °C for 30 s, and the extension step was extended to 2 min. The single band of approximately 2 kbp that was evident when the PCR reaction was subjected to electrophoresis in 1 % (w/v) agarose with TAE buffer (20) was excised, and subsequently purified using glass milk (22). The fragment and the expression vector pT7-7 (25) were then digested with the restriction endonucleases *Nde* I (New England Biolabs Inc.) and *EcoR* I (Bethesda Research Laboratories/Life Technologies Inc.) for 12 hours at 25 °C. The fragments of interest were purified by agarose gel electrophoresis and glass milk extraction, and ligated using T4 DNA ligase according to the manufacturers specifications (New England Biolabs Inc.). The resulting ligated mixture was transformed into chemically competent *E. coli* strain JM103 cells (20). The plasmid DNA was isolated from 18 colonies (20); and of the 9 colonies which contained the genes for *T. aquaticus* SCS, two were chosen for DNA sequencing and protein expression. Plasmid DNA for sequencing was isolated from the JM103 transformed cells using the QIAGEN midi plasmid purification kit (QIAGEN Inc.) according to the manufacturer's directions, and sequenced using an Applied Biosystems Model 373 Automated Sequencer. Both strands of the second clone (called "pT7-7Taq12") were sequenced by repeated rounds of sequencing and primer design.

*Expression of the Translationally Linked Genes for the  $\alpha$ - and  $\beta$ -Subunits of Thermus aquaticus SCS* Protein from both of the *T. aquaticus* SCS clones that were initially chosen for DNA sequencing (pT7-7Taq12 and 13) was also expressed after transformation of the plasmid DNA into *E. coli* strain BL-21(DE-3) (26). This strain of *E. coli* contains a copy of the  $\lambda$  bacteriophage genome integrated into the *E. coli* genome. The integrated  $\lambda$  genome contains a copy of the T7 RNA polymerase gene under control of the

*lac* UV5 promoter, that is inserted into the gene for the integrase protein. Thus, production of the T7 RNA polymerase in this system can be induced by IPTG. The expression plasmid pT7-7 contains a copy of the strong T7 RNA polymerase promoter and the ribosome binding site from the T-7 phage gene 10 placed appropriately upstream from the *Nde* I restriction endonuclease site (25).

The transformed BL-21(DE-3) cells were grown at 37 °C to mid log phase (0.7  $A_{600nm}$ ), and protein production was induced by the addition of 1 mM IPTG. Samples of culture (1 ml) were then taken at various times. The cells in each sample were harvested by centrifugation at 4 °C for 5 min at 15,000 x g. The cell pellets were resuspended in 200  $\mu$ l of sonication buffer (100 mM KCl, 0.1 mM EDTA, 0.1 mM PMSF, 1 mM benzamidine, 10 mM 2-mercaptoethanol, 1 % (v/v) glycerol, and 100 mM potassium phosphate, pH 7.4) and frozen at -20 °C. These samples were then thawed and sonicated for 30 s, three times, using a Biosonic III sonicator (Brownwill Scientific) set at an intensity of 35 and equipped with the fine probe. They were then centrifuged again for 10 min at 15,000 x g and 4 °C, and the pellet and supernatant fractions were separated. Samples were then subjected to SDS-PAGE: 200  $\mu$ l of SDS-PAGE loading buffer (50 mM Tris, pH 6.6, 2.5% (w/v) SDS, 1 mM 2-mercaptoethanol, and 35% glycerol) was added to both the pellet and supernatant fractions. Proteins in the supernatant (60  $\mu$ l) and the resuspended pellet (30  $\mu$ l) were separated by SDS-PAGE, and the resulting gel was examined after fixing the gel in 10 % (v/v) acetic acid, 45 % (v/v) methanol, and staining using coomassie blue. As a control, cells containing the plasmid pT7-7 with no insert were subjected to the same treatment.

The supernatant fractions were also tested for SCS activity (the formation of succinyl-CoA) under saturating concentrations of all substrates (100  $\mu$ M CoA, 10 mM succinate and 400  $\mu$ M ATP or GTP) in a total volume of 1 ml of assay medium containing 50 mM KCl, 10 mM MgCl<sub>2</sub>, 50 mM Tris HCl, pH 7.4. The pellet was resuspended in 6 M guanidine HCl and incubated overnight at 4 °C. In an attempt to refold the dissociated

proteins, the denaturant was removed by dialysis for 18 h in Tris HCl, pH 7.5, in the presence of 5 mM 2-mercaptoethanol and 1 % (v/v) glycerol. The resultant solutions were tested for SCS activity in the same manner as for the supernatant fractions.

*Mutagenesis of the Start Codon and the Ribosome Binding Site of the  $\alpha$ -Subunit Gene of *T. aquaticus* SCS.* The start codon of the gene for the  $\alpha$ -subunit of *T. aquaticus* SCS was changed from GTG to ATG in an effort to improve expression of the  $\alpha$ -subunit. Site-directed mutants were made in three PCR reactions using standard protocols for the PCR and overlap extension as described in Ho *et al*(27). The mutagenic PCR was carried out in the following two steps (Appendix 3): In the first step two DNA fragments were generated that had overlapping ends. One fragment was amplified using the 5' flanking primer and the complement of the internal mutagenic primer. The second fragment was amplified using the internal mutagenic primer and the 3' flanking primer. In the second step the two fragments were combined by using both fragments as the template in a PCR reaction with both the 5' and 3' flanking primers. The reaction buffer for PCR was identical to that used for PCR of the subunit genes of *N. crassa* SCS, except that the concentration of each primer was 0.25  $\mu$ M, and 100 ng of pT7-7Taq12 DNA was used as the template DNA (28). The 5' flanking primer was 5' (222) CAT CCT GGG CAT GAA CAT CA (241) 3', the 3' flanking primer was 5' (1470) GAT CTC GTC AAT GGT GTC GGC (1451) 3', the internal mutagenic primers were 5' (1123) GGA GGT GCG GCA TGA TCC TGG TG (1145) 3' and its complement. The numbers in parentheses denote the position of the first and last nucleotide of the primer, and the letter in bold print represents a different nucleotide from that in the wild-type *T. aquaticus* SCS. The annealing temperature was 65 °C. The mutant fusion product and the vector pT7-7Taq12 were digested with *Ssr* I (which cleaves at position 664) and *Avr* II (which cleaves at position 1274) according to the manufacturer's specifications (New England Biolabs Inc.). The fragments were separated by electrophoresis in 1% (w/v) agarose in TAE buffer (20), excised and then purified using glass milk (22). The mutant fragment was ligated to the

vector fragment using T4 DNA ligase (15 °C, 8 h). The resulting mutant plasmids were then used to transform competent JM103 *E. coli* cells (20). The presence of the ATG codon and the absence of other mutations, was verified by DNA sequencing using an Applied Biosystems Model 373 Automated Sequencer. The resulting expression plasmid was called pT7-7Taq<sub>ATG</sub>.

In a further effort to improve the expression of *T. aquaticus* SCS, the GC rich ribosome binding site for the  $\alpha$ -subunit gene was changed to one rich in AT. The mutagenesis was done using a procedure similar to that above except for the following modifications: 1. The internal mutagenic primers were: 5' (1116) AAT GAA AGG AGG TAA CAT ATG ATC CTA GTT AAT AAA GAG ACC CGC GTC CTG (1166) 3' and 5' (1151) TTT ATT AAC TAG GAT CAT ATG TTA CCT CCT TTC ATT GCC ACG GTG ACC TTG (1101) 3'. 2. In order to produce a mutant fusion product in the third PCR reaction (Appendix 3), the products of the first two PCR reactions were treated with T4 DNA polymerase in order to remove any 3' overhanging A's that *Taq* polymerase may have added. In addition, 9 cycles of the third PCR reaction were carried out in the absence of the 3' and 5' flanking primers in order to increase the concentration of the correctly annealed mutant fusion product prior to amplification using the flanking primers. The annealing temperature for these 9 cycles was 62 °C. The annealing temperature for the additional cycles, which contained the flanking primers, was 65 °C (the same as above). The cloning and sequencing of the mutant fusion product was also carried out as described above. The expression plasmid that was produced was called pT7-7Taq<sub>RBS</sub>.

*Expression of T. aquaticus SCS from pT7-7Taq<sub>ATG</sub> and pT7-7Taq<sub>RBS</sub>* The ability of both expression vectors to express *T. aquaticus* SCS was initially assessed using the *E. coli* strain BL-21(DE-3) in the same manner as for the original clone, except that only one time point at 4 h was taken. Due to the high level of endogenous SCS activity present in the BL-21 strain, it was difficult to detect any additional SCS activity of any expressed *T. aquaticus* SCS. Therefore, the pT7-7Taq<sub>ATG</sub> and pT7-7Taq<sub>RBS</sub> plasmids were expressed in

the SCS null strain TK3D18 (29). TK3D18 was transformed with either pT7-7Taq<sub>ATG</sub> or pT7-7Taq<sub>RBS</sub> and pGP1-2. The plasmid pGP1-2 (25) confers resistance to kanamycin, expresses a temperature sensitive  $\lambda$  repressor, and contains the T7 polymerase under control of the  $\lambda$  pL promoter. Thus, colonies which were resistant to both kanamycin and ampicillin were selected for expression in a manner analogous to the expression from the BL-21 (DE-3) strain, except that the cells were grown initially at 30 °C to mid log phase and then induced by shifting the temperature to 42 °C. This temperature shift inactivated the  $\lambda$  repressor, induced the production of T7 polymerase and thus induced the production of *T. aquaticus* SCS. The presence of SCS subunits in both the pellet and supernatant fractions was assayed by SDS-PAGE, in the same way as for the original *T. aquaticus* SCS clones. The SCS activity present in the supernatant fraction was also assayed both before and after heating to 70 °C for 30 min to assess the stability of the enzyme.

*Purification and Refolding of T. aquaticus SCS from Inclusion Bodies.* The inclusion bodies that resulted from the expression of pT7-7Taq<sub>RBS</sub> in TK3D18 culture were purified by the methods described by Mukhopadhyay (30). After expression, the cell pellet was resuspended in 50 ml of 25 % (w/v) sucrose, 1 mM EDTA, 0.1 % (w/v) sodium azide, and 50 mM Tris HCl, pH 7.0. The cells were lysed by incubation in the presence of 50 mg of lysozyme (Sigma-Aldrich Canada Ltd.) for 10 min at 22 °C, followed by addition of 100 ml of 1 % (v/v) Triton X-100, 1% (w/v) sodium deoxycholate, 100 mM NaCl, 0.1% (w/v) sodium azide, 20 mM Tris HCl, pH 7.5 for another 10 min. DNase (final concentration = 0.02 mg/ml) and MgCl<sub>2</sub> (final concentration = 5 mM) were added, and the digest was incubated for 20 min at 22 °C. The inclusion bodies were subsequently pelleted by centrifugation at 8000 rpm for 20 min. The supernatant was kept to test for any SCS activity, and the inclusion bodies were purified by four cycles of homogenization in 0.5 % (v/v) Triton X-100, 100 mM NaCl, 1 mM EDTA, 0.1 % (w/v) sodium azide, and 50 mM Tris HCl, pH 8.0, followed by centrifugation (8000 rpm, 20 min). The pellet was then washed with 50 mM Tris, pH 8.0, 1 mM EDTA, and 0.1 % (w/v) sodium azide to remove



any residual triton solution. The ability of 1.5 M, 2.0 M or 6 M guanidine HCl to extract the *T. aquaticus* SCS from the pellet was tested by homogenization in each of these solutions followed by centrifugation (8000 rpm, 20 min). The presence of *T. aquaticus* SCS in the pellet, of these washes and extractions was assayed by SDS-PAGE. Samples from the supernatant fractions of these washes and extractions were checked immediately for the ability to catalyze the formation of succinyl-CoA both before and after heating to 70 °C for 30 min.

The *T. aquaticus* SCS in the supernatant fractions was refolded by two methods. In the first, the supernatant fraction was dialyzed for 18 h at 22 °C against 5 mM 2-mercaptoethanol, 0.1 % (v/v) glycerol in 50 mM Tris HCl, pH 7.5. In the second, the supernatant fraction of the 2.0 M and 6.0 M guanidine HCl extractions was rapidly diluted 1:20 (v/v) into 0.67 M L-arginine, 50 mM potassium phosphate , pH 7.4 with constant mixing, followed by incubation for 18 h at 22 °C (31). The ability of samples of these fractions to catalyze the production succinyl-CoA was then assayed before and after heating to 70 °C for 30 min.

*Direct Sequencing of the PCR Product Generated from T. aquaticus Genomic DNA.* The low yields of soluble and thermostable *T. aquaticus* SCS prompted an investigation of the changes in the deduced amino acid sequence of *T. aquaticus* SCS when compared to the sequences from *T. flavus* and *T. aquaticus* B. To find out whether these changes were due to strain to strain variation, or to errors that occurred during PCR, the products of two separate PCR reactions were sequenced directly. The PCR from genomic DNA was carried out with the same primers and in the same manner as for the original clones. The product was then purified for sequencing using the QIAquick PCR purification kit (QIAGEN Inc.) according to the manufacture's specifications, and sequenced as described before.

*Independent Cloning of the T. aquaticus  $\alpha$ - and  $\beta$ -Subunit Genes and Their Assembly into an Expression Vector that Is Not Translationally Coupled.* The PCR

reactions for both the  $\alpha$ - and  $\beta$ -subunit genes were carried out under the same conditions as for the original clones, except for the primers. The sequence of the 5' primer for the  $\alpha$ -subunit was 5' (1116) AAT GAA AGG AGG TAA CAT ATG ATC CTA GTT AAT AAA GAG ACC CGC GTC CTG (1166) 3' and the sequence for the 3' primer was 5' CCG GAT GAA TTC CAG CCC AGG GCC TTC TTG ACC AG 3'. The sequence of the 5' primer for the  $\beta$ -subunit was 5' CGA TGC CAT ATG AAC CTG CAC GAG TAT CAA GCG 3' and the sequence for the 3' primer was 5' (1151) TTT ATT AAC TAG GAT CAT ATG TTA CCT CCT TTC ATT GCC ACG GTG ACC TTG (1101) 3'. Again, the numbers in parentheses denote the position of the first and last nucleotide of the primer, the bold letters indicate nucleotides that were different from those in the original wild-type *T. aquaticus* SCS, and the underlined letters represent restriction enzyme sites. The PCR products were cloned into the cloning vector pCR2.1 using the Invitrogen TA cloning kit (Invitrogen Corp.), according to the manufacturer's specifications. For the  $\alpha$ -subunit gene, plasmid DNA was isolated from six white colonies (20), four of which contained the gene. One was chosen and was called pCR2.1Taq $\alpha$ . For the  $\beta$ -subunit, one of the six colonies that were examined contained the gene for the  $\beta$ -subunit. This plasmid construct was called pCR2.1Taq $\beta$ . The plasmid DNA was isolated and sequenced in the same manner as for the original clones. The cloning strategy is shown in Figure 2-1. The  $\alpha$ -subunit gene was sub-cloned into the expression vector pT7-7 by first, digestion of pCR2.1Taq $\alpha$  and pT7-7 with *Nde* I (New England Biolabs Inc.) and *EcoR* I (Bethesda Research Laboratories/Life Technologies Inc.) according to the manufacturer's specifications, second, isolation of the appropriate fragments from 1 % (w/v) agarose gels, third, ligation using T4 DNA ligase (New England Biolabs Inc.) according to the manufacturer's directions and fourth, transformation to the *E. coli* strain BL-21 (DE-3) (20). Plasmid DNA was isolated from colonies that grew on plates containing 50  $\mu$ g/ml ampicillin. All six of the colonies that were examined contained the gene for the  $\alpha$ -subunit. One was chosen and called pT7-7Taq $\alpha$  (Fig. 2-1A). The gene for the  $\beta$ -subunit was sub-

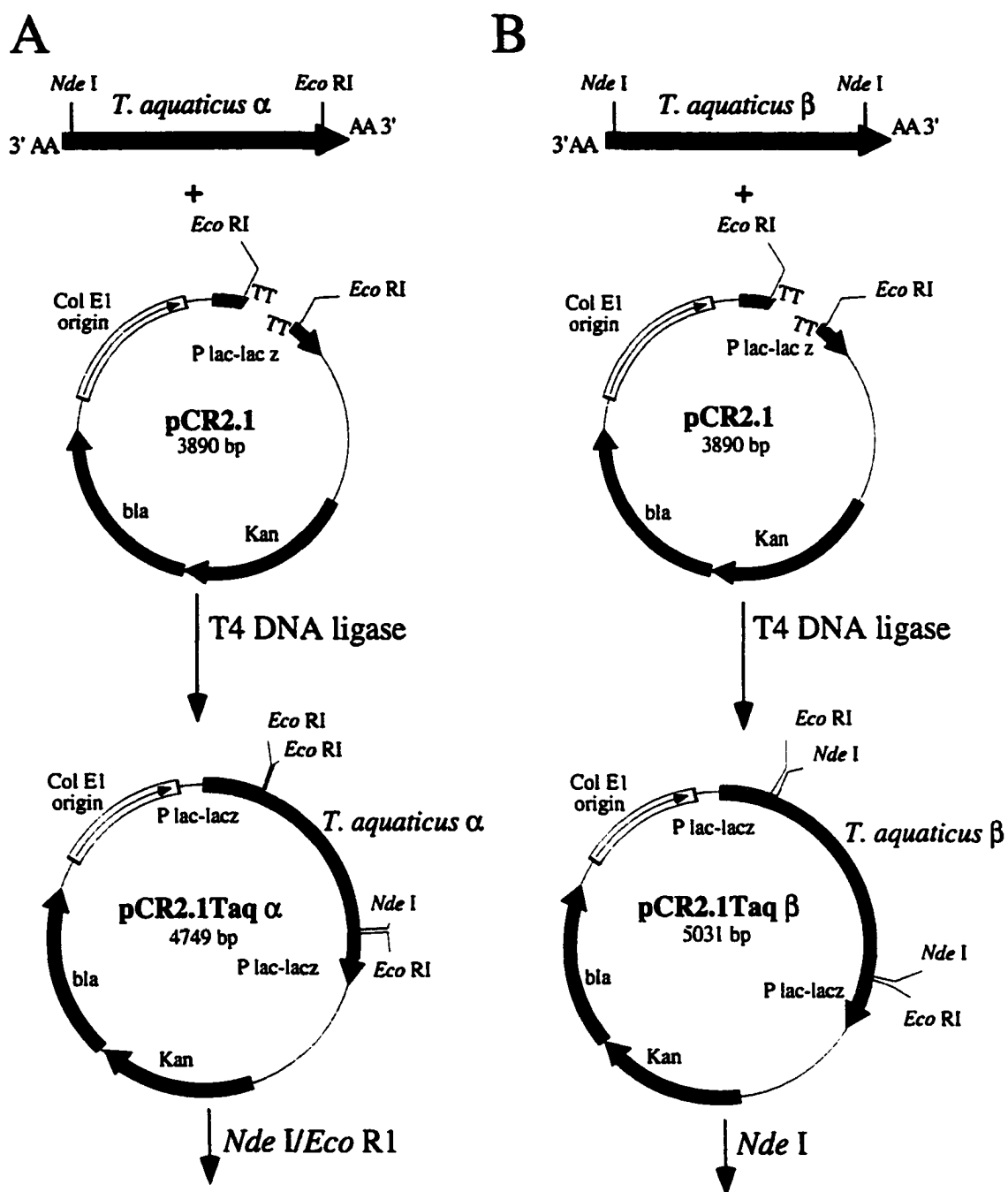
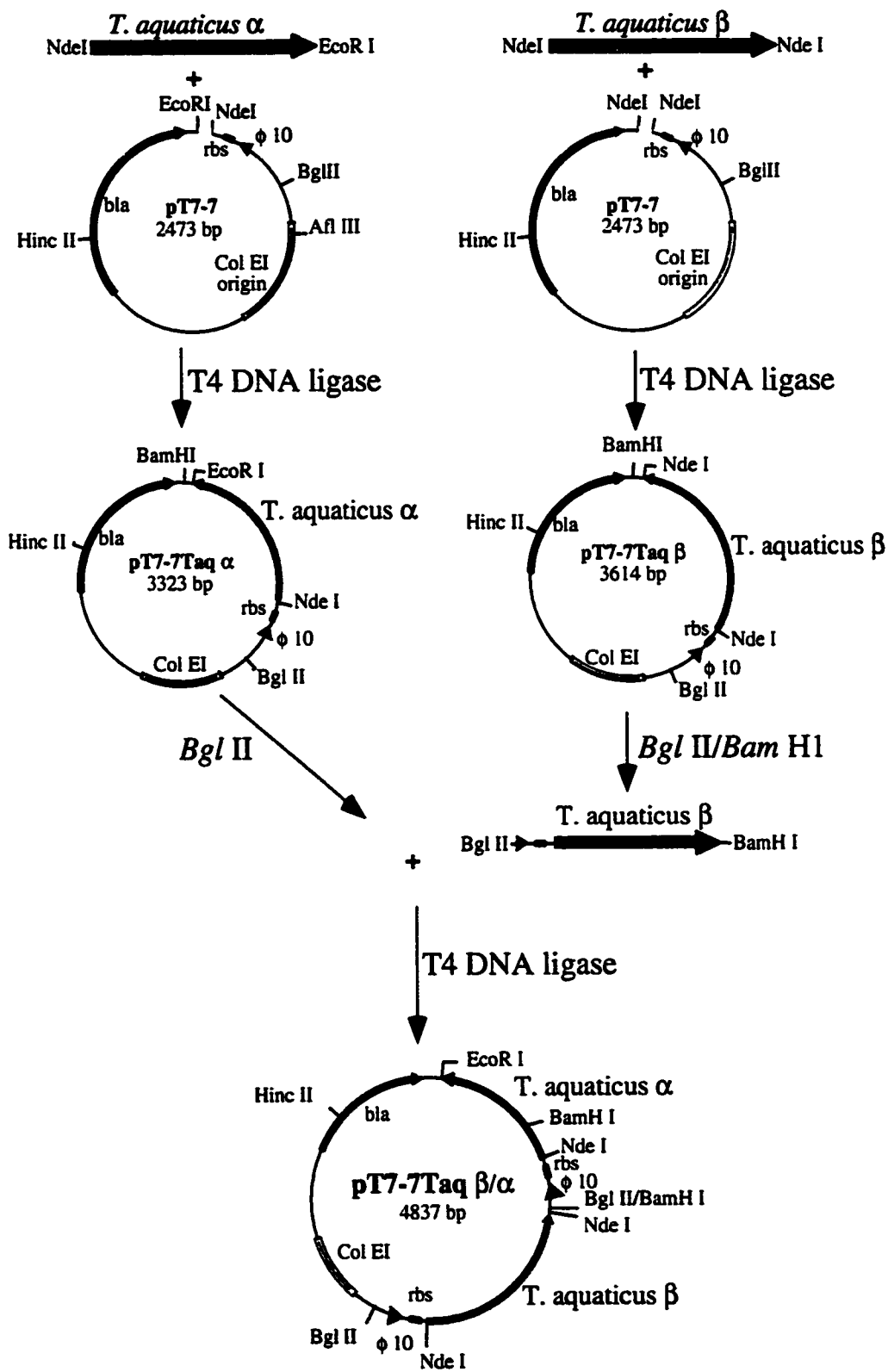


**Figure 2-1. Cloning scheme for the cloning and assembly of the  $\alpha$ - and  $\beta$ -subunit of *T. aquaticus* SCS. A. Cloning of *T. aquaticus*  $\alpha$ -subunit into the TA cloning vector pCR2.1. B. Cloning of *T. aquaticus*  $\beta$ -subunit into the TA cloning vector pCR2.1. C. The sub-cloning of the genes for the  $\alpha$ - and  $\beta$ -subunit into the expression vector pT7-7 and assembly into the whole enzyme expression vector pT7-7Taq $\beta/\alpha$ . The genes for the subunits are shown in red, the T-7gene  $\phi 10$  promoter and ribosome binding site are shown as a blue arrow and rectangle, respectively.**

C



cloned into pT7-7 in a similar manner, except that only *Nde* I was used to digest the vector (pT7-7) and insert (pCR2.1Taq $\beta$ ) plasmids. The plasmid DNA from six colonies was examined and two were found to contain the insert in the correct orientation. One was chosen and called pT7-7Taq $\beta$  (Fig. 2-1B). To create an expression vector that expressed both the  $\alpha$ - and  $\beta$ -subunit genes, pT7-7Taq $\beta$  was digested with *Bgl* II and *Bam*H I (New England Biolabs Inc.), and the vector pT7-7Taq $\alpha$  was digested with *Bgl* II. The appropriate fragments were ligated, transformed, and plasmid DNA was isolated as described before. Seven of eight colonies contained the correct insert in the proper orientation where both the  $\alpha$ - and  $\beta$ -subunits are expressed in the same direction. One was chosen and called pT7-7Taq $\beta/\alpha$  (Fig. 2-1C).

*Comparison of the Levels of Expression of T. aquaticus SCS Subunits and Whole Enzyme when Cells are Grown at 22 °C and 37 °C.* The plasmids pT7-7Taq $\alpha$ , pT7-7Taq $\beta$ , and pT7-7 $\beta/\alpha$  were expressed in the *E. coli* strain BL-21 (DE-3) grown at either 22 °C or 37 °C in the same way as was done for the original clones. Similarly, samples of the cultures were taken at various times and fractionated into supernatant and pellet fractions that were analyzed by SDS-PAGE. The supernatant fractions were assayed for their ability to catalyze the formation of succinyl-CoA at 22 °C, as usual. To assess the thermophilicity of the *T. aquaticus* enzyme, the supernatant fractions were also incubated at 70 °C for 30 min and then assayed for SCS activity at 70 °C. Due to the drop in pH that is observed when Tris buffer is heated, the buffer for the assay mixture was 10 mM potassium phosphate, pH 7.4 instead of Tris HCl.

*Labeling of the T. aquaticus SCS with [<sup>35</sup>S]-Methionine.* To investigate the stability of whole enzyme and its subunits *in vivo*, a pulse chase experiment using <sup>35</sup>S-methionine was carried out using the methods of Tabor (25). Cultures of BL-21(DE-3) cells containing pT7-7Taq $\alpha$ , pT7-7Taq $\beta$ , or pT7-7Taq $\beta/\alpha$  were grown at 37 °C overnight in LB broth (20) containing 0.1 mg/ml ampicillin, diluted 1/40 in the same broth, and allowed to grow at 22 °C or 37 °C until the absorbance at 600 nm had reached 0.5. 1.5 ml

of cells were then pelleted, washed with M9 media, resuspended in M9 medium containing 0.005% (w/v) of all the amino acids except Cys and Met, and allowed to grow further at either 22 °C or 37 °C for 60 min. Protein expression was then induced by the addition of IPTG to a final concentration of 1 mM, and cells were grown for a further 20 min before the addition of rifampicine (final concentration to 0.4 mg/ml) to inhibit the *E. coli* RNA polymerase. Cells were then allowed to grow for 60 min before labeling with 1.5  $\mu$ l (10  $\mu$ Ci) of  $^{35}$ S methionine for 5 min at 37 °C or 11 min at 22 °C followed by chasing with 300  $\mu$ l of 0.5 % (w/v) cold methionine. Samples of 200  $\mu$ l were taken at various times, and the cell debris and soluble fractions were separated as described by Horwich *et al.* (32). Cells were pelleted by centrifugation, resuspended in 8.0 ml of ice cold lysis buffer (25 % (w/v) sucrose 50 mM Tris HCl, pH 7.4), and incubated with 2.0 mg/ml lysozyme for 5 min at 37 °C. TENTA buffer (50 mM Tris HCl, pH 7.4, 1 % (v/v) 5 mM EDTA, 150 mM NaCl, Triton X-100) was added followed by incubation for 20 min at 37 °C. The lysed cells were then centrifuged at 15,000 x g for 15 min, and the pellet and supernatant fractions were separated. SDS-PAGE loading buffer was added to each fraction, and a sample of each fraction corresponding to 50  $\mu$ l of initial culture was analyzed by SDS-PAGE followed by autoradiography and quantification by phosphorimagery.

*N-terminal Sequencing and Mass Spectrometry of the Subunits of T. aquaticus SCS.* *T. aquaticus* SCS was partially purified by heating the BL-21 (DE-3) lysates to 70 °C for 30 min and centrifugation (14,000 rpm, 15 min) to remove the coagulated proteins. For N-terminal sequencing, the subunits were separated by SDS-PAGE, and then electroblotted onto a PVDF membrane. The membrane was then lightly stained using coomassie blue in 25 % (v/v) methanol and the bands which corresponded to the  $\alpha$ - and  $\beta$ -subunits were excised. These subunits were then sequenced by Edman degradation with a Hewlett Packard 1005A peptide sequencer. For mass spectrometry, the subunits were further purified using the same HPLC system as was used for separation of the *E. coli* SCS

subunits (see Chapter 3, Materials and Methods). The mass spectrometry was also performed in the same manner.

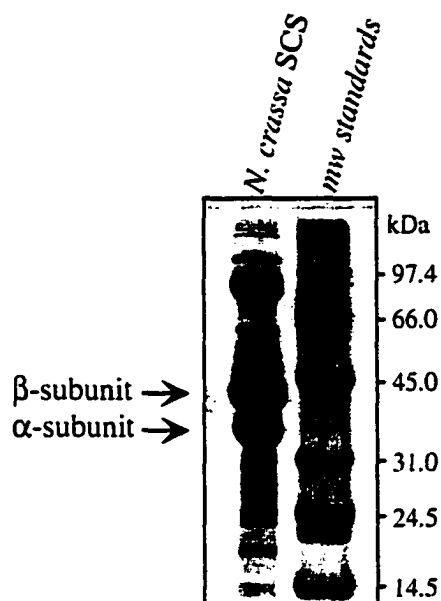
## Results and Discussion

### SECTION I: Cloning of *Neurospora crassa* SCS.

*Cloning of a Fragment of the  $\beta$ -subunit of *N. crassa* SCS.* An attempt was made to clone the ATP-specific SCS from the fungus *N. crassa* because of the hypothesis that the sequence information from the ATP-specific SCS would provide clues as to the determinants of the nucleotide specificity of SCS when compared to the sequences of the GTP-specific (pig heart) and the multi-specific *E. coli* SCS. The first step in cloning *N. crassa* SCS was to determine some amino acid sequence information which could be used to design primers for PCR. The SCS enzyme from *N. crassa* was first partially purified; and the subunits were separated by SDS PAGE (Fig. 2-2A) and blotted onto PVDF membranes. The N-terminus of each of the subunits was sequenced by Edman degradation, giving the sequences shown in Figure 2-2B. The DNA design of the sequence of the 5' primers for both the  $\alpha$ - and  $\beta$ -subunits were based on the region of the N-terminal amino acid sequence which had the lowest codon degeneracy. The design of the downstream 3' primers were based on sequences that were absolutely conserved in all species of SCS. In the case of the  $\alpha$ -subunit, this sequence was in the active site phosphohistidine loop (RMGHAGA). In the case of the  $\beta$ -subunit, it was a conserved sequence in the C-terminal half of the  $\beta$ -subunit (NIFGGIVR).

These primers were then used to probe a cDNA library of *N. crassa* sequences by PCR. The amplified fragments from PCR were subsequently cloned into pUC19 and sequenced. A sequence (Figure 2-3) similar to sequences of the  $\beta$ -subunit of SCS from other species was found. It is interesting to note, despite the eukaryotic origin of *N. crassa*

A



B

$\beta$ -subunit: NH<sub>2</sub>-M-K-I-H-E-Y-Q-G-K-E-I-L-R-K-F-G-V-A-V-P

$\alpha$ -subunit: NH<sub>2</sub>-S-I-L-T-N-K-D-T-K-V-I-T-Q-G-I-T-G-K-T-G

**Figure 2-2. Sequencing the N-terminus of the subunits of *N. crassa* SCS.** A. SDS-PAGE of partially purified *N. crassa* SCS. B. Amino acid sequence of the N-terminus of each subunit of *N. crassa* SCS. The subunits from the gel shown in (A) were electroblotted onto PVDF membrane, excised and sequenced by Edman degradation.



1 ATG AAA ATT CAC GAG TAT CAA GGT AAA GAA ATC CTG CGC CAG TTC GGC GTA ACC GTG CCG  
 1 met lys ile his glu tyr gln gly lys glu ile leu arg gln phe gly val thr val pro  
  
 61 CGC GGC ATT CCT TGC ATG TCG GTC GAC GAA GTC GAA GCG GCT GCC CAG AAG CTC GGC GGC  
 21 arg gly ile pro cys met ser val asp glu val glu ala ala ala gln lys leu gly gly  
  
 121 CCG GTG TGG GTC GTC AAG GCC CAG ATC CAT GCA GGC GGC CGC GGC AAG GGC-**GGT GGC** GTG  
 41 pro val trp val val lys ala gln ile his ala gly gly arg gly lys gly **gly gly** val  
  
 181 AAG GTG GCC AAG TCC ATC GAG CAG GTC AAG GAA TAC GCC AAC CAG ATC ATG GGC ATG CAG  
 61 lys val ala lys ser ile glu gln val lys glu tyr ala asn gln ile met gly met gln  
  
 241 CTG ATC ACC CAC CAG ACC GGC GCT GAA GGC CAG AAG GTG CGT CGC CTG CTG ATC GAA GAA  
 81 leu ile thr his gln thr gly ala glu gly gln lys val arg arg leu leu ile glu glu  
  
 101 GGC GCC GAC ATC AAG AAG GAA CTG TAC GTT TCC CTG GTC ACC GAC CGC GTC TCG CAA AAG  
 30 gly ala asp ile lys lys glu leu tyr val ser leu val thr asp arg val ser gln lys  
  
 361 GTC GTG CTG ATG GCC TCC AGC GAA GGC GGC ATG GAC ATC GAA GAA GTT GGC CAC AGC AAC  
 121 val val leu met ala ser ser glu gly gly met asp ile glu glu val gly his ser asn  
  
 421 CCG GAA AAA ATC CAC AAC GTC ATC ATC GAT CCG ATC GAT GGC CTG ACC GAC GCC CAA GCC  
 141 pro glu lys ile his asn val ile ile asp pro ile asp gly leu thr asp ala gln ala  
  
 481 GAC GAC GTG GCT GCC AAG ATC GGC GTG GCC GCT GAA TCG ATC CCG GCC GCT CGC CAG AAC  
 161 asp asp val ala ala lys ile gly val ala ala glu ser ile pro ala ala arg gln asn  
  
 541 CTG CAA GGC CTG TAC AAG GCT TAC TGG GAA ACC GAC GCT TCC CTG GCT GAA ATC AAC CCC  
 181 leu gln gly leu tyr lys ala tyr trp glu thr asp ala ser leu ala glu ile asn pro  
  
 601 CTG ATC CTG ACC GGC GAC GGC AAG GTC ATC GCC CTG GAC GCC AAG TTC AAC TTC GAC TCC  
 201 leu ile leu thr gly asp gly lys val ile ala leu asp ala lys phe asn phe asp ser  
  
 661 AAC GCC CTG TTC CGT CAC CCG GAA ATC GTC GCC TAC CGC GAC CTG GAC GAA GAA GAT CCG  
 221 asn ala leu phe arg his pro glu ile val ala tyr arg asp leu asp glu glu asp pro  
  
 721 GCT GAA GTC GAA GCC TCC AAG TTC GAC CTG GCC TAC ATC TCC CTG GAA GAC AAC ATC GAC  
 241 ala glu val glu ala ser lys phe asp leu ala tyr ile ser leu glu asp asn ile asp  
  
 781 TAC CTG ATC TCC GGT GCC GGC CTG GCC ATG GCC ACC ATG GAC ACC ATC AAG CTG TTC GGC  
 261 tyr leu ile ser gly ala gly leu ala met ala thr met asp thr ile lys leu phe gly  
  
 841 GGC GAG CCG GCC AAC TTC CTG GAC GTG GGC GGC GGC GCC ACC ACC GAG AAG GTC ACC GAA  
 281 gly glu pro ala asn phe leu asp val gly gly gly ala thr thr glu lys val thr glu  
  
 901 GCC TTC AAG ATC ATG CTG AAG AAC CCC GAA CTG AAG GCC ATC CTG GTT AAT ATC TTG GGG  
 301 ala phe lys ile met leu lys asn pro glu leu lys ala ile leu val asn ile leu gly  
  
 961 TGG AAT CTT GAA  
 321 trp asn leu glu

**Figure 2-3. Sequence of a fragment of the  $\beta$ -subunit of *N. crassa* SCS.**  
 The underlined nucleotides are the primer sequences, and the bold underlined amino acids indicate the borders of a deletion that is a characteristic feature of the  $\beta$ -subunit of SCS from eubacterial species.

(fungi), the alignment of the deduced amino acid sequence from the *N. crassa*  $\beta$ -subunit with other SCS sequences using the PIMA alignment program (33) indicated that it is most similar to the  $\beta$ -subunit sequence from eubacterial organisms (data not shown). This alignment is likely to be correct because the *N. crassa* sequence has a characteristic 10 amino acid deletion that distinguishes the  $\beta$ -subunit of eubacterial SCS from the  $\beta$ -subunit of eukaryotic SCS. The amino acids flanking the position of the deletion are indicated in bold in Figure 2-3. None of the fragments that were amplified using the primers directed to the  $\alpha$ -subunit resembled known  $\alpha$ -subunit sequences from other species.

*Screening a cDNA Library of N. crassa for the  $\alpha$ - and  $\beta$ -subunit Genes.* Since a fragment of the gene for the  $\alpha$ -subunit of SCS could not be cloned by screening the cDNA library using PCR, antiserum to the  $\alpha$ -subunit of rat liver SCS was used to screen an expression library of *N. crassa* sequences. In preliminary trials, this antiserum was shown to crossreact with *N. crassa* SCS. However, it also crossreacted with some components of a lysate of the *E. coli* strain Y1090, which was used as the bacterial lawn for plaque formation. Therefore, prior to the use of the antiserum for screening, the antiserum was purified by repeated incubation with nitrocellulose blots that were impregnated with lysates of *E. coli* Y1090. A western blot of SCS from pig heart, *E. coli*, *N. crassa* and Y1090 lysate with purified antiserum is shown in Figure 2-4. Using this antiserum, initial screens of approximately  $1 \times 10^6$  plaques gave six positive signals that were present on duplicate blots. Isolation of these plaques followed by repeated screening gave strong signals in secondary and tertiary screens. A representative autoradiogram of one of the secondary screens is shown in Figure 2-5A. The pBluescript phagemids that contained the insert DNA were excised from the  $\lambda$  phage genome and sequenced. Unfortunately none of the sequences were similar to known SCS sequences.

It should be noted that the fragment of the  $\beta$ -subunit of *N. crassa* SCS that was isolated by PCR was also used to screen a cDNA library of *N. crassa* sequences. The DNA

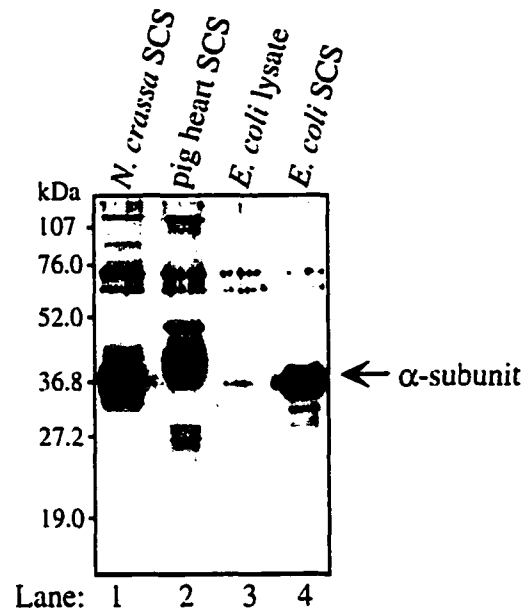


**Figure 2-4. Western blot with antibodies to the  $\alpha$ -subunit of rat liver SCS.** The subunits from *N. crassa* SCS (lane 1), pig heart SCS (lane 2), *E. coli* Y1090 lysate (lane 3) and *E. coli* SCS (lane 4) were separated by SDS-PAGE, electroblotted onto nitrocellulose membrane, and probed using purified antisera to the  $\alpha$ -subunit of rat liver SCS.

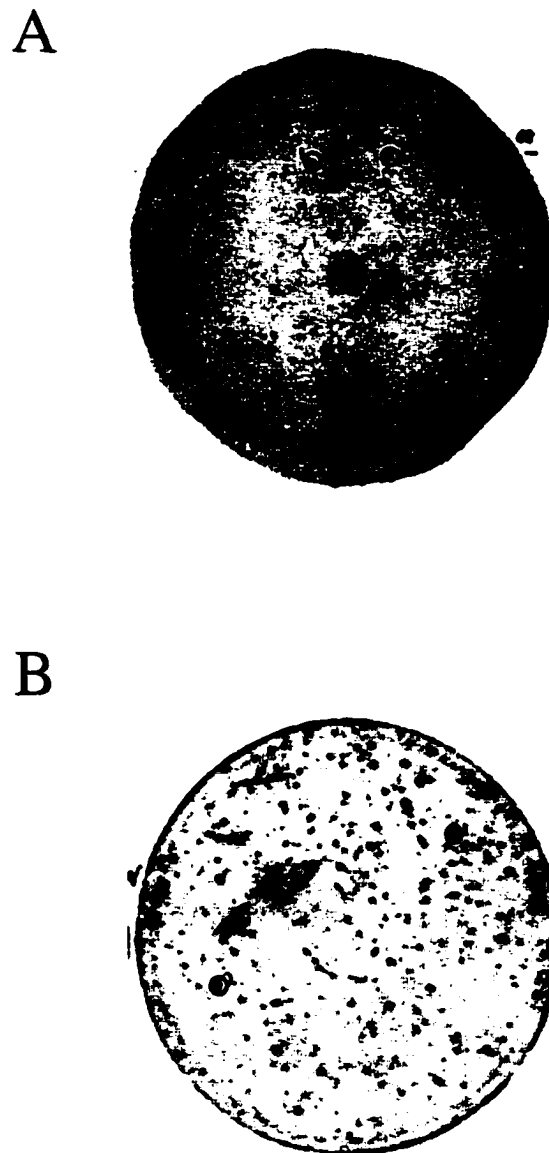


**Figure 2-5. Representative secondary screening of either (A) *N. crassa* expression library, or (B) *N. crassa* cDNA library.** In (A), *E. coli* Y1090 cells expressing a library of *N. crassa* proteins was probed with antisera raised to the  $\alpha$ -subunit of rat liver SCS. In (B), *E. coli* Y1090 cells containing a library of *N. crassa* cDNA sequences was probed with a labeled fragment of the  $\beta$ -subunit of *N. crassa* SCS. The circled and numbered positive plaques were chosen for sequencing.

fragment was labeled with digoxigenin-11-dUTP and used to probe DNA blots of the *N. crassa* library. Initial screens of approximately  $1 \times 10^6$  plaques gave nine positive signals that were present on duplicate blots. Again isolation of the positive plaques followed by re-screening gave strong positive signals (Fig. 2-5B), and again none of the sequences were similar to other SCS sequences. When the crystallographic structure of *E. coli* SCS was solved, this project was abandoned in favour of more productive avenues of exploration. Subsequent to the completion of this work it was discovered that other investigators also did not have any success in obtaining clones from this cDNA library (34).

## **SECTION II: Expression of mRNA for the GTP-specific $\beta$ -subunit of SCS in Newborn Pig Tissues.**

A previous investigation of the isoforms of the  $\alpha$ -subunit of pig SCS revealed that the PH-108 $\alpha$  isoform was regulated in a tissue specific manner (17). However, this isoform did not follow a pattern of regulation consistent with the presence of GTP-specific SCS activity. Prior to the completion of the work of Johnson *et al.* (12, 3), it was proposed that the  $\beta$ -subunit was responsible for the nucleotide specificity of SCS, and thus the mRNA for the GTP specific isoform of the  $\beta$ -subunit should be translated in a manner consistent with the expression of the GTP specific isoforms of SCS. To investigate this hypothesis, the mRNA from the  $\beta$ -subunit of GTP specific SCS was amplified by PCR from reverse transcribed mRNA from various pig tissues. The results are shown in Figure 2-6A. High levels of message were present in heart and liver, while low levels were present in muscle and brain. In heart and liver there were two separate bands, one of higher molecular weight, and one of lower molecular weight (Fig. 2-6A). As a control for the total amount of message extracted from each tissue, PCR of the mRNA for  $\beta$ -actin was performed, and approximately the same level of message was found in each tissue (Fig. 2-6B). As a negative control, PCR reactions were carried out on tissue samples that had been mock reverse-transcribed (i.e. no reverse transcriptase was added).

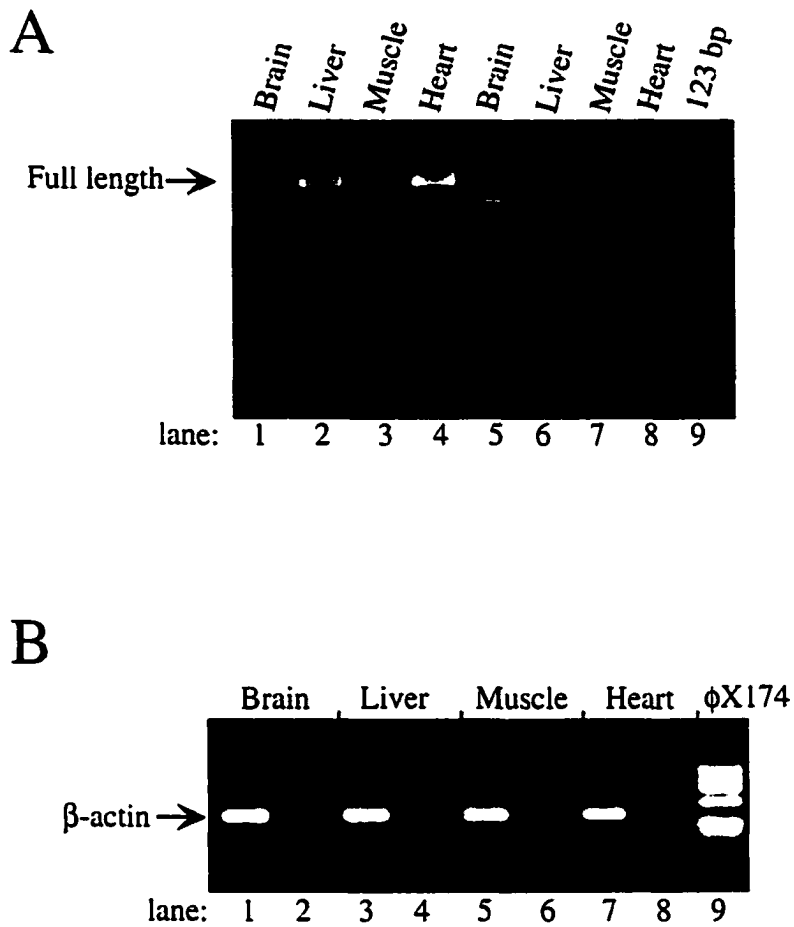


**Figure 2-6. PCR of reverse transcribed mRNA from pig tissues.** A. RT-PCR of full length  $\beta$ -subunit. Lanes 1-4 represent PCR of the full length  $\beta$ -subunit from reverse transcribed brain, liver, muscle, and heart mRNA, respectively. Lanes 5-8 represent the PCR of mock reverse transcribed mRNA where no reverse transcriptase was added. B. RT-PCR of  $\beta$ -actin mRNA. The lanes 1, 3, 5, and 7 represent the PCR of the  $\beta$ -actin gene from the same tissues as in A, and lanes 2, 4, 6, and 8 represent the PCR of mock reverse-transcribed mRNA. The standards were the 123bp ladder and  $\phi$ X174 DNA cleaved with *Hae* III.

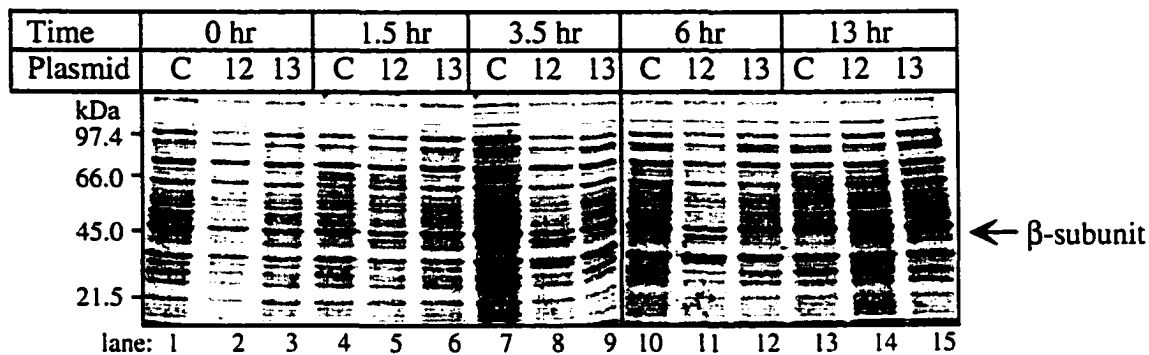
Both the higher molecular weight and lower molecular weight bands that were amplified from the reverse transcribed heart tissue in Figure 2-6A, were cloned into the TA cloning vector pCR2.1 and sequenced. The higher molecular weight band was GTP-specific SCS. Data base searches using the sequence of the lower molecular weight band did not reveal extended similarity to any other genes or proteins. The levels of the mRNA for the  $\beta$ -subunit in pig tissues were consistent with the GTP-specific activity in rat tissues, where in liver and heart it was 5 to 10 times higher than that found in brain and skeletal muscle (35). Thus, this was a preliminary indication that the  $\beta$ -subunit may be responsible for the nucleotide specificity of SCS.

### **SECTION III: Cloning and Expression of *T. aquaticus* SCS.**

*Cloning and Expression of Translationally Coupled SCS Subunit Genes from Thermus aquaticus.* To facilitate the study of the determinants of the stability of SCS, the genes for the  $\alpha$ - and  $\beta$ -subunits of SCS were cloned from a thermophilic bacterium, *Thermus aquaticus*. In *E. coli* and *T. flavus*, the genes for SCS subunits are expressed as an operon and are coupled translationally, the stop codon of the  $\beta$ -subunit overlaps with the start codon for the  $\alpha$ -subunit (36, 23). Based on the assumption that primary structure of *T. aquaticus* SCS would resemble that of *T. flavus*, the primers for PCR of *T. aquaticus* SCS were therefore designed for the start of the gene for the  $\beta$ -subunit and the end of the gene for the  $\alpha$ -subunit. PCR of genomic DNA from *T. aquaticus* resulted in the amplification of a single band of approximately 2 kbp, which was ligated into the expression vector pT7-7 and transformed into the *E. coli* strain BL-21(DE-3) for protein expression.

Two clones were chosen and were grown to mid-log phase prior to the induction of protein expression with IPTG at 37 °C. Samples were then taken at various times after induction of protein expression. As a control, protein expression was also induced in cells

A



B

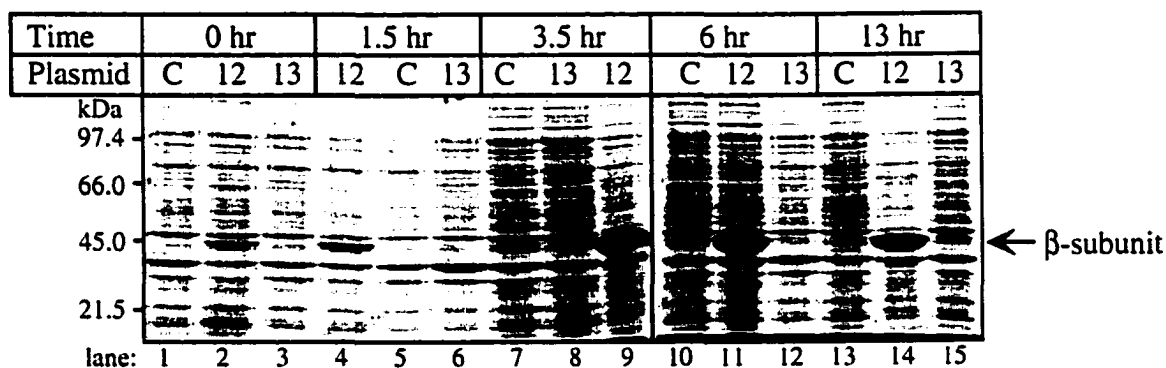


**Figure 2-7. Time course of expression of *T. aquaticus* SCS from the plasmids pT7-7Taq12 and 13.** A. SDS-PAGE of the supernatant fraction from lysates of *E. coli* BL-21(DE-3) cells that were induced for 0 h (lanes 1-3), 1.5 h (lanes 4-6), 3 h (lanes 7-9), 6 h (lanes 10-12), and 13 h (lanes 13-15). B. The pellet fractions from the same cell lysates. The cells for the samples in lanes 1, 4, 7, 10, and 13 (labeled C) contained the empty expression vector pT7-7. The cells for the samples in lanes 2, 5, 8, 11, and 14 (labeled 12) contained the *T. aquaticus* expression vector pT7-7Taq12, and lanes 3, 6, 9, 12, and 15 (labeled 13) contained pT7-7Taq13.



containing the empty expression vector pT7-7. The supernatant and pellet fractions of the cell lysate were analyzed by SDS-PAGE, and the time course of protein expression is shown in Figure 2-7. Only one of the clones expressed a significant amount of protein that was not present in the cells expressing empty vector. A band with an approximate molecular mass of 45 kDa appeared after 0 h of induction in the pellet fraction of lysed cells containing the plasmid pT7-7Taq12. This is likely to be due to leaky expression from the *lac* UV5 promoter. There is also a corresponding faint band present in the supernatant fraction after 3.5 h. The molecular mass of the  $\beta$ -subunit of *T. aquaticus* SCS as estimated by SDS-PAGE is 45 kDa, and thus this band is likely to be the  $\beta$ -subunit of *T. aquaticus* SCS. The presence of the  $\beta$ -subunit in the pellet fraction may be due to self-aggregation because of the absence of the  $\alpha$ -subunit. Consistent with the lack of expression of the  $\alpha$ -subunit, none of the supernatant fractions exhibited SCS activity greater than the background activity present in the lysates of cells containing the empty expression vector.

Both strands of the plasmid pT7-7Taq12 were sequenced, revealing a total of five amino acids that were different from the published sequences of the  $\beta$ -subunit of *T. flavus* SCS and the  $\alpha$ -subunit of *T. aquaticus* SCS. This was initially considered a strain to strain variation because another strain of *T. aquaticus*, called *T. aquaticus*-B, has six amino acid changes in the  $\alpha$ -subunit alone. The lack of expression of the  $\alpha$ -subunit may have been due to the sequences surrounding the translation start site. The start codon for the  $\alpha$ -subunit was GTG instead of the more common *E. coli* start codon, ATG. In addition, the sequence surrounding the ATG codon from -21 to +13, where the ribosome binding site should be, was 65 % GC as opposed to 12 % in the consensus sequence for ribosome binding sites in *E. coli* (reviewed in (37)). This likely reflects the thermophilicity of *T. aquaticus*, however it is also likely to be the reason for the lack of expression of the *T. aquaticus*  $\alpha$ -subunit in *E. coli*. The large differences seen in the nucleotide sequences of the ribosome binding site(s) between *T. aquaticus* and *E. coli*, may be indicative of a novel mechanism of ribosome binding site recognition and translation initiation in thermophilic

organisms. Finally, sequencing of the plasmid from the second clone (pT7-7Taq13), which did not produce any SCS protein, proceeded 48 nucleotides into the  $\beta$ -subunit gene and terminated, despite the presence of full length insert (as assayed by agarose gel electrophoresis of digested pT7-7Taq13) This may be due to the presence of secondary structure that prevented both T-7 DNA polymerase (Sequenase 2.0) and T-7 RNA polymerase from transcribing this DNA.

*Mutagenesis of the Start Codon and Ribosome Binding Site of the T. aquaticus SCS  $\alpha$ -Subunit Gene.* To improve the expression of the  $\alpha$ -subunit of SCS, the initiating GTG was mutated to ATG, both alone and in combination with changes to the ribosome binding site (Fig. 2-8A). The resulting expression plasmids, pT7-7Taq<sub>ATG</sub>, and pT7-7Taq<sub>RBS</sub> were initially tested for their ability to express *T. aquaticus* SCS in the *E. coli* strain BL-21(DE-3). Four hours after the induction of protein production, the cells were harvested and fractionated into the pellet and supernatant fractions by sonication and centrifugation, and then analyzed by SDS-PAGE (Fig. 2-8B). SCS purified directly from *T. aquaticus* by Ed Brownie was used a standard (11). The  $\alpha$ -subunit of this protein migrated as a doublet. This may be due to phosphorylated and nonphosphorylated  $\alpha$ -subunit, and has been seen in SCS from other species (11). Protein bands that migrate with the same mobility as the subunits of *T. aquaticus* SCS were evident in the pellet fraction. The levels of expression of the  $\beta$ -subunit were greater than those of the  $\alpha$ -subunit in cells that contained the pT7-7Taq<sub>ATG</sub> expression plasmid, however expression of the  $\alpha$ - and  $\beta$ -subunits was more balanced in cells which contained the pT7-7Taq<sub>RBS</sub> plasmid (compare lane 3 with lane 4 in Figure 2-8B). It was difficult to see if there was any expression of the  $\alpha$ -subunit of *T. aquaticus* SCS in the supernatant fractions, because proteins that migrated with the same mobility as the  $\alpha$ -subunit were present in the control. Despite the presence of both subunits of *T. aquaticus* SCS in the pellet fraction, no SCS activity above the background SCS activity of BL-21(DE-3) could be detected in any of the supernatant fractions. The *E. coli* strain BL-21(DE-3) expresses a relatively high amount

of *E. coli* SCS, and thus the activity of *T. aquaticus* SCS may have been masked by the background *E. coli* SCS activity. Therefore, the supernatant fractions were heated to 70 °C for 30 min to denature *E. coli* SCS, and then assayed for SCS activity. A small amount of SCS activity was evident, however the supernatant fractions from cells containing empty expression vector also had a small amount of SCS activity when treated in the same manner.

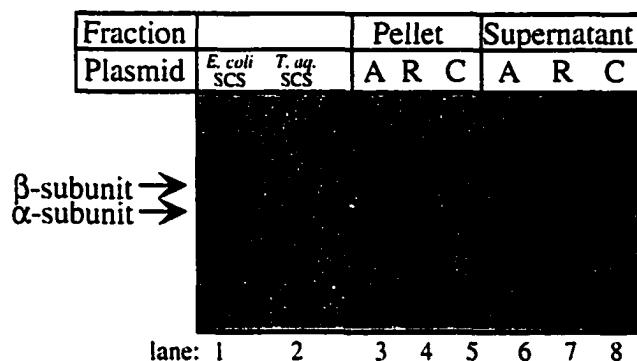
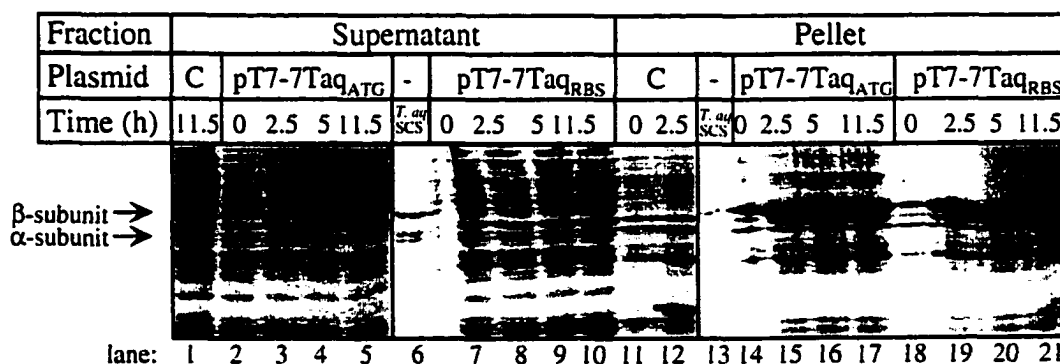
To avoid the high background of SCS activity, protein production from the expression vectors pT7-7Taq<sub>ATG</sub>, or pT7-7Taq<sub>RBS</sub> was studied in the SCS null strain TK3-D18, which does not have any background SCS activity. Cells containing these vectors were grown to mid-log phase and protein expression was induced by raising the growth temperature from 30 to 42 °C for various amounts of time. As a control, protein expression was also induced in cells containing the empty expression vector pT7-7. The cytosolic and cell debris fractions were separated by sonication followed by centrifugation, and the results of SDS-PAGE of these fractions are shown in Figure 2-8C. Again the majority of the expressed protein appeared in the pellet fractions. When the supernatant fractions were assayed for SCS activity, a small amount of activity was evident. In addition, this activity was still present after heating the cytosolic fraction to 70 °C for 30 min. This activity was not present in the supernatant fractions from cell lysates with empty expression vector. The amount of activity in the cytosolic fraction was not high enough to justify purification of *T. aquaticus* SCS from this fraction, so it was purified from the pellet fraction.

*Purification and Refolding of T. aquaticus SCS from Inclusion Bodies.* The production of *T. aquaticus* SCS was induced in TK3D18 cells containing pT7-7TaqRBS. The inclusion bodies were pelleted from cell lysates by centrifugation at low speed, and contaminating proteins were removed by homogenization in a Triton X-100 solution. SCS was then extracted from the inclusion bodies using 1.5 M, 2 M or 6 M guanidine HCl. The

**A**

pT7-7Taq<sub>ATG</sub>  
 $\alpha$ -subunit:                                   met ile leu val asn arg glu  
 GCCATGGTGGGAGGTGCGGCATGATCCTGCTGAACCGCGAG  
 $\beta$ -subunit: ala met val gly gly ala ala stop

pT7-7Taq<sub>RBS</sub>  
 $\alpha$ -subunit:                                   met ile leu val asn lys glu  
 GCAATGAAAGGAGGTAACAAATGATCCTAGTTAATAAAGAG  
 $\beta$ -subunit: ala met lys gly gly asn ile stop

**B****C**

**Figure 2-8. Expression of *T. aquaticus* SCS from the plasmids pT7-7Taq<sub>ATG</sub> and pT7-7Taq<sub>RBS</sub>.** A. The sequence changes in the start codon and ribosome binding site of the  $\alpha$ -subunit. B. SDS-PAGE of protein expression in BL-21(DE-3). Lane 1 contains *E. coli* SCS and lane 2 *T. aquaticus* SCS purified from *T. aquaticus*. Other lanes represent SDS-PAGE of the pellet (lanes 3-5) cytosolic (lanes 6-8) fractions from cells that were induced for 4 hrs. 'A' represents expression from pT7-7Taq<sub>ATG</sub>, 'R' represents expression from pT7-7Taq<sub>RBS</sub>, and 'C' represents expression from empty vector (pT7-7). C. SDS-PAGE of a time course of expression in TK3D18. As standards, lanes 6 and 13 contain *T. aquaticus* SCS. The supernatant fraction from cells with the plasmids pT7-7Taq<sub>ATG</sub> and pT7-7Taq<sub>RBS</sub> are shown in lanes 2-5 and 7-10, respectively. The pellet fractions from cells with the plasmids pT7-7Taq<sub>ATG</sub> and pT7-7Taq<sub>RBS</sub> are shown in lanes 14-17 and 18-21, respectively. As a control (labeled 'C'), the supernatant fraction from cells with empty expression vector induced for 11.5 h is shown lane 1, and the pellet those cells induced for 0 and 2.5 h are shown in lanes 11 and 12.

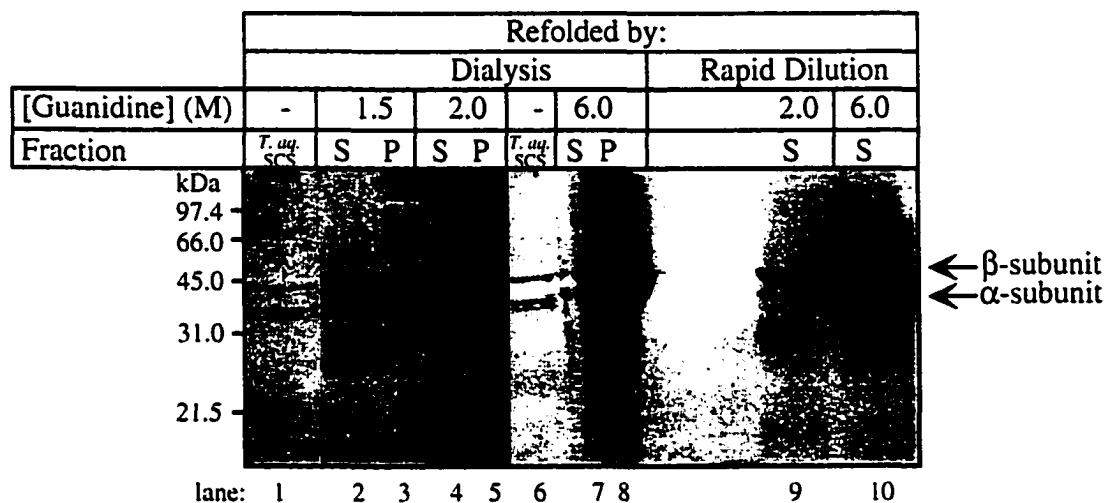


**Figure 2-9. Refolding of *T. aquaticus* SCS extracted from inclusion bodies.** SDS-PAGE of the soluble (labeled S, lanes 2, 4, 7) and insoluble (labeled P, lanes 3, 5, 8) fractions of *T. aquaticus* SCS refolded by dialysis, or the soluble fraction refolded by rapid dilution (lanes 9, 10). The material for refolding was extracted from inclusion bodies by washing with 1.5 M guanidine HCl (lanes 2, 3), 2.0 M guanidine HCl (lanes 4, 5, 9), or 6.0 M guanidine HCl (lanes 7, 8, 10). Lanes 1 and 6 contain *T. aquaticus* SCS.

extracted enzyme was refolded by two methods: either by dialysis overnight in benign buffer or by rapid dilution into 0.65 M arginine. Both the supernatant and any pellet fractions after refolding were subjected to SDS-PAGE. These results are shown in Figure 2-9. The greatest amount of SCS was extracted from the inclusion bodies by 2 M or 6 M guanidine HCl, although most of this precipitated after refolding by dialysis. Refolding by rapid dilution into arginine did not produce any precipitate, however there was a vast excess of the  $\beta$ -subunit over the  $\alpha$ -subunit. All of the supernatant fractions were also assayed for SCS activity and the results are shown in Table 2-1. The most successful extraction using these methods gave approximately 25 U per liter of culture that was not thermostable. For comparison, the yield of pure protein from preparations of *E. coli* SCS is approximately 500 U per liter of culture. Even taking into account the difference in specific activity between purified *E. coli* SCS (40 U/mg) and purified *T. aquaticus* SCS (13 U/mg) (38),

this was still a poor yield of impure enzyme. In addition, the extracted *T. aquaticus* SCS did not retain any enzymatic activity after heating to 70 °C for 30 min, indicating that it was not thermostable. Refolding of *T. aquaticus* SCS using the methods for refolding *E. coli* (39, 40) and pig heart (41) SCS were not successful.

Given that the small amount of SCS in the supernatant fraction was thermostable (Table 2-1), it was concluded that there was a problem with the folding of *T. aquaticus* SCS originally *in vivo* and subsequently *in vitro*. The *in vivo* folding problem may have been due to the unequal and rapid expression of the subunits of *T. aquaticus* SCS, or to the differences in amino acid sequence between this clone and the published sequence. To resolve these problems, I first addressed the question of whether these changes in sequence were due to strain to strain variation, or to errors in the cloning.

*Direct Sequencing of PCR Products from the T. aquaticus SCS Genes.* Two independent PCR reactions of the *T. aquaticus* SCS genes were carried out and the PCR products were sequenced directly. Both of these products matched the published

sequences (Fig 1-2 and 1-3) and neither had the changes in sequence that were observed in the original clone. This indicated that the changes were due to misincorporation of nucleotides by the *T. aquaticus* polymerase and not to strain to strain variation.

Table 2-1. SCS Activity During the Purification of Inclusion Bodies.<sup>a</sup>

Fractions:	Method of Refolding					
	No Refolding		Dialysis <sup>b</sup>		Rapid Dilution <sup>c</sup>	
70 °C for 30 min <sup>d</sup>	-	+	-	+	-	+
Supernatant	4.3 U/L	4.3 U/L	1.6 U/L	ND	ND	ND
Triton X-100	0.25 U/L	ND	0 U/L	ND	ND	ND
1.5 M Guanidine	0 U/L	ND	ND	ND	ND	ND
2.0 M Guanidine	10.5 U/L	0 U/L	1.1 U/L	ND	9.3 U/L	0 U/L
6.0 M Guanidine	25 U/L	0 U/L	0.3 U/L	ND	5.5 U/L	0 U/L

<sup>a</sup> A total of 6 L of *E. coli* TK3D18 cells were induced for 4 h and the cells harvested, lysed and the inclusion bodies were purified as described in Materials and Methods. Each fraction during this purification was assayed for the production of succinyl-CoA at 22 °C using ATP as described in Materials and Methods. 1 U is 1 μmole of succinyl-CoA formed in 1 min.

<sup>b</sup> Refolded by dialysis for 18 h at 22 °C against 50 mM Tris HCl, 5 mM 2-mercaptoethanol, and 0.1 % (v/v) glycerol, pH 7.5.

<sup>c</sup> Refolded by dilution 1:20 (v/v) into 0.67 M L-arginine, 50 mM potassium phosphate, pH 7.4 with constant vortexing, followed by incubation for 18 h at 22 °C.

<sup>d</sup> The fractions were heated to 70 °C for 30 min prior to the assay for SCS activity, in order to assess the heat stability of the enzyme.

ND not done.

*Independent Cloning and Expression of the Subunits of T. aquaticus SCS.* To address the rate of expression of each of the subunits of *T. aquaticus* SCS, expression vectors were made which expressed each subunit separately. The effect of temperature on the production of soluble protein was also examined. Using the primers that were used for the mutagenesis of the ribosome binding site, the genes for the α- and β- subunits of *T. aquaticus* SCS were amplified by PCR from genomic DNA. They were then cloned into the TA cloning vector pCR2.1 and subsequently into separate pT7-7 expression vectors

(Fig. 2-1A, B). The resulting plasmids were called pT7-7Taq $\alpha$  and pT7-7Taq $\beta$ . These clones were sequenced, and none of the changes that were observed in the original clones were observed in these clones.

When the tailspike protein of phage P22 was overexpressed in *E. coli*, it was found that the tendency of this protein to aggregate depended on the rates of expression and refolding (42). If the rate of expression exceeds the rate of refolding, the proteins come into contact with each other before they have completely folded and thus aggregate. To investigate the effect of the rate of expression of the  $\alpha$ - and  $\beta$ -subunits on the production of *T. aquaticus* SCS, each subunit was expressed at 22 and 37 °C in BL-21(DE-3) and the supernatant and pellet fractions were separated and analyzed by SDS-PAGE as described before (Fig. 2-10). Consistent with the observations for the tailspike protein (42), the expression of both subunits of *T. aquaticus* SCS produced more soluble protein at 22 °C than at 37 °C. In addition, the  $\alpha$ -subunit was expressed to a much greater extent than the  $\beta$ -subunit. This is consistent with the results of expression of individual subunits of *E. coli* and pig heart SCS (43), indicating that the  $\beta$ -subunit of SCS more prone to aggregation than the  $\alpha$ -subunit. Note that even at 37 °C, the production of soluble  $\beta$ -subunit is much greater than the levels that were observed in the original clones, indicating that the amino acid differences in the original clone were responsible for the malfolding of the  $\beta$ -subunit. This conclusion can be rationalized using sequence comparisons of *T. aquaticus* SCS with *E. coli* and pig heart SCS and the crystal structures of SCS. The first two changes, Ala 36 $\beta$  (in this clone) to Val (in the original clone) and Ile 44 $\beta$  to Thr, occur in the hydrophobic core of the N-terminal domain of the  $\beta$ -subunit, and the second two changes, Ala 369 $\beta$  to Val and Ile 370 $\beta$  to Thr, occur near the end of the C-terminal  $\alpha$ -helix, where it packs against the  $\beta$ -sheet in C-terminal domain. Thus, the changes that were observed in the original clones disrupt the folding of the  $\beta$ -subunit of SCS by interfering with the packing in the hydrophobic core. When the  $\alpha$ -subunit was expressed independently, again there was a much greater amount of soluble protein than in the



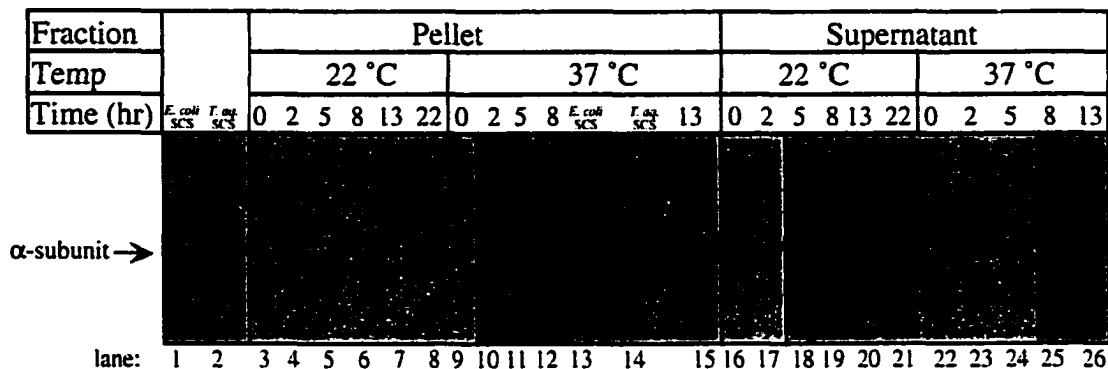
original clone. Unlike the  $\beta$ -subunit, the  $\alpha$ -subunit was never expressed to high levels, and the observed increase in soluble protein expression may simply be due to the proximal promoter and an improved ribosome binding site.

*Expression of Active, Thermostable, and Soluble T. aquaticus SCS.* To address the problem of unequal expression of the subunits of *T. aquaticus* SCS, an expression vector was constructed in which each subunit had its own promoter. This vector was called pT7-7Taq $\beta/\alpha$  (Fig. 2-1C). The effect of temperature on expression of whole enzyme from this vector in BL-21(DE-3) cells was investigated. As described for previous experiments, protein production was induced for various times at 22 and 37 °C. Again the supernatant and pellet fractions were separated and then analyzed by SDS-PAGE (Fig. 2-11). In addition, the SCS activity present in the soluble fractions was assayed both at room temperature and at 70 °C (Fig. 2-12). Similar to the expression of individual subunits, more soluble enzyme was produced when protein expression was carried out at 22 °C. Furthermore as seen in Figure 2-12, the activity of the expressed protein began to decline after 13 h when

expressed at 37 °C, whereas the activity of protein expressed at 22 °C continued to rise. The expressed enzyme was active when the assay was conducted at 70 °C. This demonstrated that the enzyme was thermostable. There was a greater increases in activity of the enzyme when the assays were conducted at 70 °C than when the assays were conducted at 22 °C. This is due to the greater specific activity of the enzyme at elevated temperatures, thus, the production of a certain amount of enzyme leads to a greater amount of succinyl-CoA production at 70 °C than at 22 °C.

The subunits of *T. aquaticus* SCS were subjected to mass spectrometry, following purification by heating to 70 °C and reverse phase HPLC. The measured mass of the  $\beta$ -subunit was 40641 Da. The predicted mass for the  $\beta$ -subunit is 40636 Da. The measured mass of the  $\alpha$ -subunit was 30510 Da, which is consistent with predicted mass of 30517 Da for the  $\alpha$ -subunit missing the N-terminal methionine residue. Edman degradation of the  $\alpha$ -

A



B

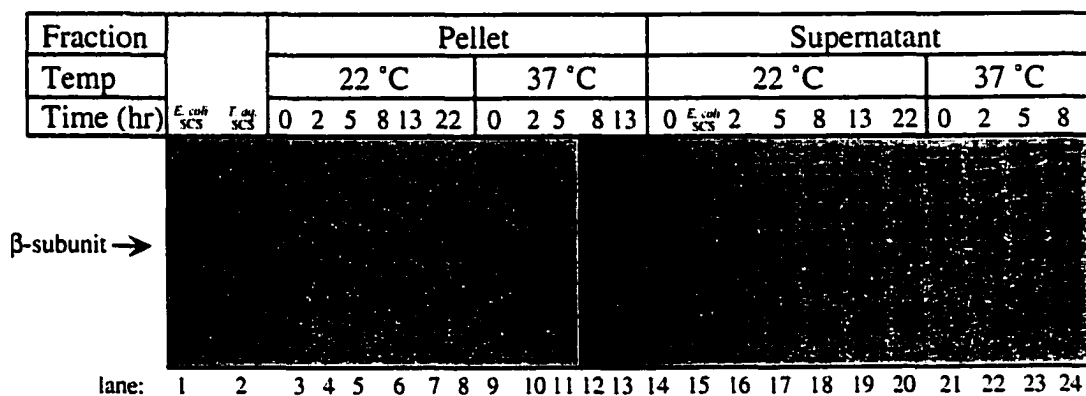
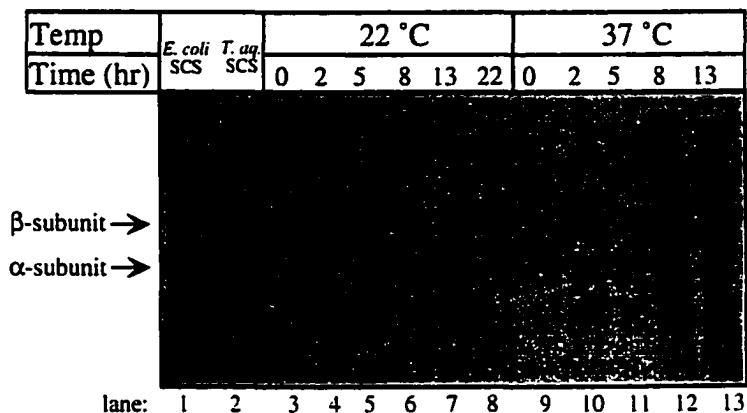


**Figure 2-10. Expression of the  $\alpha$ -subunit (A) and  $\beta$ -subunit (B) of *T. aquaticus* SCS.**  
 A. SDS-PAGE of the pellet and supernatant fractions of a time course of  $\alpha$ -subunit expression at 22°C (lanes 3-8, 16-21) and at 37 °C (lanes 9-12, 15, 22-26). As standards, Lanes 1 and 13 contain purified *E. coli* SCS, and lanes 2 and 14 contain purified *T. aquaticus* SCS. B. SDS-PAGE of the pellet and supernatant fractions of a time course of  $\beta$ -subunit expression at 22°C (lanes 3-8, 14, 16-20) and 37 °C (lanes 9-13, 21-24). Lanes 1 and 15 contain purified *E. coli* SCS, and lane 2 contains purified *T. aquaticus* SCS.

A



B

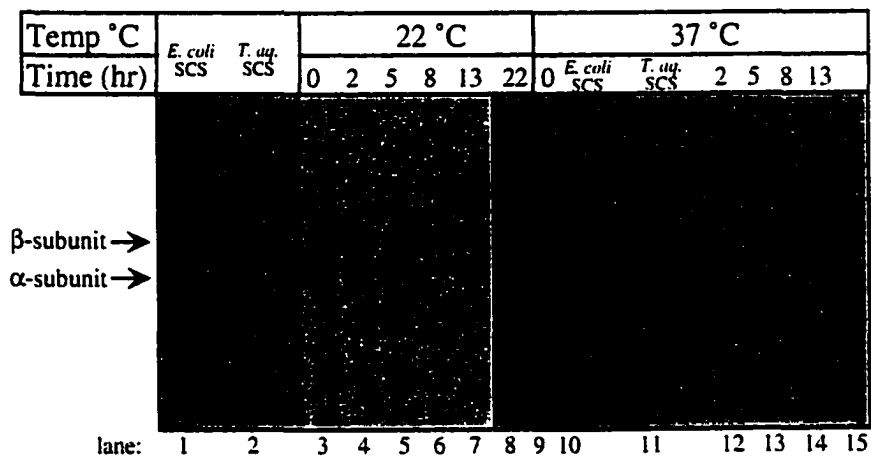


**Figure 2-11. Time course for the expression of soluble *T. aquaticus* SCS.** A. SDS-PAGE of the supernatant fractions following expression at 22 °C (lanes 3-8) and at 37 °C (lanes 9-13). As standards, lane 1 contains purified *E. coli* SCS, and lane 2, purified *T. aquaticus* SCS. B. SDS-PAGE of the pellet fractions following expression at 22 °C (lanes 3-8) and at 37 °C (lanes 9, 12-15). Again, as standards, lanes 1 and 10 contain *E. coli* SCS, and lanes 2 and 11 contain *T. aquaticus* SCS.

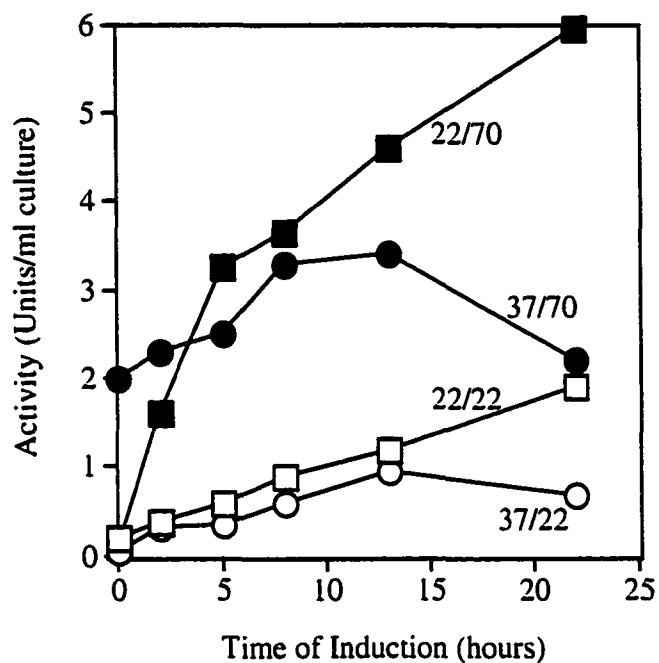


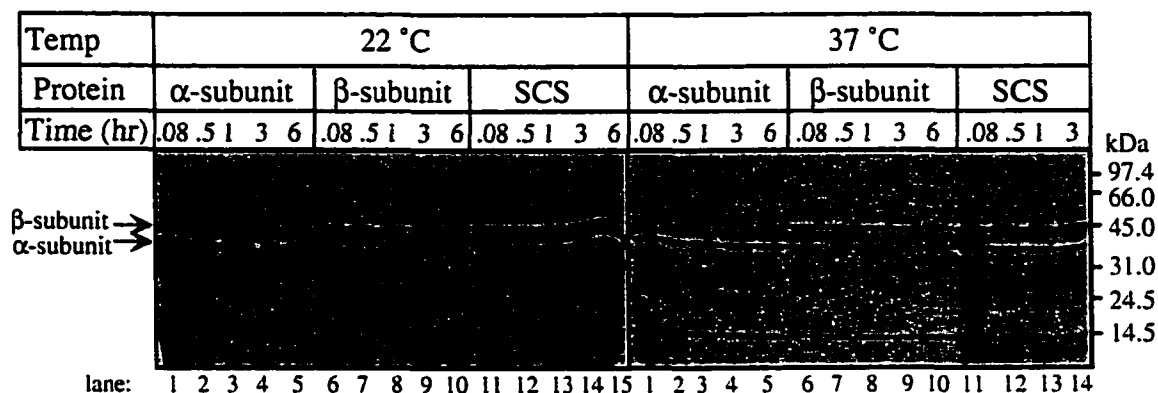
**Figure 2-12. Expression of soluble, active, and thermostable *T. aquaticus* SCS.** The supernatant fractions of a time course of whole enzyme expression at 22 °C (■, □) and 37 °C (●, ○) were assayed for SCS activity using ATP either at 22 °C (□, ○) or at 70 °C (■, ●). The activity is measured as  $\mu$ moles of succinyl-CoA production per minute per ml of culture. Note: no correction was made for the increase in the number of cells at later time points.

subunit gave the sequence ILVNKETRV, also missing the methionine. Expressed *E. coli* SCS also lacks the N-terminal methionine (Chapter 4).

*Labeling of T. aquaticus SCS with [<sup>35</sup>S]-Methionine.* To determine the half-life of whole enzyme and individual subunits *in vivo*, pulse chase experiments were performed. The whole enzyme or individual subunits were labeled with <sup>35</sup>S-methionine, followed by a chase with unlabeled methionine. To get approximately equal amounts of <sup>35</sup>S-methionine labeled protein, the labeling reaction at 22 °C was carried out for 11 min, while the labeling at 37 °C was carried out for 5 min. Samples of cells were then taken at various times after the addition of unlabeled methionine, the cells were lysed, and the supernatant and pellet fractions separated. The proteins in these fractions were then analyzed by SDS-PAGE, visualized by autoradiography (Fig. 2-13) and quantified by phosphorimager. The results of quantification of the labeling reactions after correction for the length of time of labeling, the specific activity of <sup>35</sup>S methionine, and the number of methionines in the  $\alpha$ - and  $\beta$ -subunits, are shown in Figure 2-14. Whole enzyme was stable in both the supernatant and pellet fractions; there was little degradation over the entire six hour time course. In whole enzyme expression, the ratio of  $\beta$ -subunit to  $\alpha$ -subunit is 3.8 to 1 at 22 °C and 6.8 to 1 at 37 °C. The lower rate of protein expression at 22 °C may have led to more efficient termination of transcription of the  $\beta$ -subunit (and thus less read-through), allowing relatively more RNA polymerase to initiate transcription of the  $\alpha$ -subunit.

Previous experiments by Haase-Pettingell and King (42) indicated that the rate of protein production was dependent on the temperature of induction. Consistent with those experiments, there was approximately 2 times more whole enzyme produced at 37 °C than at 22 °C (Fig 2-14A and B). It was assumed that a minimal amount of degradation occurred during the labeling reaction. This assumption may not be correct in the case of the individually expressed subunits. For example, there was approximately 2.3 times more  $\beta$ -subunit at 22 °C than at 37 °C (Fig 2-14C and D). This correlates with the rate of degradation of the  $\beta$ -subunit from the cytosol: half life of 3.5 h at 22 °C, and 1.5 h at 37 °C

A



B

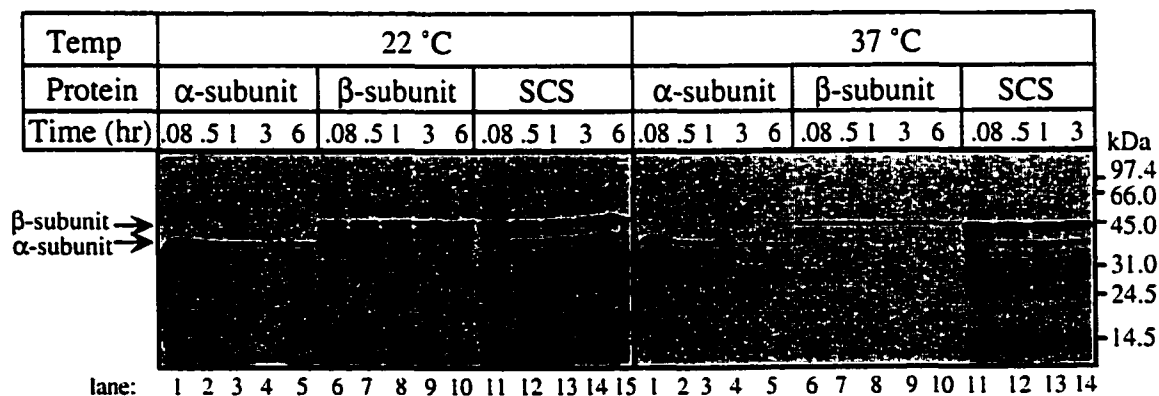


**Figure 2-13. Time course of degradation of [<sup>35</sup>S]-methionine labeled subunits and whole *T. aquaticus* SCS.** A. SDS-PAGE of labeled α-subunit (lanes 1-5), β-subunit (lanes 6-10), and whole enzyme (lanes 11-15) in the supernatant fraction. Labeling and degradation was carried out either at 22 °C or 37 °C. B. SDS-PAGE of the pellet fractions of the same time course. The positions of the molecular weight standards are shown in the right.

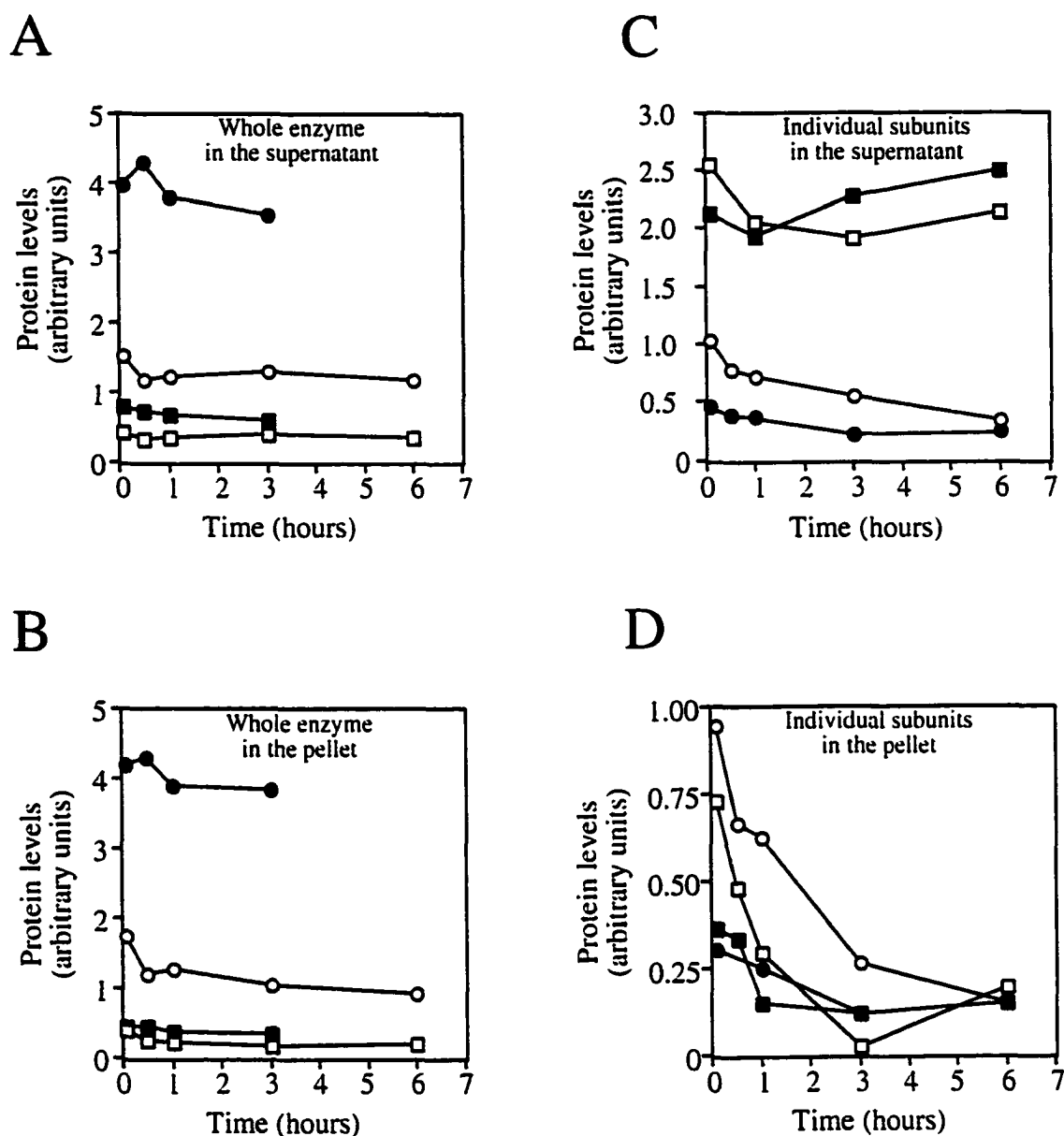


**Figure 2-14. Quantification of the degradation of [ $^{35}\text{S}$ ]-methionine labeled subunits and whole *T. aquaticus* SCS.** A and B represent quantification of whole enzyme in the supernatant and pellet fractions, respectively. C and D represent quantitation of individual subunits in the supernatant and pellet fractions, respectively. Labeling and degradation were carried out at 22 °C (○, □) or 37 °C (●, ■), and the levels of  $\alpha$ -subunit (■, □) and  $\beta$ -subunit (●, ○) were determined by phosphorimagery.

(Fig. 2-14C). Unexpectedly, the rate of degradation of the individually expressed  $\alpha$ - and  $\beta$ -subunits in the cell debris fraction was greater at 22 °C than 37 °C (Fig. 2-14D). When the individual subunits were expressed at 37 °C, there was a degradation product of approximately 14 kDa was observed in the supernatant fractions, which increased over the course of the reaction (Fig. 2-13A). Despite the increase in the rate of degradation at 22 °C, the degradation product is not present at 22 °C.



## References:

1. Murakami, K., Mitchell, T., & Nishimura, J. S. (1972) *J. Biol. Chem.* 247, 6247-6252.
2. Bailey, D. L., Wolodko, W. T., & Bridger, W. A. (1993) *Protein Sci.* 2, 1255-1262.
3. Johnson, J. D., Muhonen, W. W., & Lambeth, D. O. (1998) *J. Biol. Chem.* 273, 27573-27579.
4. McClellan, J. A., & Ottaway, J. H. (1980) *Comp. Biochem. Physiol.* 67B, 679-684.
5. Ottaway, J. H., McClellan, J. A., & Saunderson, C. L. (1981) *Int. J. Biochem.* 13, 401-410.
6. Weitzman, P. D. J., & Kinghorn, H. A. (1978) *FEBS Lett.* 88, 255-258.
7. Cha, S., Cha, C. J. M., & Parks, R. E. J. (1967) *J. Biol. Chem.* 242, 2577-2581.
8. Brownie, E. R., & Bridger, W. A. (1972) *Can. J. Biochem.* 50, 719-724.
9. Murakami, Y., & Nishimura, J. S. (1974) *Biochim. Biophys. Acta* 336, 252-263.
10. Bailey, D. L., Fraser, M. E., Bridger, W. A., James, M. N. G., & Wolodko, W. T. (1998) , *J. Mol Biol* 285, 1655-1666.
11. Brownie, E. R., & Bridger, W. A., personal communication.
12. Johnson, J. D., Mehus, J. G., Tews, K., Milavetz, B. I., & Lambeth, D. O. (1998) *J. Biol. Chem.* 273, 27580-27586.
13. Hamilton, M. L., & Ottaway, J. H. (1981) *FEBS Lett.* 123, 252-254.
14. Jenkins, T. M., & Weitzman, P. D. J. (1986) *FEBS* 205, 215-218.
15. Jenkins, T. M., Eisenthal, R., & Weitzman, P. D. J. (1988) *Biochem. Biophys. Res. Commun.* 151, 257-261.
16. Jenkins, T. M., & Weitzman, P. D. J. (1988) *FEBS Lett.* 230, 6-8.
17. Ryan, D. G., Lin, T., Brownie, E., Bridger, W. A., & Wolodko, W. T. (1997) *J. Biol. Chem.* 272, 21151-21159.
18. Wolodko, W. T., Kay, C. M., & Bridger, W. A. (1986) *Biochemistry* 25, 5420-5425.
19. Laemmli, U. K. (1970) *Nature* 227, 680.
20. Sambrook, J., Fritsch, E. F., & Maniatis, T. (1989) *Molecular Cloning: a laboratory manual*, 2 Ed., CSH Laboratory Press

21. Sanger, F., Nicklen, S., & Coulson, A. R. (1977) *Proc. Natl. Acad. Sci. USA* 74, 5463-5467.
22. Davis, D. G., Dibner, M. D., & Battey, J. F. (1986) *Basic Methods in Molecular Biology*, 1 Ed., Elsevier Science Publishing Co., Inc., New York
23. Nishiyama, M., Horinouchi, S., & Beppu, T. (1991) *Molecular & General Genetics* 226, 1-9.
24. Nicholls, D. J., Sundaram, T. K., Atkinson, T., & Minton, N. P. (1988) *Nucleic Acids Res.* 16, 9858-9858.
25. Tabor, S. (1990) in *Current Protocols in Molecular Biology* (Ausubel, F. A., Brent, R., Kingston, R. E., Moore, D. D., Seidman, J. G., Smith, J. A., & Struhl, K., eds), pp. 16.2.1-16.2.11, Greene Publishing and Wiley Interscience, New York
26. Studier, F. W., & Moffatt, B. A. (1986) *J. Mol. Biol.* 189, 113.
27. Ho, S. N., Hunt, H. D., Horton, R. N., Pullen, J. K., & Pease, L. R. (1989) *Gene* 77, 51-59.
28. Buck, D., & Guest, J. R. (1989) *Biochem. J.* 260, 737-747.
29. Froehlich, B., & Epstein, W. (1981) *J. Bacteriol.* 147, 1117-1120.
30. Mukhopadhyay. (1997) *Biotechnology* 56, 61-106.
31. Garboczi, D. N., Utz, U., Ghosh, P., Seth, A., J., K., VanTienhoven, E. A. E., Biddison, W. E., & Wiley, D. (1996) *J. Immunol* 157, 5403-5410.
32. Horwich, A. L., Low, K. B., Fenton, W. A., Hershfield, I. N., & Furtak, K. (1993) *Cell* 74, 909-917.
33. Smith, R. F., & Smith, T. F. (1992) *Protein Engineering* 5, 35-41.
34. Harkness, T., *personal communication*.
35. Weitzman, P. D. J., Jenkins, T. M., Else, A. J., & Holt, R. A. (1986) *FEBS* 199, 57-60.
36. Buck, D., Spencer, M. E., & Guest, J. R. (1985) *Biochemistry* 24, 6245-6252.
37. Gold, L., & Stormo, G. (1990) *Methods Enzymol.* 185, 89-93.
38. Brownie, E., *personal communication*.
39. Pearson, P. H., & Bridger, W. A. (1975) *J. Biol. Chem.* 250, 4451-4455.
40. Khan, I. A., & Nishimura, J. S. (1988) *J. Biol. Chem.* 263, 2152-2158.
41. Nishimura, J. S., Ybarra, J., Mitchell, T., & Horowitz, P. M. (1988) *Biochem. J.* 250, 429-434.
42. Haase-Pettingell, & King, J. (1988) *J. Biol. Chem.* 263, 4977-4983.

43. Ryan, D., *personal communication*.

**Page intentionally left blank for note taking.**

## **Chapter Three Folding of *T. aquaticus* SCS**

---

### **Introduction**

The question of how a polypeptide “matures” from a simple one dimensional sequence of amino acids to a complex three dimensional protein has been called the protein folding problem, and has been a basic question in biology for over 30 years (reviewed in (1-5)). The early work of Anfinsen and co-workers showed that proteins can fold reversibly (6, 7). This implied that the native structures of at least some small, globular proteins were in thermodynamically stable states, in conformations that were a global minimum of all of their accessible free energy states. It was later pointed out that there were far too many conformations of unfolded or partially folded polypeptides for the native conformation to be reached in a reasonable amount of time (8). To alleviate the long time required for the polypeptide to search all of conformational space to find the native conformation, Levinthal proposed the existence of protein folding pathways which directed protein folding to the native state in a reasonable amount of time (8). This proposal led to the search for relevant protein folding intermediates, and to the question of whether the intermediates were on or off the folding pathway. Due to new experimental approaches and to statistical models of protein folding, a ‘new view’ of protein folding has emerged. This new view takes into account both the presence of many conformations of the polypeptide and the search for the global minimum energy conformation in a reasonable amount of time (9-11). The analogy of energy landscapes has been used to describe this process. The landscape is shaped like a funnel with two horizontal axes representing conformational space and one vertical axis representing the energy of those conformations. The folding process is likened to skiers going down a mountain, each starts from a different point and may encounter different gullies and hills (representing folding intermediates and transition states, respectively), but all paths eventually lead to the bottom of the hill (the native conformation) (11). Thus, using the analogy of the energy landscape,

the folding intermediates that were formerly off the folding pathway (e.g. aggregation) are simply intermediates trapped in a gully with a particularly high energy transition state on the way to the native conformation.

Until recently it has been generally accepted that the early stages of protein folding are driven by the hydrophobic effect (2), that is, the clustering of hydrophobic residues away from the aqueous solvent into a hydrophobic core. For small proteins the unfolding and refolding data fit a two state kinetic model ( $D \rightleftharpoons N$ ), where denatured protein folds into the native form in a single step (12, 13). A recent model for protein folding, that is based on steric considerations of the polypeptide chain and the propensity for certain sidechains to favor the formation of specific secondary structures, has succeeded in simulating the local structures that form during the very early stages of folding without the involvement of non-local, hydrophobic, interactions (5). This implies that even a two state folding pathway proceeds in a stepwise manner, however intermediates cannot be detected. For larger proteins, a multistep process has been proposed where the first step may involve the collapse of the hydrophobic core, followed at some point by the rearrangement of residues to optimize their packing interactions (reviewed in (1, 2)). The examination of protein structures in the PDB, indicated that a polypeptide that is greater than 250 residues is just able to fold as one cooperative unit (14). Analysis of the PDB, using the existence of a domain and buried non-polar surface area as criteria, Nussinov and co-workers have defined a set of hydrophobic folding units (15). If the local residues in the polypeptide determine the initial secondary structures formed in folding, as Baldwin and Rose propose, and if there are discrete folding units in proteins, as Tsai and Nussinov propose, then this implies that proteins that have the same fold (secondary and tertiary structure) also follow the same folding pathway (or have similar energy landscapes). This seems to be the case for the cold shock protein CspB, a small all  $\beta$ -structure protein (13). This protein from *B. subtilis* is only marginally stable and folds by a rapid two state reaction. More stable

homologous proteins from *B. caldolyticus* and *T. maritima* fold by the same mechanism and with the same rates (13).

Given the similarity between the crystallographic structures of the *E. coli* and pig heart SCS (Fig. 1-13), and the extent of the similarity of the amino acid sequences between *T. aquaticus* SCS and these enzymes (57 and 47 % identity, respectively), the overall structure of the *T. aquaticus* enzyme is likely to resemble that of the *E. coli* and pig heart enzymes. If the proposals of Baldwin and Tsai are correct, the folding of the thermostable enzyme from *T. aquaticus* should be identical to the folding of the non-thermostable *E. coli* and pig heart enzymes. Thus, in this part of my studies, the folding of *T. aquaticus* SCS was investigated and compared to that of *E. coli* SCS. Toward this end, *T. aquaticus* SCS was characterized with respect to its equilibrium unfolding and its kinetics of refolding, and these results were compared to the unfolding and refolding of *E. coli* and pig heart SCS that have been done previously (16-18). In addition, an investigation of the basis for the relative stability of the *E. coli*, pig heart, and *T. aquaticus* enzymes was carried out by comparison of the amino acid differences between these enzymes. The structure of the *E. coli* enzyme, and the amino acid sequence alignment of known SCS enzymes (Fig. 1-2 and 1-3) were used to predict ion pairs in *T. aquaticus* SCS, and to evaluate their potential in stabilizing the enzyme. Moreover, the secondary structure in the model of *E. coli* SCS was also used as a basis to examine if the substitutions that occurred in the *T. aquaticus* enzyme might stabilize its secondary structure.

## Materials and Methods

*Purification of T. aquaticus SCS.* *E. coli* strain BL-21(DE-3) cells containing the plasmid pT7-7Taq $\beta/\alpha$  were grown at 22 °C to a cell density absorbance at 600 nm before the addition of IPTG to a final concentration of 0.5 mg/ml (to induce protein production from the expression vector) and further growth for 10 hours. The cells were harvested by centrifugation, resuspended in sonication buffer (100 mM KCl, 0.1 mM EDTA, 0.1 mM

PMSF, 1 mM benzamidine, 10 mM 2-mercaptoethanol, 1 % (v/v) glycerol, and 100 mM potassium phosphate, pH 7.4), and frozen at -70 °C. They were then thawed, sonicated two times for 3 min each at 4 °C using a Biosonic IV sonicator (Brownwill Scientific) set at an intensity of 70 and equipped with the large probe. The cell debris was then removed by centrifugation for 30 min at 4200 x g, and the crude supernatant was heated at 70 °C for 30 min with occasional stirring. The suspension was allowed to cool to 22 °C and then clarified by centrifugation at 4 °C for 30 min at 4200 x g. The pellet was discarded,  $(\text{NH}_4)_2\text{SO}_4$  was added to a final concentration of 20 % (w/v) and the resulting suspension was allowed to stand overnight at 4 °C. The next day the precipitate was collected by centrifugation for 30 min at 4200 x g. The pellet fraction containing *T. aquaticus* SCS was dissolved in Buffer A (10 mM potassium phosphate , 10 mM 2-mercaptoethanol, 0.1 mM EDTA, 0.1 mM PMSF, 1.0 mM benzamidine, pH 7.4) and the protein solution desalted by gel filtration through a Sephadex G-50 column prior to anion exchange chromatography. For anion exchange chromatography, the protein was bound to a Q-Sepharose fast flow column (diameter 2.5 cm, height 50 cm) which was first eluted with one liter of Buffer A, and then with a 1.5 liter linear gradient from 0 to 0.75 M KCl in Buffer A. The *T. aquaticus* SCS in fractions that eluted 0.39 and 0.42 M KCl were precipitated using 20 % (w/v)  $(\text{NH}_4)_2\text{SO}_4$  . The precipitate was then dissolved in 100 mM potassium phosphate , 10 mM 2-mercaptoethanol, pH 7.4, and *T. aquaticus* SCS further purified by gel filtration chromatography with the same buffer. For gel filtration chromatography, a Bio-Gel A 0.5M column (diameter 2.5 cm, height 120 cm) was used, and *T. aquaticus* SCS eluted between 410 and 428 ml. These fractions were pooled and the enzyme stored as a suspension in 20 % (w/v)  $(\text{NH}_4)_2\text{SO}_4$ . SDS-PAGE of samples taken at various stages of the purification of *T. aquaticus* SCS are shown in Figure 3-1.



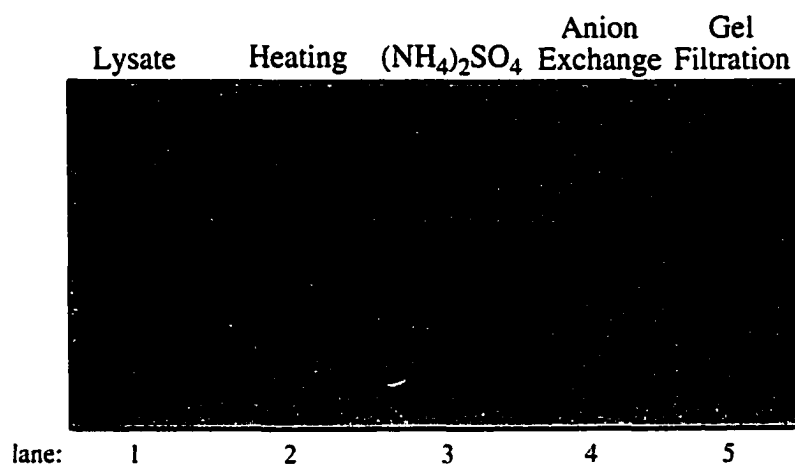


**Figure 3-1. SDS-PAGE analysis of the purification of *T. aquaticus* SCS.** Lane 1, cell lysate; lane 2, supernatant after heating to 70 °C for 30 min; lane 3, pellet fraction after a 20 % (NH<sub>4</sub>)<sub>2</sub>SO<sub>4</sub> precipitation; lane 4, pooled fractions from the Q-sepharose column; lane 5, pooled fractions after gel filtration chromatography.

*Analysis of the pH Profile of T. aquaticus SCS.* For pH profile analysis, an aliquot of the enzyme suspension in  $(\text{NH}_4)_2\text{SO}_4$  was centrifuged ( $15 \times 10^3 \times g$ , 30 min, 4 °C), and the pellet was dissolved in 500  $\mu\text{l}$  of 50 mM KCl, 0.1 mM EDTA, 50 mM Tris HCl, pH 7.4. The resultant solution was clarified by centrifugation ( $15 \times 10^3 \times g$ , 30 min, 4 °C), and dialyzed for 16 h with three changes of the same buffer at 4 °C. The ability of *T. aquaticus* SCS to catalyze the formation of succinyl-CoA from ATP, CoA and succinate was tested over a range of pH from 6.2 to 9.6. A 1.9  $\mu\text{g}$  sample of *T. aquaticus* SCS was placed in 1 ml of a buffer containing 10 mM  $\text{MgCl}_2$ , 50 mM KCl, 0.1 mM DTT, 10 mM succinate, 0.1 mM CoA, 0.4 mM ATP and 50 mM of either MOPS (pH 6.2 - 8.2) or Tris HCl (pH 8.0 - 9.6), and the formation of the thioester bond in succinyl-CoA was measured spectrophotometrically at 235 nm. When conducted at pH 7.4 and 22 °C, this is the standard assay for SCS activity (19).

*Steady State Kinetic Analyses of T. aquaticus SCS.* For kinetic analyses, an aliquot of the enzyme suspension in  $(\text{NH}_4)_2\text{SO}_4$  was centrifuged at  $15 \times 10^3 \times g$ , for 30 min, at 4 °C), and the pellet was dissolved in 500  $\mu\text{l}$  of 50 mM KCl, 0.1 mM EDTA, 50 mM Tris HCl, pH 7.4. The resultant solution was clarified by centrifugation ( $15 \times 10^3 \times g$ , 30 min, 4 °C), and dialyzed for 16 h with three changes of the same buffer at 4 °C. The concentrations of the nucleotides and CoA were determined using their standard extinction coefficients for a 1 cm pathlength (ATP:  $E_{259 \text{ nm}} = 15.4 \text{ mM}^{-1}$ , GTP:  $E_{252 \text{ nm}} = 13.7 \text{ mM}^{-1}$ , CoA:  $E_{260 \text{ nm}} = 14.6 \text{ mM}^{-1}$ ). SCS enzymatic activity was measured spectrophotometrically in the direction of succinyl-CoA formation at 22 °C. For each substrate, the initial velocity was measured at various concentrations and at a constant concentration of the other substrates (where appropriate, 114  $\mu\text{M}$  CoA, 10 mM succinate or 405  $\mu\text{M}$  ATP or GTP) in a total volume of 1 ml containing 50 mM KCl, 10 mM  $\text{MgCl}_2$ , 50 mM Tris HCl, pH 8.0. Initial rates were measured in duplicate at each concentration of substrate, and the initial velocity data were analyzed for the  $K_{m(\text{app})}$  and  $V_{\text{max}}$  values using the ENZYME KINETICS 1.11 program for a Macintosh computer (20). Oxaloacetate, acetoacetate, and malic acid

were also tested for their ability to substitute for succinate as a substrate for SCS by using 20 mM of each and 3.4  $\mu\text{g}$  of *T. aquaticus* SCS in the spectrophotometric assay.

*Activity of T. aquaticus, E. coli and Pig Heart SCS at Different Temperatures and Denaturant Concentrations.* The stability of SCS was investigated by measuring the activity of all three enzymes at different temperatures. The activity measurements for the temperature versus activity profile of the three enzymes were carried out with similar solutions as given above, except that 10 mM potassium phosphate, pH 7.4, was used as the buffer in the assay media because of the small variation in  $\text{pK}_a$  with temperature (-0.01 pH unit from 25 to 50 °C). The amounts of enzyme used for each assay of the profile were: 3.8  $\mu\text{g}$  of *T. aquaticus* SCS, 0.87 mg of *E. coli* SCS, and 0.82 mg of pig heart SCS. The enzymes, assay media, and cuvettes were incubated in a water bath for a minimum of 15 min at each temperature. The temperature of the cuvette holders on a Varian Cary 219 spectrophotometer was kept constant at each temperature by a Polyscience Polytemp circulating water bath. The temperature was increased incrementally for each temperature point throughout the profile.

The stability of SCS was also investigated by measuring the activity of all three SCS enzymes after incubation in 60 mM potassium phosphate, pH 7.4, and different concentrations of urea (0 M - 10 M) or guanidine HCl (GuHCl) (0 M - 4.0 M) at 22 °C for 24 hours.

*Gel Filtration Chromatography of T. aquaticus SCS.* To study the quaternary structure of *T. aquaticus* SCS in the presence and absence of GuHCl, and to separate the subunits, gel filtration chromatography was performed using a Sepharose 12 HR 10/30 FPLC column, and a Varian Vista 5500 liquid chromatograph. The flow rate was 0.5 ml/min, and where needed one fraction was collected each minute. First, to study the quaternary structure of *T. aquaticus* SCS a mixture of 5 mg/ml *T. aquaticus* and 5 mg/ml pig heart SCS in 60 mM potassium phosphate, 5 mM 2-mercaptoethanol, 0.1 mM EDTA, pH 7.4 was separated by gel filtration chromatography. Next, to study the quaternary

structure of *T. aquaticus* SCS just after it has lost activity in GuHCl, 5 mg/ml *T. aquaticus* SCS was incubated for 24 hours in 1.8 M GuHCl, 60 mM potassium phosphate, 5 mM 2-mercaptoethanol, 0.1 mM EDTA, pH 7.4, and then chromatography was performed in the same buffer. To study the quaternary structure of the *T. aquaticus* SCS in 3.0 M GuHCl, 5 mg/ml *T. aquaticus* SCS was incubated for 24 hours in 3.0 M GuHCl, 60 mM potassium phosphate, 5 mM 2-mercaptoethanol, 0.1 mM EDTA, pH 7.4, and then chromatography was performed in the same buffer.

*Far UV-CD of T. aquaticus Whole Enzyme and Isolated Subunits in Guanidine HCl.* The stability of the secondary structure of *T. aquaticus* SCS in different concentrations of GuHCl was investigated using far UV circular dichroism. The buffer for UV-CD was 60 mM potassium phosphate, 5 mM 2-mercaptoethanol, 0.1 mM EDTA, pH 7.4, and various concentrations of Guanidine HCl between 0 and 7.5 M. The subunits were separated at 3.0 M GuHCl, and were then dialyzed in 60 mM potassium phosphate, 5 mM 2-mercaptoethanol, 0.1 mM EDTA, pH 7.4, and far UV-CD in different concentrations of GuHCl was performed. The concentration of whole enzyme was 9.0  $\mu\text{M}$  or 2.2  $\mu\text{M}$ , the concentration of  $\alpha$ -subunit was 16.2  $\mu\text{M}$ , and the concentration of  $\beta$ -subunit was 10.0  $\mu\text{M}$ . UV-CD measurements were made using a Jasco J-720 spectropolarimeter (Jasco Inc., Easton MD) interfaced with an Epson Equity 386/25 computer and controlled by Jasco software. The thermostatted cell holder was maintained at 25 °C with a Lauda RMS circulating water bath. The instrument was routinely calibrated with ammonium d-(+)-10 camphor sulfonate at 290.5 nm and 192 nm, and with d-(-)-pantoyllactone at 219 nm. Each sample was scanned ten times from 180 to 255 nm and data were measured every 0.05 nm and averaged. Noise reduction was then applied to remove the high frequency noise prior to calculating molar ellipticities. A cuvette with a calibrated pathlength of 0.02 cm was used for all measurements. Molar ellipticities in  $\text{deg}\cdot\text{cm}^2/\text{dmol}$  were calculated with the following equation:

$$[\Theta] = \Theta_{\text{obs}} \times \text{MRW} / (10 \times l \times c)$$

where  $\Theta_{\text{obs}}$  is the ellipticity measured in millidegrees, MRW is the mean residue weight (molecular weight divided by the number of residues),  $l$  is the optical pathlength in cm, and  $c$  is the protein concentration in mg/ml.

**Sedimentation Equilibrium Analysis.** To study the quaternary structure of *T. aquaticus* SCS before and after the loss of activity in Guanidine HCl, sedimentation equilibrium experiments were performed in the absence and in the presence of two different concentrations of GuHCl. Prior to centrifugation, samples of *T. aquaticus* SCS were dialyzed for 16 hours at 20 °C with three changes of the appropriate buffer. For analysis of the quaternary structure of *T. aquaticus* SCS in the absence of GuHCl, 20 mM potassium phosphate, 2 mM dithiothreitol, pH 7.4, was used as buffer, and three separate loading concentrations of 1.77 mg/ml, 1.31 mg/ml, and 0.8 mg/ml were used for centrifugation. For analysis in the presence of GuHCl, two concentrations of guanidine were used, one slightly before the enzyme started to lose activity (0.9 M GuHCl, 60 mM potassium phosphate, 5 mM 2-mercaptoethanol, 0.1 mM EDTA, pH 7.4), and the other slightly after the enzyme lost activity (1.8 M GuHCl, 60 mM potassium phosphate, 5 mM 2-mercaptoethanol, 0.1 mM EDTA, pH 7.4). The loading concentrations for these runs were 5 mg/ml, 3 mg/ml, and 1 mg/ml. All sedimentation equilibrium experiments were carried out at 20 °C using a Beckman XL-1 Ultracentrifuge and interference optics according to procedures outlined by the manufacturer. Sample aliquots of 110  $\mu$ l were loaded into 6 sector-CFE sample cells. This allows for the three different loading concentrations of protein to be run simultaneously. The runs at two different speeds were continued until there was no difference in scans that were taken 3 h apart.

The sedimentation equilibrium data was analyzed using a nonlinear least-squares curve-fitting algorithm (21) contained in the NonLin analysis program (22). The following equation, which is based on a single ideal species, was used to fit the data:

$$C_r = e \left[ \ln(C_r) + \frac{(1 - \bar{v}\rho)\omega}{2RT} M(r^2 - r_0^2) - BM(C_r - C_r) \right]$$

where  $C_r$  is the concentration at radius,  $r$ ;  $C_{r_0}$  is the concentration at the reference radius,  $r_0$ ;  $\bar{v}$  is the partial specific volume;  $\rho$  is the density of the solvent;  $\omega$  is the angular velocity;  $R$  is the universal gas constant;  $T$  is the temperature in degrees Kelvin;  $M$  is the molecular weight; and  $B$  is a second virial coefficient term associated with non-ideality. The convergence of each variable was considered complete when the change in the variance was less than  $1 \times 10^{-6}$ . The program Sednterp (23) was used to calculate the partial specific volume of the *T. aquaticus* SCS using the method of Cohn and Edsall (24). For the runs that contained GuHCl, the method of Laue was used to apply a correction to  $\bar{v}$  for the binding of GuHCl to the enzyme and the change in hydration (25).

*Refolding of T. aquaticus SCS.* The native enzyme was first denatured by incubation in 6 M GuHCl for 24 hours. Refolding was carried out by rapid dilution (1:20 v/v) into one of three solutions: benign buffer (60 mM potassium phosphate, 50 mM KCl, pH 7.4), or pH 7.4 arginine refold buffer (0.67 M L-arginine HCl, 60 mM potassium phosphate, pH 7.4), or pH 8.0 arginine refold buffer (0.67 M L-arginine HCl, 60 mM potassium phosphate, 50 mM Tris HCl, pH 8.0). Samples were then taken after 5 hours and assayed for their ability to catalyze the formation of succinyl-CoA at pH 8.0 in the standard manner.

The kinetics of refolding *T. aquaticus* SCS was followed in the same manner using the pH 7.4 arginine refold buffer, except that samples were taken at various times. The temperature dependence of the kinetics of refolding *T. aquaticus* SCS was investigated by rapid dilution into pH 7.4 arginine refold buffer at 12 °C, 22 °C or 37 °C. Samples were then taken at various times and assayed for the ability catalyze the formation of succinyl-CoA. The concentration dependence of the kinetics of refolding at 22 °C was investigated by the same procedure (including the dilution factor) using final protein concentrations in the refolding mixtures of 0.59 mg/ml, 0.24 mg/ml, and 0.059 mg/ml.

*Correlation Between Relative Stability and Amino Acid Substitutions in Pig heart, E. coli and T. aquaticus SCS.* SCS from pig heart, *E. coli* and *T. aquaticus* had different

relative stabilities as judged by the loss of activity with increasing temperature, and increasing concentrations of urea or GuHCl. The substitutions within the amino acid sequences between these enzymes were examined for a correlation with stability. A count was made of the number of times an amino acid in an enzyme of lower stability was changed to any other amino acid in an enzyme of higher stability. This was considered a 'more stable' substitution. The reverse was also counted, that is, the number of times an amino acid in an enzyme of higher stability was changed to any other amino acid in an enzyme of lower stability. This was considered a 'less stable' substitution. Thus, the substitution is judged based on the enzyme species being compared, not on any intrinsic property of the amino acids involved. For example, a Ser in pig heart SCS changed to a Thr in *E. coli* or *T. aquaticus* SCS was counted as a 'more stable' substitution, as was a Ser in *E. coli* SCS changed to a Thr in *T. aquaticus* SCS. But in the opposite direction, a Ser in *T. aquaticus* SCS changed to a Thr in pig heart or *E. coli* SCS, or a Ser in *E. coli* SCS changed to a Thr in pig heart SCS was counted as a 'less stable' substitution.

*Potential Ion Pairs in Pig heart, E. coli and T. aquaticus SCS.* The number of ion pairs in *E. coli*, pig heart and *T. aquaticus* SCS were compared to see if they correlated with the stability of these enzymes. The ion pairs in *E. coli* and pig heart SCS were identified by examining the crystallographic structures of these enzymes (26-28). An ion pair was postulated to exist when the NZ of Lys, or the NH1 or NH2 of Arg, were within 4.0 Å of the OD1 or OD2 of Asp, or the OE1 or OE2 of Glu. These distances were measured using the program CONTACT from the CCP4 package (29).

To predict the potential ion pairs in *T. aquaticus* SCS, the sequence alignments of *E. coli* and *T. aquaticus* SCS shown in Figures 1-2 and 1-3 were examined in conjunction with the crystal structure of *E. coli* SCS. The distances between the  $\alpha$ -carbons of the residues in *E. coli* SCS that were thought to participate in an ion pair were found to be between 4.0 Å and 12 Å. A plot of the distances between all  $\alpha$ -carbon atoms in *E. coli* SCS was constructed using the PLOTDIST set of programs written by Joe Parish (30)

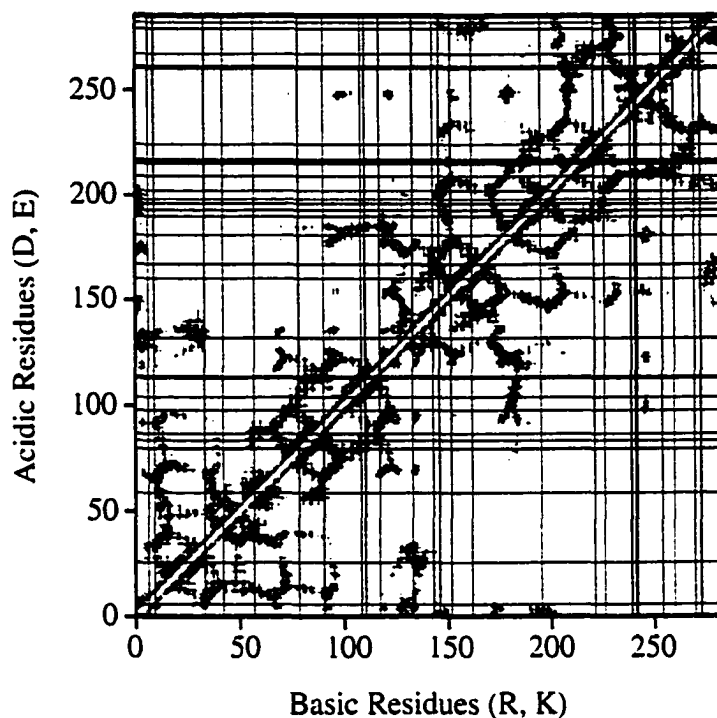


**Figure 3-2. Initial evaluation of potential ion pairs in the  $\alpha$ -subunit of *T. aquaticus* SCS.** The distances between all  $\alpha$ -carbon atoms in *E. coli* SCS were measured, and those that were between 4.0 and 12 Å were plotted on the graph above. The sequence alignment in Figure 1-2 was used to place the *T. aquaticus* amino acids in the *E. coli* numbering system. The positions of basic residues in *T. aquaticus* SCS (Arg, and Lys) were then marked by lines on the x-axis, and the positions of acidic residues were marked on the y-axis. The intersection between a basic and an acidic residue in *T. aquaticus* SCS in an area where the  $\alpha$ -carbons in *E. coli* SCS were separated by 4 - 12 Å, was further inspected for the possibility of an ion pair using the crystallographic structure of *E. coli* SCS (28).



within the package INSIGHT II (31). The amino acid alignment of *E. coli* and *T. aquaticus* SCS was used to place the *T. aquaticus* residues on this plot. Positions of the basic residues (Arg and Lys) and the acidic residues (Glu and Asp) in *T. aquaticus* SCS were marked on the x and y axes, respectively (Fig. 3-2). The criteria for initial selection of two residues that may form an ion pair was that the  $\alpha$ -carbon of a basic residue must be between 4 and 12 Å from the  $\alpha$ -carbon of an acidic residue. For one ion pair in Figure 3-2, this is where the two lines that mark the positions of the acidic and basic residues intersect with the x which denotes the residues that have  $\alpha$ -carbons spaced between 4 and 12 Å apart. After the initial selection, all of the ion pairs were visually inspected using the *E. coli* structure (28) for the possibility of an ion pair at this position. An ion pair was deemed possible if rotation of the side chain could bring the NZ of Lys, or the NH1 or NH2 of Arg, to within 4.0 Å of the OD1 or OD2 of Asp, or the OE1 or OE2 of Glu, and there were no obvious steric clashes. Only one orientation of a side chain was allowed.

*Comparison of the Pig Heart, E. coli and T. aquaticus Amino Acid Sequences for Residues that Stabilize Secondary Structure.* The amino acid sequences of these three enzymes were compared to see if there was a correlation between more stable enzymes and substitutions that potentially stabilize the appropriate secondary structure. That is, were there substitutions in corresponding  $\alpha$ -helices that would potentially lead to the additional stabilization of those  $\alpha$ -helices? Furthermore, were there substitutions in  $\beta$ -sheets that would stabilize  $\beta$ -strands? The criteria used to judge the potential of a residue to stabilize either  $\alpha$ -helix or  $\beta$ -strand was based on the survey of the PDB conducted by Levitt (32), who found that there was a bias in the type of amino acids found in helices or stands. The residues A, C, L, M, E, Q, H, and K were found more often in  $\alpha$ -helices (in this order of frequency). The residues V, I, F, Y, W, and T were found more often in  $\beta$ -strand (in this order of frequency). The propensity for residues to be in turns was not examined. The secondary structure of the *E. coli* enzyme was used to determine if a residue was in either  $\beta$ -sheet or in  $\alpha$ -helix. A count was made of the number of times an amino acid in an

enzyme of lower stability, and in a specific secondary structure (helix or strand), was changed to a different amino acid, which had a higher propensity for the appropriate secondary structure, in an enzyme of higher stability. This was considered a stabilizing substitution. A count was also made of the number of times an amino acid in an enzyme of lower stability, and in a specific secondary structure (helix or strand), was changed to a different amino acid, which had a lower propensity for the appropriate secondary structure, in an enzyme of higher stability. This was considered a destabilizing substitution. It was not counted if a residue, which had  $\beta$ -strand propensity, and was found in an  $\alpha$ -helix was changed to another residue with  $\beta$ -strand propensity. Neither was it counted if a residue, which had  $\alpha$ -helix propensity, and was found in a  $\beta$ -strand was changed to another residue with  $\alpha$ -helix propensity.

## Results

*Characterization of the Quaternary Structure of T. aquaticus SCS.* SCS enzymes exhibit either a dimeric quaternary structure, consisting of one  $\alpha$ -subunit and one  $\beta$ -subunit, as seen in pig heart SCS, or a tetrameric structure consisting of a dimer of  $\alpha\beta$ -dimers, as seen in *E. coli* SCS. The quaternary structure of *T. aquaticus* SCS was evaluated by both gel filtration chromatography and sedimentation equilibrium (Fig. 3-3). A mixture of purified *T. aquaticus* SCS and pig heart SCS was run on a gel filtration column and the elution profile revealed two separate peaks (Fig. 3-3A). The first, peak, eluting at 11.5 ml was *T. aquaticus* SCS, and the second, peak eluting at 12.5 ml was pig heart SCS (Fig. 3-3A). The identity of SCS in each peak was confirmed by its ability to catalyze the formation of succinyl-CoA from succinate, CoA, and either ATP or GTP. Pig heart SCS can only utilize GTP, whereas *T. aquaticus* SCS can use either. This elution profile closely resembled the elution profile of a mixture of *E. coli* and pig heart SCS observed using the same column (33). Since the differences in molecular weight between

the subunits of *E. coli*, *T. aquaticus*, and pig heart were small on the scale examined by gel filtration, these results indicated that *T. aquaticus* SCS was probably a tetramer.

The quaternary structure of *T. aquaticus* SCS was also elucidated by sedimentation equilibrium. Sedimentation equilibrium runs were conducted using three initial loading concentrations and two separate rotor speeds (Fig. 3-3B). The results fit a model where *T. aquaticus* SCS was a non-dissociating species with a molecular weight of  $1.35 \times 10^5$ . As calculated from the amino acid sequence, the weight for tetrameric *T. aquaticus* SCS would be 142970. Thus, it was concluded that the quaternary structure of *T. aquaticus* SCS is a tetramer.

*Enzymology of T. aquaticus SCS.* The ability of *T. aquaticus* SCS to catalyze the formation of succinyl-CoA from ATP, CoA and succinate was measured at various pH values, and the results are shown in Figure 3-4. The pH profile for *T. aquaticus* SCS was essentially a symmetrical peak with the maximal activity occurring between pH 8.0 and 8.4. The maximal activity of *E. coli* and pig heart SCS occurs at pH 7.4 (34).

The kinetic parameters of *T. aquaticus* SCS were evaluated by steady state analysis of initial rates of succinyl-CoA formation at 22 °C and the results were plotted using Hanes-Wolf plots (35, 20) (Fig. 3-5). These plots were used because they gave better correlation coefficients than the more commonly used double reciprocal plots. The  $K_{m(app)}$  values for all of the substrates except GTP are well within an order of magnitude of the values that have been determined for *E. coli* SCS (reviewed in (36)). The value of  $K_{m(app)}$  for GTP was approximately 15 times less than the value of *E. coli* SCS for the same substrate. Like other SCS enzymes, *T. aquaticus* could not use oxaloacetate, acetoacetate, or malic acid as substrates. As would be expected for a thermophilic enzyme, operating well below its optimal temperature, the maximum velocity of succinyl-CoA production at room temperature was considerably lower than that which has been measured for the *E. coli* and pig heart enzymes at room temperature.

To evaluate the thermal stability, and to estimate the maximal velocity of *T. aquaticus* SCS, the formation of succinyl-CoA catalyzed by *T. aquaticus* SCS was measured at elevated temperatures. The severe dependence of the pH of Tris buffer on temperature necessitated the use of phosphate, as the buffering species. Unfortunately, as a consequence, the rate of reaction was reduced both by product inhibition, and by a non-optimal pH of 7.4. The enzyme aliquot for each assay was taken from a stock solution that was incubated at each assay temperature (raised incrementally) for a minimum of 15 min. For comparison, the ability of pig heart and *E. coli* SCS to catalyze the formation of succinyl-CoA at elevated temperatures was also measured (Fig. 3-6). Pig heart SCS ceased to function at 49 °C, slightly lower than *E. coli* SCS at 55 °C, and both enzymes were observed to precipitate from the stock solution at these temperatures. In contrast, *T. aquaticus* SCS remained soluble and continued to function at all of the temperatures that could be measured. The increase in the activity of *T. aquaticus* SCS approached a plateau at approximately 66 °C, consistent with the optimal growth temperature reported for *T. aquaticus* of 70 - 80 °C (37). Although this would seem to indicate that the enzyme had reached its maximal velocity, the spontaneous hydrolysis of succinyl-CoA becomes significant at these temperatures, and thus these values of enzymatic activity may have been anomalously low. The rate of hydrolysis of succinyl-CoA at 75 °C was not dependent on its own concentration at approximately 40 μM (data not shown). If the rate of hydrolysis of succinyl-CoA is not at all dependent on concentration, the maximum rate of synthesis of succinyl-CoA by *T. aquaticus* SCS in the presence of 10 mM phosphate was 28.8 U/mg, which is consistent with the values that were observed for *E. coli* and pig heart SCS at room temperature.

*Equilibrium Unfolding of T. aquaticus SCS.* To compare the stabilities of *T. aquaticus*, *E. coli*, and pig heart SCS, to chemical denaturation, the activity of each enzyme was measured after incubation for 24 hours in various concentrations of either urea or

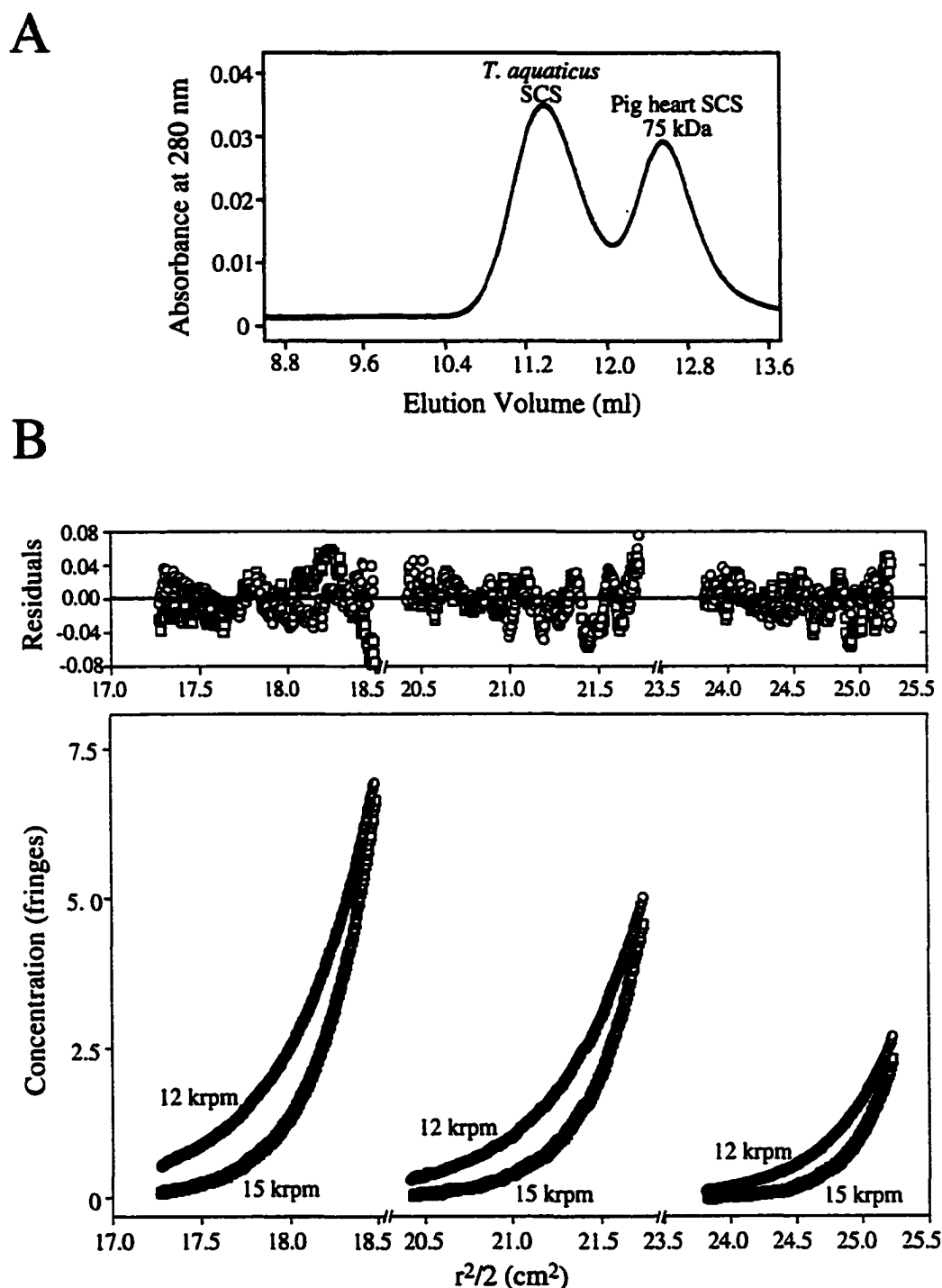


**Figure 3-3. Determination of the quaternary structure of *T. aquaticus* SCS.** A. Gel filtration of a mixture of *T. aquaticus* SCS and pig heart SCS. B. Sedimentation equilibrium of *T. aquaticus* SCS. The three sectors of the ultracentrifugation cell were loaded, each with a different initial protein concentration, 1.77 ( $\square$ ,  $\circ$ ), 1.31 ( $\square$ ,  $\circ$ ), and 0.8 mg/ml ( $\square$ ,  $\circ$ ) run at two speeds  $12 \times 10^3$  (circles) and  $15 \times 10^3$  rpm (squares). The data were best fit to a single-species model, represented by the lines drawn through the data points. The residuals for this fit are plotted in the upper panel, and the square root of the variance was 0.0156.

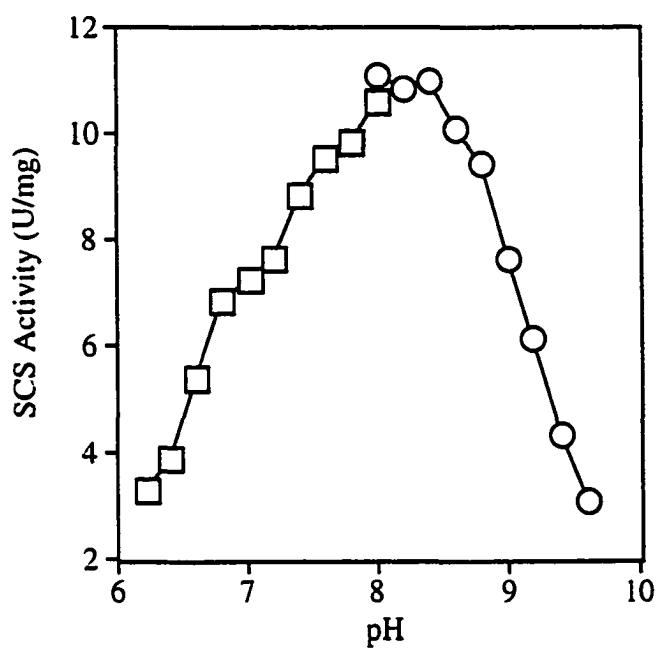


**Figure 3-4.** The pH profile of the activity of *T. aquaticus* SCS. The activity of *T. aquaticus* SCS was measured at different pH values in either (□) MOPS or (○) Tris HCl. The buffers are described in Materials and Methods.

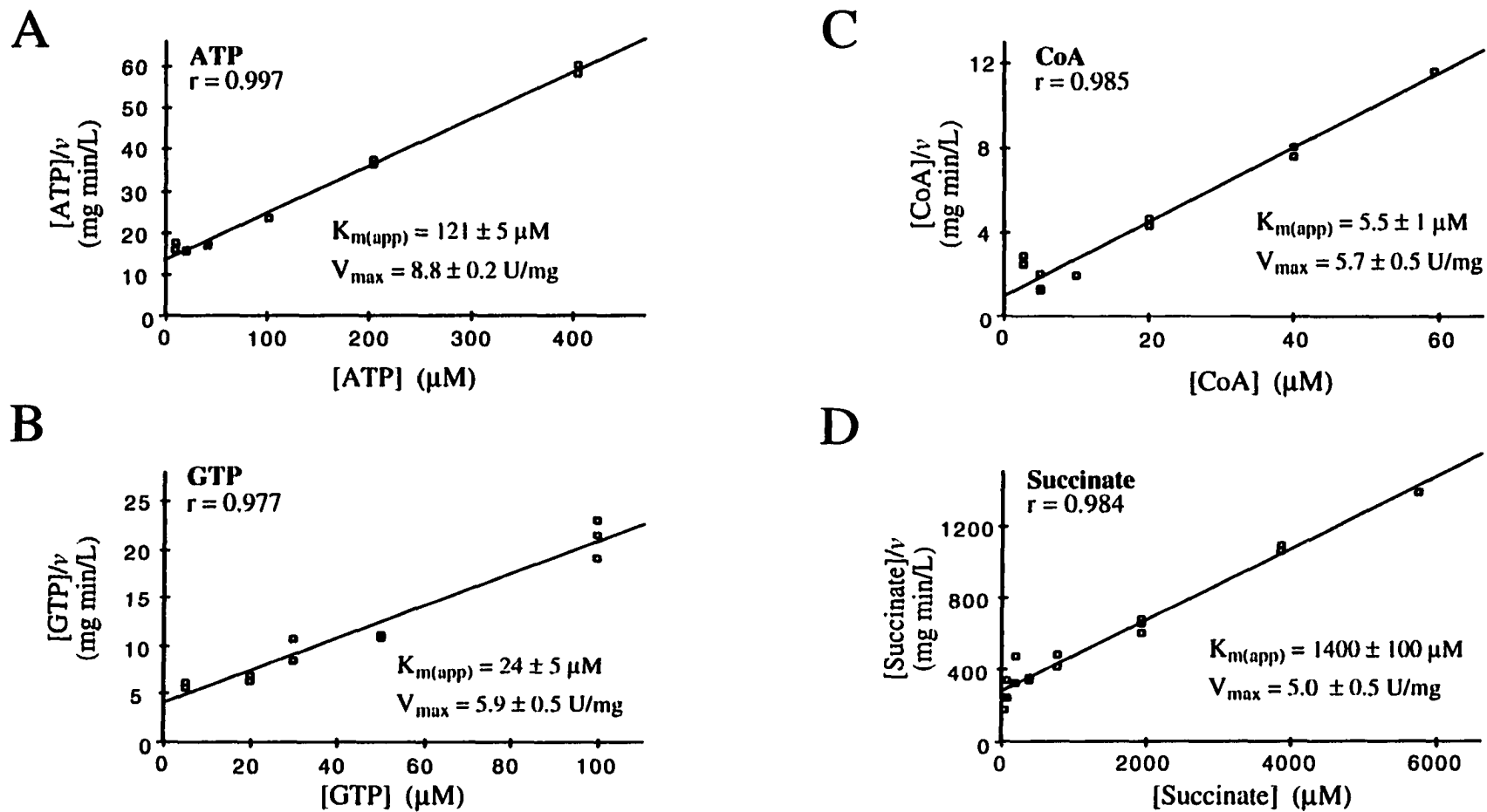


**Figure 3-5. Hanes-Wolf plots for *T. aquaticus* SCS.** The 1 mL reaction mixtures contained 50 mM KCl, 10 mM MgCl<sub>2</sub>, 50 mM Tris HCl, pH 8.0, and saturating concentrations of all substrates (114 μM CoA, 10 mM succinate, and 405 μM ATP or GTP) except for ATP in panel A, GTP in panel B, CoA in panel C, and succinate in panel D. The data were analyzed using the program ENZYME KINETICS (20). The y-intercept of the least squares line indicates the value of  $K_{m(app)}/V_{max}$ , and the slope indicates the value of  $1/V_{max}$ . The correlation coefficient of the line is indicated, as is the estimated error in the values of  $K_{m(app)}$  and  $V_{max}$ .

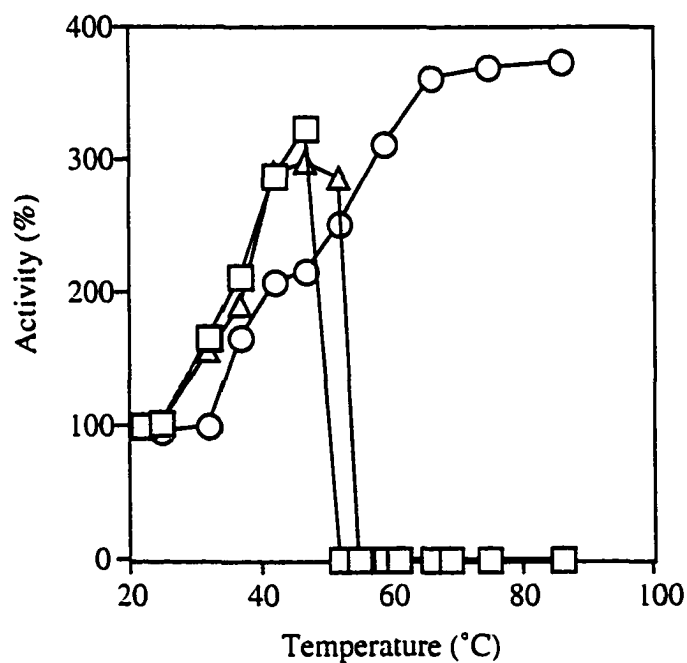


**Figure 3-6. Temperature profile of SCS.** The ability of *T. aquaticus* (○), *E. coli* (Δ), and pig heart (◻) SCS to catalyze the formation of succinyl-CoA was assayed at incremental temperatures following incubation in a water bath for a minimum of 15 min at each temperature. The activity plotted is relative to the activity at 22 °C, which was set at 100 %.



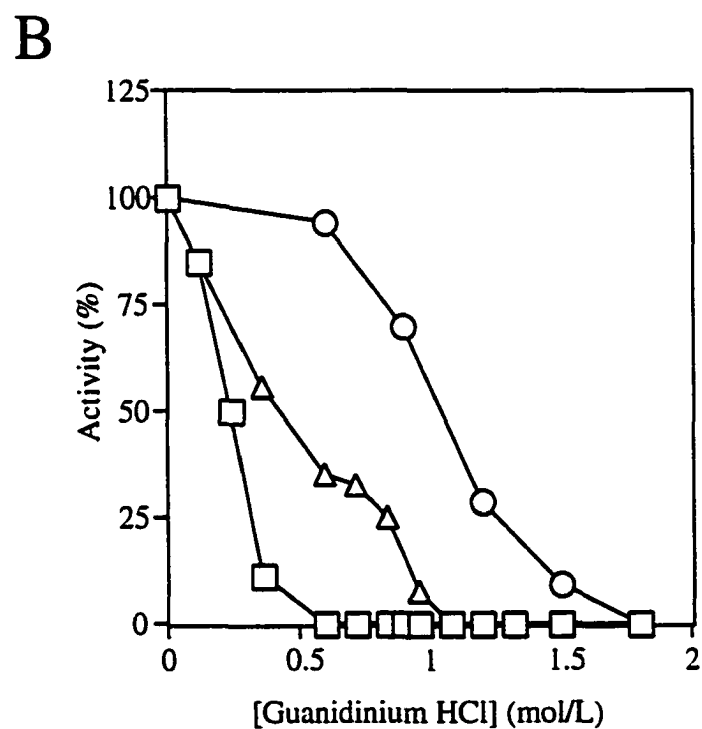
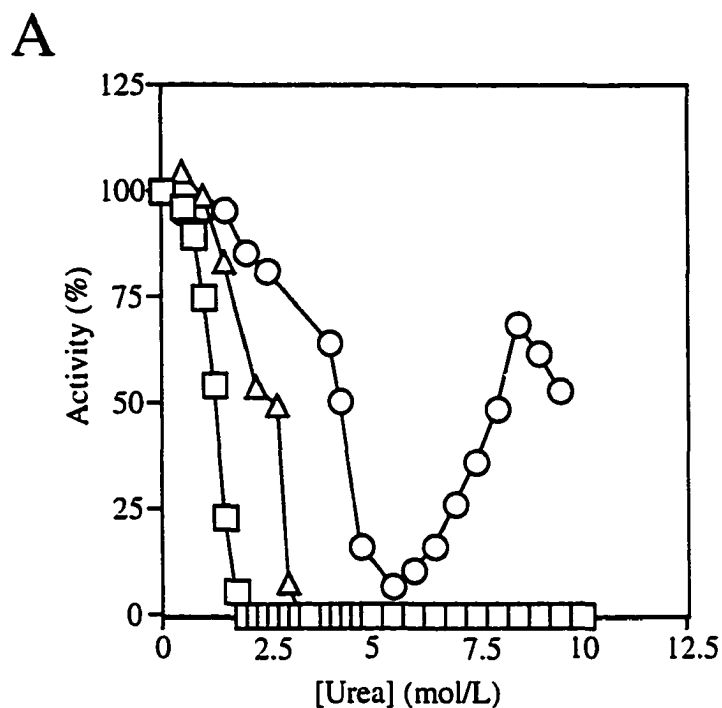


**Figure 3-7. Denaturation of SCS.** The ability of *T. aquaticus* (○), *E. coli* (Δ), and pig heart (□) SCS to catalyze the formation of succinyl-CoA in various concentrations of urea (A) and guanidine HCl (B) was assayed following incubation for 24 hours at 22 °C in each concentration of denaturant.

guanidine HCl (Fig. 3-7). Pig heart SCS was most sensitive to denaturants, *T. aquaticus* SCS was most resistant and *E. coli* SCS was intermediate. In urea, *T. aquaticus* SCS was observed to lose activity between 4 M and 5.5 M where, remarkably, it regained activity with increasing concentrations of urea until reaching 70 % of its original activity in 8.5 M urea (Fig. 3-7A). This behavior may have been due to aggregation at the intermediate concentrations of urea, although no precipitation was observed. Lactate dehydrogenase from the thermophile *Thermotoga maritima* has been shown to aggregate at intermediate concentrations of guanidine HCl (38).

When the equilibrium unfolding of *E. coli* SCS in GuHCl was studied, the activity of *E. coli* SCS was lost prior to the denaturation of the protein as monitored by far-UV CD (39). In addition, there were two transitions in the denaturation of *E. coli* SCS by GuHCl with a marked plateau between. The existence of distinct intermediates in the unfolding process was indicated by the presence of two transitions as monitored by far-UV CD, and the fact that the loss of activity did not correspond to the loss of secondary structure. To see if the equilibrium unfolding of the thermophilic enzyme from *T. aquaticus* followed the same pattern, the changes in ellipticity at 220 and 222 nm were measured as a function of denaturant concentration using either 2.2 or 9.0  $\mu$ M enzyme (Fig. 3-8). Unfolding was reversible at all GuHCl concentrations, and was not dependent on the concentration of enzyme. This is consistent with a very small dissociation constant for the dissociation of whole enzyme into subunits (recall that the sedimentation experiments indicated that the enzyme was a non-dissociating tetramer). Reminiscent of the observations with the *E. coli* enzyme (39), there were two transitions in the denaturation curve. The first (labeled 1 in Fig. 3-8) occurred at a  $[\text{GuHCl}]_{1/2}$  value of 2.2 M and the second (labeled 2 in Fig. 3-8) at a  $[\text{GuHCl}]_{1/2}$  value of 3.7 M. As would be expected for a more stable enzyme, the transitions occurred at higher GuHCl concentrations than those observed for the *E. coli* enzyme (39). Similar to the results with the *E. coli* enzyme, the activity of *T. aquaticus* SCS was lost prior to the loss of secondary structure. The *T. aquaticus* enzyme had lost all

SCS activity in 1.8 M GuHCl, while the changes in the molar ellipticity did not even begin until 2.0 M, indicating the presence of multiple intermediates in the unfolding process.

To investigate the nature of the intermediates in the unfolding of *T. aquaticus* SCS, sedimentation equilibrium, gel filtration, SDS-PAGE, and far-UV circular dichroism were used. First, sedimentation equilibrium experiments were performed on *T. aquaticus* SCS in either 0.9 or 1.8 M GuHCl (Figures 3-9 and 3-10, respectively). Recall: in 0.9 M GuHCl, *T. aquaticus* SCS had lost little activity (Fig 3-7B). In 1.8 M GuHCl *T. aquaticus* SCS had lost all of its activity (Fig. 3-7B), however the secondary structures (monitored by changes in the ellipticity at 220 and 222 nm) were still intact (Fig. 3-8). Similar to the results observed earlier in benign buffer (Fig. 3-3), the data for sedimentation equilibrium of *T. aquaticus* SCS in 0.9 M GuHCl fit a model of a non-dissociating species with a molecular weight of  $1.44 \times 10^5$ . However the results were more complicated in 1.8 M GuHCl. Moreover, the sedimentation equilibrium data did not fit any of the models for self-associating or dissociating species. The best fit of the data for 1.8 M GuHCl was a single species with an apparent molecular weight of  $3.51 \times 10^5$ . However this fit is not good, as can be seen by the plot of the residuals and the best fit line drawn through the data points in Figure 3-10. By visual inspection, the protein concentrations in the bottom of the centrifuge cell looked much higher than those in 0.9 M GuHCl did, there was no precipitate or large scale aggregation evident at the bottom of the cell. The only valid conclusion that may be drawn is that in 1.8 M GuHCl, *T. aquaticus* SCS behaves as a high molecular weight oligomer.

The results of gel filtration chromatography in the presence of 1.8 M GuHCl are shown in Figure 3-11A (for comparison the elution profiles of *T. aquaticus* and pig heart SCS in benign buffer are also shown). In 1.8 M GuHCl, there was one major peak that eluted around 8 ml and one minor peak that eluted at approximately 9.7 ml. The exclusion volume for this column was 6.2 ml. SDS-PAGE analyses of the proteins in each of these

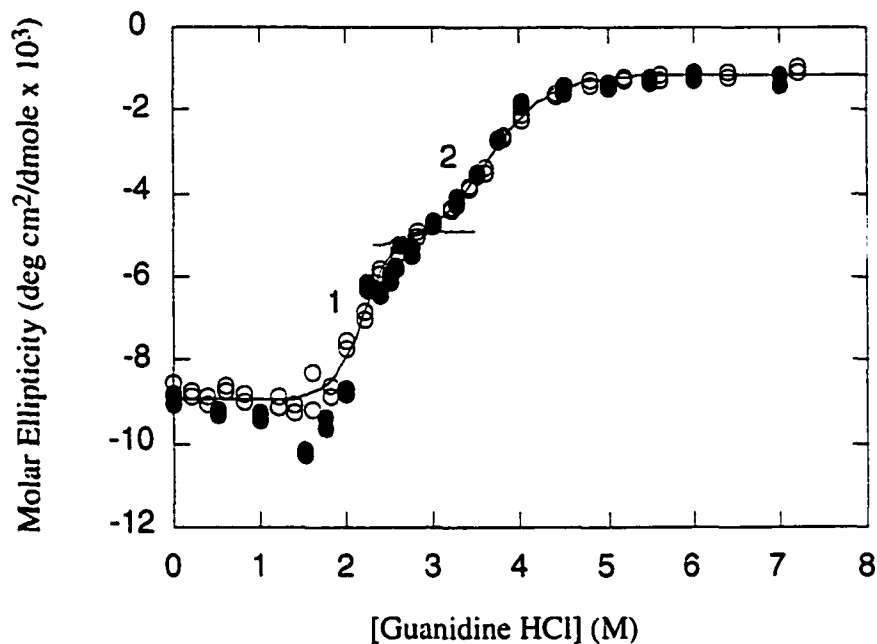


**Figure 3-8. Denaturation of *T. aquaticus* SCS monitored by CD.** Either 2.2  $\mu\text{M}$  (●), or 9.0  $\mu\text{M}$  (○) *T. aquaticus* SCS was incubated for 24 hours in solutions containing various concentrations of guanidine HCl, and the ellipticity was measured at 220 and 222 nm. The best fit line for each transition (labeled 1 and 2) was calculated separately according to  $y=a+b/(1+\exp(c-x)/d)$  using the SIGMA PLOT program (61). The values of the correlation coefficients were 0.987, and 0.998 for the lower and upper transitions, respectively. The values for  $\Delta G_{\text{H}_2\text{O}}$  and  $m$  (as defined in the footnote to Table 3-1) were obtained from replots of the data in each transition, and are given in Table 3-1.

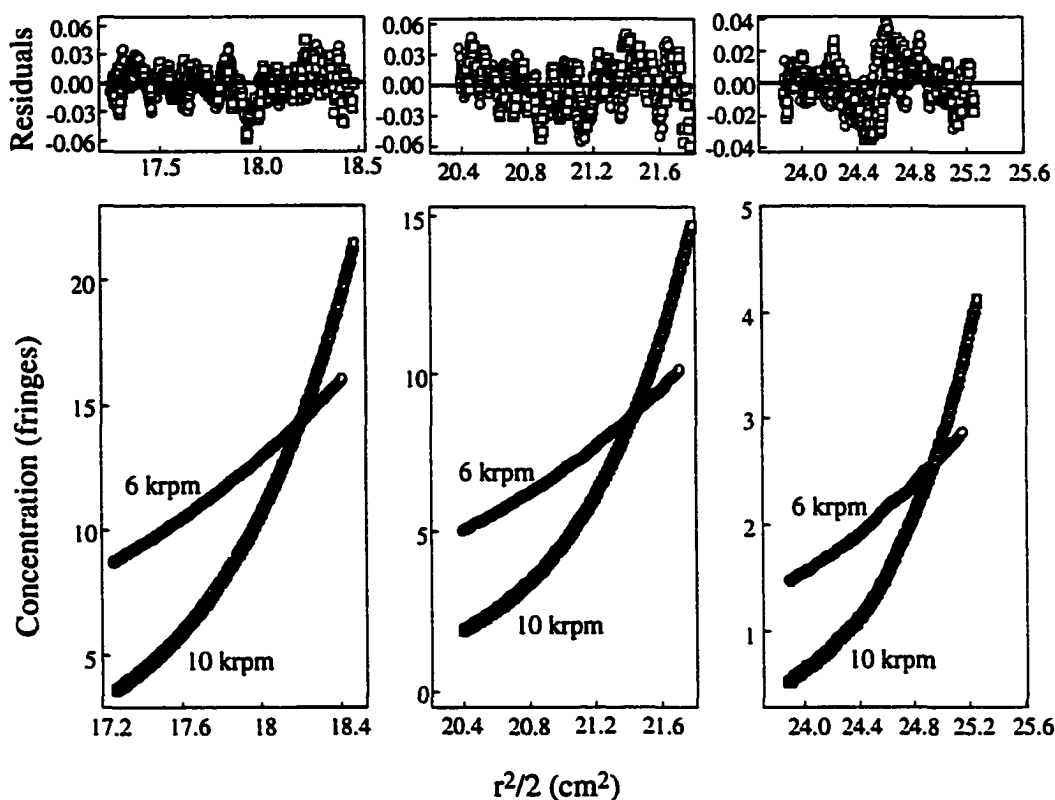


**Figure 3-9. Quaternary structure determination of *T. aquaticus* SCS in 0.9 M guanidine HCl, pH 7.4.** Sedimentation equilibrium of *T. aquaticus* SCS. The three sectors of the ultracentrifugation cell were loaded each with a different initial protein concentration, 5 mg/ml ( $\square$ ,  $\circ$ ), 3 mg/ml ( $\square$ ,  $\circ$ ), and 1 mg/ml ( $\square$ ,  $\circ$ ) and the rotor run at two speeds  $6 \times 10^3$  (circles) and  $10 \times 10^3$  rpm (squares). The data were best fit a single-species model, represented by the lines drawn through the data points. The residuals for this fit are plotted in the upper panel. The square root of the variance was 0.0177.

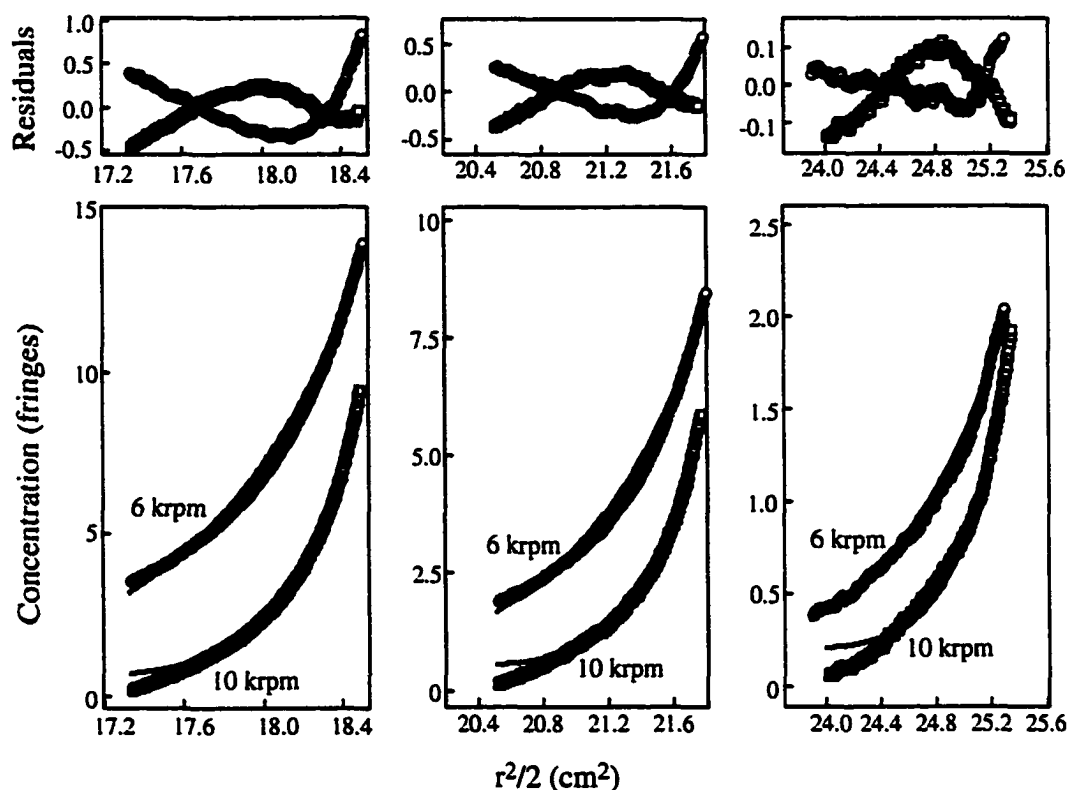


**Figure 3-10. Quaternary structure determination of *T. aquaticus* SCS in 1.8 M guanidine HCl, pH 7.4.** Sedimentation equilibrium of *T. aquaticus* SCS. The three sectors of the ultracentrifugation cell were loaded each with a different initial protein concentration, 5 mg/ml ( $\square$ ,  $\circ$ ), 3 mg/ml ( $\square$ ,  $\circ$ ), and 1 mg/ml ( $\square$ ,  $\circ$ ), and the rotor run at two speeds,  $6 \times 10^3$  (circles) and  $10 \times 10^3$  rpm (squares). The data were best fit a single-species model, represented by the lines drawn through the data points. The residuals for this fit are plotted in the upper panel.

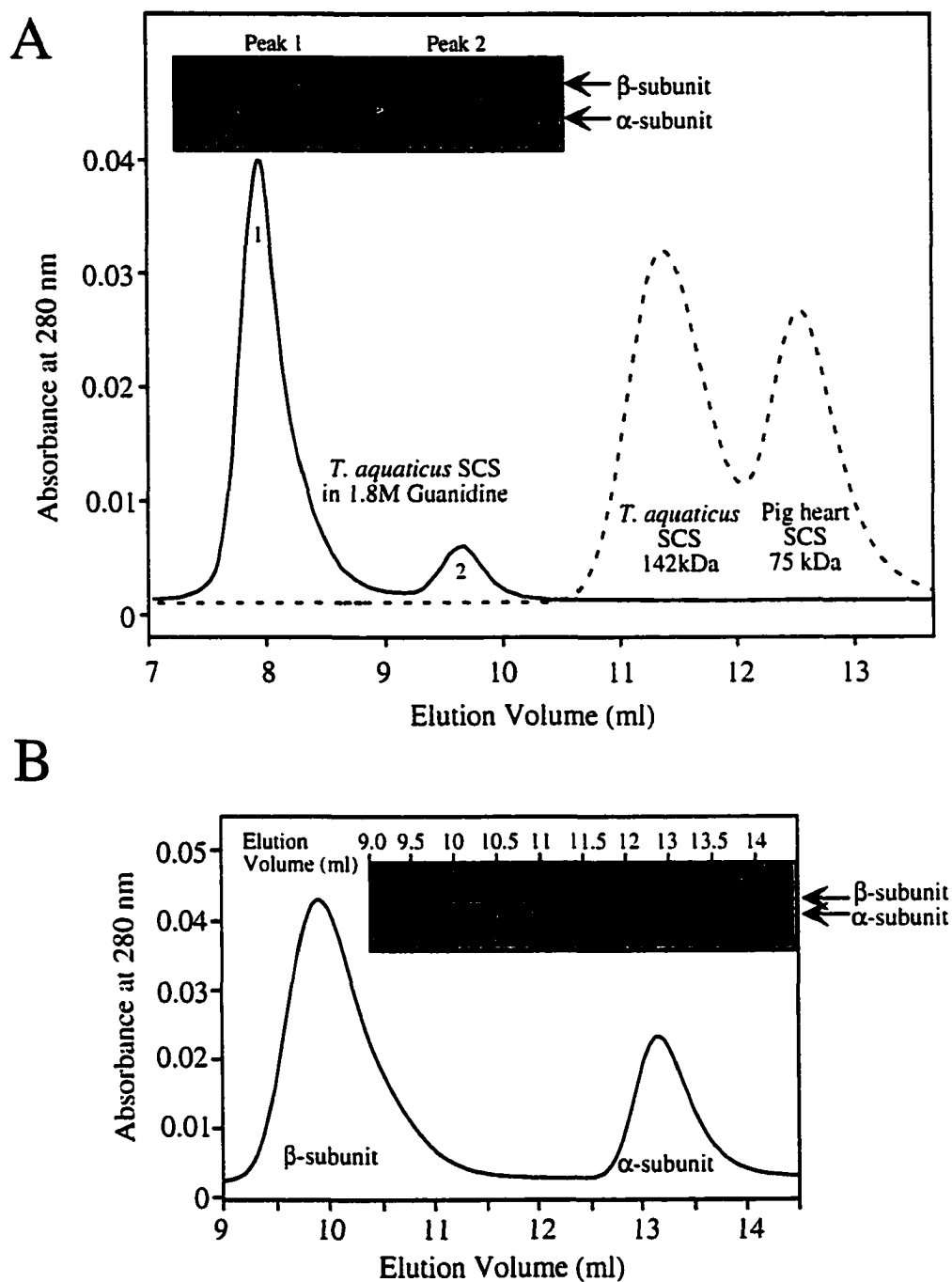


**Figure 3-11. Gel filtration chromatography of *T. aquaticus* SCS in 1.8 and 3 M guanidinium HCl.** A. The solid line represents elution profile of *T. aquaticus* SCS in the presence of 1.8 M GuHCl, carried out as described in Materials and Methods. The inset shows SDS-PAGE analysis of proteins in each of the two peak fractions, labeled peak 1 and 2. For reference, the elution profile of a mixture of *T. aquaticus* and pig heart SCS carried out in benign buffer on the same column is indicated by the dashed line. B. The elution profile from gel filtration chromatography performed on *T. aquaticus* SCS in the same buffer as in A, except the GuHCl concentration was 3.0 M. The inset shows SDS-PAGE analysis of various fractions collected from the column. The exclusion volume of the column was 6.2 ml.

peaks revealed that the major peak consisted of a mixture of  $\alpha$ - and  $\beta$ -subunits, with the  $\beta$ -subunit predominating (Fig. 3-11A, inset). The minor peak consisted of primarily  $\alpha$ -subunit. Thus, the loss of at least some of the  $\alpha$ -subunit of SCS in 1.8 M GuHCl is consistent with the loss of SCS activity (Fig. 3-7), as neither of the subunits can catalyze the formation of succinyl CoA alone. These results are consistent with the results of sedimentation equilibrium experiments if some the  $\alpha$ -subunit has dissociated from the tetramer and left  $\alpha\beta_2$ , which forms a higher molecular weight oligomer.

The denaturation studies of *T. aquaticus* SCS in GuHCl (Fig. 3-8), showed that there were two transitions in the plot of molar ellipticity *versus* the concentration of GuHCl. To investigate the nature of the intermediate that exists between these two transitions, gel filtration chromatography of *T. aquaticus* SCS was performed in 3 M GuHCl. Two peaks were observed in the elution profile (Fig. 3-11B), the first eluted around 10 ml, and the second eluted around 13.1 ml. The proteins in various fractions were analyzed by SDS-PAGE and the results are shown in the inset of Figure 3-11B. The first peak consisted of essentially  $\beta$ -subunit, and the second of  $\alpha$ -subunit alone. This raised the possibility that the first transition seen in the denaturation studies corresponded to the dissociation/unfolding of  $\alpha$ -subunit from the tetramer of *T. aquaticus* SCS, and that the second transition reflected the unfolding of the remaining enzyme.

To see if each subunit retained its native structure in the absence of the other subunit, the  $\alpha$ - and  $\beta$ -subunits were separated, and far-UV circular dichroism was carried out on individual subunits in benign buffer (Fig. 3-12A). The summation of the two spectra for the individual subunits resulted in a spectrum which closely resembled the spectrum of native enzyme in the same buffer (Fig. 3-12B). This indicated that the subunits can adopt a native fold independently, and thus major conformational changes are not required to form whole enzyme from the subunits.



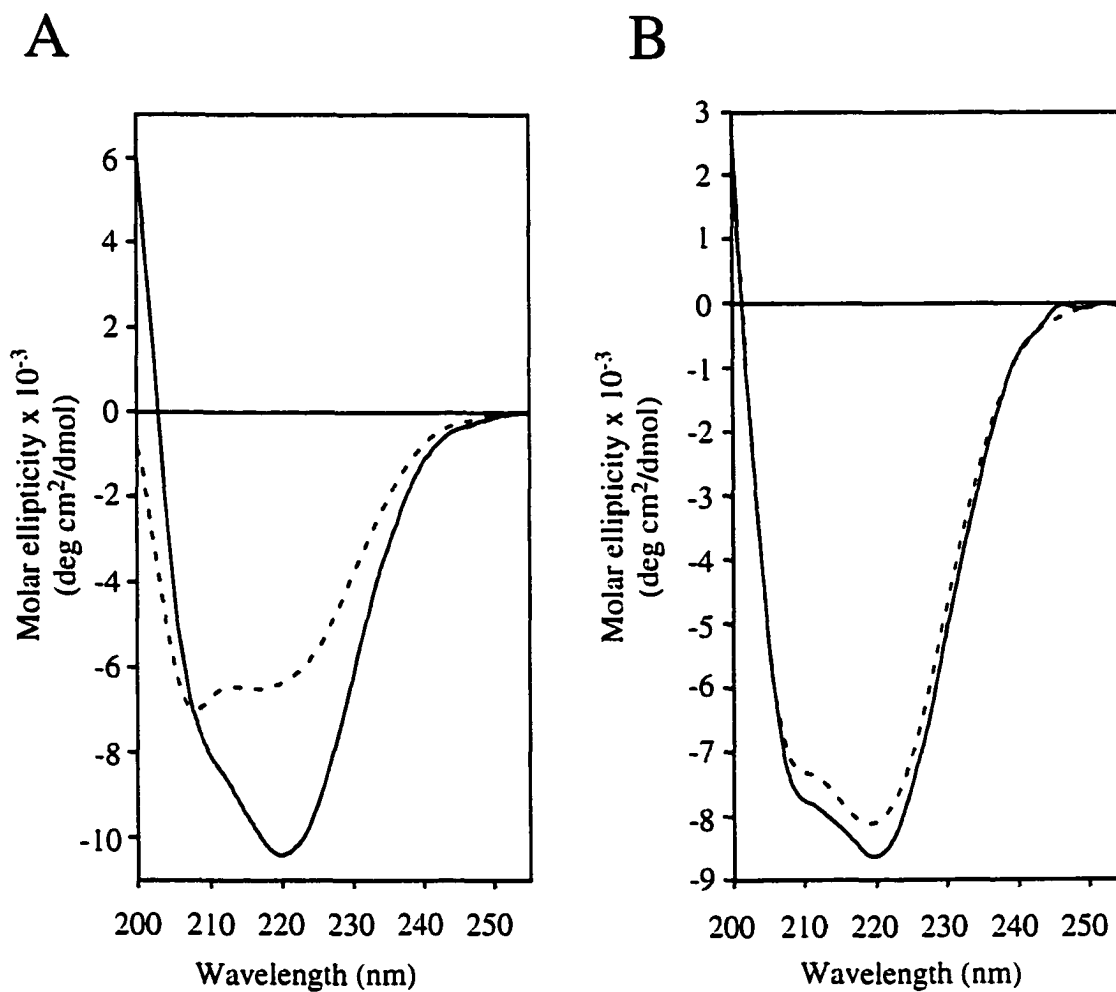


**Figure 3-12. Separated subunits of *T. aquaticus* retain their native conformation in benign buffer.** A. Far UV-CD spectra of the  $\alpha$ -subunit (dashed line) and  $\beta$ -subunit (solid line) of *T. aquaticus* SCS collected at 22 °C (see Materials and Methods for experimental details). B. Far UV-CD spectrum of *T. aquaticus* SCS whole enzyme (solid line) and the spectrum obtained by summing those in panel A (dashed line).

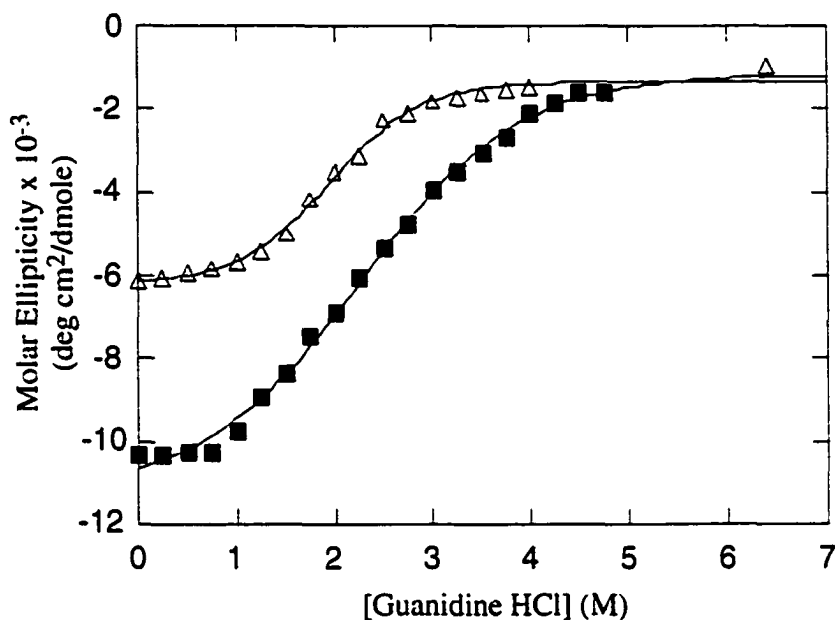


**Figure 3-13. Denaturation of *T. aquaticus* SCS subunits monitored by far-UV CD.** Purified  $\alpha$ -subunit (■) or  $\beta$ -subunit ( $\Delta$ ) was incubated individually for 24 hours in solutions containing various concentrations of GuHCl, and ellipticity at 222 nm was measured. See Materials and Methods for experimental details) The best fit line for each transition is shown and was calculated according to  $y=a+b/(1+\exp(c-x)/d)$  using the SIGMA PLOT program (61). The values for  $\Delta G_u^{H_2O}$  and  $m$  were obtained from replots of the transitions and are given in Table 3-1.

To investigate the possibility that the denaturation of whole enzyme was simply a sum of the denaturation of the subunits, the denaturation of each of the subunits alone in GuHCl was monitored by far-UV CD. The changes in molar ellipticity at 222 nm were measured as a function of denaturant concentration and the results plotted in Figure 3-13. The unfolding transitions for both the  $\alpha$ - and  $\beta$ -subunits were cooperative and were reversible at all denaturant concentrations. When the denaturation curves for the two separate subunits were added together, they did not resemble the denaturation curve for the whole enzyme, indicating that the denaturation of whole enzyme is not simply a sum of the

Table 3-1 Thermodynamic Parameters for the Unfolding of *T. aquaticus* SCS.

Protein	$[\Delta G_u^{H_2O}]_{app}^a$ (kJ/mol)	$m^a$ kJ/mol/M	Correlation coefficient <sup>a</sup>	$[GuHCl]_{1/2}^b$ (M)
Whole enzyme first transition	$29 \pm 4$	$13 \pm 2$	0.986	2.2
Whole enzyme second transition	$25 \pm 1$	$7.1 \pm 0.4$	0.998	3.7
$\alpha$ -subunit	$6.7 \pm 0.4$	$3.1 \pm 0.2$	0.998	2.19
$\beta$ -subunit	$10.0 \pm 0.8$	$5.4 \pm 0.4$	0.997	1.95

<sup>a</sup> These values were calculated by extrapolation of a replot of the molar ellipticities using the equation  $\Delta G = -RT \ln K$ , where  $K = (\Theta_N - \Theta_{obs}) / (\Theta_{obs} - \Theta_U)$ ;  $\Theta_N$  is the molar ellipticity observed at 0 M GuHCl, and  $\Theta_U$  is the molar ellipticity observed at the maximum concentration of GuHCl, and  $\Theta_{obs}$  is the observed molar ellipticity (40). In the vicinity of the transition the resulting plot was fit to the equation  $\Delta G = \Delta G_u^{H_2O} - m[GuHCl]$  (reviewed in (12)) with the correlation coefficient listed.

<sup>b</sup> These values were obtained by interpolation from the graphs, and are consistent with the values obtained by the calculation  $[GuHCl]_{1/2} = [\Delta G_u^{H_2O}]_{app} / m$ .

denaturation of the individual subunits. Values of  $[\Delta G_u^{H_2O}]_{app}$  and  $m$  for the transitions of the individual subunits and of the whole enzyme were calculated from replots using the molar ellipticity data (40, 12). These are summarized in Table 3-1. The value for  $[\Delta G_u^{H_2O}]_{app}$  is the free energy of unfolding which represents the stability of the protein in

water, and the value for  $m$  is proportional to the amount of surface area that is exposed upon denaturation (12). All of the thermodynamic parameters associated with the transitions for the individual subunits were lower than those for the whole enzyme, indicating that the complex of the subunits (native enzyme) is more stable than the isolated subunits. Thus, the denaturation of whole enzyme is not simply a sum of the denaturation of individual subunits, even though the subunits retain most of their native conformation when isolated. It should be noted that for whole enzyme, the calculation of  $[\Delta G_u^{H_2O}]_{app}$  assumed a two state transition for a monomer, which was obviously not correct. However, the proper calculation for a heterotetramer requires knowledge of the various association constants, and was thus not possible. In addition, the prevalent species just prior to the beginning of the first transition in the denaturation of *T. aquaticus* SCS was observed to be a high molecular weight oligomer (Fig. 3-11A) of uncertain composition with unknown association constants.

*Refolding of T. aquaticus SCS.* The experimental conditions for refolding both denatured pig heart and *E. coli* SCS have been reported (16, 18). Refolding of *E. coli* SCS from separated subunits has been well characterized with respect to its dependence on pH, temperature, and protein concentration (16). Since the *T. aquaticus* enzyme has the same oligomeric structure as the *E. coli* enzyme, I wished to investigate whether the refolding of *T. aquaticus* SCS follows the same path as does *E. coli* SCS.

Initially, the refolding of *T. aquaticus* SCS was attempted by rapid dilution into 60 mM potassium phosphate, 50 mM KCl, pH 7.4, in which denatured *E. coli* SCS refolds well. This buffer is called "Benign" in Figure 3-14. However in the case of *T. aquaticus* SCS, precipitate formed in the refolding solution, and less than 50 % of the original activity was recovered after refolding in this buffer. In addition, when heated to 75 °C for one hour, or to 86 °C for 20 min, the enzymatic activity that was recovered at room temperature was not stable (Fig. 3-14). Denatured *T. aquaticus* SCS did not refold under the conditions that were used for refolding pig heart SCS (18) (data not shown). The refolding

of *T. aquaticus* SCS was successful when refolding was carried out by rapid dilution into 0.67 M arginine, 60 mM potassium phosphate, pH 7.4 (41). 100 % of the original activity was recovered when the refolding was conducted in arginine pH 7.4 (Fig. 3-14). However this activity was not stable after heating. As can also be seen in Figure 3-14, only 50 % of the original activity was recovered from refolding conducted at a higher pH, 0.67 M arginine, 60 mM potassium phosphate, 50 mM Tris HCl, pH 8.0, and this activity was also not stable to heating. No precipitate was observed in either the pH 7.4 or pH 8.0 refolding mixtures. The thermostability of *T. aquaticus* SCS was restored by exchanging the arginine buffer for benign buffer (using a Millipore spin filter) after refolding in the arginine buffer was complete (Fig 3-14). Two conclusions can be drawn from these results. 1. Since *T. aquaticus* SCS cannot be refolded in buffers used for *E. coli* and pig heart SCS, the refolding of denatured *T. aquaticus* SCS does not follow the same path as these enzymes. This conclusion is reinforced by the observation that the *E. coli* and pig heart enzymes cannot be refolded by rapid dilution into the arginine refolding buffer (data not shown). 2. Although there was full recovery of activity from the arginine refolding buffer, pH 7.4, when assayed at 22 °C, the refolding is not complete and *T. aquaticus* SCS remains only partially folded in this solution.

*The Kinetics of Refolding T. aquaticus SCS.* To further investigate the refolding of *T. aquaticus* SCS, the dependence of the kinetics of refolding on the temperature and protein concentration was examined. Denatured *T. aquaticus* SCS was refolded by rapid dilution into 0.67 M arginine, 60 mM potassium phosphate, pH 7.4, at 12, 22 and 37 °C. Samples were taken and assayed for SCS activity at 22 °C (Fig. 3-15A). The results indicated that the refolding of *T. aquaticus* SCS was temperature dependent, and the rate of refolding followed apparent first order kinetics. Omission of phosphate from the buffer did not affect the rate of refolding (data not shown). The data for the refolding was fit to first order kinetics, and the rate constants for the recovery of activity were obtained using the program

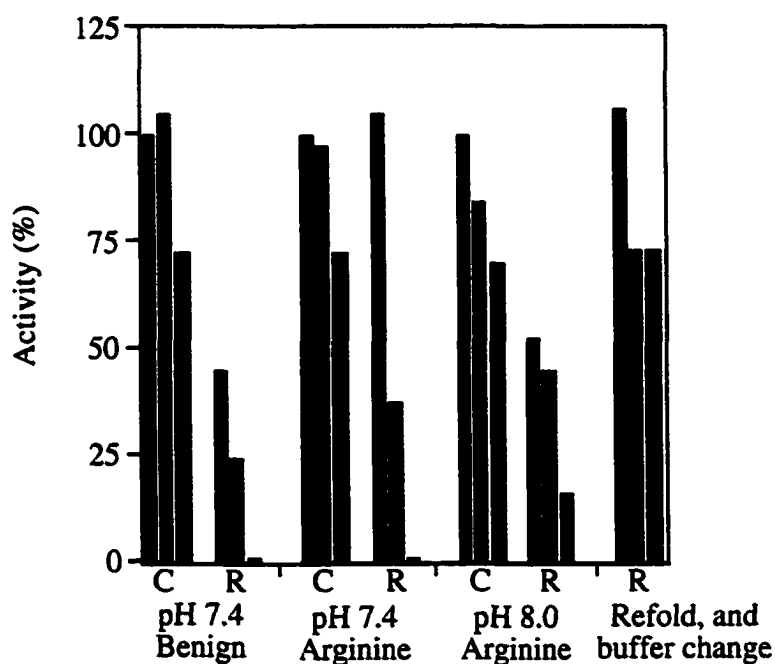


**Figure 3-14. The refolding of *T. aquaticus* SCS requires high concentrations of arginine and buffer exchange.** Denatured *T. aquaticus* SCS was refolded (labeled R) by rapid dilution (1:20) into benign buffer, or into pH 7.4 arginine buffer, or into pH 8.0 arginine buffer, or first by rapid dilution into pH 7.4 arginine refold buffer followed by buffer exchange into benign buffer. Following dilution, the refolding solutions were incubated for 5 hours at 22 °C, and the SCS activity was either measured immediately at 22 °C (shown in blue), or after incubation for one hour at 75 °C (shown in orange), or after incubation for 20 min at 80 °C (shown in red). Control samples of native enzyme (labeled C) were not denatured prior to rapid dilution. The recovered activity was calculated as a percentage based on the activity of the control sample that had not been heated.

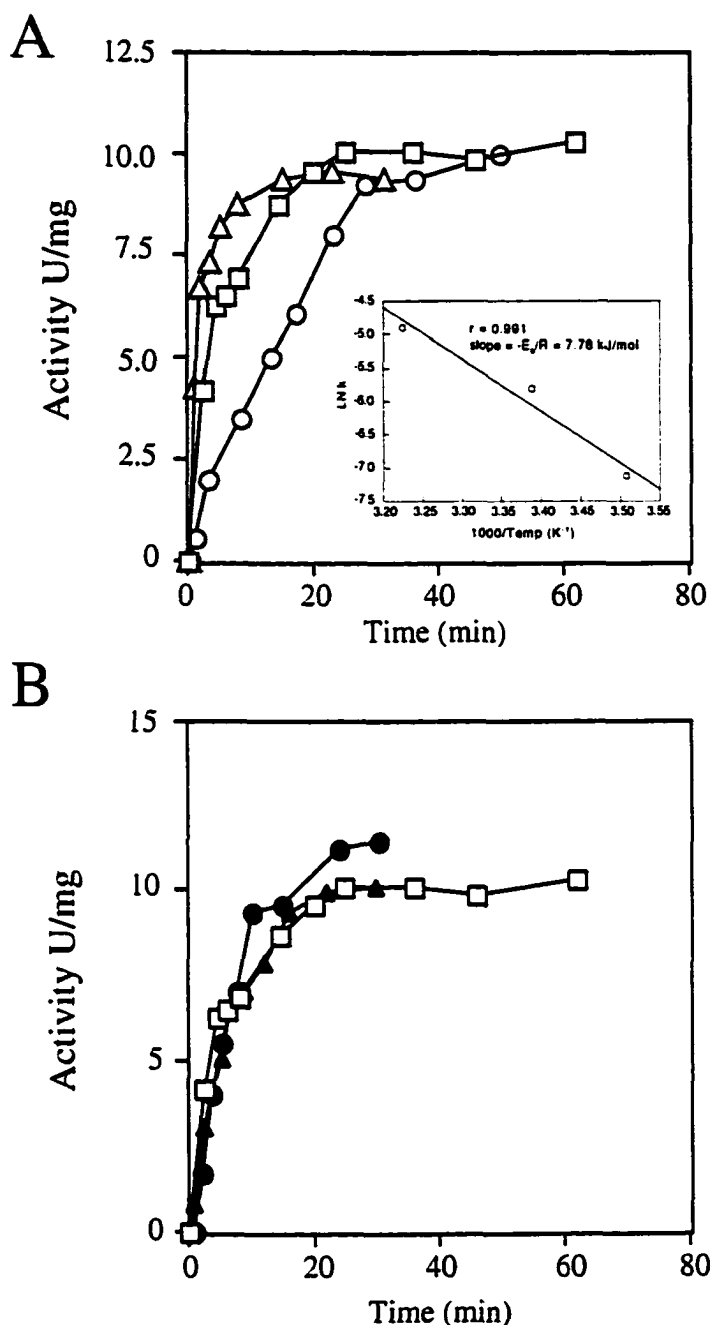


**Figure 3-15. Temperature and concentration dependence of the kinetics refolding of *T. aquaticus* SCS.** Denatured *T. aquaticus* SCS in 6 M Guanidine HCl was refolded by rapid dilution (1:20) into pH 7.4 arginine buffer. Samples were taken at various times after the initiation of refolding and assayed for SCS activity. In panel A, denatured *T. aquaticus* SCS at a final concentration of 0.59 mg/ml, was refolded at 12 °C (○), 22 °C (□), or 37 °C (△). The first order rate constants were evaluated at 12 °C ( $8.06 \times 10^{-4} \text{ s}^{-1}$ ,  $r = 0.996$ ), 22 °C, ( $3.00 \times 10^{-3} \text{ s}^{-1}$ ,  $r = 0.990$ ), and 37 °C, ( $7.53 \times 10^{-3} \text{ s}^{-1}$ ,  $r = 0.980$ ); and were plotted against the respective temperatures as shown in the inset. The slope and the correlation coefficient of the linear fit are indicated. In panel B, denatured *T. aquaticus* SCS at a final concentration of 0.59 mg/ml (□), 0.24 mg/ml (▲), or 0.059 mg/ml (●) was refolded at 22 °C.

KALIDAGRAPH (42), and replotted using an Arrhenius plot (see inset in Figure 3-14A). From this plot, the energy of activation ( $E_a$ ) associated with the refolding of *T. aquaticus* SCS estimated to be 64.7 kJ/mol.

The concentration dependence of refolding of *T. aquaticus* SCS was also examined with a final protein concentration of 0.59, 0.23, and 0.059 mg/ml in the refolding mixture. Denatured *T. aquaticus* SCS was refolded in the same manner as described for the temperature dependence study, but assayed for activity only at 22 °C (Fig. 3-15B). Consistent with the results of the equilibrium unfolding of *T. aquaticus* SCS, the kinetics of refolding also were not dependent on the concentration of protein tested.

*Characterization of the Partially Folded T. aquaticus SCS.* Despite the high recovery of activity after refolding, the initial experiments had indicated that refolded *T. aquaticus* SCS was not thermostable (see above). To assess the stability of the “refolded” form of *T. aquaticus* SCS, its ability to catalyze the formation of succinyl-CoA at different temperatures was measured in the same manner used initially for the *E. coli*, pig heart and *T. aquaticus* enzymes (Fig. 3-16). The “refolded” form is much less thermostable than the native form of *T. aquaticus* SCS, and only slightly more stable than the *E. coli* enzyme (compare Fig. 3-6 and 3-16). Nevertheless, refolded *T. aquaticus* SCS appeared to have full activity at 22 °C when assayed in the standard manner under saturating conditions of substrates.

The kinetic parameters of refolded *T. aquaticus* SCS were evaluated by steady state analysis of initial rates of succinyl-CoA formation at 22 °C. Differences in the apparent kinetic parameters as compared to the native enzyme, could indicate an area of the enzyme that is perturbed in the refolded enzyme. The results of the kinetic analysis were plotted using Hanes-Wolf plots (Fig. 3-17). The apparent kinetic parameters were essentially the same as those of the native enzyme. Remarkably, the instability of refolded *T. aquaticus* SCS did not disturb substrate binding or catalysis at 22 °C.



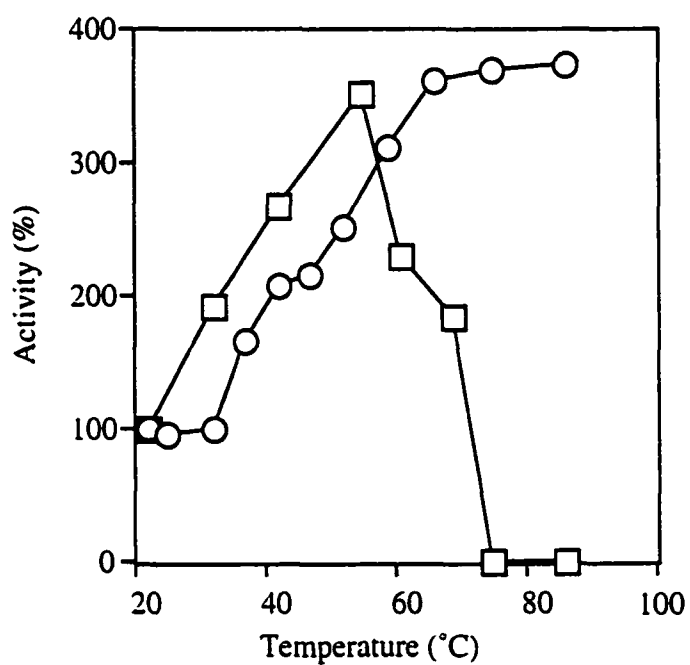


**Figure 3-16. Temperature dependence profile of native and refolded *T. aquaticus* SCS.** The ability of native (○), and refolded (◻) *T. aquaticus* SCS to catalyze the formation of succinyl-CoA at various temperatures was assayed following incubation in a water bath for a minimum of 15 min at each temperature. See Materials and Methods for experimental details

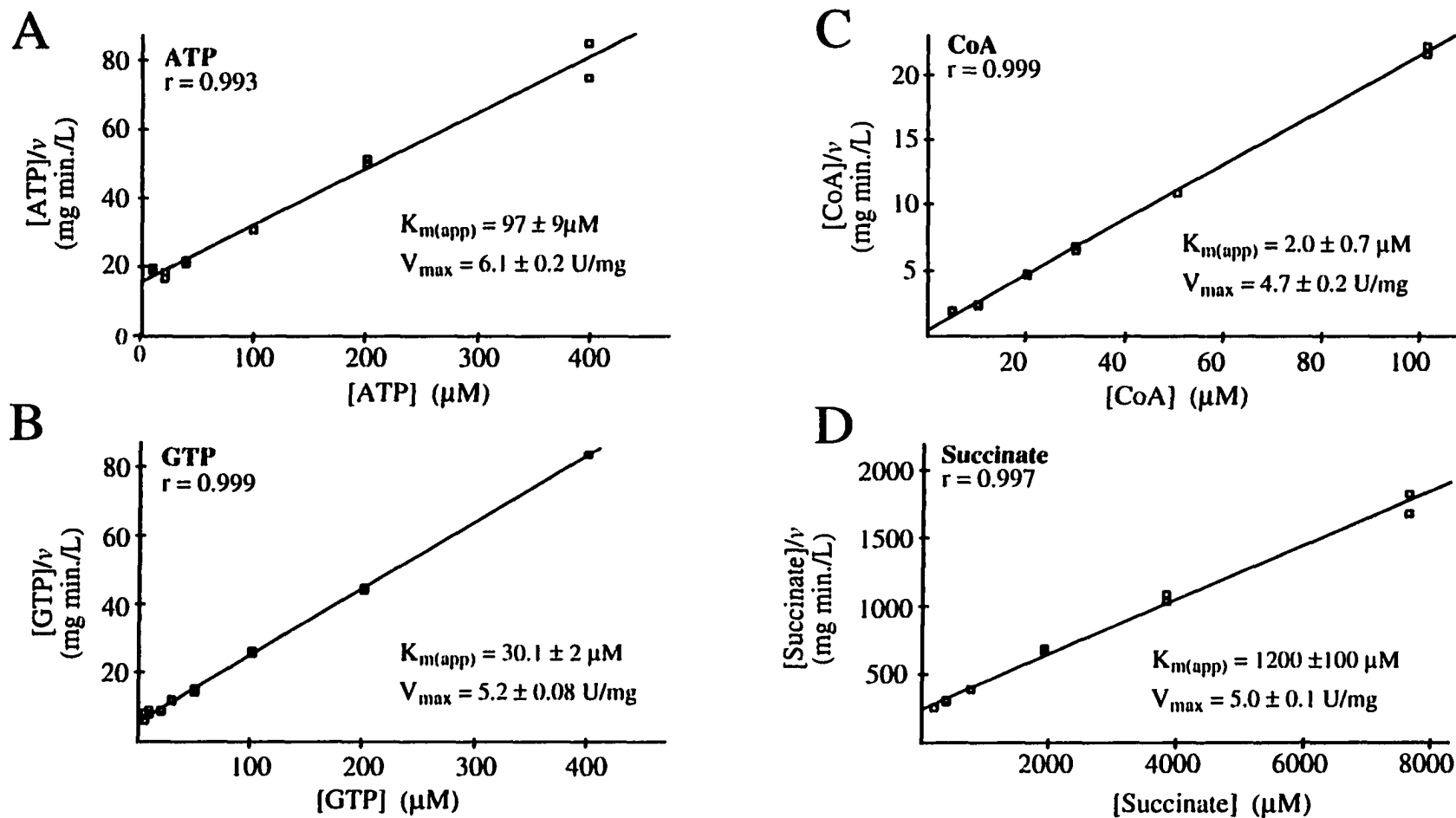


**Figure 3-17. Hanes-Wolf plots for refolded *T. aquaticus* SCS.** The 1 mL reaction mixtures contained 50 mM KCl, 10 mM MgCl<sub>2</sub>, 50 mM Tris HCl, pH 8.0, and saturating concentrations of all substrates (115 μM CoA, 10 mM succinate, and 405 μM ATP or GTP) except for ATP in panel A, GTP in panel B, CoA in panel C, and succinate in panel D. The data were analyzed using the program ENZYME KINETICS (20). The y-intercept of the least squares line indicates the value of  $K_{m(app)}/V_{max}$ , and the slope indicates the value of  $1/V_{max}$ . The correlation coefficient of the line is indicated, as is the estimated error in the values of  $K_{m(app)}$  and  $V_{max}$ .

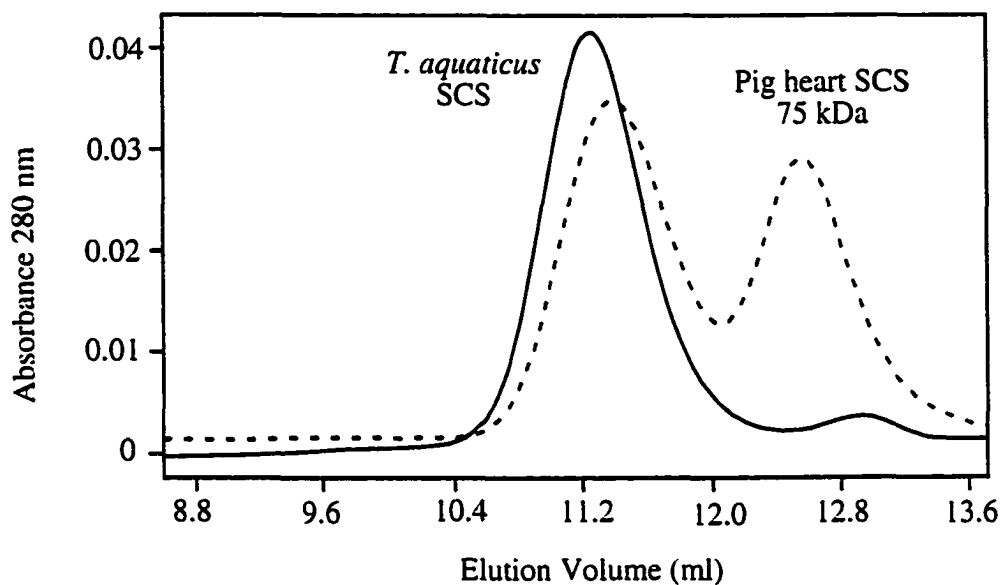


**Figure 3-18. Gel filtration chromatography of refolded *T. aquaticus* SCS.** The solid line represents the elution profile of refolded *T. aquaticus* SCS in the pH 7.4 arginine refold buffer. For reference, the gel filtration of a mixture of native *T. aquaticus* and pig heart SCS in benign buffer is indicated by the dashed line. See Materials and Methods for experimental details.

For the dimeric form of *E. coli* SCS, the kinetic parameters remained the same as the wild-type enzyme, however the dimer was less soluble and less stable than the wild-type tetramer (33). In addition, studies on the conformational stability of dimeric proteins has indicated that dimerization (from monomers) leads to a substantial increase in stability (43). To investigate the possibility that the instability of *T. aquaticus* SCS was due to the formation of dimeric and not tetrameric enzyme, gel filtration chromatography of refolded enzyme was performed (Fig. 3-18). The peak of refolded *T. aquaticus* SCS eluted around 11.2 ml, essentially where native *T. aquaticus* SCS eluted from the same column, and well before dimeric pig heart SCS. This result indicated that refolded *T. aquaticus* SCS was tetrameric.

*Comparison of the Pig Heart, E. coli and T. aquaticus SCS Amino Acid Sequences.* The basis for the relative stabilities of pig heart, *E. coli*, and *T. aquaticus* SCS was examined comparing amino acid sequences in conjunction with structural information from the pig heart and *E. coli* SCS structures (26-28). Direct comparison of the amino acid composition of the three enzymes is shown in Figure 3-19. The two relative trends observed going from pig heart SCS to *E. coli* SCS to *T. aquaticus* SCS: first, a decrease in the number of Ser, Asn, Gln, Cys, and Phe, and second, an increase in the number of Arg, Ala, Val, and Met.

Analysis of the general amino acid composition only counts the net change in the number of each amino acid, and ignores the context dependence of the substitutions. That is, specific amino acids may be lost (e.g. Leu and Ile) in favor of other similar amino acids (e.g. Val). This deficiency was addressed by looking at the nature of the amino acid substitutions between the three enzymes using the sequence alignments shown in Figures 1-2 and 1-3. In Figure 3-20, the substitutions of any amino acid for every other amino acid are compiled in a frequency chart. The values listed are the number of times a given amino acid from a less stable protein is substituted with a specific amino acid in a more stable protein. Recall that pig heart SCS was less stable than *E. coli* SCS which, in turn, was

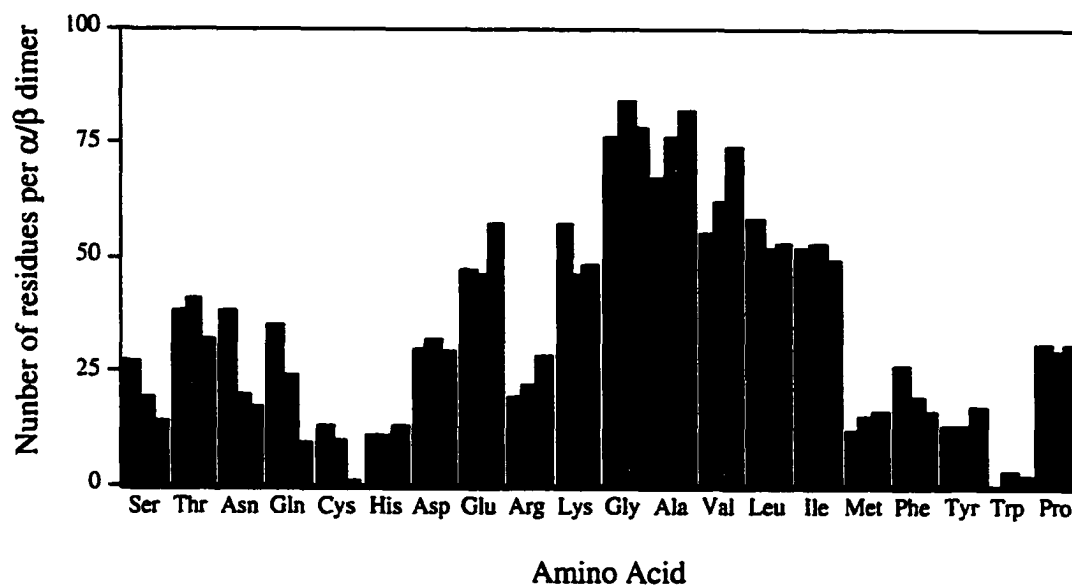


**Figure 3-19. Comparison of the amino acid composition of different SCS enzymes.** The amino acid composition of the  $\alpha$ - and  $\beta$ -subunits of SCS from pig heart (in blue), *E. coli* (in orange), and *T. aquaticus* (in red) are shown. The sequences used are shown in Figures 1-2 and 1-3, and the database accession numbers are given in Appendix 1.

### Amino Acids in More Stable SCS Enzymes

		Uncharged Polar					Charged					Non-Polar										
		S	T	N	Q	C	H	D	E	R	K	G	A	V	L	I	M	F	Y	W	P	
Amino Acids in Less Stable SCS Enzymes	Uncharged Polar	S	-	9	0	0	0	2	0	6	1	3	2	14	1	0	0	2	1	1	0	0
		T	9	-	1	2	0	2	2	6	4	6	1	6	6	7	5	0	0	4	0	0
		N	3	5	-	1	0	1	5	<b>8</b>	<b>9</b>	11	2	4	3	2	0	0	0	2	0	1
		Q	0	5	2	-	0	3	6	<b>8</b>	<b>9</b>	5	1	2	3	<b>10</b>	<b>8</b>	2	0	1	0	2
		C	0	5	0	0	-	0	0	0	0	1	0	7	3	4	3	1	0	0	0	0
	Charged	H	0	0	0	0	0	-	0	3	1	3	0	1	4	0	1	2	0	0	0	
		D	1	4	2	2	0	3	-	8	4	5	4	0	0	0	0	0	1	1	0	3
		E	2	3	<b>5</b>	<b>5</b>	0	0	6	-	3	11	7	14	3	5	<b>9</b>	2	2	0	0	3
		R	0	1	<b>5</b>	<b>5</b>	0	0	1	<b>8</b>	-	8	1	2	3	2	<b>9</b>	0	0	1	0	1
		K	2	8	<b>6</b>	<b>8</b>	0	1	4	10	11	-	7	8	8	1	0	4	0	1	0	8
	Non-Polar	G	0	4	1	0	0	0	1	4	4	2	-	12	3	1	0	0	0	2	0	0
		A	<b>6</b>	1	1	1	3	2	<b>9</b>	10	1	4	14	-	12	7	3	5	1	4	1	4
		V	1	3	1	1	0	0	1	3	1	4	3	14	-	9	27	5	1	1	0	4
		L	2	2	1	0	0	3	1	<b>10</b>	3	3	1	9	<b>21</b>	-	<b>26</b>	4	10	1	0	0
		I	0	0	<b>4</b>	<b>3</b>	0	1	0	<b>9</b>	<b>9</b>	2	0	8	<b>35</b>	19	-	1	4	1	1	3
		M	0	0	1	1	0	0	1	1	1	0	0	0	2	2	3	-	1	0	1	0
		F	0	0	1	0	0	2	0	0	1	4	2	6	1	15	4	1	-	6	1	0
		Y	0	0	0	0	0	0	0	0	0	4	0	2	2	2	0	1	4	-	2	0
		W	0	0	0	0	0	0	0	0	0	0	0	0	1	0	1	0	0	1	-	0
		P	0	3	2	0	0	0	2	0	2	9	2	4	2	1	1	1	1	0	0	-

**Figure 3-20. Amino acid replacements in more stable SCS enzymes.** The number of times an amino acid from a less stable enzyme in each row was replaced by an amino acid in a more stable enzyme in the column is shown. Amino acids that showed a directional bias are indicated in bold print. For example, there were more Leu<sub>less stable enzyme</sub> substituted for Val<sub>more stable enzyme</sub> (21) than there were Val<sub>less stable enzyme</sub> substituted for Leu<sub>more stable enzyme</sub> (9). A directional bias was deemed to exist when there were at least 4 more substitutions in one direction than in the other, and the ratio of the number of substitutions in each direction was greater than 2. The totals for each grouping of amino acids is shown in large print in the boxes, red indicates changes in the less stable to more stable direction (e.g. Uncharged Polar<sub>less stable</sub> → Polar<sub>more stable</sub>) and blue represents changes in the opposite direction (e.g. Polar<sub>less stable</sub> → Uncharged Polar<sub>more stable</sub>). The total number of conservative substitutions is indicated in yellow.

less stable than *T. aquaticus* SCS (see for example Fig 3-6 and 3-7). For discussion, the amino acids are grouped into three categories based on their side chains: uncharged polar, charged polar, and nonpolar (44). Conservative substitutions (substitutions for amino acids within the same group) were by far the largest number of substitutions. This was especially evident for Val, Ile, and Leu. The other trend observed was the substitution of uncharged polar amino acids in “less stable” SCS for any others in “more stable” SCS. This is consistent with what Haney *et al.* found in a comparison of genes from a thermophilic and a mesophilic *Methanococcus* species (45). It has been suggested that an increase in the volume of hydrophobic residues is one way proteins can increase their stability (46-48). In more stable SCS there is a slight tendency for a greater number of hydrophobic amino acids that have smaller side chains. The most biased substitutions in the non-polar group are  $L_{\text{less stable}} \rightarrow V_{\text{more stable}}$ ,  $I_{\text{less stable}} \rightarrow A_{\text{more stable}}$ , and  $F_{\text{less stable}} \rightarrow A_{\text{more stable}}$ , all of which effectively decrease the size of the side chain.

Comparison of the amino acid sequences of several enzymes that have thermophilic and mesophilic counterparts revealed that helix stabilizing residues were favored in the thermophilic proteins (46). The SCS sequences were examined to see if there was a tendency for substitution of residues that would potentially stabilize the appropriate secondary structures in the more stable proteins. The pig heart, *E. coli*, and *T. aquaticus* SCS amino acid sequences were compared using the secondary structure from the *E. coli* enzyme as a reference (28). The substitutions from a less stable protein to a more stable protein were counted based on whether the substitutions in the more stable protein stabilized or destabilized the secondary structure in which it resided. Only  $\alpha$ -helices or  $\beta$ -sheets were considered. The list of residues that stabilized each secondary structure was taken from the survey of the PDB done by Levitt (32). There were 220 substitutions that stabilized their corresponding secondary structure in the more stable SCS, and there were 193 substitutions that destabilized their corresponding secondary structure. Thus, there was only a slight “improvement” in the stabilization of secondary structures in the more

stable SCS sequences. In addition, in the amino acid sequence of *T. aquaticus*, there are two proline residues that would occur in the center of  $\alpha$ -helices based on *E. coli* SCS, indicating that these  $\alpha$ -helices in *T. aquaticus* SCS are either shortened or broken in the center.

Comparison of the crystal structures of mesophilic and thermophilic enzymes has revealed several features that were correlated with thermophilicity (46, 49, 47, 50, 48). One of these was an increase in the number of intrasubunit ion pairs. The ion pairs between side chains in *E. coli* and pig heart SCS were identified using the crystallographic structures of these enzymes (26, 28). The potential ion pairs in *T. aquaticus* were predicted using the amino acid sequence alignment of *E. coli* and *T. aquaticus* SCS shown in Figures 1-2 and 1-3 as described in Materials and Methods. Tabulation of the ion pairs in *E. coli* SCS, and pig heart SCS, and the potential ion pairs in *T. aquaticus* SCS are tabulated in Table 3-2 below. There are more intrasubunit ion pairs in the *E. coli* enzyme than in the pig heart enzyme, and even more potential ion pairs in the *T. aquaticus* enzyme. Furthermore, there is also an additional number of potential intersubunit ion pairs in *T. aquaticus* SCS.

Table 3-2. Ion Pairs in SCS from Pig Heart<sup>a</sup>, *E. coli*<sup>a</sup>, and *T. aquaticus*<sup>b</sup>.

Enzyme Source	Intrasubunit Ion Pairs		Intersubunit Ion Pairs	
	$\alpha$ -subunit	$\beta$ -subunit	$\alpha_1/\beta_1$	$\alpha_1/\beta_2$
Pig Heart	8	13	3	na <sup>c</sup>
<i>E. coli</i>	11	20	3	4
<i>T. aquaticus</i>	18	27	7	7

<sup>a</sup> Evaluated using the program CONTACT from the CCP4 package and the crystallographic structures of either pig heart or *E. coli* SCS (26, 28).

<sup>b</sup> Evaluated using the structure of *E. coli* SCS and the sequence alignment in Figures 1-2 and 1-3 as outlined in Materials and Methods.

<sup>c</sup> Not applicable, because pig heart SCS is a dimeric enzyme that consists of only one  $\alpha$ -subunit and one  $\beta$ -subunit. The *T. aquaticus* and *E. coli* enzymes are heterotetramers with two of each subunit.



## Discussion

It has been proposed that the folding of polypeptides follows an energy landscape that is shaped like a funnel with the most stable (native) form at the bottom (9-11). If folding intermediates exist for a given protein, then they are represented by valleys in this landscape. The transition states on the way to the native state are represented by peaks in this landscape. Thus, the energy landscape for a protein that shows a two state transition between folded and unfolded forms is a smooth funnel. In addition, it has been proposed that discrete folding units exist (15). Taken together these would imply that proteins having the same protein fold should also fold in the same manner. This has been shown to be the case for the cold shock protein Csp B, which undergoes a two state transition (13). To consider this implication in a system that has a "rough" energy landscape, the folding of a thermophilic enzyme, *T. aquaticus* SCS, was compared to that of a previously investigated mesophilic enzyme, *E. coli* SCS.

*Equilibrium Unfolding of T. aquaticus SCS, and Comparison to E. coli SCS.* The equilibrium unfolding of *E. coli* SCS has a number of intermediates (17) and thus has a "rough" energy landscape. The activity of *E. coli* SCS in increasing concentrations of GuHCl was lost prior to any observed changes in optical measurements (fluorescence, or far-UV CD), and two transitions were evident in measurements by far-UV circular dichroism (17), reflecting changes in secondary structure. These results implied the existence of multiple intermediates during the unfolding of *E. coli* SCS. In similar ways the equilibrium unfolding of *T. aquaticus* SCS also implied a number of intermediates. Like *E. coli* SCS, the whole enzyme lost all catalytic activity prior to any changes in secondary structure, and measurements of the ellipticity in different concentrations of GuHCl revealed two transitions. As would be expected for a thermophilic enzyme, these transitions occurred at higher GuHCl concentrations ( $[\text{GuHCl}]_{1/2}$  of 2.2 M and 3.7 M) than the corresponding transitions for the *E. coli* enzyme ( $[\text{GuHCl}]_{1/2}$  of 0.75 M, and 1.68 M). Re-analysis of the Nishimura and Kahn data for the denaturation of *E. coli* SCS in GuHCl

as monitored by CD (39) produced values for  $[\Delta G_u^{H_2O}]_{app}$  and  $m$  associated with *E. coli* SCS. The  $[\Delta G_u^{H_2O}]_{app}$  is an estimate of the stability of the protein in the absence of denaturant, and  $m$  is proportional to the increase in solvent accessible surface area upon unfolding (40, 51, 12). The  $[\Delta G_u^{H_2O}]_{app}$  values for the unfolding of *E. coli* SCS were, 10.9 kJ/mol, and 12.3 kJ/mol, for the first and second transitions, respectively. Consistent with the relative values observed for the  $[GuHCl]_{1/2}$  these values for  $[\Delta G_u^{H_2O}]_{app}$  are 2-3 times less than those determined for the *T. aquaticus* enzyme (Table 3-1). The  $m$  values for the denaturation of *E. coli* SCS (14.6 kJ/mol/M for the first transition, and 7.3 kJ/mol/M for the second) compare favorably to the values of  $m$  for the *T. aquaticus* enzyme (13 and 7.1 kJ/mol/M, respectively), indicating that the domains being denatured in *T. aquaticus* SCS expose approximately the same surface area to the solvent as those in *E. coli* SCS. This would imply that the intermediates in the equilibrium unfolding of *T. aquaticus* SCS resemble those in the unfolding of *E. coli* SCS. Further investigation of the changes in fluorescence of the *T. aquaticus* enzyme and of the intermediates present in the unfolding of the *E. coli* enzyme in various concentrations of guanidine should be completed prior to the assertion of equivalence between these pathways.

The analysis of the intermediates in the equilibrium unfolding of *T. aquaticus* SCS revealed two intermediates. First after the enzyme had lost catalytic activity in GuHCl, but before there were any changes in the molar ellipticity, the results from gel filtration chromatography and sedimentation equilibrium indicated the presence of high molecular weight species deficient in the  $\alpha$ -subunit. Thus, the loss in activity was either due to oligomerization or due to the dissociation of some of the  $\alpha$ -subunit. Second, at concentrations of GuHCl between the two transitions observed by far-UV CD, the intermediate species of SCS present were partially folded and separated subunits, and the first transition reflected the partial denaturation of part of at least one of the subunits. This was concluded because gel filtration chromatography had shown that the subunits were

separated, and equilibrium denaturation of the isolated subunits had shown that denaturation of whole enzyme was not simply the sum of the denaturation of each subunit.

*Thermodynamic Constants Derived from the Equilibrium Unfolding.* The equilibrium denaturation of either separated subunits or whole *T. aquaticus* SCS in various concentrations of GuHCl was used to calculate the corresponding values of  $[\Delta G_u^{H_2O}]_{app}$ , and  $m$ . Neither of these values for the individual subunits coincided with the values for either transition associated with unfolding the whole enzyme, indicating that neither of these transitions corresponded solely to the denaturation either subunit. The values of  $[\Delta G_u^{H_2O}]_{app}$  for the isolated subunits were significantly lower than those for the whole enzyme, indicating that in the heterotetramer, the subunits are stabilized by association with each other. The  $m$  value for the isolated  $\alpha$ -subunit was 1.35 times less than the  $m$  value for the  $\beta$ -subunit, consistent with 1.7, the ratio of the mass of the  $\beta$ -subunit to the mass of the  $\alpha$ -subunit, and an approximate estimation of surface exposed. Summation of the  $m$  values for the two transitions in the whole enzyme gives a value of 20.1 kJ/mol·M for the denaturation of whole enzyme. Within experimental error this is consistent with a value of 17 kJ/mol·M derived by summation of  $m$  values for the isolated subunits times 2 (two of each subunit make up the tetramer). This indicated that the surface area exposed by denaturation of the individual subunits was approximately the same as that exposed by denaturation of the native enzyme. The 3 kJ/mol·M difference may reflect the surface area between the subunits. This implied that the isolated subunits retain most of their native structure, which is consistent with the results of far-UV CD of the isolated subunits (Fig 3-12).

The values of  $[\Delta G_u^{H_2O}]_{app}$  for *T. aquaticus* SCS (29 and 25 kJ/mol), although higher than those for the *E. coli* enzyme, are in the mid-range of the values that have been measured for other, primarily mesophilic proteins (20-60 kJ/mol) (52). This indicates that the thermal stability of *T. aquaticus* SCS does not arise from an increase in the  $[\Delta G_u^{H_2O}]_{app}$ , but rather from a change in the dependence of the  $\Delta G_u^{H_2O}$  on temperature. For proteins,

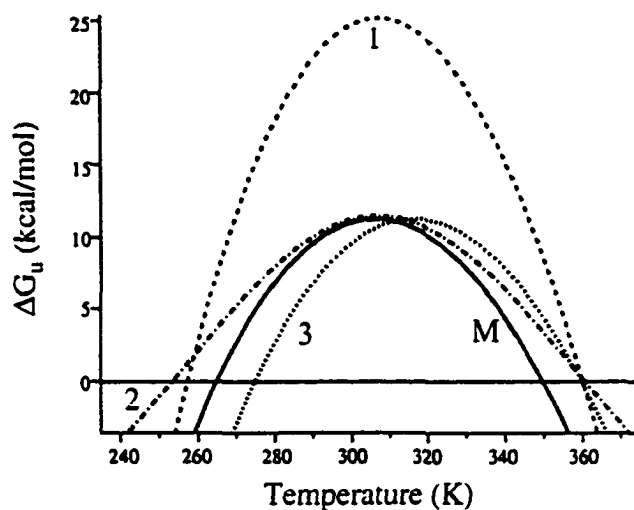


**Figure 3-21. Models for the dependence of free energy on temperature.** Curve M (solid line) represents the relationship between the free energy of unfolding,  $\Delta G_u$ , and temperature for a typical mesophilic protein. Curve 1 (dashed line), the thermophilic protein has greater stability over all temperatures. Curve 2 (dashed and dotted line), the magnitude of  $\Delta G_u$  depends less on temperature. Curve 3 (dotted line) the relationship between  $\Delta G_u$  and temperature is the same as that for the mesophilic protein, but is shifted to a higher temperature. This figure was taken from Beadle *et al.*(54).

the dependence of the free energy of unfolding,  $\Delta G_u$ , on temperature graphically describes a parabola (40), and several models have been proposed to explain the thermal stability of thermophilic proteins (53, 54) (Fig. 3-21). A thermophilic enzyme could have a greater  $\Delta G_u$  over all temperatures (Fig. 3-21, curve 1), or the dependence of  $\Delta G_u$  on temperature could be either flattened or shifted to higher temperatures (Fig. 3-21, curves 2 or 3, respectively). The thermal stability of *T. aquaticus* SCS likely does not arise entirely from the model represented by curve 1 because its  $\Delta G_u$  is no higher than that of other mesophilic proteins. However, it also does not arise entirely from either of the other models, because they predict that the  $\Delta G_u$  should be lower or equal to that for the *E. coli* protein at room temperature. Thus, the thermal stability of *T. aquaticus* SCS arises from a combination of these models. It is more stable than *E. coli* SCS at 22 °C, and is either less dependent on temperature or its optimal stability is shifted to a higher temperature. These possibilities can be distinguished by repeating the denaturation of *T. aquaticus* SCS in GuHCl at different temperatures.

*Kinetics of Refolding T. aquaticus SCS.* To extend the comparison between the folding of the thermophilic *T. aquaticus* SCS, and mesophilic SCS from *E. coli*, the kinetics of refolding of *T. aquaticus* SCS was examined. The conditions under which pig heart SCS (18) or *E. coli* SCS (16, 39) were refolded could not be used for the refolding of *T. aquaticus* SCS, nor could the conditions developed for the refolding of *T. aquaticus* SCS be used for the refolding of pig heart or *E. coli* SCS. This indicated that the refolding of these enzymes *in vitro* were quite different from one another. Further investigation of the kinetics of refolding of *T. aquaticus* SCS required the use of arginine in the refolding solution. It has been proposed that co-solvents such as glycerol, sorbitol, trehalose, lysine and arginine facilitate refolding by preferentially increasing the solvation of the native form of the protein of interest (55-57). Studies on RNase A have indicated that arginine also bound protein lowering its stability (57). Thus, the mechanism of the arginine mediated refolding of *T. aquaticus* SCS likely involves both of these effects, 1. an increase in the

solvation of the native form of *T. aquaticus* SCS, and 2. by providing a scaffold for the folding.

The rates of refolding *T. aquaticus* SCS in solutions containing arginine followed apparent first order kinetics (Fig 3-15), indicating that the rate limiting step in refolding was a unimolecular conformational change. An Arrhenius plot of the apparent first order rate constants of the refolding reactions at the different temperatures showed that the energy of activation for this conformational change was 65 kJ/mol. The corresponding value for *E. coli* SCS is 21.8 kJ/mol (16). These relative values are consistent with the respective growth temperatures for *E. coli* and *T. aquaticus*. The *T. aquaticus* enzyme can have a higher activation energy for folding than the *E. coli* enzyme because there is more thermal energy at the optimal growth temperature for *T. aquaticus*.

Consistent with the conclusion that the rate limiting step in refolding *T. aquaticus* SCS was a unimolecular conformational change, the rate of refolding was not concentration dependent over a 10 fold range in concentration. This is in contrast to the refolding of the *E. coli* enzyme, which is concentration dependent over the same concentration range (16).

*An Intermediate in the Refolding of T. aquaticus SCS.* The efficiency of refolding of a denatured enzyme is generally judged by the recovery of catalytic activity. However for a few proteins the recovery of activity does not correlate with recovery of the native structure (58-60). Refolding of *T. aquaticus* SCS in arginine buffer resulted in full recovery of enzymatic activity when measured at 22 °C, however the protein was no longer thermostable. To investigate the source of this instability, a full set of kinetic experiments, and gel filtration chromatography were conducted. All of the results with the refolded protein were indistinguishable from those of native *T. aquaticus* SCS. In fact, the  $K_{m(app)}$  values for substrates were slightly lower for refolded *T. aquaticus* SCS than for the native enzyme, implying intact and functional active sites. Thus, the source of the instability in *T. aquaticus* SCS is likely to be in the protein core. This has been shown to be the case in two other proteins that have been examined. Refolded  $\beta$ -lactoglobulin also exhibited a complete

recovery of its ligand binding activity, but was less stable than wild type enzyme. Significantly, both the binding of monoclonal antibodies and the lifetime of tryptophan phosphorescence were altered by refolding (58, 60). In the case of *E. coli* alkaline phosphatase, maximal enzymatic activity was regained after only one hour, while the lifetime of tryptophan phosphorescence did return to native values for several days (59). Refolded SCS from *T. aquaticus* does not recover its thermal stability in arginine buffers after 2 weeks. It does however recover its thermal stability after approximately 5 hours when the buffer is changed to a minimal phosphate/KCl buffer. There is one tryptophan in each of the  $\alpha$ - and  $\beta$ -subunits that could be used to monitor phosphorescence to investigate the possibility that the instability is due to poor packing in the hydrophobic core.

*Sequence Analysis of Three SCS Enzymes of Increasing Stability.* A number of comparison studies have examined the sequences and crystallographic structures of mesophilic proteins and their thermophilic counterparts, and have concluded that several factors contribute to the thermophilicity of proteins (46, 49, 47, 50, 48, 45). These include the following: 1) an increase in the number of  $\alpha$ -helix stabilizing residues, 2) an increase in the volume of buried hydrophobic residues, 3) an increase in ion pairs and hydrogen bonds between a charged residue and a neutral residue, and 4) a decrease in the surface to volume ratio of the protein. Examination of the amino acid sequences of the pig heart, *E. coli* and *T. aquaticus* SCS revealed that a number of seemingly minor changes in sequence are responsible for the increased stability of *E. coli* SCS when compared to pig heart SCS and of *T. aquaticus* SCS when compared to *E. coli* SCS. Consistent with the extensive survey of amino acid sequences from mesophilic and thermophilic proteins from *Methanococcus* species conducted by Haney *et al.* (45), the uncharged polar residues in less stable SCS were predominantly changed to almost any other residue in sequences of the more stable enzymes. In the amino acid sequences of the more stable enzymes, there was also a slight increase in the number of residues that would potentially stabilize the secondary structures in which they reside. There was also an increase in the number of ion pairs or potential ion

pairs in the more stable enzymes. In contrast to previous studies, the volume of the hydrophobic residues decreased because the conservative substitutions were in favour of residues with smaller side chains. However there was an increase in the total number of hydrophobic residues, which may lead to an increase in the total volume buried non-polar residues. Overall, these changes are not major since the thermodynamic parameters that were determined for *T. aquaticus* SCS indicated that although the *T. aquaticus* enzyme was more stable than the *E. coli* enzyme, it was still in the mid range of mesophilic proteins.

To summarize, the results of equilibrium unfolding of *T. aquaticus* SCS implied that the intermediates present at equilibrium may be similar to those present during the equilibrium unfolding of *E. coli* SCS. This supported the hypothesis that the folding of proteins with similar protein structures should be similar, as is the case for the folding of CspB (13). However, when the recovery of activity was monitored, the refolding of denatured *T. aquaticus* SCS did not even remotely resemble that of *E. coli* SCS, indicating that the paths that these enzymes take to reach those equilibrium intermediates are different. To further investigate those paths, it would be interesting to see if the recovery of secondary structure was the same in *T. aquaticus* SCS as in *E. coli* SCS.



**References:**

1. Jaenicke, R. (1991) *Biochemistry* 30, 3147-3161.
2. Levitt, M., Gerstein, M., Huang, E., Subbiah, S., & Tsai, J. (1997) *Annu. Rev. Biochem.* 66, 549-579.
3. Callender, R. H., Dyer, R. B., Gilmanshin, R., & Woodruff, W. H. (1998) *Annu. Rev. Phys. Chem.* 49, 173-202.
4. Baldwin, R. L., & Rose, G. D. (1999) *Trends Biochem. Sci.* 24, 26-33.
5. Baldwin, R. L., & Rose, G. D. (1999) *Trends Biochem. Sci.* 24, 77-83.
6. Anfinsen, C. B., Haber, E., Sela, M., & White, F. H. J. (1961) *Proc. Natl. Acad. Sci. USA* 47, 1309-1314.
7. Anfinsen, C. B. (1973) *Science* 181, 223-230.
8. Levinthal, C. (1968) *J. Chim. Phys.* 65, 44-45.
9. Baldwin, R. L. (1994) *Nature* 369, 183-184.
10. Baldwin, R. L. (1995) *J. Biomolec. NMR* 5, 103-109.
11. Dill, K. A., & Hue, S. C. (1997) *Nature Struct. Biol.* 4, 10-19.
12. Myers, J. K., Pace, N. C., & Scholtz, M. J. (1995) *Prot. Sci* 4, 2138-2148.
13. Perl, D. e. a. (1998) *Nat. Struct. Biol.* 5, 229-235.
14. Garel, J. R. (1992) *Folding of large proteins: Multidomain and multisubunit proteins* (Creighton, T. E., Ed.), W. H. Freeman and Company, New York
15. Tsai, C., & Nussinov, R. (1997) *Prot. Sci.* 6, 24-42.
16. Wolodko, W. T., & Bridger, W. A. (1987) *Biochem. Cell Biol.* 65, 452-457.
17. Khan, I. A., & Nishimura, J. S. (1988) *J. Biol. Chem.* 263, 2152-2158.
18. Nishimura, J. S., Ybarra, J., Mitchell, T., & Horowitz, P. M. (1988) *Biochem. J.* 250, 429-434.
19. Moffet, F. J., & Bridger, W. A. (1970) *J. Biol. Chem.* 245, 2758-2762.
20. Stanislawski, J. (1991), ENZYME KINETICS v1.11, Trinity Software, Campton, NH.
21. Johnson, M. L., Corriea, J. J., Yphantis, D. A., & Halvorson, H. R. (1981) *Biophys. J.* 36, 575-588.
22. Yphantis, D. A. (1991), NONLIN, Mansfield Center, Connecticut.

23. Hayes, D. B., Laue, T., & J., P. (1995-1998), SEDENTERP v1.01 University of New Hampshire, NH.
24. Cohn, E. J., & Edsall, J. T. (1943) in *Proteins, Amino acids and Peptides as Ions and Dipolar Ions* (Rheinhold, ed), pp. 157, New York
25. Laue, T. M., Shah, B. D., Ridgeway, T. M., & Peltier, S. L. (1992) *Computer-aided interpretation of analytical sedimentation data for proteins*. Analytical Ultracentrifugation in Biochemistry and Polymer Science. (Harding, S. E., Rowe, A. J., & Horton, J. C., Eds.), Royal Society of Chemistry, Cambridge
26. Fraser, M. E. *personal communication*.
27. Wolodko, W. T., Fraser, M. E., James, M. N. G., & Bridger, W. A. (1994) *J. Biol. Chem.* 269, 10883-10890.
28. Fraser, M. E., James, M. N. G., Bridger, W. A., & Wolodko, W. T. (1999) *J. Mol. Biol.* 285, 1633-1653.
29. Collaborative Computational Project, (1994) *Acta Cryst. D50*, 760-763.
30. Parish, J. (1999) *personal communication*.
31. Insight II Ed., MSI, Sandiego, CA
32. Levitt, M. (1978) *Biochemistry* 17, 4277-4285.
33. Bailey, D. L., Fraser, M. E., Bridger, W. A., James, M. N. G., & Wolodko, W. T. (1998) , *J. Mol Biol* 285, 1655-1666.
34. Wolodko, *personal communication*.
35. Hanes, C. (1932) *Biochem. J.* 26, 1406-1421.
36. Bridger, W. A. (1974) in *The Enzymes* (Boyer, P. D., ed) Vol. X, 3 Ed., pp. 581-606, Academic Press Inc., New York
37. Brock, T. D., & Freeze, H. (1969) *J. Bacteriol.* 98, 289-297.
38. Dams, T., Ostendrop, R., Ott, M., Rukat, K., & Jaenicke, R. (1996) *Eur. J. Biochem* 240, 274-279.
39. Kahn, I. A., & Nishimura, J. S. (1988) *J. Biol. Chem.* 263, 2152-2158.
40. Pace, C. N. (1975) *Crit. Rev. Biochem.* 3, 1-43.
41. Garboczi, D. N., Utz, U., Ghosh, P., Seth, A., J., K., VanTienhoven, E. A. E., Biddison, W. E., & Wiley, D. (1996) *J. Immunol* 157, 5403-5410.
42. KALIDAGRAPH v3.0, Synergy Software, Reading PA
43. Neet, K. E., & Timm, D. E. (1994) *Protein Sci.* 3, 2167-2174.

44. Voet, D., & Voet, J. G. (1995) *Biochemistry*, 2nd Ed., John Wiley and Sons, Inc., New York
45. Haney, P. J., Badger, J. H., Buldak, J. L., Reich, C. L., Woese, C. R., & Olsen, G. J. (1999) *Proc. Natl. Acad. Sci.* 96, 3578-3583.
46. Argos, P., Rossman, M. G., Grau, U. M., Zuber, H., Frank, G., & Tratschin, J. (1979) *Biochemistry* 18, 5698-5703.
47. Davies, G., J., Gamblin, S. J., Littlechild, J. A., & Watson, H. C. (1993) *Proteins* 15, 283-289.
48. Tanner, J. J., Hecht, R. M., & Krause, K. L. (1996) *Biochemistry* 35, 2597-2609.
49. Lim, H. M., & Pene, J. J. (1988) *Gene Anal. Techniques* 5, 32-39.
50. Krino, H., Aoki, M., Aoshima, M., Hayashi, Y., Ohba, M., Yamagishi, A., Wakagi, T., & Oshima, T. (1994) *Eur. J. Biochem.* 220, 275-281.
51. Strotle, D. (1989) *J. Biol. Chem.* 264, 5315-5318.
52. Pace, C. N. (1990) *Trends Biotechnol.* 8, 93-98.
53. Nojima, H., Ikai, A., Oshima, T., & Noda, H. (1977) *J. Mol. Biol.* 116, 429-442.
54. Beadle, B. M., Base, W. A., Wilson, D. B., Gilkes, N. R., & Shoichet, B. K. (1999) *Biochemistry* 38, 2570-2576.
55. Lin, T., & Timasheff, S. N. (1996) *Prot. Sci.* 5, 372-381.
56. Cacace, M. G., Landau, E. M., & Ramsden, J. J. (1997) *Quant. Rev. Biophys.* 30, 241-277.
57. Guife, X., & Timasheff, S. N. (1997) *Prot. Sci.* 6, 211-221.
58. Hattori, M., Ametani, A., Katakura, Y., Shimizu, M., & Kaminogawa, S. (1993) *J. Biol. Chem.* 268, 22414-22419.
59. Subramaniam, V., Bergenham, N., Gafni, A., & Steel, D. G. (1995) *Biochemistry* 34, 1133-1136.
60. Subramaniam, V., Steel, D. G., & Gafni, A. (1996) *Prot. Sci.* 5, 2089-2094.
61. Norby, J., Rubenstein, S., Tuerke, T., Schwallie Farmer, C., Forood, R., Bennington, J. (1983) SIGMA PLOT v4.11, Jandel Scientific.

**Page intentionally left blank for note taking.**

## **Chapter Four      Photoaffinity Labeling of *E. coli* SCS with 8-N<sub>3</sub>-ATP<sup>1</sup>**

### **Introduction**

Previous work had implied that the nucleotide binding site is located in the  $\beta$ -subunit of SCS. The cloning and characterization of the ATP- and GTP-specific isozymes from pigeon breast and liver revealed that they consist of the same  $\alpha$ -subunit but different  $\beta$ -subunits (1, 2). This implies that the nucleotide specificity of SCS resides with the  $\beta$ -subunit. Although this implication contradicts an earlier study that suggested that the nucleotide-binding site was present in the  $\alpha$ -subunit (3), it is consistent with the crystal structure of the *E. coli* enzyme. Both of the two nucleotide-binding (Rossmann) folds in the  $\alpha$ -subunit are occupied, one by bound CoA, and the other by the loop that contains the active-site phosphohistidine (4). However, there are two unoccupied potential nucleotide-binding sites in the  $\beta$ -subunit: a third Rossmann fold in the C-terminal domain (4), and the "ATP-grasp" fold in the N-terminal domain (5, 6). The residues lining each of these sites are well conserved amongst known amino acid sequences of SCS. Figures 4-1 and 4-2 show nucleotide modeled into each of these domains.

The location of each of these potential nucleotide-binding sites relative to the bound CoA and the active-site phosphohistidine would have direct and different consequences to our understanding of the catalytic mechanism of SCS. If the nucleoside triphosphate were bound in the C-terminal domain of the  $\beta$ -subunit (Fig. 4-1), no substantial conformational change would be required for phosphorylation/dephosphorylation of the active-site histidine (partial reaction (1), in Chapter 1). If the nucleotide were bound in the N-terminal domain of the  $\beta$ -subunit, then the active-site phosphohistidine is 35 Å away (Fig. 4-2B), and a major conformational change would therefore be required to bring the phosphohistidine into proximity with the nucleoside diphosphate (6).

---

<sup>1</sup> A version of this chapter has been published: Joyce, M. A., Fraser, M. E., Brownie, E. R., James, M. N. G., Bridger, W. A., Wolodko, W. T. (1999) *Biochemistry* 38, 7273-7283.

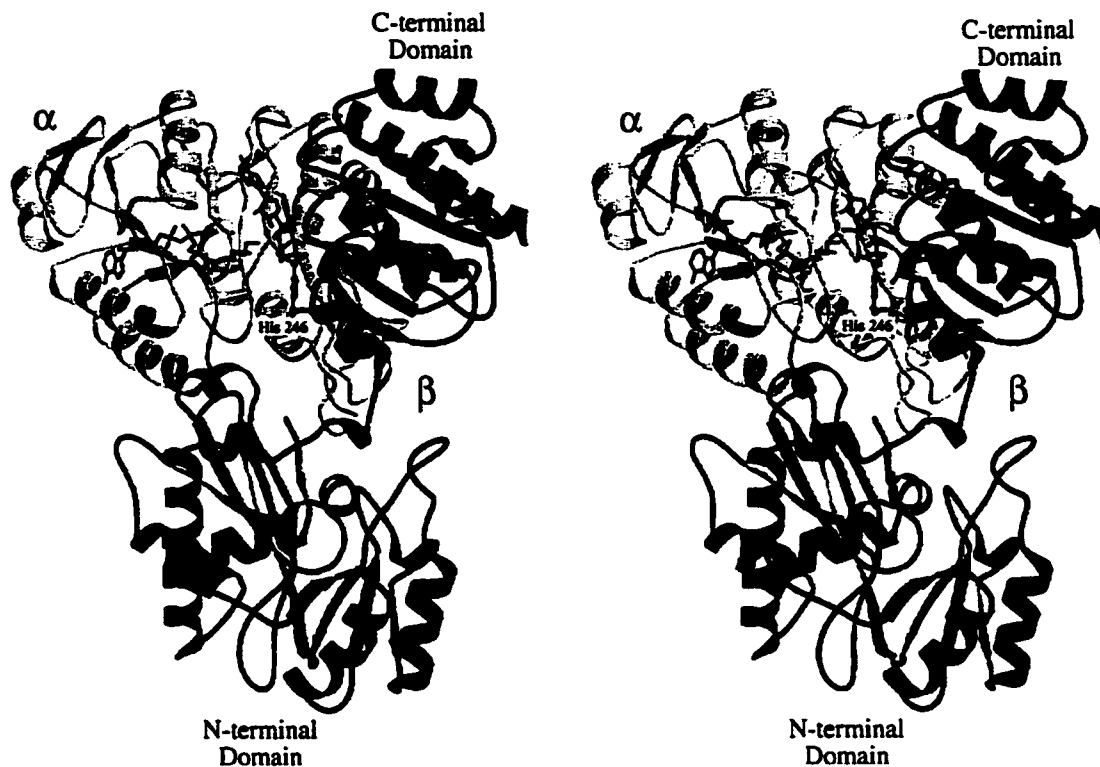
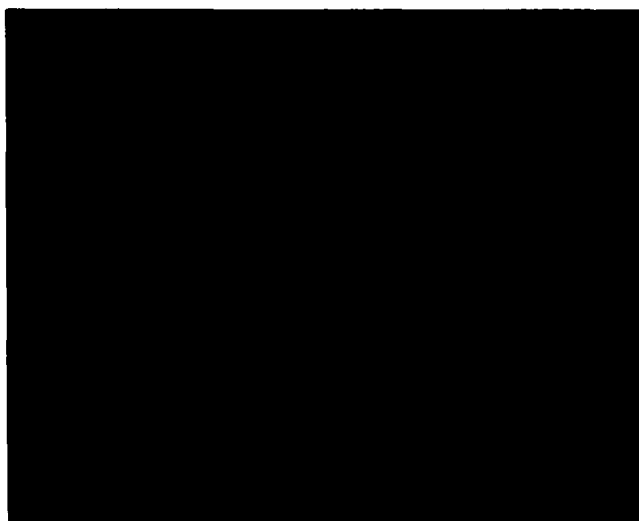


**Figure 4-1. Stereo ribbon diagram of an  $\alpha\beta$ -dimer of SCS with ATP modeled into the C-terminal domain of the  $\beta$ -subunit. The  $\alpha$ -subunit is shown in yellow, the  $\beta$ -subunit in green, the active site phosphohistidine is displayed as a mauve ball and stick model. The molecules of CoA and ATP are displayed as stick models in cyan and red, respectively.**

A



B

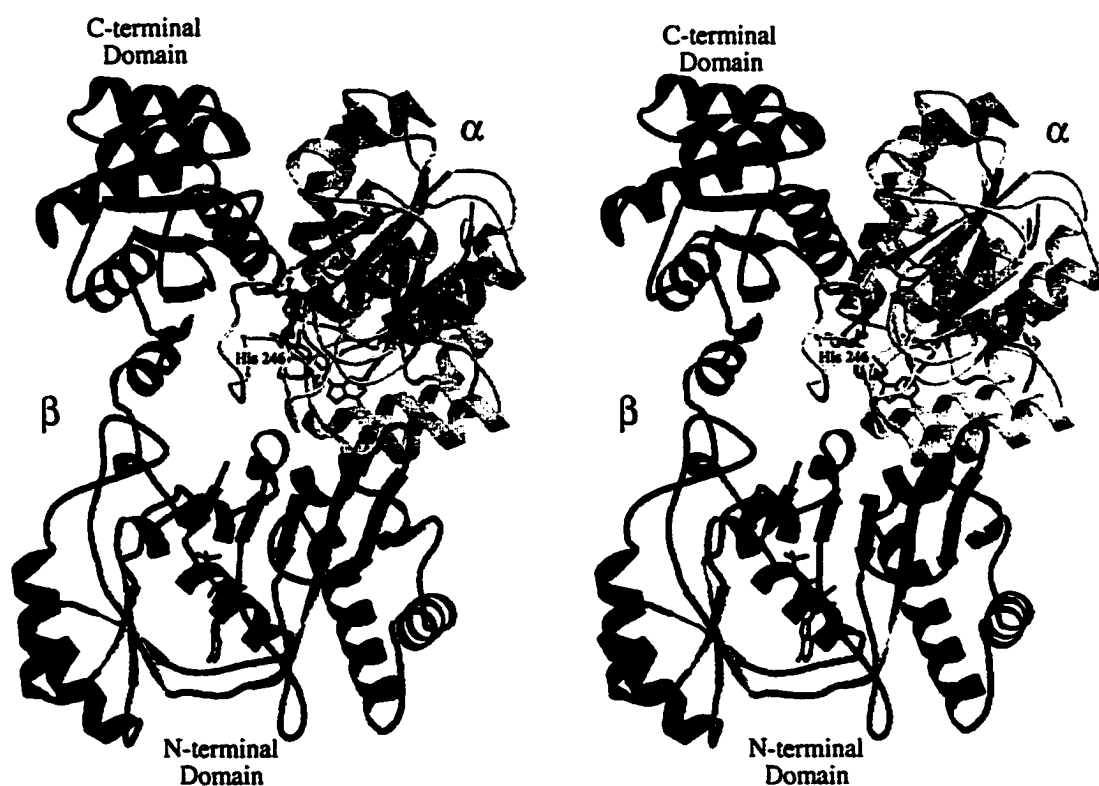


**Figure 4-2. Modeling of ADP into the N-terminal domain of the  $\beta$ -subunit of SCS.** (A) Ribbon diagram of a superposition of the N-terminal domain of the  $\beta$ -subunit (shown in green) of SCS on D-ala:D-ala ligase (shown in grey). The superposition was based on the c- $\alpha$  positions of 101 atoms with an rms deviation of 2.286 Å. (Appendix 3) (B) Stereo ribbon diagram of ADP modeled into the N-terminal domain of the  $\beta$ -subunit of an  $\alpha\beta$ -dimer of SCS based on the superposition shown in (A). The  $\alpha$ -subunit of SCS is shown in yellow, the  $\beta$ -subunit in green, the active site phosphohistidine and the CoA molecule are displayed as stick models in mauve and cyan, respectively. The ADP molecule is shown in red. The model has been rotated by approximately 180° with respect to that shown in Figure 3-1.

The location of the nucleotide binding site was investigated by using the photoaffinity analogue 8-N<sub>3</sub>-ATP. This avoids the pitfalls of experiments using oxidized CoA disulfide, where the ability of oxidized CoA disulfide to bind to the substrate binding site was investigated indirectly using desulfo-CoA (7). These characteristics led to specific incorporation of 8-N<sub>3</sub>-ATP into the nucleotide binding site.

The focus of the present study was to determine the location of the nucleotide-binding site in *E. coli* SCS using the photoaffinity analogue 8-N<sub>3</sub>-ATP. 8-N<sub>3</sub>-ATP was chosen for two related reasons. First, 8-N<sub>3</sub>-ATP is stable in the dark, and this allowed for the investigation of its suitability as a substrate for SCS. Second, a free radical is thought to be generated upon the irradiation of 8-N<sub>3</sub>-ATP, and thus the reactive species should react with any proximal groups, and not be dependent on the presence of a specific side chain. A free radical reactive species is also expected to have a relatively short lifetime reducing the amount of non-specific labeling of the protein. To investigate the suitability of 8-N<sub>3</sub>-ATP as an affinity analogue for use with SCS, a number of studies were carried out. The ability of 8-N<sub>3</sub>-ATP to label SCS in a manner consistent with its behavior as a substrate was investigated. In addition, the inactivation of SCS by 8-N<sub>3</sub>-ATP, the kinetic relationship between ATP and 8-N<sub>3</sub>-ATP, and the stoichiometry of 8-N<sub>3</sub>-ATP photolabeling of SCS were evaluated. The photoaffinity analogue, 8-N<sub>3</sub>-ATP, was then used to label SCS, and the location of the bound label was determined by the isolation of photolabeled tryptic peptides.

## Materials and Methods

*Photolabeling of E. coli SCS by [ $\alpha$ -<sup>32</sup>P]-8-N<sub>3</sub>-ATP.* Wild-type *E. coli* SCS was over-expressed and purified according to the methods of Wolodko *et al.* (8, 4). The ATP analogue, 8-N<sub>3</sub>-ATP, was purchased from Sigma-Aldrich Canada Ltd., and [ $\alpha$ -<sup>32</sup>P]-8-N<sub>3</sub>-ATP (2-10 Ci/mmol) from ICN Pharmaceuticals, Inc. For the saturation studies, 5  $\mu$ g of SCS in 30  $\mu$ l of a solution containing 50 mM KCl, 10 mM MgCl<sub>2</sub>, 1  $\mu$ M succinate, 0.12



$\mu\text{M}$  CoA, and 50 mM MOPS, pH 7.4 was incubated for 15 s on ice with the appropriate concentration of [ $\alpha$ - $^{32}\text{P}$ ]-8- $\text{N}_3$ -ATP (0.1-0.3 Ci/mmol). Conditions were identical for the pH range studies, except that either 50 mM MOPS, pH 7.8 or 50 mM MES, pH 6.4 were used in place of 50 mM MOPS, pH 7.4. The sample was then irradiated for 30 s, 2 min., or 5 min. using a hand-held UV6L Mineralight UV lamp ( $I = 360 \mu\text{W}/\text{cm}^2$ ,  $\lambda = 254 \text{ nm}$ ) from a distance of 2 cm. The reaction was quenched by the addition of 1  $\mu\text{l}$  of 0.25 M DTT. Next, 20  $\mu\text{l}$  of SDS-PAGE loading buffer (2.5% (w/v) SDS, 1 mM 2-mercaptoethanol, 35% (v/v) glycerol, and 50 mM Tris HCl, pH 6.6) was added to the samples, which were then heated to 96 °C for 5 min prior to analysis by SDS-PAGE using a 12% (w/v) polyacrylamide gel (9). Phosphorimaging of the photolabeled SCS was carried out using a Fujix BAS 1000 phosphorimager. Exposure of the imaging plate was usually complete in 2-3 hours. For inhibition of the photolabeling, 2 mM ATP or 3 mM GTP was included in the buffer during the photolabeling procedure. Apparent dissociation constants were determined by analysis of the labeling data using the program ENZYME KINETICS 1.11 (10).

*Inactivation of SCS Activity by 8- $\text{N}_3$ -ATP.* The procedure was identical to the procedure for the saturation of photolabeling, except that 2.6  $\mu\text{g}$  of SCS and non-radioactive 8- $\text{N}_3$ -ATP were used. After quenching, 8  $\mu\text{l}$  of each sample was assayed for SCS activity using a spectrophotometric assay that measures the formation of the thioester bond of succinyl-CoA at 235 nm (11). To study the protection of SCS from inactivation by 8- $\text{N}_3$ -ATP, 2 mM ATP or GTP was included in the buffer.

*Determination of the  $K_m$  (app) of SCS for 8- $\text{N}_3$ -ATP.* Kinetic reactions were conducted at 22 °C and started by the addition of 16.5  $\mu\text{g}$  of SCS in 10  $\mu\text{l}$  to 1 ml of a buffer containing 10 mM  $\text{MgCl}_2$ , 10 mM succinate, 100  $\mu\text{M}$  CoA, 20 mM Tris HCl, pH 7.4 and various concentrations of 8- $\text{N}_3$ -ATP. The rate of formation of succinyl-CoA was monitored spectrophotometrically at 235 nm in duplicate at each concentration. The data were analyzed using the program SIGMA PLOT (12). The curve was fitted using the Hill

equation:  $v = V_{\max}[S]^n/(K + [S]^n)$ , where  $v$  is the velocity of SCS in  $\mu\text{moles}/\text{min}/\text{mg}$ ,  $V_{\max}$  is the maximum velocity,  $[S]$  is the concentration of 8- $\text{N}_3$ -ATP,  $K$  is a constant, and  $n$  is the Hill coefficient (13).

*Investigation of the Kinetic Relationship between 8- $\text{N}_3$ -ATP and ATP.* Kinetic measurements were carried out to determine whether 8- $\text{N}_3$ -ATP was competitive with ATP in the synthesis of succinyl-CoA by SCS. The buffers used for these reactions were identical to those used for the determination of the  $K_{m(\text{app})}$  of SCS for 8- $\text{N}_3$ -ATP. The reactions were initiated using 0.12 - 0.24  $\mu\text{g}$  of SCS. The rate of formation of succinyl-CoA in reactions containing various concentrations of ATP (ranging from 5  $\mu\text{M}$  to 400  $\mu\text{M}$ ) and 8- $\text{N}_3$ -ATP (0, 29, 58, and 100  $\mu\text{M}$ ) was monitored. The velocity data were analyzed using the program ENZYME KINETICS 1.11 (10).

*Photolabeling and Mass Spectrometry of SCS Subunits.* Photolabeled SCS for mass spectrometry was prepared by irradiation of 30  $\mu\text{g}$  of SCS in 400  $\mu\text{l}$  of a buffer containing 50 mM KCl, 10 mM  $\text{MgCl}_2$ , 50 mM MOPS, pH 7.4, and either 400  $\mu\text{M}$  or 724  $\mu\text{M}$  8- $\text{N}_3$ -ATP. Irradiation was carried out in a Southern New England Ultraviolet Co. RPM200 UV box (reactor  $\lambda = 350$  nm) for 7 min at 4 °C. The  $\alpha$ - and  $\beta$ -subunits were then separated by reverse phase HPLC using a Vydac 4.6 x 250 mm  $\text{C}_8$  column on a Varian Vista series 5000 liquid chromatography system equipped with a Hewlett Packard 1040 HPLC diode array detector. The mobile system consisted of 0.05% (v/v) trifluoroacetic acid in water (A) and 0.05% (v/v) trifluoroacetic acid in acetonitrile (B). The gradient for HPLC was either 2% (v/v) B/min, or 2% (v/v) B/min for 20 min followed by 0.5% (v/v) B/min for 40 min, at a flow rate of 1 ml/min. Fractions containing the separated subunits were analyzed using a Fisons VG Quatro triple quadrupole mass spectrometer with an electrospray ionization source running in positive mode. The running buffer for the mass spectrometry was 50% (v/v) acetonitrile/water, and 0.1% (v/v) trifluoroacetic acid flowing at a rate of 10  $\mu\text{l}/\text{min}$ . The quadrupoles were scanned 10-15 times at a rate of 10s/scan, and

summed to produce the final spectrum. Several multiply charged species in a series were then used to calculate the mean molecular mass.

*Photolabeling of SCS by 8-N<sub>3</sub>-ATP for Purification and Sequencing or Mass Spectrometry of Labeled Peptides.* Photolabeled SCS was prepared by irradiation for 1 min of a total of 566 µg SCS in 500 µl split into three similar aliquots containing 50 mM KCl, 10 mM MgCl<sub>2</sub>, 400 µM [ $\alpha$  <sup>32</sup>P]-8-N<sub>3</sub>-ATP (30 Ci/mol), and 50 mM MOPS, pH 7.4, on ice. Irradiation ( $\lambda = 254$  nm) was carried out from a distance of 2 cm. The aliquots were pooled, and the photolabeling quenched by the addition of 3 µl of 1 M DTT. Labeled protein was separated from free analogue in the reaction mixture on a 20 ml Sephadex G-50 column previously equilibrated with 20 mM Tris HCl, pH 8.0. The labeled SCS eluted after the first 8 ml in a total volume of 3 ml. Labeled SCS was digested at 37 °C with 20 µg of modified sequencing grade trypsin (Boehringer Mannheim). After 12 hours, the pH was adjusted to pH 6.0 with 3 µl of 11.6 M HCl to stop the reaction, and 3 ml of 5 mM DTT, 100 mM ammonium acetate, pH 6.0 was added.

An Al<sup>3+</sup> affinity column (Chelating Sepharose Fast Flow, purchased from Pharmacia Biotech Inc.) was prepared and chromatography performed according to the methods of Jayaram and Haley (14): 5 ml of iminodiacetic acid Chelating Sepharose Fast Flow was washed successively with 3 x 25 ml volumes of water, buffer A (5 mM DTT, 100 mM (NH<sub>4</sub>)<sub>2</sub>SO<sub>4</sub>, pH 6.0), buffer B (5 mM DTT, 0.5 mM NaCl, 100 mM (NH<sub>4</sub>)<sub>2</sub>SO<sub>4</sub>, pH 6.0), buffer A, buffer C (5 mM DTT, 5 M urea, 100 mM (NH<sub>4</sub>)<sub>2</sub>SO<sub>4</sub>, pH 6.0) and buffer A. A 5 ml portion of the "washed" resin was then placed in a column, the flow rate was adjusted to approximately 0.5 ml/min, and the digested SCS was loaded onto this column. The labeled peptides associated with the Al<sup>3+</sup> column because of the charges on the phosphates of the analogue. The column was then washed successively with 2 x 30 ml of each of buffer A, buffer B, buffer A, buffer C, and buffer A. The final elution step was carried out with 100 mM ammonium acetate, 10 mM sodium pyrophosphate, pH 8.0. The radiolabeled peptides eluted in the final step. Aliquots of 5 µl of each fraction were assayed

for radioactivity using a Beckman LS 7800 liquid scintillation counter. The fractions containing radioactivity were pooled and further purified by reverse phase HPLC using the same column and HPLC system that was used for purification of the subunits. The HPLC gradient was isocratic for 30 min at 0% (v/v) B to allow elution of the flowthrough. This was followed by a gradient of 1% (v/v) B/min with a flow rate of 0.5 ml/min. Fractions of 0.5 ml were collected and aliquots assayed for radioactivity using a Beckman LS 7800 liquid scintillation counter. The peptides containing radioactivity were sequenced by Edman degradation with a Hewlett Packard 1005A peptide sequencer. Mass spectrometry was performed using a VG Quatro electrospray mass spectrometer in the same manner as for the subunits. The fractions that eluted from the  $Al^{+3}$  column during the washes were also assayed by reverse phase HPLC using the same system and gradient as for the radioactive fractions except that there was no isocratic gradient and the flow rate was 1 ml/min.

## Results

Several methods were used to determine if 8- $N_3$ -ATP was an appropriate photoaffinity analogue of ATP for studies with SCS. It was shown that 8- $N_3$ -ATP labels SCS in a saturable manner that was coincident with the inactivation of SCS. It was also shown that 8- $N_3$ -ATP was a substrate for SCS and, upon irradiation, labeled the  $\beta$ -subunit with a stoichiometry of one 8- $N_3$ -ATP per  $\beta$ -subunit.

*Photolabeling of SCS by 8- $N_3$ -ATP.* Irradiation of SCS in the presence of [ $\alpha$ - $^{32}P$ ]-8- $N_3$ -ATP resulted in the photolabeling of SCS at pH 6.4 and 7.8 (Fig. 4-3). Control samples of SCS were not labeled by [ $\alpha$ - $^{32}P$ ]-8- $N_3$ -ATP when incubations were carried out in the dark, nor when the irradiation step was carried out prior to the addition of SCS (Fig. 4-3, lanes 1 and 2). Irradiation of SCS for 30 s at pH 7.4 resulted in saturable labeling of SCS with [ $\alpha$ - $^{32}P$ ]-8- $N_3$ -ATP (Fig. 4-4). As evident from the autoradiograms, photolabeling occurred predominantly in the  $\beta$ -subunit (Fig. 4-4A). Some labeling of the

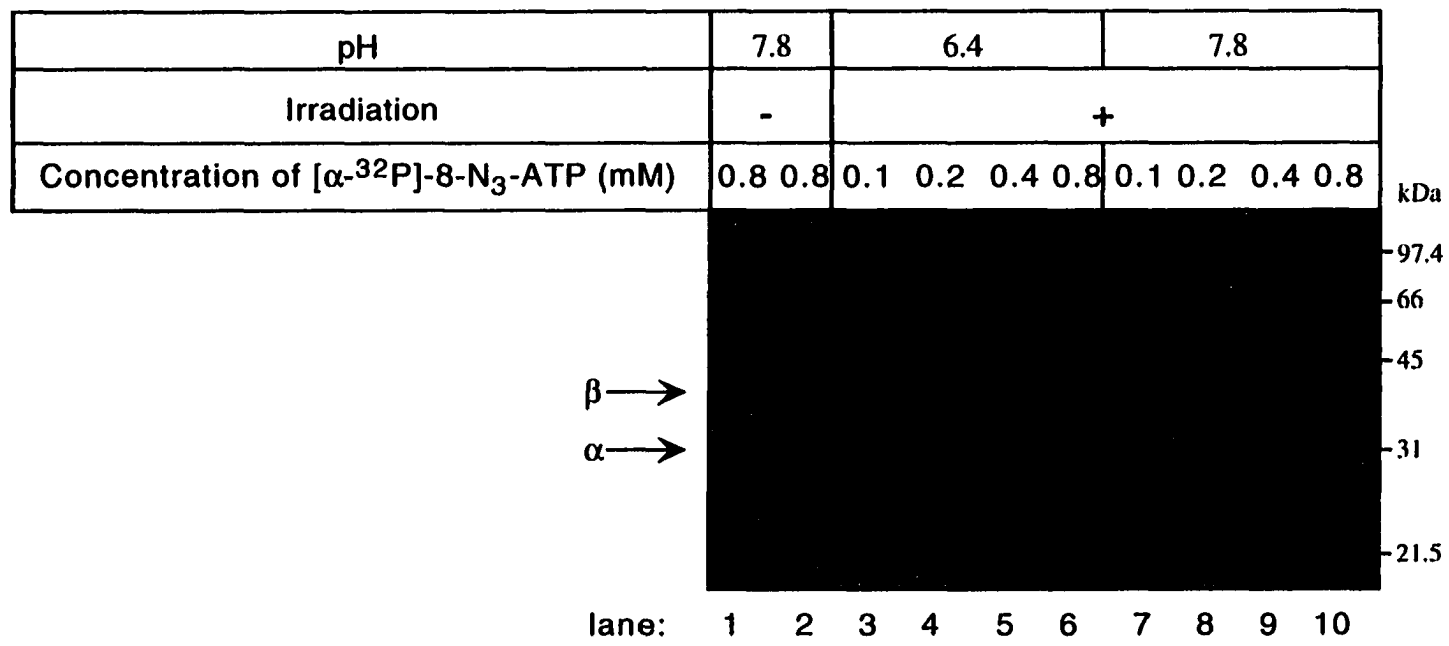


**FIGURE 4-3. Autoradiogram of SCS photolabeled at pH 6.4 and 7.8 as analyzed by SDS-PAGE.** The sample in lane 1 was incubated in the dark in the presence of [ $\alpha$ - $^{32}$ P]-8-N $_3$ -ATP for 2 min. prior to the addition of DTT (to stop the reaction). The sample in lane 2 was irradiated prior to the addition of SCS. Lanes 3-6 contain SCS irradiated for 2 min. in the presence, respectively, of 0.1, 0.2, 0.4, and 0.8, mM [ $\alpha$ - $^{32}$ P]-8-N $_3$ -ATP in 50 mM MES, pH 6.4. In lanes 6-10, 50 mM MOPS, pH 7.8 was used. The positions of molecular weight standards are indicated to the right of the autoradiogram.

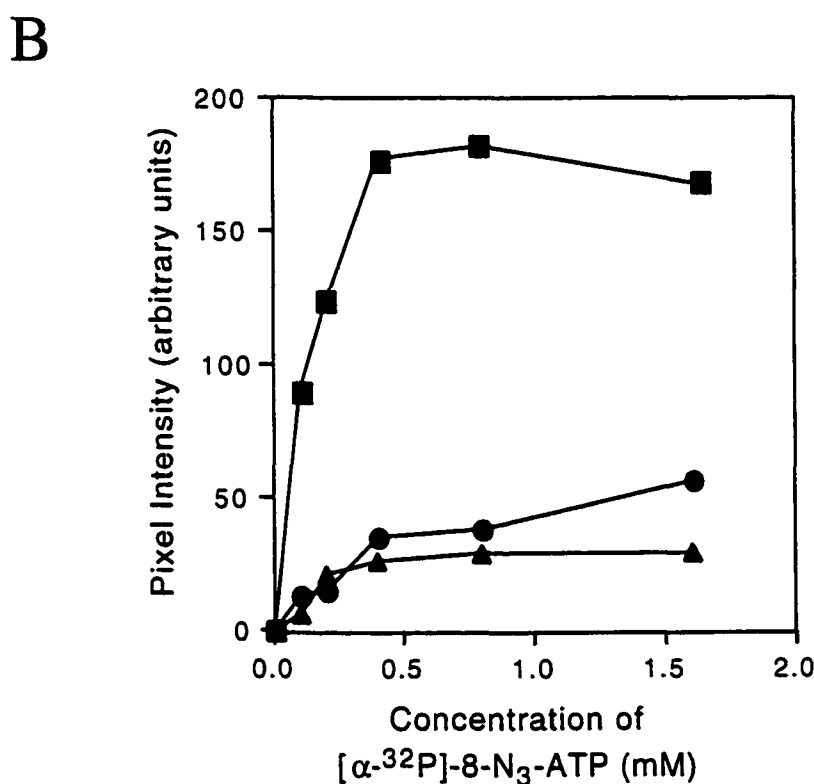
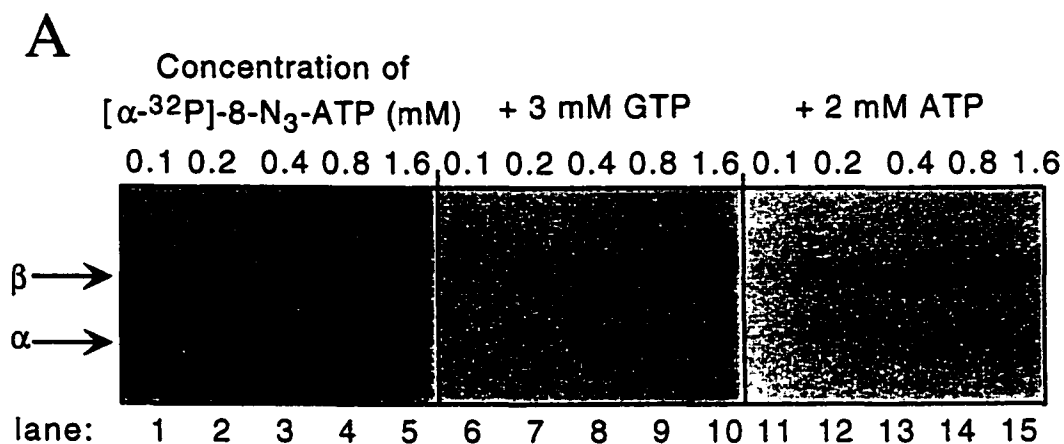
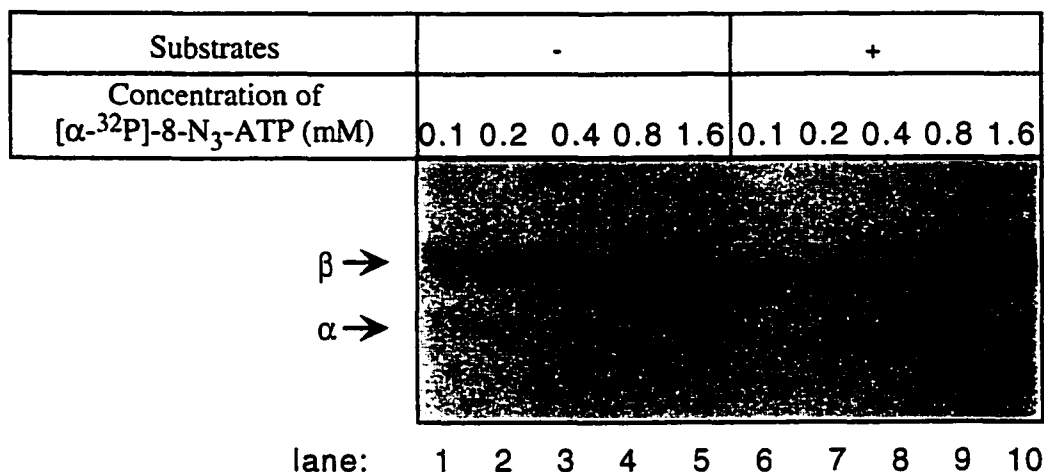


**FIGURE 4-4. Saturation of photolabeling of SCS by [ $\alpha$ - $^{32}$ P]-8-N $_3$ -ATP, and prevention of photolabeling by ATP and GTP. A. Autoradiogram of photolabeled SCS analyzed by SDS-PAGE. Lanes 1-5 contain SCS irradiated for 30 seconds in the presence, respectively, of 0.1, 0.2, 0.4, 0.8, and 1.6 mM [ $\alpha$ - $^{32}$ P]-8-N $_3$ -ATP. In lanes 6-10, 3 mM GTP was included during irradiation. In lanes 11-15, 2 mM ATP was included during irradiation. B. Quantitation of the incorporation of [ $\alpha$ - $^{32}$ P]-8-N $_3$ -ATP into the  $\beta$ -subunit of SCS by phosphorimagery: ■, with 8-N $_3$ -ATP alone (corresponding to lanes 1-5 in panel A); ●, plus 3 mM GTP (corresponding to lanes 6-10); ▲, plus 2 mM ATP (corresponding to lanes 11-15).**

$\alpha$ -subunit was observed at the highest concentrations of analogue tested (at  $\lambda = 254$  nm) and may have resulted from low affinity for nucleotide leading to non-specific labeling (15). Labeling was inhibited by the addition of 2 mM ATP or 3 mM GTP (Fig. 4-4), indicating that the binding of 8-N<sub>3</sub>-ATP was specific for the nucleotide-binding site of SCS. The extent of labeling by [ $\alpha$ -<sup>32</sup>P]-8-N<sub>3</sub>-ATP was dependent on the concentration of the analogue, and saturation of labeling of the  $\beta$ -subunit was observed at approximately 0.5 mM (Fig. 4-4B). Photolabeling of SCS is slightly greater in the presence of succinate and CoA (Fig. 4-5). From a Hanes-Wolf plot of the data from labeling in the presence of substrates, the value of  $K_{d(app)}$  for 8-N<sub>3</sub>-ATP was estimated to be 54  $\mu$ M (Fig. 4-5B). A better estimate of  $K_d$  for 8-N<sub>3</sub>-ATP would require that the analogue not be altered by the enzyme. Although the labeling was carried out on ice to retard catalysis by the enzyme, there may still have been some turnover of analogue. This is likely to be the reason for the increase in labeling that is observed in the presence of substrates. The value of the  $K_{d(app)}$  derived from labeling experiments carried out in the absence of succinate and CoA was 90  $\mu$ M (Fig. 4-5B). These  $K_{d(app)}$  values for 8-N<sub>3</sub>-ATP were consistent with the values of  $K_{m(app)} = 70$   $\mu$ M (this study) and  $K_{d(app)} = 68$   $\mu$ M (16) determined at 25 °C for ATP and ADP, respectively, and were therefore considered reasonable.

*Is 8-N<sub>3</sub>-ATP a Substrate for SCS?* In order to determine if 8-N<sub>3</sub>-ATP behaves as a substrate for SCS, in a manner consistent with the labeling, a kinetic analysis of the associated enzymatic activity was performed. Initial rates of formation of succinyl-CoA were measured in solutions containing various concentrations of 8-N<sub>3</sub>-ATP and saturating concentrations of succinate and CoA. The plot of velocity of SCS activity versus concentration of 8-N<sub>3</sub>-ATP was sigmoidal (Fig. 4-6), and a Hill plot was used to determine the kinetic constants. The value of  $K_{0.5V_{max}}$  extrapolated from the graph was 210  $\mu$ M, and the  $V_{max}$  was 0.074  $\mu$ moles/min/mg. This value for  $K_{0.5V_{max}}$  is comparable to the value of

A



B

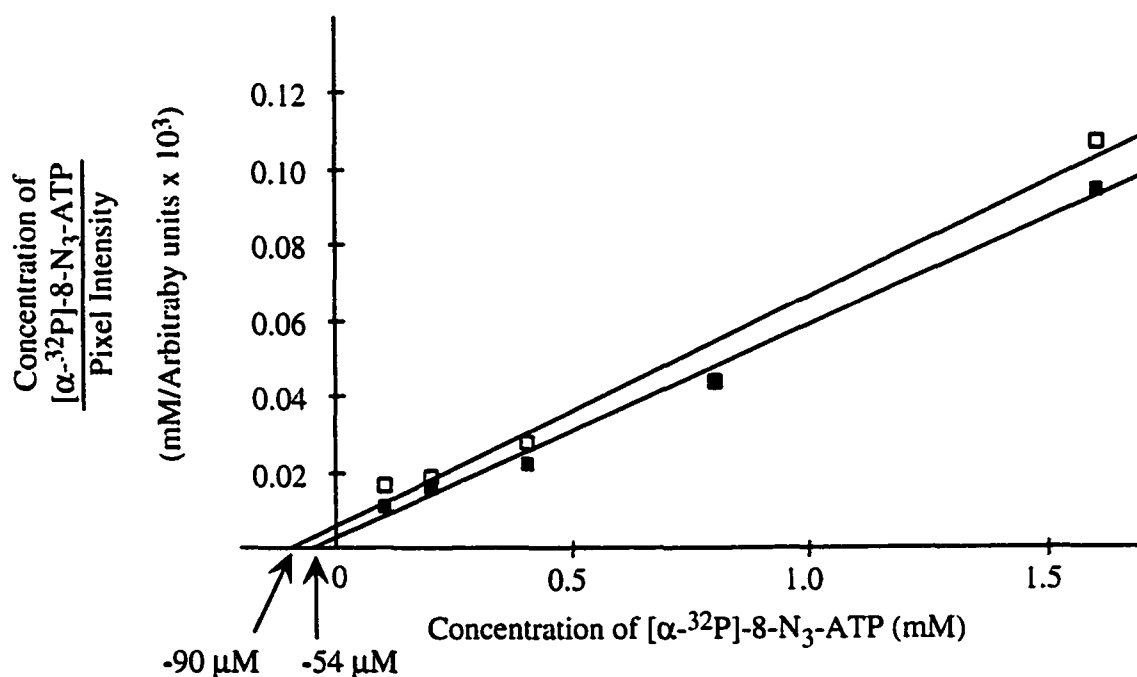


**Figure 4-5. Photolabeling of SCS by in the absence and presence of substrates.** A. Autoradiogram of photolabeled SCS analyzed by SDS-PAGE. Lanes 1-5 contain SCS irradiated in the presence, respectively, of 0.1, 0.2, 0.4, 0.8, 1.6 mM  $[\alpha\text{-}^{32}\text{P}]\text{-8-N}_3\text{-ATP}$ , and in the absence of other substrates. In lanes 6-10, 1  $\mu\text{M}$  succinate and 0.12  $\mu\text{M}$  CoA were included. (B) A Hanes plot of the quantitation of the incorporation of  $[\alpha\text{-}^{32}\text{P}]\text{-8-N}_3\text{-ATP}$  into the  $\beta$ -subunit of SCS: ( $\square$ ), in the absence of substrates (corresponding to lanes 1-5), and ( $\blacksquare$ ), in the presence of substrates (corresponding to lanes 6-10). The correlation coefficients for the two plots were 0.986 and 0.996. The error in the  $K_{m(\text{app})}$  values is approximately 30  $\mu\text{M}$ . The data were plotted and analysed using the program ENZYME KINETICS (10).



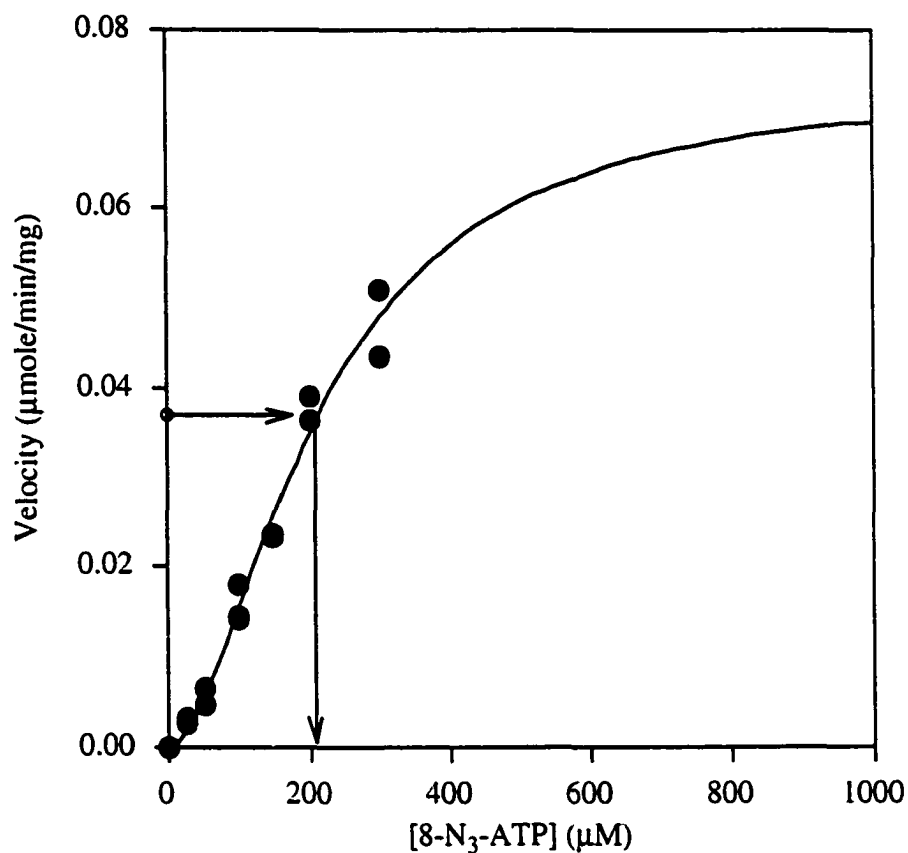


**Figure 4-6. Plot of the initial velocity of SCS activity versus concentration of 8-N<sub>3</sub>-ATP.** The reaction mixtures contained: 10 mM MgCl<sub>2</sub>, 10 mM succinate, 100 mM CoA, 20 mM Tris HCl, pH 7.4, and various concentrations of 8-N<sub>3</sub>-ATP (●). Also shown is the best fit curve calculated by the program SIGMA PLOT (12) using the Hill equation ( $v=V_{\max}[8\text{-N}_3\text{-ATP}]^n/(K + [8\text{-N}_3\text{-ATP}]^n$ ). The derived constants were  $V_{\max} = 0.074$  μmoles/min/mg,  $n = 1.7$ , and  $K = 12000$ . The correlation coefficient was 0.980. The interpolation of the value for  $K_{0.5V_{\max}}$  is indicated by the arrows.

90  $\mu\text{M}$  for  $K_{d(\text{app})}$  obtained from the labeling experiments, and consistent with 8- $\text{N}_3$ -ATP acting as a substrate. The value of  $V_{\text{max}}$  was approximately 500 times less than that observed using ATP.

*Does 8- $\text{N}_3$ -ATP Compete with ATP for Binding to SCS?* Because SCS has a low value for  $V_{\text{max}}$  when using 8- $\text{N}_3$ -ATP as a substrate, 8- $\text{N}_3$ -ATP can be treated as an “inhibitor” of SCS in order to qualitatively assess whether it is competitive with respect to ATP. Double reciprocal plots of the velocity of SCS versus the concentration of ATP indicated that the maximum velocity of SCS at high concentrations of ATP is the same for presence of 8- $\text{N}_3$ -ATP ranging from 0 to 100  $\mu\text{M}$  (Fig. 4-7). This suggests that 8- $\text{N}_3$ -ATP and ATP compete for the same form of the enzyme. The inhibition of SCS by 100  $\mu\text{M}$  8- $\text{N}_3$ -ATP resembled the product inhibition of SCS by ADP that was observed by Moffet and Bridger (17).

*Inactivation of SCS by 8- $\text{N}_3$ -ATP.* Irradiation of SCS in the presence of 8- $\text{N}_3$ -ATP resulted in the loss of SCS activity (Fig. 4-8). This inactivation was concentration dependent and the activity of SCS was inversely related to the degree of photoincorporation of [ $\alpha$   $^{32}\text{P}$ ]-8- $\text{N}_3$ -ATP into the  $\beta$ -subunit of SCS. The presence of ATP or GTP protected SCS from both photoincorporation and inactivation. When samples were irradiated for 30 s, inhibition to 45% of the initial activity was observed at the highest concentrations of analogue tested (Fig. 4-8A). Irradiation for longer lengths of time (for example, 5 min) in the presence of 8- $\text{N}_3$ -ATP resulted in greater labeling and total inactivation of SCS, and both were inhibited by the addition of ATP or GTP (Fig. 4-8B).

*Mass Spectrometry of SCS Subunits Labeled by 8- $\text{N}_3$ -ATP.* To determine the stoichiometry of labeling, electrospray mass spectrometry was performed on photolabeled  $\alpha$ - and  $\beta$ -subunits separated by HPLC. The results of reverse phase HPLC are shown in Figure 4-9. The  $\alpha$ - and  $\beta$ -subunits are clearly resolved with the  $\beta$ -subunit eluting later than the  $\alpha$ -subunit. In untreated samples the  $\beta$ -subunit has greater absorbance at 210 nm,

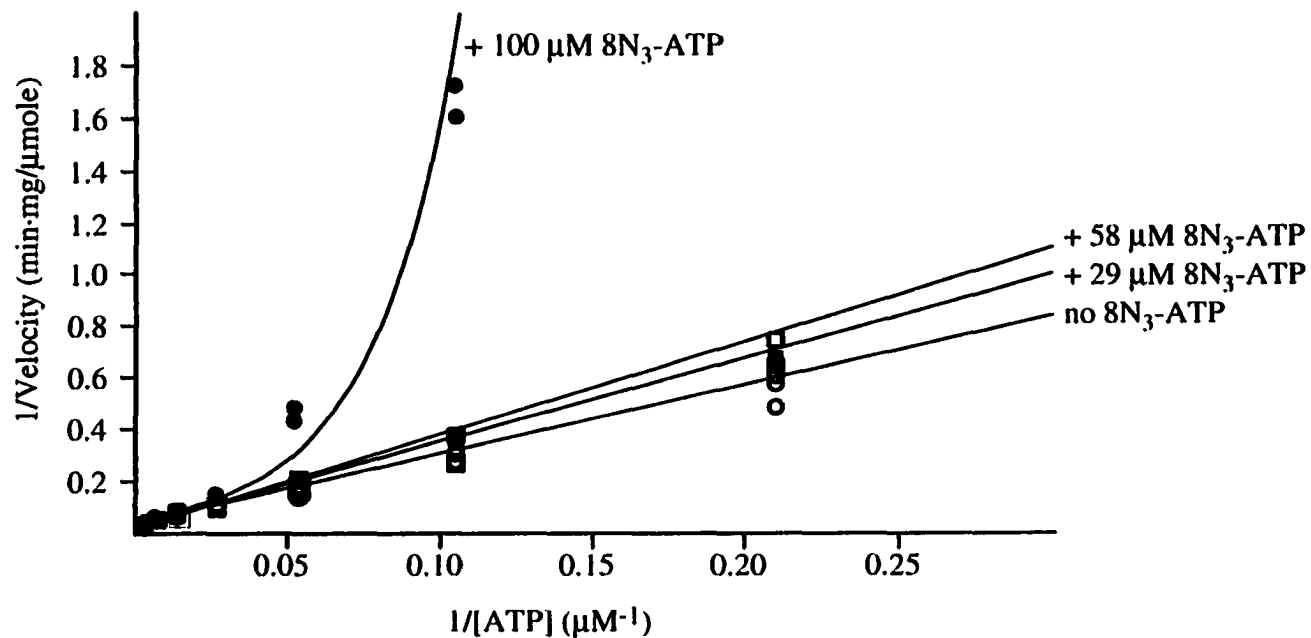


**Figure 4-7. Reciprocal plots showing the "inhibition" of SCS by  $8\text{-N}_3\text{-ATP}$  with ATP as the variable substrate.** The reaction mixtures contained: 10 mM  $\text{MgCl}_2$ , 10mM succinate, 100 mM CoA, and 20 mM Tris HCl, pH 7.4, and various concentrations of ATP plus, no  $8\text{-N}_3\text{-ATP}$  (○), or 29  $\mu\text{M}$   $8\text{-N}_3\text{-ATP}$  (■), or 58  $\mu\text{M}$   $8\text{-N}_3\text{-ATP}$  (□), or 100  $\mu\text{M}$   $8\text{-N}_3\text{-ATP}$  (●). The correlation coefficients for both the plots of 29  $\mu\text{M}$  and 58  $\mu\text{M}$   $8\text{-N}_3\text{-ATP}$  was 0.976. The data were plotted and analyzed using the program ENZYME KINETICS (10).

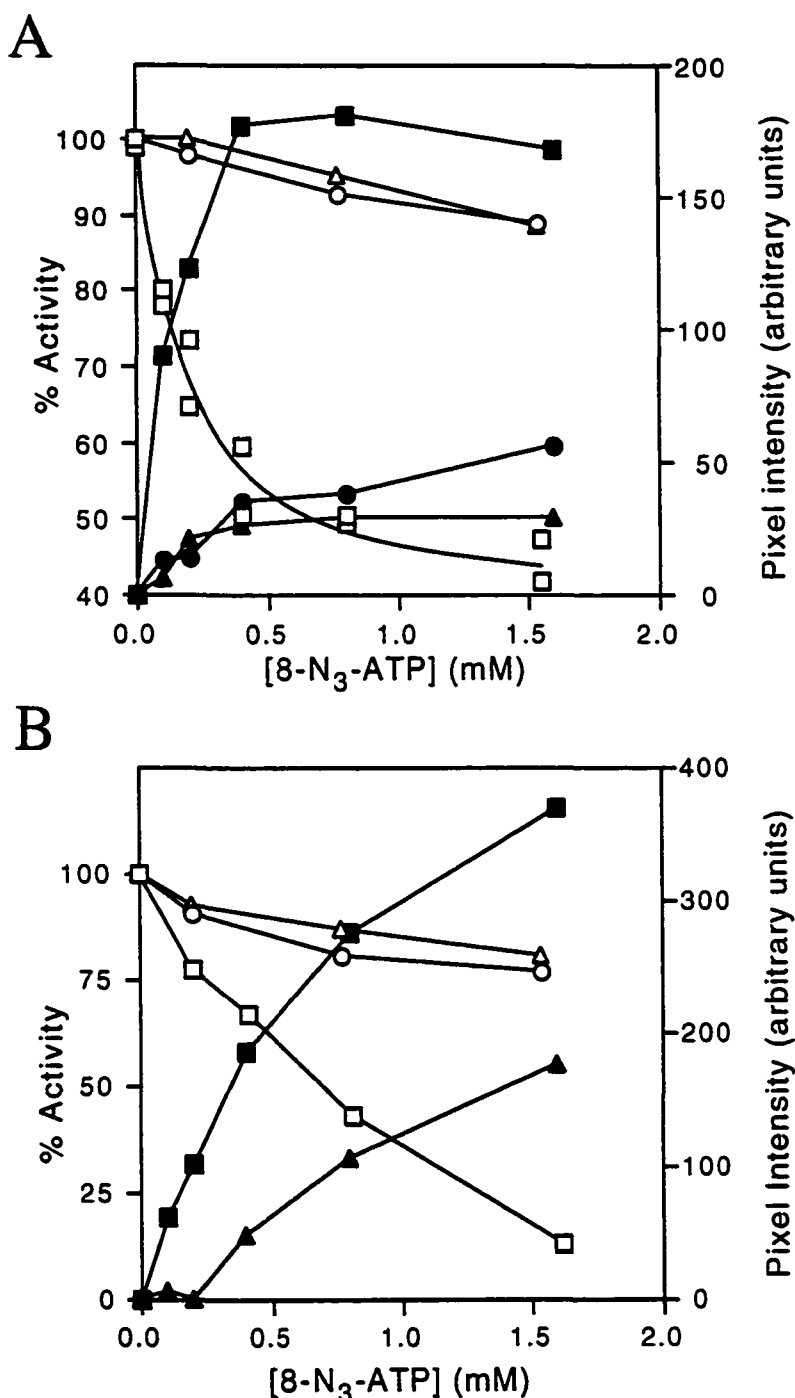


**FIGURE 4-8. Correlation of photolabeling of the  $\beta$ -subunit with inhibition of SCS.** Irradiation was carried out for 30 s (panel A) or 5 min (panel B). Open symbols represent measurements of the enzymatic activity of SCS after irradiation in the presence of various amounts of 8-N<sub>3</sub>-ATP. Closed symbols represent photoincorporation of 8-N<sub>3</sub>-ATP into the  $\beta$ -subunit as assayed by phosphorimager after photolabeling with [ $\alpha$ -<sup>32</sup>P] 8-N<sub>3</sub>-ATP and separation by SDS-PAGE.  $\square$ ,  $\blacksquare$  represent irradiation in the presence of only 8-N<sub>3</sub>-ATP (0.1, 0.2, 0.4, 0.8, and 1.6 mM).  $\Delta$ ,  $\blacktriangle$  represent SCS irradiated in the presence of 8-N<sub>3</sub>-ATP and ATP ( $\Delta$ , 2 mM;  $\blacktriangle$ , 2 mM in A and 1 mM in B).  $\circ$ ,  $\bullet$  represent SCS irradiated in the presence of 8-N<sub>3</sub>-ATP and 2 mM GTP.

consistent with the relative molecular weight of the subunits (Fig. 4-9A). Irradiation of SCS at 350 nm resulted in a decrease in the relative absorbance of the  $\beta$ -subunit when compared to the  $\alpha$ -subunit (compare Fig 4-9A with B). The results of mass spectrometry of the isolated subunits are shown in Figure 4-10. When irradiation at 350 nm was carried out in the absence of 8-N<sub>3</sub>-ATP, there were two species present in HPLC fractions containing the  $\alpha$ -subunit and one in the fractions containing the  $\beta$ -subunit (Fig. 4-10A and B). In the case of the  $\alpha$ -subunit the major species had a mass of 29645 Da, corresponding to the predicted mass of 29647 Da for purified  $\alpha$ -subunit that lacks the N-terminal methionine (18, 19). The major species was 82 Da smaller than the minor species (Fig. 4-10A), corresponding to the mass of H<sub>2</sub>PO<sub>3</sub> (81 Da) and indicating that the major portion of the population of the  $\alpha$ -subunit was dephosphorylated. In the case of the  $\beta$ -subunit (Fig. 4-10B), the only species present had a mass of 41397 Da, that of the unmodified  $\beta$ -subunit (41394 Da). When 400  $\mu$ M 8-N<sub>3</sub>-ATP was added to the reaction mixture, again two species were observed in the case of the  $\alpha$ -subunit (Fig. 4-10C); however, the species of higher mass was now prominent. This indicated that the  $\alpha$ -subunit was phosphorylated during the course of the labeling reaction, in keeping with the conclusion that 8-N<sub>3</sub>-ATP was acting as a substrate. Two species were also observed in HPLC fractions containing the  $\beta$ -subunit when SCS was irradiated in the presence of 8-N<sub>3</sub>-ATP (Fig. 4-10D). The smaller of the two had a mass of 41404 Da and the larger species had a mass of 41985 Da. The difference between the two masses corresponds to one 8-N<sub>3</sub>-ATP (520 Da) and an extra 61 Da. The extra mass may be due to one Mg<sup>2+</sup> ion (24 Da) and one K<sup>+</sup> ion (39 Da) chelating to the 8-N<sub>3</sub>-ATP or it may be due to two molecules of NO (60 Da, total). The NO molecules may have arisen from the liberation of N<sub>2</sub><sup>•</sup> during irradiation, which could have reacted with oxygen, and subsequently attached to the protein. The reaction of oxygen with nitrophenyl azides has been shown to occur during low power irradiation of these compounds (20). When irradiation was carried out in the presence of a saturating concentration of 8-N<sub>3</sub>-ATP (800  $\mu$ M), the mass spectra of both subunits contained more

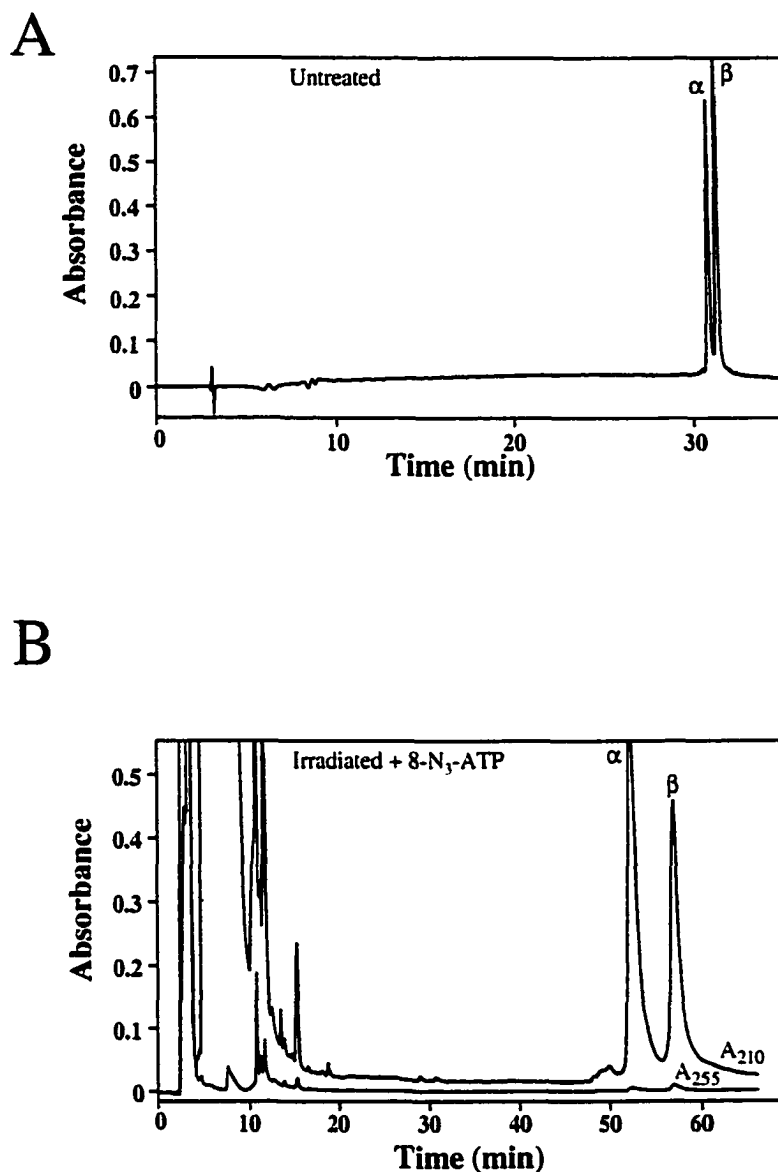


**FIGURE 4-9. Reverse phase HPLC of SCS photolabeled by 8-N<sub>3</sub>-ATP.** SCS protein shown in panel A was not treated, and that in panel B was irradiated in the presence of 400 mM 8-N<sub>3</sub>-ATP. The separation shown in panel A was carried out with a linear gradient of 2% (v/v) acetonitrile-TFA/min with a flow rate of 1 ml/min as described in Materials and Methods. The solid lines represent absorbance at 210 nm, as well as, in panel B, at 255 nm. The separation shown in panel B was carried out with a linear gradient of 2% (v/v) B/min for 20 min, followed by a gradient of 0.5% (v/v) B/min, all with a flow rate of 1ml/min.

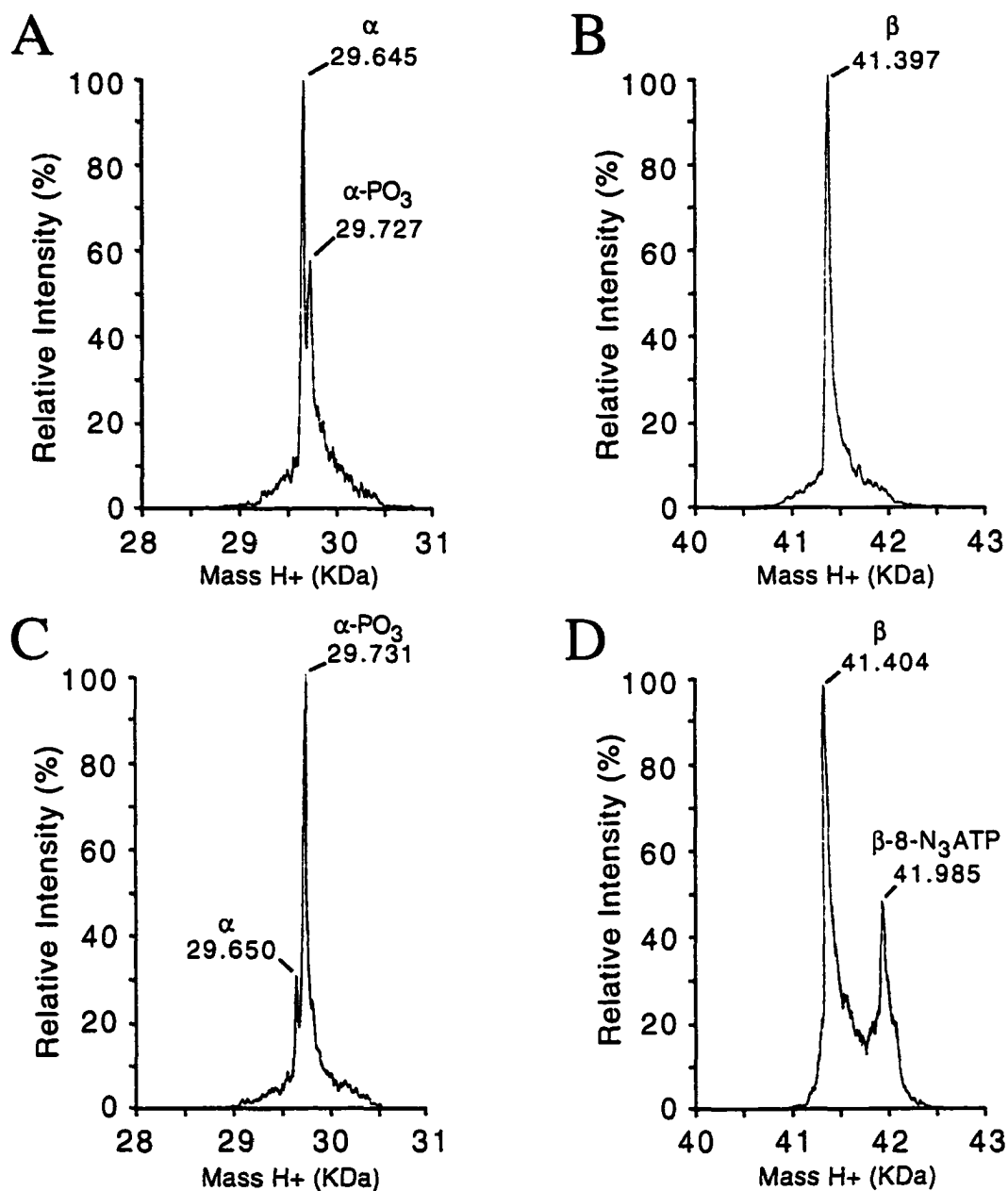


**FIGURE 4-10. Electrospray mass spectra of the subunits of SCS.** SCS was irradiated either in the absence (A and B) or presence (C and D) of  $8\text{-N}_3\text{-ATP}$ . The subunits were separated by reverse phase HPLC, shown in Figure 4-9, followed by mass spectrometry of the isolated subunits (see Materials and Methods for specific details). The results for the  $\alpha$ -subunit are shown in (A) and (C), and those for the  $\beta$ -subunit in (B) and (D).

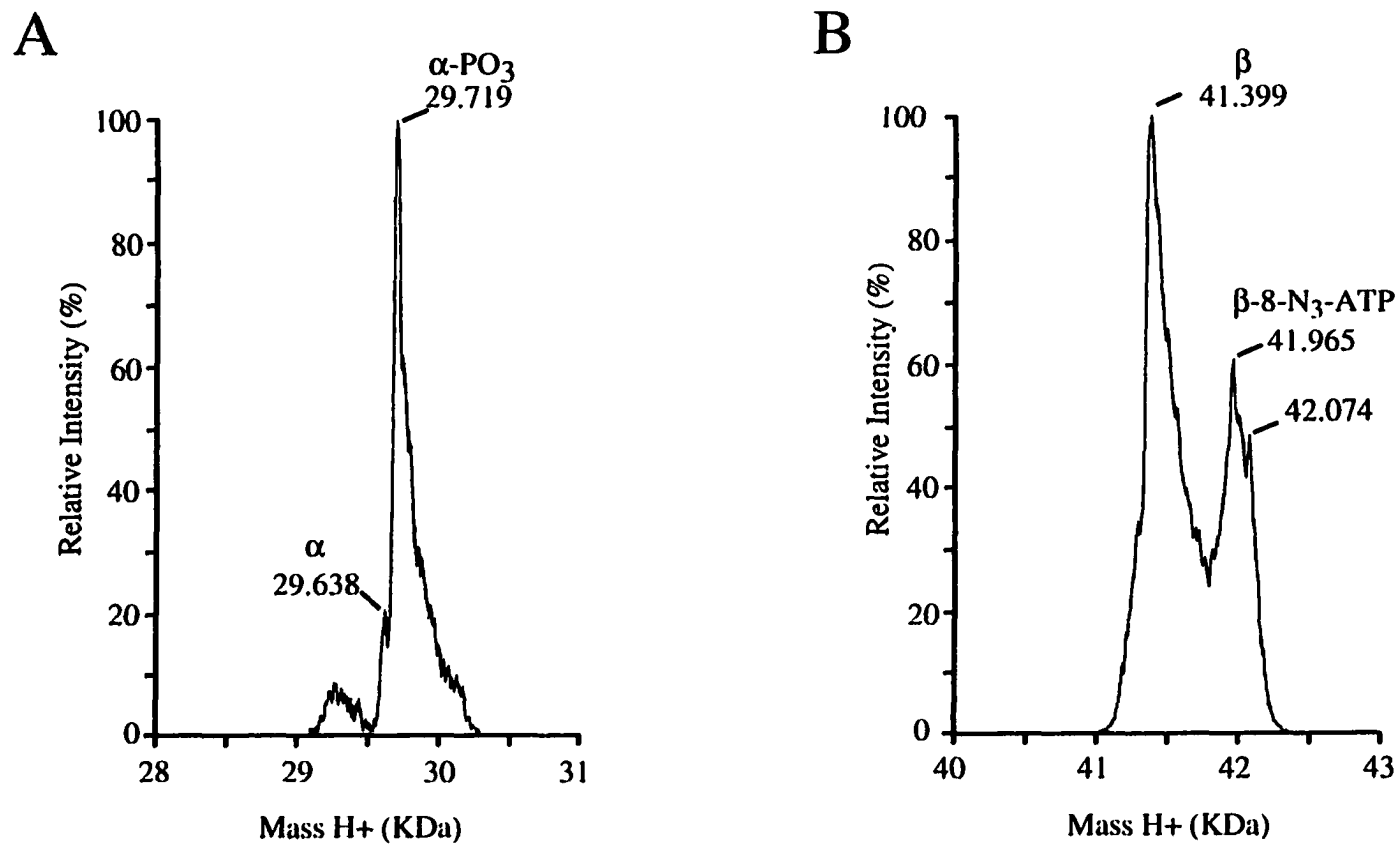


**FIGURE 4-11. Electrospray mass spectra of the subunits of SCS irradiated in the presence of a saturating concentration of 8-N<sub>3</sub>ATP.** SCS was irradiated in the presence of 724  $\mu$ M 8-N<sub>3</sub>-ATP, and the subunits were separated by reverse phase HPLC. This was followed by mass spectrometry of the isolated subunits (see Materials and Methods for specific details). The  $\alpha$ -subunit is shown in panel A, and the  $\beta$ -subunit is shown in panel B.



“noise”. However, there was no evidence of  $\alpha$ -subunit which had been modified by even one 8-N<sub>3</sub>-ATP (Fig 4-11A), and there was an increase in the relative amount of the  $\beta$ -subunit species labeled with one 8-N<sub>3</sub>-ATP (Fig. 4-11B). These observations support the earlier interpretation that under the harsher conditions of the initial experiments (Fig. 4-3), the labeling of the  $\alpha$ -subunit was non-specific. Note: irradiation at 350 nm gave rise to a limited number of products and therefore an easily interpretable mass spectrum, whereas irradiation at 254 nm led to the complex production of multiple products. The large decrease in the relative absorbance of the  $\beta$ -subunit after irradiation at 254 nm observed during reverse phase HPLC (data not shown) also indicated that damage was induced by irradiation at this wavelength.

*Isolation of 8-N<sub>3</sub>-ATP Photolabeled Peptides from SCS.* To determine the location of the 8-N<sub>3</sub>-ATP binding site, peptide fragments of photolabeled SCS were generated by tryptic digestion, purified and then analyzed by amino acid sequencing and mass spectrometry. Photolabeling of SCS was carried out by irradiation of SCS at 254 nm for 1 min in the presence of 400  $\mu$ M [ $\alpha$ -<sup>32</sup>P]-8-N<sub>3</sub>-ATP. As a compromise, the wavelength of 254 nm was used to maximize the yield of labeled peptides, and the mid-range concentration of 400  $\mu$ M analogue to minimize non-specific labeling. Typically 0.42 moles of [ $\alpha$ -<sup>32</sup>P]-8-N<sub>3</sub>-ATP were incorporated per mole of SCS. Following digestion, labeled peptides were separated from unlabeled peptides by Al<sup>3+</sup> affinity chromatography (14). After washing the loaded column with buffers containing low salt, high salt, and urea to disrupt non-specific electrostatic and hydrophobic interactions that may cause unlabeled peptides to be retained on the column, 85% of the radioactivity initially bound to the column remained bound (Fig. 4-12). Reverse phase HPLC of the of the flowthrough and wash fractions from this column revealed no labeled peptides in these washes. In addition, two peptides were depleted from the flowthrough fraction (data not shown). The bound radioactivity was eluted from the affinity column using 10 mM pyrophosphate, and pooled.

Subsequent reverse phase HPLC analysis of these pooled fractions revealed three major peaks with radioactivity (Fig. 4-13). The first peak, containing most of the total radioactivity, appeared in the HPLC flow through fractions which eluted before the beginning of the chromatogram (data not shown). No peptide was found in these fractions. Similar losses of radioactive label have been observed in other studies that have used azido analogues (21, 14). The other two peak fractions containing significant radioactivity eluted at 37 and 42 minutes (at a flow rate of 0.5 ml/min), respectively (Fig. 4-13). Although the yields of the purified peptides were low (approximately 20 pmol), these peptides displayed a ratio of  $A_{210\text{ nm}}/A_{255\text{ nm}}$  close to one, consistent with the presence of the aromatic adenine moiety. Edman degradation analysis of the peptide in the peak that eluted at 42 minutes gave the following sequence: VVFMAS<sup>T</sup>EGGVEAEKVAEETPHLLHK. This corresponds to a tryptic peptide from amino acid residue 121 to 146 of the  $\beta$ -subunit of SCS. The mass of the material in this fraction was 3368 Da as determined by mass spectrometry (Fig. 4-14B). This corresponds to the mass of the peptide (2850.5 Da) plus the mass of the analogue (520 Da). There was an additional mass of 3416 in this fraction, which may be the same peptide with two bound  $Al^{+3}$  ions. In SCS, there are no tryptic peptides with a mass of 3416, either with or without the analogue. The material in the peak that eluted at 37 minutes was also subjected to mass spectrometry and revealed two major species of mass 1466 (Fig. 4-14A) and 520 Da. This corresponds to a tryptic peptide from amino acid residue 107 to 119 of the  $\beta$ -subunit and a detached analogue. Obviously, the ionization of the labeled peptide during mass spectroscopy had caused the photoinsertion bond to break. Unfortunately we were unable to sequence this peptide. Nevertheless both of these results are consistent with a nucleotide-binding site being located in the N-terminal domain of the  $\beta$ -subunit.

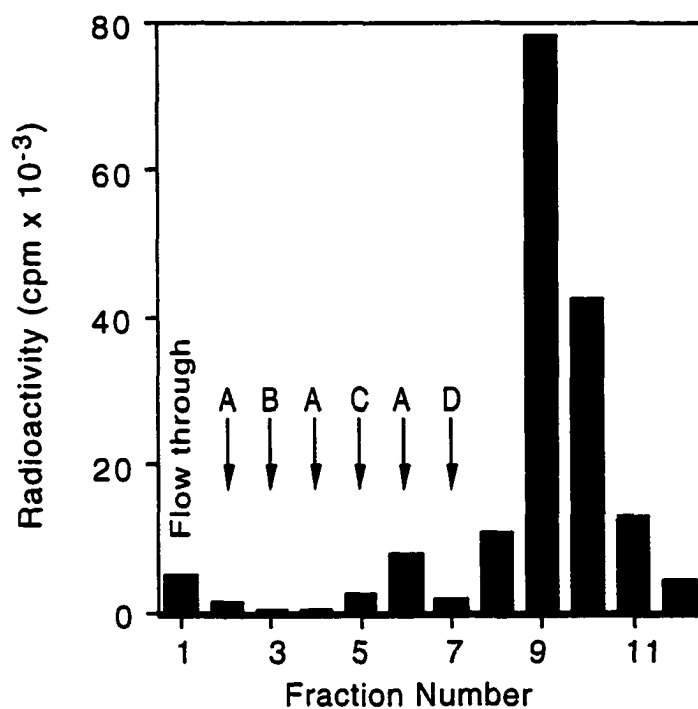


**FIGURE 4-12. Purification of photolabeled peptides of SCS by  $\text{Al}^{+3}$  affinity chromatography.** The  $\text{Al}^{+3}$  affinity column was loaded with the tryptic digest of SCS photolabeled with 8- $\text{N}_3$ -ATP and washed sequentially with the solutions indicated: A (5 mM DTT, 100 mM  $(\text{NH}_4)_2\text{SO}_4$ , pH 6.0), B (5 mM DTT, 0.5 M NaCl, 100 mM  $(\text{NH}_4)_2\text{SO}_4$ , pH 6.0), C (5 mM DTT, 8 M urea, 100 mM  $(\text{NH}_4)_2\text{SO}_4$ , pH 6.0), and D (5 mM DTT, 10 mM pyrophosphate, 100 mM  $(\text{NH}_4)_2\text{SO}_4$ , pH 8.0). The  $^{32}\text{P}$ -levels were determined as described in Materials and Methods.

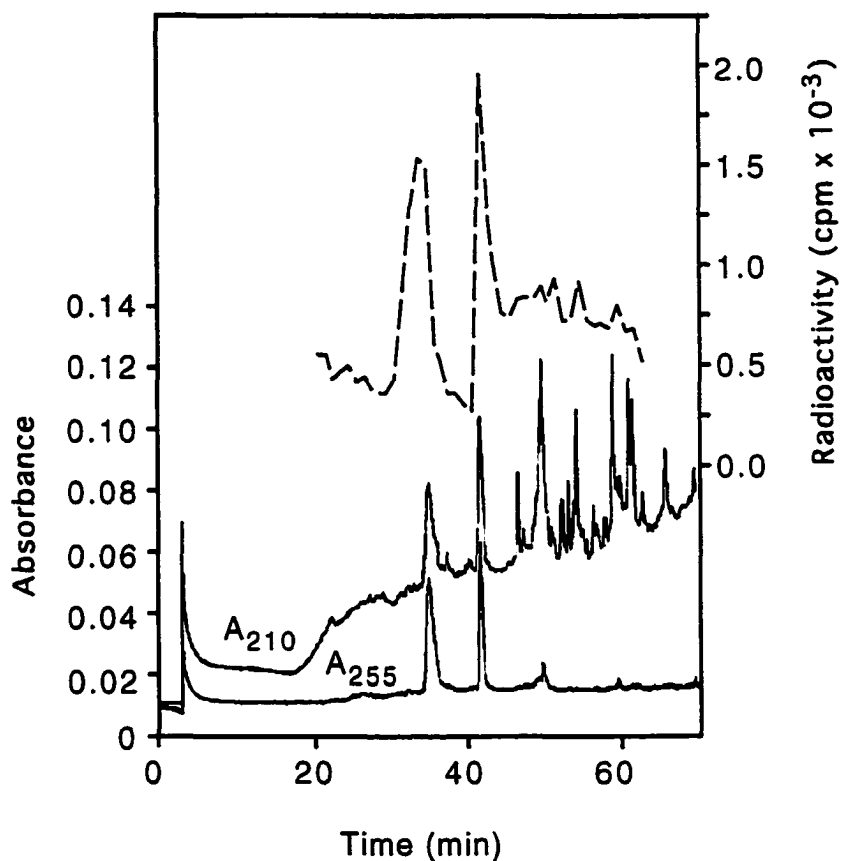


**FIGURE 4-13. Purification of photolabeled peptides of SCS reverse phase HPLC.** Separations were carried out with a linear gradient of 1% (v/v) acetonitrile-TFA/min with a flow rate of 0.5 ml/min as described in Materials and Methods. The solid lines represent absorbance at 210 or 255 nm, and the dashed line represents the radioactivity associated with 0.5 ml fractions as assayed by liquid scintillation counting.

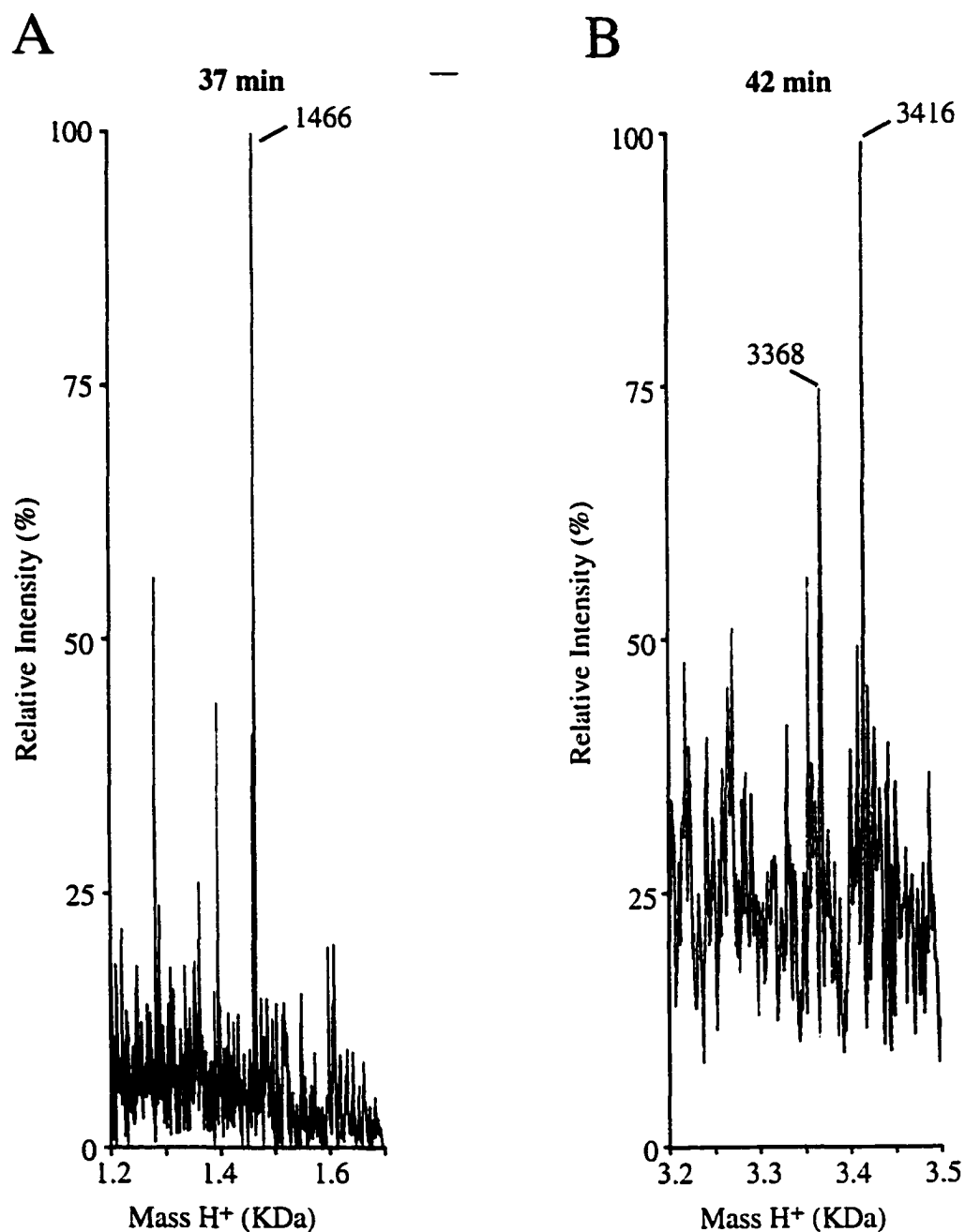


**FIGURE 4-14. Electrospray mass spectra of tryptic peptides from photolabeled SCS.** SCS was irradiated in the presence of 8-N<sub>3</sub>-ATP, digested with trypsin, and the peptides were purified by Al<sup>3+</sup> affinity chromatography and reverse phase HPLC. This was followed by mass spectrometry of the isolated peptides (see Materials and Methods for specific details). The peptide that eluted from reverse phase HPLC at 37 min is shown in panel A, and the peptide that eluted at 42 min is shown in panel B.

## Discussion

This study was undertaken to determine the location of the nucleotide-binding site of *E. coli* SCS by using 8-N<sub>3</sub>-ATP to specifically label peptides from the β-subunit. From the labeling results it was concluded that the nucleotide likely binds in the ATP-grasp fold of the N-terminal domain and not in the Rossmann fold of the C-terminal domain. Binding of the nucleotide in the N-terminal domain requires that the catalytic His 246α interacts alternately at two sites, site I where CoA and, presumably, succinate bind, and site II where the nucleotide binds. NMR spectroscopy presented evidence for a “flip” between two conformations of the phosphorylated histidine (Fig. 1-10) (22). His 246α is part of a loop that could swing to shuttle the histidine residue between the two sites during each catalytic cycle.

A number of methods were used to show that 8-N<sub>3</sub>-ATP was a suitable analogue of ATP for use with SCS. The photolabeling of SCS by 8-N<sub>3</sub>-ATP occurred over a range in pH, was saturable and inhibited by the nucleotide substrates of *E. coli* SCS. The addition of substrates to the photolabeling reaction resulted in a slight improvement in the amount of label incorporated. In view of the inability of phosphorylated SCS to bind ATP (23), the increase in labeling is likely due to catalytic turnover by the enzyme. In addition, the activity of SCS decreased reciprocally in conjunction with photolabeling. The  $K_{d (app)}$  observed for 8-N<sub>3</sub>-ATP from photolabeling was within one order of magnitude the  $K_m$  for ATP and to the  $K_{d(app)}$  for ADP (Table 4-1).

Table 4-1: Summary of Kinetic Parameters of SCS for ATP, ADP or 8-N<sub>3</sub>-ATP

	$K_m (app)$ (μM)	$K_d (app)$ (μM)	$K_{0.5 v_{max}}$ (μM)
ATP	70	-	-
ADP <sup>a</sup>	12	68	-
8-N <sub>3</sub> -ATP	-	+substrates 54, -substrates 90	210

<sup>a</sup> Obtained from the work of Moffet *et al.* (17, 24)

In only one respect the behavior of SCS with 8-N<sub>3</sub>-ATP did not reflect the natural substrate, ATP. The velocity versus concentration of substrate plots for 8-N<sub>3</sub>-ATP were sigmoidal, not the typical rectangular hyperbola that was observed with ATP (17). This could be indicative of a cooperative mechanism where the binding of the first 8-N<sub>3</sub>-ATP induces a change in the enzyme structure that favors the binding of subsequent molecules of 8-N<sub>3</sub>-ATP. However, a cooperative mechanism for nucleotide binding has not been observed for SCS. Mass spectrometry of whole subunits indicated that there was only one molecule of 8-N<sub>3</sub>-ATP bound per  $\beta$ -subunit when the concentration of 8-N<sub>3</sub>-ATP was 4 times  $K_{0.5V_{max}}$ . Thus, it is unlikely that there is an allosteric site which may have given rise to a sigmoidal curve. A functional dimer of *E. coli* SCS, created by mutagenesis of ion pair residues at the tetramer interface, showed no significant changes in kinetic parameters when compared to the wild-type tetramer (25). This indicated that the two active sites in the tetramer do not interact, and thus cooperatively cannot arise via "cross-talk" between the two active sites in the tetramer. A sigmoidal curve can be manifest in other ways. The first possibility is the presence of a contaminant which modifies the substrate irreversibly (26). The DTT that was used during the purification of SCS could have modified the 8-N<sub>3</sub>-ATP, however extensive dialysis in the absence of reductant prior to kinetic and photolabeling experiments should have removed any residual DTT. The second explanation for a sigmoidal curve is the presence of multiple orders of substrate addition and product release (27, 26). An extensive mathematical treatment of this phenomenon has been done for a two substrate system by Sweeny *et al.* Detailed kinetic measurements of *E. coli* SCS carried out by Moffet *et al.* (17) concluded that the major reaction pathway is the addition of ATP to free enzyme followed by the random addition of succinate or CoA, before the release of products. However, there were indications that other minor pathways exist (16, 24, 4). Thus the comparatively low  $k_{cat}$  observed for 8-N<sub>3</sub>-ATP may allow minor pathways to become more significant. This could lead to the manifestation of a sigmoidal curve through the competition of multiple reaction pathways.

Photolabeling with 8- $N_3$ -ATP marked two tryptic peptides that are part of the nucleotide binding site in the N-terminal domain of the  $\beta$ -subunit (Figure 4-15). In the crystal structure, residues 121-146 $\beta$  include a loop that corresponds to the loop that closes over the nucleotide-binding site in DD-ligase. Residues 107-119 $\beta$  lie under this loop in SCS, and residue Glu 107 $\beta$  has a counterpart in DD-ligase that forms hydrogen bonds with the ribose hydroxyl groups of ADP. Based on the structure of ADP in complex with DD-ligase, the 8- $N_3$ -ATP analogue could not bind in the *anti* conformation without the azido group clashing with the ribose. Rotation of the adenine ring toward the *syn* conformation would allow the analogue to fit, albeit poorly (recall:  $K_{0.5V_{max}} = 210 \mu\text{M}$ ). Moreover, such a rotation would present the azido group to residue Glu 107 $\beta$  and toward residue Gly 130 $\beta$  of the loop (the closest residues within the two peptide segments), thus facilitating the observed photolabeling. In keeping with this argument, the preferred conformation of ATP analogues with substituents at the 8-position is *syn* in solution (28-30).



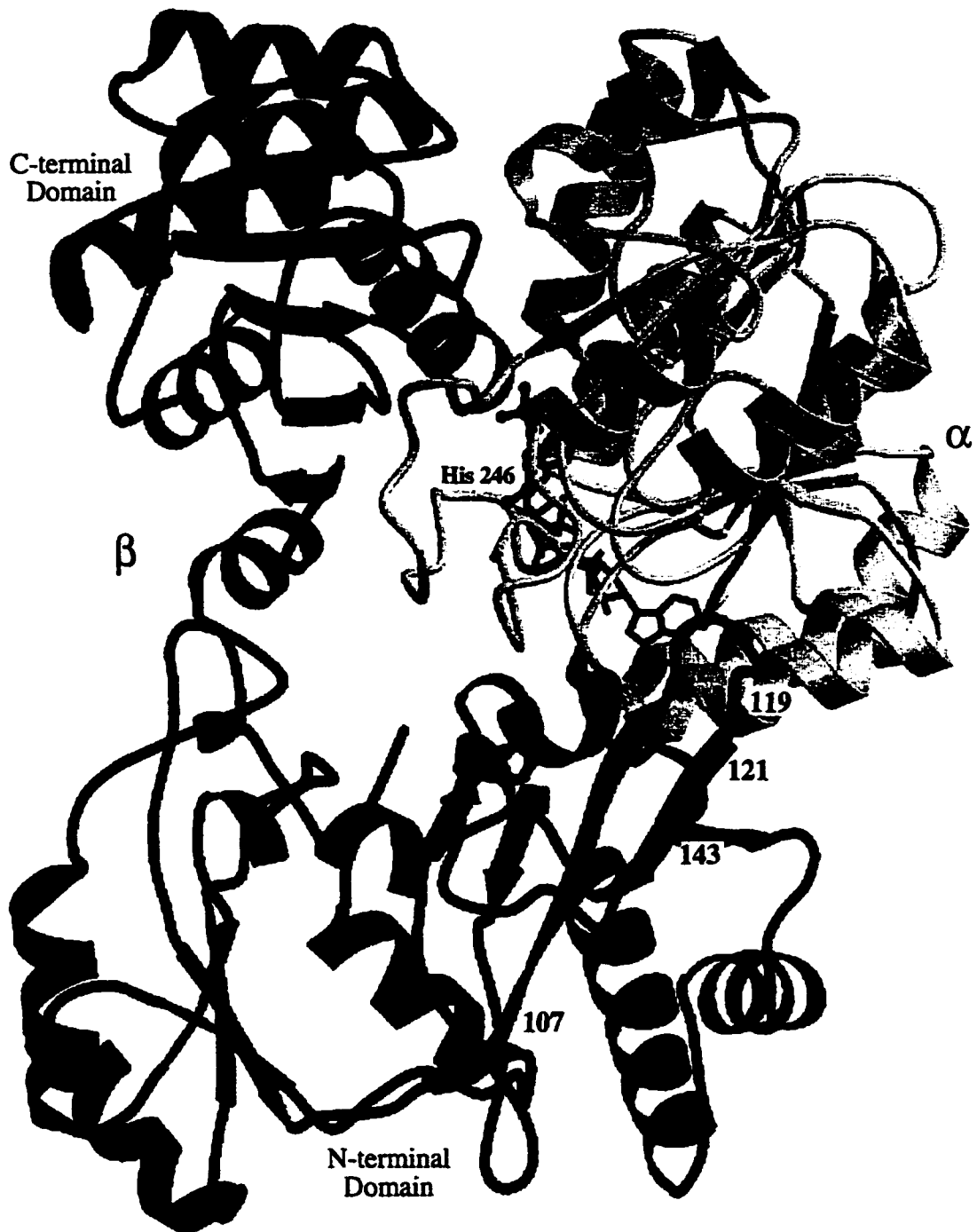


**Figure 4-15.** Ribbon diagram of one  $\alpha\beta$ -dimer of *E. coli* SCS. The  $\alpha$ -subunit is shown in yellow, and the  $\beta$ -subunit is shown in green. The active site phosphohistidine is shown in black and the CoA molecule is shown in red. The two peptides that were labeled by [ $\alpha$ - $^{32}\text{P}$ ] 8- $\text{N}_3$ -ATP, 107-119 and 121-143, are shown in light blue and dark blue, respectively. Residues 107 $\beta$  and 130 $\beta$  within these peptides are closest to the proposed site of nucleotide binding.

**References:**

1. Johnson, J. D., Mehus, J. G., Tews, K., Milavetz, B. I., & Lambeth, D. O. (1998) *J. Biol. Chem.* 273, 27580-27586.
2. Johnson, J. D., Muhonen, W. W., & Lambeth, D. O. (1998) *J. Biol. Chem.* 273, 27573-27579.
3. Pearson, P. H., & Bridger, W. A. (1975) *J. Biol. Chem.* 250, 8524-8529.
4. Wolodko, W. T., Fraser, M. E., James, M. N. G., & Bridger, W. A. (1994) *J. Biol. Chem.* 269, 10883-10890.
5. Murzin, A. G. (1996) *Curr. Opin. in Struct. Biol.* 6, 386-394.
6. Fraser, M. E., James, M. N. G., Bridger, W. A., & Wolodko, W. T. (1999) *J. Mol. Biol.* 285, 1633-1653.
7. Collier, G. E., & Nishimura, J. S. (1978) *J. Biol. Chem.* 253, 4938-4943.
8. Wolodko, W. T., Kay, C. M., & Bridger, W. A. (1986) *Biochemistry* 25, 5420-5425.
9. Laemmli, U. K. (1970) *Nature* 227, 680.
10. Stanislawski, J. (1991) Vol. 63, ENZYME KINETICS v1.11, Trinity Software, Campton, NH
11. Bridger, W. A., Ramaley, R. F., & Boyer, P. D. (1969) *Methods Enzymol.* 13, 70-75.
12. Norby, J., Rubenstein, S., Tuerke, T., Schwallie Farmer, C., Forood, R., & Bennington, J. (1993), 4.11 Ed., Jandel Scientific
13. Hill, A. V. (1910) *Journal of Physiology* 40, 4-7.
14. Jayaram, B., & Haley, B. E. (1994) *J. Biol. Chem.* 269, 3233-3242.
15. Potter, R. L., & Haley, B. E. (1983) *Methods Enzymol.* 91, 613-633.
16. Moffet, F. J., Wang, T., & Bridger, W. A. (1972) *J. Biol. Chem.* 247, 8139-8144.
17. Moffet, F. J., & Bridger, W. A. (1970) *J. Biol. Chem.* 245, 2758-2762.
18. Bridger, W. A. (1974) in *The Enzymes* (Boyer, P. D., ed) Vol. X, 3 Ed., pp. 581-606, Academic Press Inc., New York
19. Buck, D., Spencer, M. E., & Guest, J. R. (1985) *Biochemistry* 24, 6245-6252.
20. Liang, T., & Schuster, G., B. (1987) *J. Am. Chem. Soc.* 109, 7803-7810.
21. King, S. M., Kim, H., & Haley, B. E. (1991) *Methods Enzymol.* 196, 449-466.

22. Vogel, H. J., & Bridger, W. A. (1983) *Biochem. Soc. Trans.* 11, 315-323.
23. Bowman, C. M., & Nishimura, J. S. (1975) *J. Biol. Chem.* 250, 5609-5613.
24. Moffet, F. J., & Bridger, W. A. (1973) *Can. J. Biochem.* 51, 44-55.
25. Bailey, D. L., Fraser, M. E., Bridger, W. A., James, M. N. G., & Wolodko, W. T. (1998) , *J. Mol. Biol* 285, 1655-1666.
26. Westley, J. (1969) *Enzymic Catalysis*, 1 Ed. (Halvorson, H. O., Roman, H. L., & Bell, E., Eds.), Harper and Row, New York
27. Sweeny, J. R., & Fisher, J. R. (1968) *Biochemistry* 7, 561-565.
28. Tavale, S. S., & Sobel, H. M. (1970) *J. Mol. Biol.* 48, 109-123.
29. Ikehara, M., Uesugi, S., & Yoshida, K. (1972) *Biochemistry* 11, 830-836.
30. Ikehara, M., Uesugi, S., & Yoshida, K. (1972) *Biochemistry* 11, 836-842.

**Page intentionally left blank for note taking.**

## **Chapter Five Mutagenesis of Residues in Two Potential Nucleotide Binding Sites in *E. coli* SCS**<sup>1</sup>

### **Introduction**

In order further to probe the location of the nucleotide binding site on SCS, site-directed mutagenesis of *E. coli* SCS was carried out in parallel with the investigations that used the photoaffinity analogue 8-N<sub>3</sub>-ATP. Based on the x-ray crystallographic structure of SCS, there were two potential nucleotide binding sites to be considered for investigation. One was the Rossmann fold in the C-terminal domain of the  $\beta$ -subunit (1), and the other was the ATP grasp fold in the N-terminal domain of the  $\beta$ -subunit (2, 3).

Indirect support for a nucleotide-binding site being possibly in the C-terminal domain of the  $\beta$ -subunit is two-fold. First, previous studies have indicated that oxidized CoA disulfide forms a disulfide bond with Cys 325 $\beta$  and inactivates SCS (4, 5). The relative levels of protection of *E. coli* SCS from this modification afforded by ATP and GTP were consistent with the relative affinity of the enzyme for ATP and GTP (data not shown). Furthermore examination of a 2F<sub>o</sub>-F<sub>c</sub> electron density map of the x-ray crystallographic model of *E. coli* SCS revealed density trailing from Cys 325 $\beta$  to a position between Phe 22 $\alpha$  and Ile 322 $\beta$  (3). This density was discontinuous and had been modeled using water molecules, However it may represent a CoA molecule bound to Cys 325 $\beta$  and present at low occupancy. There is similar more continuous density trailing from Cys 325 $\beta$  in a 2F<sub>o</sub>-F<sub>c</sub> electron density map of the dephosphorylated form of *E. coli* SCS (Chapter 6). Second, an ATP molecule can be modeled into this Rossmann fold with the  $\gamma$ -phosphate of ATP superimposed on the phosphate of the phosphohistidine, and the adenosine ring positioned in a hydrophobic patch between the side chains of Ile 322 $\beta$  and Phe 22 $\alpha$  (Fig. 5-1). Binding of ATP in this location would thus provide a reason for the protection of SCS from inactivation by oxidized CoA disulfide, that is observed with

---

<sup>1</sup> A version of this chapter has been published: Joyce, M. A., Fraser, M. E., Brownie, E. R., James, M. N. G., Bridger, W. A., Wolodko, W. T. (1999) *Biochemistry* 38, 7273-7283.

nucleotide triphosphates. The loop containing Ile 322 $\beta$  may be anchored by an ion pair formed between Arg 324 $\beta$  and Asp 326 $\beta$ . In addition, these two residues are conserved amongst SCS enzymes that use ATP, whereas they are Asn and Ala, respectively, in SCS enzymes that are specific for GTP (6, 7).

The original prediction that a nucleotide-binding site resides in the N-terminal domain of the  $\beta$ -subunit of *E. coli* SCS was based on structural similarity between the ATP-grasp fold in the N-terminal domain of the  $\beta$ -subunit and the nucleotide-binding fold found in glutathione synthetase (8) and D-ala:D-ala ligase (DD-ligase) (9). Many of the residues that contact the ADP molecule in the nucleotide-binding folds of both glutathione synthetase and DD-ligase are also found in the N-terminal domain of the  $\beta$ -subunit (Fig. 5-2A) (3). In addition, there is a sulfate ion bound in the N-terminal domain of the  $\beta$ -subunit in the crystal structure of *E. coli* SCS (1). This sulfate ion is 1.4 Å from the  $\beta$ -phosphate of the ADP in DD-ligase, when the structure of DD-ligase is superimposed onto the N-terminal domain of the  $\beta$ -subunit (3). The amino acid sequence of the loop which binds the sulfate ion (51-AGGRGKXGGV-60) is conserved in all known SCS sequences.

The focus of the present study was to differentiate between the two potential locations of the nucleotide-binding site in *E. coli* SCS. Towards this end, site-directed mutagenesis studies of conserved residues within each of the potential nucleotide-binding sites were carried out. The possible roles of these residues in catalysis by SCS were evaluated by measuring the kinetic parameters of the mutant proteins, and determining their ability to catalyze the partial phosphorylation reactions involving either nucleotide (partial reaction (1) in Chapter 1) or succinyl-CoA and  $P_i$  (partial reactions (2) and (3) in Chapter 1). In addition, mutation of a single residue in the N-terminal domain of the  $\beta$ -subunit altered the nucleotide specificity of *E. coli* SCS.

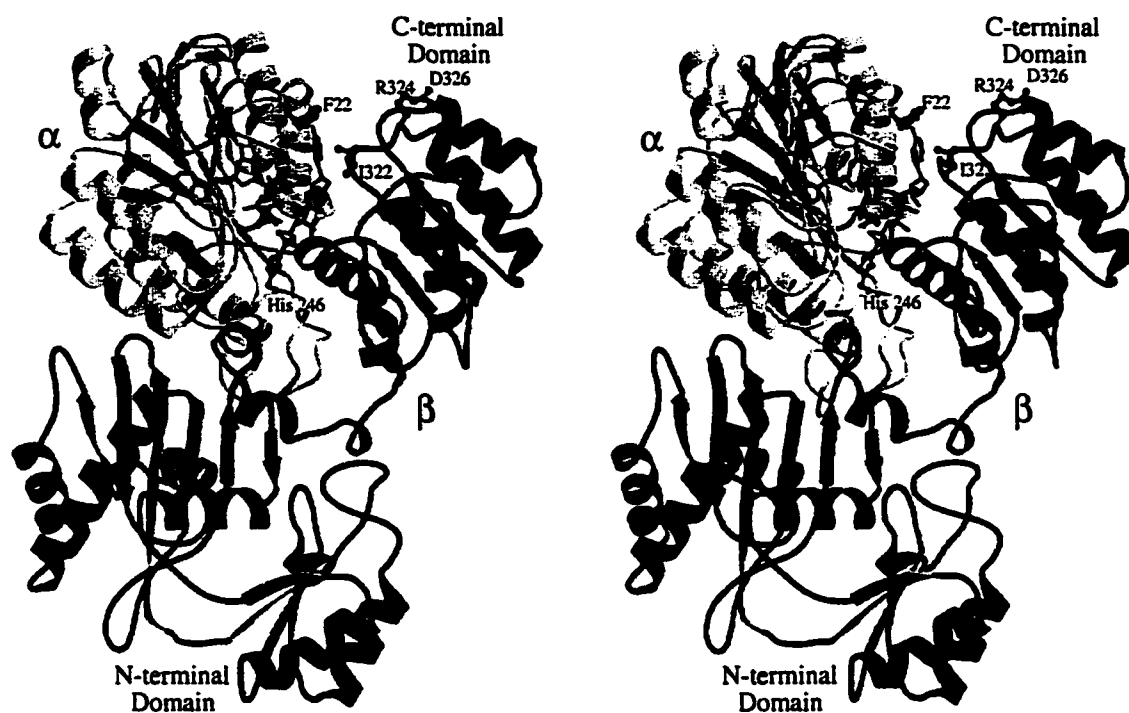


**Figure 5-1. Stereo diagram of ATP modeled into the C-terminal domain of the  $\beta$ -subunit of SCS showing some of the residues that may effect nucleotide binding. The  $\alpha$ -subunit is shown in yellow, the  $\beta$ -subunit in green, and the active site phosphohistidine is displayed as a mauve ball and stick model. The molecules of CoA and ATP are drawn as stick models in cyan and red, respectively. The side chains of Ile 322 $\beta$ , Arg 324 $\beta$ , and Asp 326 $\beta$  which were mutated, as well as Phe 22 $\alpha$ , are depicted as ball and stick models.**

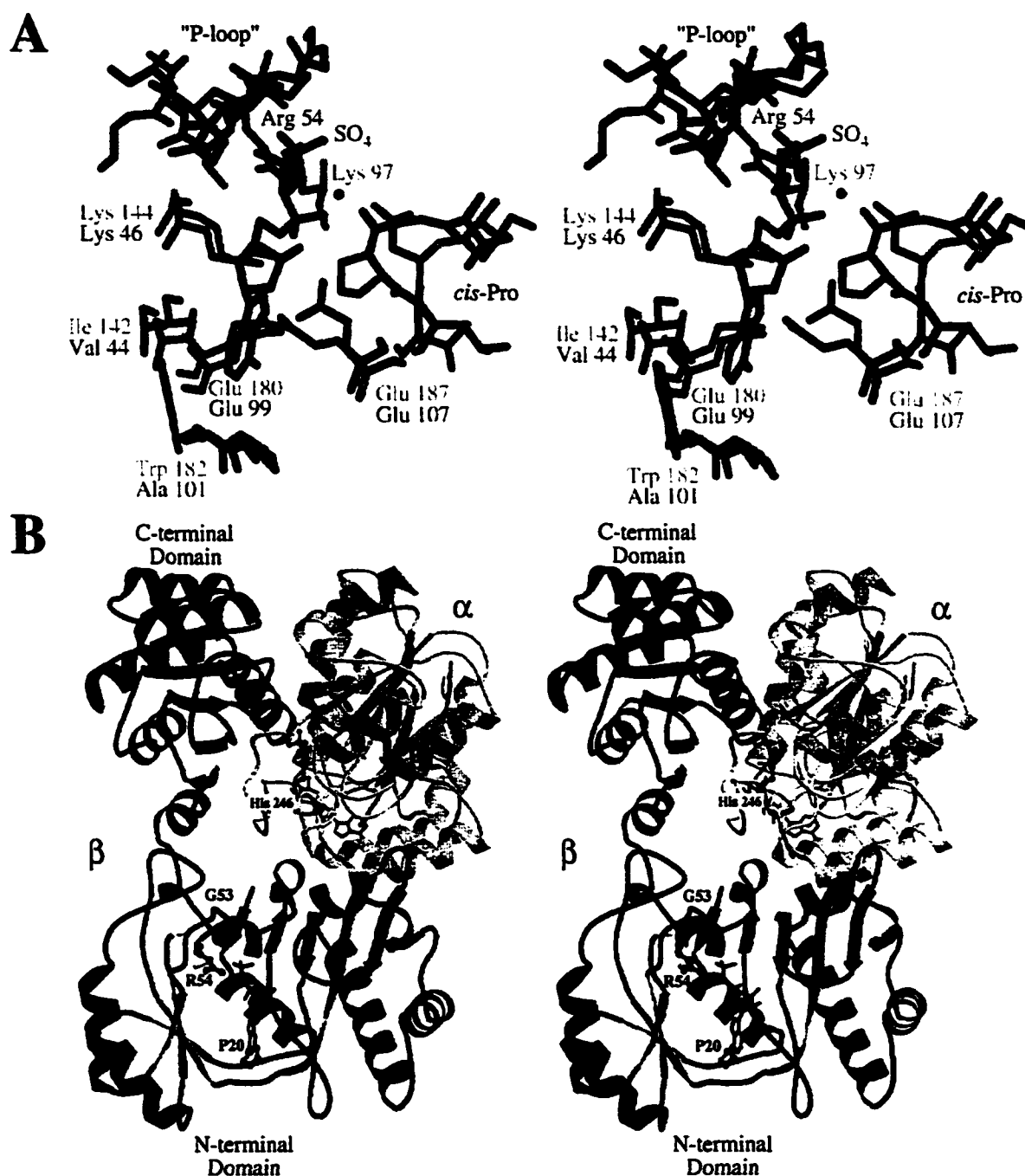


**Figure 5-2. Modeling of ADP into the N-terminal domain of the  $\beta$ -subunit of SCS.** (A) Stereo view of the superposition of the N-terminal domain of the  $\beta$ -subunit of SCS (backbone shown in green) on D-ala:D-ala ligase (backbone shown in grey). This diagram is based on two superpositions, one with residues from the small sub-domain of the N-terminal domain (shown on the left in this diagram) and one with residues from the large sub-domain (shown on the right). The residues used in the superpositions are given in Appendices 4 and 5. (B) Convergent stereo ribbon diagram of an ADP molecule modeled into the N-terminal domain of SCS based on the superposition of the small sub-domain. The  $\alpha$ -subunit of SCS is shown in yellow, the  $\beta$ -subunit in green, and the active site phosphohistidine (His 246 $\alpha$ ) and the CoA molecule are displayed as stick models in mauve and cyan, respectively. The ADP molecule is coloured red, and the side chains of the mutated residues are labeled.



## Materials and Methods

*Construction of Site-directed Mutants in the  $\beta$ -subunit of SCS.* Site-directed mutants were made in three steps using standard protocols for the PCR and overlap extension (10). The reaction buffer for PCR was identical to that used for PCR in Chapter 2, except that 0.25  $\mu$ M of each primer was used, and 100 ng of pGS202 was used as template DNA (11). The primers used for construction of the mutant plasmids are shown in Table 5-1.

**Table 5-1. Primers for Mutagenic PCR<sup>a</sup>.**

**Mutations in the N-terminal Domain of the  $\beta$ -subunit:**

5' flanking primer: (located in the  $\lambda$  Pr promoter) 5' TTTTACCTCTGGCGGTGATA 3'

3' flanking primer (597) 5' GGGTTGATTTTCGATCAACGC 3' (577)

**Internal Mutagenic Primers:**

**P20 $\beta$ Q Mutant:**

(49) 5' TACCAGCACAGGTGGGTTATG 3' (69) and its complement

**G53 $\beta$ V-R54 $\beta$ E Double Mutant:**

(143) 5' GTTCACGCTGGTGTGGAGGGTAAAGCGGGC 3' (172) and complement

**Mutations in the C-terminal Domain of the  $\beta$ -subunit**

5' flanking primer: (411) 5' AAGAACTCCGCACCTGATC 3' (431)

3' flanking primer: (1157) 5' CCTCCACTGCGGCAACAACC 3' (1137)

**Internal Mutagenic Primers:**

**I322 $\beta$ A Mutant:<sup>b</sup>**

(954) 5' CTTGCGCGGTg/cCCGTTTCGTTGC 3' (976) and complement

**R324 $\beta$ N-D326 $\beta$ A Double Mutant:**

(959) 5' GCGGTATCGTTAACTGCGCTCTGATCGCTG 3' (988) and complement

<sup>a</sup> The nucleotides that are different from the wild-type sequence are shown in bold, and the numbers in parentheses denote the position of the first and last nucleotide of the primer. The abbreviations used for naming the mutants are: the first letter is one letter code for the wild-type amino acid, the number denotes the position of the amino acid, greek symbol denotes the  $\alpha$ - or  $\beta$ -subunit, and the second letter is the one letter code for the mutant amino acid.

<sup>b</sup> The primer for the I322 $\beta$ A mutation was actually a mixture of two primers which differed by one nucleotide, shown in lower case.

Each PCR reaction was initially heated at 96 °C for 5 min to denature the template DNA, followed by 30 cycles of annealing for 30 s at a temperatures between 57 °C and 67 °C, polymerase extension for 45 s at 72 °C and denaturation for 30 s at 96 °C using a Techne PHC-2 thermocycler. The mutant fusion product for the mutations P20βQ and G53βV-R54βE and the vector pGS202 were digested with *Nde* I (which cleaves at position 1) and *Bst* XI (which cleaves at position 557) according to the manufacturer's specifications (New England Biolabs Inc.). The fragments were separated by electrophoresis in 1% (w/v) agarose in TAE buffer (12), excised and purified using glass milk (13). Each mutant fragment was ligated to the vector fragment using T4 DNA ligase (15 °C, 8 h). The resulting mutant plasmids were then used to transform competent JM103 *E. coli* cells (12). The procedures for preparing the mutants I322βA and R324βN-D326βA were identical to those described above except that the restriction enzyme *Bpu* 1102 I (which cleaves at position 1132) was used instead of *Nde* I. The mutants G53βV-R54βE-I322βA and G53βV-R54βE -R324βN were constructed by ligating the *Nde* I - *Bst* XI fragment from the G53βV-R54βE mutant into identically digested vectors from the I322βA and R324βN mutants. The presence of mutations in all constructs was verified by DNA sequencing using an Applied Biosystems Model 373 Automated Sequencer. The mutations I322βG-R324βP and I322βA-D326βN arose serindipidously in the PCR reaction mixture for the generation of the I322βA mutation because of low annealing temperatures during PCR.

*Expression and Purification of SCS Mutants.* Cells of the SCS null strain TK3D18 (14) were transformed with the mutant plasmids. Mutant proteins were expressed and purified by methods described previously (15, 1). All mutant proteins were produced in high yields (approximately 30 to 100 mg/l of culture), and were purified to homogeneity as evaluated by SDS-PAGE and staining with coomassie blue (Fig. 5-3). During purification using chromatographic methods, the elution profiles of all mutant proteins were identical to those of wild-type enzyme. The mutant proteins were stored as suspensions in solutions containing 50% (w/v)  $(\text{NH}_4)_2\text{SO}_4$  at 4 °C. The purified mutant proteins did not appear to

have any changes in secondary structure compared to wild-type SCS as determined by UV-CD from 180 to 255 nm (Fig. 5-4). For UV-CD, each mutant protein was centrifuged ( $15 \times 10^3 \times g$ , 30 min, 4 °C), and the pellet was dissolved in 500  $\mu$ l of 50 mM KCl, 0.1 mM EDTA, 50 mM Tris HCl, pH 7.4. The resultant solution was clarified by centrifugation ( $15 \times 10^3 \times g$ , 30 min, 4 °C), and dialyzed for 16 h with three changes of the same buffer at 4 °C. The protein concentrations were approximately 1.1 - 1.7 mg/ml. The far-UV CD measurements were carried out essentially as described in Chapter 2. The mean residue weight for wild-type SCS was 105.080, for P20 $\beta$ Q 105.033, for G53 $\beta$ V-R54 $\beta$ E 105.141, for I322 $\beta$ A 105.018, for R324 $\beta$ N 105.018, for I322 $\beta$ A-R324 $\beta$ N 104.910, for I322 $\beta$ G-D326 $\beta$ N 105.016, and for R324 $\beta$ N-D326 $\beta$ A 104.953.

*Steady State Kinetic Analyses of SCS Mutants.* For kinetic analyses, an aliquot of the appropriate  $(\text{NH}_4)_2\text{SO}_4$  suspension was centrifuged ( $15 \times 10^3 \times g$ , 30 min, 4 °C), and the pellet was dissolved in 500  $\mu$ l of 50 mM KCl, 0.1 mM EDTA, 50 mM Tris HCl, pH 7.4. The resultant solution was clarified by centrifugation ( $15 \times 10^3 \times g$ , 30 min, 4 °C), and dialyzed for 16 h with three changes of the same buffer at 4 °C. The concentration of the protein was determined spectrophotometrically using the extinction coefficient determined for wild-type SCS at 280 nm ( $E_{1\%}^{1\text{cm}} = 5.0$ ) (16). The concentrations of the nucleotides and CoA were determined using their standard extinction coefficients for a 1 cm pathlength (ATP:  $E_{259\text{ nm}} = 15.4 \text{ mM}^{-1}$ , GTP:  $E_{252\text{ nm}} = 13.7 \text{ mM}^{-1}$ , CoA:  $E_{260\text{ nm}} = 14.6 \text{ mM}^{-1}$ ). The  $K_{m(\text{app})}$  and  $k_{\text{cat}}$  values in the direction of succinyl-CoA formation were determined at 22 °C. For each substrate, the initial velocity was measured at various substrate concentrations and at a constant concentration of the other substrates (where appropriate, 115  $\mu$ M CoA, 60 mM succinate or 510  $\mu$ M ATP or GTP) in a total volume of 1 ml containing 50 mM KCl, 10 mM  $\text{MgCl}_2$ , 50 mM Tris HCl, pH 7.4. Initial rates were measured in duplicate at each concentration of substrate, and the initial velocity data were

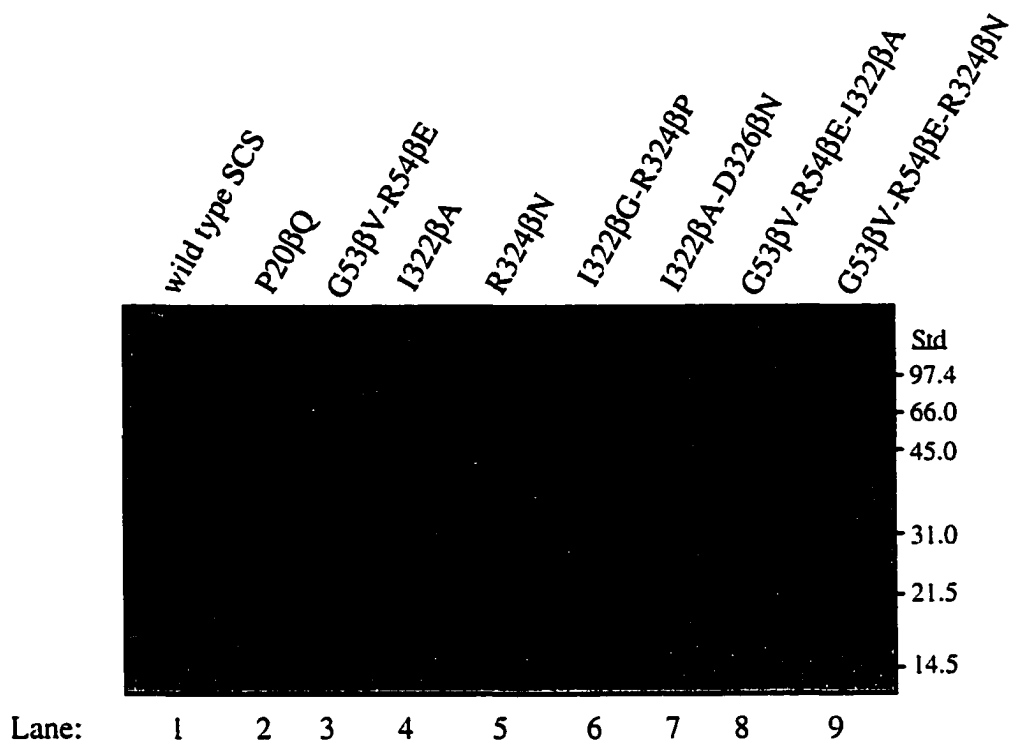


**Figure 5-3. SDS-PAGE of purified mutants of *E. coli* SCS.** Lane 1, wild -ype SCS; lane 2, protein with the mutation P20 $\beta$ Q; lane 3, G53 $\beta$ V-R54 $\beta$ E; lane 4, I322 $\beta$ A; lane 5, R324 $\beta$ N; lane 6, I322 $\beta$ G-R324 $\beta$ P; lane 7, I322 $\beta$ A-D326 $\beta$ N; lane 8, G53 $\beta$ V-R54 $\beta$ E-I322 $\beta$ A; and lane 9, G53 $\beta$ V-R54 $\beta$ E-R324 $\beta$ N.

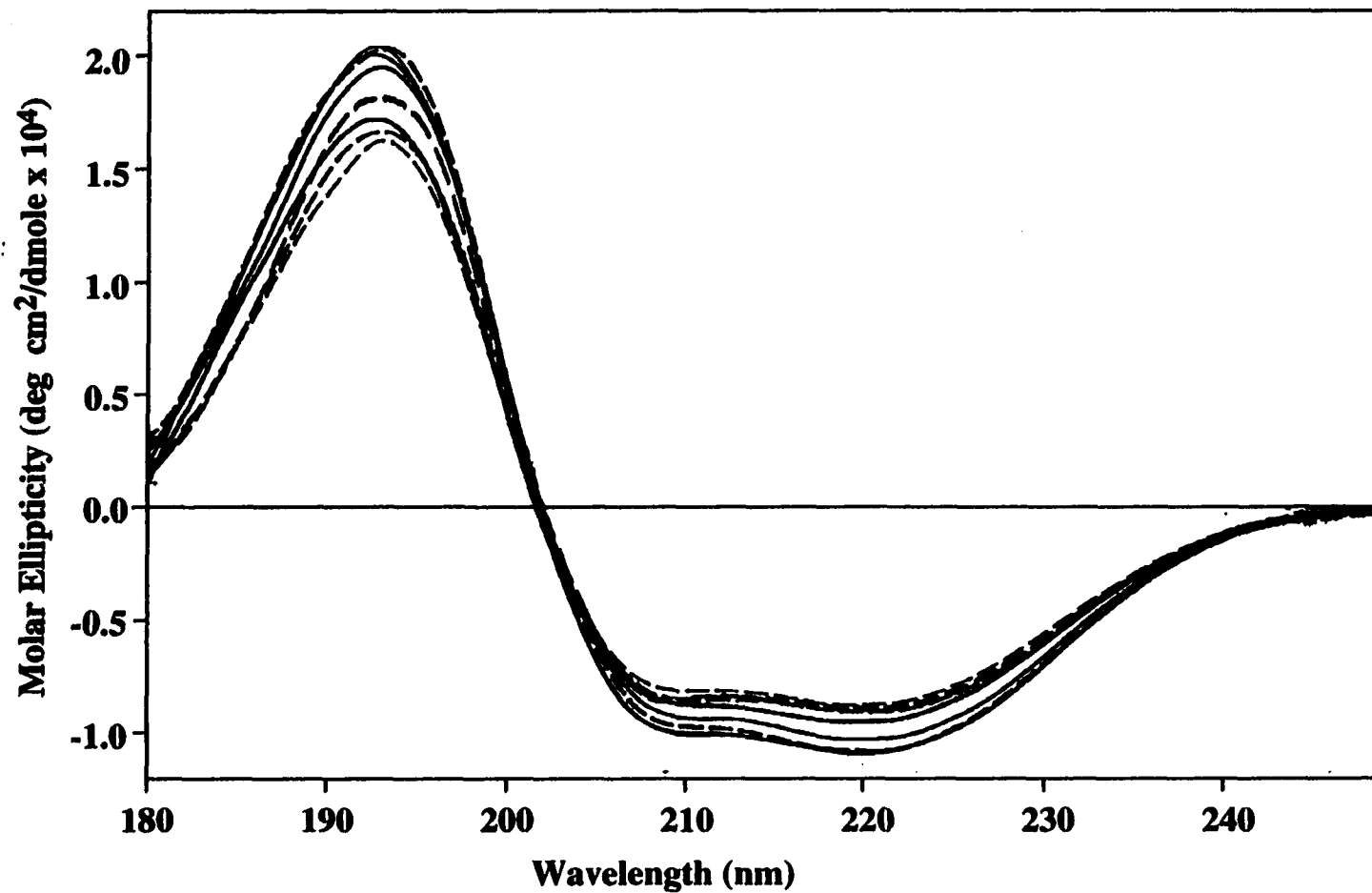


**Figure 5-4 Analysis of wild-type and mutant SCS by far-UV circular dichroism.** Wild-type SCS (—) and SCS proteins with the mutations P20 $\beta$ Q (—), G53 $\beta$ V-R54 $\beta$ E (---), I322 $\beta$ A (—), R324 $\beta$ N (---), I322 $\beta$ G-R324 $\beta$ P (---), I322 $\beta$ A-D326 $\beta$ N (---), and R324 $\beta$ A-D326 $\beta$ N (---) were analyzed by far-UV CD as described in Materials and Methods.

analyzed using the ENZYME KINETICS 1.11 program for a Macintosh computer (17). The  $k_{cat}$  values were obtained by division of the value for  $V_{max}$  by the molar concentration of active sites (i.e. per  $\alpha\beta$ -dimer) used in the experiments.

*Phosphorylation Reactions Catalyzed by SCS Mutants.* Phosphorylation of SCS by ATP or GTP (partial reaction (1)), was carried out at 22 °C in 30  $\mu$ l of a buffer containing 10 mM  $MgCl_2$ , 50 mM KCl, 50 mM Tris HCl, pH 7.4 with 1 mM [ $\gamma$ - $^{32}P$ ]-ATP or [ $\gamma$ - $^{32}P$ ]-GTP (approximately 0.3 Ci/mmol). Reactions were started by the addition of 5  $\mu$ g of SCS in 2  $\mu$ l, and incubated for various lengths of time before the addition of 15  $\mu$ l of SDS-PAGE loading buffer to stop the reactions. Phosphorylation of SCS in the opposite direction by succinyl-CoA and  $P_i$  (partial reactions (2) and (3)), was done in the same buffer except that [ $\gamma$ - $^{32}P$ ]-ATP or [ $\gamma$ - $^{32}P$ ]-GTP was replaced by 0.3 mM succinyl-CoA and 1 mM  $^{32}P_i$  (approximately 0.3 Ci/mmol). The results were analyzed via SDS-PAGE (12% (w/v) polyacrylamide gels) and autoradiography, with the radioactively labeled bands quantified by phosphorimaging. Exposure of the image plate was complete in 1 to 2 hours.

## Results

*Site-Directed Mutagenesis of Residues in the N-terminal Domain of the  $\beta$ -Subunit.* Residues Gly 53 $\beta$  and Arg 54 $\beta$  in the N-terminal domain were chosen for mutation. These residues are present in the conserved A51 $\beta$ -V60 $\beta$  loop: Gly 53 $\beta$  has hydrogen bonding and Arg 54  $\beta$  ionic interactions with the sulfate ion in the crystal structure of *E. coli* SCS (Fig. 5-2A) (3). It was reasoned that mutation of these residues would disrupt their interactions with the terminal phosphates of the nucleotide if nucleotide were bound at this site. The location of the mutated residues in relation to a molecule of ADP modeled into the N-terminal domain is shown in Figure 5-2B.

The kinetic parameters for the G53 $\beta$ V-R54 $\beta$ E double mutant were determined by steady-state analysis of initial rates of succinyl-CoA formation, and the results were plotted

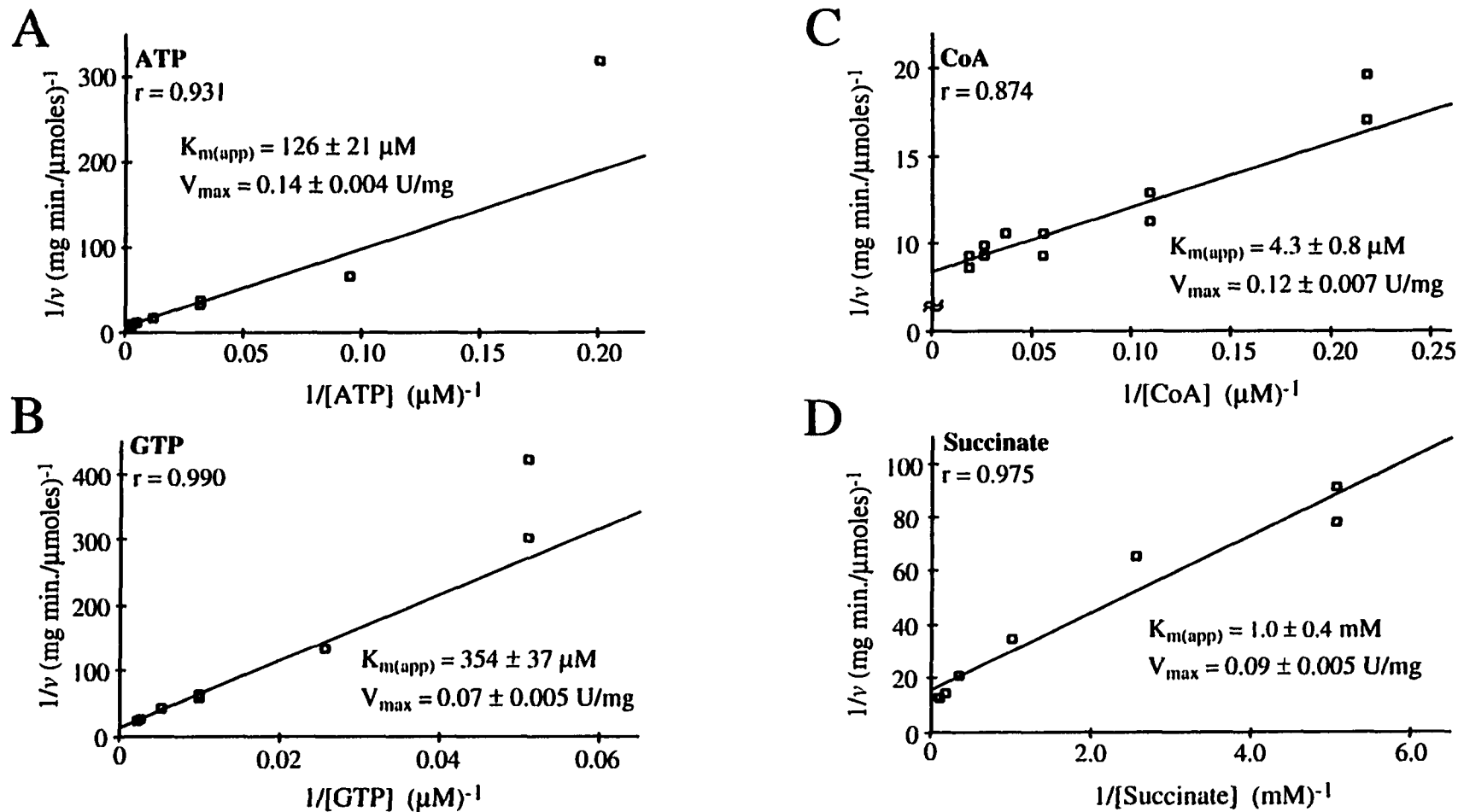


**Figure 5-5. Double reciprocal plots of the rate of succinyl-CoA formation versus substrate concentration for SCS with the mutation G53βV-R54βE.** The 1 ml reaction mixtures contained 50 mM KCl, 10 mM MgCl<sub>2</sub>, 50 mM Tris HCl, pH 7.4, and saturating concentrations of all substrates (115 μM CoA, 60 mM succinate, and 510 μM ATP or GTP) except: ATP in panel A; GTP in panel B; CoA in panel C; succinate in panel D. The data were analyzed using the program ENZYME KINETICS (17). The y-intercept of the least squares line gives the value of 1/V<sub>max</sub>, and the slope has the value of K<sub>m(app)</sub>/V<sub>max</sub>. The correlation coefficient of the line is indicated, as is the estimated error in the values of K<sub>m(app)</sub> and V<sub>max</sub>.

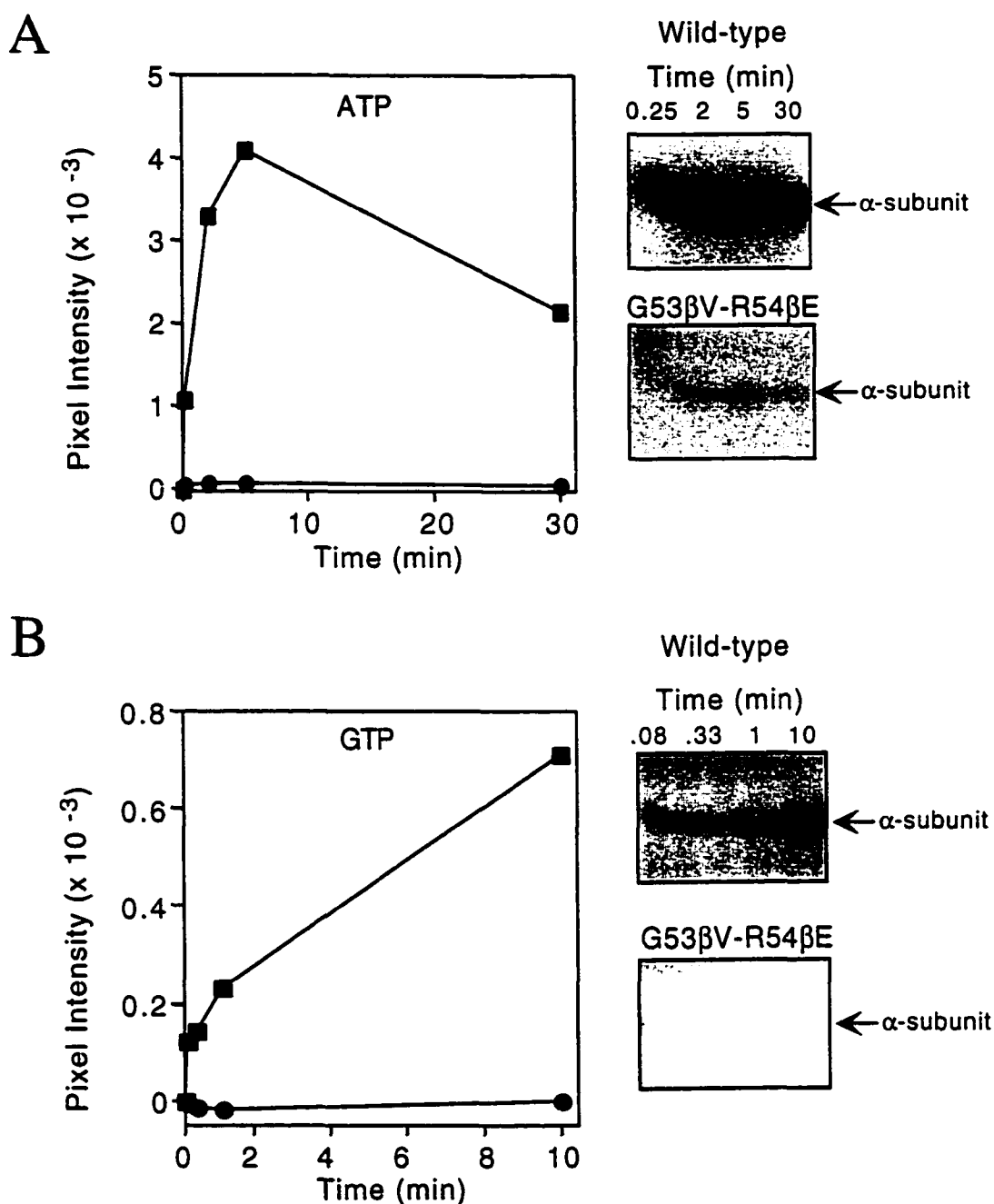
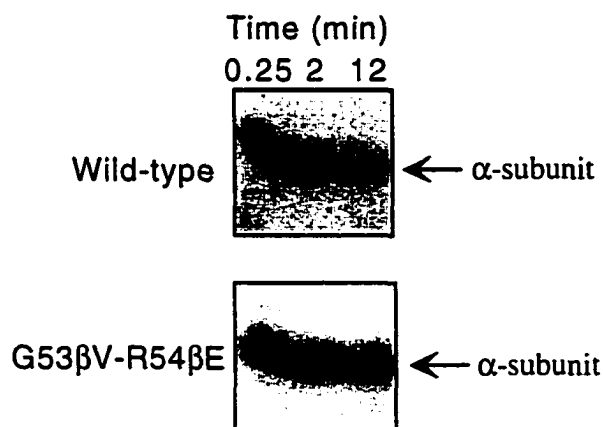


**Figure 5-6. Time course of the phosphorylation by NTP of wild-type and one mutant of SCS with changes in the N-terminal domain of the  $\beta$ -subunit.** Wild-type and mutant SCS were incubated in the presence of (A) [ $\gamma$ - $^{32}$ P] ATP, (B) [ $\gamma$ - $^{32}$ P] GTP. Samples were taken at various times, and the subunits were separated by SDS-PAGE. The gels were then analyzed by phosphorimager, and the results are shown on the left: wild-type SCS ( $\blacksquare$ ), and protein with the mutation G53 $\beta$ V-R54 $\beta$ E ( $\bullet$ ). Autoradiograms of the gels are shown on the right.



A



B

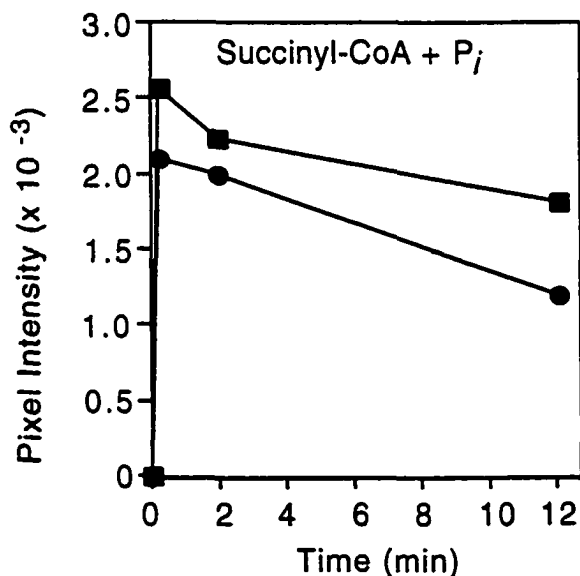


**Figure 5-7.** Time course of the phosphorylation by succinyl-CoA and  $P_i$  of wild-type and one mutant of SCS with changes in the N-terminal domain of the  $\beta$ -subunit. Wild-type and mutant SCS were incubated in the presence of succinyl-CoA and  $^{32}P_i$ . Samples were taken at various times, and the subunits were separated by SDS-PAGE. Autoradiograms of the gels are shown in panel (A). The gels were analyzed by phosphorimagery, and the results are shown in panel (B): wild-type SCS (■), and protein with the mutation G53 $\beta$ V-R54 $\beta$ E (●).

**Table 5-2: Apparent Kinetic Parameters of Wild-Type and Mutant SCS Proteins<sup>a</sup>**

Protein	Succinate	CoA	ATP	ATP	ATP	GTP	GTP	GTP
	$K_{m(\text{app})}$	$K_{m(\text{app})}$	$K_{m(\text{app})}$	$k_{\text{cat}}$	$k_{\text{cat}}/K_{m(\text{app})}$	$K_{m(\text{app})}$	$k_{\text{cat}}$	$k_{\text{cat}}/K_{m(\text{app})}$
	(mM)	( $\mu\text{M}$ )	( $\mu\text{M}$ )	( $\text{min}^{-1}$ )	( $\times 10^{-3} \text{M}^{-1} \text{s}^{-1}$ )	( $\mu\text{M}$ )	( $\text{min}^{-1}$ )	( $\times 10^{-3} \text{M}^{-1} \text{s}^{-1}$ )
Wild-type	0.25	4.0	70	2684	639	394	1471	62.2
<b>Mutations in the N-terminal Domain of the <math>\beta</math>-subunit</b>								
P20 $\beta$ Q	1.6	3.7	131	1065	135	73	807	184
G53 $\beta$ V-R54 $\beta$ E	1.0	4.3	126	7.8	1.03	354	5.0	0.235
<b>Mutations in the C-terminal Domain of the <math>\beta</math>-subunit</b>								
I322 $\beta$ A	14	17	90	533	98.7	239	521	36.3
R324 $\beta$ N	1	10	20	852	710	106 <sup>b</sup>	ND <sup>c</sup>	-
I322 $\beta$ G-R324 $\beta$ P	80	19	12	284	411	60	72	20.0
I322 $\beta$ A-D326 $\beta$ N	20	16	30	494	273	149	271	30.4
R324 $\beta$ N-D326 $\beta$ A	3.6	13	95	3124	548	374 <sup>b</sup>	ND <sup>c</sup>	-
<b>Mutations in both the N- and C-terminal Domains of the <math>\beta</math>-subunit</b>								
G53 $\beta$ V-R54 $\beta$ E-I322 $\beta$ A	0.70	0.15	83	0.92	0.18	5.8	0.36	1.0
G53 $\beta$ V-R54 $\beta$ E-R324 $\beta$ N	0.29	2.7	82	2.6	0.53	17	0.92	0.92

<sup>a</sup> Measured by following the production of succinyl-CoA spectrophotometrically at 235 nm. See Materials and Methods for specific details.

<sup>b</sup> An estimate based on measurements using a single GTP concentration (300  $\mu\text{M}$ ) which is comparable to the  $K_{m(\text{app})}$  value for the wild-type enzyme.

<sup>c</sup> not determined

using a weighted double reciprocal plot (Fig. 5-5). Kinetic analysis of the G53 $\beta$ V-R54 $\beta$ E mutant protein revealed one major difference when compared to wild-type SCS, an approximate 300-fold decrease in  $k_{cat}$  with either ATP or GTP (Table 5-2). The values of  $K_{m(app)}$  for the other substrates remained comparable to those of wild-type enzyme.

To determine which partial reactions for phosphorylation of SCS were impaired by these mutations, single turnover experiments were performed with [ $\gamma$ - $^{32}$ P]-ATP, or [ $\gamma$ - $^{32}$ P]-GTP (partial reaction (1)), or succinyl-CoA and  $^{32}$ P $_i$  (partial reactions (2) and (3)). The  $\alpha$ -subunit of the G53 $\beta$ V-R54 $\beta$ E mutant protein was not phosphorylated by either [ $\gamma$ - $^{32}$ P]-ATP or [ $\gamma$ - $^{32}$ P]-GTP (Fig. 5-6A and 5-6B, respectively), but was fully phosphorylated by succinyl-CoA and  $^{32}$ P $_i$  (Fig. 5-7). These results are consistent with Gly 53 and/or Arg 54 of the  $\beta$ -subunit playing a role during transfer of the  $\gamma$ -phosphate of ATP or GTP (bound in the N-terminal domain) to the active-site histidine of the  $\alpha$ -subunit.

Two residues that may be involved in determining the nucleotide specificity of SCS were predicted from the superposition of the N-terminal domain of *E. coli* and pig heart SCS on DD-ligase (3), in combination with sequence comparisons of SCS enzymes (Fig. 1-3) with different nucleotide specificities. One residue, Glu 99 $\beta$  of *E. coli* SCS superimposes with Glu 180 of DD-ligase, the residue that makes a hydrogen bond with the amino group at the 6 position of the adenine ring of ADP (Fig. 5-2A). GTP has a keto group at the 6 position of the guanine ring, and SCS specific for GTP contains an alanine residue at the corresponding location (Fig. 5-8) (6, 7). The second residue that can provide specificity is located at position 20 $\beta$ . The GTP-specific enzymes have a glutamine residue postulated to form a hydrogen-bond with the O6 of GTP (Fig. 5-8). However, *E. coli* SCS and the ATP-specific enzymes (7) have a proline residue at this position. To investigate one of these possible determinants of nucleotide specificity, the proline residue was mutated to glutamine, reasoning that the change should increase the affinity of the *E. coli* enzyme for GTP.

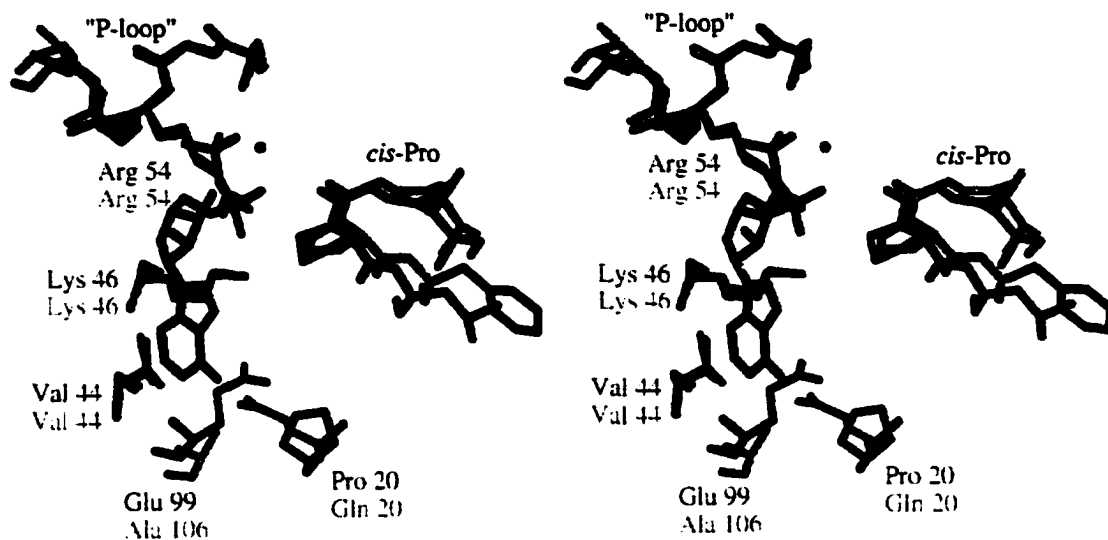


**Figure 5-8. Stereo view of the superposition of residues from the N-terminal domains of *E. coli* and pig heart SCS on the ADP from DD-ligase.** The superposition of *E. coli* SCS (shown with green backbone atoms) on the ADP and Mg<sup>2+</sup> ion from DD-ligase (shown as a red ball and stick model and a blue sphere, respectively). This view is approximately the same as that shown in Figure 5-2A. The residues used for the superposition of *E. coli* and pig heart SCS (shown with grey backbone atoms) are given in Appendix 6.

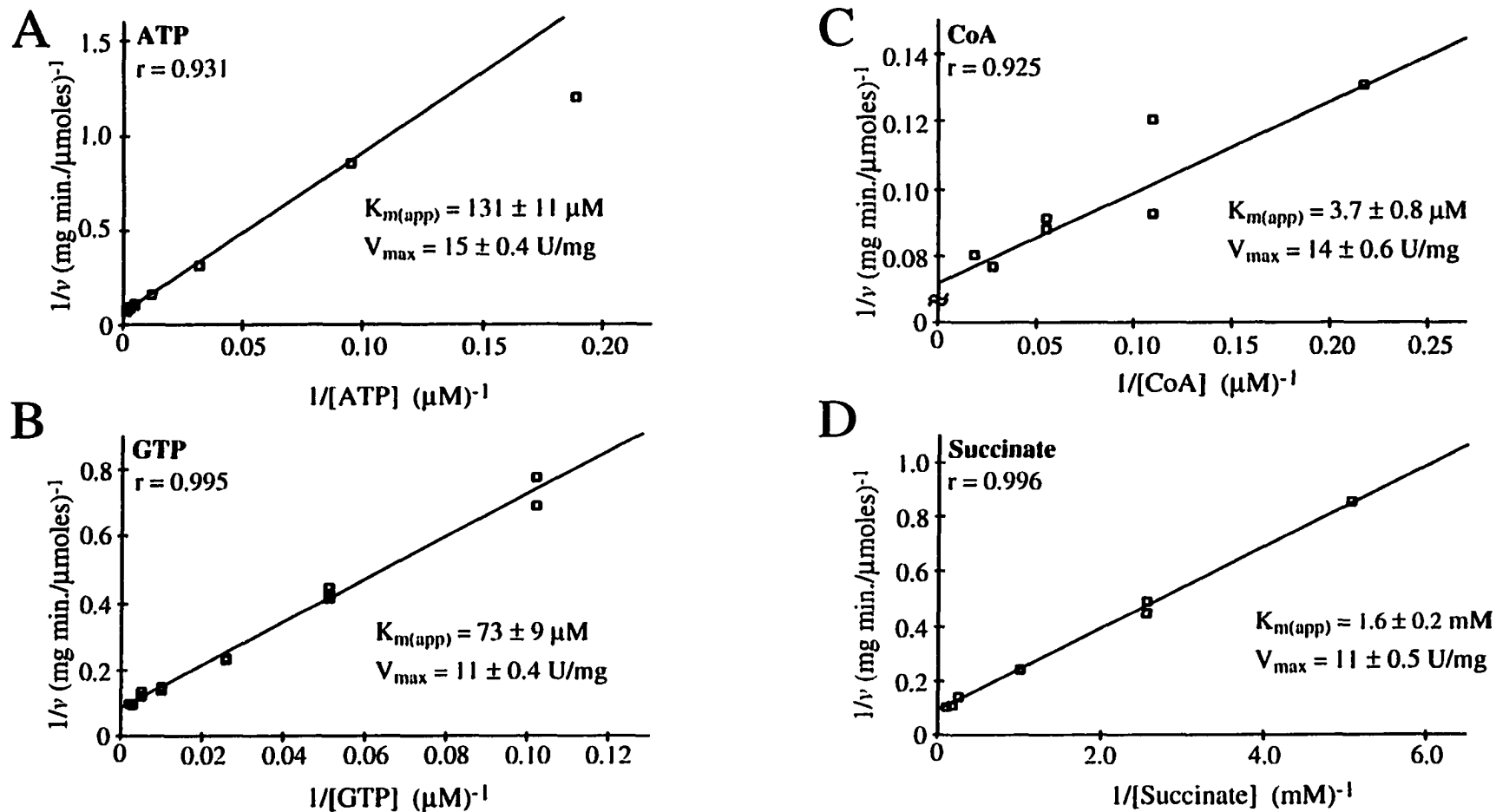


**Figure 5-9. Double reciprocal plots of the rate of succinyl-CoA formation versus substrate concentration for protein with the mutation P20βQ.** The 1 ml reaction mixtures contained 50 mM KCl, 10 mM MgCl<sub>2</sub>, 50 mM Tris HCl, pH 7.4, and saturating concentrations of all substrates (115 μM CoA, 60 mM succinate, and 510 μM ATP or GTP) except: ATP in panel A; GTP in panel B; CoA in panel C; succinate in panel D. The data were analyzed using the program ENZYME KINETICS (17). The y-intercept of the least squares line gives the value of 1/V<sub>max</sub>, and the slope has the value of K<sub>m(app)</sub>/V<sub>max</sub>. The correlation coefficient of the line is indicated.

The mutant P20 $\beta$ Q was prepared and analyzed in a similar manner to the G53 $\beta$ V-R54 $\beta$ E mutant. The results of the kinetic analyses (shown in Fig. 5-9, and summarized in Table 5-2) revealed that while the  $K_{m(\text{app})}$  for ATP had increased slightly, that for GTP had decreased by over five times. Furthermore, a comparison of the  $k_{\text{cat}}/K_{m(\text{app})}$  ratios for ATP and GTP clearly demonstrated that GTP was a better substrate than ATP for the P20 $\beta$ Q mutant, which was opposite to that observed for wild-type SCS. This result supports the hypothesis that Gln 20 $\beta$  forms a hydrogen bond with the O6 of GTP in the mutant protein, and that this residue is involved in determining the nucleotide specificity of SCS.

*Site-directed Mutagenesis of Residues in the C-terminal Domain of the  $\beta$ -subunit.*

Given that a large conformational change in SCS would be required if nucleotide was bound in the N-terminal domain of the  $\beta$ -subunit, it was important to consider the evidence from modeling and separate studies using oxidized CoA disulfide that indicated that the Rossmann fold in the C-terminal domain of the  $\beta$ -subunit may also bind nucleotide. In this light, three conserved residues in the C-terminal domain of the  $\beta$ -subunit that were implicated by modeling studies were chosen for mutation. The residues Ile 322 $\beta$ , Arg 324 $\beta$  and Asp 326 $\beta$  were mutated (singly and in combination) to probe this potential site (Fig. 5-1). It was reasoned that mutation of these residues would disrupt a loop in the Rossmann fold, and thus disrupt any putative nucleotide binding in the C-terminal domain of the  $\beta$ -subunit.

The mutant proteins were prepared and analyzed in a similar manner to that described earlier. Steady-state kinetic analyses of the proteins with mutations in the C-terminal domain of the  $\beta$ -subunit (Figures 5-10 to 5-13) revealed few differences in kinetic parameters when compared to wild-type SCS (summarized in Table 5-2). The major changes observed were increases in the values of  $K_{m(\text{app})}$  for succinate and CoA. For example, the I322 $\beta$ G-R324 $\beta$ P mutant protein had an increase in the value of  $K_{m(\text{app})}$  for succinate of approximately 320 times that of wild-type SCS. Together these results implied

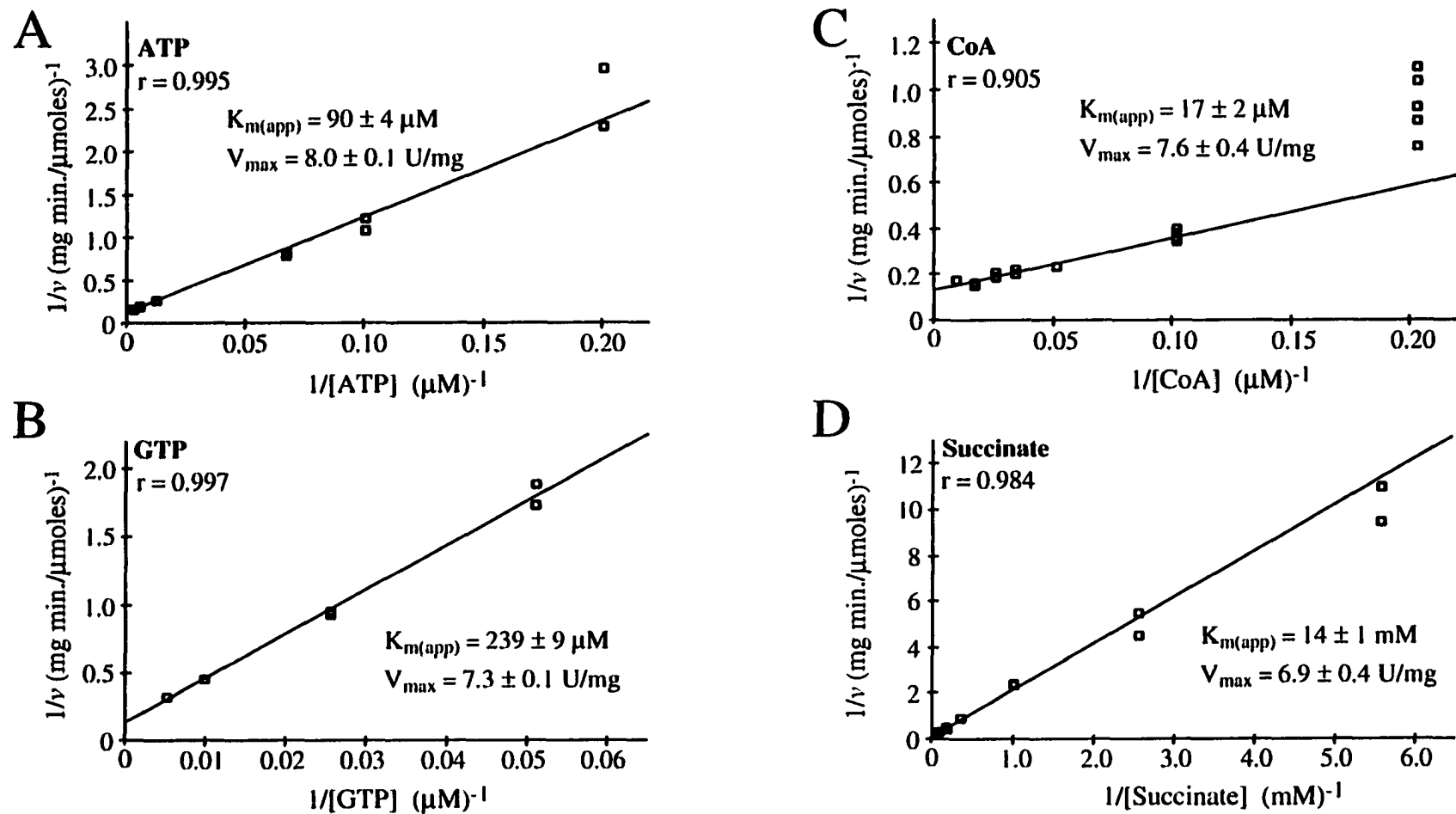


**Figure 5-10. Double reciprocal plots of the rate of succinyl-CoA formation versus substrate concentration for protein with the mutation I322 $\beta$ A.** The 1 ml reaction mixtures contained 50 mM KCl, 10 mM MgCl<sub>2</sub>, 50 mM Tris HCl, pH 7.4, and saturating concentrations of all substrates (115  $\mu$ M CoA, 60 mM succinate, and 510  $\mu$ M ATP or GTP) except: ATP in panel A; GTP in panel B; CoA in panel C; succinate in panel D. The data were analyzed using the program ENZYME KINETICS (17). The y-intercept of the least squares line gives the value of  $1/V_{max}$ , and the slope has the value of  $K_{m(app)}/V_{max}$ . The correlation coefficient of the line is indicated.

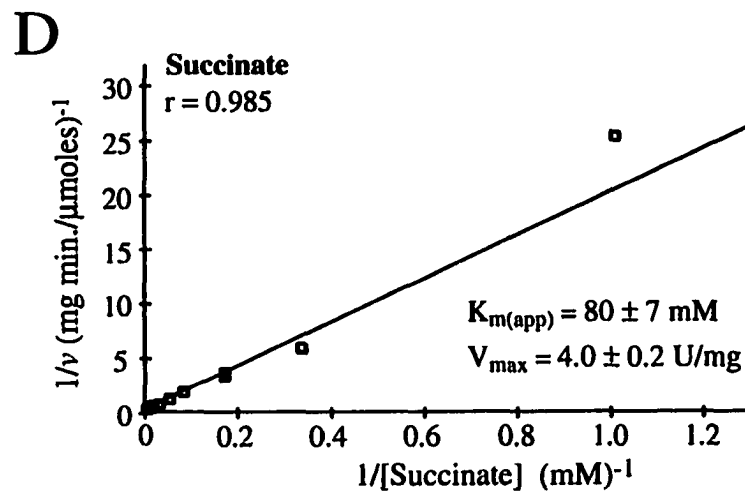
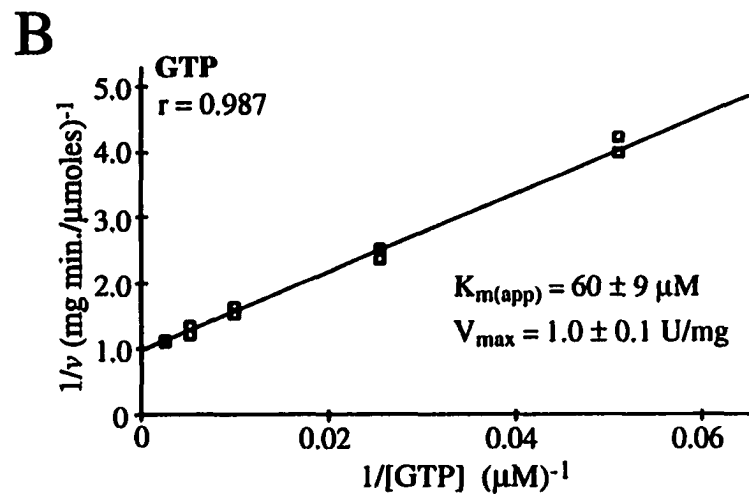
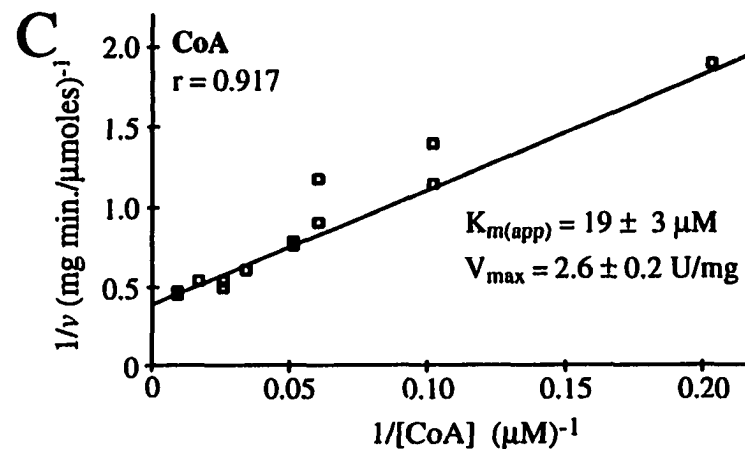
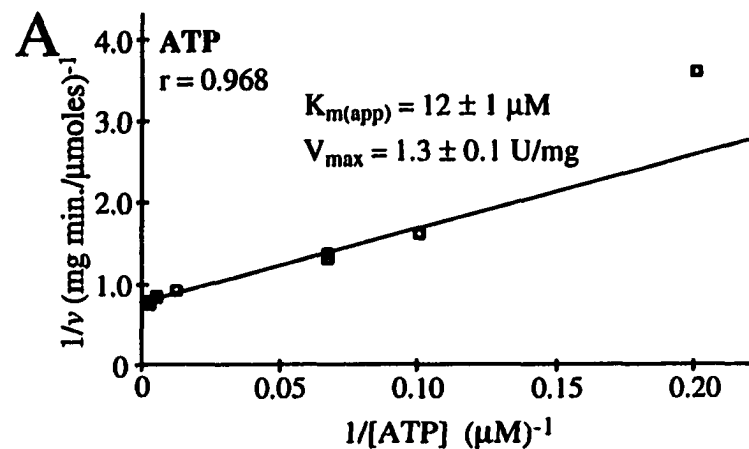


**Figure 5-11. Double reciprocal plots of the rate of succinyl-CoA formation versus substrate concentration for protein with the mutation I322βG-R324βP.** The 1 ml reaction mixtures contained 50 mM KCl, 10 mM MgCl<sub>2</sub>, 50 mM Tris HCl, pH 7.4, and saturating concentrations of all substrates (115 μM CoA, 60 mM succinate, and 510 μM ATP or GTP) except: ATP in panel A; GTP in panel B; CoA in panel C; succinate in panel D. The data were analyzed using the program ENZYME KINETICS (17). The y-intercept of the least squares line gives the value of  $1/V_{max}$ , and the slope has the value of  $K_{m(app)}/V_{max}$ . The correlation coefficient of the line is indicated.



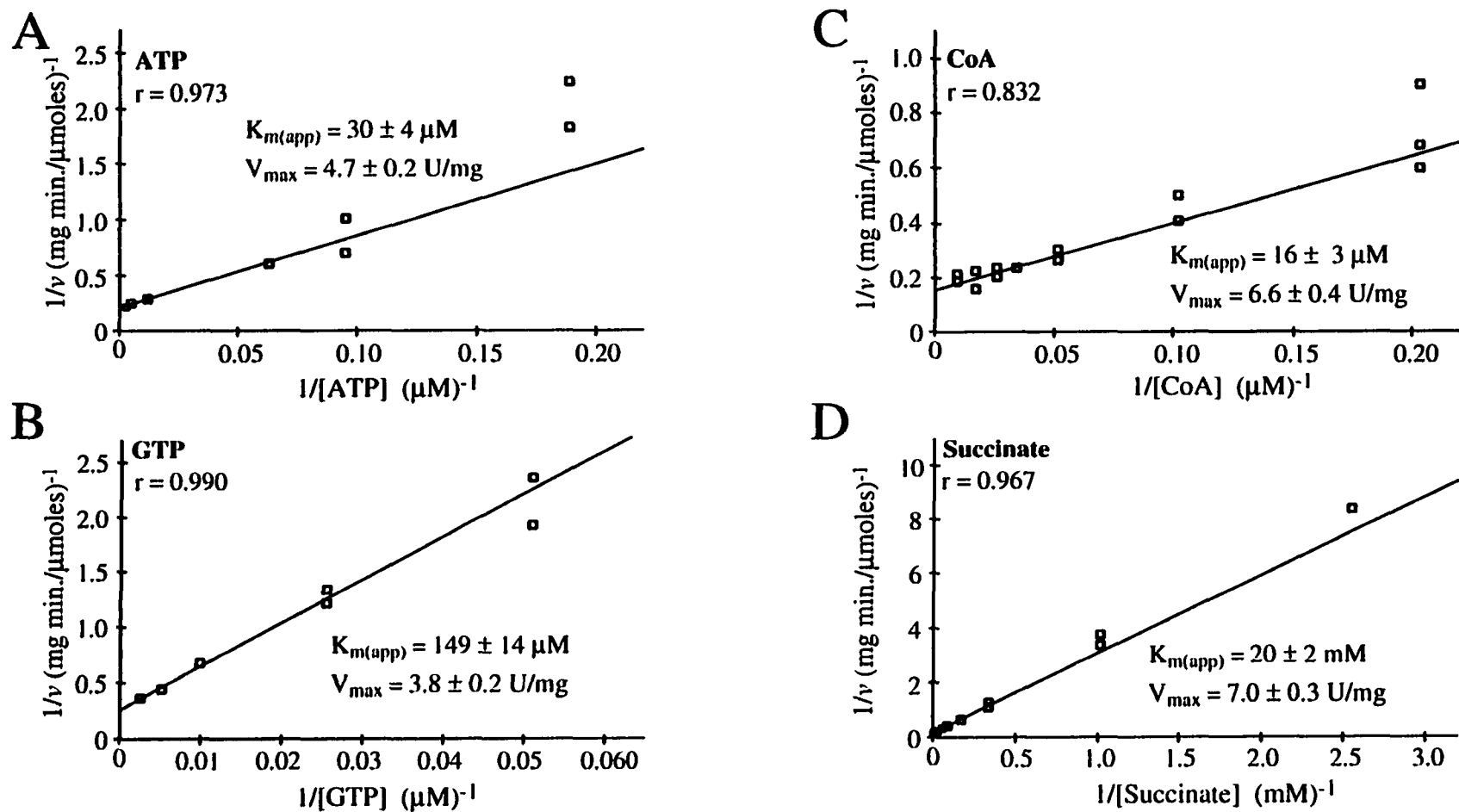


**Figure 5-12. Double reciprocal plots of the rate of succinyl-CoA formation versus substrate concentration for protein with the mutation I322βA-D326βN.** The 1 ml reaction mixtures contained 50 mM KCl, 10 mM MgCl<sub>2</sub>, 50 mM Tris HCl, pH 7.4, and saturating concentrations of all substrates (115 μM CoA, 60 mM succinate, and 510 μM ATP or GTP) except: ATP in panel A; GTP in panel B; CoA in panel C; succinate in panel D. The data were analyzed using the program ENZYME KINETICS (17). The y-intercept of the least squares line gives the value of  $1/V_{max}$ , and the slope has the value of  $K_{m(app)}/V_{max}$ . The correlation coefficient of the line is indicated.

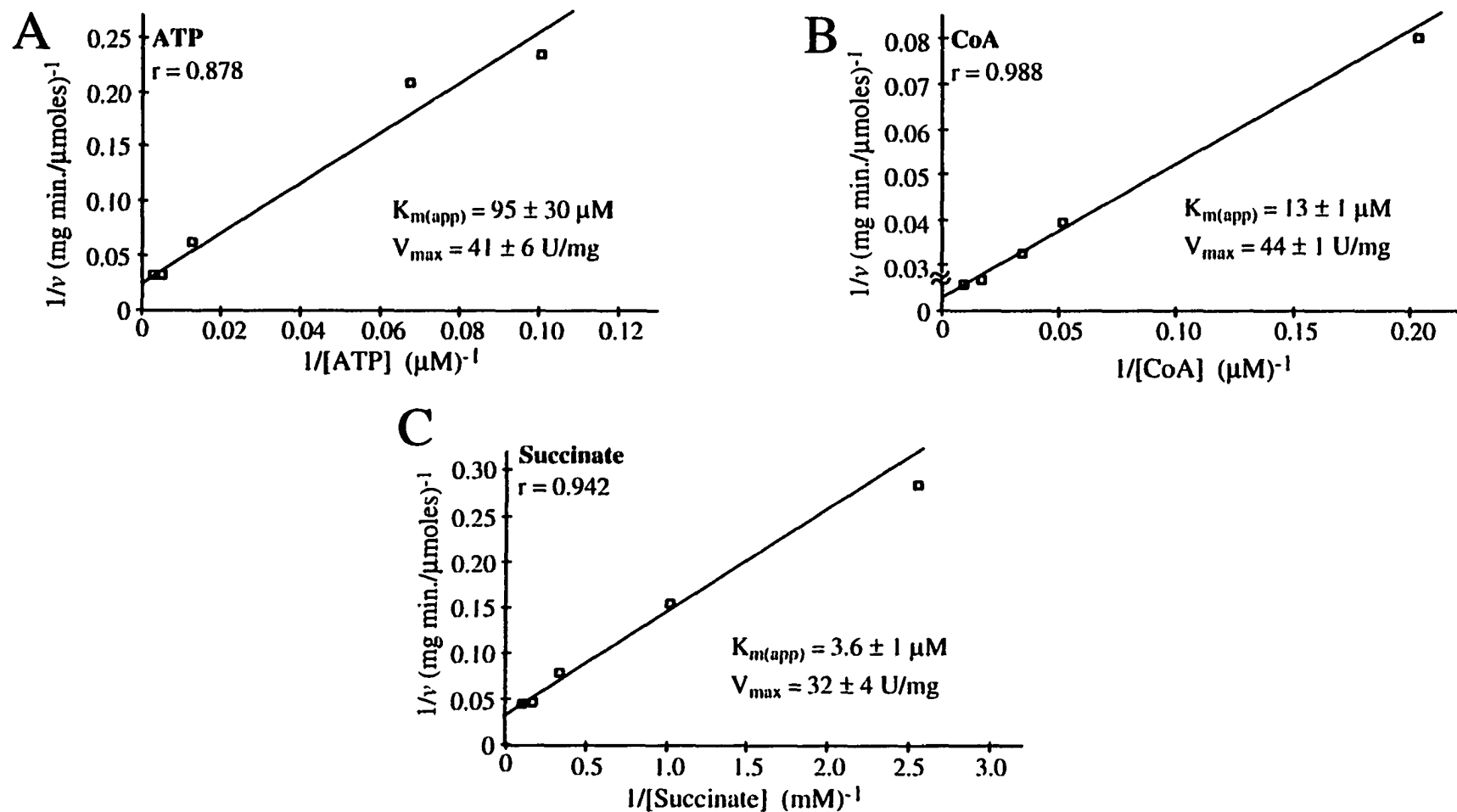


**Figure 5-13. Double reciprocal plots of the rate of succinyl-CoA formation versus substrate concentration for protein with the mutation R324 $\beta$ N-D236 $\beta$ A.** The 1 ml reaction mixtures contained 50 mM KCl, 10 mM MgCl<sub>2</sub>, 50 mM Tris HCl, pH 7.4, and saturating concentrations of all substrates (115  $\mu$ M CoA, 60 mM succinate, and 510  $\mu$ M ATP or GTP) except: ATP in panel A; CoA in panel B; succinate in panel C. The data were analyzed using the program ENZYME KINETICS (17). The y-intercept of the least squares line gives the value of  $1/V_{max}$ , and the slope has the value of  $K_{m(app)}/V_{max}$ . The correlation coefficient of the line is indicated.

that Ile 322 $\beta$ , Arg 324 $\beta$  and Asp 326 $\beta$  are proximal to the succinate/CoA binding sites. However, it is interesting to note that there was a decrease in the value of  $K_{m(\text{app})}$  for nucleotides when either Arg 324 $\beta$  and Asp 326 $\beta$  were changed (these two residues form an ion pair in *E. coli* SCS). Changing both residues to those found in pig heart SCS (R324 $\beta$ N-D326 $\beta$ A) returned the values of  $K_{m(\text{app})}$  for nucleotides to those found in wild-type SCS.

To determine which of the phosphorylation reactions may be impaired by these mutations, single turnover experiments were performed with [ $\gamma$ - $^{32}\text{P}$ ]-ATP or [ $\gamma$ - $^{32}\text{P}$ ]-GTP (partial reaction (1)), or succinyl-CoA and  $^{32}\text{P}_i$  (partial reactions (2) and (3)). The rate of phosphorylation of mutant proteins by [ $\gamma$ - $^{32}\text{P}$ ]-ATP (Fig. 5-14A) or [ $\gamma$ - $^{32}\text{P}$ ]-GTP (Fig. 5-14B) was equal to or faster than wild-type SCS. The increase in the rate of phosphorylation of mutant proteins by GTP was greater than the rate increase observed for ATP when both are compared to wild-type enzyme. This may be due to the use of a sub-saturating level of GTP at  $2xK_m$ , whereas that of ATP was  $10xK_m$ . Thus, this rate increase may reflect the changes in the  $K_{m(\text{app})}$  for GTP and not  $k_{\text{cat}}$ . The rate of phosphorylation by succinyl-CoA and  $^{32}\text{P}_i$  (partial reactions (2) and (3)) had decreased when compared to wild-type SCS (Fig. 5-15). These results were opposite to those observed for the mutations tested in the N-terminal domain of the  $\beta$ -subunit, and consistent with the conclusion that Ile 322 $\beta$ , Arg 324 $\beta$  and Asp 326 $\beta$  are not involved with binding nucleotide.

These results demonstrated the pleiotropic effect of mutations in the C-terminal domain of the  $\beta$ -subunit. The major effect was an increase in the value of  $K_{m(\text{app})}$  for succinate, and a decrease in the rate of partial reactions involving  $\text{P}_i$  and succinyl-CoA. However, the value of  $K_{m(\text{app})}$  for nucleotide decreased and the rate of the partial reaction involving nucleotide increased. Given the hypothesis that the nucleotide binding site resides in the N-terminal domain of the  $\beta$ -subunit, and given the long distance of these mutations in the C-terminal domain from the N-terminal domain, the effect of these mutations on the kinetic parameters involving nucleotide was unexpected, and prompted

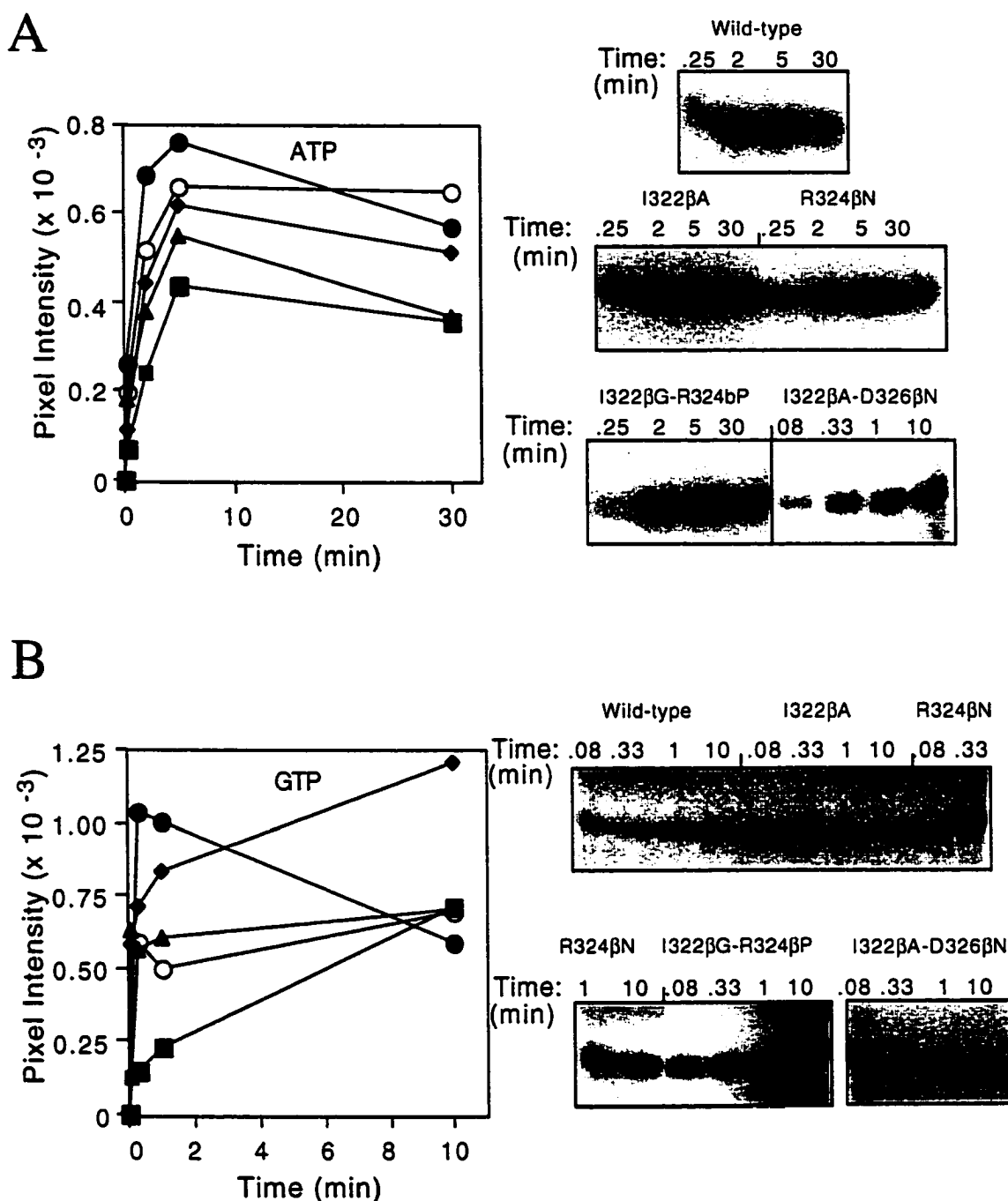


**Figure 5-14.** Time course of the phosphorylation by NTP of wild-type SCS and mutants with changes in the C-terminal domain of the  $\beta$ -subunit. Wild-type and mutant SCS were incubated in the presence of [ $\gamma$ - $^{32}$ P] ATP (A), or [ $\gamma$ - $^{32}$ P] GTP (B). Samples were taken at various times, and the subunits were separated by SDS-PAGE. The gels were then analyzed by phosphorimetry and the results are shown on the left: wild-type SCS(■), protein with the mutation I322 $\beta$ A(●), R324 $\beta$ N(▲), I322 $\beta$ G-R324 $\beta$ P (◆), and I322 $\beta$ A-D326 $\beta$ N(O). Autoradiograms of the gels showing the  $\alpha$ -subunit are on the right.

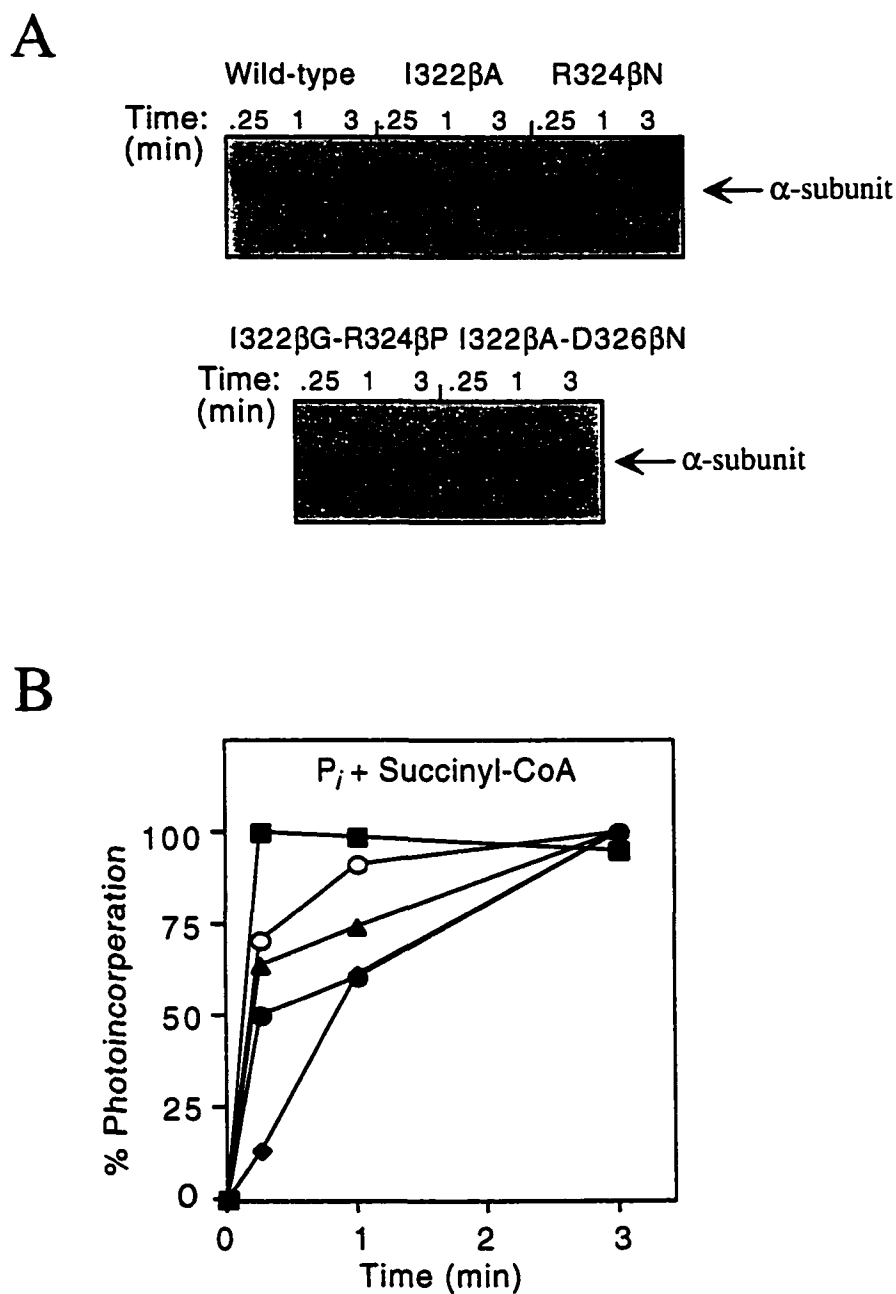


**Figure 5-15.** Time course of the phosphorylation by  $P_i$  and succinyl-CoA of wild-type SCS and mutants with changes in the C-terminal domain of the  $\beta$ -subunit. Wild-type and mutant SCS were incubated in the presence of  $^{32}P_i$  and succinyl-CoA. Samples were taken at various times, and the subunits were separated by SDS-PAGE. Autoradiograms of the gels are shown in panel A. The gels were analyzed by phosphorimager and the results are shown in panel B: wild-type SCS (■), protein with the mutation I322 $\beta$ A (●), R324 $\beta$ N (▲), I322 $\beta$ G-R324 $\beta$ P (◆), and I322 $\beta$ A-D326 $\beta$ N (○).

further investigation.

*Site-Directed Mutagenesis of Residues in Both Domains of the  $\beta$ -Subunit.* Constructs containing the changes G53 $\beta$ V-R54 $\beta$ E-I322 $\beta$ A and G53 $\beta$ V-R54 $\beta$ E-R324 $\beta$ N were made, and the mutant proteins were expressed, purified, and analyzed as before. The results of the kinetic analyses of these proteins are shown in Figures 5-16 and 5-17. The data for the G53 $\beta$ V-R54 $\beta$ E-I322 $\beta$ A mutant protein were plotted using Hanes-Wolf plots because the correlation coefficients were significantly better than in weighted double reciprocal plots. This may be due to the low rates of reaction observed with this mutant protein. When the data for the G53 $\beta$ V-R54 $\beta$ E-R324 $\beta$ N mutant protein was plotted using both types of plots, the results were sufficiently similar that although the Hanes-Wolf plots gave better correlation coefficients, the more common double reciprocal plots were used. If the mutations in the N-terminal domain are absolutely independent from those in the C-terminal domain, then the changes observed in the values of  $K_{m(app)}$  and  $k_{cat}$  between the triple mutant proteins (e.g. G53 $\beta$ V-R54 $\beta$ E-R324 $\beta$ N) and the corresponding single N-domain mutant protein (e.g. G53 $\beta$ V-R54 $\beta$ E) should correspond to the changes in the values of  $K_{m(app)}$  and  $k_{cat}$  observed between wild-type SCS and the corresponding single domain mutant protein (e.g. R324 $\beta$ N). Consistent with this idea, the  $k_{cat}$  for protein with the changes G53 $\beta$ V-R54 $\beta$ E-R324 $\beta$ N was 3 times less than the  $k_{cat}$  for protein with the changes G53 $\beta$ V-R54 $\beta$ E, and the  $k_{cat}$  for protein with the change R324 $\beta$ N was 3 times less than the  $k_{cat}$  for wild type SCS (Table 5-2). In the case of mutant protein with the changes G35 $\beta$ V-R54 $\beta$ E-I322 $\beta$ A, the relationships were similar, 8 times as compared to 5 times. The mutant protein with the changes G35 $\beta$ V-R54 $\beta$ E-R324 $\beta$ N had values of the  $K_{m(app)}$  for substrates that were within one order of magnitude of the corresponding  $K_{m(app)}$  values for the mutant proteins G53 $\beta$ V-R54 $\beta$ E, and R324 $\beta$ N. However, the mutant protein with the changes G35 $\beta$ V-R54 $\beta$ E-I322 $\beta$ A had values of  $K_{m(app)}$  for substrates that were significantly lower than those of proteins with the changes G35 $\beta$ V-R54 $\beta$ E and I322 $\beta$ A.

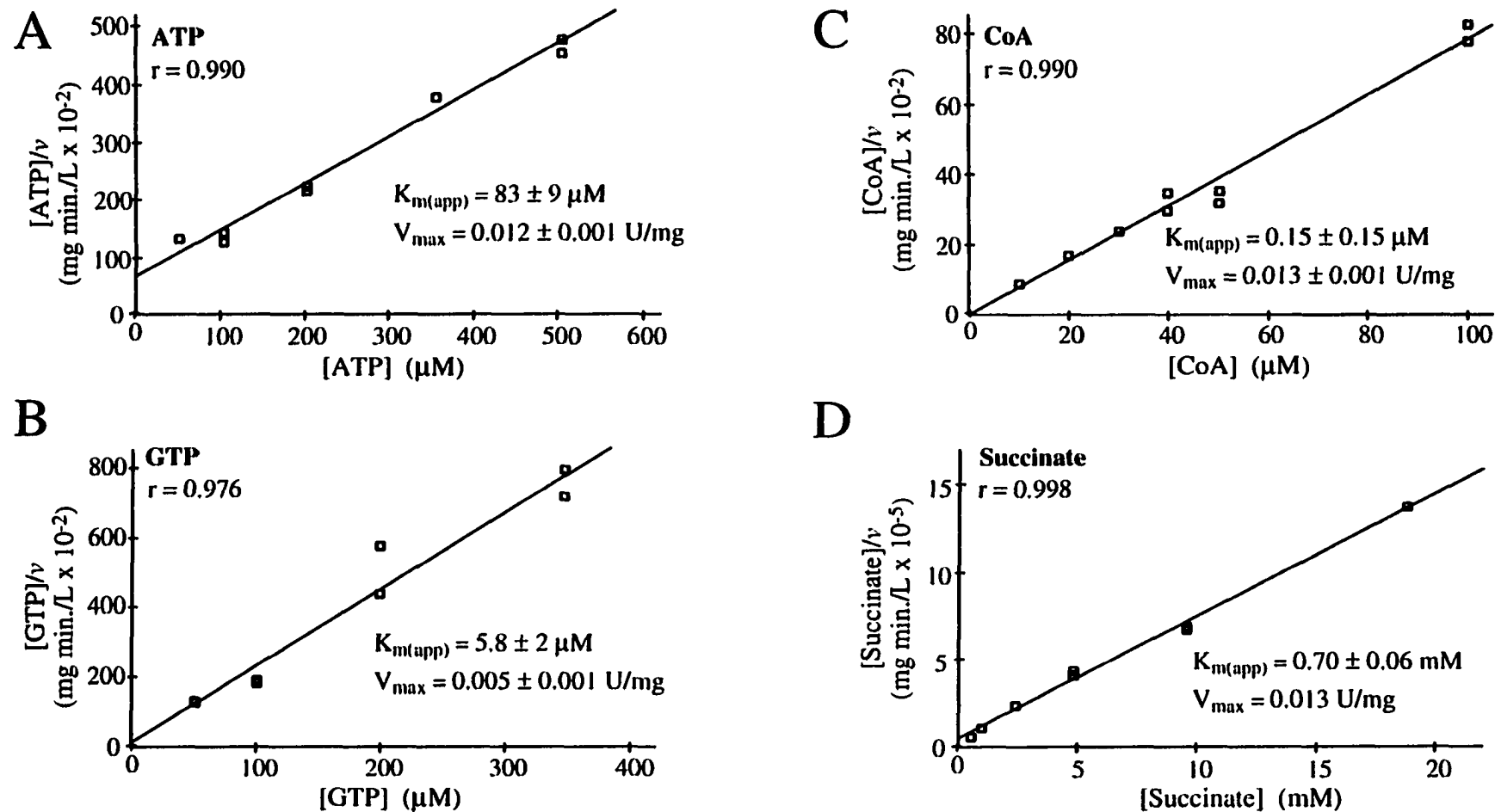


**Figure 5-16. Hanes-Wolf plots for protein with the mutation G53βV-R54βE-I322βA.** The 1 ml reaction mixtures contained 50 mM KCl, 10 mM MgCl<sub>2</sub>, 50 mM Tris HCl, pH 7.4, and saturating concentrations of all substrates (115 μM CoA, 60 mM succinate, and 510 μM ATP or GTP) except: ATP in panel A; GTP in panel B; CoA in panel C; succinate in panel D. The data were analyzed using the program ENZYME KINETICS (17). The y-intercept of the least squares line gives the value of  $K_{m(app)}/V_{max}$ , and the slope is equal to the value of  $1/V_{max}$ . The correlation coefficient of the line is indicated, as is the estimated error in the values of  $K_{m(app)}$  and  $V_{max}$ .

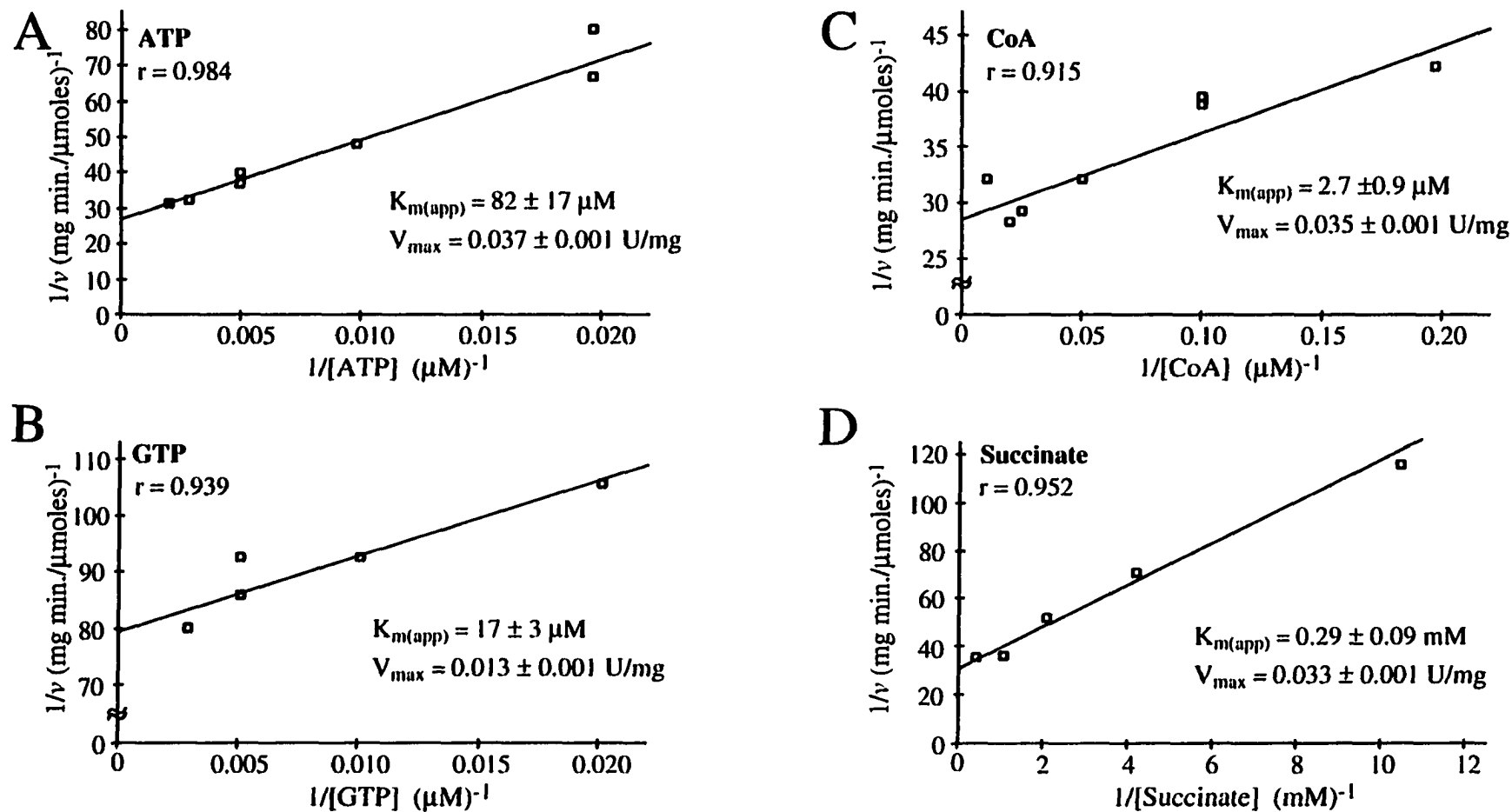


**Figure 5-17. Double reciprocal plots of the rate of succinyl-CoA formation versus substrate concentration for protein with the mutation G53βV-R54βE-R324βN.** The 1 ml reaction mixtures contained 50 mM KCl, 10 mM MgCl<sub>2</sub>, 50 mM Tris HCl, pH 7.4, and saturating concentrations of all substrates (115 μM CoA, 60 mM succinate, and 510 μM ATP or GTP) except: ATP in panel A; GTP in panel B; CoA in panel C; succinate in panel D. The data were analyzed using the program ENZYME KINETICS (17). The y-intercept of the least squares line gives the value of 1/V<sub>max</sub>, and the slope has the value of K<sub>m(app)</sub>/V<sub>max</sub>. The correlation coefficient of the line is indicated, as is the estimated error in the values of K<sub>m(app)</sub> and V<sub>max</sub>.



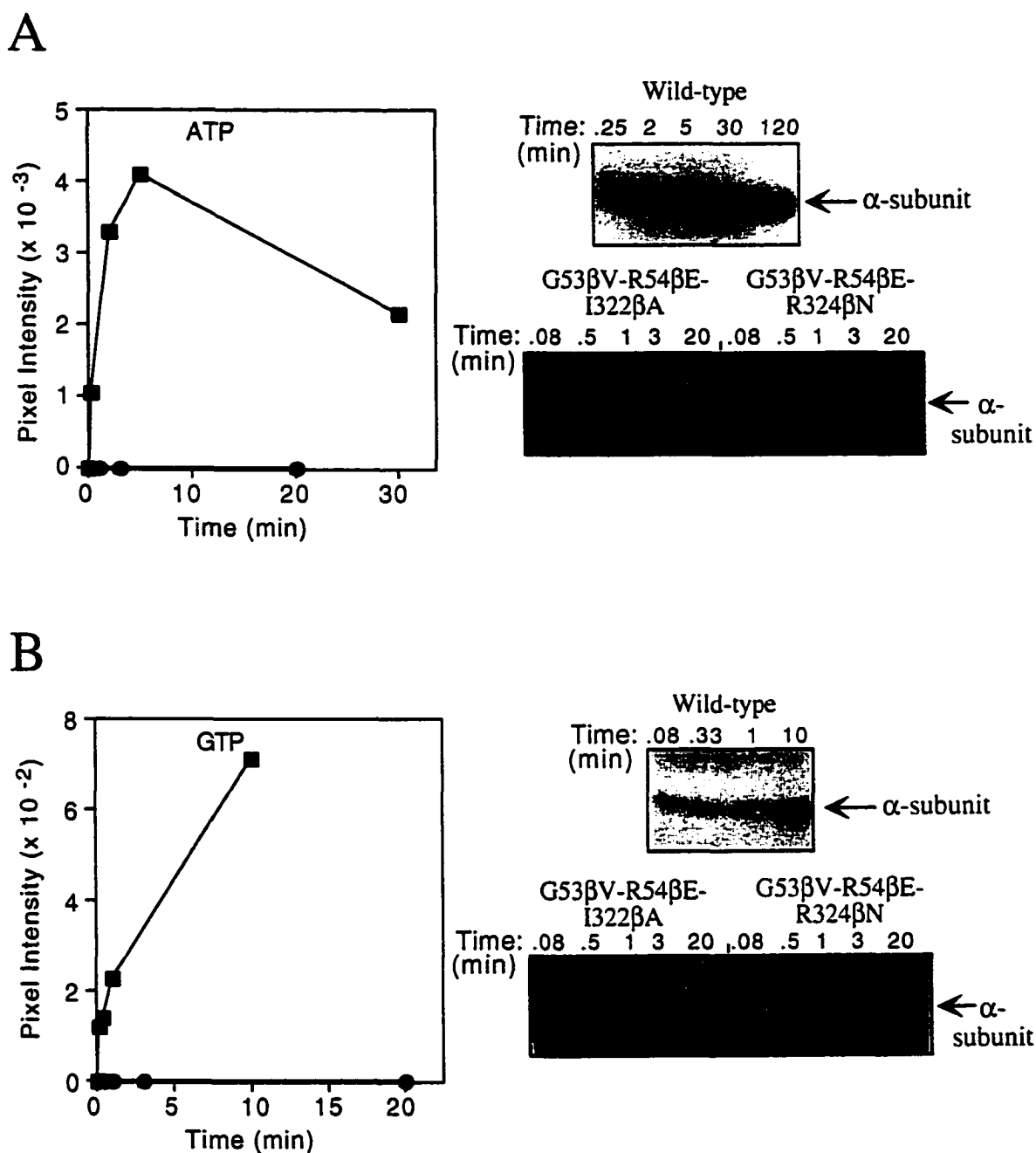


**Figure 5-18. Time course of the phosphorylation by NTP of wild-type and mutant SCS with changes in both domains of the  $\beta$ -subunit.** Wild-type and mutant SCS were incubated in the presence of [ $\gamma$ - $^{32}$ P] ATP (A), or [ $\gamma$ - $^{32}$ P] GTP (B). Samples were taken at various times, and the subunits were separated by SDS-PAGE. The gels were then analyzed by phosphorimager and the results are shown on the left: wild-type SCS ( $\blacksquare$ ), protein with the mutation G53 $\beta$ V-R54 $\beta$ E-I322 $\beta$ A ( $\blacktriangle$ ), and G53 $\beta$ V-R54 $\beta$ E-R324 $\beta$ N ( $\bullet$ ). Autoradiograms of the gels showing the  $\alpha$ -subunit are on the right.

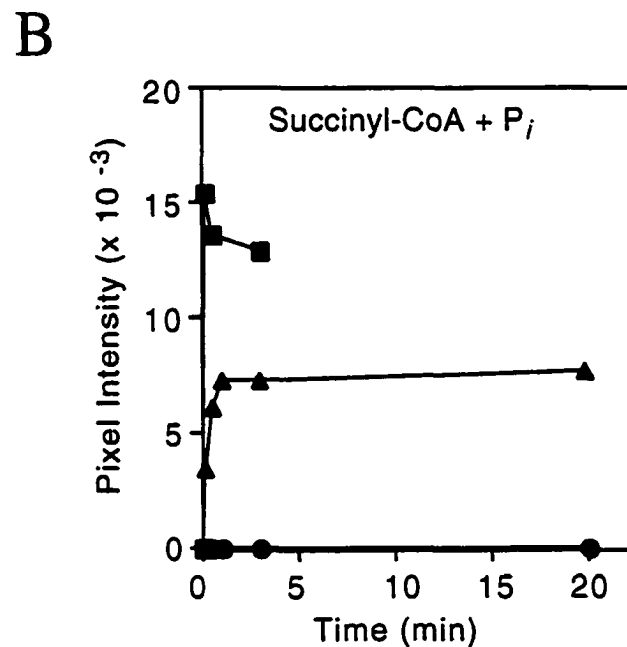
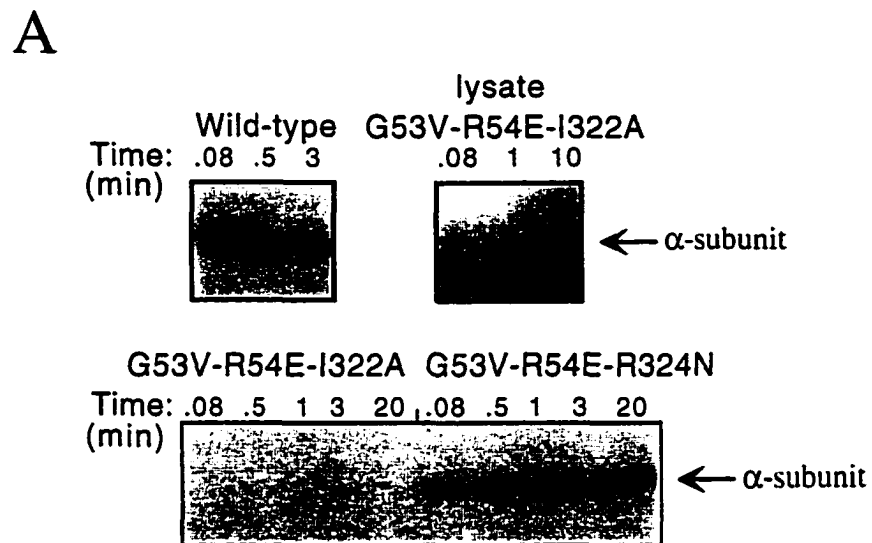


**Figure 5-19. Time course of the phosphorylation by succinyl-CoA and  $P_i$  of wild-type and mutant SCS with changes in both domains of the  $\beta$ -subunit.** Wild-type and mutant SCS were incubated in the presence of  $^{32}P_i$  and succinyl-CoA. Samples were taken at various times, and the subunits were separated by SDS-PAGE. Autoradiograms of the gels are shown in panel A. The gels were then analyzed by phosphorimager and the results are shown in panel B: wild-type SCS (■), protein with the mutation G53 $\beta$ V-R54 $\beta$ E-I322 $\beta$ A (▲), and G53 $\beta$ V-R54 $\beta$ E-R324 $\beta$ N (●).

If the mutations in the C- and N-terminal domain are completely independent, the partial reactions catalyzed by the proteins containing mutations in both domains of the  $\beta$ -subunit (e.g. G35 $\beta$ V-R54 $\beta$ E-R324 $\beta$ N) should be a combination of the partial reactions catalyzed by proteins containing mutations in each of the domains (e.g. G35 $\beta$ V-R54 $\beta$ E and R324 $\beta$ N). Consistent with the behavior of the G35 $\beta$ V-R54 $\beta$ E mutant protein, neither of the triple mutants were phosphorylated by [ $\gamma$ - $^{32}$ P]-ATP (Fig. 5-18A) or [ $\gamma$ - $^{32}$ P]-GTP (Fig. 5-18B). When compared to wild-type protein, the phosphorylation of both the G35 $\beta$ V-R54 $\beta$ E-I322 $\beta$ A and G35 $\beta$ V-R54 $\beta$ E-R324 $\beta$ N mutant proteins by succinyl-CoA and  $^{32}$ P<sub>i</sub> was impaired (Fig. 5-19). The rate of phosphorylation of G35 $\beta$ V-R54 $\beta$ E-R324 $\beta$ N mutant protein by succinyl-CoA and  $^{32}$ P<sub>i</sub> was comparable to that observed for protein with the mutation R324 $\beta$ N. The phosphorylation of G35 $\beta$ V-R54 $\beta$ E-I322 $\beta$ A mutant protein by succinyl-CoA and  $^{32}$ P<sub>i</sub> was not detected in purified preparations of this mutant. When lysates of the SCS null strain containing constructs that expressed this mutant were made and tested for their ability to be phosphorylated by succinyl-CoA and P<sub>i</sub>, phosphorylation was observed (Fig. 5-19A). The results indicate that the effects of mutations in the N-terminal domain of the  $\beta$ -subunit are essentially independent from the effects of mutations in the C-terminal domain of the  $\beta$ -subunit.

## Discussion

This study was undertaken to differentiate between two possible locations of the nucleotide-binding site in the  $\beta$ -subunit of *E. coli* SCS. The results of this study support and extend the results of the affinity labeling study that used 8-N<sub>3</sub>-ATP (Chapter 4). Mutation of residues in the N-terminal domain of the  $\beta$ -subunit affected predominantly kinetic parameters involving nucleotide and partial reaction (1), indicating that these residues were proximal to the nucleotide binding site. Mutations in the C-terminal domain primarily affected the kinetic parameters involving succinate and CoA and partial reactions

(2) and (3), indicating that these residues were proximal to the CoA and succinate binding sites. Therefore it was concluded that the nucleotide binds in the ATP-grasp fold of the N-terminal domain of the  $\beta$ -subunit and not in the Rossmann fold of the C-terminal domain. Binding of the nucleotide in the N-terminal domain requires that the catalytic His 246 $\alpha$  interacts alternately at two sites, site I where CoA and, presumably, succinate bind, and site II where the nucleotide binds. NMR spectroscopy presented evidence for a "flip" between two conformations of the phosphorylated histidine (18). His 246 $\alpha$  is part of a loop that is postulated to swing and shuttle the histidine residue between the two sites during each catalytic cycle.

The specific mutations that were made in the C-terminal domain of the  $\beta$ -subunit affected the partial reactions involving CoA and succinate, but not nucleotide. From the relative increase in the kinetic parameters observed for these two substrates (Table 5-2) succinate and CoA are poorer substrates for the mutants than for the wild-type enzyme. It was thus not surprising that the mutants were more slowly phosphorylated by succinyl-CoA and  $P_i$  (Fig. 5-15). The effect of these mutations can be rationalized from examination of the x-ray crystallographic structure of *E. coli* SCS (3). The effects on the CoA binding site are likely to arise from the interaction between the loop which contains Ile 322 $\beta$  and the  $\alpha$ -helix that contains Phe 22 $\alpha$ . This helix is part of the Rossmann fold in the  $\alpha$ -subunit that binds CoA. The effects on the  $K_{m(\text{app})}$  for succinate may arise because the loop containing Ile 322 $\beta$  is adjacent to a conserved glycine rich loop that is proximal to the phosphohistidine. This loop contains a series of glycine residues whose main chain amino groups could stabilize the negative charge on the non-reactive carboxyl group succinate. Furthermore, the disruption of the succinate and CoA binding sites would indirectly affect the movement of the phosphohistidine loop. If the conformation of SCS with the phosphohistidine loop bound in the  $\alpha$ -subunit (as seen in the crystal structure) were destabilized, the rate of phosphorylation by succinyl-CoA and  $P_i$  at site I would be reduced while the rate of phosphorylation by nucleotide at site II would be increased. These are the

effects observed with the proteins with mutations in the C-terminal domain (Figures. 5-14 and 5-15). Similar, but more pronounced effects, were observed by Luo and Nishimura for protein with the mutation H142 $\alpha$ N (19). This mutant protein was “practically devoid of enzyme activity”, but was thiophosphorylated and de-thiophosphorylated by ATP $\gamma$ S and ADP, respectively, at a rate much greater than that for wild-type enzyme. However, when succinate and CoA were used for de-thiophosphorylation, the rate was much slower than that for wild-type enzyme. The kinetic parameters of the mutant protein R324 $\beta$ N-D326 $\beta$ A, which are similar to those of wild-type SCS, can also be rationalized by examination of the crystal structures of both *E. coli* (3) and pig heart SCS (20). In the structure of *E. coli* SCS, there is an ion pair between R324 $\beta$  (which is part of the I322 $\beta$  loop) and D326 $\beta$  (which is in the adjacent helix). In the structure of pig heart SCS, the side chain of Asn 324 $\beta$  is a helix capping residue in the adjacent  $\alpha$ -helix. Thus mutation of both residues restored the stabilization of the loop containing I322 $\beta$ .

The mutagenesis of selected residues in the N-terminal domain of the  $\beta$ -subunit affected the binding of nucleotide or the catalysis of partial reaction (1) involving nucleotide, but not the binding of the other substrates or catalysis of partial reactions ((2) and (3)) involving succinyl-CoA and P<sub>i</sub>. The positions of these mutated residues are shown as ball and stick models in Figure 5-2. As demonstrated by the significant changes observed in the catalytic efficiency of the mutant proteins compared to the wild-type enzyme (Table 5-2), the residues Gly 53 $\beta$  and Arg 54 $\beta$  are likely to be involved in transfer of the  $\gamma$ -phosphate of nucleotide triphosphate to and from the active site histidine, and the residue at position 20 $\beta$  has a role in determining the nucleotide specificity of SCS.

**References:**

1. Wolodko, W. T., Fraser, M. E., James, M. N. G., & Bridger, W. A. (1994) *J. Biol. Chem.* 269, 10883-10890.
2. Murzin, A. G. (1996) *Curr. Opin. in Struct. Biol.* 6, 386-394.
3. Fraser, M. E., James, M. N. G., Bridger, W. A., & Wolodko, W. T. (1999) *J. Mol. Biol.* 285, 1633-1653.
4. Collier, G. E., & Nishimura, J. S. (1978) *J. Biol. Chem.* 253, 4938-4943.
5. Mann, C. J., Hardies, S. C., & Nishimura, J. S. (1989) *J. Biol. Chem.* 264, 1457-1460.
6. Bailey, D. L., Wolodko, W. T., & Bridger, W. A. (1993) *Protein Sci.* 2, 1255-1262.
7. Johnson, J. D., Mehus, J. G., Tews, K., Milavetz, B. I., & Lambeth, D. O. (1998) *J. Biol. Chem.* 273, 27580-27586.
8. Hara, T., Kato, H., Katsube, Y., & Oda, J. (1996) *Biochem.* 35, 11967-11974.
9. Fan, C., Moews, P. C., Walsh, C. T., & Knox, J. R. (1994) *Science* 266, 439-443.
10. Ho, S. N., Hunt, H. D., Horton, R. N., Pullen, J. K., & Pease, L. R. (1989) *Gene* 77, 51-59.
11. Buck, D., & Guest, J. R. (1989) *Biochem. J.* 260, 737-747.
12. Sambrook, J., Fritsch, E. F., & Maniatis, T. (1989) *Molecular Cloning: a laboratory manual*, 2 Ed., CSH Laboratory Press
13. Davis, D. G., Dibner, M. D., & Battey, J. F. (1986) *Basic Methods in Molecular Biology*, 1 Ed., Elsevier Science Publishing Co., Inc., New York
14. Froehlich, B., & Epstein, W. (1981) *J. Bacteriol.* 147, 1117-1120.
15. Wolodko, W. T., Kay, C. M., & Bridger, W. A. (1986) *Biochemistry* 25, 5420-5425.
16. Krebs, A., & Bridger, W. A. (1974) *Can. J. Biochem.* 52, 594-598.
17. Stanislawski, J. (1991) Vol. 63, 1.11 Ed., Trinity Software, Campton, NH
18. Vogel, H. J., & Bridger, W. A. (1983) *Biochem. Soc. Trans.* 11, 315-323.
19. Lou, G.-X., & Nishimura, J. S. (1991) *J. Biol. Chem.* 266, 20781-20785.
20. Fraser, M. E. *personal communication.*

**Page intentionally left blank for note taking.**

## Chapter Six      Studies of the ADP-Bound Form of *E. coli* SCS<sup>1</sup>

---

### Introduction

Succinyl-CoA synthetase (SCS) catalyzes the reversible interchange of purine nucleoside diphosphate, succinyl-CoA and P<sub>i</sub> with purine nucleoside triphosphate, succinate and CoA via a phosphorylated histidine (His 246 $\alpha$ ) intermediate (reviewed in (1) and (2)). As with other enzymes that bind nucleotides, Mg<sup>2+</sup> ions are required, and the “true” substrate is probably a nucleotide-Mg<sup>2+</sup> complex. Universally, SCS consists of two subunit types designated  $\alpha$  and  $\beta$ ; the catalytic unit carrying out the interchange is an  $\alpha\beta$ -dimer. This is true even for SCS from *E. coli*, a heterotetramer, which has been shown to consist of two  $\alpha\beta$ -dimers that are catalytically independent (3). In the crystal structure of *E. coli* SCS, the  $\alpha$ -subunit is seen to bind one of the substrates, CoA, and has a loop that includes the histidine residue (H246 $\alpha$ ) phosphorylated during catalysis (4). Based on the sequences of different  $\beta$ -subunits from isoforms of SCS in pigeon, Johnson *et al.* proposed that the  $\beta$ -subunit confers the nucleotide specificity (5), implying that the  $\beta$ -subunit binds the nucleotide. Consistent with this implication, evidence from the recognition of a new structural motif (6), from the comparison of SCS with other enzymes possessing this motif (7), and from the results of studies using a photoactivated ATP analogue and site-directed mutagenesis (8) delimited the nucleotide binding site to an ATP-grasp fold in the  $\beta$ -subunit. The CoA-binding site and the proposed nucleotide binding ATP-grasp fold are located approximately 35 Å apart in SCS, and have been designated site I and site II, respectively (8). Catalysis of the full reaction would necessitate the movement of His 246 $\alpha$  between these two sites, thus explaining why the formation of an active catalytic unit requires both  $\alpha$ - and  $\beta$ -subunits.

---

<sup>1</sup> A version of this chapter has been accepted for publication: Joyce, M. A., Fraser, M. E., James, M. N. G., Bridger, W. A., Wolodko, W. T. (1999) accepted for publication in *Biochemistry*.



Similar to other enzymes that contain a phosphohistidine, His 246 $\alpha$  of SCS has been shown to be phosphorylated on the N $\epsilon$ 2 atom of the histidine sidechain (9, 4, 7). However, in solution, the prevalent isomer of histidine has the lone pair of electrons on N $\delta$ 1 (10). This pair of electrons presumably initiates the nucleophilic attack on either nucleoside triphosphate or succinyl phosphate, creating the phosphohistidine. Vogel and Bridger predicted that an anionic group could stabilize the minor tautomeric form of His 246 $\alpha$  with the proton on N $\delta$ 1, thus facilitating the production of the N $\epsilon$ 2 isomer of phosphohistidine (11, 12). In site I, Glu 208 $\alpha$  is positioned to fulfill this role (4, 7).

In this chapter, the x-ray crystallographic results of soaking crystals of *E. coli* SCS with high concentrations of ADP and Mg<sup>2+</sup> ions are reported, proving that the ADP·Mg<sup>2+</sup> complex binds in the ATP-grasp fold of the N-terminal domain of the  $\beta$ -subunit. The specific interactions of the nucleotide-Mg<sup>2+</sup> complex with SCS are described in some detail and compared to other ATP binding proteins. In addition, a hypothetical model of the histidine-containing loop in the “down” position where it can interact with the nucleotide in site II is presented. Evidence for the participation of two glutamate residues in the phosphoryl transfer reactions that occur at each site (those involving succinate and CoA, at site I, and those involving nucleotide, at site II) is also presented. The participation of the glutamate residue in site II was predicted by the hypothetical model and by Fraser *et al.* (7).

## Materials and Methods

*Protein Purification and Crystallization.* SCS was overexpressed in the *E. coli* strain JM103 transformed with the expression plasmid pGS202 (4) and purified as previously described (13). Crystals of phosphorylated SCS were grown by microdialysis from precipitant solutions consisting of 1.93 M ammonium sulfate, 50 mM potassium phosphate and 0.5 mM CoA, pH 7.3 (14).

*Soaking of ADP into Crystals of SCS.* Several experiments were carried out with the design of successive trials based on the results of the preceding ones, before achieving a complex of nucleotide and the enzyme in the crystals.

In the first experiment, the membrane surrounding the dialysis button was cut away to allow excess protein to diffuse away from the crystals. After 4.5 h, the open buttons were transferred to freshly prepared precipitant solutions containing 1 mM ADP (greater than 15 times  $K_d$  (15)). Magnesium ions were not added since they would have formed an insoluble precipitate with the phosphate and ammonium ions. The crystals were left to soak for 48 h at room temperature prior to data collection.

The successful experiment was inspired by the work of Ray, Jr. *et al.*, who presented stratagems to lower the salt concentration prior to conducting a substrate soak (16). The dialysis buttons were transferred to a solution containing 1.85 M ammonium sulfate in 50 mM MOPS, pH 7.3 to lower the concentrations of the sulfate and phosphate ions. After approximately 24 h, the buttons were transferred to a solution containing 1.85 M ammonium sulfate, 50 mM MOPS, 5 mM  $MgCl_2$  and 0.53 mM ADP, pH 7.2. The crystals were allowed to soak for an additional 24 h before the buttons were transferred to a solution containing 1.8 M ammonium sulfate, 50 mM MOPS, 10 mM  $MgCl_2$  and 4.7 mM ADP, pH 7.2. After 20 h, the membrane was removed, and the buttons were transferred to the final soaking solution containing 1.8 M ammonium sulfate, 50 mM MOPS, 50 mM  $MgCl_2$  and 10.5 mM ADP, pH 7.2 for 5 h prior to mounting the crystals for data collection.

*Data Collection, Processing and Refinement.* The data were collected on beamline 6A2 at the Photon Factory in Japan using 1.0 Å x-rays with the screenless Weissenberg camera (17). The methods for data collection and processing using the program WEISS have been previously described (4). The statistics for two data sets, the first experiment and the successful experiment, are presented in Table 6-1.

Table 6-1. Statistics for the Two X-ray Diffraction Data Sets.

	First Experiment	Successful Experiment
Space group	P4 <sub>3</sub> 22	P4 <sub>3</sub> 22
tetramers/asymmetric unit	2	2
Number of crystals	6	6
Resolution	2.9 Å	3.3 Å
Observations	258739	195264
at high resolution (range)	19746 (3.02Å - 2.89Å)	15389 (3.54 - 3.33Å)
Unique reflections	45002	31753
at high resolution (range)	6283 (3.08 - 2.90Å)	4445 (3.51 - 3.30Å)
Data completeness	98.7%	99.0%
at high resolution (range)	96.9% (3.08 - 2.90Å)	98.4% (3.51 - 3.30Å)
R <sub>merge</sub> <sup>a</sup>	9.2%	16.4%
at high resolution (range)	35.0% (3.02Å - 2.89Å)	37.8% (3.54 - 3.33Å)

<sup>a</sup>  $R_{\text{merge}} = (\sum \sum |I_i - I|) / \sum \sum I$ , where  $I_i$  is the measured intensity of an individual reflection, and  $I$  is the mean value for all equivalent measurements of this reflection.

Each data set was scaled to the high resolution data set for native SCS (7), and SIGMAA-weighted electron density maps (18) were calculated using programs from the BIOMOL package (Gröningen, Holland). The program TOM (ALBERTA/CALTECH version 3.0) (19) was used to view the electron density maps and to build the molecular models into the electron density peaks. The atomic coordinates and B-factors were refined using the CNS suite of programs with standard protocols (20-26) over several rounds. Both torsion angle simulated annealing refinement and conjugate gradient minimization refinement were performed with maximum likelihood targets. Non-crystallographic symmetry restraints were applied to all atoms except those of residues at the crystal contacts. The programs PROCHECK (27) and WHATCHECK (28) were used to judge

the stereochemistry and the weights for the restraints. WHATCHECK was also used to improve the unit cell dimensions. Changes in R free were used to judge the refinement protocol. For the 3.3 Å data, no water molecules were included in the final mode and two B-factors were used for each residue, one for the main chain atoms and one for the side chain atoms.

**Table 6-2. Primers for Mutagenesis via PCR<sup>a</sup>.**

---

**Mutations of Glu 208 $\alpha$ :**

5' flanking primer: (37) 5' GCCCGCTATGGCTTACCAGC 3' (57)

<sup>b</sup>3' flanking primer (in the mcs of pGS202) 5' GGTCGACGAATTCCGGACA 3'

Internal Mutagenic primers:

E208 $\alpha$ D:

(1778) 5' CGTGATGATCGGTGATATCGGCGGTAGCG 3' (1807) and its complement

E308 $\alpha$ Q:

(1778) 5' CGTGATGATTGGCCAGATCGGCGGTA 3' (1804) and complement

**Mutations of Glu 197 $\beta$ :**

5' flanking primer: (37) 5' GCCCGCTATGGCTTACCAGC 3' (57)

3' flanking primer: (1157) 5' CCTCCACTGCGGCAACAACC 3' (1137)

Internal Mutagenic primers:

E197 $\beta$ A and E197 $\beta$ D:

<sup>c</sup>(580) 5' GCGTTGATC(**a/g/c**)(**a/c**)(**g/c**)ATCAACCCG 3' (601) and complement

E197 $\beta$ Q:

(579) 5' GGCGTTGATCCAAATCAACC 3' (599) and complement

---

<sup>a</sup> The nucleotides that are different from the wild-type sequence are shown in bold, and the numbers in parentheses denote the position of the first and last nucleotide of the primer. Position 1 is the A of the start codon, ATG, for the  $\beta$ -subunit.

<sup>b</sup> The 3' flanking primer was in the multiple cloning site (MCS) of pGS202, downstream of the  $\alpha$ -subunit.

<sup>c</sup> The primer for the E197 $\beta$ A and E197 $\beta$ D mutations was actually a mixture of primers, shown in lower case.

*Site Directed Mutagenesis of Glu 208 $\alpha$  and Glu 197 $\beta$ .* Site-directed mutants were made in three steps using standard protocols for the PCR and overlap extension (29)

similar to that used in Chapters 2 and 5. The primers for mutagenesis are given in Table 6-2. The mutant fusion product for the mutation E208 $\alpha$ Q and the vector pGS202 were digested according to the manufacturer's specifications (New England Biolabs Inc.) with *Ava* I (which cleaves at position 1715) and *Eco* RI (which cleaves in the multiple cloning site, downstream of the  $\alpha$ -subunit). The fragments were separated and ligated using the methods described in Chapter 3, and then used to transform competent JM103 *E. coli* cells (30). The plasmid construct containing the mutation E208 $\alpha$ D was obtained from Dr. David Ryan (31). The mutant fusion product for the mutations E197 $\beta$ A, E197 $\beta$ D, E197 $\beta$ Q and the vector pGS202 were digested with *Bst* XI (which cleaves at position 557) and *Bpu* 1102 I (which cleaves at position 1132). The fragments were then treated in the same manner as was done for the E208 $\alpha$  mutant constructs. The presence of mutations in all constructs was verified by DNA sequencing using an Applied Biosystems Model 373 Automated Sequencer.

*Expression and Purification of SCS Mutants.* The mutant proteins were expressed and purified by the same methods that were used in Chapter 5. The purity of the mutant proteins was evaluated by SDS-PAGE and staining with coomassie blue.

*Steady State Kinetic Analyses of SCS Mutants.* The kinetic analyses of these mutant proteins were conducted and analyzed using the methods described in Chapter 5, except for the saturating concentrations of the substrates. The concentrations used here were: 129  $\mu$ M CoA, 10 mM succinate, and 441  $\mu$ M ATP.

*Phosphorylation Reactions Catalyzed by SCS Mutants.* The mutant proteins were tested for their ability to catalyze the partial reactions involving either nucleotide (partial reaction (1) in Chapter 1) or succinyl-CoA and  $P_i$  (partial reactions (2) and (3) in Chapter 1). Phosphorylation of these mutant proteins by ATP, GTP, or by succinyl-CoA and  $P_i$  were conducted using the same buffers and conditions as in Chapter 5, except that lysates of cells that expressed the mutant proteins were used instead of pure protein. Protein expression from the cells containing the mutant constructs was synchronized. The amount

of protein used for phosphorylation was quantified using SDS-PAGE, by staining with coomassie blue and analyzing the extent of expression of the  $\beta$ -subunit of SCS using a Bio-Rad Gel Doc 1000 and the accompanying software.

## Results

*Crystallographic Structures of SCS Soaked with ADP.* The differences from the native data ( $R_{\text{diff}} = 100\% \times \sum ||F_{\alpha(\text{native})}| - k |F_{\alpha(\text{soak})}|| / \sum |F_{\alpha(\text{native})}|$ ) were 10.8% and 23.6% for the data from the first and successful experiments, respectively. Initial difference maps in the first experiment showed clearly that the active site histidine residue was not phosphorylated, and that there was electron density for a phosphate (or sulfate) ion bound nearby in site I (Fig. 6-1). In the successful experiment, in addition to the dephosphorylated enzyme, there was electron density for the nucleotide and a  $\text{Mg}^{2+}$  ion in the N-terminal domain of each  $\beta$ -subunit, site II (Fig. 6-2). Moreover, in the  $2|F_{\alpha(\text{soak})}| - |F_{\alpha(\text{native})}|, \alpha_{(\text{native})}$  maps, the electron density of the surrounding protein and each molecule of coenzyme A was well defined<sup>1</sup>. The models were modified to include the observed conformational differences in the protein and the  $\beta$ -phosphate of the ADP molecule was substituted for the sulfate ion, then refined. The results of the refinement are outlined in Table 6-3. A sample of the electron density from the refined model of dephosphorylated enzyme from the first experiment, around the vicinity of the active site histidine is shown in Figure 6-3. The electron density associated with the ADP- $\text{Mg}^{2+}$  complex in the refined model of the successful experiment is shown in Figure 6-4.

In both dephosphorylated models of SCS, the hydroxyl group of Ser 153 $\alpha$  had rotated to form a hydrogen bond (3 Å) with one oxygen atom of the phosphate ion (Fig. 6-5). This is the only change common to the two structures in the vicinity of the active site

---

<sup>1</sup> During refinement of the model of dephosphorylated SCS, additional density from Cys 325 $\beta$  became evident, reminiscent of that observed in the native structure of SCS (4). This represents anomalous binding of CoA. Only the pantoic acid and  $\beta$ -mercaptoethylamine portion of a CoA molecule could be modeled into this density on chain B and refined.

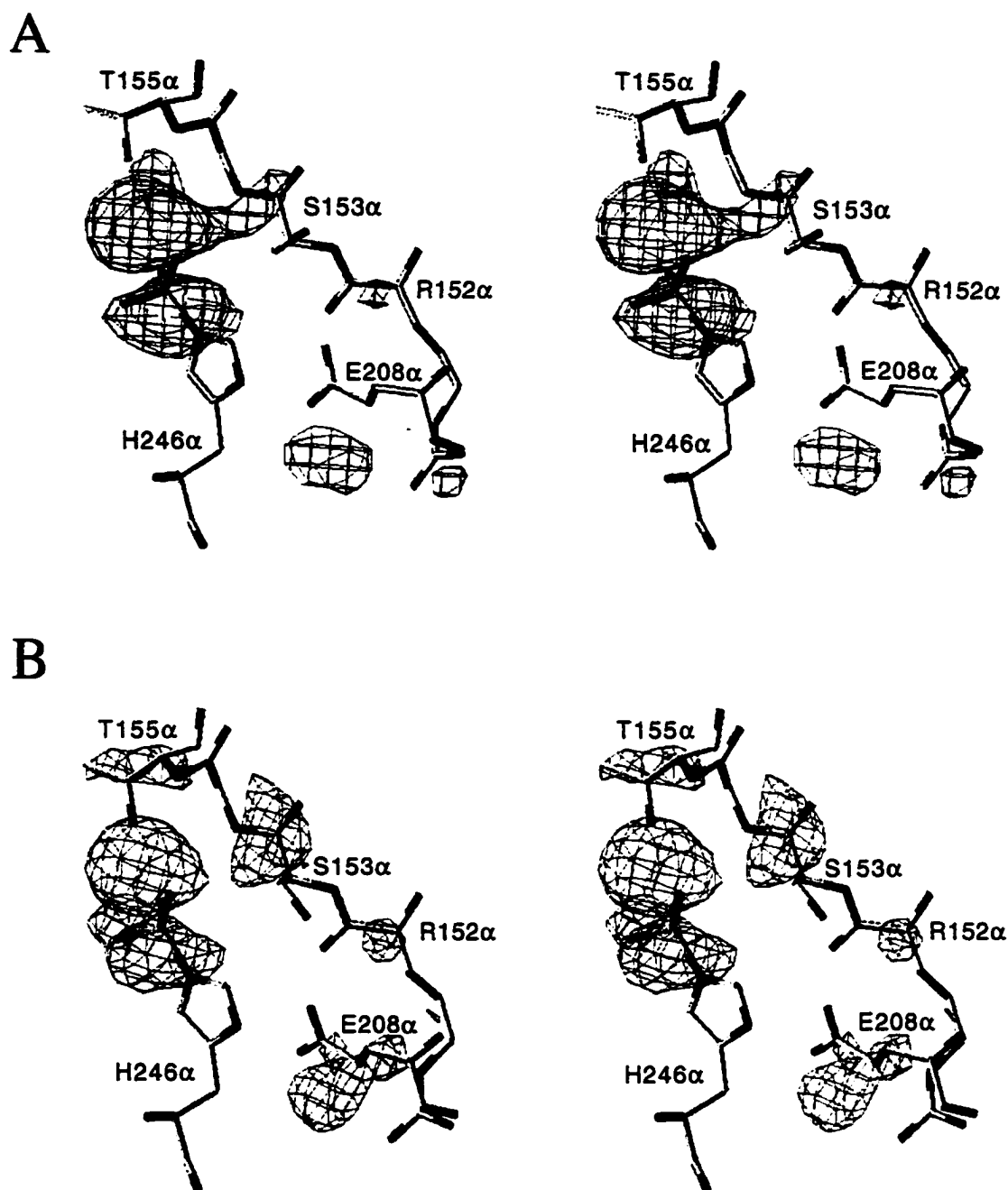


**Figure 6-1. Stereo diagrams of difference electron density in the  $\alpha$ -subunit.** Panel A, chain A; panel B, chain D of the SCS tetramer. The data were from the first experiment, and the vicinity of the active site phosphohistidine, His 246 $\alpha$ , is shown. Shown is the initial difference electron density from the  $|F_{\alpha(\text{soak})}| - |F_{\alpha(\text{native})}|$  map generated using phases from the native structure of SCS and contoured at  $-3.3\sigma$  (red lines) and  $+3.3\sigma$  (green lines). Amino acid residues of the native model are yellow, with nitrogen atoms in blue and oxygen in red. Figures 6-2 to 6-5 were drawn using the program O (46).

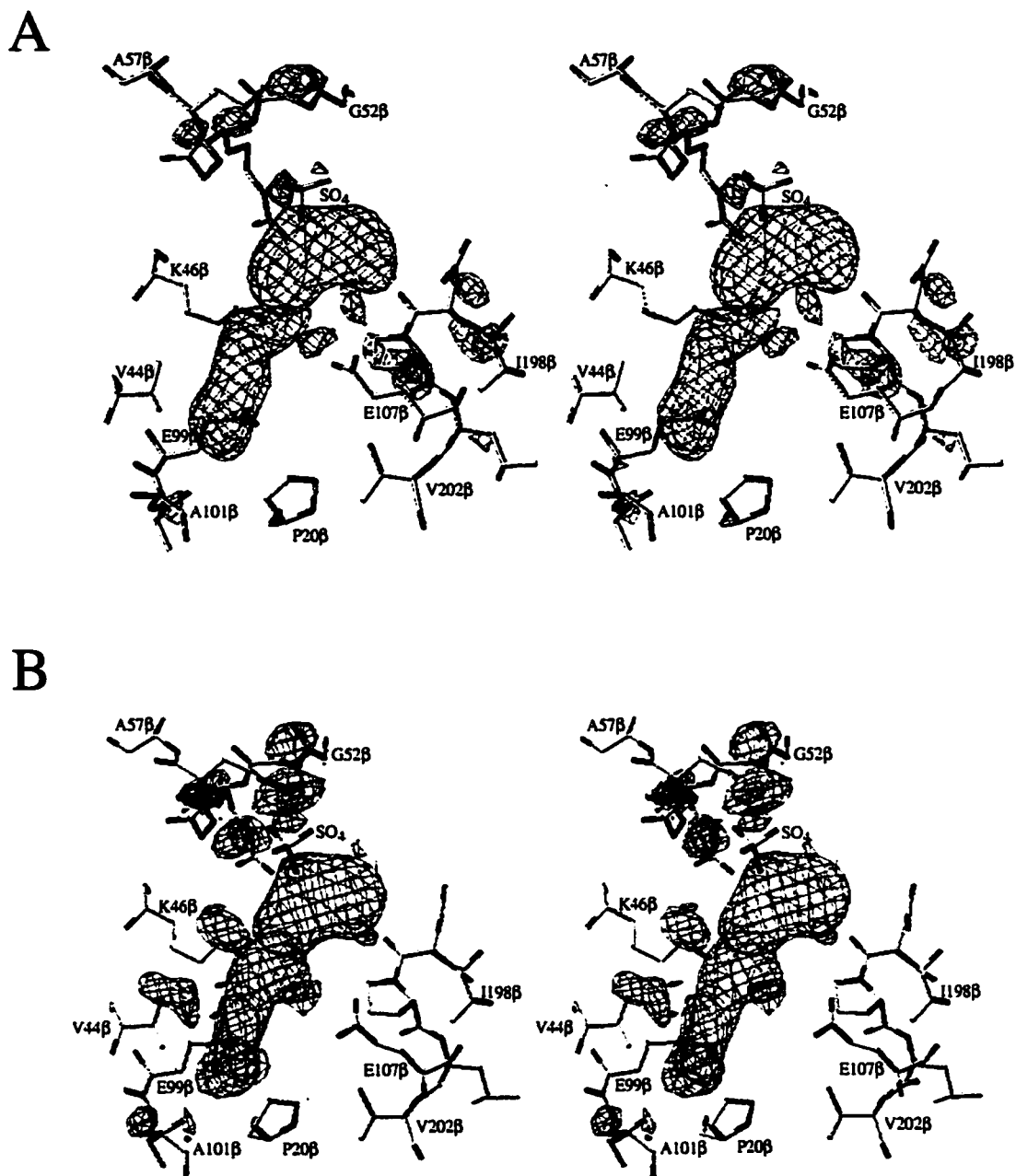
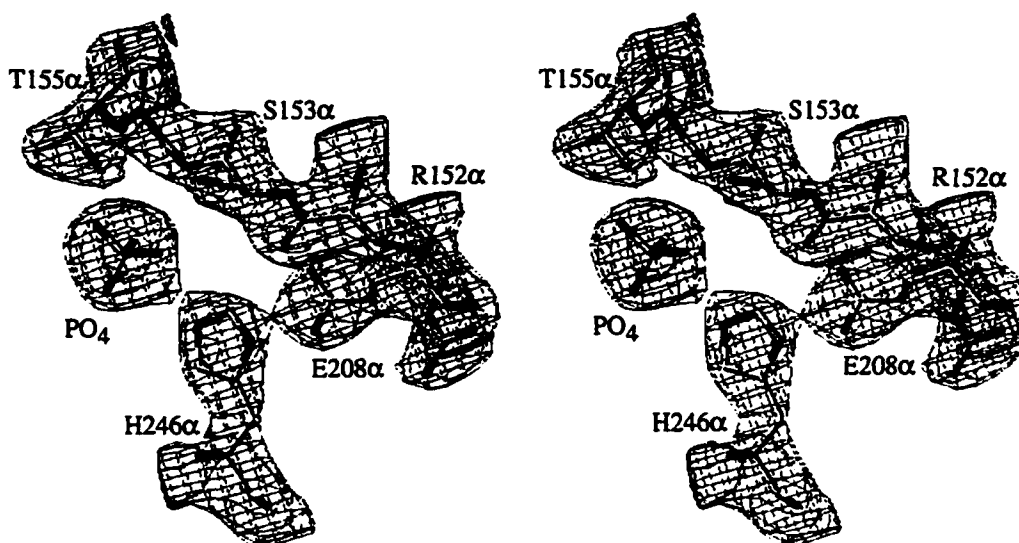


**Figure 6-2. Stereo diagrams of difference electron density in the N-terminal domain of the  $\beta$ -subunit.** The data were from the successful experiment soaking crystals of SCS with ADP and  $Mg^{2+}$  ions. Panel A, chain B; panel B, chain E of the SCS tetramer. Shown is the initial difference electron density from the  $|F_{o(\text{soak})}| - |F_{o(\text{native})}|$  map generated using phases from the native structure of SCS and contoured at  $-3.3\sigma$  (red lines) and  $+3.3\sigma$  (green lines) is shown. Amino acid residues of the native model are yellow, with nitrogen atoms in blue and oxygen in red.



A



B

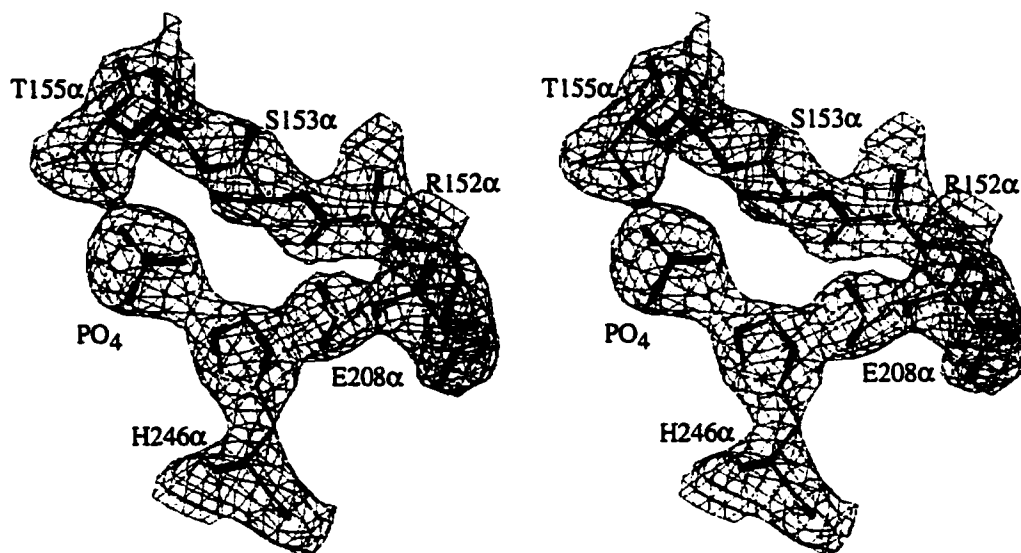
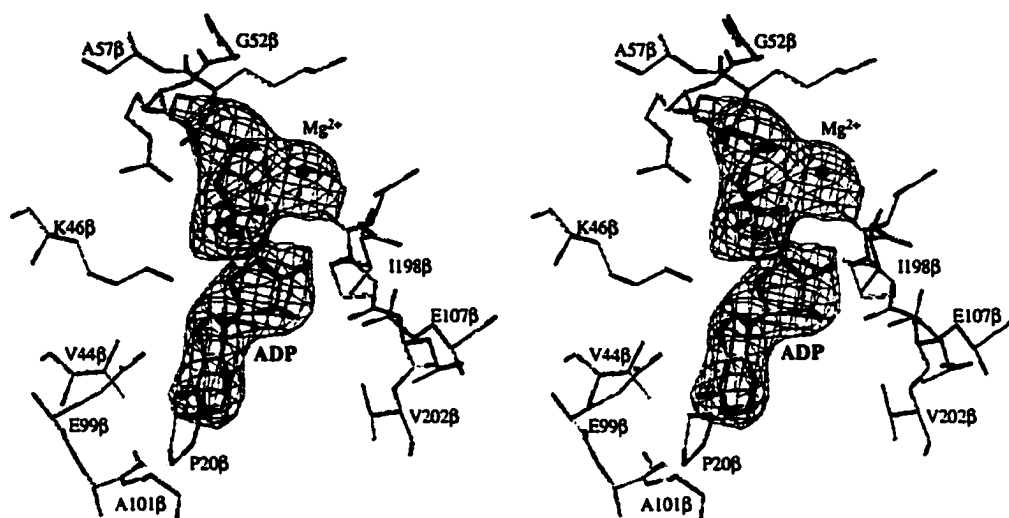


**Figure 6-3. Stereo diagrams of electron density in the  $\alpha$ -subunit.** Panel A, chain A; panel B, chain D of the SCS tetramer. The vicinity of the active site histidine, His 246 $\alpha$ , is shown. Shown is electron density (contoured at  $1.5\sigma$ ) from the  $2|F_o| - |F_c|$  map generated using the calculated phases from the final model of dephosphorylated SCS from the first experiment. Amino acid residues within the density are from the final model, and are depicted in yellow, with nitrogen atoms in blue and oxygen atoms in red.

A



B

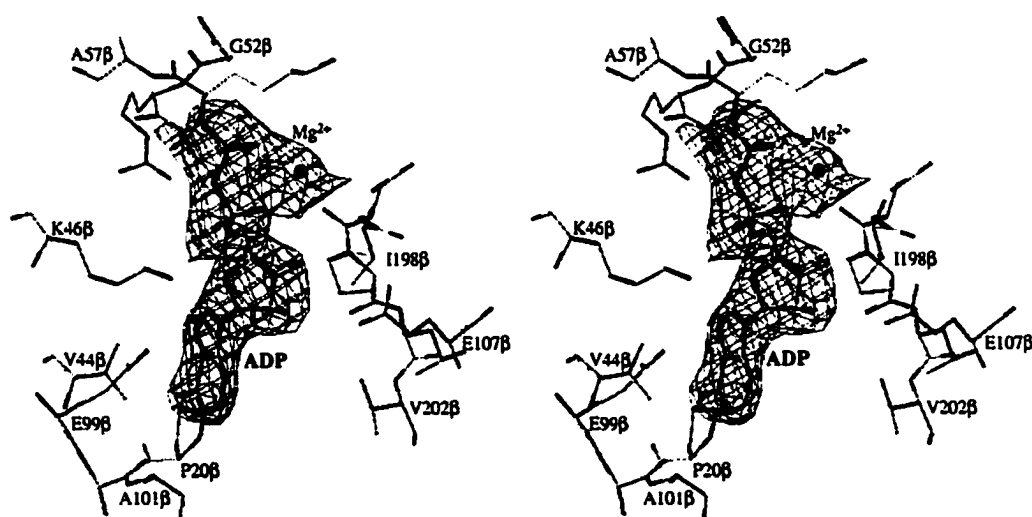


**Figure 6-4. Stereo diagrams of electron density in the N-terminal domain of the  $\beta$ -subunit.** The data were from the successful experiment soaking crystals of SCS with ADP and  $Mg^{2+}$  ions. Panel A, chain B; panel B, chain E of the SCS tetramer. Shown is electron density of the ADP- $Mg^{2+}$  complex (contoured at  $1.5\sigma$ ) from the  $2|F_o| - |F_c|$  map generated using the phases from the final model of ADP- $Mg^{2+}$  complex bound to the dephosphorylated SCS. Amino acid residues from the final model are yellow, with nitrogen atoms in blue, and oxygen atoms in red, and the  $Mg^{2+}$  ion is shown as a black dot.

histidine residue, other than the dephosphorylation, that is greater than the lower limit of significance of the experiment. The His 246 $\alpha$  loop is still associated with the C-terminal domain of the  $\alpha$ -subunit, site I.

**Table 6-3. Refinement Statistics.**

	First Experiment	Successful Experiment
Cell dimensions	a = b = 98.82 Å c = 404.68 Å $\alpha = \beta = \gamma = 90^\circ$	a = b = 99.86 Å c = 407.15 $\alpha = \beta = \gamma = 90^\circ$
Number of data	45002 (20 - 2.9Å)	31753 (20 - 3.3Å)
R-factor <sup>a</sup>	17.2 % (20 - 2.9Å)	19.1 % (20 - 3.3Å)
R <sub>free</sub> <sup>b</sup>	22.8 % (20 - 2.9Å)	24.7 % (20 - 3.3Å)
Number of protein atoms	9892	9892
Number of water molecules	330	0
Number of ligand atoms	133	168
Rms deviations from ideal geometry:		
Bond lengths	0.016 Å	0.017 Å
Bond angles	1.9°	1.9°
Ramachandran plot statistics for 1110 non-proline and non-glycine residues:		
Number in most favored regions	1008 (90.8%)	946 (85.2%)
Number in additional allowed regions	100 (9.0%)	158 (14.2%)
Number in generously allowed regions	0 (0%)	4 (0.4%)
Residues in disallowed regions	2 (0.2%)	2 (0.2%)

<sup>a</sup>  $R = \sum ||F_o| - |F_c|| / \sum |F_o|$

<sup>b</sup> R-factor based on data excluded from the refinement (11 %)

The refined model of the ADP molecule bound to SCS is shown in Figure 6-6A. The ADP molecule lies in the cleft between the two subdomains that constitute the N-terminal domain of the  $\beta$ -subunit. The smaller subdomain includes a four-stranded  $\beta$ -sheet and two  $\alpha$ -helices. The larger subdomain has as its core a six-stranded  $\beta$ -sheet. In the

structure of the ADP molecule, the adenine ring is oriented anti to the ribose ring with a  $\chi$  angle (O4\*-C1\*-N9-C4) of  $-154^\circ$  (Figure 6-6A). The observed conformation of the ADP molecule complexed with the  $Mg^{2+}$  ion is depicted in Figure 6-6B. Residues of the protein that interact with this complex are presented schematically. The adenine ring is sandwiched between the hydrophobic side chains of Val 44 $\beta$  and Leu 212 $\beta$ . The amino group at C6 of the adenine moiety forms hydrogen bonds with one carboxyl oxygen atom of Glu 99 $\beta$  (interatomic distance of 3.1 Å) and the main chain carbonyl oxygen atom of Ala 100 $\beta$  (3.3 Å). The N1 nitrogen atom of the adenine base accepts a hydrogen bond from the main chain amide nitrogen atom of Thr 102 $\beta$  (2.9 Å). The ribose sugar is held by a hydrogen bond from the 2'-hydroxyl group to one oxygen atom of the carboxyl group of Glu 107 $\beta$  (3.2 Å). The  $\epsilon$ -amino group of Lys 46 $\beta$  forms ionic interactions with the  $\alpha$ -phosphate group and the guanidino group of Arg 54 $\beta$  interacts with both the  $\alpha$ - and the  $\beta$ -phosphate groups. Two of the terminal oxygen atoms of the  $\beta$ -phosphate group form hydrogen bonds with the main-chain amide nitrogen atoms of residues 53-55 $\beta$ . The  $Mg^{2+}$  ion is coordinated by five oxygen atoms, one from each of the  $\alpha$ - and  $\beta$ -phosphate groups, one from each of the side chains of Asp 213 $\beta$  and Asn 199 $\beta$ , and the fifth from the main chain carbonyl group of Asn 199 $\beta$  (see Figure 6-7 and the Discussion).

One important difference between the two dephosphorylated structures is located far from the nucleotide binding site. In site I of the SCS model derived from the successful experiment, the electron density showed that the side chains of Cys 123 $\alpha$  and Pro 124 $\alpha$  have "flipped" so that the side chain of the proline residue now packs into the protein interior in the space previously occupied by the sulfhydryl group of the cysteine residue (Fig. 6-8). The cysteine side chain is exposed and forms a disulfide bond with the sulfhydryl group of the CoA molecule. We do not know the relevance of the Cys-Pro flip.

*Modeling of the Active Site Loop into Site II.* Since the nucleotide binds in the N-terminal domain of the  $\beta$ -subunit (site II) and the phosphorylated His 246 $\alpha$  is observed  $\sim 35$  Å away at site I, we postulated that the loop containing this histidine residue must

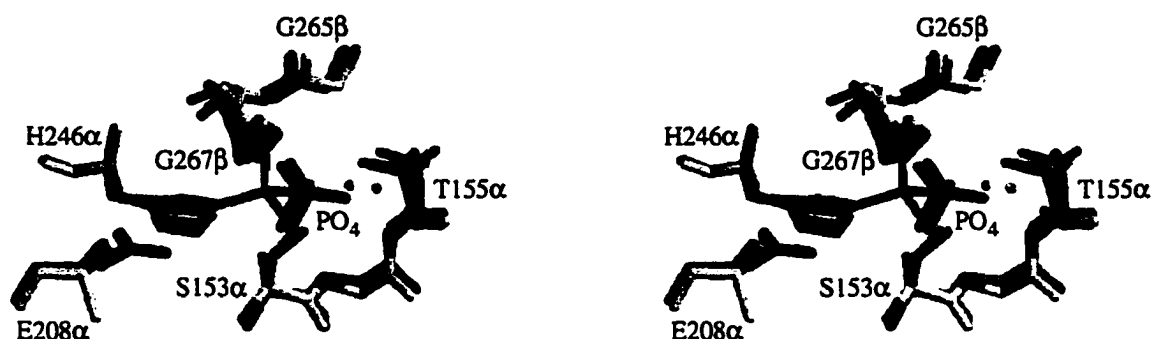


**Figure 6-5. Superposition of native and dephosphorylated SCS around the phosphohistidine.** The backbone of the ADP-bound model of SCS is yellow, with nitrogen atoms in blue. The side chains are coloured according to residue type, the phosphate from this model is shown in red, and the water molecule, W62, is blue. The residues, phosphate ion and water W65 from the refined model of the first experiment are shown in magenta. The residues and a water, Q246, from the native SCS model are shown in grey. The residues used in these superpositions are given in Appendix 7.

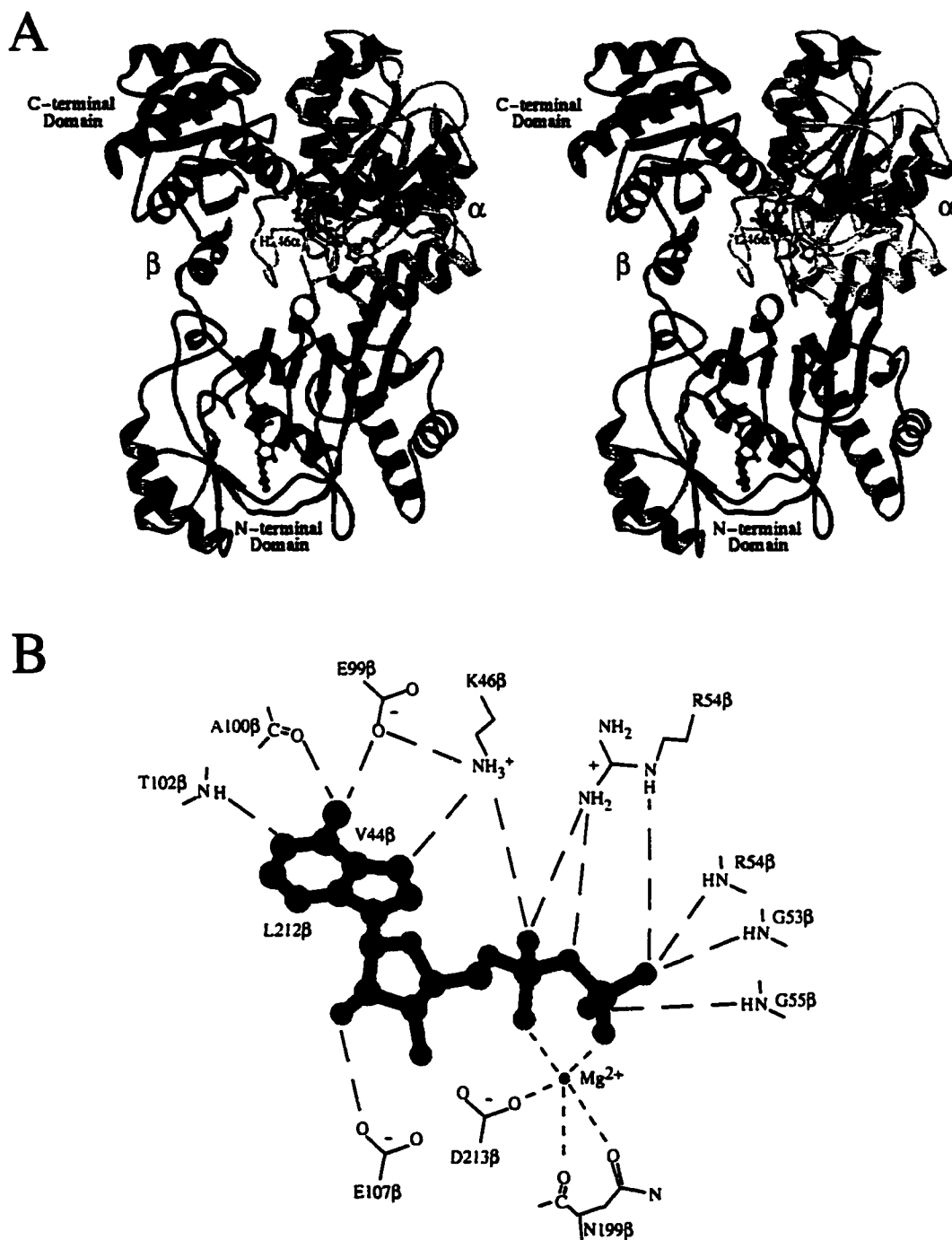
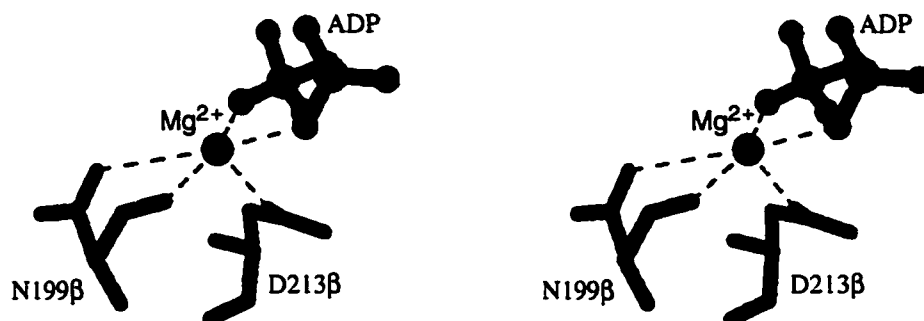


**Figure 6-6. Nucleotide binding site of SCS.** A. Stereo ribbon diagram of one  $\alpha\beta$ -dimer (chains A and B) of *E. coli* SCS with the bound ADP shown as a red ball and stick model. The  $\alpha$ -subunit is coloured yellow (except for the side chain of His 246 $\alpha$  and the phosphate ion which are red), the  $\beta$ -subunit is green, and the molecule of CoA is shown as a cyan ball and stick model. B. Ball and stick model of the ADP- $Mg^{2+}$  complex showing its conformation when bound to SCS. Surrounding residues of SCS that interact with this complex are presented schematically. The long dashed lines show possible hydrogen bonding interactions. Val 44 $\beta$  and Leu 212 $\beta$  have hydrophobic interactions with the adenine ring. The  $Mg^{2+}$  ion is depicted by a magenta sphere, and is chelated by five ligands as shown by short dashed lines.

A



B

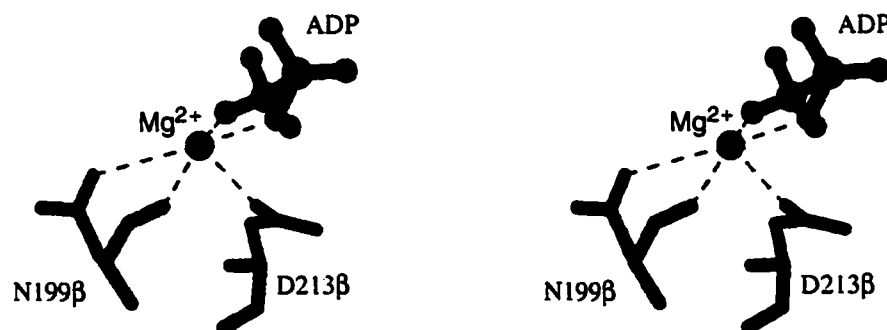


**Figure 6-7. Stereo diagrams showing the coordination of the  $Mg^{2+}$  ion in the  $\beta$ -subunits of SCS.** In panel A the coordination observed in chain B is shown, and in panel B the coordination in chain E is shown. The  $Mg^{2+}$  ion is coloured magenta, and the phosphates from the ADP molecule are shown as a red ball and stick model. The side chains are coloured according to residue type, and the the backbone of residues that interact with the  $Mg^{2+}$  ion are green with the oxygen atoms in red.

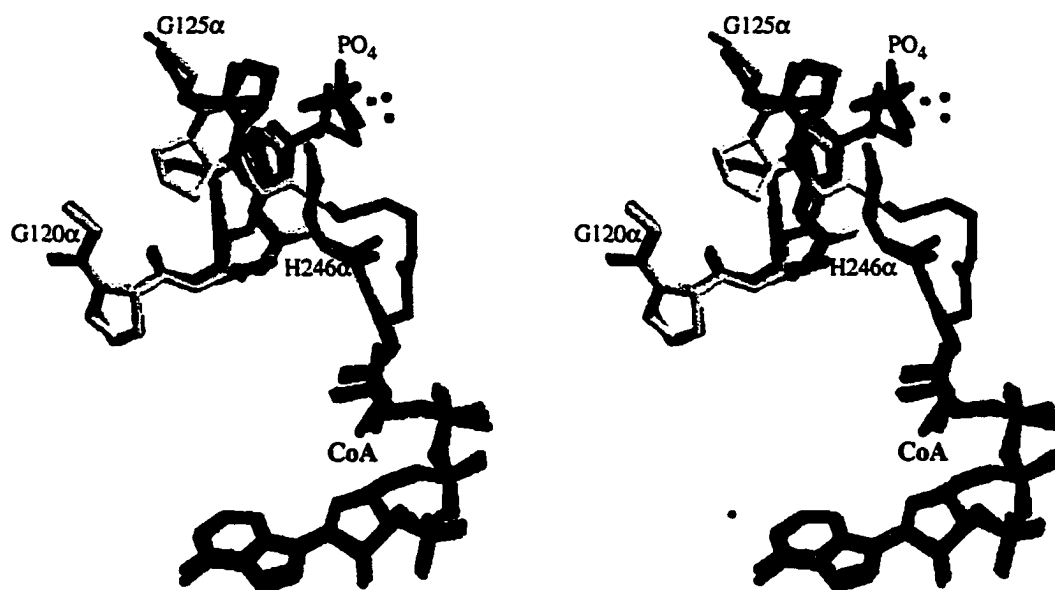


**Figure 6-8. Superposition of native and dephosphorylated SCS around the CoA.** The backbone from the ADP-bound model of SCS is yellow, and the phosphate, and CoA are shown in red. The water molecule from this model, W62, is shown as a blue dot. The residues, CoA, phosphate ion, and water W65 from the refined model of the first experiments are magenta. The residues, CoA, and water Q246 from the model of native SCS are grey. The residues used in these superpositions are given in Appendix 7.

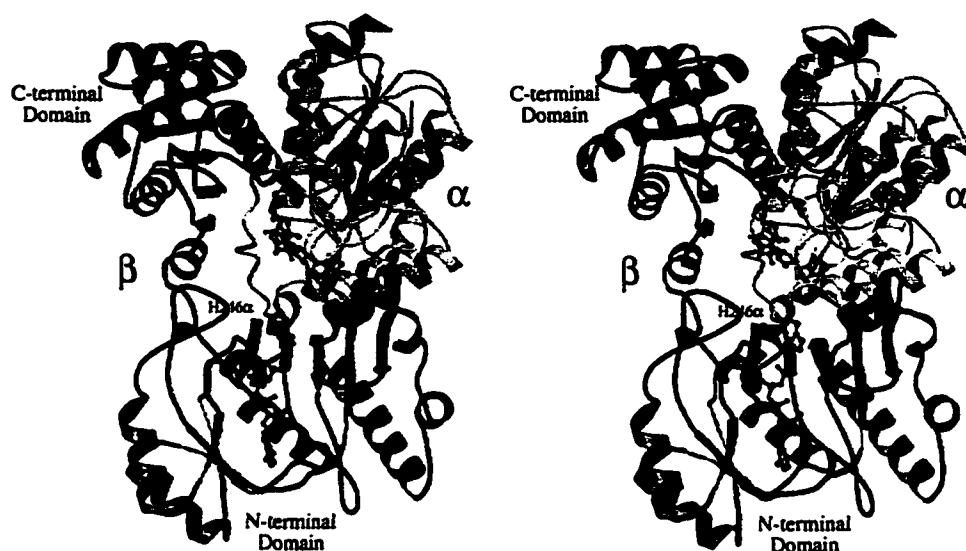


“swing” between the two sites during catalysis (7). Now, presuming that the  $\gamma$ -phosphate group of ATP has the same orientation relative to the imidazole ring as does the phosphate ion in the dephosphorylated structure, the oxygen atom O4 of the phosphate ion can be positioned on one of the terminal oxygen atoms of ADP to model ATP<sup>2</sup>. The terminal oxygen atom chosen as the  $\beta,\gamma$ -bridging atom of ATP was the one that allowed the modeled  $\gamma$ -phosphate group to coordinate the Mg<sup>2+</sup> ion. This choice is consistent with the structures of ATP analogues bound to carbamoyl phosphate synthetase (32) and synapsin I (33). This positioning orients as well a possible conformation of the His 246 $\alpha$  loop prior to phosphorylation at site II. For this modeling, the loop was detached from the rest of the  $\alpha$ -subunit by breaking the C $\alpha$ -C bond of residue 241 $\alpha$  and the N-C $\alpha$  bond of residue 253 $\alpha$ , and the loop was rotated about the position of the C $\alpha$  atom of residue 253 $\alpha$  so that the angle at the  $\beta,\gamma$ -bridging oxygen atom of ATP was approximately 109°. The movement orients the imidazole ring so that N $\delta$ 1 is directed towards Glu 197 $\beta$ . We had predicted earlier that Glu 197 $\beta$  would form a hydrogen bond with N $\delta$ 1 of the imidazole ring when His 246 $\alpha$  is bound at site II (7). To improve the model, the torsion angles along the polypeptide chain were adjusted so that the hydrophobic side chains of residues Met 244 $\alpha$ , Ile 250 $\alpha$  and Ile 251 $\alpha$  interacted with Leu 195 $\beta$  and Val 113 $\beta$ , and so that the termini of the loop were directed toward residues 240 $\alpha$  and 254 $\alpha$ . The loop was reattached, and the geometry of residues 239 $\alpha$ -242 $\alpha$  and residues 251 $\alpha$ -256 $\alpha$  was regularized. This model of the His 246 $\alpha$  loop in site II is depicted in Figure 6-9. It must be emphasized that this conformation of the loop is purely hypothetical, based only on the knowledge that His 246 $\alpha$  must move from where it is seen in the structure to where the nucleotide binds. Lending credence to this model is the fact that residues of the  $\beta$ -subunit that would interact with the active site loop are conserved in known sequences of SCS. For example, residues equivalent to 113 $\beta$  and 195 $\beta$  are usually hydrophobes; 115 $\beta$  is usually Asp, but can be Glu; 134 $\beta$  and 197 $\beta$  are Glu; and 215 $\beta$  is predominantly Lys, but

---

<sup>2</sup> The modeling was done using the program TOM (19).

A



B

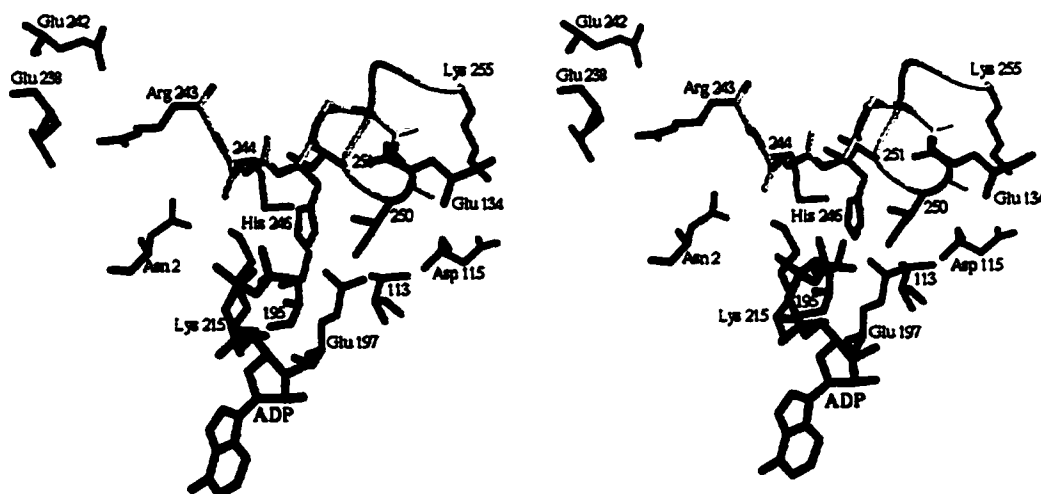


**Figure 6-9. Model of the His 246 $\alpha$  loop at site II.** A. Stereo ribbon diagram of an  $\alpha\beta$ -dimer of SCS with the hypothetical model of the His 246 $\alpha$  loop at site II. The ATP molecule is represented by a red ball and stick model, and the CoA by a cyan ball and stick model. B. Stereo diagram of the residues that may interact when the His 246 $\alpha$  loop is at site II. The residues of the His 246 $\alpha$  loop are shown with yellow backbone atoms with selected nitrogen atoms shown in blue. The residues of the  $\beta$ -subunit which may interact with the loop are shown with green backbone atoms. The side chains are coloured according to residue type, and the ATP molecule is red.

can be Arg. This model in the complete  $\alpha\beta$ -dimer is shown in Figure 6-9A. A comparison of Figure 6-9A with Figure 6-6A points out that there is space for the loop to move unencumbered by any other part of SCS.

*Site-Directed Mutagenesis of a Glutamate Residue in Each of Site I and II.* Vogel and Bridger predicted that an anionic group would be required to stabilize one tautomeric form to ensure the presence of the lone pair of electrons on the Ne2 position of the active site histidine (11, 12). In site I, Glu 208 $\alpha$  is positioned to fulfill this role (4, 7). In site II, Glu 197 $\beta$  may fulfill this role (7). In the absence of these sidechains, the lone pair of electrons would preferentially reside on the N $\delta$ 1 of the histidine as it does when histidine is free in solution (10). Consequently the Ne2 would be protonated, and thus unable to initiate nucleophilic attack on the phosphorus atom of either succinyl-phosphate (at site I), or ATP (at site II).

To assess the role of Glu 208 $\alpha$  (in site I), it was mutated to Asp to shorten the sidechain by one methylene group, or to Gln to eliminate the charge on the sidechain. The kinetic parameters for both of the Glu 208 $\alpha$  mutants were determined by steady-state analyses of initial rates of succinyl-CoA formation, and the results were plotted using Hanes-Wolf plots (Fig. 6-10 and 6-11). Kinetic analyses of the E208 $\alpha$ D and E208 $\alpha$ Q mutant proteins revealed that  $K_{m(\text{app})}$  and  $k_{\text{cat}}$  values for succinate and CoA that were comparable to those of wild-type enzyme (Table 6-4). However for the E208 $\alpha$ D mutant, the  $K_{m(\text{app})}$  values for ATP and GTP were 4 and 6 times lower, respectively, than those of wild-type enzyme; and for the E208 $\alpha$ Q mutant, the corresponding  $K_{m(\text{app})}$  values were 2 and 35 times less, respectively (Table 6-4). Such parallel changes were not observed for the  $k_{\text{cat}}$  values associated with the nucleotides. Whereas the values of  $k_{\text{cat}}$  for the E208 $\alpha$ D mutant protein were comparable to those for wild-type SCS, kinetic analyses of the E208 $\alpha$ Q mutant protein revealed a reduction in the  $k_{\text{cat}}$  value of approximately 5000 times.

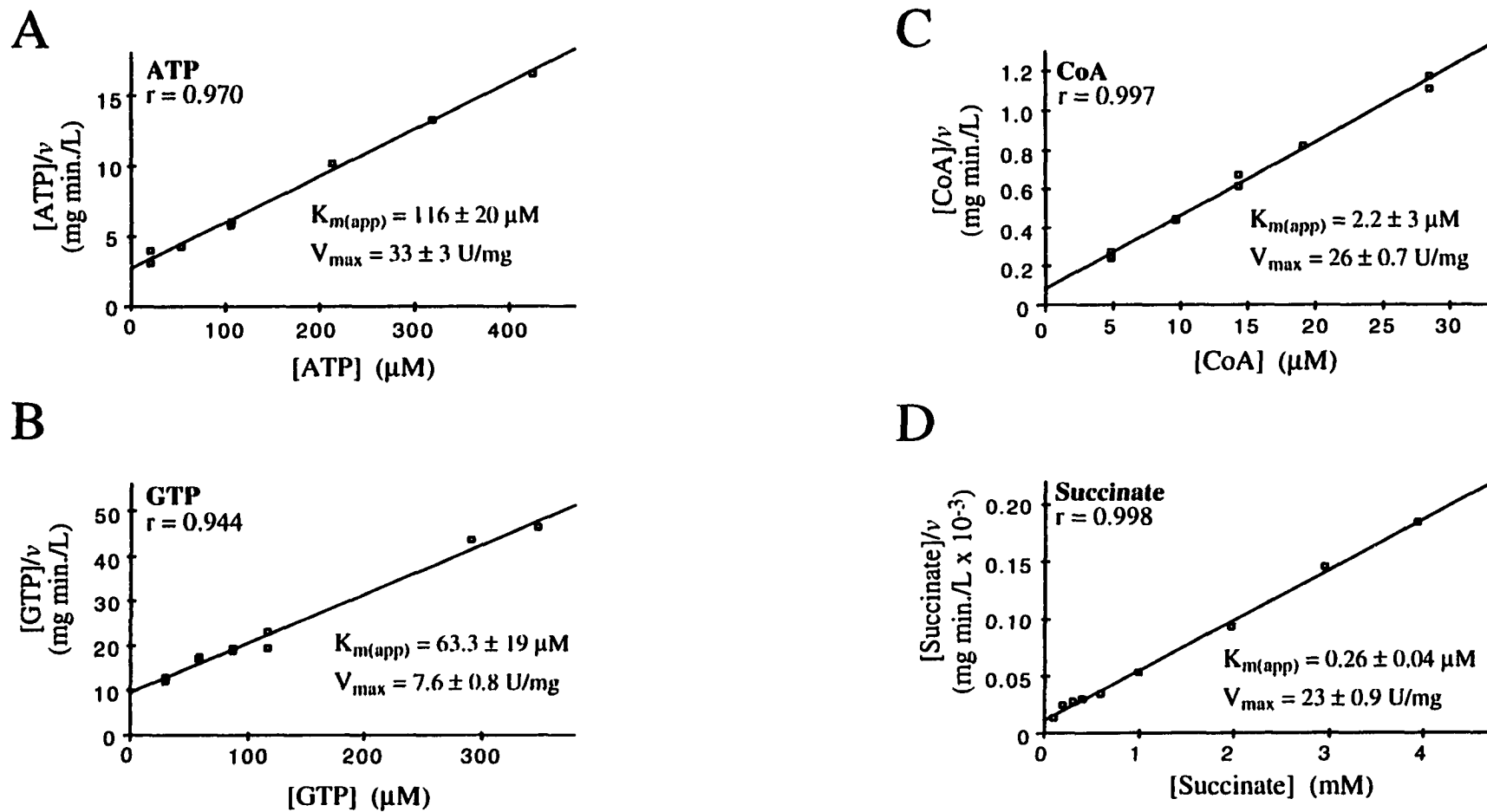


**Figure 6-10. Hanes-Wolf plots for the *E. coli* SCS mutant E208βD.** The 1 ml reaction mixtures contained 50 mM KCl, 10 mM MgCl<sub>2</sub>, 50 mM Tris HCl, pH 7.4, and saturating concentrations of all substrates (129 μM CoA, 10 mM succinate, and 441 μM ATP or GTP) except for ATP in panel A, GTP in panel B, CoA in panel C, and succinate in panel D. The y-intercept of the least squares line gives the value of  $K_{m(app)}/V_{max}$ , and the slope has the value of  $1/V_{max}$ . The correlation coefficient of the line is indicated.

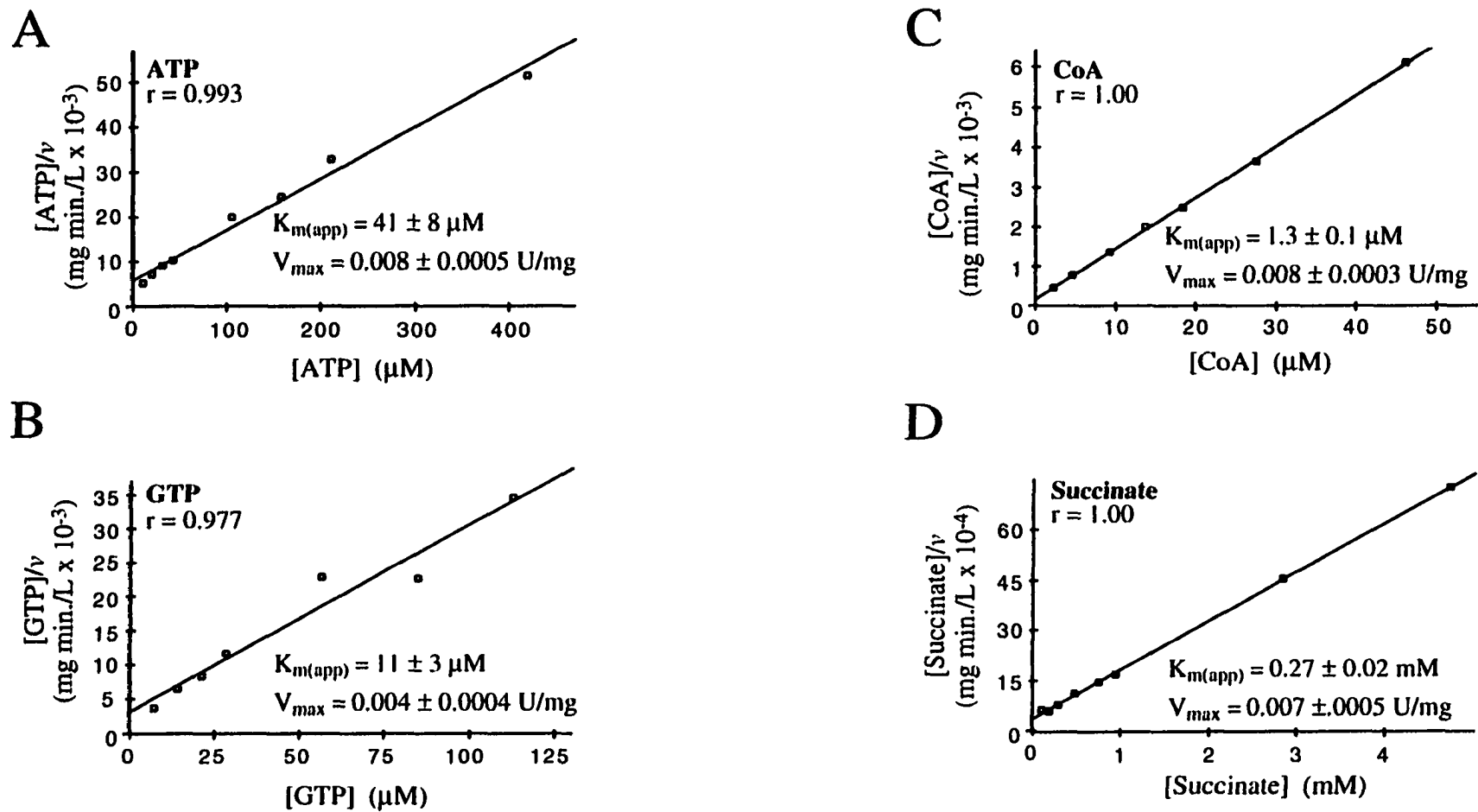


**Figure 6-11. Hanes-Wolf plots for the *E. coli* SCS mutant E208 $\beta$ Q.** The 1 ml reaction mixtures contained 50 mM KCl, 10 mM MgCl<sub>2</sub>, 50 mM Tris HCl, pH 7.4, and saturating concentrations of all substrates (129  $\mu$ M CoA, 10 mM succinate, and 441  $\mu$ M ATP or GTP) except for ATP in panel A, GTP in panel B, CoA in panel C, and succinate in panel D. The y-intercept of the least squares line gives the value of  $K_{m(app)}/V_{max}$ , and the slope has the value of  $1/V_{max}$ . The correlation coefficient of the line is indicated.

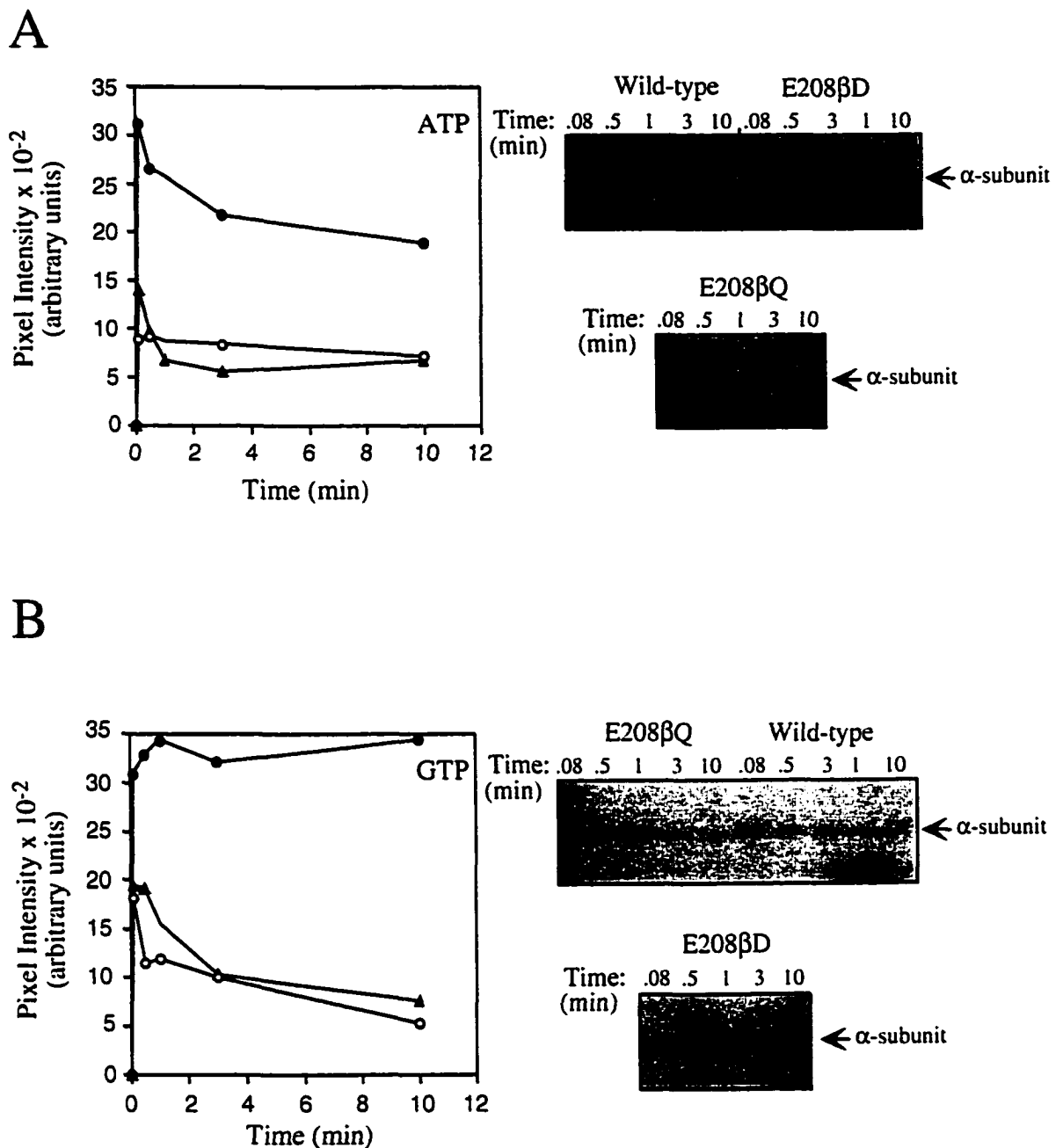


**Figure 6-12. Time course of the phosphorylation by NTP of wild-type SCS and the Glu 208 $\beta$  mutant protein.** Wild-type and mutant SCS were incubated in the presence of [ $\gamma$ - $^{32}$ P] ATP, panel A or [ $\gamma$ - $^{32}$ P] GTP, panel B. Samples were taken at various times, and the subunits were separated by SDS-PAGE. The gels were then analyzed by phosphorimetry and the results are shown on the left: wild-type SCS (O), protein with the mutation E208 $\beta$ D (●), and E208 $\beta$ Q (▲). Autoradiograms of the gels are shown on the right.

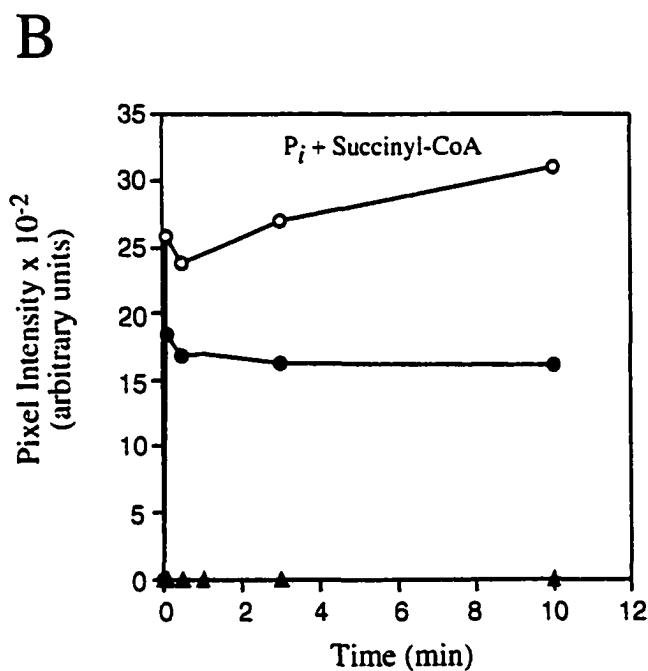
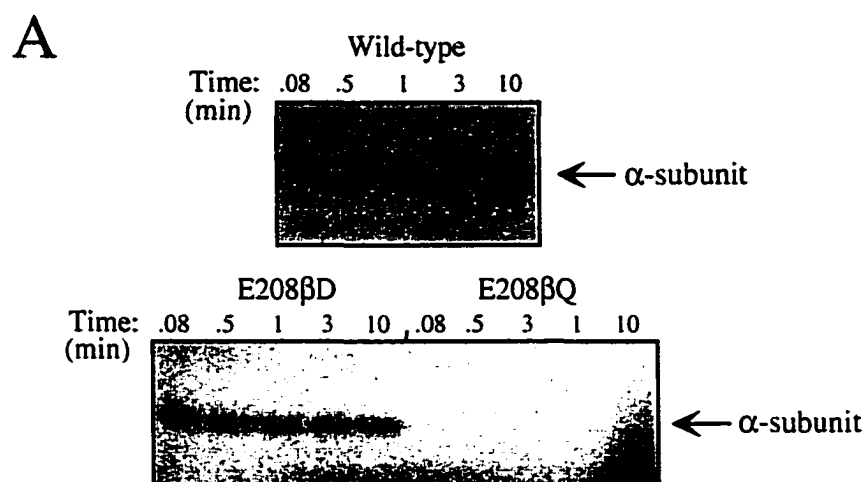


**Figure 6-13. Time course of phosphorylation by succinyl-CoA and  $P_i$  of wild-type SCS and the Glu 208 $\beta$  mutant protein.** Wild-type and mutant SCS were incubated in the presence of  $^{32}P_i$  and succinyl-CoA. Samples were taken at various times, and the subunits were separated by SDS-PAGE. Autoradiograms of the gels are shown in panel A. The gels were analyzed by phosphorimager, and the results are shown in panel B: wild-type SCS (○), protein with the mutation E208 $\beta$ D (●), and E208 $\beta$ Q (▲).

To determine which partial reactions for phosphorylation of SCS were impaired by these mutations, single turnover experiments were performed with [ $\gamma$ - $^{32}\text{P}$ ]-ATP, or [ $\gamma$ - $^{32}\text{P}$ ]-GTP (partial reaction (1)), or succinyl-CoA and  $^{32}\text{P}_i$  (partial reactions (2) and (3)). Consistent with the results of the steady state kinetic analysis, the rate of phosphorylation of the  $\alpha$ -subunit of the E208 $\alpha$ D mutant by ATP, GTP, or succinyl-CoA and  $\text{P}_i$  was comparable to that of wild-type protein (Figures 6-12 and 6-13). However, the  $\alpha$ -subunit of the E208 $\alpha$ Q mutant protein was only phosphorylated by ATP or GTP (Fig. 6-12), but not by  $\text{P}_i$  and succinyl-CoA (Fig. 6-13). These results are consistent with the participation of Glu 208 $\alpha$  in partial reactions (2) and/or (3), which are thought to occur at site I.

To assess the role of Glu 197 $\beta$  (in site II), it was mutated to Asp to shorten the sidechain by one methylene group, to Gln to eliminate the charge on the sidechain, or to Ala to eliminate the sidechain. Protein with the mutation E197 $\beta$ A was inactive. The kinetic parameters for the remaining Glu 197 $\beta$  mutants were determined by steady-state analysis of initial rates of succinyl-CoA formation, and the results were plotted using Hanes-Wolf plots (Fig. 6-14 and 6-15). Kinetic analysis of the E197 $\beta$ D mutant protein revealed that  $k_{\text{cat}}$  values and  $K_{\text{m(app)}}$  values for all substrates were comparable to those of wild-type enzyme (Table 6-4). Similar to the results for the E208 $\alpha$ Q mutant, kinetic analysis of the E197 $\beta$ Q mutant revealed a decrease in the value of  $k_{\text{cat}}$  of 3000 fold using ATP, and 7000 fold using GTP when compared to the values of wild-type enzyme. The  $K_{\text{m(app)}}$  values for all of the substrates were comparable to those of wild-type enzyme, except for GTP which had decreased by approximately 18 times.

The rates of phosphorylation of the Glu 197 $\beta$  mutants with ATP, GTP or succinyl-CoA and  $\text{P}_i$  were determined, and the results are shown in Figures 6-16 and 6-17. The E197 $\beta$ A mutant was not phosphorylated by ATP, GTP, or  $\text{P}_i$  and succinyl-CoA. Consistent with the steady state kinetic analysis, and similar to the E208 $\alpha$ D mutant, the rate of phosphorylation of the E197 $\beta$ D mutant by ATP, GTP, or succinyl-CoA and  $\text{P}_i$  was



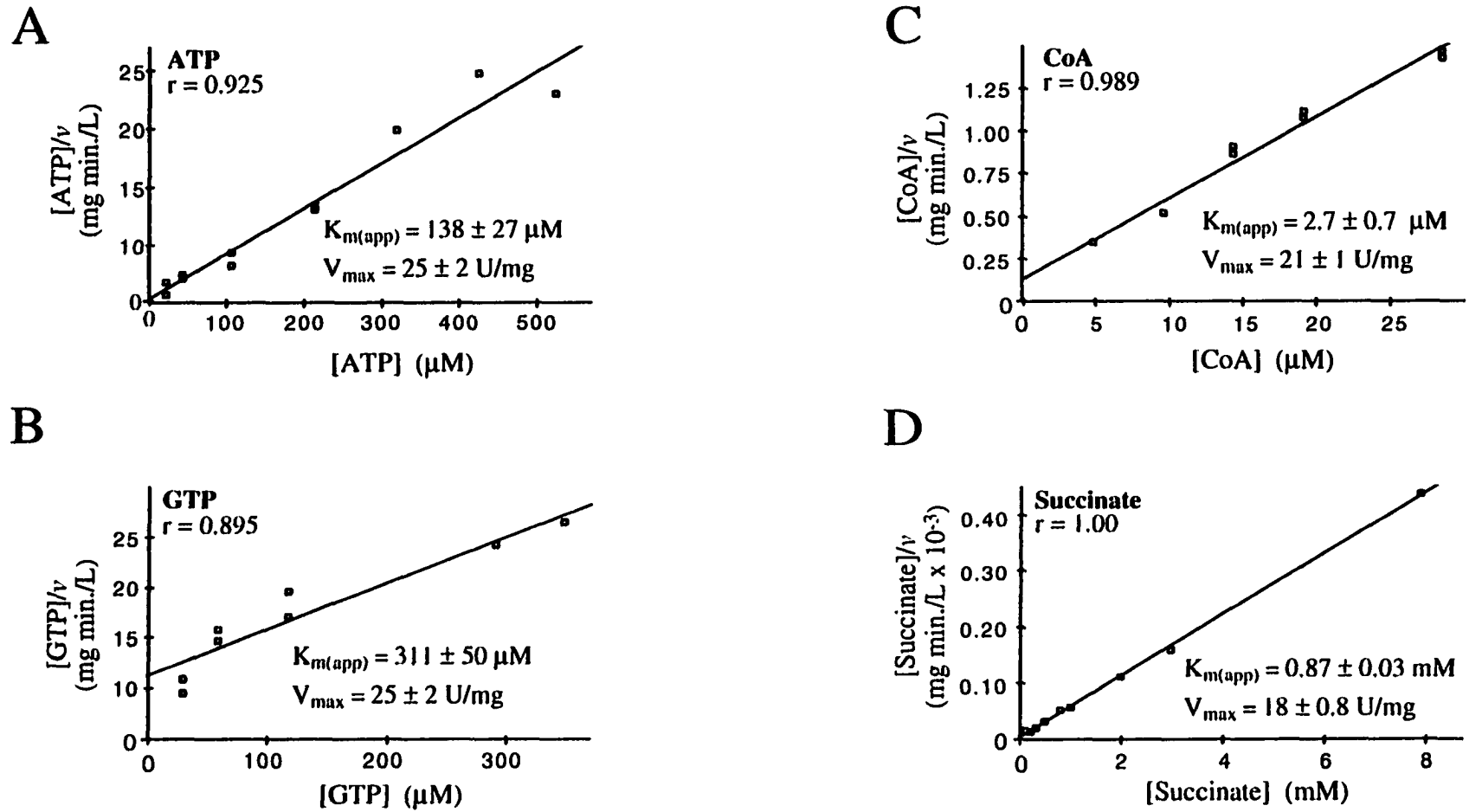


**Figure 6-14. Hanes-Wolf plots for the *E. coli* SCS mutant E197 $\beta$ D.** The 1 ml reaction mixtures contained 50 mM KCl, 10 mM MgCl<sub>2</sub>, 50 mM Tris HCl, pH 7.4, and saturating concentrations of all substrates (129  $\mu$ M CoA, 10 mM succinate, and 441  $\mu$ M ATP or GTP) except for ATP in panel A, GTP in panel B, CoA in panel C, and succinate in panel D. The y-intercept of the least squares line gives the value of  $K_{m(app)}/V_{max}$ , and the slope has the value of  $1/V_{max}$ . The correlation coefficient of the line is indicated.

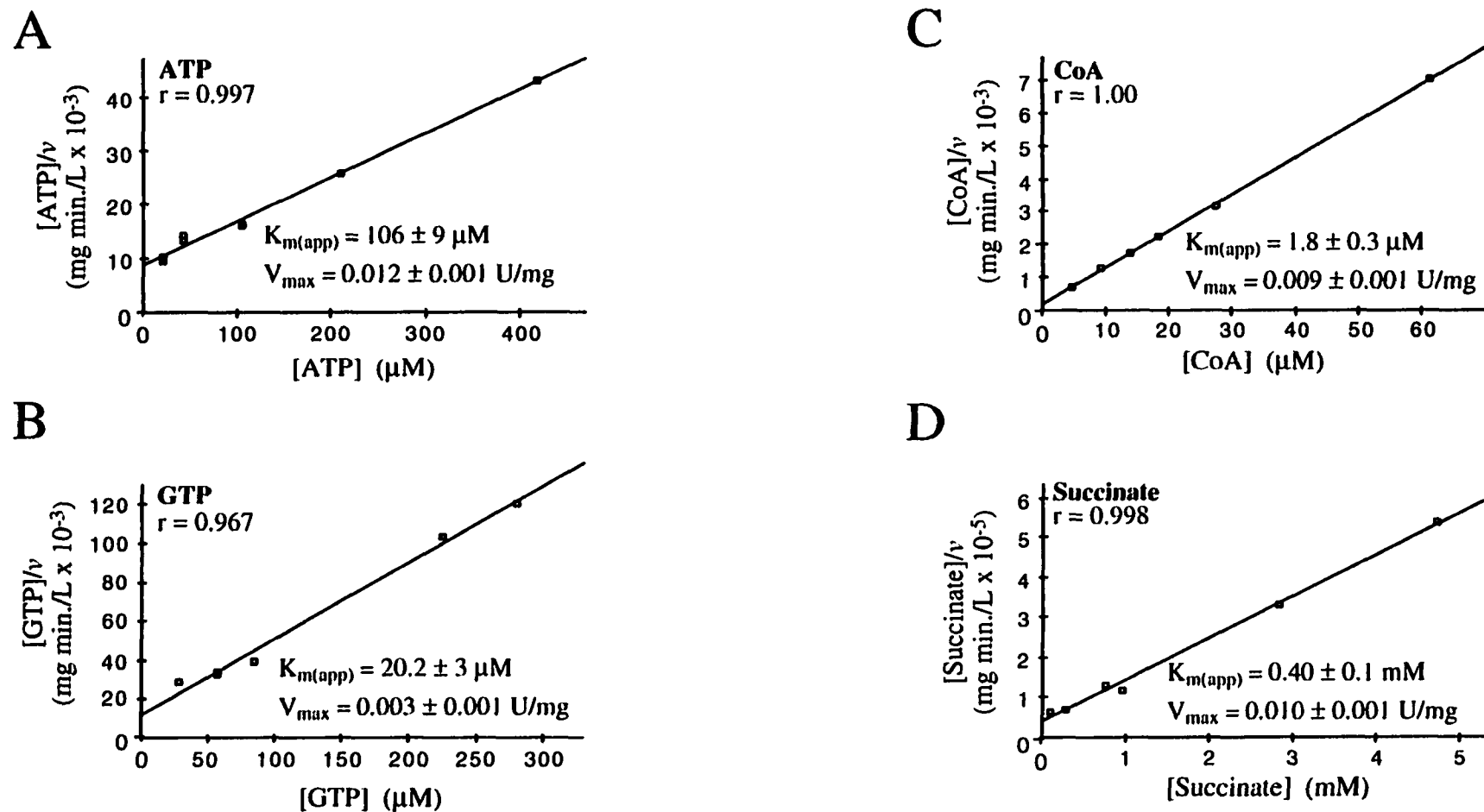


**Figure 6-15. Hanes-Wolf plots for the *E. coli* SCS mutant E197βQ.** The 1 ml reaction mixtures contained 50 mM KCl, 10 mM MgCl<sub>2</sub>, 50 mM Tris HCl, pH 7.4, and saturating concentrations of all substrates (129 μM CoA, 10 mM succinate, and 441 μM ATP or GTP) except for ATP in panel A, GTP in panel B, CoA in panel C, and succinate in panel D. The y-intercept of the least squares line gives the value of  $K_{m(app)}/V_{max}$ , and the slope has the value of  $1/V_{max}$ . The correlation coefficient of the line is indicated.

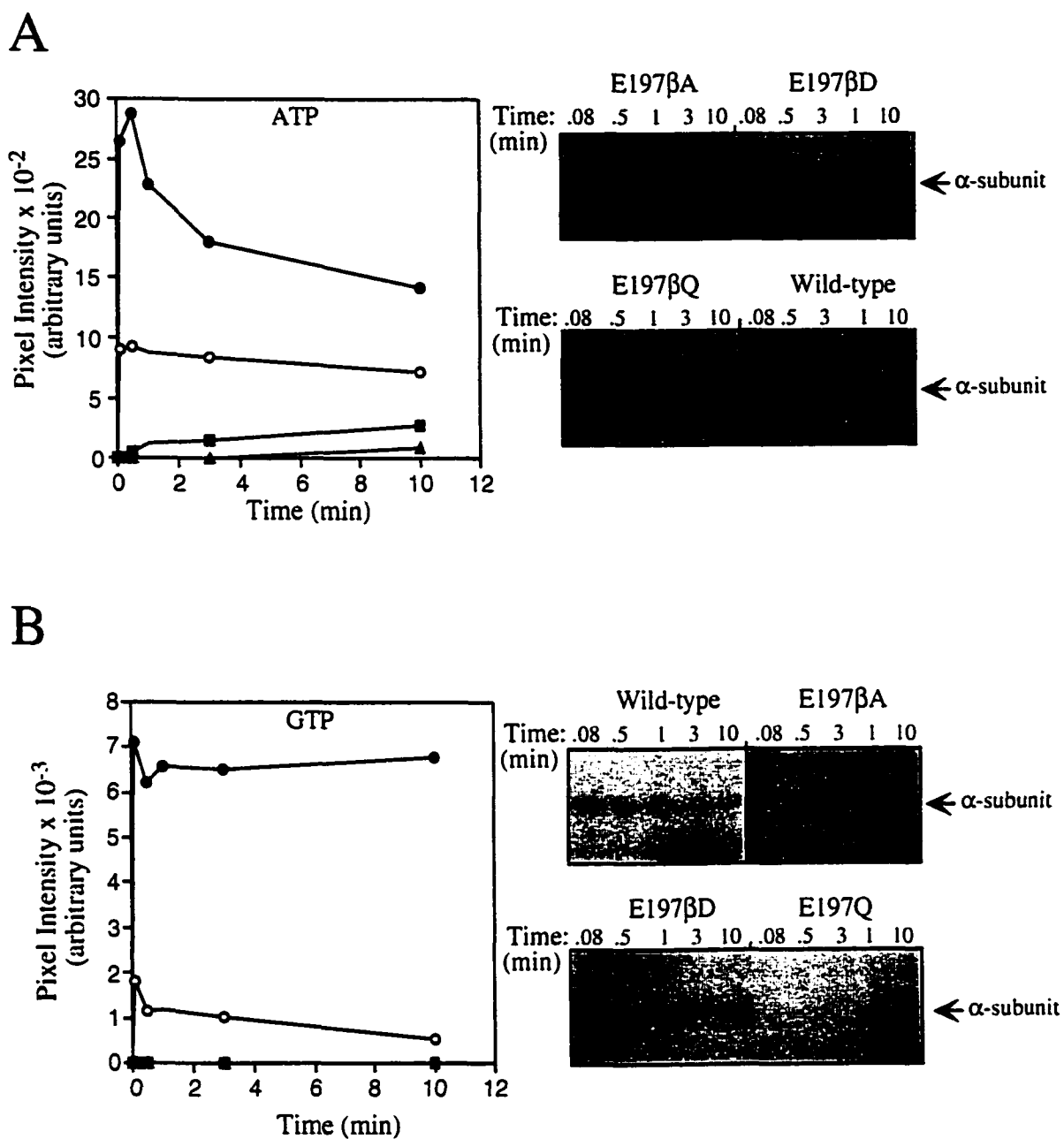


**Figure 6-16. Time course of phosphorylation by NTP of wild-type SCS and the Glu 197 $\beta$  mutant protein.** Wild-type and mutant SCS were incubated in the presence of [ $\gamma$ - $^{32}$ P] ATP in panel A, or [ $\gamma$ - $^{32}$ P] GTP in panel B. Samples were taken at various times, and the subunits were separated by SDS-PAGE. The gels were then analyzed by phosphorimager and the results are shown on the left: wild-type SCS (○), protein with the mutation E197 $\beta$ A (■), E197 $\beta$ D (●), and E197 $\beta$ Q (▲). Autoradiograms of the gels are shown on the right.

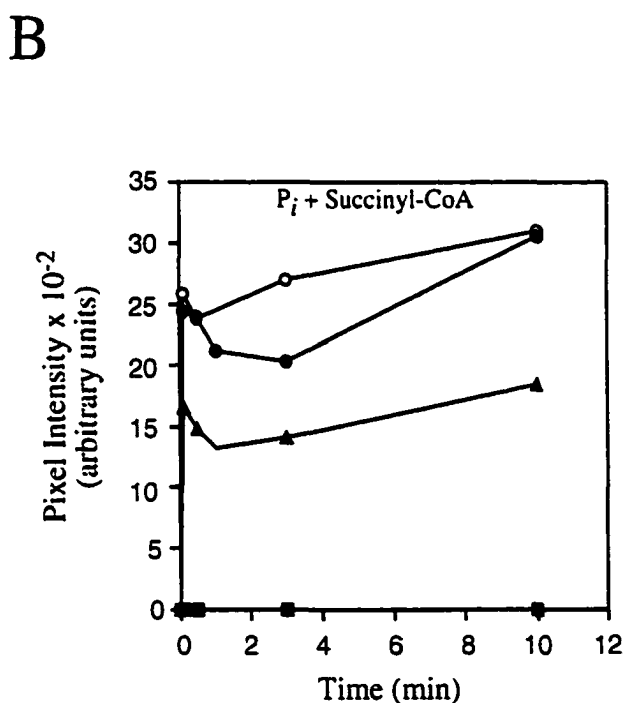
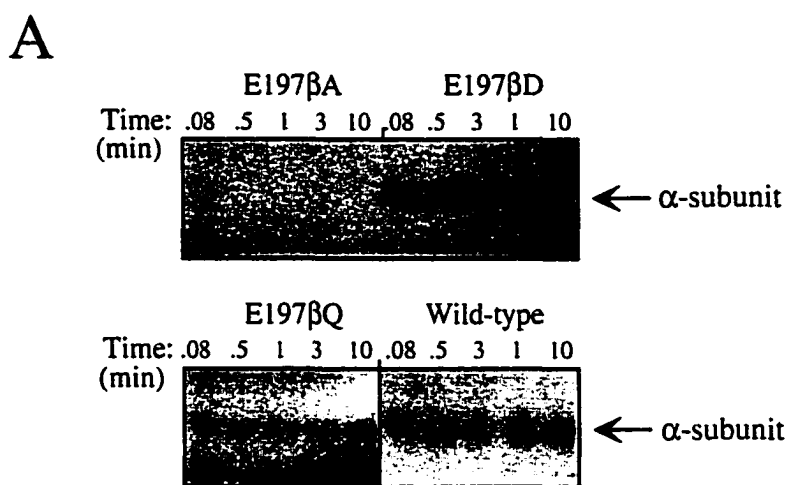


**Figure 6-17. Time course of phosphorylation by succinyl-CoA and  $P_i$  of wild-type SCS and the Glu 197 $\beta$  mutant protein.** Wild-type and mutant SCS were incubated in the presence of  $^{32}P_i$  and succinyl-CoA. Samples were taken at various times, and the subunits were separated by SDS-PAGE. Autoradiograms of the gels are shown in panel A. The gels were analyzed by phosphorimetry, and the results are shown in panel B: wild-type SCS (○), protein with the mutation E197 $\beta$ A (■), E197 $\beta$ D (●), and E197 $\beta$ Q (▲).

similar to that of wild-type protein. The E197 $\beta$ Q mutant was not phosphorylated by either ATP or GTP, but was phosphorylated by succinyl-CoA and P<sub>i</sub> at rates that were similar to those of wild-type protein. These results are the reciprocal to those of the E208 $\alpha$ Q mutant, and are consistent with the participation of Glu 197 $\beta$  in the partial reaction involving nucleotide at site II.

Table 6-4: Kinetic Parameters of Wild-type and Mutant SCS Proteins<sup>a</sup>

Protein	Succinate K <sub>m(app)</sub> (mM)	CoA K <sub>m(app)</sub> ( $\mu$ M)	ATP K <sub>m(app)</sub> ( $\mu$ M)	ATP k <sub>cat</sub> (min <sup>-1</sup> )	GTP K <sub>m(app)</sub> ( $\mu$ M)	GTP k <sub>cat</sub> (min <sup>-1</sup> )
Wild-type	0.25	4.0	70	2684	394	1471
Mutations of Glu 208 $\alpha$ (site I)						
E208 $\alpha$ D	0.26	2.2	116	2343	63.3	539.6
E208 $\alpha$ Q	0.27	1.3	41.2	0.57	11	0.28
Mutations of Glu 197 $\beta$ (site II)						
E197 $\beta$ D	0.87	2.7	138	1775	311	1775
E197 $\beta$ Q	0.40	1.8	106	0.85	20.2	0.21

<sup>a</sup> Measured by following the production of succinyl-CoA spectrophotometrically at 235 nm (See Materials and Methods of specific details).

## Discussion

*Crystallographic Structures of SCS Soaked with ADP.* The results of the first experiment are relevant to the idea that ADP causes dephosphorylation. Since the phosphohistidine can be hydrolyzed nonenzymatically at low pH, it is possible that a drop in pH during the ADP soak was responsible for the dephosphorylation. However, in control experiments, it was verified that the pH did not drop below neutrality upon the addition of ADP. Furthermore, as a negative control, trials with nonhydrolyzable nucleotide analogues under identical conditions did not result in dephosphorylation of the enzyme, demonstrating that ADP is responsible for the dephosphorylation. The fact that ADP was not observed bound in the crystal structure can be attributed to low occupancy.

At the concentration of ADP used in this experiment, ADP would not be a good competitor for the sulfate and phosphate ions present at high concentration in the precipitant solution. A sulfate or phosphate ion is seen in both this and the native structure (7) bound to the N-terminal domain of the  $\beta$ -subunit. As proved by the structure of the ADP-complex with SCS in the successful experiment, the  $\beta$ -phosphate of the nucleotide replaces the sulfate or phosphate ion at this location. Hence, in addition to nonspecific ionic effects, there would be direct competition for the binding site by sulfate and phosphate ions.

Based on the results of the first soaking experiment, several modifications were made to the protocols for subsequent experiments culminating in success. The significant changes were lowering as much as possible the concentration of competing ions (e.g. the precipitant sulfate ions), exchanging the buffer (i.e. removing the phosphate ions) so that magnesium ions could be added, and increasing the concentrations of the substrates, ADP and  $Mg^{2+}$  ions. The requirement for the excessively high concentration of nucleotide was also demonstrated by an experiment in which the ADP in the final step was replaced by 10 mM  $\beta,\gamma$ -methyleneadenosine 5'-triphosphate (AMPPCP). This nonhydrolyzable analogue of ATP has a  $K_i$  value of 0.38 mM (11), more than an order of magnitude higher than the  $K_m$  for ATP or ADP (34, 15). The enzyme was dephosphorylated by ADP in the preceding steps but the concentration of AMPPCP was not sufficiently high for it to compete with the sulfate ion and bind in the N-terminal domain of the  $\beta$ -subunit.

Although the binding site for the ADP- $Mg^{2+}$  complex has been identified, full details of the binding cannot be described due to the limited resolution of the data. The soaking experiments caused a deterioration in the crystals. The data to 2.9 Å resolution were used in the analysis of the first experiment, but data to only 3.3 Å resolution were used in the successful experiment. It is likely that the crystals are less well ordered after the soaking experiments because the enzyme must change conformation to bind better the ADP- $Mg^{2+}$  complex. Figure 6-18 shows a superposition of the nucleotide-bound structure with the native structure. Parts of the smaller subdomain have moved relative to the rest of

the enzyme, however the helices of this subdomain have not. These helices are constrained because they pack against a second tetramer in the crystals (cf. Figure 7(a) in reference (7)). However, even these helices can eventually move, since the crystals shattered when left to soak longer than 48 h. Due to the low resolution of the data, the coordinate errors for the well-ordered atoms in the two models are rather high, estimated as 0.6-0.7 Å (35, 18). In the final refinement of the model from the successful experiment, no water molecules were included. So although it might have been expected that the  $Mg^{2+}$  ion would be octahedrally coordinated by six oxygen atoms, in the structure of the complex with SCS, the ion is coordinated by five oxygen atoms of the protein (Fig. 6-7). In this model, the sixth position is open to the solution and presumably it would be filled by an oxygen atom from a water molecule. Likewise, although a phosphate ion has been modeled next to His 246 $\alpha$ , this ion may be a sulfate.

The observed changes in the structure of the protein that accommodate the binding of the ADP- $Mg^{2+}$  complex are relatively small. The inner loop (residues 48 $\beta$  to 59 $\beta$ ) that complexes the free sulfate ion in the native structure is shifted in towards the cleft to bind the  $\beta$ -phosphate of ADP. The neighboring loop (residues 82 $\beta$  to 90 $\beta$ ) also shifts so that its interactions with the inner loop can be maintained (Fig. 6-18). The side chain carboxylate group of Asp 213 $\beta$  provides one ligand for the  $Mg^{2+}$  ion. In so doing, the hydrogen bond observed in the native structure between one carboxylate oxygen atom and the nitrogen atom of Gly 214 $\beta$  must be broken (Fig. 6-19). The plane of the peptide bond between Asp 213 $\beta$  and Gly 214 $\beta$  is rotated in the complex relative to the native structure, and the carbonyl oxygen atom adopts a position more favorable to accept a hydrogen bond (3.2Å) from the amide nitrogen atom of Asn 199 $\beta$ . The use of the side chain oxygen atom, O $\delta$ 1, of Asn 199 $\beta$  to coordinate the  $Mg^{2+}$  ion disrupts hydrogen bonding interactions in the

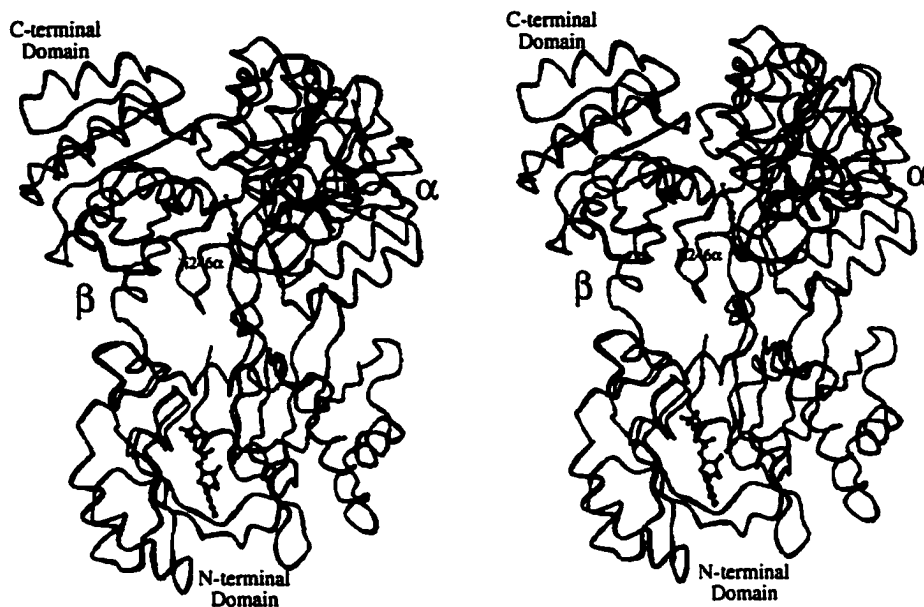


**Figure 6-18. Stereo diagram superposing the ADP-bound and native models of an  $\alpha\beta$ -dimer to show the conformational shift.** The ball and stick model of the ADP molecule and the corresponding  $C\alpha$ -trace are coloured red. The  $C\alpha$ -trace of the native enzyme and the ball and stick model of the bound sulfate ion are green, while the side chain of His 246 $\alpha$  is blue. The residues used in this superposition are given in Appendix 7.



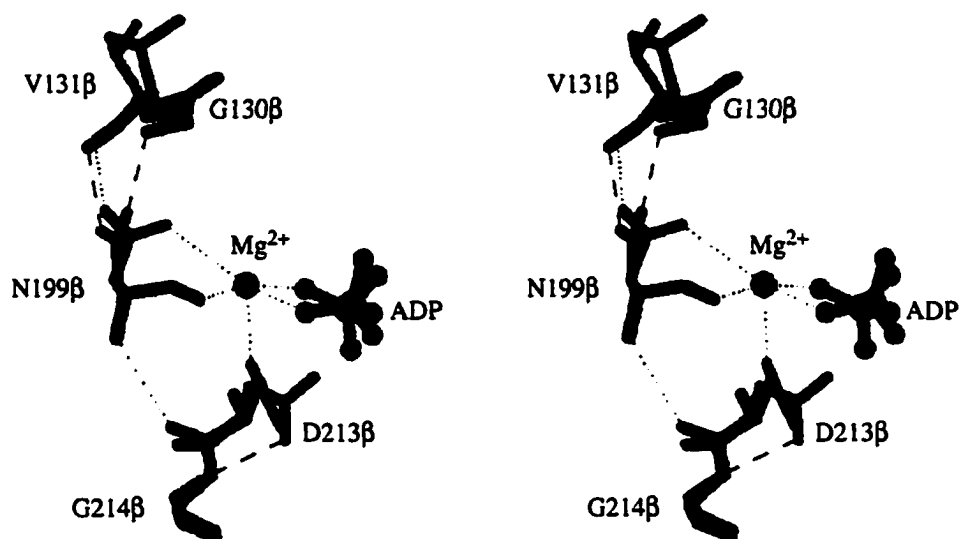


**Figure 6-19. Changes in the vicinity of the  $Mg^{2+}$  ion.** The native model and the ADP-bound model are superimposed. The native model is shown in grey. The potential hydrogen bonds in the native model are shown as long dashed lines. The ADP-bound model is green, and the potential hydrogen bonds and  $Mg^{2+}$  coordination is indicated by short dashed lines. The  $Mg^{2+}$  ion is coloured magenta, and the phosphates from the ADP molecule are shown as a red ball and stick model. The oxygen atoms are coloured red and the nitrogen atoms blue.

native structure between the side chain amido group of Asn 199 $\beta$  and the amide nitrogen atom of Gly 130 $\beta$  (Fig 6-19). Residues Gly 130 $\beta$  and Val 131 $\beta$  are part of one tryptic peptide labeled by 8-N<sub>3</sub>-ATP (8). The location of these residues in a ribbon diagram of the N-terminal domain of the  $\beta$ -subunit is indicated by an asterisk in Figure 6-20A. The loop containing these residues is structurally analogous to the "lid" over the nucleotide in DD-ligase (36) and glutathione synthetase (37), two other enzymes possessing the ATP-grasp fold (6). Primarily due to the absence of a "lid", 47% of the ADP molecule when bound by SCS is accessible to solvent, in contrast to 2% when bound by DD-ligase.<sup>3</sup> Surprisingly, there is very little change in the position of Glu 107 $\beta$ . By analogy to DD-ligase, the carboxylate group of this side chain was expected to form hydrogen bonds with the 2'- and 3'-hydroxyl groups of the ribose moiety (7). Instead, only one oxygen atom of the carboxylate group interacts with the 2'-hydroxyl group, and this with the long distance of 3.2 Å (Fig 6-20B). This is similar to the binding in synapsin I (33).

The ADP-Mg<sup>2+</sup> complex is bound, with only these small changes, by residues of both subdomains of the N-terminal domain of the  $\beta$ -subunit. This contrasts with the earlier hypothesis that the two subdomains would close, so that each would superpose with its counterpart of DD-ligase (7). Instead, when the superposition of the two structures is based on the ADP molecules<sup>4</sup>, the  $\beta$ -strands of the smaller subdomain superpose quite well, while those of the larger subdomains do not (Fig. 6-20A). Instead, the  $\beta$ -strands of this subdomain of SCS are in the same plane as those of DD-ligase, but there is an angle of about 20° between the directions of the strands. It may be that the orientation of one subdomain with respect to the other need not be identical among structures possessing the ATP-grasp fold. However one may be left to wonder if SCS is in the conformation it would adopt when binding the ADP-Mg<sup>2+</sup> complex in solution.

---

<sup>3</sup> The surface areas of the molecules accessible to solvent were calculated using the program MS (38).

<sup>4</sup> The superposition was done using the program SUPPOS from the BIOMOL package (Gröningen, Holland).

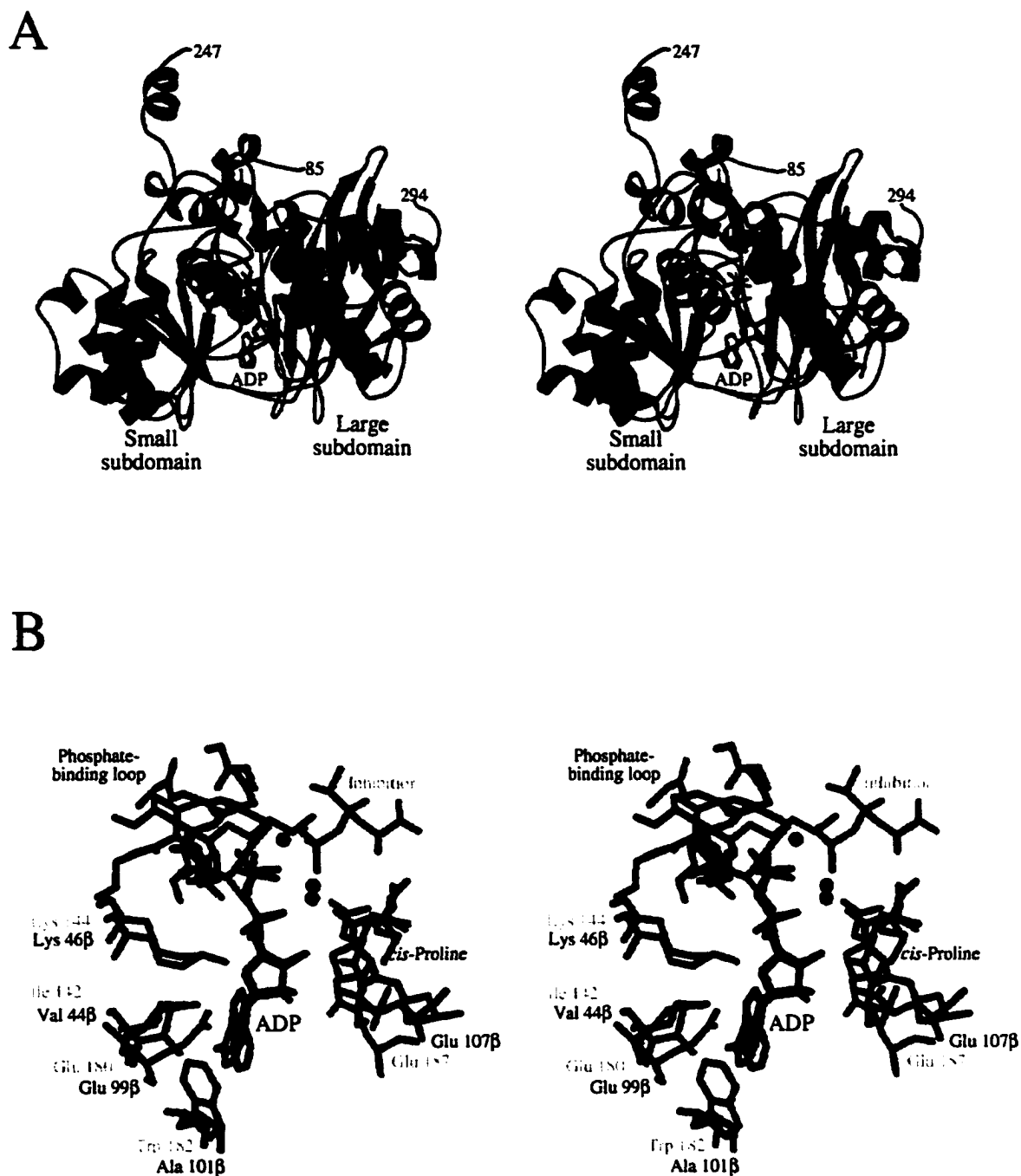


**Figure 6-20. Stereo diagram of the superposition of the ADP in SCS with that in DD-ligase.** A. Ribbon diagram of the N-terminal domain of the  $\beta$ -subunit of SCS (shown in green) superimposed on DD-ligase (shown in grey) based on bound ADP molecule. The ADP in SCS is shown as a red ball and stick model, while that in DD-ligase is grey. B. Close-up view of the nucleotide binding sites of SCS and DD-ligase from the superposition shown in panel A. The backbone of SCS is shown in green, and that of DD-ligase is grey. The sidechains are coloured according to residue type. The  $Mg^{2+}$  ion in SCS is magenta while those in DD-ligase are grey. The phosphoramidate inhibitor from DD-ligase is also shown.

These are the first structures observed of dephosphorylated SCS. In the native, phosphorylated structure, there was a water molecule bound to the phosphoryl group of chain A at site I (7). It was postulated that this water molecule was in the position that the oxygen atom of succinate might adopt prior to the transfer of the phosphoryl group from the phosphohistidine. This interpretation is supported by the dephosphorylated structures wherein one of the oxygen atoms of the phosphate ion (O4) adopts this position (Fig. 6-5). Interactions between the protein and the other three oxygen atoms are similar in the phosphorylated and dephosphorylated structures, with the exception of the previously mentioned change in  $\chi_1$  of Ser 153 $\alpha$ . This change allows the O $\gamma$  atom of Ser 153 $\alpha$  to interact with oxygen atom O1 of the phosphate ion. The environments of the three oxygen atoms covalently attached to the phosphorus atom could be maintained as the phosphoryl group is transferred from the phosphohistidine to form succinyl-phosphate and released as a phosphate ion at site I. These three oxygen atoms would be in the equatorial plane, while the nitrogen atom of the imidazole ring and the fourth oxygen atom would adopt the axial positions about the phosphorus atom in the trigonal bipyramidal transition state.

*Comparison of the ADP-Bound Form of SCS to Other Nucleotide Binding Proteins.* As noted before, the N-terminal domain of SCS is a member of the class of nucleotide binding folds called the ATP-grasp fold (4, 39, 6, 40-43, 7). As such, it displays remarkable similarity to other members of this group, the majority of the residues that make contacts with the ADP have equivalent residues in other proteins that contain the ATP-grasp fold. Table 6-5 lists the residues that are equivalent between SCS and a representative member of the ATP grasp family, DD-ligase (36). These residues are involved primarily in binding the adenosine moiety and  $\alpha$ -phosphate.

Table 6-5. Equivalent Residues that Contact the ADP Mg<sup>2+</sup> Complex in SCS and DD-ligase.<sup>a</sup>

Residue in SCS	Residue in DD-ligase	Function
Val 44 $\beta$	Ile 142	Hydrophobic interaction with adenine.
Leu 212 $\beta$ and Val 104 $\beta$	Met 259 and Leu 269	Hydrophobic interaction with adenine.
Lys 46 $\beta$	Lys 144	H-bond with N7 of adenine and ionic interaction with the $\alpha$ -phosphate group.
Glu 99 $\beta$ , and the main chain carbonyl group of Ala 100 $\beta$	Glu 180, and the main chain carbonyl group of Lys 181	H-bond with N6 of adenine.
main chain amide of Thr 102 $\beta$	main chain amide of Leu 183	H-bond with N1 of adenine
Glu 107 $\beta$	Glu 187	H-bond with the 2' OH of the ribose sugar.
Asp 213 $\beta$	Glu 270	Coordination of the Mg <sup>2+</sup> ion.
main chain carbonyl of Asn 199 (precedes a cis-Pro bond)	side chain of Asp 257 (no cis-Pro)	Coordination of the Mg <sup>2+</sup> ion.

<sup>a</sup> Judging the equivalence of these residues was based on the superposition of the ADP molecule in SCS with that in DD ligase, using the program SUPPOS from the BIOMOL package (Gröningen, Holland).

Equally interesting, are the residues that have different interactions. In DD-ligase, Trp 182 forms the part of the hydrophobic pocket where the adenine ring resides; the equivalent residue in SCS is Ala 101 $\beta$ . This difference is likely to underlie the specificity of *E. coli* SCS to accommodate both ATP and GTP. A large hydrophobic residue at this position would sterically clash with the amino group on the C2 atom of guanine. In pig heart SCS specific for GTP, this residue is also Ala. Moreover, in mammalian SCS specific for ATP, this residue is Arg or Lys, whose side chains would also obstruct the amino group on the C2 atom of guanine. A second difference between SCS and DD-ligase is observed in the Mg<sup>2+</sup> binding site. One of the coordination positions of the Mg<sup>2+</sup> in SCS

is formed by the main chain carbonyl oxygen of Asn 199 $\beta$ , which is involved in a cis-proline bond with Pro 200 $\beta$ . This cis-proline bond positions the carbonyl group to “substitute” for the side chain of the equivalent residue in DD-ligase, Asp 257. Furthermore, as a consequence of the cis-proline bond, the residue in SCS equivalent to Met 259 in DD-ligase is not in position to make hydrophobic interactions with the adenine ring. Instead, this role is fulfilled by L212 $\beta$  in SCS. A third difference between SCS and DD-ligase is observed in the conformation of the inner loop, (residues 53 $\beta$  to 55 $\beta$  in SCS) that interacts with the  $\alpha$ - and  $\beta$ -phosphate groups of ADP (Fig. 4-19B). Although Thoden *et al.* (32) postulated that the Type III' reverse turn seen to bind the nucleotide in carbamoyl phosphate synthetase (32), glutathione synthetase (37), and DD-ligase (36) may be common to all proteins of this family, SCS and pyruvate phosphate dikinase (44) are the current exceptions. Because pyruvate phosphate dikinase transfers the  $\gamma,\beta$ -pyrophosphate group of ATP as a single unit, the conformation of this loop would be expected to be different. In SCS, the guanidino portion of the side chain of Arg 54 $\beta$  interacts with the phosphates of ADP, “replacing” Lys 97 of DD-ligase (36), Lys 125 of glutathione synthetase (37) or Arg 675 of carbamoyl phosphate synthetase (32), residues that are not part of the reverse turn.

The ATP-grasp fold, as represented by DD-ligase, displays remarkable structural similarity in the area around the nucleotide to an unrelated class of nucleotide binding proteins, represented by cAMP dependent protein kinase (cAPK) (40, 41, 43). Given the high degree of similarity observed between the nucleotide binding domains of SCS and DD-ligase, the structural similarity to cAPK extends to SCS, especially around the AMP portion of the ADP molecule. For both of these folds (the ATP-grasp and the cAPK fold), the binding site for nucleotide resides between two domains (in SCS these domains have been designated the smaller and larger subdomains of the nucleotide binding fold), one smaller, dominated by a 4-5 stranded antiparallel  $\beta$ -sheet, and one larger domain (43). In all there are 10 segments (103 residues) from these two domains (43) that are similar in the

ATP grasp and cAPK nucleotide binding folds. For six of the 10 segments, the connectivity is similar to that in SCS. The structural similarity extends throughout the bound nucleotide and the residues that interact with it, to the bound  $Mg^{2+}$  ions, several water molecules, and to a network of hydrophobic and electrostatic interactions (43). A superposition of the N-terminal domain of the  $\beta$ -subunit of SCS and cAPK is shown in Figure 6-21.

These enzymes (DD-ligase and cAPK) also display some structural similarity to a third nucleotide binding fold, the allosteric effector site found in ribonucleotide reductase (RNR R1) (42). There are 23 equivalent residues in these proteins, some of which serve to orient the AMP portion of the ligand (42). Counterparts to these residues are observed in SCS. A superposition of the N-terminal domain of the  $\beta$ -subunit of SCS and RNR R1 is shown in Figure 6-22. The main chain amide nitrogen of Thr 102 $\beta$  (corresponding to L183 in DD-ligase, V123 in cAPK, and N18 in RNR R1) forms a hydrogen bond with the N1 of the adenine, and the main chain carbonyl oxygen atom of Ala 100 $\beta$  (corresponding to K181 in DD-ligase, E121 in cAPK, and R16 in RNR R1) forms a hydrogen bond with the N6 amino group of adenine. The side chain oxygen atom of Glu 99 $\beta$  (corresponding to E180 in DD-ligase, and E15 in RNR R1) also forms a hydrogen bond with the N6 amino group of adenine, and Lys 46 $\beta$  (corresponding to K144 in DD-ligase, K72 in cAPK, and K9 in RNR R1) makes ionic interactions with the  $\alpha$ -phosphate group of the nucleotide. Val 44 $\beta$  (corresponding to I142 in DD-ligase, A70 in cAPK, and V57 in RNR R1) packs against one side of the adenine ring, and Leu 212 $\beta$  (corresponding to M154 in DD-ligase, and V57 in cAPK) packs against the other side of the purine ring. A third hydrophobic contact with the nucleotide that is present in DD-ligase, cAPK, and RNR R1 occurs where Ala 100 $\beta$  is located in *E. coli* SCS. Presumably the absence of a large side chain at this position allows *E. coli* SCS to bind both ATP and GTP.

The nucleotide binding site of SCS also has some more limited similarity to the representative member of the small G-proteins, H-ras p21, where nucleotide is observed

bound on the edge of a parallel  $\beta$ -sheet (45). The conformation of Gly 53 $\beta$ -Arg 54 $\beta$ -Gly 55 $\beta$  in SCS is reminiscent of the conformation of three residues (Gly 15-Lys 16-Ser 17) of the phosphate-binding loop H-ras p21 (45). Each binds the  $\beta$ -phosphate of the nucleotide; however, if the three residues in the two proteins are superposed, the nucleotides are oriented in opposite directions, so that the  $\alpha$ -phosphate of ADP bound to SCS superposes with the  $\gamma$ -phosphate of the nucleotide bound to H-ras p21. When the superposition is based on the nucleotide diphosphate molecules observed in these structures<sup>5</sup>, there are several specific residues that have equivalent positions, but unlike the previous examples, neither the secondary structure nor the connectivity is similar (Fig 6-23). For example, hydrophobic interactions are made between the nucleotide and residues on either side of the adenine or guanine ring. Hydrophobic contacts are made between one side of the purine ring and Leu 212 $\beta$  in SCS, or Phe 28 in p21. On the other side of the purine ring, they are made by Val 44 $\beta$  in SCS, and by the methylene portion of the sidechain of Lys 117 in p21. The hydrogen bond between the main chain amide nitrogen of Thr 102 $\beta$  and the N1 of adenine in SCS is equivalent to a hydrogen bond between the N1 of guanine and the oxygen atom of the side chain of Asp 119 in p21. In SCS, glutamate 107 $\beta$  makes a hydrogen bond with the 2' hydroxyl group of the ribose, similar to the hydrogen bond between the main chain carbonyl oxygen atom of Asp 30 and the 2' OH of the ribose in p21. In SCS, the interaction between the guanidinium group of Arg 54 $\beta$  and the  $\beta$ -phosphate of ADP is equivalent to the interaction between the amino group of Lys 16 and the  $\beta$ -phosphate group in p21.

Thus, there exists considerable similarity between structures that bind nucleotide, regardless of the protein fold in which the nucleotide binds. This would indicate that convergent evolution produces different proteins that to fold in a variety of ways to produce similar local interactions with a specific ligand. The similarity in the chemical groups and

---

<sup>5</sup> The superposition was done using the command `lsq_explicit` in the program O (46), specifying all common atoms between the ADP, and GMPPCP molecules. The RMSD between the NDP portion of the two nucleotides was 1.455 Å



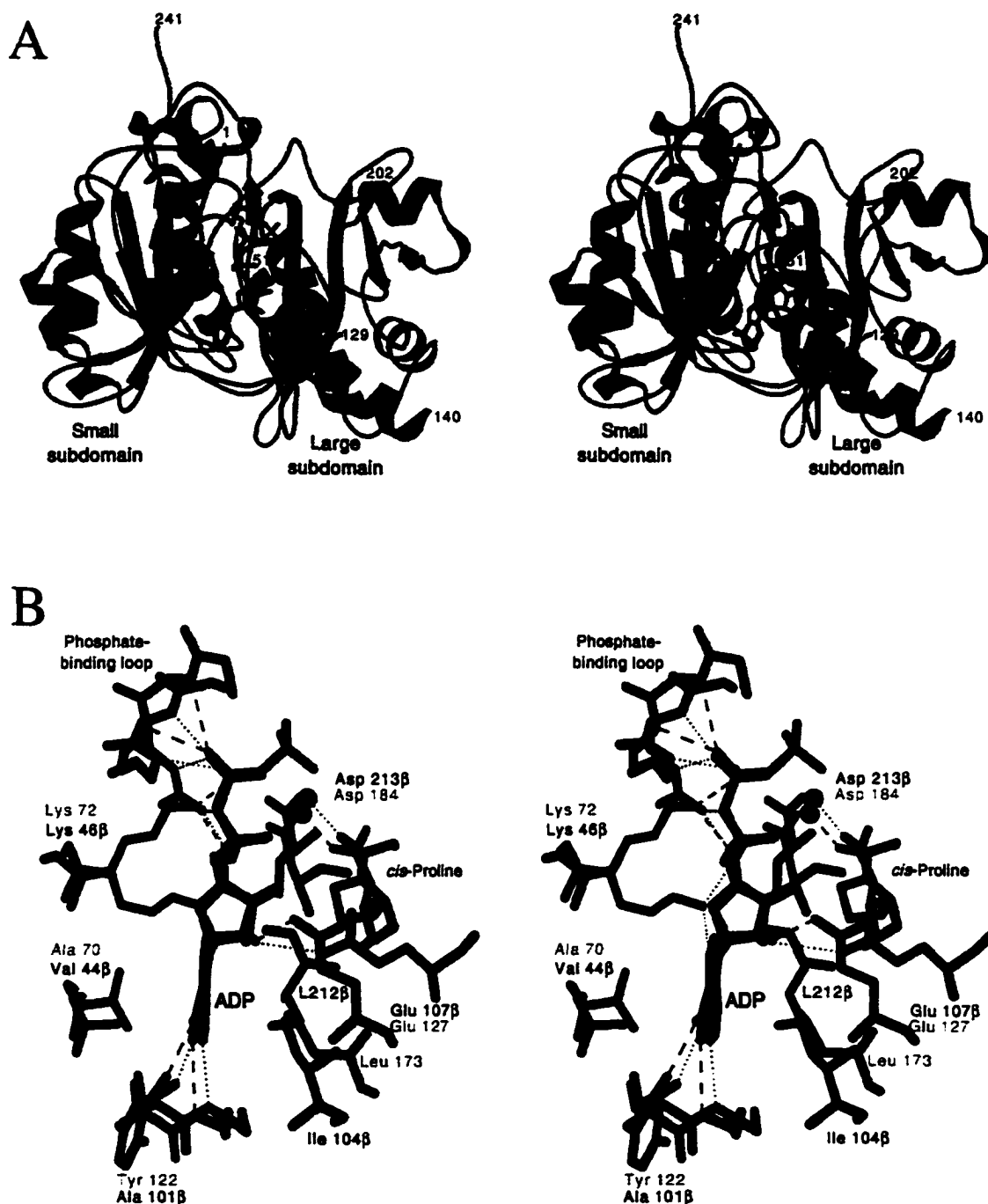


**Figure 6-21. Stereo diagram of the superposition of the ADP in SCS with that in cAMP dependent protein kinase (cAPK).** A. Ribbon diagram of the N-terminal domain of the  $\beta$ -subunit of SCS (shown in green) superimposed on cAPK (shown in grey) based on bound ADP molecule. The ADP in SCS is shown as a red ball and stick model, while that in cAPK is grey. B. Close-up view of the nucleotide binding sites of SCS and cAPK from the superposition shown in panel A. The backbone of SCS is shown in green, and that of cAPK is grey. The sidechains are coloured according to residue type. The  $Mg^{2+}$  ion in SCS is magenta while those in cAPK are grey. Hydrogen bonds from the nucleotide to the protein are coloured according to the nucleotide colour. The PDB accession number for cAPK is 1CDK.

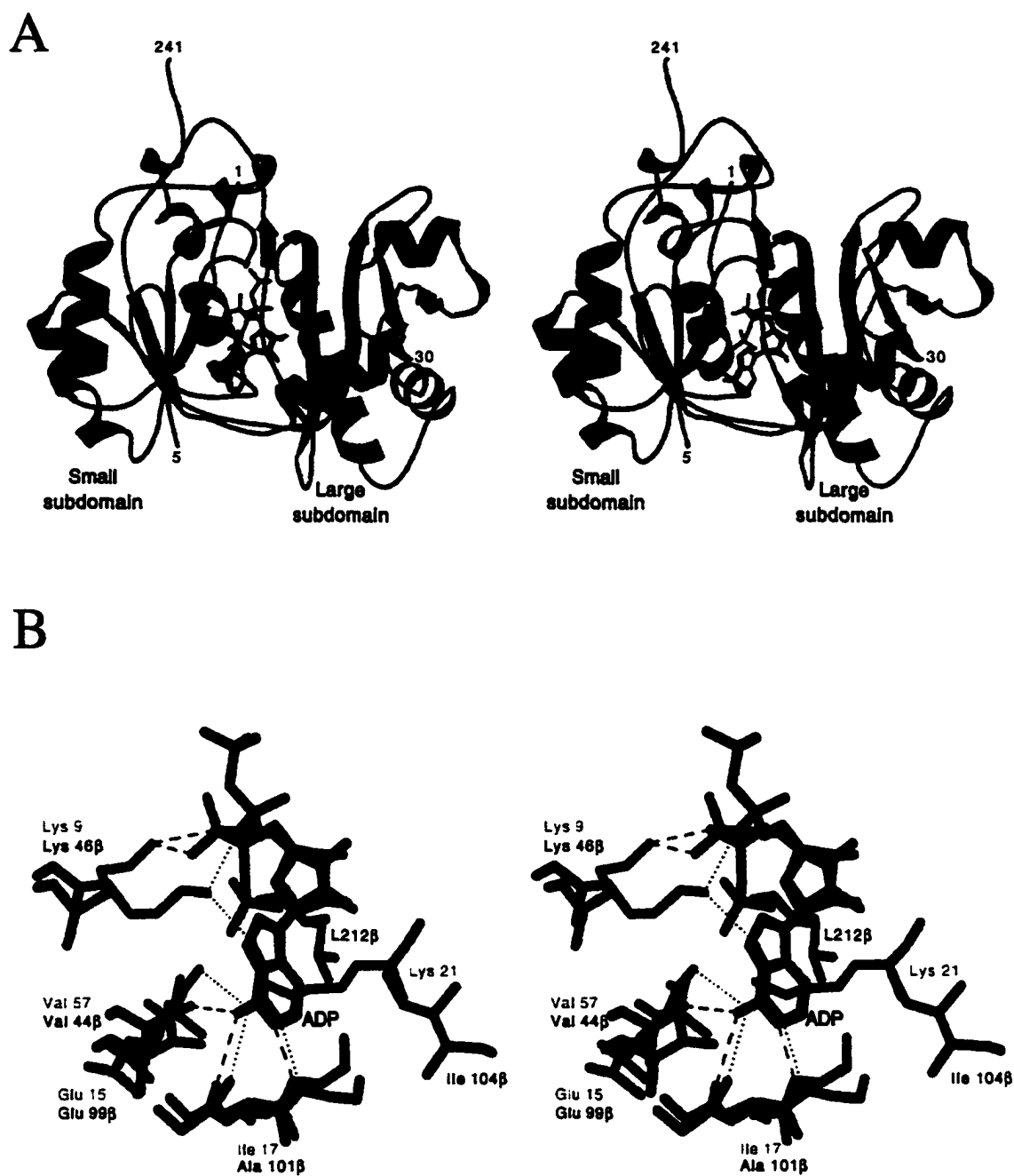


**Figure 6-22. Stereo diagram of the superposition of the ADP in SCS with that in Ribonucleotide reductase (RNR1).** A. Ribbon diagram of the N-terminal domain of the  $\beta$ -subunit of SCS (shown in green) superimposed on RNR1 (shown in grey) based on bound ADP molecule. The ADP in SCS is shown as a red ball and stick model, while that in RNR1 is grey. B. Close-up view of the nucleotide binding sites of SCS and RNR1 from the superposition shown in panel A. The backbone of SCS is shown in green, and that of RNR1 is grey. The sidechains are coloured according to residue type. The  $Mg^{2+}$  ion in SCS is magenta while those in RNR1 are grey. Hydrogen bonds from the nucleotide to the protein are coloured according to the nucleotide colour. The PDB accession number for RNR1 is 3R1R.

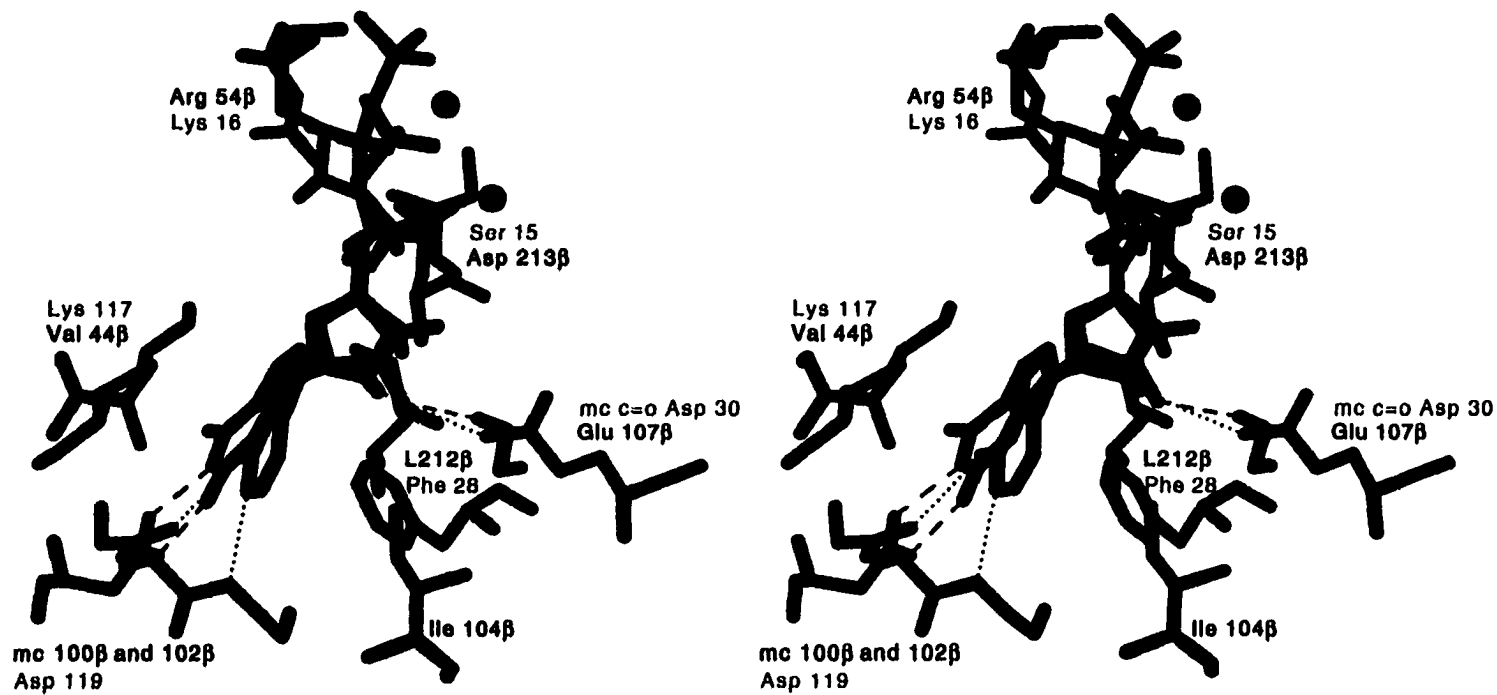


**Figure 6-23.** Stereo diagram of the superposition of the ADP in SCS with that in p21 ras. Close-up view of the nucleotide binding sites of SCS and p21 ras. The backbone of SCS is shown in green, and that of p21 ras is grey. The sidechains are coloured according to residue type. The Mg<sup>2+</sup> ion in SCS is magenta while those in p21 ras are grey. Hydrogen bonds from the nucleotide to the protein are coloured according to the nucleotide colour. The PDB accession number for p21 ras is 6Q21.

structures that are used by nature to bind nucleotide likely reflect the limited number of productive interactions with nucleotide that are possible, while allowing for functionality. Thus, there is greater similarity (between different nucleotide binding proteins) in the amino acids which are proximal to the AMP portion of the nucleotide, than there is in the amino acids that bind the functional portion of the nucleotide, the  $\beta$ - and  $\gamma$ -phosphoryl groups.

*Modeling and Mutagenesis of E. coli SCS.* The mechanism for the reaction catalyzed by SCS has been envisioned as a series of nucleophilic attacks with phosphorylated histidine residue as an intermediate (1). The nucleophilic attack by the active site histidine on the phosphoryl group of either succinyl-phosphate (proposed to occur in site I), or on the  $\gamma$ -phosphoryl group of ATP (proposed to occur in site II) requires a free electron pair. In SCS, the phosphohistidine has been shown to be the N $\epsilon$ 2 isomer (47, 4, 7). This would imply that the free electron pair must have been on the N $\epsilon$ 2 atom of the imidazole ring, despite the preference of free histidine in solution to have the electron pair on N $\delta$ 1 (10). Vogel and Bridger predicted that the presence of an ionic group proximal to N $\delta$ 1 would favour the formation of the isomer of histidine with the free electrons on the N $\epsilon$ 2 atom (48, 12). The identification of the nucleotide binding site in the N-terminal domain of the  $\beta$ -subunit, 35Å from the active site histidine and the bound CoA molecule in the  $\alpha$ -subunit, implies that the partial reactions that involve succinyl-CoA and P<sub>i</sub> and those that involve nucleotide are carried out at separate sites. These have been designated site I and site II, respectively (8). There is a relevant glutamate residue located in each of these two sites. In site I, Glu 208 $\alpha$  interacts with the N $\delta$ 1 atom of the active site phosphohistidine as seen in the crystal structure of SCS (4, 7). In other enzymes that have a covalent histidine intermediate, the presence of a hydrogen bond between the non-phosphorylated nitrogen atom (either N $\delta$ 1 or N $\epsilon$ 3) of an active site histidine and a hydrogen bond acceptor seems to be a common theme (49-53). In site II, Glu 197 $\beta$  was predicted to interact with the N $\delta$ 1 atom of H246 $\alpha$  in a similar manner based on the hypothetical model shown in Figure 6-9. Mutagenesis of these glutamate residues in each

site was carried out to examine their role in the phosphoryl transfer catalyzed by SCS. When these residues were mutated separately to glutamine, the activity of the mutant enzymes was reduced by approximately 3-4 orders of magnitude. In addition, the mutation E208 $\alpha$ Q inhibited only phosphorylation by  $P_i$  and succinyl-CoA in site I, and the mutation E197 $\beta$ Q inhibited only phosphorylation by nucleotide in site II (Figures 6-12, 6-13, 6-17 and 6-18). The effect of these mutations was not due to disruption of the substrate binding sites, because the  $K_{m(app)}$  values resembled those of wild-type SCS (Table 6-4). Since the side chain of glutamine can still accept a hydrogen bond, the charge on the native glutamate residues must be important for the phosphorylation of SCS. This is consistent with the prediction that the lone pair of electrons reside on the N $\epsilon$ 2 atom of His 246 $\alpha$  in order to initiate nucleophilic attack on the phosphoryl group of succinyl-phosphate or the  $\gamma$ -phosphate of nucleotide triphosphate (11). When E208 $\alpha$  and E197 $\beta$  were mutated separately to aspartate, the activity of the mutant proteins was very similar to that of wild-type protein, indicating that shortening the side chain by one methylene group had no effect on SCS. This can be explained by an accommodating movement of either the His 246 $\alpha$  loop, or the aspartate residue, or by the presence of an intervening water molecule that could make hydrogen bonds with the sidechain carboxylate group of the aspartate and the N $\delta$ 1 of His 246 $\alpha$ . In the case of Glu 197 $\beta$ , elimination of the side chain by mutation to alanine resulted in enzyme that was practically devoid of activity. The results of these mutagenesis experiments supported the prediction of Vogel and Bridger that production of the intermediate phosphohistidine requires the presence of an anionic group to stabilize the isomer of histidine with the lone pair of electrons on the N $\epsilon$ 2 atom (11, 12). Moreover, the results of the experiments with the E197 $\beta$  mutants also provide some credence for the hypothetical model, and illustrate the usefulness of these types of models for predicting and testing the role of various residues in the enzyme mechanism. The validity of other possible interactions proposed by the hypothetical model must be tested by mutagenesis, or by the solution of a crystallographic structure of SCS with the His 246 $\alpha$  loop down in site

II. In this vein, the ability of SCS to catalyze its dephosphorylation in the crystal without cracking the crystal, makes SCS a candidate for kinetic crystallography.

### References:

1. Bridger, W. A. (1974) in *The Enzymes* (Boyer, P. D., ed) Vol. 10, 3rd Ed., pp. 581-606
2. Nishimura, J. S. (1986) in *Advances in Enzymology* (Meister, A., ed) Vol. 58, pp. 141-172, Wiley, New York
3. Bailey, D. L., Fraser, M. E., Bridger, W. A., James, M. N. G., & Wolodko, W. T. (1999) *J. Mol. Biol.* 285, 1655-1666.
4. Wolodko, W. T., Fraser, M. E., James, M. N. G., & Bridger, W. A. (1994) *J. Biol. Chem.* 269, 10883-10890.
5. Johnson, J. D., Muhonen, W. W., & Lambeth, D. O. (1998) *J. Biol. Chem.* 273, 27573-27579.
6. Murzin, A. G. (1996) *Curr. Opin. in Struct. Biol.* 6, 386-394.
7. Fraser, M. E., James, M. N. G., Bridger, W. A., & Wolodko, W. T. (1999) *J. Mol. Biol.* 285, 1633-1653.
8. Joyce, M. A., Fraser, M. E., Brownie, E. R., James, M. N. G., Bridger, W. A., & Wolodko, W. T. (1999) *Biochemistry* 38, 7273-7283.
9. Hultquist, D. E., Moyer, R. W., & Boyer, P. D. (1966) *Biochemistry* 5, 322-331.
10. Blomberg, F., Maurer, W., & Ruterjans, H. (1977) *J. Am. Chem. Soc.* 94, 8149-8159.
11. Vogel, H. J., & Bridger, W. A. (1982) *J. Biol. Chem.* 257, 4834-4842.
12. Vogel, H. J., & Bridger, W. A. (1983) *Biochem. Soc. Trans.* 11, 315-323.
13. Wolodko, W. T., Kay, C. M., & Bridger, W. A. (1986) *Biochemistry* 25, 5420-5425.
14. Wolodko, W. T., James, M. N. G., & Bridger, W. A. (1984) *J. Biol. Chem.* 259, 5316-5320.
15. Moffet, F. J., Wang, T., & Bridger, W. A. (1972) *J. Biol. Chem.* 247, 8139-8144.
16. Ray, J., W.J., Bolin, J. T., Puvathingal, J. M., Minor, W., Liu, Y., & Muchmore, S. W. (1991) *Biochemistry* 30, 6866-6875.
17. Sakabe, N. (1991) *Nucl. Instrum. Meth. in Phys. Res.* A303, 448-463.

18. Read, R. J. (1986) *Acta Cryst. A*42, 140-149.
19. Jones, T. A. (1985) *Methods Enzym.* 115, 157-171.
20. Engh, R. A., & Huber, R. (1991) *Acta Cryst. A*47, 392-400.
21. Brunger, A. T. (1992) *Nature* 355, 472-474.
22. Kleywegt, G. J., & Brunger, A. T. (1996) *Structure* 4, 897-904.
23. Pannu, N. S., & Read, R. J. (1996) *Acta Cryst. A*52, 659-668.
24. Adams, P. D., Pannu, N. S., Read, R. J., & Brunger, A. T. (1997) *Proc. Natl. Acad. Sci. USA* 94, 5018-5023.
25. Brunger, A. T., Adams, P. D., & Rice, L. M. (1997) *Structure* 5, 325-336.
26. Brunger, A. T., Adams, P. D., Clore, G. M., Delano, W. L., Gros, P., Grosse-Kunstleve, R. W., Jiang, J.-S., Kuszewski, J., Jilges, N., Pannu, N. S., Read, R. J., Rice, L. M., Simonson, T., & Warren, G. L. (1998) *Acta Cryst. D*54, 905-921.
27. Laskowski, R. A., MacArthur, M. W., Moss, D. S., & Thornton, J. M. (1993) *J. Appl. Cryst.* 26, 283-291.
28. Hooft, R. W. W., Vriend, G., Sander, C., & Abola, E. E. (1996) *Nature* 381, 272.
29. Ho, S. N., Hunt, H. D., Horton, R. N., Pullen, J. K., & Pease, L. R. (1989) *Gene* 77, 51-59.
30. Sambrook, J., Fritsch, E. F., & Maniatis, T. (1989) *Molecular Cloning: a laboratory manual*, 2 Ed., CSH Laboratory Press
31. Ryan, D. personal communication.
32. Thoden, J. B., Wesenberg, G., Raushel, F. M., & Holden, H. M. (1999) *Biochemistry* 38, 2347-2357.
33. Esser, L., Wang, C., Hosaka, M., Smagula, C. S., Sudhof, T. C., & Deisenhofer, J. (1998) *EMBO J.* 17, 977-984.
34. Moffet, F. J., & Bridger, W. A. (1970) *J. Biol. Chem.* 245, 2758-2762.
35. Luzzati, V. (1952) *Acta Cryst.* 5, 802-810.
36. Fan, C., Moews, P. C., Walsh, C. T., & Knox, J. R. (1994) *Science* 266, 439-443.
37. Hara, T., Kato, H., Katsube, Y., & Oda, J. (1996) *Biochemistry* 35, 11967-11974.
38. Connolly, M. L. (1983) *Science* 221, 709-713.
39. Fan, C., Moews, P. C., Shi, Y., Walsh, C. T., & Knox, J. R. (1995) *Proc. Natl. Acad. Sci. USA* 92, 1172-1176.
40. Kobayashi, N., & Go, N. (1997) *Eur. Biophys. J.* 26, 135-144.

41. Kobayashi, N., & Go, N. (1997) *Nat. Struct. Biol.* 4, 6-7.
42. Denessiouk, K. A., Lehtonen, J. V., & Johnson, M. A. (1998) *Prot. Sci.* 7, 1768-1771.
43. Denessiouk, K. A., Lehtonen, J. V., & Johnson, M. A. (1998) *Prot. Sci.* 7, 1136-1146.
44. McGuire, M., Huang, K., Kapadia, G., Herzberg, O., & Dunaway-Mariano, D. (1998) *Biochemistry* 37, 13463-13474.
45. Pai, E. F., Kregel, U., Petsko, G. A., Goody, R. S., & Kabsch, W. (1990) *EMBO Journal* 9, 2351-2359.
46. Jones, T. A., Zou, J. Y., Cowan, S. W., & Kjeldgaard, M. (1991) *Acta Cryst.* A47, 110-119.
47. Hildebrand, J. G., & Spector, L. B. (1969) *J. Biol. Chem.* 244, 2606-2613.
48. Vogel, H. J., Bridger, W. A., & Sykes, B. D. (1982) *Biochemistry* 21, 1126-1132.
49. Herzberg, O., Reedy, P., Sutrina, S., Saier, M. H., Reizer, J., & Kapadia, G. (1992) *Proc. Natl. Acad. Sci. USA* 89, 2499-2503.
50. Jia, Z., Quail, W., Waygood, B., & Dalbaere, L. T. J. (1993) *J. Biol. Chem.* 268, 22490-22501.
51. Moréra, S., Lascu, I., Dumas, C., LeBras, G., Brizzo, P., Véron, M., & Janin, J. (1994) *Biochemistry* 33, 459-567.
52. Herzberg, O., Chen, C. C. H., Kapadia, G., McGuire, M., Carroll, L., Noh, S. J., & Dunaway-Mariano, D. (1996) *Proc. Natl. Acad. Sci. USA* 93, 2652-2657.
53. Wedekind, J. E., Frey, P. A., & Rayment, I. (1996) *Biochemistry* 35, 11560-11569.



**Page intentionally left blank for note taking.**

## **Chapter Seven Conclusions and Final Discussion**

---

### **Summary**

The studies contained in this thesis revolved around the investigation of two major themes. The first theme of this thesis concerned the folding and stability of *T. aquaticus* SCS. The second and more prominent was an elucidation of the location of the nucleotide binding site, and evaluation of the role of some residues involved in substrate binding and catalysis by SCS.

*Folding and Stability of T. aquaticus SCS.* Comparison of the equilibrium unfolding of *T. aquaticus* SCS with that of *E. coli* SCS (1) indicated that the unfolding of the two enzymes was similar despite their differences in stability. Unlike equilibrium unfolding, the kinetics of the refolding of SCS from *T. aquaticus* were very different from those of *E. coli* or pig heart SCS (2-4). These results demonstrated that although the species present at equilibrium may be similar, the folding paths that the different enzymes take to reach those species are different (Chapter 3).

The thermodynamic parameters derived from studying the equilibrium unfolding of *T. aquaticus* SCS showed that although the *T. aquaticus* enzyme was more stable than the *E. coli* enzyme, it was still in the mid-range of the stability values of mesophilic proteins at room temperature (5). Thus, the stabilization of *T. aquaticus* SCS does not arise from a wholesale increase in the  $\Delta G_u^{\text{H}_2\text{O}}$ , but rather from a change in the dependence of the  $\Delta G_u^{\text{H}_2\text{O}}$  on temperature. Consistent with this, the amino acid substitutions that were observed when sequences of SCS enzymes of increasing stability were aligned and examined were not changes which would intuitively be thought to lead to an increase in stability. For example, there was no increase in the size of hydrophobic residues. Only a slight increase in the number of residues that could stabilize the secondary structure in which they occur. There was an increase in the number of potential ion pairs. However,

in staphylococcal nuclease, elimination of existing ion pairs had only a minor effect on the  $\Delta G_u^{H_2O}$  values (6). In addition, despite the recovery of activity and of quaternary structure, the refolding of *T. aquaticus* SCS in buffer containing arginine was not complete, and full recovery of enzymatic activity at high temperatures required a subsequent change in buffer (Chapter 3).

*The Nucleotide Binding Site of SCS.* The second and more prominent theme of this thesis concerned the location of the nucleotide binding site of SCS and the evaluation of residues involved in substrate binding and catalysis. To locate the nucleotide binding site, *E. coli* SCS was labeled with 8-N<sub>3</sub>-ATP and following tryptic digestion, labeled peptides were isolated and identified. Reference to the x-ray crystallographic structure of *E. coli* SCS (7, 8) revealed that the labeled peptides were located in the larger subdomain of the N-terminal domain of the  $\beta$ -subunit, far (approximately 35Å) from the location of the active site histidine (Chapter 4).

The nucleotide binding site in the N-terminal domain of the  $\beta$ -subunit was further examined by investigation of the role of residues predicted to be involved in nucleotide binding in the N-terminal domain of the  $\beta$ -subunit. Mutation of two residues (G53 $\beta$  and R54 $\beta$ ), that in the crystallographic structure of native *E. coli* SCS were involved in binding a sulfate ion in the N-terminal domain of the  $\beta$ -subunit, revealed that they were vital to the formation of a phosphorylated enzyme intermediate from nucleoside triphosphate, but were not required for the formation of phosphorylated enzyme from P<sub>i</sub> and succinyl-CoA. Mutation of another residue in the N-terminal domain of the  $\beta$ -subunit, Pro 20 $\beta$ , demonstrated that residues at this position play an important role in determining the nucleotide specificity of SCS (Chapter 5). In addition, the roles of residues in the C-terminal domain of the  $\beta$ -subunit were also examined. It was important to examine the role of these residues for three reasons: 1. ATP was remarkably specific in protecting SCS from inactivation by oxidized-CoA disulfide (ATP 4-10 times better than ADP or GTP at protecting *E. coli* SCS from inactivation. data not shown). Oxidized CoA disulfide (o-

CoAS<sub>2</sub>) binds to Cys 325 $\beta$ , which is in a Rossmann fold in the C-terminal domain of the  $\beta$ -subunit (9, 10). 2. ATP could be modeled into this domain with the  $\gamma$ -phosphate of ATP superimposed on the phosphate of the phosphohistidine. 3. At that time, crystals of phosphorylated SCS had been soaked with ADP and had resulted in the dephosphorylation of the enzyme without cracking the crystal (Chapter 6). At that point, it seemed probable that small conformational changes in the C-terminal domain of the  $\beta$ -subunit could occur in the crystal form. Mutagenesis of I322 $\beta$ , R324 $\beta$ , D326 $\beta$ , in the C-terminal domain (individually or in combination), was found to have a much more pleiotropic effect than those in the N-terminal domain. Mutations in the C-terminal domain affected primarily the substrate binding and/or catalysis of partial reactions involving succinyl-CoA and P<sub>i</sub> (Chapter 5). These results reduced the likelihood that the Rossmann fold in the C-terminal domain of the  $\beta$ -subunit was the nucleotide binding site of SCS.

Location of the nucleotide binding site in the N-terminal domain of the  $\beta$ -subunit of SCS was proven by soaking *E. coli* SCS crystals with high concentrations of ADP and Mg<sup>2+</sup> ions. Additional electron density observed in the N-terminal domain could be fitted and refined by an ADP·Mg<sup>2+</sup> complex (Chapter 6). Subsequent comparison of the nucleotide binding site in SCS to the nucleotide binding sites in other proteins, based on the position of the bound nucleotide, revealed that seemingly unrelated protein folds often utilize similar residues in similar positions to bind the nucleotide.

In SCS, a consequence of the nucleotide binding in the N-terminal domain of the  $\beta$ -subunit is that the phosphohistidine loop must swing between two sites during a catalytic cycle. Site I is delineated by the location of the CoA molecule and the active site histidine residue seen in the crystallographic structures of SCS (7, 8). Site I is located between the C-terminal domains of a  $\beta$ -subunit and  $\alpha$ -subunit in an  $\alpha\beta$ -dimer. This is where reactions involving CoA, P<sub>i</sub>, and presumably succinate take place (partial reactions (2) and (3) from Chapter 1). Site II is 35Å away from site I in the N-terminal domain of the  $\beta$ -subunit, delineated by the location of the nucleotide binding site. Site II is where the reaction

involving nucleotide take place (partial reaction (1) from Chapter 1). A hypothetical model of the His 246 $\alpha$  loop down in site II was constructed. This model predicted a role for a number of conserved residues in stabilizing the loop in site II. Amongst these residues was Glu 197 $\beta$ , which had been previously predicted to play a similar role in site II as Glu 208 $\alpha$  did in site I (8). In site I, the sidechain oxygen atom of Glu 208 $\alpha$  makes a hydrogen bond to the N $\delta$ 1 atom of the active site histidine, ensuring that the free pair of electrons reside on the N $\epsilon$ 2 atom (Fig. 1-7 and 6-2). In proteins that have a covalently modified histidine at the active site, the presence of a residue that makes a hydrogen bond with the unmodified nitrogen atom of the active site histidine seems to be a general requirement (11-15). As described in Chapter 6, mutagenesis of Glu 208 $\alpha$  in site I, or Glu 197 $\beta$  in site II revealed each could fulfill this requirement on the formation of the phosphoenzyme intermediate from the appropriate substrates (P, and succinyl-CoA, at site I, and ATP or GTP, at site II, Chapter 6).

## Significance and Future Perspectives

*Investigation of the Folding of T. aquaticus SCS.* The folding process of oligomeric proteins has been proposed to consist of three phases, the partial folding of monomeric units preceding the assembly of these units into immature oligomers, and the further folding of the immature oligomers into the native state (16, 17). In the case of *T. aquaticus* SCS, the refolding (as measured by the recovery of enzymatic activity) is not concentration dependent. Thus, the first phase, the initial folding of the monomeric units (the  $\alpha$ - and  $\beta$ -subunits), must be the rate limiting step in the overall folding of *T. aquaticus* SCS. Therefore, the second phase, the assembly of the monomeric units into oligomeric protein, occurs much faster than the initial folding of the monomeric units. This hypothesis is consistent with the observation that the secondary structure of isolated individual subunits (as measured by far-UV CD) closely resembles that of the subunits in whole enzyme. These results indicate that the third phase, the folding that is subsequent to the

assembly of the subunits is relatively minor. This may be a general characteristic of thermophilic proteins, because a protein that acquires most of its secondary structure after association has been predicted to be prone to aggregation (18). Aggregation is expected to be a greater problem in thermophiles than in mesophiles because of the higher growth temperature.

The incomplete refolding of *T. aquaticus* SCS in arginine buffers is of particular interest to those who are interested in refolding proteins that have been purified from inclusion bodies, some of which are used in clinical applications (reviewed in (19, 20)). Despite the full recovery of activity at room temperature and the recovery of the correct quaternary structure, *T. aquaticus* SCS was no longer thermostable. This is the third example of a protein that regains its activity prior to the recovery of the true native structure (21-23). These studies demonstrate the danger of using the recovery of enzymatic activity as a measure of the recovery of the native structure, and illustrates the need for complete characterization of refolded proteins prior to their use, especially in clinical applications.

*Comparison of the Folding of Thermophilic and Mesophilic SCS.* Recent proposals for the existence of discrete folding units and the mechanism for the early stages of protein folding have implied that proteins which have the same secondary and tertiary structure should also fold in the same manner, regardless of the final stability of the protein (24-26). Studies comparing the kinetics of unfolding and refolding of mesophilic and thermophilic Csp B have shown that this is indeed the case for this small, all  $\beta$ -structure protein (27). The equilibrium unfolding of *T. aquaticus* SCS resembles that of *E. coli* SCS, implying that the intermediates that are present at equilibrium are similar regardless of the stability of the protein. The nature of the intermediates that are present during the unfolding of *E. coli* and *T. aquaticus* SCS need to be further investigated to confirm this. When the kinetics of refolding were investigated using the recovery of activity as a measure of refolding, the refolding of *T. aquaticus* SCS was not in any way similar to that of either *E. coli* or pig heart SCS. These results indicated that, contrary to the implications of recent

hypotheses about the mechanism of protein folding, the refolding of SCS was not determined by the secondary and tertiary structure of the enzyme (assuming that the structure of the *T. aquaticus* enzyme resembles that of the *E. coli* enzyme). However, the recovery of activity occurs very late in protein folding, and the early events of folding may yet be similar. The early kinetics of protein folding can be monitored using a stopped flow apparatus which measures either CD (secondary structure) or fluorescence (aromatic groups in the protein core).

The thermodynamic parameters that were derived from the unfolding studies of *T. aquaticus* SCS indicated that although the thermophilic enzyme was more stable than the mesophilic enzyme, the value for  $\Delta G_u^{H_2O}$  was still in the mid-range of values reported for protein stabilities. This observation has now been made for several thermophilic proteins (28-30, 27, 31), and indicated that the *T. aquaticus* SCS is stabilized not by a general increase in stability of the folded protein, but by a change in the temperature dependence of the  $\Delta G_u^{H_2O}$ . In view of these findings, investigations which examine the effect of different amino acid substitutions on the stability of proteins and peptides should be expanded to examine the effects of these substitutions on the temperature dependence of  $\Delta G_u^{H_2O}$ . The amino acid substitutions that are observed in thermophilic proteins could be used as a guide for these investigations.

*The Substrate Binding Sites of SCS.* The studies on the location of the nucleotide binding site in SCS have identified the second of three substrate binding sites. The binding site for the third substrate, succinate, has been not been found yet. To locate this binding site, the tetrahedral hemithioacetal formed from succinic semialdehyde and CoA could be used in place of CoA when growing crystals under the same conditions as for the native enzyme (7). This transition state analogue had a  $K_i$  of 4.3  $\mu\text{M}$  with SCS (32).

*Comparison of the Catalytic Mechanism of SCS to that of Other Synthetases and Phosphotransferases.* The location of the nucleotide binding site in the N-terminal domain of the  $\beta$ -subunit, 35Å from site I requires that a conformational change occur during each

cycle of catalysis to shuttle the His 246 $\alpha$  loop between sites I and II. This places SCS among a growing number of enzymes that require intermediates generated at one site to traverse large distances before reaction at a second site (14, 33). In SCS and pyruvate phosphate dikinase, a covalently linked histidine is used to transfer phosphoryl groups to other substrates, and in carbamoyl phosphate synthetase, the intermediates diffuse between active sites separated by 96Å. This is unlike other synthetases and ligases where the first substrate is either adenylated or phosphorylated directly, and the adenylyl or phosphoryl group subsequently acts as a leaving group for the incoming substrate, all at a single active site (34-41). These enzymes often have a loop that shields the active site from bulk water, and prevents the intermediates from escape. Since the loop over the active site often interacts with the substrates, it is likely that the presence of all substrates in the active site is required for the formation of an active site conformation that can catalyze the initial phosphoryl transfer (34, 35). For example, in GMP synthetase each of the three substrates is bound in a separate domain, and substrate binding of one of the substrates (XMP) has been proposed to lead to the formation of a closed complex that is catalytically competent (37). In SCS, the formation of a stable phosphorylated intermediate (phosphohistidine) allows the enzyme to react in either direction with the availability of substrates. This is consistent with the proposed metabolic roles of SCS, functioning in one direction to generate NTP in the citric acid cycle, and in the other to generate succinyl-CoA in ketone body metabolism and in biosynthesis.

*Investigation of the Proposed Conformational Change in SCS.* The large conformational change that would be required to complete a catalytic cycle needs further investigation. Which residues are responsible for stabilizing the His 246 $\alpha$  loop in each of the two active sites? What is the "trigger" that induces this loop to move to its location in site II? Using the ability of NTP to phosphorylate SCS as an assay, the effect of mutations in site I and II either directly on the catalytic steps, or on the movement of the loop cannot be distinguished.



The solution of the structure of SCS with the His 246 $\alpha$  loop down in site II by x-ray crystallography would identify the residues involved in the conformational change and those involved in the catalysis of partial reaction (1) at site II. Mutagenesis of specific residues that are thought to stabilize the His 246 $\alpha$  loop in site I, as seen in the crystallographic structures of SCS, may help to destabilize the loop in this position sufficiently for SCS to be crystallized with the loop down in site II. The co-crystallization of dephosphorylated SCS in the presence of non-hydrolyzable (AMPPNP or AMPPCP) and transition state analogues (ADP + AlF<sub>4</sub><sup>-</sup> or NO<sub>3</sub><sup>-</sup>) of ATP may also favor the conformation of SCS with the loop in site II. However, crystals of SCS in the presence of ATP or ADP of sufficient quality have been difficult to obtain. In this vein, one of the original reasons for cloning SCS from *T. aquaticus* was to obtain sufficient quantities for crystallization. This has now been done (Chapter 2). It is thought that thermostable enzymes crystallize more readily than their mesophilic counterparts. Thus, suitable crystals of the thermophilic enzyme in the presence of analogues of ATP may be obtained. In addition, the ability of *E. coli* SCS to be dephosphorylated while in the crystal form (Chapter 6) makes it a good candidate for kinetic crystallography, perhaps using 'caged' ATP analogues (42, 43, 39).

In the absence of a crystallographic structure of the His 246 $\alpha$  loop down in site II, the questions posed at the beginning of this section can be answered in two ways. The first is using phosphorus NMR. Vogel and Bridger found NMR evidence for two exchanging conformations of the phosphohistidine in SCS (44). The addition of a competitive inhibitor of succinate, 2,2' difluorosuccinate, and CoA induced a single conformation (44). The second conformation alone could not be detected because the NMR signal from the terminal phosphate group of ATP or ADP overlapped with the phosphohistidine signal (44). This problem may be avoided by using the ADP analogue ADP- $\beta$ S. ADP- $\beta$ S is an inhibitor of SCS (assayed in the direction of succinyl-CoA synthesis) that is competitive with ATP, and has an associated value of  $K_{i(\text{app})}$  of 137  $\mu\text{M}$  (data not shown). In addition, it is not a

substrate for the enzyme in the direction of ATP synthesis (data not shown). The presence of a sulphur atom on the terminal phosphate group of ADP should shift the NMR signal sufficiently to allow detection of the second conformation of the phosphohistidine. In combination with site-directed mutagenesis the role of residues suggested by the hypothetical model in Chapter 6 can be ascertained.

The second method that could be used to investigate the conformational changes in SCS involves the use of synthetic peptides which resemble the His 246 $\alpha$  loop. If a synthetic peptide that resembles the loop could be phosphorylated by SCS, the residues that are involved in the catalysis of phosphoryl transfer and those that are involved in binding the loop could be easily distinguished because peptide binding and phosphorylation could be examined separately. In order for SCS to be able to phosphorylate the synthetic peptide, the His 246 $\alpha$  loop must be first removed. The His 246 $\alpha$  loop of SCS does not have any definite secondary structure (7, 8), and resembles a forearm with each strand of the loop on either side of the arm, and the phosphohistidine located at the fingertips (Fig. 4-7). At the elbow of the forearm, the two strands of the active site loop are close together, and a deletion (actually a substitution of 2-4 glycine residues for the residues from 235 $\alpha$  to 256 $\alpha$ ) of the active site loop could be made here without much disruption of the secondary structure. Synthetic peptides could then be made and the affinity of various peptides for the enzyme, and the ability of the enzyme to phosphorylate these peptides could be easily examined. In combination with site specific mutagenesis, this could provide a quick and easy method for the examination of residues involved in the conformational change.

Many of the residues that are implicated by the hypothetical model to stabilize the His 246 $\alpha$  loop in site II (Chapter 6) are candidates for mutagenesis, as are the residues that interact with the loop when it is up in site I as seen in the crystal structures. The effect of the E208 $\alpha$ Q and E197 $\beta$ Q mutations on the conformation of the active site loop could be studied using either of the methods outlined above. Good candidates for residues involved in triggering the conformational change are Glu 134 $\beta$ , and Asp 115 $\beta$  which are well

conserved in all SCS species, but do not seem to be fulfilling any function in the nucleotide binding site. Glu 134 $\beta$  resides in the loop in SCS that is analogous to the loop in DD-ligase which closes over the nucleotide binding site (Fig. 6-20) (34). In the hypothetical model with the His 246 $\alpha$  down in site II, the side chain of Glu 134 $\beta$  can interact with the main chain nitrogen atoms of residues Ala 247 $\alpha$  and/or Gly 248 $\alpha$ . Asp 115 $\beta$  resides at the end of a strand in the  $\beta$ -sheet that forms the core of the larger subdomain of the N-terminal domain of the  $\beta$ -subunit. In the hypothetical model Asp 115 $\beta$  is approximately 5 Å from Lys 255 $\beta$  which is conserved in SCS from eubacterial and mammalian species. This strand (that Asp 155 $\beta$  is on) is next to the strand that contains cis-proline 200 $\beta$ , the carbonyl of the preceding residue coordinates the Mg<sup>2+</sup> and thus could respond to bound nucleotide triphosphate bringing it closer to Lys 255 $\beta$  and thus stabilizing the loop in site II.

*Investigation of Residues Directly Involved in Catalysis by SCS.* The role of a number of residues in catalysis was examined by site-directed mutagenesis. Gly 53 $\beta$  and/or Arg 54 $\beta$  were shown to be essential to phosphoryl transfer from ATP to the active site histidine (Chapter 5). The structure of the ADP-bound form of SCS revealed that the main chain nitrogen atom of Gly 53 $\beta$  made a hydrogen bond with an oxygen atom on the  $\beta$ -phosphate and the side chain of Arg 54 $\beta$  made ionic interactions with the  $\alpha$ - and  $\beta$ -phosphate groups of ADP (Chapter 6). When ATP and the active site histidine are in site II, the sidechain of Arg 54 $\beta$  may move to aid in the transfer of the  $\gamma$ -phosphate of ATP to the histidine.

The role of a glutamate in each of site I (Glu 208 $\alpha$ ) and site II (Glu 197 $\beta$ ) was also examined. An acidic sidechain was found to be essential for phosphoryl transfer at the appropriate site. Clearly, the role of other residues in catalysis should be examined. Specifically, the role of Ser 153 $\alpha$ , which changes conformation to form a hydrogen bond with the free phosphate in dephosphorylated enzyme (Chapter 6) can be examined by mutagenesis to alanine. The binding of phosphate can then be measured by equilibrium

dialysis. The partial reactions catalyzed by SCS (see Chapter 1) can also be probed by phosphorylation of the mutant enzyme with either nucleoside triphosphate, or succinyl-CoA and  $P_i$ . The partial reactions can be further dissected by studying the phosphorylation of the mutant enzyme by succinyl-phosphate (45, 46), and the dephosphorylation by ADP (to make ATP), or by succinate and dethioCoA (to make succinyl-phosphate), or by succinate and CoA (to make succinyl-CoA) (47, 48).

Another candidate for examination is Cys 123 $\alpha$ , which is found in a covalent linkage to CoA in the ADP-bound form of SCS (Chapter 6). The final step in the reaction of SCS in the direction of succinyl-CoA formation is the displacement of the phosphoryl group from succinyl-phosphate by the thiol group of CoA (Fig. 1-7) (49). Nucleophilic attack of the thiol group of CoA on the carbonyl group of succinyl-phosphate requires deprotonation of the thiol, and Cys 123 $\alpha$  is the only appropriate residue in a position to perform this role. A coordinated six atom reaction scheme can be envisioned (Fig 7-1), where the sidechain of Cys 123 $\alpha$  removes the proton from the thiol of CoA, the sulphur atom of CoA attacks the carbonyl oxygen of succinyl-phosphate, and the oxyanion so generated abstracts the proton from Cys 123 $\alpha$ . When the oxyanion collapses, the proton is taken by the departing phosphate group. This scheme explains the conservation of Cys 235 $\alpha$  in different species of SCS. Amino acid sequence alignments show that this residue is usually cysteine but can be serine or threonine. Thus, the covalent bond between Cys 123 $\alpha$  and the thiol of the CoA molecule in the ADP-bound form of SCS is an artifact due to the lack of reducing agent in the soak conditions, but is reflective of the proximity and reactivity of Cys 123 $\alpha$ . If Cys 123 $\alpha$  is important in the last step of the reaction mechanism, then phosphorylation and dephosphorylation of the enzyme by succinyl-CoA and  $P_i$ , and by succinate and CoA, respectively should be the only partial reactions that are inhibited by mutation of this residue to alanine. Phosphorylation of mutant enzyme by NTP or succinyl-phosphate should not be affected, nor should the dephosphorylation of the enzyme by desulfo-CoA and succinate (forming succinyl-phosphate).

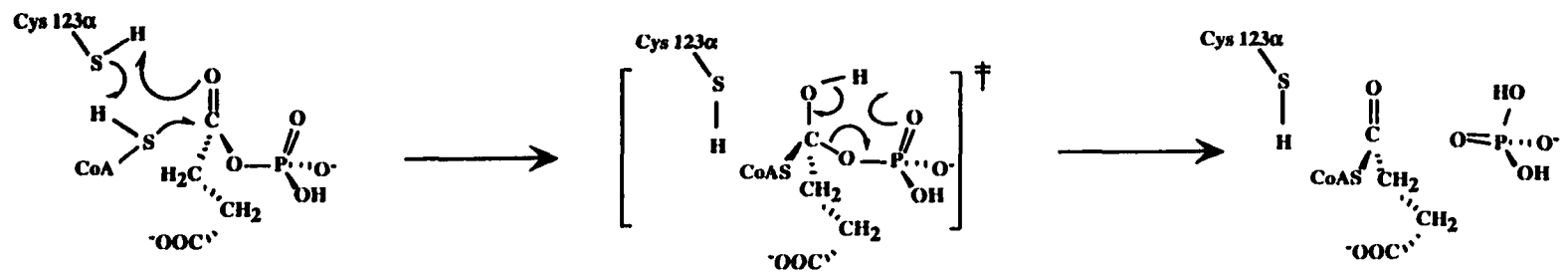


**Figure 7-1. Proposed mechanism of the nucleophilic attack of the thiol group of CoA on succinyl-phosphate. The arrows indicate the direction of electron flow.**

*Investigation of the Function of the Rossmann Fold in the C-terminal Domain of the  $\beta$ -subunit.* The location of the catalytic nucleotide binding site in the N-terminal domain of the  $\beta$ -subunit leaves open the following question: What is the function, if any, of the Rossmann fold in the C-terminal domain of the  $\beta$ -subunit? The first experiments that were conducted to investigate the nucleotide binding site of SCS used oxidized CoA disulfide, and were not included in this thesis. These experiments provided hints that the nucleotide binding site was not in the Rossmann fold in the C-terminal of the  $\beta$ -subunit, proximal to the phosphohistidine. Furthermore they indicated that this Rossmann fold may have a function.

Previous investigations had shown that oxidized CoA disulfide (o-CoAS<sub>2</sub>) inhibits SCS by binding in the C-terminal domain of the  $\beta$ -subunit (9, 10). In *E. coli* SCS, ATP protected the enzyme from this inactivation by o-CoAS<sub>2</sub>. In addition, this protection was very specific for ATP: the presence of ATP in the inactivation reaction reduced the initial rate of inactivation by 20 times, while the presence of ADP or GTP at the same concentrations only reduced the initial rate of inactivation by 5 or 2 times, respectively (data not shown). Although the relative degree of protection provided by ATP and GTP reflected the relative values of the  $K_m$  for ATP and GTP, the relative degree of protection provided by ATP and ADP was not consistent with the relative  $K_m$  values for ATP and ADP, which are approximately the same (Table 1-2). When the same experiments were done using GDP/GTP-specific pig heart SCS, the pattern of protection was the same. ATP still protected the enzyme from inactivation by o-CoAS<sub>2</sub> to a much greater extent than GTP or ADP did. The protection of pig heart SCS by ATP was remarkable because, in spectrophotometric assays of the activity of pig heart SCS, the inhibition of succinyl-CoA production by ATP could not be detected. These results indicated: 1. Since the protection of *E. coli* and pig heart SCS by ATP or GTP did not match the nucleotide specificity of the two enzymes, and o-CoAS<sub>2</sub> had been shown to bind in the C-terminal domain of the  $\beta$ -subunit, the catalytic nucleotide binding site did not reside in the C-terminal domain of the

$\beta$ -subunit. 2. ATP binds to GDP/GTP-specific pig heart SCS, possibly in the C-terminal domain of the  $\beta$ -subunit.

Since there was an indication that ATP was binding to the GTP/GDP-specific pig heart enzyme, the question became: what was it doing? Some preliminary experiments were performed to answer this question. Since only relatively low concentrations of NTP can be used in the spectrophotometric assay (up to approximately 400  $\mu$ M), the phosphorylation of pig heart SCS (by GTP or by succinyl-CoA and  $P_i$ ) was used to examine the effect of higher concentrations of ATP on pig heart SCS. Phosphorylation of pig heart SCS by  $P_i$  and succinyl-CoA was inhibited in a sigmoidal manner by ATP, with a complete loss in activity between 0.75 and 1.5 mM ATP (data not shown). Phosphorylation of pig heart SCS by GTP was inhibited more gradually by ATP concentrations between 0.75 and 3.0 mM (data not shown). This is the first indication that SCS is inhibited by non-substrate nucleotides, and should be investigated further by using kinetic studies and site directed mutagenesis. The inhibition of GDP/GTP-specific pig heart SCS by ATP is consistent with the proposed role for the enzyme in ketone body metabolism, shutting down the utilization of ketone bodies when the intracellular concentration of ATP reaches a sufficient level. To aid the investigation of the function of the C-terminal domain of the  $\beta$ -subunit in pig heart SCS, the mutations A326 $\beta$ D, and N324 $\beta$ R-A326 $\beta$ D that were constructed in the Rossmann fold in the C-terminal domain of the  $\beta$ -subunit, should be studied further (the numbering system for the residues is that in *E. coli* SCS).

*The End.*

**References:**

1. Kahn, I. A., & Nishimura, J. S. (1988) *J. Biol. Chem.* 263, 2152-2158.
2. Pearson, P. H., & Bridger, W. A. (1975) *J. Biol. Chem.* 250, 4451-4455.
3. Wolodko, W. T., & Bridger, W. A. (1987) *Biochem. Cell Biol.* 65, 452-457.
4. Nishimura, J. S., Ybarra, J., Mitchell, T., & Horowitz, P. M. (1988) *Biochem. J.* 250, 429-434.
5. Pace, C. N. (1990) *Trends Biotechnol.* 8, 93-98.
6. Meeker, A. K., Garcia-Moreno, E., & Shortle, D. (1996) *Biochemistry* 35, 6443-6449.
7. Wolodko, W. T., Fraser, M. E., James, M. N. G., & Bridger, W. A. (1994) *J. Biol. Chem.* 269, 10883-10890.
8. Fraser, M. E., James, M. N. G., Bridger, W. A., & Wolodko, W. T. (1999) *J. Mol. Biol.* 285, 1633-1653.
9. Collier, G. E., & Nishimura, J. S. (1978) *J. Biol. Chem.* 253, 4938-4943.
10. Mann, C. J., Hardies, S. C., & Nishimura, J. S. (1989) *J. Biol. Chem.* 264, 1457-1460.
11. Herzberg, O., Reedy, P., Sutrina, S., Saier, M. H., Reizer, J., & Kapadia, G. (1992) *Proc. Natl. Acad. Sci. USA* 89, 2499-2503.
12. Jia, Z., Quail, W., Waygood, B., & Dalbaere, L. T. J. (1993) *J. Biol. Chem.* 268, 22490-22501.
13. Moréra, S., Lascu, I., Dumas, C., LeBras, G., Brizzo, P., Véron, M., & Janin, J. (1994) *Biochemistry* 33, 459-567.
14. Herzberg, O., Chen, C. C. H., Kapadia, G., McGuire, M., Carroll, L., Noh, S. J., & Dunaway-Mariano, D. (1996) *Proc. Natl. Acad. Sci. USA* 93, 2652-2657.
15. Wedekind, J. E., Frey, P. A., & Rayment, I. (1996) *Biochemistry* 35, 11560-11569.
16. Jaenicke, R. (1987) *Prog. Biophys. Mol. Biol.* 49, 117-237.
17. Jaenicke, R. (1991) *Biochemistry* 30, 3147-3161.
18. Jaenicke, R., & Rudolf, R. (1986) *Methods Enzymol.* 131, 218-250.
19. Guise, A. D., West, S. M., & Chaudhuri, J. B. (1996) *Mol. Biotech.* 6, 53-63.
20. Mukhopadhyay. (1997) *Biotechnology* 56, 61-106.
21. Hattori, M., Ametani, A., Katakura, Y., Shimizu, M., & Kaminogawa, S. (1993) *J. Biol. Chem.* 268, 22414-22419.



22. Subramaniam, v., Bergenham, N., Gafni, A., & Steel, D. G. (1995) *Biochemistry* 34, 1133-1136.
23. Subramaniam, v., Steel, D. G., & Gafni, A. (1996) *Prot. Sci.* 5, 2089-2094.
24. Tsai, C., & Nussinov, R. (1997) *Prot. Sci.* 6, 24-42.
25. Baldwin, R. L., & Rose, G. D. (1999) *Trends Biochem. Sci.* 24, 26-33.
26. Baldwin, R. L., & Rose, G. D. (1999) *Trends Biochem. Sci.* 24, 77-83.
27. Perl, D. e. a. (1998) *Nat. Struct. Biol.* 5, 229-235.
28. Nojima, H., Ikai, A., Oshima, T., & Noda, H. (1977) *J. Mol. Biol.* 116, 429-442.
29. Knapp, S., Karsikoff, A., Berndt, K. D., Christova, P., Atanasov, B., & Ladenstein, R. (1992) *J. Mol. Biol.* 264, 1132-1144.
30. McCrary, B. S., Edmonstom, S. P., & Shriver, J. W. (1996) *J. Mol. Biol.* 264, 784-805.
31. Beadle, B. M., Base, W. A., Wilson, D. B., Gilkes, N. R., & Shoichet, B. K. (1999) *Biochemistry* 38, 2570-2576.
32. Schwartz, B., Vogel, K. W., & Drueckhammer, D. G. (1996) *J. Org. Chem.* 61, 9356-9361.
33. Thoden, J. B., Holden, H. M., Wesenberg, G., Raushel, F. M., & Rayment, I. (1997) *Biochemistry* 36, 6305-6316.
34. Fan, C., Moews, P. C., Walsh, C. T., & Knox, J. R. (1994) *Science* 266, 439-443.
35. Hara, T., Kato, H., Katsube, Y., & Oda, J. (1996) *Biochem.* 35, 11967-11974.
36. Poland, B. W., Fromm, H. J., & Honzatko, R. B. (1996) *J. Mol. Biol.* 264, 1013-1027.
37. Tesmer, J. G., Klem, T. J., Deras, M. L., Davisson, V. J., & Smith, J. L. (1996) *Nat. Struct. Biol.* 3, 74-86.
38. Berry, M. B., & Phillips, G. N. (1998) *Proteins* 32, 276-288.
39. Kack, H., Gibson, K. J., Lindqvist, Y., & Schneider, G. (1998) *Proc. Natl. Acad. Sci. USA* 95, 5495-5500.
40. Rizzi, M., Bolognesi, M., & Coda, A. (1998) *Structure* 6, 1129-1140.
41. Schmitt, E., Moulinier, L., Fujiwara, S., Imanaka, T., Thierry, J. C., & Moras, D. (1998) *EMBO J.* 17, 5227-5237.
42. Schlichting, I., Almo, S. C., Rapp, G., Wilson, K., Kyriakos, P., Lentfer, A., Wittinghofer, A., Kabsch, W., Pai, E. F., Petsko, G. A., & Goody, R. S. (1990) *Nature* 345, 309-345.

43. Cepus, V., Ulbrich, C., Allin, C., Troullier, A., & Gerwert, K. (1998) *Methods. Enzymol* 291, 223-245.
44. Vogel, H. J., & Bridger, W. A. (1982) *J. Biol. Chem.* 257, 4834-4842.
45. Nishimura, J. S., & Meister, A. (1965) *Biochemistry* 4, 1457-1462.
46. Hildebrand, J. G., & Spector, L. B. (1969) *J. Biol. Chem.* 244, 2606-2613.
47. Grinnell, F., & Nishimura, J. S. (1969) *Biochemistry* 8, 4126-4130.
48. Wolodko, W. T., Brownie, E. R., O'Connor, M. D., & Bridger, W. A. (1983) *J. Biol. Chem.* 258, 14116-14119.
49. Bridger, W. A. (1974) in *The Enzymes* (Boyer, P. D., ed) Vol. X, 3 Ed., pp. 581-606, Academic Press Inc., New York

Appendix 1. Table of Data Base Accession Numbers for Subunits of SCS <sup>a</sup>

Abbreviation	Species	$\alpha$ -subunit	$\beta$ -subunit
ARATH1	<i>Arabidopsis thaliana</i> 1	X69138	AJ001808
ARATH2	<i>Arabidopsis thaliana</i> 2	AJ001807	-
ARCFL1	<i>Archaeoglobus fulgidus</i> 1	AE000996	AE000996
ARCFL2	<i>Archaeoglobus fulgidus</i> 2	AE000954	AE000954
AQUAE1	<i>Aquifex aeolicus</i> 1	AE000748	AE000748
AQUAE2	<i>Aquifex aeolicus</i> 2	AE000761	AE000733
BACSU	<i>Bacillus subtilis</i>	P80865	P80886
CAEEL1	<i>Caenorhabditis elegans</i> 1	M88968	Z68004
CAEEL2	<i>Caenorhabditis elegans</i> 2	AF003389	P53589
CHLTR	<i>Chlamydia trachomatis</i>	AE001354	AE001354
COXBU	<i>Coxiella burnetii</i>	P53591	X77919
DICDI	<i>Dictyostelium discoideum</i>	S65966	-
ECOLI1	<i>Escherichia coli</i> 1	AE000176	P07460
ECOLI2	<i>Escherichia coli</i> 2	P77187	-
HAEIN	<i>Haemophilus influenzae</i>	U32799	U32799
HUMAN-A	Human ADP/ATP	-	AF058953
HUMAN-G	Human GDP/GTP	-	AF058954
METTH	<i>Methanobacterium thermoautotrophicum</i>	AE000839	AE000875
METJA	<i>Methanococcus jannachii</i>	E64455	Q57663
Malate	<i>Methylobacterium extorquens</i> (Malate thiokinase)	C55230	P53594
MOUSE-A	Mouse ADP/ATP	-	AF058955
MOUSE-A	Mouse GDP/GTP	-	AF058956
MYCTU	<i>Mycobacterium tuberculosis</i>	P71558	P71559
NEOFR	<i>Neocallimastix frontalis</i>	-	X84222
PIG-A	Pig ADP/ATP	-	AF061966
PIG-G	Pig GDP/GTP	-	P53590
PIG57	Pig heart 57	AF008588	-
PIG108	Pig heart 108	AF008589	-
BIRD	Pigeon	AF035394	-
BIRD-A	Pigeon ADP/ATP	-	AF043540
BIRD-G	Pigeon GDP/GTP	-	AF043541
PYRHO	<i>Pyrococcus horikoshii</i>	AP000007	-
RAT	Rat	P13086	-
RICPR	<i>Rickettsia prowazekii</i>	O08371	O05966
SACCE	<i>Saccharomyces cerevisiae</i>	S61696	P53312
SCHPO	<i>Schizosaccharomyces pombe</i>	Z98529	AL034491
STRCO	<i>Streptomyces coelicolor</i>	AL031013	AL031013
	<i>Synechocystis</i> sp	D90913	D90901
THEAQ	<i>Thermus aquaticus</i>	X56033	S15950
THEFL	<i>Thermus aquaticus flavus</i>	X54073	X54073
TRIVA1	<i>Trichomonas vaginalis</i> 1	U87096	U87093
TRIVA2	<i>Trichomonas vaginalis</i> 2	U87097	U87094
TRIVA3	<i>Trichomonas vaginalis</i> 3	U87098	U87095

<sup>a</sup> Accession numbers are from the following data banks: beginning in A or U, GenBank<sup>TM</sup>; beginning in P or O, Swiss-Prot; beginning in M, X, or Z, EMBL; beginning in C, E, or S, PIR.

## Appendix 2.

Strains of *E. coli*

JM103 (*endA1, hsdR, supE, sbcBC, thi-1, strA, Δ(lac-pro), F'[traD36, lacI<sup>q</sup>ZΔM15, proAB<sup>+</sup>]*)<sup>a</sup>

BL21(DE3) (*hsdS gal[λcIts857 ind1 Sam7 nin5 lacUV5-T7 gene1]*)<sup>b</sup>

TK3D18 (*Δ(kdp-suc)D18 Δ(gal-bio)*)<sup>c</sup>

Y1090 (*Δ(lac)U169, Δ(lon), araD139, strA, supF, mcrA, trpC22::Tn10, pMC9*)

XL1-Blue (*recA1, endA1, gyrA96, thi-1, hsdR17, supE44, relA1, lac [F' proAB lacI<sup>q</sup>Z ΔM15 Tn10 (tet<sup>r</sup>)]*)

INVα-F' (*F' endA1, recA1, hsdR17 (r<sub>k</sub><sup>-</sup> m<sub>k</sub><sup>+</sup>), supE44, thi-1, gyrA96, relA1, Ø80lacZΔM15, Δ(lacZYA-argF)U169*)

<sup>a</sup> Used for propagation and sequencing of plasmid DNA.

[Hanrahan, D. (1983) *J. Mol. Biol.*, 166, 557-580]

<sup>b</sup> Used for expression of cDNA inserts cloned into expression vectors.

[Studier, F. W., & Moffatt, B. A. (1986) *J. Mol. Biol.*, 189, 113-130]

<sup>c</sup> Used for expression of cDNA inserts cloned into expression vectors.

[Froelich, B. & Epstein, W. (1981) *J. Bacteriol.*, 147, 1117-1120]

## Appendix 3

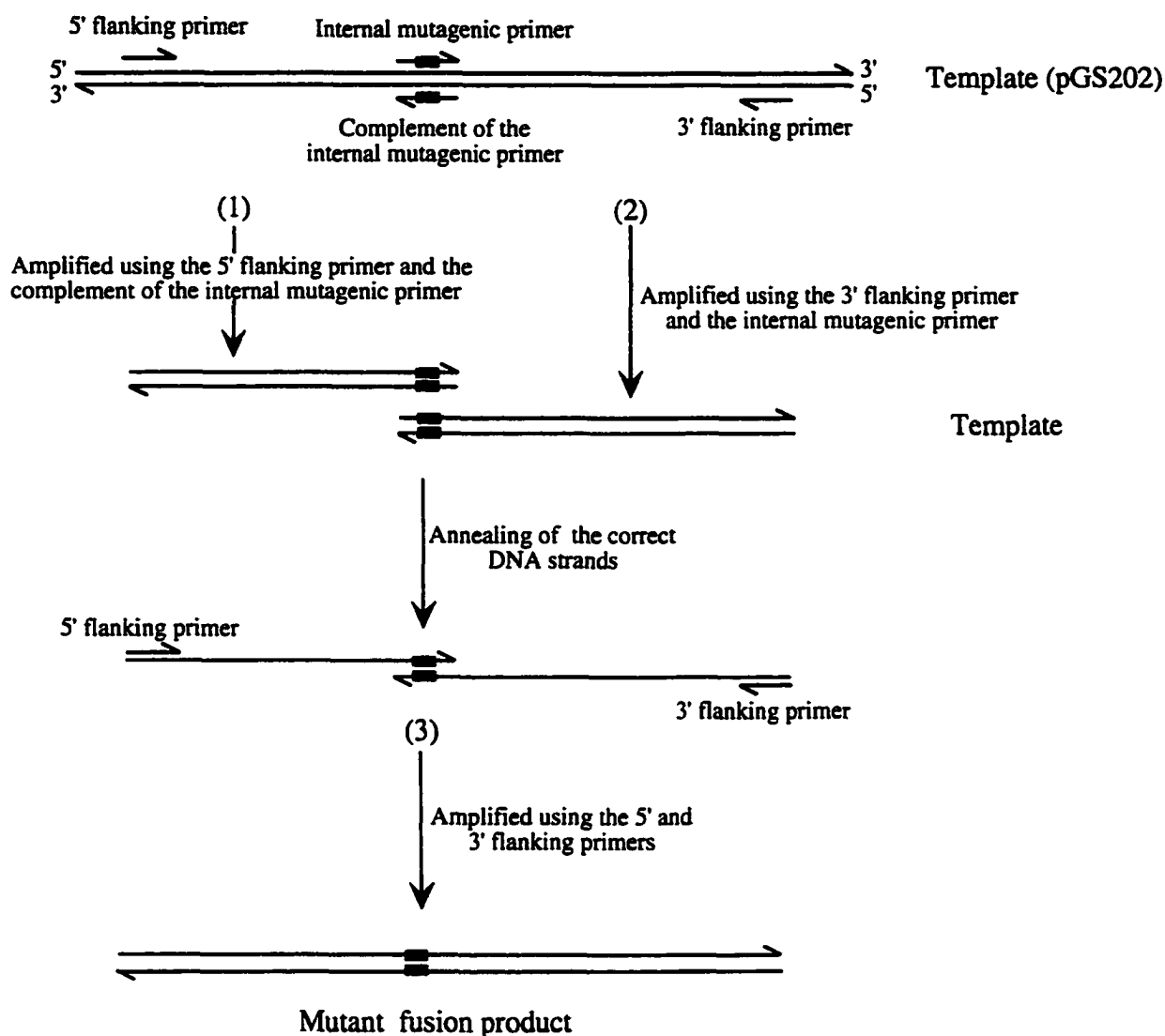


Diagram of site-directed mutagenesis by overlap extension. The site of mutagenesis is indicated by the small closed rectangle. The 3' ends of the DNA strands are indicated by the arrow heads. The primers are represented by short black arrows. In the first step, two separate PCR reactions are carried out. In the first reaction (1), the left half of the mutant fusion product is amplified. In the second reaction (2), the right half of the mutant fusion product is amplified. Following amplification, the two fragments are purified by agarose gel electrophoresis and used as the template for the third PCR reaction (3). The DNA strands which anneal to give the full length mutant fusion product are shown in blue.

## Appendix 4.

Residues Used in the Structural Alignment of the Small Subdomain of the N-terminal Domain of the  $\beta$ -subunit of *E. coli* SCS with DD-ligase.<sup>ab</sup>


---

DD-ligase	2	TDKI	5
<i>E. coli</i> SCS	A206	IGEI	A209
DD-ligase	45	VDVTQ	49
<i>E. coli</i> SCS	B284	ANFLD	B288
DD-ligase	95	MDKLRSKLLWQGAGLPVAPWVALTR	119
<i>E. coli</i> SCS	B3	LHEYQAKQLFARYGLPAPVGYACT	B27
DD-ligase	136	ALGLPVIVKPSR	147
<i>E. coli</i> SCS	B38	IGAGPWVVKCQV	B49
DD-ligase	153	GMSKVVAENALQDALRL	169
<i>E. coli</i> SCS	B59	GVKVVNSKEDIRAFEN	B75
DD-ligase	174	DEEV LIEK WLSGP	186
<i>E. coli</i> SCS	B93	VNQLVEAATDIA	B105
DD-ligase	187	EFTV	190
<i>E. coli</i> SCS	B107	ELYL	B110
DD-ligase	256	IDVMLDSDGQFYLLA	271
<i>E. coli</i> SCS	B199	NPLVITKQGD L ICLDG	B214
DD-ligase	281	SLVPM	285
<i>E. coli</i> SCS	B132	EIEKV	B136

---

<sup>a</sup> The prefix A denotes residues from the  $\alpha$ -subunit of *E. coli* SCS, while B denotes residues from the  $\beta$ -subunit.

<sup>b</sup> The alignment was performed initially using the C- $\alpha$  positions of residues 139 to 146 from DD-ligase and residues 41 $\beta$  to 48 $\beta$  from SCS, and subsequently improved using the program O<sup>1</sup> with a distance cut-off of 3.8 Å. The root mean squared deviation of the C- $\alpha$  positions was 1.960 Å.

<sup>1</sup> Jones, T. A., Zou, J. Y., Cowan, S. W., & Kjeldgaard, M. (1991) *Acta Cryst.* A47, 110-119.

## Appendix 5.

### Residues Used in the Structural Alignment of the Large Subdomain of the N-terminal Domain of the $\beta$ -subunit of *E. coli* SCS with DD-ligase.<sup>a,b</sup>

---

DD-ligase	25	AVLA	28
<i>E. coli</i> SCS	A254	GKGT	A257
DD-ligase	91	SALS	94
<i>E. coli</i> SCS	B2	NLHE	B5
DD-ligase	183	LSGPEFTVAIL	193
<i>E. coli</i> SCS	B103	DIAKELYLGAV	B113
DD-ligase	200	SIRI	203
<i>E. coli</i> SCS	B125	ASTE	B128
DD-ligase	226	PAGLE	230
<i>E. coli</i> SCS	B166	KLGLE	B170
DD-ligase	233	QEANL	237
<i>E. coli</i> SCS	B173	LVQQF	B177
DD-ligase	251	KGWGRI	256
<i>E. coli</i> SCS	B193	LALIEI	B198
DD-ligase	257	DVMLDSGQFYLLLEANT	273
<i>E. coli</i> SCS	B200	PLVITRQGDLICLDGKL	B216

---

<sup>a</sup> The prefix A denotes residues from the  $\alpha$ -subunit of *E. coli* SCS, while B denotes residues from the  $\beta$ -subunit.

<sup>b</sup> The alignment was performed initially using the C- $\alpha$  positions of residues 187 to 191 from DD-ligase and residues 107 $\beta$  to 111 $\beta$  from SCS, and subsequently improved using the program O with a distance cut-off of 3.8 Å. The root mean squared deviation of the C- $\alpha$  positions was 1.927 Å.

## Appendix 6.

Residues Used in the Structural Alignment of *E. coli* and Pig Heart SCS.<sup>a,b</sup>


---

<i>E. coli</i>	A3	LIDKNTKVICQGFTGSQGFTHSEQAIAYGTKMVGCVTPGKGGTTHLGLPV			
Pig heart	A11	YVDKNTKVICQGFTGKQGFTHSQQALEYGTNLVGGTTPGKGGKTHLGLPV			
<i>E. coli</i>	A53	FNTVREAVAATGATASVIYVPAPFCKDSILEAIDAGIKLIITITEGIPTL			
Pig heart	A61	FNTVKEAKEQTGATASVIYVPPFFAAAAINEAIDAEVPLVVCITEGIPQQ			
<i>E. coli</i>	A103	DMLTVKVKLDEAG	A115		
Pig heart	A111	DMVRVKHRLLRQ	A123		
<i>E. coli</i>	A116	VRMIGPNCPGVITPGECKIGIQPGHIHKPGKVGIVSRSGTLTYEAVKQTT			
Pig heart	A125	TRLIGPNCPGVINPGECKIGIMPGHIIKKGRIGIVSRSGTLTYEAVHQTT			
<i>E. coli</i>	A166	DYGFQSTCVGIGGDP I PGSNF IDILEMFEKDPQTEAIVMIGEIGGSAAE			
Pig heart	A175	QVGLGQSLCVGIGGDPFNGTDFTDCLIFLNDPATEGIILIGEIGGNAEE			
<i>E. coli</i>	A216	EAAAYIKEHV	A225		
Pig heart	A225	NAAEFLKQHN	A234		
<i>E. coli</i>	A226	TKPVVGYIAGVTAPKGRMGAGAI IAGGKGTADKFAALEAAGVKTIRS			
Pig heart	A239	SKPVVSFIAGLTAPPGRRMGGAGAI IAGGKGGAKAKITALQSAGVVVMS			
<i>E. coli</i>	A276	LADIGEALKTV	A286		
Pig heart	A289	PAQLGTTIYKE	A299		
<i>E. coli</i>	B1	MNLHEYQAKQLFARYGLPAPVGYACTTPREA	B31		
Pig heart	B1	VNLQEYQSKKLMSDNGVKVARFFVASTAAAA	B31		
<i>E. coli</i>	B33	EAASKIG	B39	B42	PWVVKCQV B49
Pig heart	B33	AAAKRLN	B39	B42	EIVLKAQI B49
<i>E. coli</i>	B94	NQILVEAATDIAKELYLGAVVDRSSRRVVFMASTEGGVEIEKVAEETPHL			
Pig heart	B101	NKVMVAEALDISRETYLA I LMDRSCNGPVLVGSPOGGVDIEEVAASNPEL			
<i>E. coli</i>	B144	IHKVALDPLTGMPYQGRELAFKLGLEGKLVQOFTKIFMGLATIFLERDL			
Pig heart	B151	IFKEQIDIIEGIKDSQAQRMAENLGFGLQNLQAADQIKKLYNLFKIDA			
<i>E. coli</i>	B194	ALIEINPLVITKQGDLCIDGKLGADGNALFRQPD LREMRDQS	B236		
Pig heart	B201	TQVEVNPFGETPEGQVVCDAKINFDDNAEFRQKDI FAMD DKS	B243		
<i>E. coli</i>	B238	EDPREAQAQWELNYVALDGNIGCMVNGAGLAMGTMDIVKLHGGE PANFL			
Pig heart	B245	NEPIENEAAKSDLAYIGLDGNIACVVNGAGLAMATCDIIFLNGGK PANFL			
<i>E. coli</i>	B288	DVG	B290		
Pig heart	B295	DLG	B297		
<i>E. coli</i>	B296	ERVTEAFKIILSDDKVKAVLVNIFGGIVRCDLIADGIIGAVAEVGVNVPV			
Pig heart	B303	SAVYQAFKLLTADPKVEAILVNIFGGIVNNAI IANGITKAARELELKVPA			
<i>E. coli</i>	B346	VVRLEGNAELGAKKLADSGLNIIAAKGLTDAQQVVAAV	B385		
Pig heart	B353	VVRLEGTNVHEAQNILTNSGLPITSAVDLEDAAKKAVASV	B340		

---

<sup>a</sup> The prefix A denotes residues from the  $\alpha$ -subunit of SCS, while B denotes residues from the  $\beta$ -subunit.

<sup>b</sup> The alignment was performed initially using the C- $\alpha$  positions of residues 11 $\alpha$  to 31 $\alpha$  from pig heart SCS and residues 3 $\alpha$  to 23 $\alpha$  from *E. coli* SCS, and subsequently improved using the program O with a distance cut-off of 3.8 Å. The root mean squared deviation of the C- $\alpha$  positions was 1.363 Å.



## Appendix 7.

### Residues Used in the Structural Alignment of the Model from the First Experiment and Native *E. coli* SCS.

Fragments used in the alignment:

Chain A: 1-129, 131-152, 157-284

Chain B: 1-138, 140-174, 176-319, 323-332, 335-384

Chain D: 1-27,31-63, 65-114, 116-138, 140-153,158-167, 169-218, 220-284

Chain E: 1-289, 293-309, 311-321, 323-354, 359-372, 374-382

The alignment was performed initially using the C $\alpha$  positions of residues 245 $\alpha$  to 247 $\alpha$  from *E. coli* SCS, and subsequently improved using the program O with a distance cut-off of 0.5 Å. The root mean squared deviation of the C $\alpha$  positions for these 1294 atoms was 0.217 Å.

### Residues Used in the Structural Alignment of the Model from ADP-Bound and Native *E. coli* SCS.

Fragments used in the alignment:

Chain A: 1-41, 45-85, 87-122, 131-134, 148-160, 177-195, 198-201, 203-220, 227, 252, 259-263

Chain B: 1-17, 21-29, 47-50, 74-80, 94-98, 104-130, 132-141, 143-168, 173-204, 207-279, 282-288, 293-322, 325-333, 335-340, 342-346

Chain D: 95-98

Chain E: 1-8, 19-30, 32-35, 43-46, 48-52, 71-79, 93-94, 188-192, 198-201, 234-237

The alignment was performed initially using the C $\alpha$  positions of residues 245 $\alpha$  to 247 $\alpha$  from *E. coli* SCS, and subsequently improved using the program O with a distance cut-off of 0.5 Å. The root mean squared deviation of the C $\alpha$  positions for these 546 atoms was 0.324 Å.